water

Special Issue Reprint

Groundwater Depletion

Current Trends and Future Challenges to Mitigate the Phenomenon

Edited by
Nerantzis Kazakis, Micòl Mastrocicco and Konstantinos Chalikakis

mdpi.com/journal/water

MDPI

Groundwater Depletion: Current Trends and Future Challenges to Mitigate the Phenomenon

Groundwater Depletion: Current Trends and Future Challenges to Mitigate the Phenomenon

Guest Editors

Nerantzis Kazakis
Micòl Mastrocicco
Konstantinos Chalikakis

MDPI

Basel • Beijing • Wuhan • Barcelona • Belgrade • Novi Sad • Cluj • Manchester

Guest Editors
Nerantzis Kazakis
Department of Geology
Aristotle University of Thessaloniki
Thessaloniki
Greece

Micòl Mastrocicco
Department of Environmental, Biological and Pharmaceutical Sciences and Technologies
University of Campania "Luigi Vanvitelli"
Caserta
Italy

Konstantinos Chalikakis
EMMAH, INRAE
Avignon Université
Avignon
France

Editorial Office
MDPI AG
Grosspeteranlage 5
4052 Basel, Switzerland

This is a reprint of the Special Issue, published open access by the journal *Water* (ISSN 2073-4441), freely accessible at: https://www.mdpi.com/journal/water/special_issues/Groundwater_Depletion.

For citation purposes, cite each article independently as indicated on the article page online and as indicated below:

Lastname, A.A.; Lastname, B.B. Article Title. *Journal Name* **Year**, *Volume Number*, Page Range.

ISBN 978-3-7258-8375-2 (Hbk)
ISBN 978-3-7258-8376-9 (PDF)
https://doi.org/10.3390/books978-3-7258-8376-9

© 2026 by the authors. Articles in this reprint are Open Access and distributed under the Creative Commons Attribution (CC BY) license. The reprint as a whole is distributed by MDPI under the terms and conditions of the Creative Commons Attribution-NonCommercial-NoDerivs (CC BY-NC-ND) license (https://creativecommons.org/licenses/by-nc-nd/4.0/).

Contents

Nerantzis Kazakis, Micol Mastrocicco and Konstantinos Chalikakis
Groundwater Depletion: Current Trends and Future Challenges to Mitigate the Phenomenon
Reprinted from: *Water* **2024**, *16*, 2385, https://doi.org/10.3390/w16172385 . . . . . **1**

Petrut-Liviu Bogdan, Valentin Nedeff, Mirela Panainte-Lehadus, Dana Chitimuș, Narcis Barsan and Florin Marian Nedeff
Delineation of Groundwater Potential Zones Using Geospatial Techniques. Case Study: Roman City and the Surrounding Area in the Northeastern Region, Romania
Reprinted from: *Water* **2024**, *16*, 3013, https://doi.org/10.3390/w16213013 . . . . . **3**

Mathieu Bertrand, Catherine Bertrand, Naomi Mazzilli, Sylvain Gigleux, Sophie Denimal, Rémi Valois, et al.
Advancing the Understanding of Complex Piezometric Information: A Methodological Approach Integrating Long-Term Piezometry, Surface Nuclear Magnetic Resonance, and Fracture Analysis Using Insights from the "Calcaires du Barrois" Series, France
Reprinted from: *Water* **2024**, *16*, 1700, https://doi.org/10.3390/w16121700 . . . . . **19**

Ahmed Shalby, Bakenaz A. Zeidan, Katarzyna Pietrucha-Urbanik, Abdelazim M. Negm and Asaad M. Armanuos
Modelling Approach for Assessment of Groundwater Potential of the Moghra Aquifer, Egypt, for Extensive Rural Development
Reprinted from: *Water* **2024**, *16*, 1562, https://doi.org/10.3390/w16111562 . . . . . **44**

Maria Perraki, Vasilios Skliros, Petros Mecaj, Eleni Vasileiou, Christos Salmas, Ioannis Papanikolaou and Georgios Stamatis
Identification of Microplastics Using μ-Raman Spectroscopy in Surface and Groundwater Bodies of SE Attica, Greece
Reprinted from: *Water* **2024**, *16*, 843, https://doi.org/10.3390/w16060843 . . . . . **66**

Eleni-Anna Nanou, Konstantinos Perdikaris, Panagiotis Tserolas and Eleni Zagana
Recharge Assessment in Greek Karst Systems: Methodological Considerations and Implications
Reprinted from: *Water* **2024**, *16*, 568, https://doi.org/10.3390/w16040568 . . . . . **86**

Min Liu, Zhenlong Nie, Le Cao, Lifang Wang and Huixiong Lu
Nature-Based Solutions for the Restoration of Groundwater Level and Groundwater-Dependent Ecosystems in a Typical Inland Region in China
Reprinted from: *Water* **2024**, *16*, 33, https://doi.org/10.3390/w16010033 . . . . . **103**

Dimitrios Malamataris, Anna Chatzi, Konstantinos Babakos, Vassilios Pisinaras, Evangelos Hatzigiannakis, Barbara A. Willaarts, et al.
A Participatory Approach to Exploring Nexus Challenges: A Case Study on the Pinios River Basin, Greece
Reprinted from: *Water* **2023**, *15*, 3949, https://doi.org/10.3390/w15223949 . . . . . **120**

Ploutarchos Tzampoglou and Constantinos Loupasakis
Hydrogeological Hazards in Open Pit Coal Mines–Investigating Triggering Mechanisms by Validating the European Ground Motion Service Product with Ground Truth Data
Reprinted from: *Water* **2023**, *15*, 1474, https://doi.org/10.3390/w15081474 . . . . . **152**

Georgios Louloudis, Christos Roumpos, Emmanouil Louloudis, Eleni Mertiri and Georgios Kasfikis
Repurposing of a Closed Surface Coal Mine with Respect to Pit Lake Development
Reprinted from: *Water* **2022**, *14*, 3558, https://doi.org/10.3390/w14213558 . . . . . **168**

Kashif Mehmood, Bernhard Tischbein, Martina Flörke and Muhammad Usman
Spatiotemporal Analysis of Groundwater Storage Changes, Controlling Factors, and Management Options over the Transboundary Indus Basin
Reprinted from: *Water* **2022**, *14*, 3254, https://doi.org/10.3390/w14203254 . . . . . **194**

Mattia Gaiolini, Nicolò Colombani, Gianluigi Busico, Fabrizio Rama and Micòl Mastrocicco
Impact of Boundary Conditions Dynamics on Groundwater Budget in the Campania Region (Italy)
Reprinted from: *Water* **2022**, *14*, 2462, https://doi.org/10.3390/w14162462 . . . . . **214**

Christopher Papadopoulos, Mike Spiliotis, Fotios Pliakas, Ioannis Gkiougkis, Nerantzis Kazakis and Basil Papadopoulos
Hybrid Fuzzy Multi-Criteria Analysis for Selecting Discrete Preferable Groundwater Recharge Sites
Reprinted from: *Water* **2022**, *14*, 107, https://doi.org/10.3390/w14010107 . . . . . **231**

Constantinos Loupasakis and Ploutarchos Tzampoglou
Reply to Louloudis et al. Comments on "Tzampoglou, P.; Loupasakis, C. Hydrogeological Hazards in Open Pit Coal Mines–Investigating Triggering Mechanisms by Validating the European Ground Motion Service Product with Ground Truth Data. *Water* 2023, *15*, 1474"
Reprinted from: *Water* **2025**, *17*, 2436, https://doi.org/10.3390/w17162436 . . . . . **257**

Georgios Louloudis, Christos Roumpos, Eleni Mertiri and Petros Kostaridis
Comment on Tzampoglou, P.; Loupasakis, C. Hydrogeological Hazards in Open Pit Coal Mines–Investigating Triggering Mechanisms by Validating the European Ground Motion Service Product with Ground Truth Data. *Water* 2023, *15*, 1474
Reprinted from: *Water* **2025**, *17*, 2343, https://doi.org/10.3390/w17152343 . . . . . **261**

water

MDPI

Editorial

Groundwater Depletion: Current Trends and Future Challenges to Mitigate the Phenomenon

Nerantzis Kazakis [1,*], Micol Mastrocicco [2] and Konstantinos Chalikakis [3]

[1] Laboratory of Hydrogeology, Department of Geology, Faculty of Natural Sciences, University of Patras, 26504 Rion, Greece
[2] Department of Environmental, Biological and Pharmaceutical Sciences and Technologies, University of Campania "Luigi Vanvitelli", Via Vivaldi 43, 81100 Caserta, Italy; micol.mastrocicco@unicampania.it
[3] UMR 1114 EMMAH (AU-INRAE), Avignon Université, 84029 Avignon, France; konstantinos.chalikakis@univ-avignon.fr
* Correspondence: nkazakis@upatras.gr

Groundwater constitutes the primary source of drinking water for more than two billion people across the globe. Additionally, groundwater contributes to food and energy security, as well as human health and ecosystem preservation. However, groundwater depletion is a common phenomenon worldwide. This phenomenon appears when extraction surpasses the recharge of the aquifer, and it is triggered by the socioeconomic framework and controlled by the aquifer regime. Groundwater depletion can lead to seawater intrusion in coastal aquifers, a reduction in river base flow, upconing of deep geothermal water, and increased pumping costs. Groundwater depletion has been reported on both a global and regional scale. This Special Issue, entitled "Groundwater Depletion: Current Trends and Future Challenges to Mitigate the Phenomenon", attempts to highlight the efficiency and adequacy of global and regional strategies to mitigate the phenomenon and to promote the transition from regional to aquifer scale. Additionally, it is critically important to appraise the role of climate variability, management practices, and the monitoring of groundwater reserves. The Special Issue also provides the state-of-the-art of tools and methods to map, model, and forecast the phenomenon.

Particularly, this Special Issue includes 11 articles, providing all aspects of the groundwater depletion phenomenon in several different countries incorporating aquifers with different hydrogeological conditions. In an article by Papadopoulos et al. (Contribution 1), the fuzzy logic approach was used to develop a multi-criteria model for the selection of groundwater recharge sites. The model was developed for the aquifer system in the agricultural plain of the Prefecture of Xanthi in northeast Greece. In the unconfined aquifers of the Campania region in southern Italy, a simulation model was obtained in order to determine the dynamic and the impact of boundary conditions on groundwater budget. The non-uniform extinction depth is highlighted as the most influential in aquifer dynamics, while both sea level and rivers scarcely affect groundwater budgets (Contribution 2). Contribution 3 estimated the groundwater storage changes/anomalies (GWCs) in the Indus River Basin, using data from GRACE and the WaterGAP Hydrological Model. Groundwater storage is mainly triggered in the study area by climatic variations and increased pumping for irrigation.

Contribution 4 suggested the use of a closed-surface coal mine as lake to store water and use it for energy production, irrigation, and as a recreation park. Tzampoglou and Loupasakis (Contribution 5) used satellite and in situ data to provide evidence of the overexploitation of the aquifer in the Amyntaio basin, both by dewatering wells of an open-pit coal mine and irrigation wells. Contribution 6 introduced a comprehensive methodology for water resource management, including "framing", "mapping", "involvement", "co-production", and "sharing" phases. Contribution 7 suggested a nature-based solution for the restoration of groundwater level decline in the Gansu Province of China. Contribution 8

provided the results of the APLIS model for the estimation of groundwater recharge in Karst aquifers in southern Greece. The occurrence of microplastics was identified in the groundwater of SE Attica, Greece (Contribution 9). Contribution 10 highlighted the complementarity of long-term piezometric data combined with hydrogeophysics and fracture analysis to understand complex aquifer structure and groundwater dynamics. Groundwater flow dynamics were estimated using a numerical model (FEFLOW) in the Moghra desert of Egypt (Contribution 11).

We wish to extend our gratitude to the authors who contributed to this Special Issue, to the reviewers for their invaluable support, and to the organizers and staff of MDPI for their dedication in bringing this issue to completion and publication.

We believe that this work will stimulate researchers to quantify groundwater depletion at several sites worldwide and suggest strategies to mitigate the phenomenon at the aquifer scale.

Conflicts of Interest: The authors declare no conflict of interest.

List of Contributions:

1. Papadopoulos, C.; Spiliotis, M.; Pliakas, F.; Gkiougkis, I.; Kazakis, N.; Papadopoulos, B. Hybrid Fuzzy Multi-Criteria Analysis for Selecting Discrete Preferable Groundwater Recharge Sites. *Water* **2022**, *14*, 107. https://doi.org/10.3390/w14010107.
2. Gaiolini, M.; Colombani, N.; Busico, G.; Rama, F.; Mastrocicco, M. Impact of Boundary Conditions Dynamics on Groundwater Budget in the Campania Region (Italy). *Water* **2022**, *14*, 2462. https://doi.org/10.3390/w14162462.
3. Mehmood, K.; Tischbein, B.; Flörke, M.; Usman, M. Spatiotemporal Analysis of Groundwater Storage Changes, Controlling Factors, and Management Options over the Transboundary Indus Basin. *Water* **2022**, *14*, 3254. https://doi.org/10.3390/w14203254.
4. Louloudis, G.; Roumpos, C.; Louloudis, E.; Mertiri, E.; Kasfikis, G. Repurposing of a Closed Surface Coal Mine with Respect to Pit Lake Development. *Water* **2022**, *14*, 3558. https://doi.org/10.3390/w14213558.
5. Tzampoglou, P.; Loupasakis, C. Hydrogeological Hazards in Open Pit Coal Mines–Investigating Triggering Mechanisms by Validating the European Ground Motion Service Product with Ground Truth Data. *Water* **2023**, *15*, 1474. https://doi.org/10.3390/w15081474.
6. Malamataris, D.; Chatzi, A.; Babakos, K.; Pisinaras, V.; Hatzigiannakis, E.; Willaarts, B.A.; Bea, M.; Pagano, A.; Panagopoulos, A. A Participatory Approach to Exploring Nexus Challenges: A Case Study on the Pinios River Basin, Greece. *Water* **2023**, *15*, 3949. https://doi.org/10.3390/w15223949.
7. Liu, M.; Nie, Z.; Cao, L.; Wang, L.; Lu, H. Nature-Based Solutions for the Restoration of Groundwater Level and Groundwater-Dependent Ecosystems in a Typical Inland Region in China. *Water* **2024**, *16*, 33. https://doi.org/10.3390/w16010033.
8. Nanou, E.-A.; Perdikaris, K.; Tserolas, P.; Zagana, E. Recharge Assessment in Greek Karst Systems: Methodological Considerations and Implications. *Water* **2024**, *16*, 568. https://doi.org/10.3390/w16040568.
9. Perraki, M.; Skliros, V.; Mecaj, P.; Vasileiou, E.; Salmas, C.; Papanikolaou, I.; Stamatis, G. Identification of Microplastics Using μ-Raman Spectroscopy in Surface and Groundwater Bodies of SE Attica, Greece. *Water* **2024**, *16*, 843. https://doi.org/10.3390/w16060843.
10. Bertrand, M.; Bertrand, C.; Mazzilli, N.; Gigleux, S.; Denimal, S.; Valois, R.; Girod, L.-M.; Cinkus, G.; Busquet, V.; Chalikakis, K. Advancing the Understanding of Complex Piezometric Information: A Methodological Approach Integrating Long-Term Piezometry, Surface Nuclear Magnetic Resonance, and Fracture Analysis Using Insights from the "Calcaires du Barrois" Series, France. *Water* **2024**, *16*, 1700. https://doi.org/10.3390/w16121700.
11. Shalby, A.; Zeidan, B.A.; Pietrucha-Urbanik, K.; Negm, A.M.; Armanuos, A.M. Modelling Approach for Assessment of Groundwater Potential of the Moghra Aquifer, Egypt, for Extensive Rural Development. *Water* **2024**, *16*, 1562. https://doi.org/10.3390/w16111562.

Disclaimer/Publisher's Note: The statements, opinions and data contained in all publications are solely those of the individual author(s) and contributor(s) and not of MDPI and/or the editor(s). MDPI and/or the editor(s) disclaim responsibility for any injury to people or property resulting from any ideas, methods, instructions or products referred to in the content.

water

MDPI

Article

Delineation of Groundwater Potential Zones Using Geospatial Techniques. Case Study: Roman City and the Surrounding Area in the Northeastern Region, Romania

Petrut-Liviu Bogdan [1,2,*], Valentin Nedeff [1], Mirela Panainte-Lehadus [1], Dana Chitimuș [1], Narcis Barsan [1] and Florin Marian Nedeff [1]

[1] Faculty of Engineering, Vasile Alecsandri University of Bacau, 157 Calea Marasesti, 600115 Bacau, Romania; vnedeff@ub.ro (V.N.); mirelap@ub.ro (M.P.-L.); dana.chitimus@ub.ro (D.C.); narcis.barsan@ub.ro (N.B.); florin_nedeff@ub.ro (F.M.N.)

[2] National Administration "Romanian Waters"—Siret River Basin Administration, Cuza Voda No. 1, 600274 Bacau, Romania

* Correspondence: bogdan.p.liviu@gmail.com

Abstract: Effective groundwater management is crucial under the current climatic conditions, addressing both qualitative and quantitative aspects. An important step in delineating groundwater potential zones involves remote sensing (RS) data and geographic information systems (GISs), facilitating resource assessment, and the implementation of suitable field data management. This study introduces the delineation of potential groundwater zones using seven layers and the Multi-Criteria Decision Analysis (MCDA) method. Satty's Analytic Hierarchy Process (AHP) was employed to rank the seven selected parameters, contributing to the advancement of groundwater research and resource assessment. All seven thematic layers (Rainfall, Geology, Land Use/Land Cover, Drainage Density, Elevation, Slope, and Soil) were prepared and analyzed to delineate groundwater potential zones. The resulting groundwater potential zone map was categorized into four classes, Very Good, Good, Moderate, and Poor, covering areas of 81.53 km^2 (45.1%), 56.36 km^2 (31.2%), 19.54 km^2 (10.8%), and 23.17 km^2 (12.8%) of the total area, respectively. The accuracy of the output was validated by comparing it with information on groundwater prospects in the area, and the overall accuracy of the method was approximately 72%. High-yield boreholes were drilled and concentrated in the Very Good groundwater potential zones, while low-yield ones were developed in the Poor areas.

Keywords: groundwater potential; multi-criteria decision-maker; AHP; GIS techniques; remote sensing

1. Introduction

Climate change plays a significant role in and has important implications for groundwater resources and the hydrological cycle [1–4]. In recent decades, due to a growing global population, the demand for freshwater has increased substantially, with the necessity of water for irrigation and industrialization leading to more frequent instances of water scarcity [5–8].

Groundwater is one of the most important resources, stored in various geological formations, showing variations in quantity and quality, as well as different parameters, including temperature, chemistry, flow direction, and interactions with surface water systems [9–13]. Preserving and conserving groundwater resources is a pressing issue of the 21st century, with water management posing a significant challenge for governments worldwide [11,14,15].

The study area is located in the Siret River Basin, and the primary source of supply comes from groundwater, specifically from the ROSI03 aquifer, a phreatic groundwater body, utilized in varying proportions: 67.7% for meeting the population's demands, 2.3% for agriculture, and 30% for industrial sector [16]. The examined region is positioned

upstream from the confluence of two major rivers, namely the Moldova River and the Siret River, situated in the Siret River watershed, and is primarily characterized as an agricultural zone.

The conventional methodologies employed for the identification, delineation, and mapping of groundwater potential zones primarily rely on on-site surveys utilizing geophysical, geological, and hydrogeological tools, but these methods are typically characterized by high costs and time-intensive processes [4,14,17]. The introduction of geospatial tools in the field of geosciences is an efficient approach, particularly when it comes to groundwater exploration before resorting to conventional exploration and exploitation techniques [18]. Remote sensing technologies (RI) and the Geographic Information System (GIS) provide a rapid and cost-effective method for estimating underground resources [19–21]. In the context of delineating groundwater potential zones and mapping them, this study employs a combination of GIS technology and the Analytical Hierarchy Process (AHP). AHP, developed by Thomas Saaty in 1980, proves to be an effective method for simplifying complex decision-making through direct comparisons to a series of pairwise comparisons and for summarizing result integration [22]. Choosing AHP for this study was a decision based on the advantages of the method, particularly its ability to utilize multi-criteria decision-making for integrating diverse thematic layers, which is essential for delineating groundwater potential zones. Although other methods such as Machine Learning, Fuzzy Logic, and Artificial Neural Networks exist, AHP was selected for its simplicity, ease of application, and validation in various studies [14,23,24]. Furthermore, AHP is a suitable technique for ensuring result consistency, thereby minimizing subjective influences in the decision-making process [25]. The GIS was used to perform weighted overlay analysis on the layer maps, considering the priorities determined by the AHP, resulting in the identification of potential groundwater zones [26–28].

Various studies worldwide have focused on identifying potential groundwater zones utilizing GIS and mathematical models. For instance, Shreeya Baghel et al. [14] in their study on groundwater potential in the catchment of the Mahandi Basin, D. C. Jhariya et al. [10] in their paper assessing groundwater potential zones in Raipur city, India, Aysha Akter et al. [21] with the study predicting groundwater potential zones using GIS techniques, and Mustafa et al. [29] in their study of the Demirci district (Turkey) highlighted the effective integration of various factors, including geology, geomorphology, rainfall, land use/land cover (LULC), drainage density, slope, groundwater level depth, and soil texture. These studies employed the weighted index analytical hierarchy process (AHP) method to develop groundwater potential models, contributing to a clear understanding of groundwater potential. These findings affirm the method's utility across varied geographical contexts and suggest that the results obtained are similar to those presented in this study.

Taking all aspects into consideration, the primary goal of this study, which combines AHP with RS and GIS, is to outline, recognize, and map groundwater potential zones to facilitate the sustainable management of water resources in the region.

2. Materials and Methods

The present study was conducted in the northeast of Romania on the east part of Neamț county. The region of interest (ROI) described in this paper is situated in the south extremity of Fălticeni Plateau, to the confluence of two major rivers, Moldova on the west boundary and Siret on the east boundary [30]. The study area has a total surface of 180.6 square km, shown in Figure 1. The coordinate system used in this study is Stereo 70(EPSG31700), specific to Romania and and for all maps used in this article. For better international recognition, the equivalent coordinates in WGS 84(EPSG4326) are provided as follows: the study area is located between latitudes 46°54′28.22″ N and 47°05′30.26″ N, and longitudes 26°46′43.81″ E and 26°58′15.50″ E.

The area comprises the city of Roman, with the highest economic and industrial development, and the surrounding northern municipalities, which, in general, are predominantly

characterized by agricultural activities [31]. The average elevation of the study area varies from 175 to 260 m above the mean sea level.

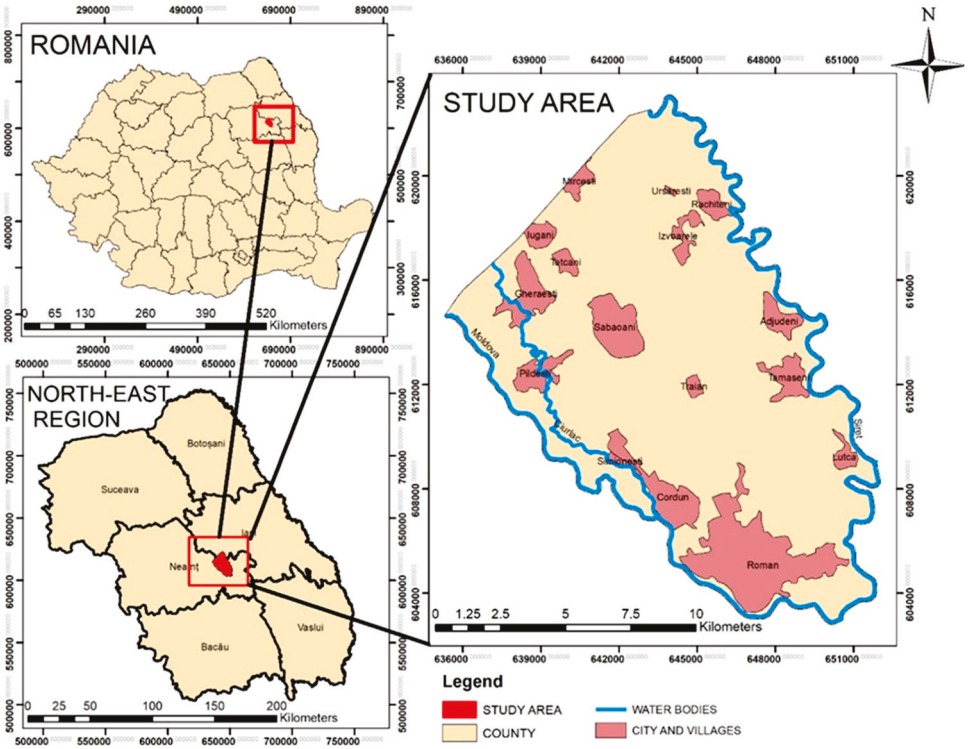

Figure 1. Study area.

2.1. Data Acquisition

In the process of identifying potential groundwater zones within the region of interest (ROI), a variety of geospatial techniques were employed. The methodology involves digital image processing, digital elevation model (DEM) evaluation, and field studies including hydrogeological data.

To delineate the groundwater potential zone (GPZ) for the study area, seven parameters such as geology, rainfall, slope, drainage density, Land Use and Cover (LULC), soil and elevation, as presented in Table 1, were analyzed. One of the datasets required for the study is represented by the digital elevation model (DEM) which has been acquired from the United States Geological Survey through the Shuttle Radar Topography Mission (SRTM) with a resolution of 30 m (cell size = 30 × 30 m/pixel). The DEM was used to delineate the boundaries of the ROI, drainage density and the slope using different techniques and spatial tools in ArcGis 10.8 software. Precipitation data were acquired from pluviometric gauging stations belonging to the Siret River Basin Administration Bacău. The data were processed to create rainfall maps with ArcGIS software using the IDW interpolation tool. The geological data were processed by digitizing the Geological map of Romania, L-25-IX, 13 Piatra Neamț at a scale of 1:200,000, and the soil data were prepared by digitizing the Soil Map of Romania at a scale of 1:200,000. The Land Use and Land Cover (LULC) map was generated from LANDSAT 8 OLI (Operational Land Imager) data from 2020 with a 30 m resolution using supervised image classification in ArcGIS10.8.

The entire workflow process is described in Figure 2 according to the data shown in Table 1. This representation summarizes the steps involved in delineating groundwater potential zones, integrating various data. This visualization aids in effectively communicating the methodology employed and facilitates a deeper understanding of the groundwater potential assessment process.

Table 1. Principal database used in groundwater potential study.

S. No	Data Used	Parameters	Scale/Resolution	Source	Application
1	Elevation Data	Drainage Density, Slope, Location of the study area	30 m	[32]	Boundary Area, Calculate GWPZ
2	Meteorological data	Rainfall map	30 m	[16,33]	Calculate GWPZ
3	Soil Map	Soil Texture, Soil type	1:200,000	[34]	Calculate GWPZ
4	Geological Map	Geology type	1:200,000	[35]	Calculate GWPZ
5	LANDSAT 8 OLI	Land Use and Cover map (LULC)	30 m	[31]	Calculate GWPZ
6	Hydrogeological maps	Hydrogeological data (groundwater table, groundwater flow rate)	1:200,000	[33]	Result Validation

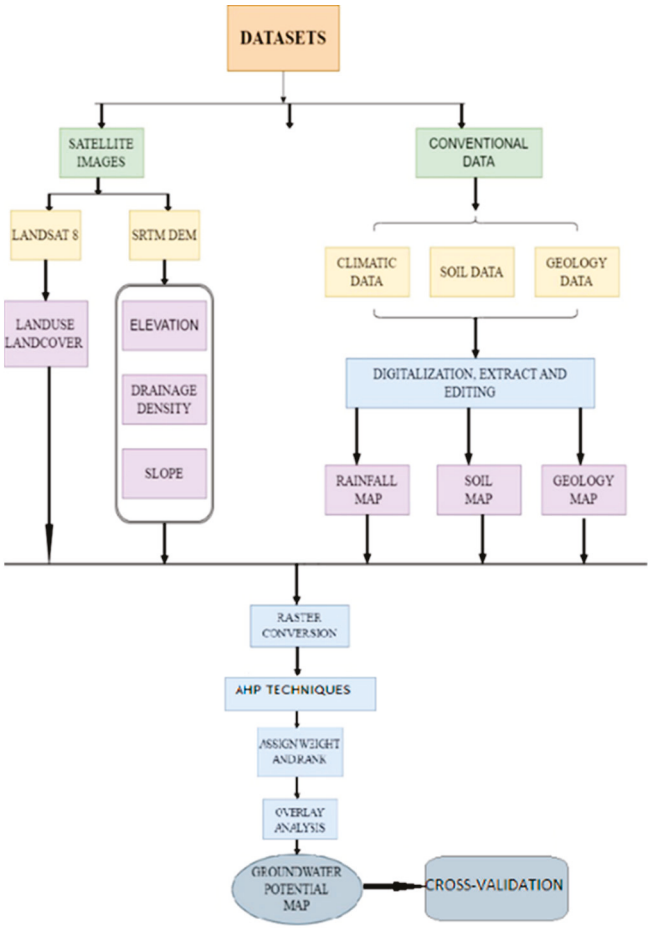

Figure 2. Flowchart.

2.2. Multi-Criteria Decision Analysis Using AHP

Analytical Hierarchical Process (AHP) is one of the most used and well-known GIS method for delineating groundwater potential zones by integrating all thematic layers. In this study, we used seven different layers with sub-criteria that have a different weight in controlling groundwater flow and storage in the area. These factors are weighted according to their local impact on the presence of groundwater and expert judgement/opinion. In the specialized literature, there are studies that establish similar weights for factors, depending on their importance in different hydrogeological contexts [5,10,14].

The Analytical Hierarchy Process (AHP), first introduced by L. Saaty, is a technique for multicriteria decision-making [36]. It utilizes a pairwise comparison matrix to determine

scale ratios between different criteria. According to Saaty's scale, presented in Tables 2 and 3, in pairwise comparisons, a value of 1 is assigned to two thematic layers when they are considered to have equal importance for groundwater potential, while a value of 9 is given to represent extreme importance in such pairs [22]. According to each layer importance, we created a pairwise comparison matrix for seven variables, presented in Table 4. Various weights were allocated to thematic layers, reflecting their significance in terms of water retention capacity. The total weight (TW) was obtained by the total value of the scale weight divided by the cumulative number of parameters for all thematic layers [22]. The Normalized Pairwise Comparison Matrix (NPCM) was constructed by calculating ratios derived from the division of the total value and each individual judgment value within the same column. Following that, the total of these ratio values within each row was divided by the count of parameters in the pairwise comparison matrix [37].

Table 2. Analytical Hierarchy Process scale [22,36].

Intensity of Importance	Definition	Explanation
1	Equal importance	Two elements contribute equally to the goal
3	Moderate importance	Experience and judgment slightly favor one element over another
5	Strong Importance	Experience and judgment strongly favor one element over another
7	Very strong importance	One element is favored very strongly over another, and its dominance is demonstrated in practice
9	Extreme importance	The evidence favoring one element over another is of the highest possible order of affirmation
2,4,6,8 used to express intermediate values preference in weights		

The Consistent Ratio (CR) is used to validate the accuracy of the weights derived from the normalized pairwise comparison matrix. It compares the ratio between the Consistency Index (CI) and a Random Consistency Index (RI) that depends on the number of criteria used [25]:

$$CR = CI/RI \tag{1}$$

where CI is the Consistency Index; and RI is the Random Consistency Index (values obtained from Saaty's standard (Table 3)).

$$CI = (\lambda_{max} - n)/(n - 1) \tag{2}$$

where n is the number of criteria (layers); and λ_{max} is the average value of the Consistency Index (Eigen value).

Table 3. Saaty's ratio index for different values of n [37].

N	1	2	3	4	5	6	7
RI	0	0	0.58	0.89	1.12	1.24	1.32

According to Saaty, if CR is equal to 0.1 or less, it is acceptable to continue the analysis, but if the consistency value is greater than 0.1, it is necessary for the judgment to be revised [36].

$$\text{Maximum Eigen value } (\lambda_{max}) = 7.37$$

$$n = 7$$

$$\text{Consistency Index CI} = (\lambda_{max} - n)/(n - 1) = 0.06$$

$$\text{Random Index} = 1.32$$

$$\text{Consistency Ratio (CR)} = CI/RI = 0.047$$

Table 4. Pairwise comparation matrix for all thematic layers.

Variable	Rainfall	Geology	LULC	Drainage Density	Elevation	Slope	Soil	Normalized Weight
Rainfall	1	2	4	3	2	3	3	0.28
Geology	1/2	1	4	4	1	3	3	0.21
LULC	1/4	1/4	1	1/3	1/4	1/3	1	0.05
Drainage Density	1/3	1/4	3	1	1/3	1/2	3	0.09
Elevation	1/2	1	4	3	1	2	3	0.19
Slope	1/3	1/3	3	2	1/2	1	3	0.12
Soil	1/3	1/3	1	1/3	1/3	1/3	1	0.06

2.3. Weighted Overlay Analysis (WOA)

Following the transformation to a cell size of 30 × 30 m, the thematic layers were reclassified using the obtained weighting values. Weighted Overlay Analysis (WOA) is a method that empowers users to address intricate spatial site suitability factors by integrating diverse input parameters, leading to the delineation of groundwater potential zones (GZPs). In the Weighted Overlay Analysis (WOA) tool, all reclassified raster maps are overlaid and appropriate weights are assigned. The generated raster layer was categorized into four groups of groundwater potential zones (GPZs) using consistent weight ranges in accordance with recommendations from the United Nations' Food and Agricultural Organization [38].

$$S = \sum_{i=1}^{n} (wi.xi), \tag{3}$$

where S is the total GPZ score; wi denotes the weight of the GPZ criteria; xi indicates the sub-criteria score of i GPZ criteria; and n represents the total number of GPZ criteria.

Each sub-criteria in each thematic layer received scores ranging from 1 to 5, taking into consideration favorable conditions and their importance in identifying groundwater zones. The least suitable sub-parameters were assigned a minimum score of 1, and the highest suitable sub-parameters were assigned a maximum score of 5, while sub-parameters of moderate suitability were given intermediate values for groundwater potential zone (GPZ) identification, as presented in Table 5.

Table 5. Percentage influence and scale value of individual themes for the overlay analysis.

Parameter	Influence (%)	Sub-Criteria	Feature Weight
RAINFALL	28	650.73–667.57 mm	2
		667.58–681.04 mm	3
		694.52–710.14 mm	3
		681.05–694.51 mm	3
		710.14–728.8 mm	3
GEOLOGY	21	Holocene gravel and sand deposits	4
		Pleistocene diluvial and proluvial deposits	1
		Holocene recent alluvium	3

Table 5. *Cont.*

Parameter	Influence (%)	Sub-Criteria	Feature Weight
LULC	5	Water bodies	3
		High vegetation	3
		Low vegetation	3
		Agriculture land	3
		Built-up area	1
DRAINAGE DENSITY	9	0–0.31 km/km^2	4
		0.32–0.88 km/km^2	3
		0.89–1.4 km/km^2	3
		1.5–2.0 km/km^2	2
		2.1–3.3 km/km^2	1
ELEVATION	19	175.5–189.9 m	4
		190.0–201.2 m	3
		201.3–216.8 m	2
		216.9–233.5 m	2
		233.6–260.4 m	1
SLOPE	12	0.0–1.3%	5
		1.4–3.8%	4
		3.9–8.6%	3
		8.7–16.0%	2
		16.1–53%	1
SOIL	6	Clay and silt loam	2
		Soil with variate texture	2
		Sandy loam	3
		Marshes and pounds	4
		Clayey	1

Verification and validation of the obtained GWPZ map were conducted by comparing the groundwater yield data from eleven boreholes provided by the Siret River Basin Administration in Bacău.

3. Results and Discussion

The following sections explore the outcomes and discussion of this study. This part involves the creation of thematic layers, delineation of groundwater zones, and the evaluation of map accuracy through validation. This is accomplished by comparing actual yield descriptions with the expected yield class derived from the predictive map.

3.1. Rainfall

One of the main factors influencing groundwater recharge in the study area is represented by precipitation. The intensity and duration of rainfall play an important role in infiltration dynamics. High-intensity, short-duration rain events tend to limit infiltration, favoring surface runoff, whereas low-intensity, long-duration rainfall supports greater infiltration, which can be fundamental for groundwater recharge and sustainable water resource management. The spatial distribution of the multiannual rainfall map was classified into five categories, which include (650.73–667.57) mm/year, (667.58–681.04) mm/year,

(681.05–694.51) mm/year, (694.52–710.14) mm/year, and (710.14–728.8) mm/year, as presented in Figure 3a. It is noticeable that the precipitation amounts gradually decrease near the study area's boundary.

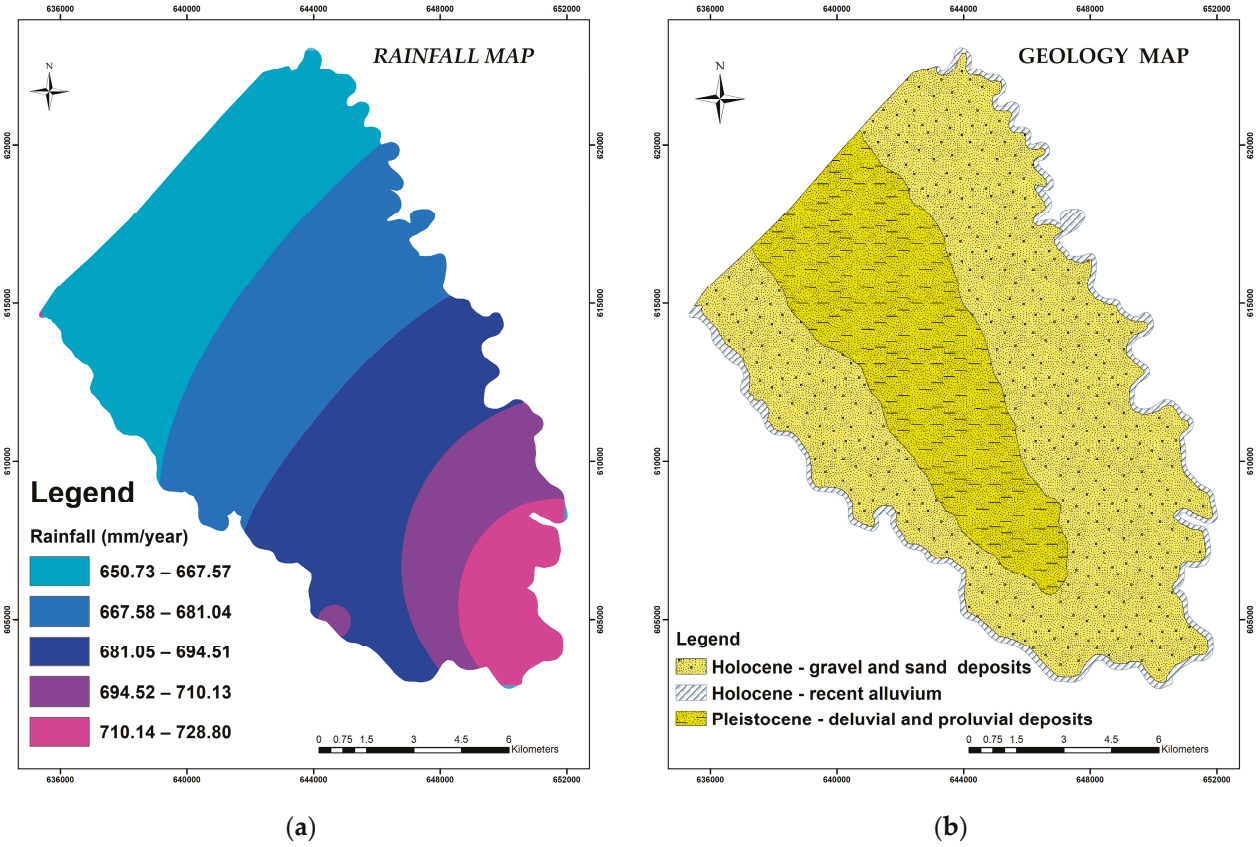

Figure 3. (**a**) Spatial distribution of precipitation; (**b**) geology map of the interest area.

3.2. Geology

Geology plays a critical role in determining the characteristics and distribution of groundwater, influencing the porosity and permeability of groundwater potential in an area, and is used in various analyzed studies where geological maps are integrated into GIS. A comparison between the geological layer used in this study and those in existing literature shows significant similarities in methodology and application [10,14]. A substantial area within the study region, presented in Figure 3b, is marked by Holocene gravel and sand deposits, while higher elevation zones display Pleistocene diluvial and proluvial deposits. According to the lithological characteristics, a higher feature weight was assigned to Holocene deposits, while a lower weight was assigned to Pleistocene deposits.

3.3. Land Use Land Cover (LULC)

Land Use and Land Cover (LULC) data are important in providing essential information regarding infiltration, soil moisture, groundwater, and surface water, and these offer perspectives on groundwater requirements. The study area's land classification was categorized into five classes, which included water bodies, high vegetation, low vegetation, agricultural land, and built-up areas presented in Figure 4a. The predominant category in the study area is represented by agricultural land, accounting for 60.2% of the total area, with a concentration in the central part of the region. Built-up areas are notably prevalent in the southern part, particularly around the Roman city and its adjacent counties. The land use and land cover were validated using Google satellite images and ground-truthing data, with a Kappa coefficient of 0.71, and the overall classification accuracy was found to be 76%, as previously reported in other studies [31]. Based on various criteria such

as water transmission and storage capacity, the "Built-Up Area" category received a low feature weight score of 1, while the remaining classes were assigned higher feature weights in general.

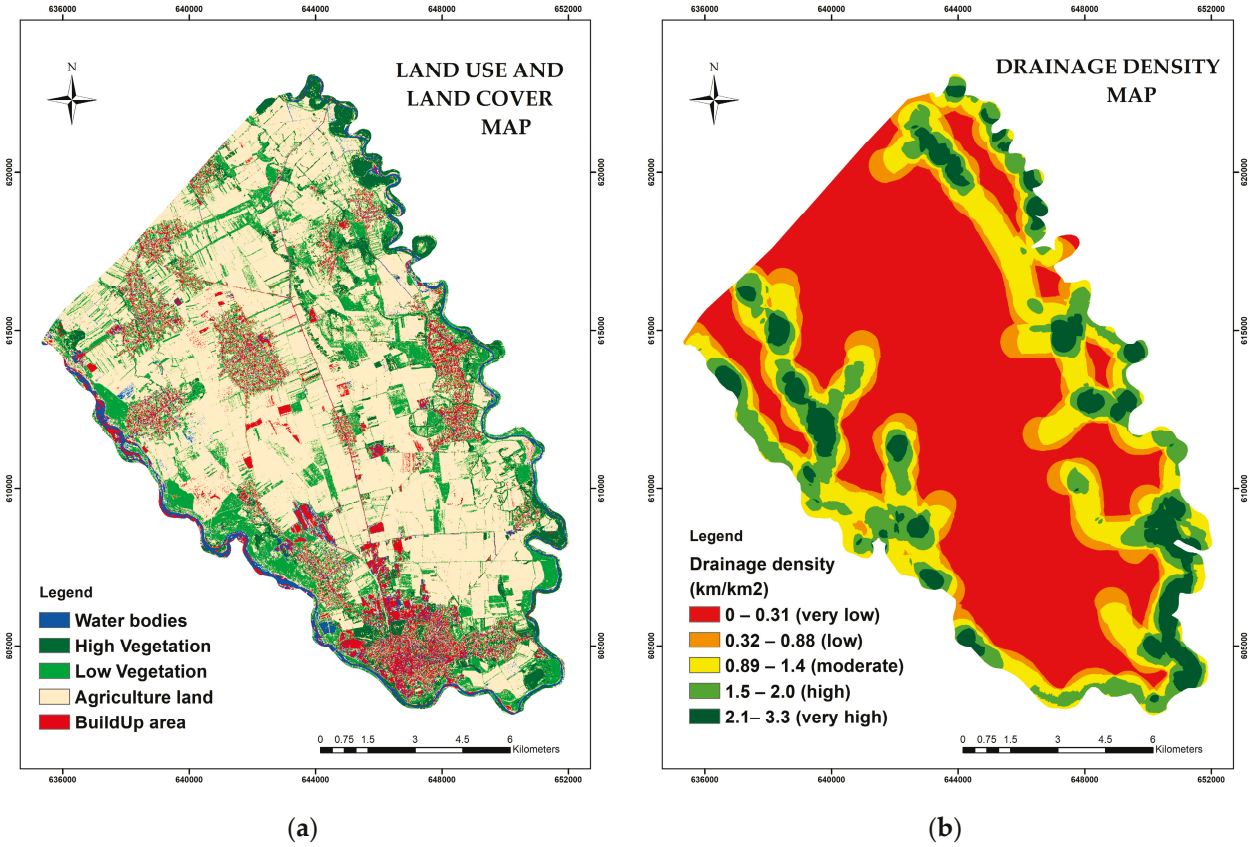

(**a**) (**b**)

Figure 4. (**a**) Land use and Land Cover map; (**b**) drainage density map.

3.4. Drainage Density

Drainage density is obtained by dividing the total length of all the rivers in a drainage basin by the total area of the drainage basin [39]. It is a fundamental indicator of hydrological landscapes, and it serves as a valuable tool for analyzing landforms in the context of groundwater potential [10]. It plays a crucial role in determining both infiltration rates and the characteristics of the underlying lithology [40]. In this context, a region with low drainage density is more favorable for high groundwater potential compared to a region with high drainage density. This is why, in this research, a higher weight was assigned to areas with low drainage density. The drainage density was reclassified and sorted into the following categories presented in Figure 4b: Very low (0–0.31 km/km^2), Low (0.32–0.88 km/km^2), Moderate (0.89–1.4 km/km^2), High (1.5–2.0 km/km^2), and Very high (2.1–3.3 km/km^2).

3.5. Elevation

The elevation information collected by the Shuttle Radar Topography Mission (SRTM) was used to create visual representations or maps of the terrain using ArcGis software. To verify the accuracy of the SRTM data with a 30 m resolution, the digital model (DEM) was compared with ground control measurements taken in 206 points using a GNSS RTK system. The maximum error observed was 0.7 m at point P198, while the minimum error recorded was −1.3 m at point P68, resulting in a median error of −0.19 m. This error can be considered acceptable for this type of digital terrain model, as illustrated in Figures 5 and 6.

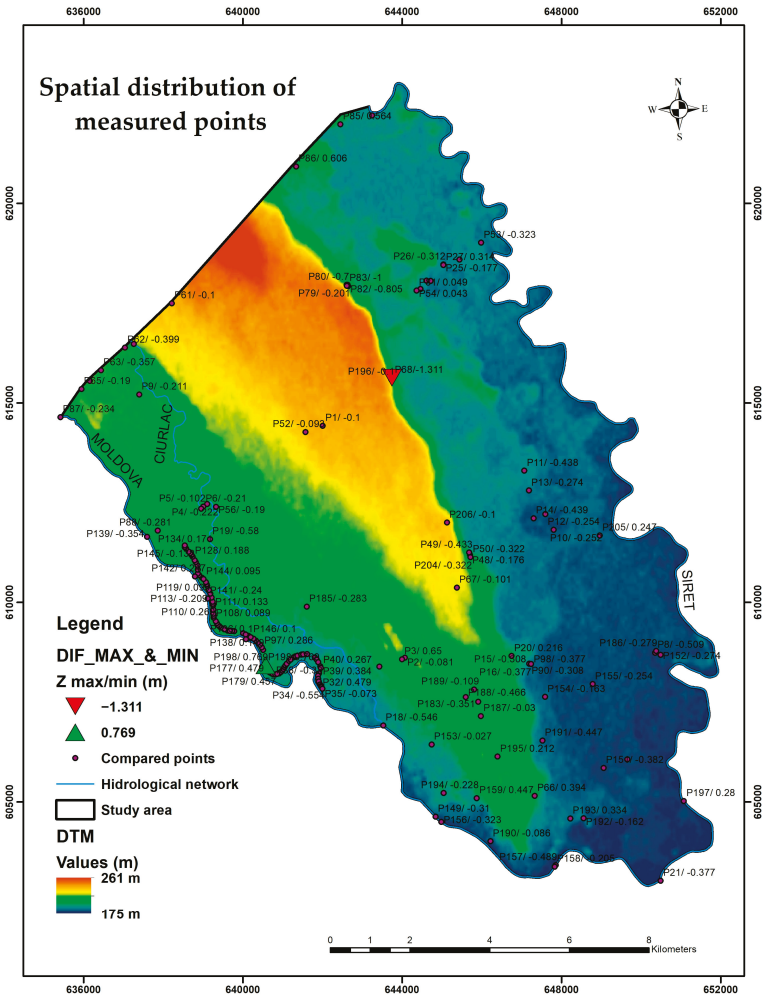

Figure 5. Spatial distribution of compared points.

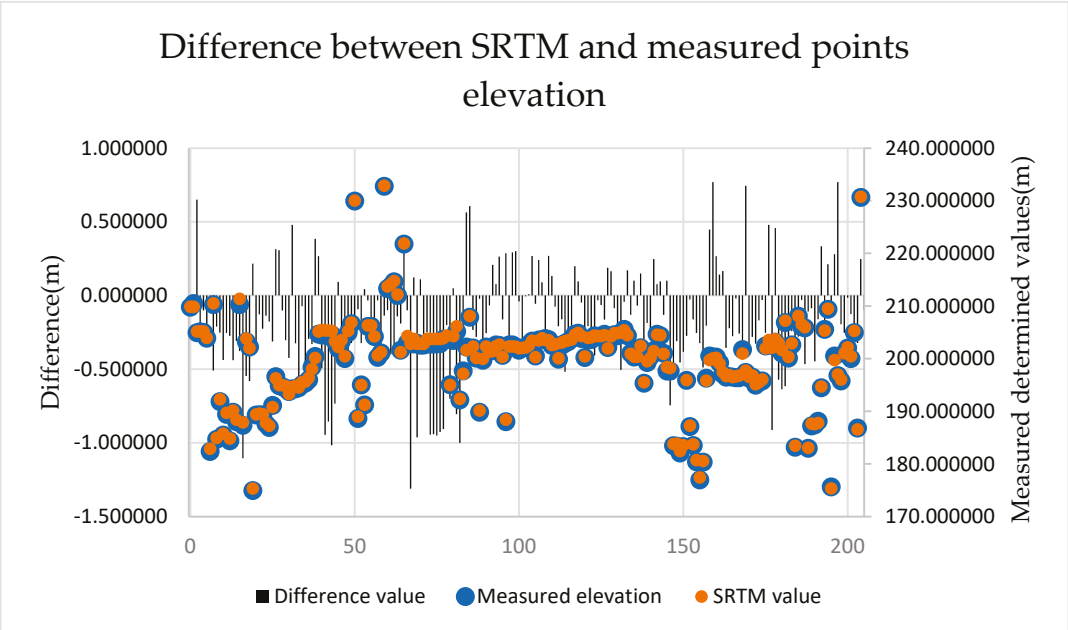

Figure 6. Difference between SRTM elevation and measured point elevation.

In the study area, the elevations range from a minimum of 175 m to a maximum of 261 m. In this case, low rankings were assigned to areas with higher elevations, while high rankings were designated for those with lower elevations. This ranking takes into account various hydrological characteristics, such as infiltration rates, run-off patterns, and slope steepness. The elevation was reclassified into five categories, ranging from low to high, as illustrated in Figure 7a. Different feature weights were assigned to these categories: a weight of 3 for the lower elevation zones, which range from 175.5 m to 201.2 m; a weight of 2 for the moderate elevation zones, spanning from 201.3 m to 216.8 m; and a weight of 1 for the highest elevation zone, covering the range from 233.6 m to 260.4 m.

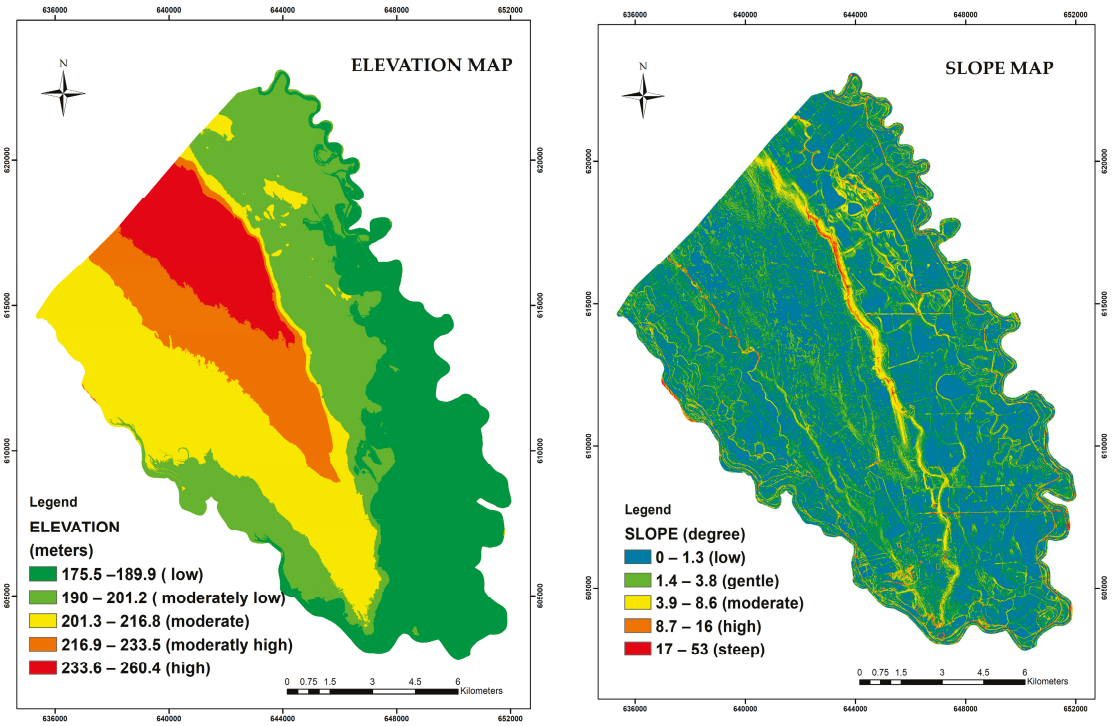

(**a**) (**b**)

Figure 7. (**a**) Elevation map; (**b**) slope map.

3.6. Slope

Slope, a crucial determinant of runoff and infiltration rates, is influenced by the spacing of contour lines. In general, closely spaced contours in vector representation indicate steeper slopes, while in raster representation, each cell provides a slope value where lower values suggest a flatter terrain and higher values denote steeper slopes. The slope values were reclassified and grouped into five categories, like in Figure 7b: Low (0–1.3), Gentle (1.4–3.8), Moderate (3.9–8.6), High (8.7–16.0), and Steep (17–53). Higher slopes result in reduced recharge as precipitation water quickly flows down steep slopes during rainfall events. Therefore, a lower weight (1) was assigned to steep slopes, while a higher weight (3) was allocated for low-to-gentle slopes.

3.7. Soil

Soil serves as a crucial parameter for identifying potential groundwater occurrence zones. In the study area, five soil types are present, including sandy loam, soil with variable texture, clay and silt loam, clay soil, and marshes and ponds (as shown in Figure 8). The soil's texture plays a vital role in controlling surface runoff and the infiltration of rainwater. Sandy soil has a low runoff rate and high groundwater potential, whereas clay and silty loam soil have a high runoff rate and very low groundwater storage capacity.

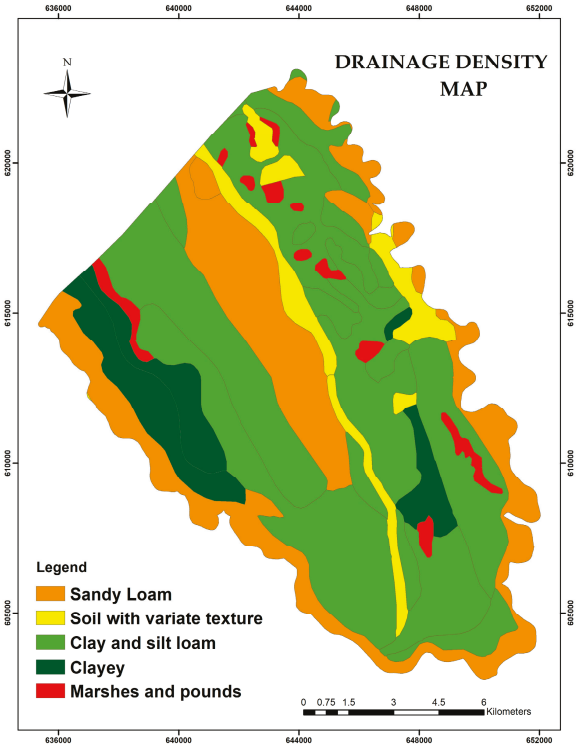

Figure 8. Soil map.

3.8. Ground Water Potential Zones and Validation

Ground Water Potential Zones

The result of the groundwater potential map in the study area indicated four distinct zones, representing areas with Very Good, Good, Moderate, and Poor groundwater potential, as shown in Figure 9 and Table 6.

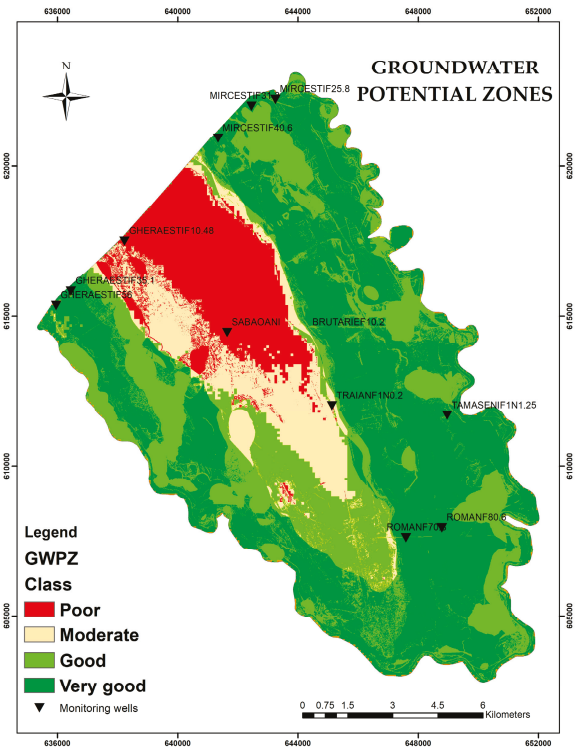

Figure 9. Groundwater potential map of the study area.

Table 6. Groundwater potential zones area.

Class	Area (sq. km.)	Area (%)
Poor	23.17	12.8
Moderate	19.54	10.8
Good	56.36	31.2
Very Good	81.53	45.1

Regions with Very Good and Good groundwater potential are generally located in low-altitude areas, such as along rivers, and on their terraces, and in regions with low slopes. Precipitation is a significant factor in the classification of these areas, but the values are relatively close between classes due to the relatively small size of the study area. Geology plays a crucial role, with areas characterized by lithology with high permeability and water storage capacity, such as sandy deposits, sand, or recent alluvial deposits primarily on terraces and riverbeds, indicating a higher potential for groundwater resources.

The accuracy assessment of the forecasting model is crucial to avoid errors and enhance the decision-making process in environmental studies. The potential zones derived from the integration of various techniques, including Remote Sensing (RS), Geographic Information Systems (GISs), and Multi-Criteria Decision Analysis (MCDA), were cross-validated with data from eleven boreholes in the study area. The spatial distribution of the 11 boreholes can be classified as plausible, considering that they are spread across the entire area, in zones with different geology, exposed soils with various characteristics, and in areas with significant elevation differences. The comparison between the predicted and actual yield data from the pumping test, as outlined in Table 7, highlights the accuracy of the prediction, standing at 72.7%. This validation confirms the reliability and precision of the methodology utilized in this study.

The accuracy verification of the predicted values is determined as follows:

Total number of boreholes = 11.

Number of boreholes with matching values between actual and expected yield = 8.

Number of boreholes with differing values between actual and expected yield = 3.

Prediction accuracy = $(8/1) \times 100 = 72.7\%$.

Table 7. Validation of groundwater potential zones area.

S. No.	Borehole	Longitude	Latitude	Top Aquifer	Aquifer Bed	Yield from Drilled Borehole (L/s)	Actual Yield Description	Expected Yield Class from the Prediction Map	Agreement Between Expected and Actual Yields
1	Roman F7	647,590.50	607,626.57	4.30	6.30	1.71	Good	Good–Very Good	Agree
2	Roman F8	648,789.46	607,947.26	3.60	6.30	0.60	Moderate	Good–Very Good	Disagree
3	Tamaseni F1N	648,965.90	611,672.02	5.30	8.90	1.25	Good	Good–Very Good	Agree
4	Traian F1N	645,126.58	611,998.20	23.40	27.80	0.20	Poor	Poor–Moderate	Disagree
5	Gheraesti F5	635,949.01	615,347.45	1.40	6.50	6.00	Very Good	Very Good	Agree
6	Gheraesti F3	636,440.61	615,816.37	4.00	7.90	5.10	Very Good	Very Good	Agree
7	Gheraesti F1	638,219.22	617,495.75	9.80	14.80	0.48	Poor	Poor	Agree
8	Mircesti F4	641,338.54	620,925.06	11.20	12.80	0.60	Moderate	Good–Very Good	Disagree
9	Mircesti F3	642,450.36	621,983.51	5.70	7.50	1.30	Good	Good–Very Good	Agree
10	Mircesti F2	643,245.01	622,203.72	6.50	9.80	5.80	Very Good	Good–Very Good	Agree
11	Sabaoani B1	641,640.80	614,460.89	21.80	22.60	0.20	Poor	Poor	Agree

4. Conclusions

The present study aims to delineate groundwater potential zones in the eastern part of Neamț county, where groundwater plays a crucial role, particularly for domestic use. Additionally, groundwater is utilized in the industrial sector, with the city of Roman being a focal point due to its significant economic and industrial development. The study area is predominantly characterized by agricultural land, accounting for 60.2% of the total region, with a concentration in the central part. This sector relies on both river and groundwater, making efficient water management essential. The groundwater potential map classifies areas into Very Good (45.1%), Good (31.2%), Moderate (10.8%), and Poor (12.8%) potential zones. The demarcation of these zones is notably influenced by factors such as precipitation, geology, and elevation. The validation of this model was conducted using observation boreholes, resulting in an accuracy assessment of 72.7%.

The obtained result is comparable with similar studies in the literature that used the same techniques. For example, a study conducted in the Ambo area of the Blue Nile Basin in Ethiopia achieved an accuracy of 69.5% [23], and another study on landslides in the Upper Wabe–Shebele River Basin of Southeastern Ethiopia reported a higher accuracy of 81% [24].

Even though the hydrogeological conditions, climate, hydrology, and geographical location differ, by applying the same techniques, which take into account the weight of various factors, it is observed that the obtained results show good accuracy. This strengthens the case for using these techniques in the delineation of groundwater potential zones.

Identifying areas with groundwater potential is critical for the economic development of the region. This research represents an important step in making decisions regarding the selection of sites for water consumers, as well as in the sustainable use of resources. Additionally, it is essential for regional development planning to understand how to manage resources and reduce the risks associated with their depletion.

Therefore, it can be concluded that these results are valuable for planning new projects and expanding existing ones that involve groundwater utilization in the study area, making significant contributions to the sustainable planning and development of water resources in the region.

Author Contributions: Conceptualization, P.-L.B.; Methodology, P.-L.B.; Formal Analysis, P.-L.B.; Investigation, P.-L.B.; Writing—Original Draft, P.-L.B.; Writing—Review and Editing, N.B.; Visualization, M.P.-L., D.C. and F.M.N.; Supervision, V.N. All authors have read and agreed to the published version of the manuscript.

Funding: This research received no external funding.

Data Availability Statement: The datasets used and/or analyzed during the current study are available from the corresponding author upon reasonable request.

Conflicts of Interest: The authors declare no conflicts of interest.

References

1. Taylor, R.G.; Scanlon, B.; Döll, P.; Rodell, M.; van Beek, R.; Wada, Y.; Longuevergne, L.; Leblanc, M.; Famiglietti, J.S.; Edmunds, M.; et al. Ground water and climate change. *Nat. Clim. Chang.* **2013**, *3*, 322–329. [CrossRef]
2. Fitts, C.R. *Groundwater Science*; Elsevier: Amsterdam, The Netherlands, 2002.
3. Croitoru, A.-E.; Minea, I. The impact of climate changes on rivers discharge in Eastern Romania. *Theor. Appl. Climatol.* **2015**, *120*, 563–573. [CrossRef]
4. Senanayake, I.P.; Dissanayake, D.M.D.O.K.; Mayadunna, B.B.; Weerasekera, W.L. An approach to delineate groundwater recharge potential sites in Ambalantota, Sri Lanka using GIS techniques. *Geosci. Front.* **2016**, *7*, 115–124. [CrossRef]
5. Abijith, D.; Saravanan, S.; Singh, L.; Jennifer, J.J.; Saranya, T.; Parthasarathy, K.S.S. GIS-based multi-criteria analysis for identification of potential groundwater recharge zones—A case study from Ponnaniyaru watershed, Tamil Nadu, India. *HydroResearch* **2020**, *3*, 1–14. [CrossRef]
6. Bond, N.R.; Burrows, R.M.; Kennard, M.J.; Bunn, S.E. Chapter 6—Water Scarcity as a Driver of Multiple Stressor Effects. In *Multiple Stressors in River Ecosystems*; Sabater, S., Elosegi, A., Ludwig, R., Eds.; Elsevier: Amsterdam, The Netherlands, 2019; pp. 111–129.

7. Brown, A.; Matlock, M.D. A review of water scarcity indices and methodologies. *White Pap.* **2011**, *106*, 19.
8. Irimia, O.; Tomozei, C.; Valentin, N.; Lehadus, M.P. Experimental results regarding the groundwater quality in rural zone in Romania. *Int. Multidiscip. Sci. GeoConf. SGEM* **2017**, *17*, 463–470.
9. Nasir, M.J.; Khan, S.; Zahid, H.; Khan, A. Delineation of groundwater potential zones using GIS and multi influence factor (MIF) techniques: A study of district Swat, Khyber Pakhtunkhwa, Pakistan. *Environ. Earth Sci.* **2018**, *77*, 367. [CrossRef]
10. Jhariya, D.C.; Khan, R.; Mondal, K.C.; Kumar, T.K.I.; Singh, V.K. Assessment of groundwater potential zone using GIS-based multi-influencing factor (MIF), multi-criteria decision analysis (MCDA) and electrical resistivity survey techniques in Raipur city, Chhattisgarh, India. *AQUA—Water Infrastruct. Ecosyst. Soc.* **2021**, *70*, 375–400. [CrossRef]
11. Mace, R. *The Importance of Groundwater Sustainability*; Springer International Publishing: Cham, Switzerland, 2023; pp. 1–20.
12. Ionuț, M.; Iosub, M.; Boicu, D. Groundwater Resources from Eastern Romania under Human and Climatic Pressure. *Sustainability* **2020**, *12*, 10341. [CrossRef]
13. Cochiorca, A.; Nedeff, V.; Bârsan, N.; Sandu, I.; Emilian, M.; Chiţimus, D.; Irimia, O. Surface Water and Groundwater Quality Evaluation in a Mining Area. *Rev. Chim.* **2020**, *71*, 124–131. [CrossRef]
14. Baghel, S.; Tripathi, M.P.; Khalkho, D.; Al-Ansari, N.; Kumar, A.; Elbeltagi, A. Delineation of suitable sites for groundwater recharge based on groundwater potential with RS, GIS, and AHP approach for Mand catchment of Mahanadi Basin. *Sci. Rep.* **2023**, *13*, 9860. [CrossRef] [PubMed]
15. Venkatesan, G.; Pitchaikani, S.; Saravanan, S. Assessment of Groundwater Vulnerability Using GIS and DRASTIC for Upper Palar River Basin, Tamil Nadu. *J. Geol. Soc. India* **2019**, *94*, 387–394. [CrossRef]
16. Romanian Water National Administration. *River Basin Management Plan for Hydrographic Basin SIRET 2023-2027*; Romanian Water National Administration Siret River Basin; Romanian Water National Administration: Bucharest, Romania, 2022.
17. Singh, P.; Thakur, J.K.; Kumar, S. Delineating groundwater potential zones in a hard-rock terrain using geospatial tool. *Hydrol. Sci. J.* **2013**, *58*, 213–223. [CrossRef]
18. Nampak, H.; Pradhan, B.; Abd Manap, M. Application of GIS based data driven evidential belief function model to predict groundwater potential zonation. *J. Hydrol.* **2014**, *513*, 283–300. [CrossRef]
19. Hinton, J. GIS and remote sensing integration for environmental applications. *Int. J. Geogr. Inf. Syst.* **1996**, *10*, 877–890. [CrossRef]
20. Jaiswal, R.; Mukherjee, S.; Krishnamurthy, J.; Saxena, R. Role of remote sensing and GIS techniques for generation of groundwater prospect zones towards rural development--an approach. *Int. J. Remote Sens.* **2003**, *24*, 993–1008. [CrossRef]
21. Akter, A.; Uddin, A.M.H.; Wahid, K.B.; Ahmed, S. Predicting groundwater recharge potential zones using geospatial technique. *Sustain. Water Resour. Manag.* **2020**, *6*, 24. [CrossRef]
22. Saaty, T.L. How to make a decision: The analytic hierarchy process. *Eur. J. Oper. Res.* **1990**, *48*, 9–26. [CrossRef]
23. Haile, M.; Yadeta, J.; Gambe, L. Delineation of groundwater potential zones using geo-spatial and AHP techniques: Ambo area, Blue Nile Basin, Ethiopia. *Sustain. Water Resour. Manag.* **2022**, *8*, 36. [CrossRef]
24. Sheko, S.; Moges, A.; Ulsido, M. Assessing Groundwater Potential Zones and Their Implications for Landslides in the Upper Wabe-Shebele River Basin of Southeastern Ethiopia. *J. Eng.* **2024**, *2024*, 7044576. [CrossRef]
25. Saaty, T.L. Decision making with the analytic hierarchy process. *Int. J. Serv. Sci.* **2008**, *1*, 83–98. [CrossRef]
26. Madrucci, V.; Taioli, F.; de Araújo, C.C. Groundwater favorability map using GIS multicriteria data analysis on crystalline terrain, Sao Paulo State, Brazil. *J. Hydrol.* **2008**, *357*, 153–173. [CrossRef]
27. Achu, A.; Thomas, J.; Reghunath, R. Multi-criteria decision analysis for delineation of groundwater potential zones in a tropical river basin using remote sensing, GIS and analytical hierarchy process (AHP). *Groundw. Sustain. Dev.* **2020**, *10*, 100365. [CrossRef]
28. Ghosh, D.; Mandal, M.; Karmakar, M.; Banerjee, M.; Mandal, D. Application of geospatial technology for delineating groundwater potential zones in the Gandheswari watershed, West Bengal. *Sustain. Water Resour. Manag.* **2020**, *6*, 14. [CrossRef]
29. Topuz, M.; Deniz, M. Application of GIS and AHP for land use suitability analysis: Case of Demirci district (Turkey). *Humanit. Soc. Sci. Commun.* **2023**, *10*, 115. [CrossRef]
30. Posea, G. *Geomorfologia României*; Editura Fundaţiei România de Mâine: Bucharest, Romania, 2002; pp. 27–40.
31. Bogdan, P.-L.; Nedeff, V.; Barsan, N.; Panainte-Lehaduș, M.; Chitimus, D.; Nedeff, F.; Tomozei, C. Applications of the GIS and Remote Sensing methods in the Land use and cover maps. Case study: Roman city and the surroundings of the Northern side area. In Proceedings of the 2022 8th International Conference on Energy Efficiency and Agricultural Engineering (EE&AE), Ruse, Bulgaria, 30 June–2 July 2022; pp. 1–5. [CrossRef]
32. Jet Propulsion Laboratory, NASA. *NASA Shuttle Radar Topography Mission Global 1 Arc Second*; Jet Propulsion Laboratory, NASA: La Cañada Flintridge, CA, USA, 2013. [CrossRef]
33. Romanian Water Administration—Siret River Basin Administration. *Basin Forecast Service, Hydrology, Hydrogeology—Data Archive*; Romanian Water Administration: Bucharest, Romanian, 2022.
34. Florea, N.; Bălăceanu, V.; Munteanu, I.; Asvadurov, H.; Conea, A.; Oancea, C.; Cernescu, N.; Popovăţ, M. *The Soil Map of Romania at the Scale 1: 200,000*; Legenda Generală. (The Soil Map of Romania at the scale 1: 200,000. General Legend); National Institute for Research and Development in Pedology, Agrochemistry and Environmental Protection—ICPA Bucharest: Bucharest, Romania, 1994; p. 1.
35. Alexandrescu, G.; Joja, T.; Mirauta, E. *Geological map of Romania (1:200,000), Sheet Piatra Neamt*; Harta Geologica 1:200,000; HG-13; Romania Institutul Geologic: Bucharest, Romania, 1968.
36. Saaty, T.L. A scaling method for priorities in hierarchical structures. *J. Math. Psychol.* **1977**, *15*, 234–281. [CrossRef]

37. Saaty, T.L. *The Analytic Hierarchy Process*; McGrawhill Juc.: New York, NY, USA, 1980.
38. FAO. The State of Food and Agriculture 2019. In *Moving Forward on Food Loss and Waste Reduction*; United Nation's Food and Agricultural Organization: Rome, Italy, 2019. [CrossRef]
39. Horton, R.E. Erosional development of streams and their drainage basins; hydrophysical approach to quantitative morphology. *Geol. Soc. Am. Bull.* **1945**, *56*, 275–370. [CrossRef]
40. Roy, S.; Hazra, S.; Chanda, A.; Das, S. Assessment of groundwater potential zones using multi-criteria decision-making technique: A micro-level case study from red and lateritic zone (RLZ) of West Bengal, India. *Sustain. Water Resour. Manag.* **2020**, *6*, 4. [CrossRef]

Disclaimer/Publisher's Note: The statements, opinions and data contained in all publications are solely those of the individual author(s) and contributor(s) and not of MDPI and/or the editor(s). MDPI and/or the editor(s) disclaim responsibility for any injury to people or property resulting from any ideas, methods, instructions or products referred to in the content.

water

MDPI

Article

Advancing the Understanding of Complex Piezometric Information: A Methodological Approach Integrating Long-Term Piezometry, Surface Nuclear Magnetic Resonance, and Fracture Analysis Using Insights from the "Calcaires du Barrois" Series, France

Mathieu Bertrand [1,2,*], Catherine Bertrand [1], Naomi Mazzilli [3], Sylvain Gigleux [2], Sophie Denimal [1], Rémi Valois [3], Lise-Marie Girod [1,2], Guillaume Cinkus [3], Valentine Busquet [1,2] and Konstantinos Chalikakis [3,*]

1 UMR6249 ChronoEnvironnement (CNRS-UFC), University of Franche-Comté, 25000 Besançon, France; catherine.bertrand@univ-fcomte.fr (C.B.); sophie.denimal@univ-fcomte.fr (S.D.); lise-marie.girod@mines-paristech.fr (L.-M.G.); vambusquet@orange.fr (V.B.)
2 Agence Nationale pour la Gestion des Déchets Radioactifs (Andra), RD960, BP9, 55290 Bure, France; sylvain.gigleux@andra.fr
3 UMR 1114 EMMAH (AU-INRAE), Avignon Université, 84029 Avignon, France; naomi.mazzilli@univ-avignon.fr (N.M.); remi.valois@univ-avignon.fr (R.V.); guillaume.cinkus@univ-avignon.fr (G.C.)
* Correspondence: mathieu.bertrand@univ-fcomte.fr (M.B.); konstantinos.chalikakis@univ-avignon.fr (K.C.)

Abstract: This study aims to analyze spatio-temporal piezometric data and integrate them with geological, geotechnical, and geophysical data to enhance their interpretation. The research focuses on a site located in the Meuse and Haute-Marne departments of France, which has been under investigation since 1994 as part of the surface facilities characterization for the Meuse-Haute-Marne underground laboratory and the CIGEO (Centre Industriel de stockage Géologique) Andra project. These investigations span different spatial and temporal scales. We observed the contribution of water masses associated with external forcing and identified two types of aquifer responses: a rapid response to rainfall events when fractures are well-connected, and minor reactivity at the matrix level. Additionally, we demonstrated that the matrix compartment can be finely characterized through a combined interpretation of piezometric response analysis, fracture analysis, and surface nuclear magnetic resonance (SNMR) soundings. The methodology developed in this project offers an improved understanding of karst piezometry and/or unsaturated zone extension, which is essential for comprehend ding flow dynamics and better constraining the functioning of karst aquifers. Furthermore, this site serves as an ideal workshop for studying flow in fractured media, providing valuable insights into hydrodynamic behavior in complex subsurface environments.

Keywords: hydrogeology; karst; piezometric analysis; fracturing; SNMR

1. Introduction

Karst aquifers generally have significant water resources and reserves, which are still relatively under-utilized and in some regions of the world represent the essential, if not the only, resource [1–3]. As a result, the search for new water resources (water for food, water shortage support, agriculture...) leads to an increasing interest in karst systems, either to optimize seasonal exploitation (active management) or to establish systems to protect quality (protection perimeters and protection works) or quantity (sizing of works in urbanized areas) [1]. Additionally, studying these systems is essential during geotechnical or civil engineering investigations [4].

If karst aquifers are first to be studied using a descriptive and comparative approach [5], then piezometric records are fundamental data for characterizing these systems. They are measured in the field, either at the source or by direct measurement of the water

column in the borehole [6]. It is an essential measure for understanding the behavior of an aquifer [7,8], for characterizing and evaluating its functioning and its hydrodynamic parameters (storage coefficient and hydraulic conductivity) [9–12], and also for detecting interactions between different structures during its operation [13]. These parameters can be extracted by analyzing signals acquired under active stress (usual hydraulic tests) or passive stress (tidal effect, [14]). These data are essential for the exploitation of water resources [15,16] as well as for civil engineering investigations [17,18].

However, in complex systems such as karst aquifers, the structure and the functioning of aquifers are difficult to understand due to the high heterogeneity degree and the different types of porosity that are involved in groundwater circulation. Indeed, the piezometric levels measured in boreholes are influenced by different types of water volumes coming from the matrix, fractures, or conduits [19–21]. Boreholes that are only a few meters apart can have piezometric levels that differ significantly, in part due to different dynamics between matrix and fractures and/or karst conduits. These differences in piezometric levels may also be due to varying degrees of saturation within the aquifer. Water circulation in this type of environment is thus constrained by hydrodynamic heterogeneities, which induce preferential circulation and, therefore, non-uniform water (and pressure) transfers [22,23], with a continuum between very fast, non-dispersive flows (piston or conduit flows) and very slow, highly dispersive flows (diffuse flows) [24–26]. Borehole logs, wall imaging techniques, and core analysis provide high-resolution fracturing information. Combined with hydraulic tests, they provide relevant information on the hydrodynamic functioning of the aquifer, such as fracturing, karstification degree, and connectivity. Nonetheless, the obtained information only reflects the well spatial scale, so there is a high uncertainty far from the wells. In these subsurface geological environments, flows are generally not linked to a particular structure or homogeneous reservoir but are distributed at all scales [27]. This complexity poses the problem of detecting, measuring (and being representative of), and monitoring these flows in 4D [19,28].

Non-intrusive techniques such as geophysical methods can complement and spatialize the geological and hydrogeological knowledge gained by analyzing the water levels in boreholes [29]. These methods are based on analyzing the propagation of physical variables (e.g., electromagnetic field, acoustic waves). This propagation is influenced by various factors, including the presence or absence of water in the environment being studied [30]. Among these methods, surface nuclear magnetic resonance (SNMR) provides a signal directly linked to the presence of groundwater. The initial amplitude of the SNMR signal is directly related to the presence of mobile water in the subsurface, while its relaxation time can be related to pore size [31,32]. This method thus provides direct information on groundwater hydrodynamic properties in karst environments [33].

When industrial activities are spread out above or within fractured and/or karstified aquifers, it is important to develop a comprehensive hydrodynamic functioning model to ensure the durability of the resources and minimize related risks. As an example, the French National Agency for the Management of Radioactive Waste (Andra) aims to securely dispose of high and low-intermediate level long-lived radioactive waste at the CIGEO (Centre Industriel de stockage Géologique) project (Meuse, France). The work support zone, and the ramp zone facilities, will be used for digging and building the underground structures located at a depth of approximately 500 m and for receiving and inspecting waste packages and preparing them for transfer to the underground facilities via a ramp these zones measuring around 550 hectares lies on the "Calcaires du Barrois" series. The basal part of the "Calcaires du Barrois" is the dominant formation at the outcrop, consisting of a complex hydrosystem with two horizons of differing permeability. The upper horizon is fractured, resulting from the decompression and cryoturbation phenomena of the last deglaciations, while the underlying horizon exhibits diffuse karstification. However, this karstification is not concentrated enough to produce large-scale dissolution features such as caves or metric drains. To properly size surface facilities and reservoir access shafts, a better understanding of the flow dynamics within

this formation is essential. Additionally, the hydrogeological characterization of the "Calcaires du Barrois" is a key part of the project, aimed at establishing an effective environmental monitoring network.

The hydrodynamic behavior of the "Calcaires du Barrois" is directly linked to the fracturing of the environment. Numerous geological and geotechnical investigations have been conducted over hundreds of boreholes at this site over the years, providing data on fracturing, and petrophysics. Piezometry and hydrodynamics investigation has been conducted according to dozens of piezometers. Nineteen boreholes were re-used as piezometers. These were selected from an area of 13 km^2 as they have provided good quality data series for more than 8 years. Because this density of investigation is not often available for studying karst systems [29], we designed this project to use these facilities to study the hydrogeologic complexities of this "fractured-rock karst site".

We decided to bring together the data collected at the study site and evaluate the data as a whole, complemented by SNMR. This investigation is directly related to the presence of mobile water in the subsurface and provides direct information on the hydrodynamic properties of mobile groundwater in karst environments. It is particularly suited to the study area. We thus combined (1) the analysis of long piezometric records with (2) full fracture analysis from borehole logs and (3) geophysical measurements to gain further insight into the complex "Calcaires du Barrois" system. This approach is used to shed more light on hydrodynamic responses and their origins in the complex "Calcaires du Barrois" system. We also provide methodological insights that are easily transposable to other studies aiming at water body characterization in karst environments.

2. Context

2.1. Study Site

The Meuse/Haute-Marne region is located on the south-eastern edge of the Paris Basin, between the valleys of the Marne and the Meuse rivers (France, Figure 1A) and, more precisely, in the outcrop zone of the Upper Jurassic formations ("Calcaires du Barrois" series), at the boundary of the presence of Cretaceous terrains. The "Calcaires du Barrois" series is a succession of limestone strata (Sublithographic limestone, Dommartin limestone, "Oolithe de Bure" formation, and Decayed limestones) and a marl layer that is approximately 10 m thick ("Pierre Chaline" formation), separating the Sublithographic limestone and the Dommartin limestone. The Kimmeridgian marls form the bedrock on which the sedimentary sequence rests (Figure 1A,B,D). This series dips northwest towards the center of the Paris Basin with an average dip of about 1 degree [34]. This shallow dip is associated with a plateau morphology: the "Calcaires du Barrois" series plateau. This plateau is cut by relatively narrow, incised valleys. It is bordered to the east by the Ormançon River and to the west by the Saulx River. Between these two rivers flow the Bureau and Orge rivers, tributaries of the Saulx.

The study site covers 13 km^2 and is located at the head of the Orge catchment. It is bounded by the Orge River to the west and the Bureau River to the east (Figure 1C). These two rivers are characterized by dry periods from April to October. The Bureau joins the Orge near Bure (Figure 1A). In this sector, only the Sublithographic limestone is exposed. In detail, this limestone is composed of five levels, which are distinguished by variations in facies (multi-centimetric limestone-mudstone alternation at the bottom of the series) and thickness (up to 15 m for level N5) (Figure 1B).

Between 2002 and 2023, rainfall was measured at the CMHM (Centre Meuse-Haute-Marne) site with a weather station (hourly and daily). The average annual rainfall (over 21 years) recorded at the CMHM was 946 mm. The annual precipitation at CMHM ranged between 750 mm (in 2004) and 1200 mm (in 2007).

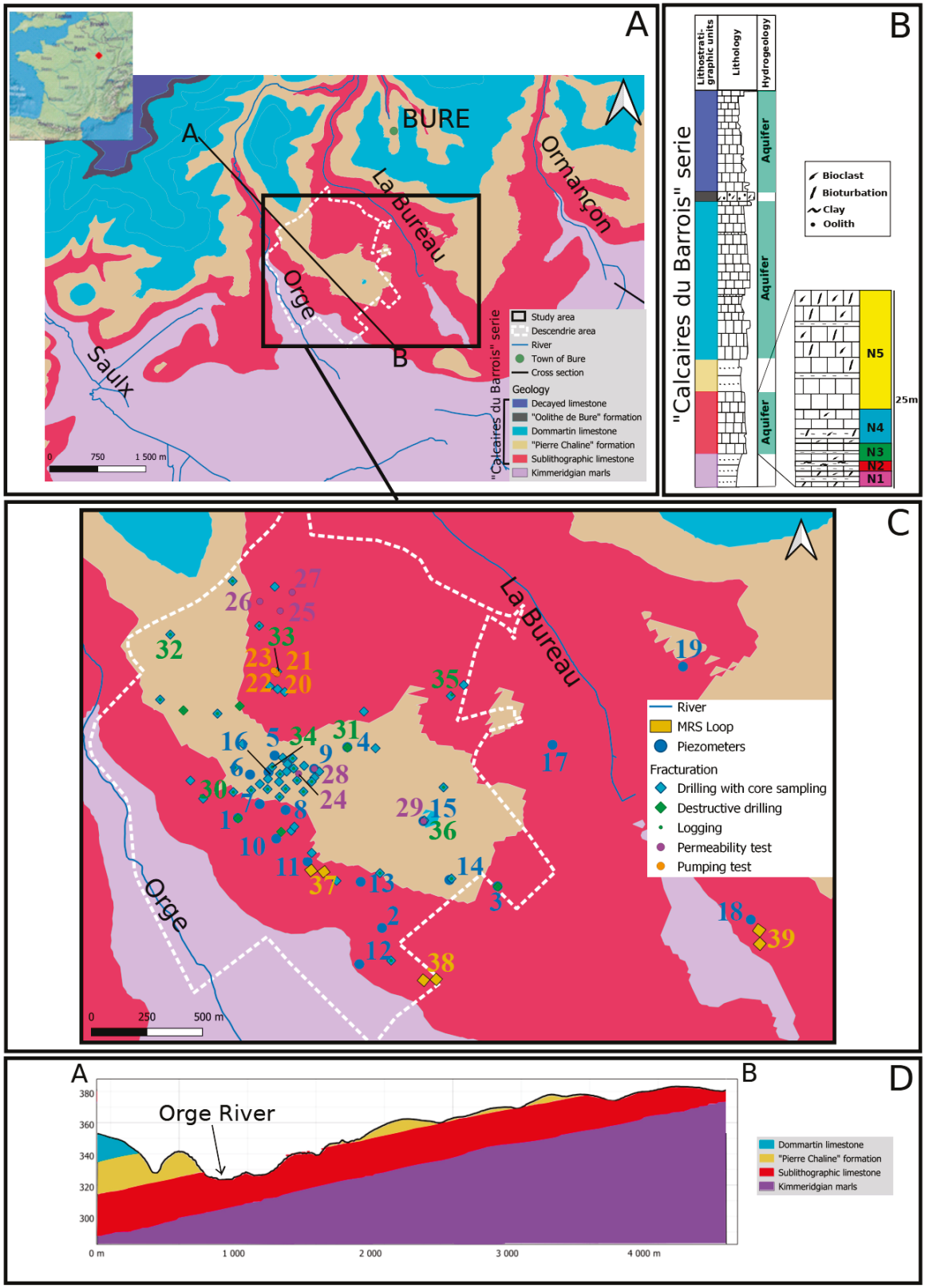

Figure 1. (**A**)—Geological map of the study area. The white dashes represent the location of the future waste reception, control, and preparation area of the CIGEO site area called Descendrie area. (**B**)—Lithostratigraphic succession of the study area and location of the aquifers in this succession. (**C**)—Focus on the study area, showing the location of piezometers, geological boreholes, and SNMR soundings. The numbers correspond to the piezometer names in Appendix A. (**D**)—North-West (**A**)/South-East (**B**) cross-section with vertical exaggeration (10×).

2.2. Geological and Hydrogeological Characteristics of the "Calcaires du Barrois" Series

The local hydrogeological system of the "Calcaires du Barrois" series consists of three more-or-less well-connected aquifer levels where the series is complete (Figure 1B). These are, from the bottom to the top [34]:

- The Sublithographic limestones (25 m thick) are lithographic micritic limestones with rare bioclastic beds and rare marly interbeds of decimetric thickness.
- The Dommartin limestones (63 m thick) consist of about 25 m of micritic limestones with bioclastic beds and marl interbeds at the base, an interval of about 25 m of micritic limestones with very rare bioclasts and bioclastic packstones at the top of this interval, and about 13 m of micritic limestones with very little bioclasticity at the top of the Dommartin limestones.
- The Decayed limestones (36 m—thick), which correspond to micritic limestones with little bioclasticity.

These levels are separated by aquitards such as the "Pierre Chaline" formation, a predominantly marly level, and the "Oolithe de Bure" formation, formed by a massive bed of beige limestone with oolites and a sparitic matrix. Depending on the degree of fracturing, these aquitards can be relatively permeable. The Kimmeridgian marl with exogyres that underlie the "Calcaires du Barrois" series forms an impermeable layer. The upper and lower limestone layers contained in these marls are also aquifers to a lesser extent. The aquifers in this series supply numerous springs with low flow rates [34].

The water table in the Sublithographic limestones is unconfined in the upstream part of the catchment but becomes captive north of the town of Bure under the "Pierre Chaline" formation. The water table in the Dommartin limestones is semi-captive due to the limited extent of the Oolithe de Bure. Over the extent of the study area, the water table in the Decayed limestones is unconfined.

Karstification is well developed within the "Calcaires du Barrois" series. In addition, typical karst features can be observed at the surface (sinkholes, wells). Speleological explorations to the north-west of the area [35] have highlighted the extensive development of karstification in the "Calcaires du Barrois" series. In the study area, numerous losses and resurgences of the Orge and Ormançon have been observed where these rivers cross the "Pierre Chaline" marls [36].

3. Data and Methods

The proposed methodology is based on spatial analysis of piezometric and fracture records, coupled with imaging and monitoring of water content using the SNMR method.

3.1. Hydrogeological Investigations: Piezometry Analyses

The extensive instrumentation at the site provides a considerable amount of borehole data. Our first objective was to extract from these records statistical or correlative indicators of the hydrodynamic behavior of the structures, and then to use these indicators to establish groups of similar hydrodynamic functioning.

Seven piezometric time series indicators were defined in this project:

1. The variance, which is measured via time series variation coefficient, an indicator of the dispersion of the distribution of piezometric levels.
2. The maximum amplitude (difference between the "Calcaires du Barrois" series base and the water level extremum piezometric levels). The base of the "Calcaires du Barrois" series is used as a reference to compare the height of piezometric variations measured in the boreholes.
3. The slopes of piezometric rises and recession. The positive and negative slopes of the piezometric curves provide information on the rate of piezometric rise and the rate at which wells are drying up. These indicators are determined by studying the derivative of piezometric variations as a function of time. These derivatives are calculated at all points of a hydrograph using the finite difference method. The indicators provide

information on the hydrodynamic parameters of the system. They therefore provide an insight into the structure of the system, such as the relative fracture density in the vicinity of the studied piezometers.

4. System inertia or memory effect. This parameter quantifies the time taken for an event to affect the chronicle or, in other words, the time n taken for an event occurring at time t to not affect the event recorded at time $t + n$. The inertia of the system is expressed by the autocorrelation function [37]. This function is a measure of the degree of dependence on events in the same chronicle by assessing their repetitive nature. A significant memory effect reflects a certain degree of flow regulation by the system and, therefore, the importance of a capacitive character [38,39]. The memory effect is an indicator of the structure of the system and fracturing.
5. Response time and cross-correlation coefficient. These indicators examine the strength of the relationship between the input signal, rainfall, and what can be considered as an approximation of the output signal, piezometry. It is assumed that there is a causal relationship between these two variables. The cross-correlation function corresponds to the transfer function between the two signals and provides information about the structure of the system.

These indicators were grouped by hydrodynamic behavior using principal component analysis and hierarchical ascending classification (HAC).

This approach was applied to 19 piezometers spread over the Descenderie area and over two time periods (Appendix B). Four of the 19 piezometers have a continuous series of over 25 years (piezometers 16, 17, 18, and 19) and the other piezometers have a continuous series since 2016. Datasets from recordings on the 19 piezometers between November 2016 and July 2021 were selected for use in this project because they provide the longest records to harmonize the processing, and they have been homogenized at hourly time steps. Before statistical processing, an analysis of the raw data was performed to quantify the missing data for all records (water samples or well tests). Over the 8 years of recording, the missing data represent 6.5% of the total data collected from the 19 piezometers.

Data on piezometric variations (mNGF) have been continuously recorded at quarter-hourly or hourly intervals by pressure sensors (Diver, Ven Essen Instrument) (Appendix B). Ranges are 10 m for pressure with an accuracy of 0.5 cm H_2O, and between −20 °C and 80 °C with an accuracy of +/−0.1 for temperature.

3.2. Geological Investigations: Fracturing Analysis

The fracturing and diffuse karstification degrees of the "Calcaires du Barrois" series have been described using borehole logging coupled with core analysis when possible. One of the objectives was to estimate the effect of lithology on the density and vertical extent of fracturing and karstification along the marl–limestone sequence where the flows seem to occur.

We used the following logs:

1. Optical Televiewer borehole wall imaging (sensor OPTV), which provides a complete, continuous scan of the borehole and, thus, provides a developed, oriented image of the borehole walls that can be used for subsequent image processing allowing measure dips and identify and orient planes of stratification, fracturing, and schistosity, (shown in polar plots). The characteristics of the Optical Televiewer are 360° camera 2 m long and 50 mm in diameter with 1 mm resolution. The quality of the images obtained depends mainly on the acquisition conditions in the borehole: the turbidity of the water, the diameter of the borehole, and the stability of the ground.
2. Natural radioactivity logging or "Gamma Ray" (GR) measures the natural gamma radioactivity of rocks. It measures the content of naturally radioactive elements in the rocks and thus clarifies and correlates the lithological cross-section obtained by sampling the ground during drilling. In the study area, it can be used to distinguish between marl intervals (high values) and limestone intervals (low values). Correlations between boreholes are based on this measurement.

We used 54 boreholes that had been drilled in the study area; they traversed both the Sublithographic limestones and the "Pierre Chaline" formation, depending on their location (Figure 1C). Forty-eight (48) of the 54 boreholes were cored and investigated using two types of logging: optical and gamma-ray. Thirty were logged optically and by gamma-ray; one was optically logged and 17 were investigated by gamma-ray logging. Of the 6 boreholes drilled destructively, only the gamma-ray logs could be used. Drilling and logging were conducted in 2015 and 2016. In most cases, wall imaging in boreholes is not relevant below the water level due to issues with turbidity.

3.3. Geotechnics Investigations: Hydraulic Tests

Two types of hydraulic tests were carried out: (i) Lefranc tests and (ii) pumping tests, carried out after the groundwater table had stabilized.

3.3.1. Lefranc Tests

The Lefranc water test is an in situ test used to determine the value of the local permeability coefficient (KL), which may differ significantly from the bulk permeability coefficient. The Lefranc water test applies to all fine or gravelly soils below the water table, where the assumed permeability coefficient is greater than approximately 10^{-6} m/s. It can be conducted in exploratory boreholes as work progresses.

Lefranc tests are conducted either under constant load (water is injected into the borehole at a constant rate until the level in the borehole stabilizes) or under variable load (a volume of water is injected into the borehole and the drop in level is monitored as a function of time). These tests are carried out in 1 m increments as the borehole progresses.

One month after drilling completion, two constant flow injection tests were conducted throughout the borehole ({28}, {29}; Figure 1C). For {28}, the tests were carried out by injecting water at a constant rate of 0.02 l/s for 2 h and then, after a recovery time of 21 h, an injection of 0.03 L/s for 7 h. The protocol used for {29} was more or less the same in terms of injection time and recovery time. However, the injected flow rates are doubled, i.e., 0.04 L/s and then 0.06 L/s. Pressure measurements in the borehole with a DIVER pressure probe were continued for 450 h after the end of the tests. The different flow rates used for these tests were chosen by the companies conducting the geotechnical investigations.

Results of the constant load tests were based on the expression of [40], which expresses the permeability coefficient as a function of flow rate, a factor that depends only on the borehole shape and its position with respect to the aquifer boundaries, the water column height, and the borehole diameter. Only measurements recorded after stabilization were used to determine the permeability coefficient.

Twenty-six hydraulic tests (Lefranc tests) were conducted [41] by a company specialized in geotechnical studies during the destructive drilling of 4 boreholes (Figure 1C). A total of 16 slug tests were performed by injecting water at a constant rate of 1 L/s for 1 h into three boreholes {25}, {26} and {27}. Tests that did not produce significant measurements (very low infiltration) were continued for one hour with a variable load. This consisted of 10 tests, including 5 in borehole {24}, 1 in borehole {25}, 1 in borehole {27}, and 3 in borehole {26}.

3.3.2. Pumping Tests

The constant flow test, which is the most commonly used pumping test, consists of lowering the piezometric surface of the water table by pumping and measuring changes in the level of this surface, as a function of time, as well as the flow rate pumped. This allows the permeability coefficient of the tested layer and the storage factor to be determined.

The pumping was carried out in borehole {20} (source borehole) and the changes in the piezometric surface over time were monitored using 3 piezometers (observation boreholes) located 3 m {21}, 8 m {22}, and 20 m {23} from the borehole (Figure 1C).

The pump test was carried out in December 2015 according to the NF P94-130 standard [42]. The lowering of the groundwater level was measured using pressure sensors in the 3 control piezometers. The pumping test was stopped after 1 h to prevent the pump

from draining. The piezometric level was measured in the source borehole being pumped and in the 3 observation piezometers during a recovery period of 21.5 h after pumping was stopped. The interpretations of the pumping test are derived from the analytical solution developed by Moench [43] for the source borehole and from the modified Theis [44] solution for one of the observation piezometers. The analytical solution developed by Moench [43] takes into account the incomplete borehole effect and the parietal effect in a homogeneous and anisotropic-free aquifer with a drip. The analytical solution developed by Theis [44] was originally developed for use in confined aquifers, but can also be used for unconfined aquifers by correcting the drawdown data [45].

The permeability coefficient k obtained from the pumping test is the horizontal permeability coefficient of the layer. It is a global or "large" coefficient, representative of the average hydraulic behavior of the volume of the layer under test. The storage factor or S coefficient is dimensionless. It gives the change in the volume of water contained in a vertical prism with a horizontal section of unit area for a unit change in the hydraulic load.

3.4. Hydrogeophysics Investigations: Surface Nuclear Magnetic Resonance (SNMR)

We used SNMR to analyze the spatial and temporal variation of water content to estimate the location of water volumes passing through these fractured environments [30,32]. The measuring device was NUMISPoly equipment from IRIS Instruments, with a coincident transmitting/receiving eight-square loop configuration composed of two squares with 40 m sides.

SNMR signal parameters (initial amplitude E0 and observed transverse relaxation time T2*) are derived from the SNMR signal envelope assuming a mono exponential decay [33]. The SNMR water content (mobilizable water content) was derived from E0. The effective porosity in which the water is stored has been was derived from the apparent transverse relaxation time T2* [32]. The hydraulic parameters of the aquifers are then estimated qualitatively: The water content gives an image of the drainage porosity of the reservoir, and the T2* constant provides information on the characteristics of water-filled pores [46]. Measuring T2* is easier and faster than measuring T1 because the T1 assessment requires the use of a two-pulse protocol with a variable delay between pulses [47]. In the absence of magnetic heterogeneities, the T2* estimate is considered reliable [47], so we used T2* in our survey.

Several procedures have been used to improve the quality of SNMR data in this study [48]. To compensate for the fact that electromagnetic (EM) noise has a large influence on the measurement, an EM noise measurement campaign was conducted prior to drilling to select the areas with the least EM noise. An eight-square loop shape was favored to further reduce the EM noise effect on the soundings. The excitation pulse was repeated and the recording sequences were averaged to reduce the influence of random noise.

SNMR signal filtering is indispensable to improve the signal-to-noise ratio and to allow the estimation of SNMR parameters. The filtering procedure was chosen based on tests carried out using the raw noise data on a synthetic signal and performed using NumPro 12 $\times$ 2 from the SAMOVAR suite. A notch filter of the type global Narrow was used to attenuate the disturbance field due to the 50 Hz harmonics of the power lines present near the sounding [49]. The maximum noise level for the use of a stack was set at 500 nV, and the maximum average noise level was set to 50 nV. Damage to the signal caused by filtering was calculated using the RMSE (Root Mean Square Error). The RMSE compares the square root of differences between predicted and observed values.

SNMR data quality was estimated based on the average signal-to-noise ratio (S/N) [50] derived from stacked and filtered measurements [51]. The higher the S/N, the higher the reliability of the SNMR survey. We consider SNMR soundings to be of acceptable quality when the S/N is ≥ 2.

A total of 19 SNMR soundings were implemented in 3 acquisition zones, under different hydraulic regimes. Acquisition zones covered the entire sector with varying thicknesses of Sublithographic limestone (3 m, 12 m, and 25 m). In each zone, a single low-water campaign (summer 2021) and a high-water campaign (spring 2022) were conducted

to characterize the seasonal water level variations. To better assess SNMR water content dynamics, additional measurements were performed at site 38 prior and after rainfall events during both low water (7 soundings over 38 days from 23 June 2021 to 30 July 2021) and high water (9 soundings over 8 days from 5 April 2022 to 12 April 2022).

Only soundings with an average number of recording sequences (stacks) greater than 200 and a signal-to-noise ratio greater than 2.5 are presented in this paper (Table 1).

Table 1. Table of SNMR surveys and their main characteristics (name, site, date, average number of stacks, signal-to-noise (S/N) ratio, maximum depth with good resolution, rainfall in the 7 days preceding the sounding (Rainfall D-7), and the hydraulic regime.

Sounding Name	Site	Date	Average Number of Stacks	Ratio S/N	Maximum Depth Resolution (m)	Rainfall D-7 (mm)	Hydraulic Regime High-Water (HW) or Low-Water (LW)
{37}	{37}	1 March 2022	299	2.51	24.41	7.8	HW
{38}_1	{38}	23 June 2021	274	2.67	25.77	10.4	LW
{38}_2	{38}	28 June 2021	288	2.7	25.77	21.0	LW
{38}_3	{38}	11 April 2022	367	9.18	21.6	48.4	HW
{38}_4	{38}	12 April 2022	243	6.63	21.6	48.4	HW
{39}	{39}	3 March 2022	289	7.78	24.41	4.4	HW

A smooth inversion was performed with SVD (singular value decomposition) type regularization. We chose a relatively low regularization (15 for water content and 20 for T2*) based on a preconception of the geology of the soundings. A sharp contrast in hydrodynamic properties is indeed expected between the upper part, the limestone part and the marl, and the lower part of the sounding. The uncertainty in the water content is reflected in the 95% confidence interval of the SAMOVAR plots.

4. Results

4.1. Piezometric Data Processing (2016–2021)

Table 2 shows the values of the piezometric indicators determined for each borehole, together with the percentage of missing data for that borehole. These results will be used as the basis for the multi-criteria analysis that will characterize the comparative phase of this study.

Table 2. Table of values of piezometric indicators for each structure.

Name	1-Variance	2-Amplitude (m)	3-Flood Rise Gradient	3-Recovery Gradient	4-Inertia (Days)	5-Response Time (Hours)	5-Rainfall-Piezometry Correlation	Missing Data (%)
{1}	1.71	8.7	1.72×10^{-6}	-1.25×10^{-7}	69	25	0.14	1.59
{2}	1.14	8.88	1.13×10^{-6}	-1.24×10^{-7}	61	16	0.24	3.23
{3}	1.52	7.02	6.61×10^{-6}	-1.26×10^{-7}	62	37	0.18	7.05
{4}	1.7	15.93	7.88×10^{-7}	-1.91×10^{-7}	115	30	0.03	1.17
{5}	0.65	8.82	3.31×10^{-7}	-9.18×10^{-8}	40	18	0.23	0.02
{6}	0.82	6.71	5.57×10^{-7}	-1.23×10^{-7}	56	199	0.09	0.35
{7}	2.08	18.87	1.84×10^{-6}	-2.98×10^{-7}	74	16	0.17	3.77
{8}	0.45	8.11	9.26×10^{-8}	-3.98×10^{-9}	2	15	0.24	0
{9}	0.92	10.13	3.41×10^{-7}	-1.10×10^{-7}	54	18	0.2	1.59
{10}	0.88	12.89	1.49×10^{-7}	-3.35×10^{-8}	30	17	0.21	0

Table 2. *Cont.*

Name	1-Variance	2-Amplitude (m)	3-Flood Rise Gradient	3-Recovery Gradient	4-Inertia (Days)	5-Response Time (Hours)	5-Rainfall-Piezometry Correlation	Missing Data (%)
{11}	0.23	3.71	9.99×10^{-8}	-6.81×10^{-9}	8	4	0.36	0
{12}	0.4	5.11	7.88×10^{-8}	-1.32×10^{-9}	7	13	0.21	0.02
{13}	1.4	10.86	2.31×10^{-6}	-1.04×10^{-7}	74	16	0.18	0.28
{14}	0.64	4.83	4.93×10^{-9}	-5.02×10^{-10}	42	20	0.23	0.06
{15}	0.55	2.44	3.95×10^{-7}	-3.12×10^{-8}	68	176	0.1	0
{16}	0.82	10.91	6.49×10^{-7}	-1.26×10^{-8}	6	13	0.29	0.76
{17}	0.99	5.28	1.43×10^{-6}	-1.31×10^{-7}	65	100	0.16	2.28
{18}	3.2	11.66	3.79×10^{-6}	-3.63×10^{-7}	71	68	0.11	70.61
{19}	0.99	5.16	4.87×10^{-6}	-5.66×10^{-8}	60	39	0.19	29.38

4.1.1. Monocriteria Statistical Analysis

Strict Signal Indicators

For the 19 piezometers studied during the period 2016–2021, the coefficient of variation ranges from 0.23 to 3.2. This indicator is difficult to interpret in isolation from the other indicators. However, it is relevant to describe the variability of the signal. The maximum amplitude between the lowest and highest levels in each series is highly variable. It ranges from 2.4 to 18.9 m at piezometers {15} and {7}, which are about 750 m apart. The average maximum amplitude is 8.73 m with a dispersion of values of 4.2. These indicators reflect the heterogeneity of piezometric behavior in the structures.

Hydrodynamic Parameter Indicators

Piezometer {14} has the lowest rates of piezometric rise and recovery with values of 4.93×10^{-9} and -5.02×10^{-10}. The highest velocities are observed for piezometer {3}, a piezometric rise with a value of 6.6×10^{-6}, and structure {18}, for recovery with a value of -3.63×10^{-7}. The slope values give a relative indication of the rate at which changes occur once a response begins after a rainfall event. The variation in these values supports the hypothesis of a heterogeneous environment with quite different behavior from one structure to another. The variation gives an idea of the hydrodynamic characteristics of the environment around the structures.

System Structure and Fracture Indicators

The inertia values derived from interpretation of the autocorrelation functions (Table 2) again highlight a divergence in the memory effect of the system in the vicinity of the investigated structures. The values range from 2 to 115 days, 400 m apart. In general, the interpretation of the autocorrelation curves shows that the memory effect can be quite different between one structure and another, despite the short distance between them. This is the case for holes {16} and {6}, 80 m apart, with memory effects of 6 and 69 days, respectively. These results are considered to be statistically robust.

The phase shift values between input and output signals, derived from the interpretation of the rain–piezometry cross-correlation curves, reflect variable response times ranging from 4 h {11} to 8.5 days {6} (Table 2).

The associated correlation coefficients are also variable, ranging from 0.03 {4} to 0.36 {11}. In absolute terms, these "rainfall–piezometric" correlation values appear to be quite low, reflecting the inertia of the system.

4.1.2. Multi-Criteria Statistical Analysis

Multi-criteria analyses have the advantage of being able to characterize how the indicators work together and to determine which indicators are likely to discriminate between the piezometric signals from different boreholes (Principal Component Analyses (PCA)). Hierarchical Ascending Classifications classify the piezometers based on the coordinates of the points in the PCA.

The PCA was performed on all seven indicators for the 19 piezometers located in the study area. On the F1F2 axis, the percentage of information explained was 75.48%.

The distribution of the indicators in the variable space shows that all the indicators are significant on the F1F2 axes (due to their proximity to the circle of radius 1), except the slope of the flood rise (Figure 2C).

The amplitude of the variations correlates with the variance and the slopes of the piezometric rises in the series and is anti-correlated with the recovery slopes (Figure 2C). The inertia is anti-correlated with the rainfall–piezometric parameter. Response time shows no correlation with other indicators.

According to the distribution of structures in the space of individuals (Figure 2B,D), points {6} and {15} are strongly expressed on the F2 axis and seem to be discriminated by their response time.

Points {4}, {7}, and {18}, which are strongly expressed on the F1 axis, can be explained by their dispersion and variation amplitude values, which vary inversely to recovery slopes, which are also strongly expressed in the variation of these structures.

Points {8}, {11}, {12}, {14}, and {16} are expressed on the F1 axis and are strongly explained by their "rainfall–piezometry" correlation value.

On the other hand, the remaining points {1}, {2}, {3}, {5}, {9}, {10}, {13}, {17}, and {19} form a median group that is moderately expressed on both axes (Figure 2B,D).

A HAC was then used to discriminate between groups of piezometers based on the coordinates of the points in the PCA. Five groups stood out on the dissimilarity dendrogram. The HAC was performed for a significance threshold of 0.08, symbolized by a solid line on the dendrogram. At the end of this analysis, five groups stand out (Figure 2A).

The first group (A1, pink) discriminates between points {4}, {7} and {18}. This can be explained by the F1 axis, which is mainly responsible for the "rainfall–piezometry" correlation, amplitude, and dispersion. The representative piezometer in this group is {18}. The group is representative of highly transmissive behavior.

A second group (A2, red), which essentially shows "rainfall–piezometry" correlation values expressed primarily on the F1 axis, consists of points {8}, {11}, {12}, {14}, and {16}. The representative piezometer in this group is {16}. This group is related to the fracturing of the environment and therefore has a transmissive behavior.

A third group (A3, green), representing the response time indicator, is strongly expressed on the F2 axis and consists of points {6} and {15}. The representative piezometer in this group is {15}, which is typical of a capacitive environment.

A fourth group (A4, purple), the median, differs from the first by the best flood gradients, an indicator that is not very representative on the F1F2 axes and consists of points {3} and {19}. The most representative piezometer in this group is {19}. This group presents both transmissive and capacitive behavior.

A fifth and final group (A5, black), median, which has no axis and is therefore a factor of influence, consists of points {1}, {2}, {5}, {9}, {10}, {13}, and {17}. The representative piezometer in this group is {17}. This group has an above transmissive and capacitive behavior.

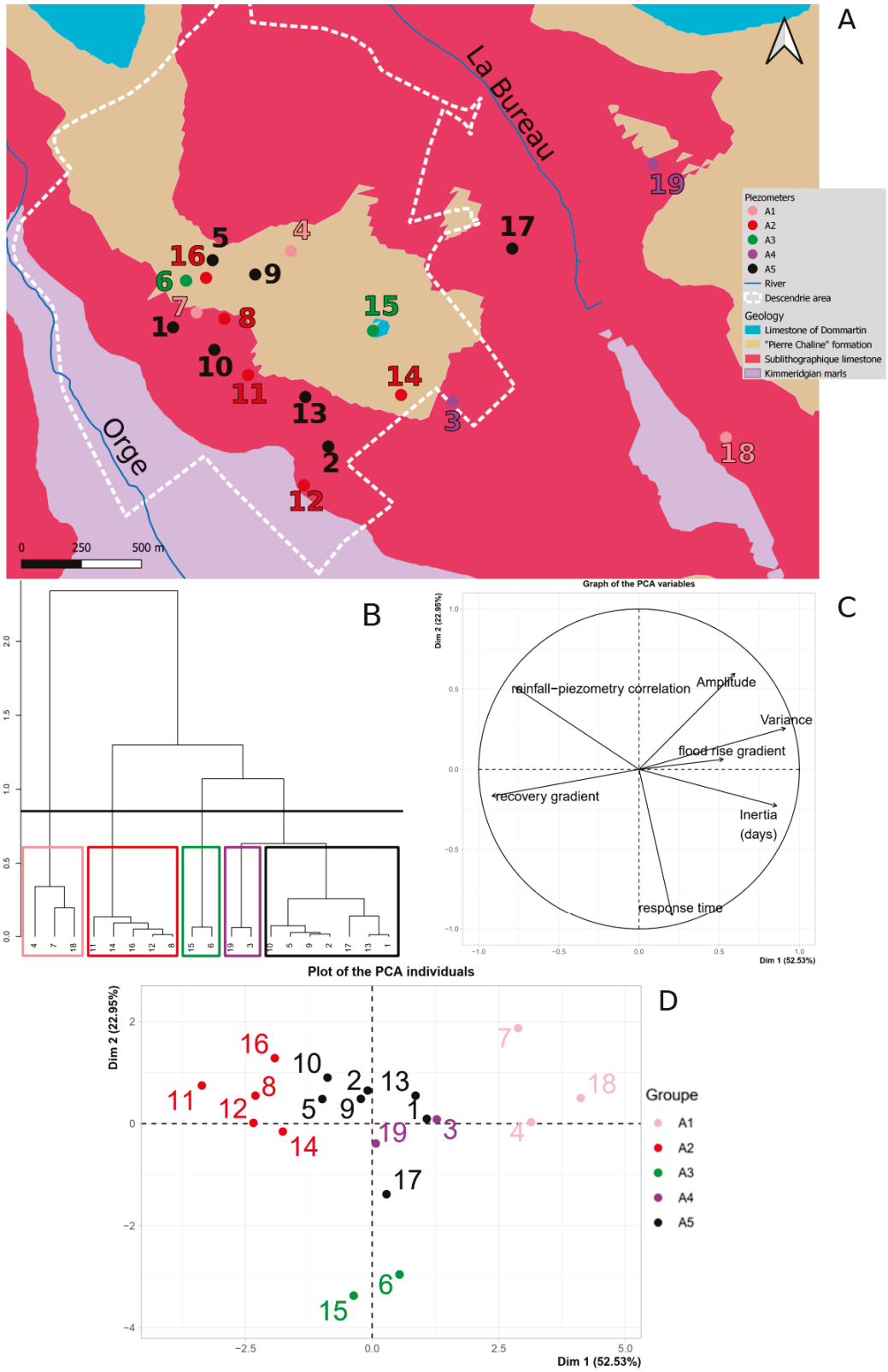

Figure 2. Result of multi-criteria statistical analysis. (**A**)—Mapping of piezometer positions according to the groups resulting from the hierarchical classification. The colors are associated with the groups determined by the hierarchical classification. (**B**)—Hierarchical classification of piezometers according to the selected criteria described in methodology. (**C**)—PCA variable graph. (**D**)—PCA individuals' graph.

4.2. Processing Geological and Geotechnical Data

4.2.1. Fracturing Data

Gamma Ray logs are used as a reference for all geological and fracture studies in the study area and are used to correlate Sublithographic limestone levels from one borehole to another. Areal fracturing has led to the development of a karst network that is visible on optical logs, as shown in Figure 3C,E,F).

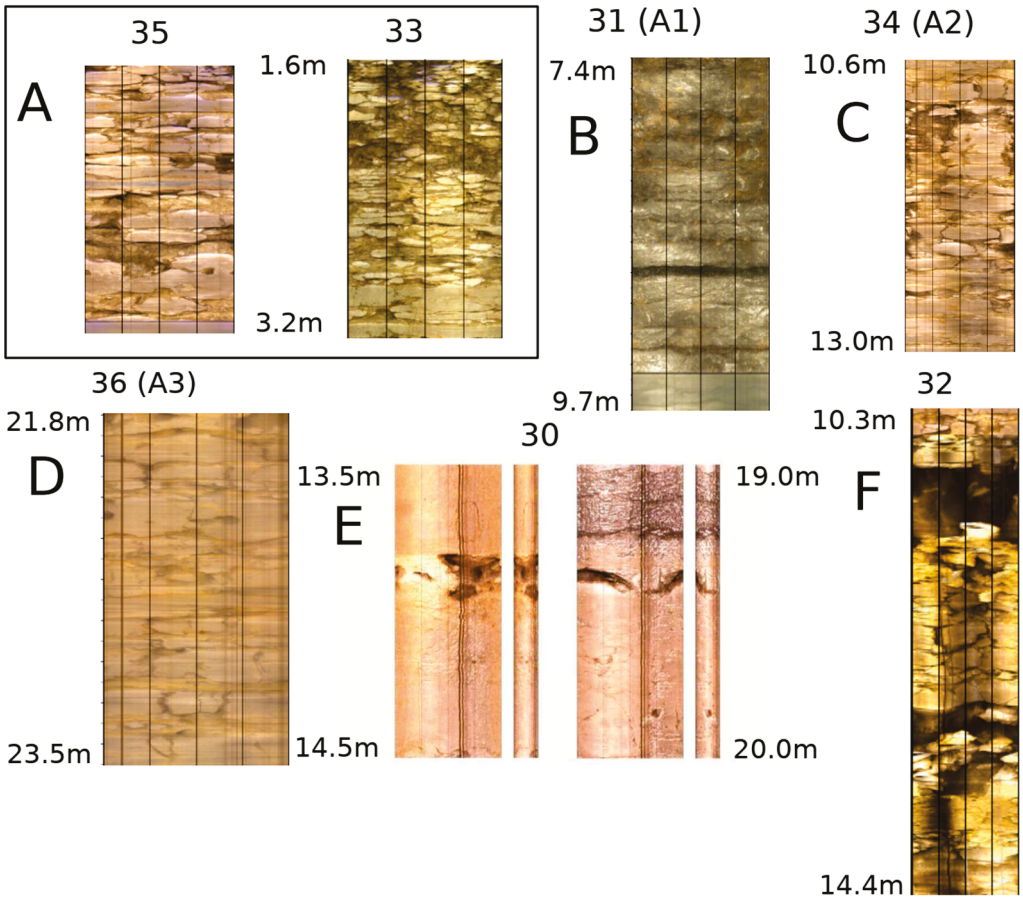

Figure 3. (**A**)—Weathered zone. (**B**)—Fracturing in a piezometer of group A1 (poorly developed fracturing). (**C**)—Fracturing in a borehole near a piezometer of group A2 {16}, with highly developed fracturing. (**D**)—Fracturing in a borehole near a Group A3 piezometer {29}, with vertical and horizontal fracturing visible. (**E**)—Dissolution marks in a borehole distant from the piezometers and therefore not able to be connected to a functioning group. (**F**)—Highly developed and partly karstified fracturing (presence of conduit) in a borehole that cannot be connected to a piezometric functioning group.

Below and sometimes at some distance from the altered surface zone (Figure 3A), centimeter-scale horizontal drains are most commonly found in the limestone intervals of the most marly levels, following the bedding planes (Figure 3B,D). These drains, which show clear traces of dissolution, are often found in the limestone interbeds of N4 and N2 (Figure 1B) or in the upper part of the Exogyres marls (Figure 3B,E,F).

Fracture orientation detected by wall imagery from 25 boreholes (3 of which are to the north of the study area) is summarized in Figure 4. A primary direction centered on N150°E is visible, with a scatter of measurements around this value. In detail (Figure 4), perpendicular directions dominate in some of the boreholes.

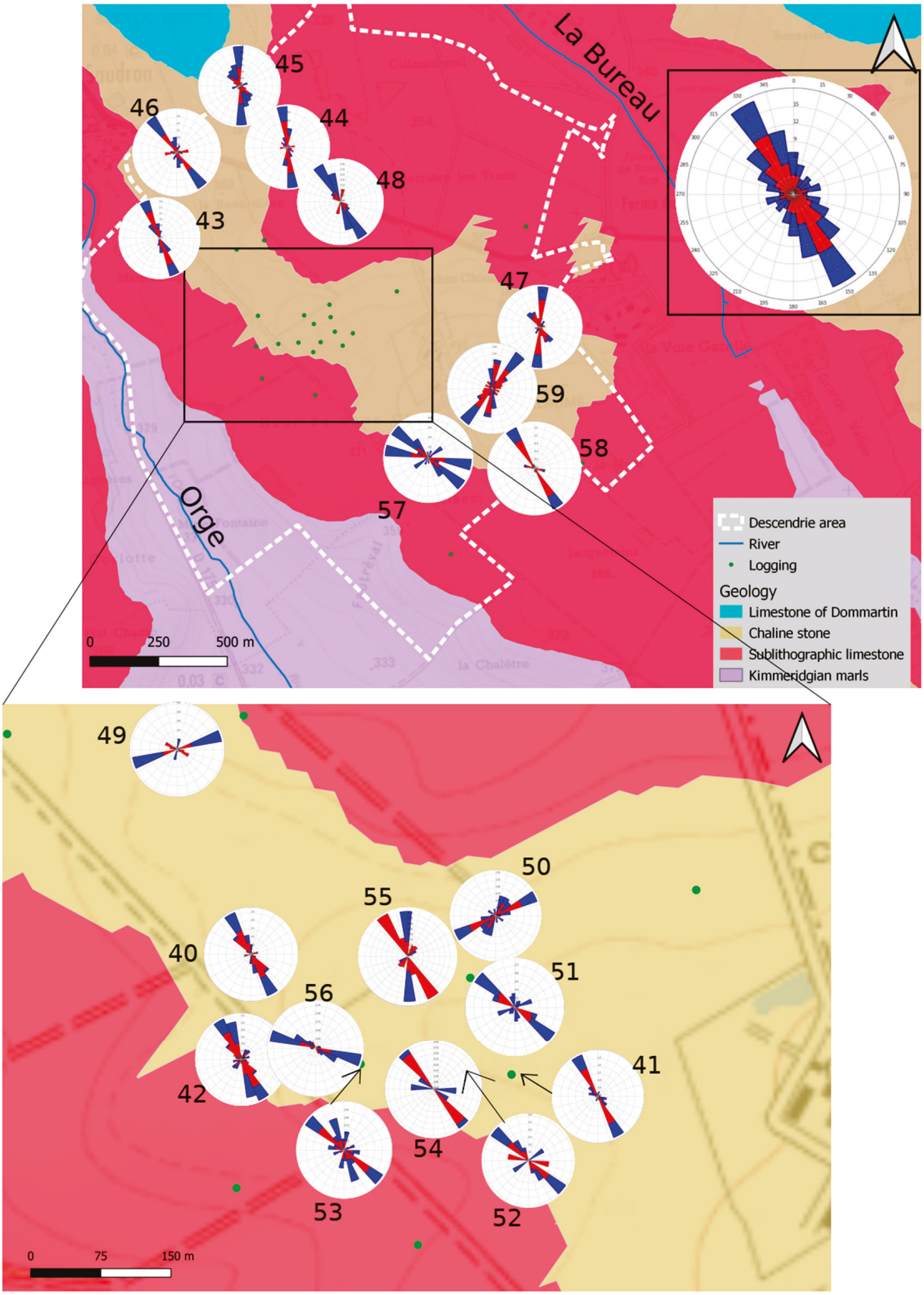

Figure 4. Map of the distribution of oriented fracturing based on optical logs, with differentiation between open fracturing (in red) and closed fracturing (in blue). The synthesis of all rose diagrams is represented by the large rose.

The fractures identified by the methods used are local and difficult to match from one borehole to another.

4.2.2. Hydraulics Tests

Lefranc Tests: Permeability on the Scale of the Borehole

Results of the tests conducted on boreholes {24}, {25}, {26}, and {27} are shown in Figure 5.

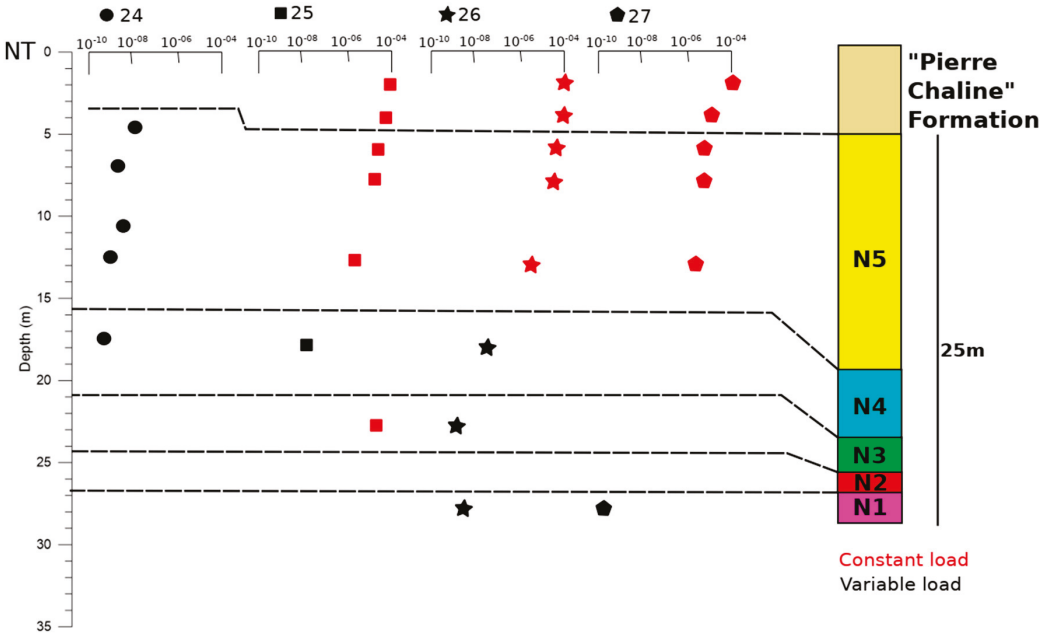

Figure 5. Permeability tests (Lefranc) at various normalized depths in relation to the natural terrain (NT). Legend colors correspond to those shown in Figure 1B.

Stratigraphically, the tests were conducted in the "Pierre Chaline" formation to a depth of 4.5 m, in the upper part of the Sublithographic limestone (N5) at depths from 4.5 m to 13.5 m, in the middle part of the Sublithographic limestone (N4) at depths from 17 to 18.5 m, and in the lower part of the Sublithographic limestone (N3 to N1) at depths from 22.5 m to 30 m. Kimmeridgian marls were also encountered in a single borehole {28}.

Permeability results from constant load tests range from 10^{-4} to 10^{-6} m/s, with permeability decreasing with depth. Permeability results from variable load tests range from 10^{-8} to 10^{-10} m/s, regardless of the formation and test depth.

The formations are permeable to semi-permeable (10^{-5} to 10^{-6} m/s) down to a depth of 17 m (N5). Then, in the middle to lower part of the Sublithographic limestone (N4 to N1), they reach values of 10^{-8} to 10^{-10} m/s. A more permeable zone at 10^{-5} m/s in the lower part of the limestone (N3) was encountered in {25}.

The permeability differences measured reflect the general anisotropy of the various lithologies of the Sublithographic limestones. However, they also reflect anisotropy on a larger scale. For example, borehole {24} crosses the upper and middle parts of the Sublithographic limestones (N5 and N4), which have low permeabilities in the order of 10^{-8} to 10^{-10} m/s, whereas it is located 800 m from the other boreholes, which have higher permeability ranges (Figure 5). The borehole {24} is also very close to Group A2 and A5 piezometers, which have more-or-less transmissive behavior.

The results for the N5 formation remain consistent among nearby boreholes {25}, {26} and {27}. For the N3 formation, the variation in values at the same depth is significant, with differences of 10^{-4} m/s between two nearby boreholes ({25} and {26}). The N3 formation contains many more marly layers than the N5 formation. This explains the much greater permeability variation within this formation and also between the two formations.

Pumping Tests: Permeability at Aquifer Scale

Analyses of the pumping test and the disturbance in the only responsive observation piezometer give permeability values between 10^{-8} and 10^{-7} m/s. The difference between these values can be explained by the fact that different volumes were studied due to the heterogeneity of the medium being excited by the tests.

The storage coefficient for both pumped and interference boreholes obtained from these tests is approximately 10^{-3} m/s.

4.3. SNMR Data

4.3.1. SNMR Signal

The lowest initial amplitude (E0) over all soundings is between 5 and 10 nV. Initial amplitudes associated with the highest pulse moments range between 1 and 5 nV. These very low initial amplitude values do, however, allow some interpretation, since the signal-to-noise ratio of the soundings (Table 1) is always greater than 2.5.

The SNMR signals are provided in Figure 6. Uncertainty bounds are derived by considering minimum and maximum values from all SNMR signal parameter sets (signal amplitude e and T2* relaxation time) that yield a 10% increase in the root mean squared error (RMSE) fitting error as compared to the optimal RMSE, as proposed by [51].

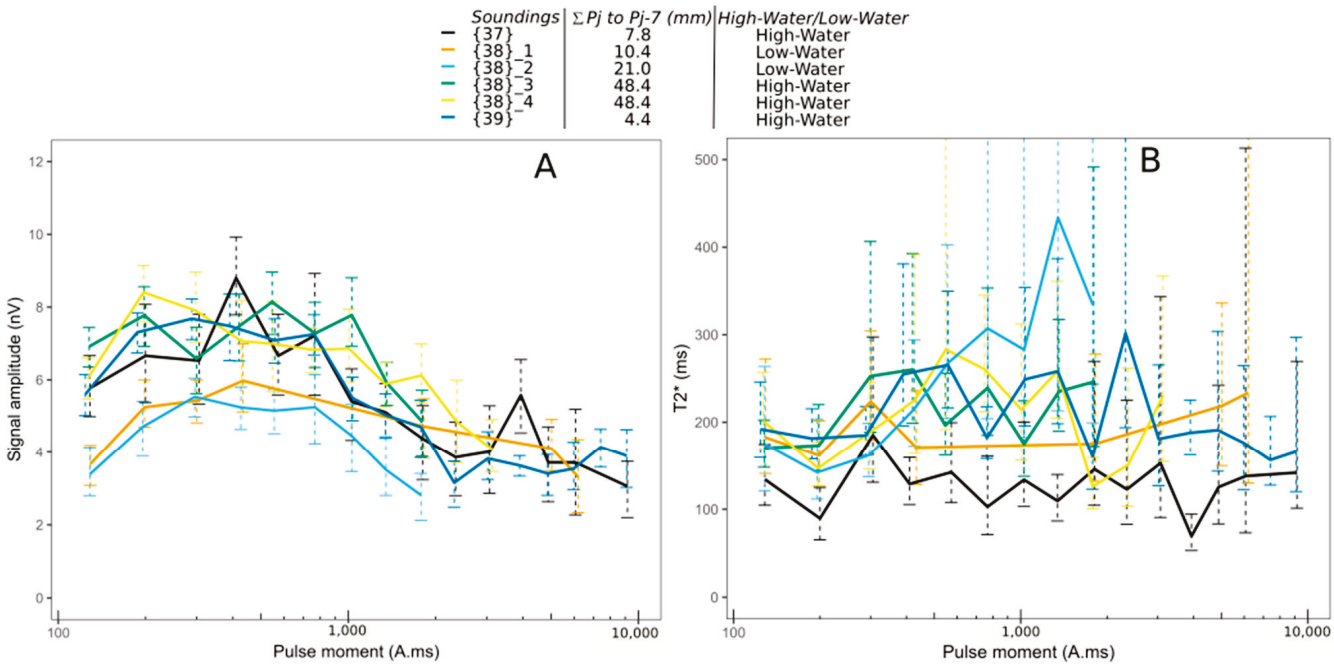

Figure 6. SNMR signal parameters as a function of the energizing pulse, for all soundings (Σ Pj to Pj − 7 = sum of rainfall over the 7 days preceding the sounding). (**A**)—Initial signal amplitude. (**B**)—Apparent transverse relaxation time T2*.

Two groups of responses stand out. The first group, consisting of soundings {38}_1 and {38}_2, has initial signal amplitudes approximately 3 nV lower at low pulse moments than the group consisting of soundings {38}_3, {38}_4, {37} and {39}, which suggests lower water content in the upper part of the sounding. High uncertainties are associated with T2* estimates. Sounding {37} stands out with relatively lower T2*, which may be associated with small porosity dimensions. These original data (Figure 6) are unaffected by any inversion artefacts. It is therefore interesting to compare these trends with the inverted results (Figure 7).

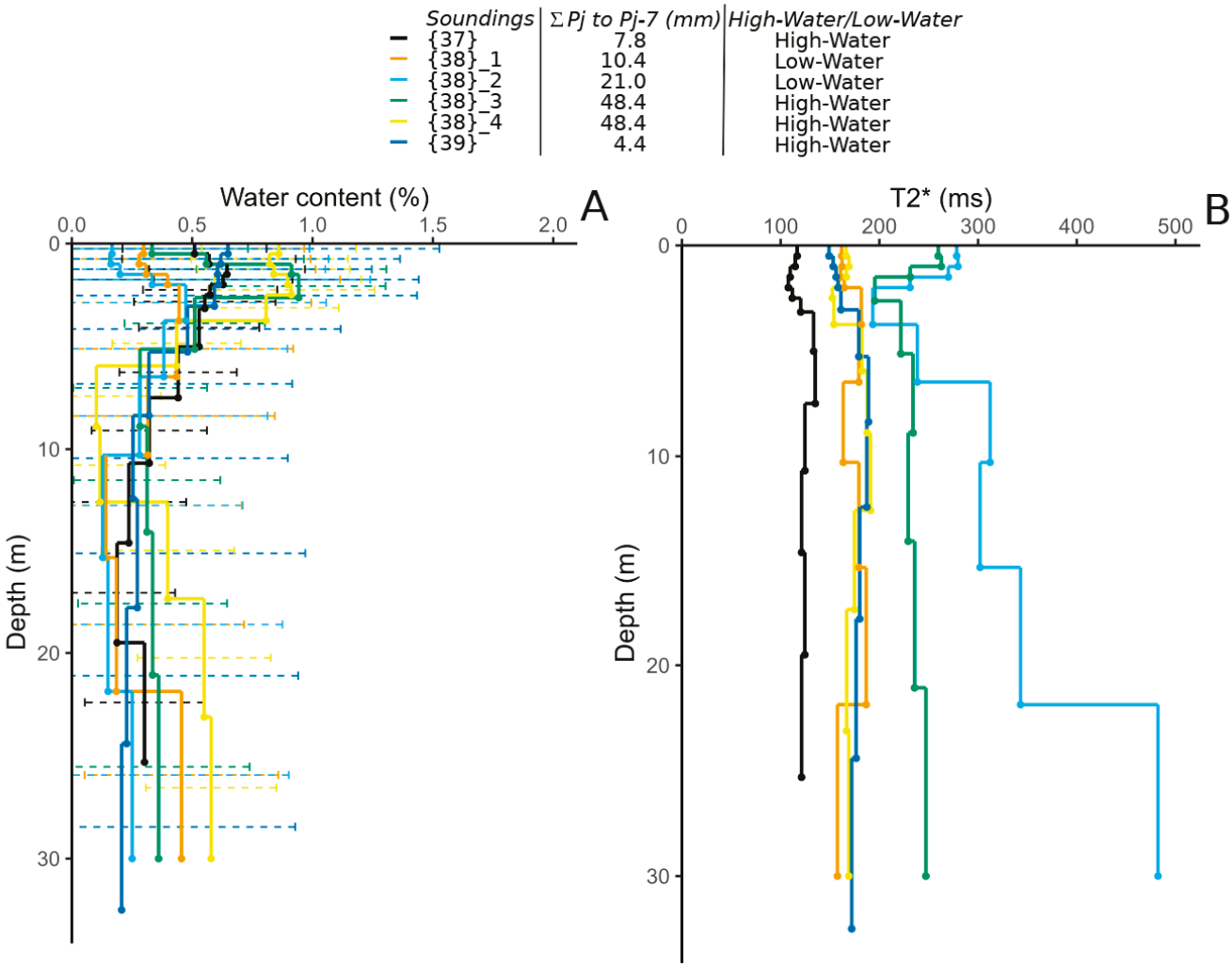

Figure 7. SNMR inversion for all sites. (**A**)—SNMR water content. (**B**)—Apparent transverse relaxation time T2*.

4.3.2. Inversion Results

The inversion results are displayed in Figure 7 with a 95% confidence interval on SNMR water content derived from the SVD inversion [52]. This approach provides an estimate of the uncertainty bounds of the water content in each layer considered separately. It accounts for the fact the buried water layers that have equal water volumes can, to some extent, yield equivalent SNMR responses. The results show very low to low water contents, which do not exceed 0.9% (1.5% considering the maximum inversion uncertainties), and that have an average value of 0.42%, with highest water content being reached in the first 0-5m (Figure 7A). These results indicate and quantify the low water storage capacity of the Sublithographic limestone matrix. In addition, the trends seen in Figure 6 are confirmed with these inverted data, since the same trends are present (two response groups and a very limited quantity of water content).

The T2* estimates are consistent with a filtered, non-inverted SNMR signal, with significantly lower values associated with Sounding {37} (see Section 4.3.1). High values associated with Sounding {38}_2 are not significant as they are associated with high signal uncertainties.

Soundings performed under different hydrologic conditions exhibit contrasting behaviors in the upper 0–5 m. Soundings {38}_1 and {38}_2 were performed in low water levels with significant antecedent precipitations. They have have lowest water content (0.3% in average). Soundings {37} and {39} were performed in high water levels with little antecedent

precipitations. The have intermediate water content (0.55% in average). Soundings {38}_3 and {38}_4 were performed in high water levels with important antecedent precipitations. The have the highest water content (0.8% in average). SNMR inversions thus evidence both a primarily seasonal time-scale variation on the limestone water content, and a significant but secondary short (daily) time-scale variation.

The uncertainties provided in Figure 7 show the minimum and maximum water content that may be associated with each water layer, taken separately. Maximum water content for a specific water layer is associated with minimum or at least reduced water content in other layers. Such representation of uncertainty is not adequate to assess the minimum and maximum water content over the whole sounding. As a complement to Figure 7, we thus provide uncertainty bounds for sounding {38} for equivalent models that yield the minimum and the maximum water volumes over the investigated depth [53] (Figure 8). The average water content is between 0.57–0.61% and 0.51–0.63% for soundings {38}_4 and {38}_3, respectively, while it is only between 0.19–0.25% and 0.33–0.35% for soundings {38}_2 and {38}_1, respectively.

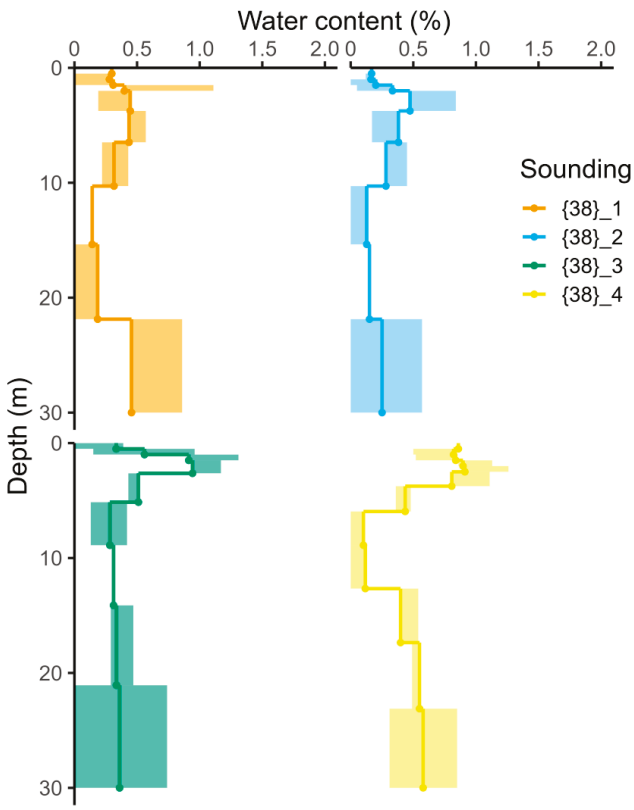

Figure 8. SNMR inversion for soundings performed at location {38}. Temporal water content variability between high ({38}_3 and {38}_4) and low ({38}_1 and {38}_2) water levels can be significant.

5. Discussion

Large borehole networks are often installed with geotechnical objectives in mind, and the data collected as part of these studies are often not linked to hydrogeological studies as such. Although these boreholes can be reused as piezometers, they were not originally designed as such. In many cases, these boreholes were dug throughout the structure and are not cased. This greatly complicates the interpretation of water level variations in response to internal or external forcing. Our study site benefits from such a network of discrete boreholes set up for geotechnical purposes. In the following discussion, we examine the strengths and weaknesses of this network, as well as possible ways of overcoming them.

5.1. Piezometric Response and Fracture Network Connectivity

Statistical analysis of these chronicles requires a large dataset and, depending on the indicators used, makes it possible to classify the different piezometric variations according to their response to rainfall. This descriptive analysis made it possible to characterize five behaviors, grouping 19 piezometers and identifying transmissive (groups A1 and A2), an inertial (group A3), and a group with mixed behaviors (groups A4 and A5) (Figure 9).

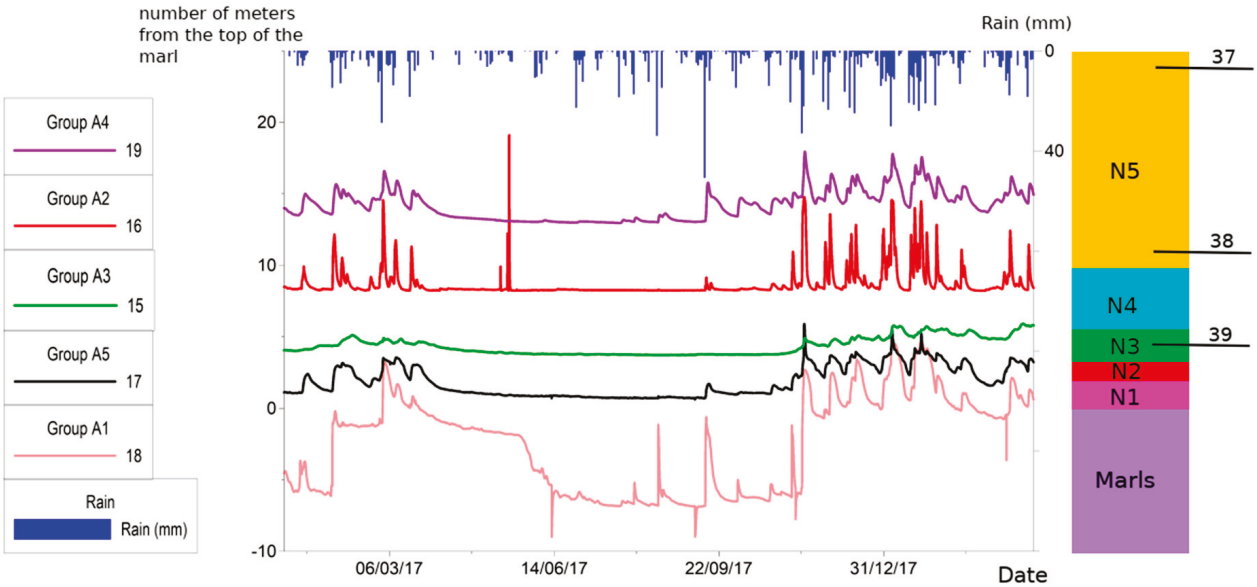

Figure 9. Classification of hydrodynamic behavior of water levels in piezometers in response to rainfall events.

Considered alone, piezometric response does allow some relevant insights into the hydrodynamics behavior. This is the case for Groups A4 and A5, where the analysis of the piezometric response provides information on the more-or-less inertial functioning of the boreholes, and suggests the presence of fractures in the process of development or a poorly connected fracture network. It is also the case for Group A1, for which neither geological drillings allowing fracture analysis, nor geophysical logs, are available near the piezometers. According to the descriptive analysis, Group A1 behaves like a permeable medium with a rapid response time to rainfall events but a relatively long memory effect with a slow decrease in water level. We associated such behavior with a moderate degree of fracturing (Figure 3B), with the rapid water level rise in the piezometer being simply due to the filling of the piezometer and not significative of the hydrodynamic response of the water table in the piezometer area. The SNMR results confirm this interpretation, as the significantly lower T2* associated with sounding {37} hints at a significative matrix contribution to the effective porosity.

Detailed fracture analysis may evidence discrete features that are not relevant for understanding hydrodynamic responses. For example, group A3 is associated with matrix functioning, despite the presence of open fractures near one piezometer in this group (Figure 3D). The orientation of these open fractures is perpendicular to the main flow, which may explain the inertial behavior of this piezometer.

In other cases, detailed fracture analysis using geological boreholes and SNMR can avoid erroneous water level dynamics interpretation. In the example provided in Figure 10, optical imaging allows to identify a karst conduit that is responsible for the regulation of the groundwater level. SNMR sounding {39}, located close to piezometer {16} (Figure 10), did not record evidence of significative water content below this fracture. We thus formulate the hypothesis that the water level below this base level does not contribute to the flow and may not be considered as representative from the water table.

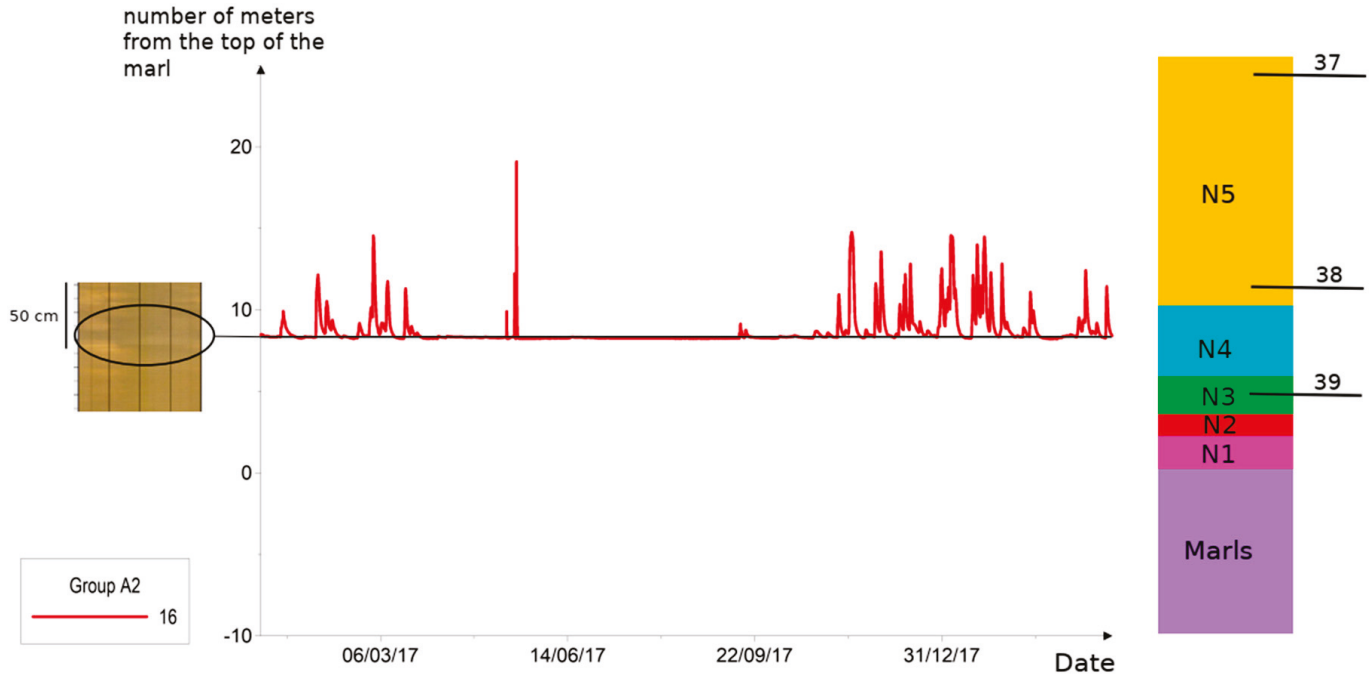

Figure 10. Link between conduit and piezometric level: the karst conduit maintains a base level in the piezometer. Only water levels above this base level contribute to the flow.

5.2. Hydraulic Tests and Local Matrix Characterization

In karstified environments, permeabilities can vary by several orders of magnitude depending on the scale of measurement (laboratory, borehole, and catchment) [27]. For each of these permeability ranges, different measurement methods are used. Hydraulic tests carried out in this study are mostly sensitive to the near borehole media.

Permeability measurements carried out indicate higher permeability at the surface of the Sublithographic limestones and lower permeability at depth in these limestones, in the marls, and in the marlier limestone layers. These values highlight a semi-permeable behavior for limestones to be impermeable when marls predominate, whereas the piezometric response tends to highlight the reactivity of the system.

In our study, the duration of the Lefranc tests is too short and the pumping test flow rates are too low to attract the more distant water contained within the carbonate matrix or connected fractures, so they mainly provide local matrix characterization.

5.3. SNMR and Water Content Quantification

Information on water mobilization in response to forcing obtained from piezometric responses, fracturing analysis, and hydraulic tests remains incomplete as they do not quantify the water saturation of the medium. SNMR measurements provide access to the water content and its variation over a wider access radius than those investigated by borehole tests or piezometric variations.

In our study, very low (3 and 8 nV) SNMR signals associated with high signal-to-noise ratio allow us to quantify very low (<0.6%) water content with significative variability.

We relate this variability to both a primarily seasonal time-scale variation of the limestone water content and a significant but secondary short (daily) time-scale variation. This result reinforces the interpretation of the piezometric behavior of matrix-like and mixed matrix/transmissive groups, with mostly seasonal matrix dynamics and daily-to-weekly fissures and fracture dynamics.

6. Conclusions

This study utilized a variety of methods to better understand the functioning of karst groundwater systems. With karst outcrops covering 10-15% of the world's continental surface [21], understanding these hydrosystems is crucial for addressing the challenges associated with the exploitation of groundwater resources. It is estimated that around 25% of the world's population relies on groundwater extracted from karst areas for drinking water [52]. Additionally, studying these systems is essential during geotechnical or civil engineering investigations [4].

Karst hydrosystems are complex due to their triple porosity (matrix, fractures, and conduits) and inherent heterogeneity. Both the fracture properties and the hydrodynamic properties of the carbonate matrix determine the functioning of karst aquifers. Piezometric information is often the basis for understanding flow organization. Many studies rely on discrete piezometric data to characterize these complex environments where flows are distributed according to permeability constraints.

Our study benefits from a large network of boreholes initially implemented for geotechnical purposes. Despite the density of this observation network, the collection of water level variations is not easily linked to the hydrogeological properties of the aquifer. While piezometric responses alone provide some insights into hydrodynamic behavior, detailed fracture analysis can reveal discrete features that are not always relevant for understanding these responses. However, in some cases, combining detailed fracture analysis from geological boreholes with SNMR is necessary to avoid erroneous interpretations of water level dynamics.

High-density and high-quality data in karst environments are rarely available due to the complexity and heterogeneity of these systems. Comprehensive datasets are crucial for accurate analysis and modeling, yet they are challenging to obtain. By leveraging the extensive and high-quality data from this unique site, we can gain valuable insights into the hydrogeologic complexities of fractured-rock karst systems, providing a strong basis for effectively understanding and managing these environments

The combination of geological, hydrogeological, and geophysical measurements in this project highlights the contribution of water masses with two types of aquifer responses: a rapid response at hourly-to-daily timescales to rainfall events in well-connected fractures, and a slower response at seasonal timescales in the matrix. The characterization of the dynamics and the quantification of the water content in the matrix and fissured/fractured compartments were enabled by the combined interpretation of piezometric response analyses and SNMR data.

Thus, coupling various separately collected measurements provides a key to understanding the aquifer as a whole. Future work could include longer pumping tests or modelling fluctuations of base groundwater levels to better assess matrix flows.

Author Contributions: Conceptualization, M.B., C.B. and N.M.; methodology, M.B., L.-M.G., V.B., N.M., R.V., K.C., C.B., S.D., S.G. and G.C.; software, M.B., N.M. and G.C.; validation, N.M., R.V. and K.C.; formal analysis, M.B.; investigation, M.B., L.-M.G. and V.B.; resources, S.G.; data curation, M.B., L.-M.G. and V.B.; writing—original draft preparation, M.B., C.B. and N.M.; writing—review and editing, C.B., N.M., K.C., R.V., S.D. and S.G.; Supervision, C.B., N.M., K.C. and S.G.; project administration, C.B., K.C. and S.G.; funding acquisition, S.G., C.B., K.C., N.M. and S.D. All authors have read and agreed to the published version of the manuscript.

Funding: This research was funded by ANDRA PhD grant number 20080158.

Data Availability Statement: Data are contained within the article.

Acknowledgments: We would like to thank the reviewers for their work and constructive comments and suggestions. We would also like to express our sincere thanks to Patricia Bobeck for her proof-reading and for her contribution to the English version of the manuscript.

Conflicts of Interest: The authors declare no conflict of interest.

Appendix A

Table A1. Links between number, name, and information.

Number	Name	Information	Number	Name	Information
1	CIG1028	Piezometry	31	CIG1031	Borehole imaging
2	CIG1029	Piezometry	32	CIG1080	Borehole imaging
3	CIG1030	Piezometry	33	CIG1088	Borehole imaging
4	CIG1031	Piezometry	34	CIG1120	Borehole imaging
5	CIG1227	Piezometry	35	CIG1122	Borehole imaging
6	CIG1228	Piezometry	36	CIG1254	Borehole imaging
7	CIG1229	Piezometry	37	EST3BIS	SNMR
8	CIG1230	Piezometry	38	EST14	SNMR
9	CIG1237	Piezometry	39	EST18	SNMR
10	CIG1245	Piezometry	40	CIG1005	Fracturing
11	CIG1246	Piezometry	41	CIG1009	Fracturing
12	CIG1247	Piezometry	42	CIG1011	Fracturing
13	CIG1248	Piezometry	43	CIG1077	Fracturing
14	CIG1249	Piezometry	44	CIG1078	Fracturing
15	CIG1250	Piezometry	45	CIG1079	Fracturing
16	EST1012	Piezometry	46	CIG1080	Fracturing
17	EST1021	Piezometry	47	CIG1086	Fracturing
18	EST1037	Piezometry	48	CIG1088	Fracturing
19	EST5071	Piezometry	49	CIG1090	Fracturing
20	CIG1023	Pumping tests	50	CIG1108	Fracturing
21	CIG1024	Pumping tests	51	CIG1114	Fracturing
22	CIG1025	Pumping tests	52	CIG1116	Fracturing
23	CIG1026	Pumping tests	53	CIG1117	Fracturing
24	CIG1137	Lefranc tests	54	CIG1118	Fracturing
25	CIG1138	Lefranc tests	55	CIG1120	Fracturing
26	CIG1139	Lefranc tests	56	CIG1121	Fracturing
27	CIG1140	Lefranc tests	57	CIG1252	Fracturing
28	CIG1237	Lefranc tests	58	CIG1253	Fracturing
29	CIG1250	Lefranc tests	59	CIG1254	Fracturing
30	CIG1011	Borehole imaging			

Appendix B

Table A2. Characteristics of the piezometers used in this study. Type and data-acquisition start dates.

Name	Depth (m)	Borehole Screen	Geological Level	Data	Data Acquisition Start On
{16}	25.5	Ø 112/122.5 mm + gravel packing	Sublithographic limestone (N1)	Pressure Temperature	13 April 1996 30 June 1999
{17}	30	Ø 113/125 mm opening 1 mm + gravel packing	Kimmeridgian marls	Pressure Temperature Sampling	4 April 2000 6 July 2000 6 July 2000
{18}	20.2	Ø 113/125 mm opening 1 mm + gravel packing	Kimmeridgian marls	Pressure Temperature Sampling	5 April 2000
{19}	39.06	Ø 119.8/125 mm	Kimmeridgian marls	Pressure Temperature	20 December 1995 10 July 1999
{1}	20	gravel packing	Kimmeridgian marls	Pressure	25 January 2016
{2}	14	gravel packing	Kimmeridgian marls	Pressure	17 February 2016
{3}	28	gravel packing	Kimmeridgian marls	Pressure	25 February 2016
{4}	30	gravel packing	Kimmeridgian marls	Pressure	27 January 2016
{5}	30.3	gravel packing	Kimmeridgian marls	Pressure Temperature	31 August 2016
{6}	30.3	gravel packing	Kimmeridgian marls	Pressure Temperature	31 August 2016
{7}	30.3	gravel packing	Kimmeridgian marls	Pressure Temperature	22 August 2016
{8}	32	gravel packing	Kimmeridgian marls	Pressure Temperature	31 August 2016
{9}	30.3	gravel packing	Kimmeridgian marls	Pressure Temperature	31 August 2016
{10}	20.3	gravel packing	Kimmeridgian marls	Pressure Temperature	18 August 2016
{11}	20.3	gravel packing	Sublithographic limestone (N1)	Pressure Temperature	16 June 2016
{12}	15.4	gravel packing	Kimmeridgian marls	Pressure Temperature	29 September 2016
{13}	30.35	gravel packing	Kimmeridgian marls	Pressure Temperature	22 August 2016
{14}	15.3	gravel packing	Sublithographic limestone (N5)	Pressure Temperature	24 November 2016
{15}	30.3	gravel packing	Sublithographic limestone (N4)	Pressure Temperature	3 August 2016

References

1. Stevanović, Z. Global Distribution and Use of Water from Karst Aquifers. *Geol. Soc. Lond. Spec. Publ.* **2018**, *466*, 217–236. [CrossRef]
2. Ravbar, N.; Šebela, S. The Effectiveness of Protection Policies and Legislative Framework with Special Regard to Karst Landscapes: Insights from Slovenia. *Environ. Sci. Policy* **2015**, *51*, 106–116. [CrossRef]
3. Hartmann, A.; Goldscheider, N.; Wagener, T.; Lange, J.; Weiler, M. Karst Water Resources in a Changing World: Review of Hydrological Modeling Approaches: Karst Water Resources Prediction. *Rev. Geophys.* **2014**, *52*, 218–242. [CrossRef]
4. Chen, C.-T.; Hu, J.-C.; Lu, C.-Y.; Lee, J.-C.; Chan, Y.-C. Thirty-Year Land Elevation Change from Subsidence to Uplift Following the Termination of Groundwater Pumping and Its Geological Implications in the Metropolitan Taipei Basin, Northern Taiwan. *Eng. Geol.* **2007**, *95*, 30–47. [CrossRef]

5. Mangin, A. Pour une meilleure connaissance des systèmes hydrologiques à partir des analyses corrélatoire et spectrale (The use of autocorrelation and spectral analyses to obtain a better understanding of hydrological systems). *J. Hydrol.* **1984**, *67*, 25–43. [CrossRef]
6. Nistor, M.M.; Rahardjo, H.; Satyanaga, A.; Hao, K.Z.; Xiaosheng, Q.; Sham, A.W.L. Investigation of Groundwater Table Distribution Using Borehole Piezometer Data Interpolation: Case Study of Singapore. *Eng. Geol.* **2020**, *271*, 105590. [CrossRef]
7. De Luca, D.A.; Lasagna, M.; Debernardi, L. Hydrogeology of the Western Po Plain (Piedmont, NW Italy). *J. Maps* **2020**, *16*, 265–273. [CrossRef]
8. Fiorillo, F. Tank-Reservoir Drainage as a Simulation of the Recession Limb of Karst Spring Hydrographs. *Hydrogeol. J* **2011**, *19*, 1009–1019. [CrossRef]
9. Bennett, G.; Van Camp, M.; Shemsanga, C.; Kervyn, M.; Walraevens, K. Assessment of Spatial and Temporal Variability of Groundwater Level in the Aquifer System on the Flanks of Mount Meru, Northern Tanzania. *J. Hydrol. Reg. Stud.* **2022**, *44*, 101212. [CrossRef]
10. Giese, M.; Reimann, T.; Bailly-Comte, V.; Maréchal, J.-C.; Sauter, M.; Geyer, T. Turbulent and Laminar Flow in Karst Conduits Under Unsteady Flow Conditions: Interpretation of Pumping Tests by Discrete Conduit-Continuum Modeling. *Water Resour. Res.* **2018**, *54*, 1918–1933. [CrossRef]
11. Praamsma, T.; Novakowski, K.; Kyser, K.; Hall, K. Using Stable Isotopes and Hydraulic Head Data to Investigate Groundwater Recharge and Discharge in a Fractured Rock Aquifer. *J. Hydrol.* **2009**, *366*, 35–45. [CrossRef]
12. Maréchal, J.-C.; Ladouche, B.; Dörfliger, N.; Lachassagne, P. Interpretation of Pumping Tests in a Mixed Flow Karst System: Pumping Tests in Karst System. *Water Resour. Res.* **2008**, *44*, W05401. [CrossRef]
13. Banks, E.W.; Simmons, C.T.; Love, A.J.; Shand, P. Assessing Spatial and Temporal Connectivity between Surface Water and Groundwater in a Regional Catchment: Implications for Regional Scale Water Quantity and Quality. *J. Hydrol.* **2011**, *404*, 30–49. [CrossRef]
14. Valois, R.; Rau, G.C.; Vouillamoz, J.-M.; Derode, B. Estimating Hydraulic Properties of the Shallow Subsurface Using the Groundwater Response to Earth and Atmospheric Tides: A Comparison With Pumping Tests. *Water Resour. Res.* **2022**, *58*, e2021WR031666. [CrossRef]
15. Bon, A.F.; Aoudou Doua, S.; Banakeng, L.A.; Narke, C.; Chouto, S.; Mbouombouo Ndam, A. Contribution of a Geostatistical Model of Electrical Conductivity in the Assessment of the Water Pollution Index of the Quaternary Aquifer of the Lake Chad Basin (Kousseri-Cameroon). *Arab. J. Geosci.* **2020**, *13*, 170. [CrossRef]
16. Dewandel, B.; Aunay, B.; Maréchal, J.C.; Roques, C.; Bour, O.; Mougin, B.; Aquilina, L. Analytical Solutions for Analysing Pumping Tests in a Sub-Vertical and Anisotropic Fault Zone Draining Shallow Aquifers. *J. Hydrol.* **2014**, *509*, 115–131. [CrossRef]
17. Castellazzi, P.; Arroyo-Domínguez, N.; Martel, R.; Calderhead, A.I.; Normand, J.C.L.; Gárfias, J.; Rivera, A. Land Subsidence in Major Cities of Central Mexico: Interpreting InSAR-Derived Land Subsidence Mapping with Hydrogeological Data. *Int. J. Appl. Earth Obs. Geoinf.* **2016**, *47*, 102–111. [CrossRef]
18. Haimson, B.C.; Doe, T.W. State of Stress, Permeability, and Fractures in the Precambrian Granite of Northern Illinois. *J. Geophys. Res.* **1983**, *88*, 7355–7371. [CrossRef]
19. Dausse, A.; Leonardi, V.; Jourde, H. Hydraulic Characterization and Identification of Flow-Bearing Structures Based on Multi-Scale Investigations Applied to the Lez Karst Aquifer. *J. Hydrol. Reg. Stud.* **2019**, *26*, 100627. [CrossRef]
20. Goldscheider, N.; Drew, D. *Methods in Karst Hydrogeology*; International Contributions to Hydrogeology; Taylor & Francis: London, UK, 2007; ISBN 978-0-415-42873-6.
21. Kiraly, L. Karstification and Groundwater Flow. *Speleogenesis Evol. Karst Aquifers* **2003**, *1*, 1–26.
22. Ford, D.C.; Williams, P.W. *Karst Hydrogeology and Geomorphology*; Chapman and Hall: London, UK, 2007. [CrossRef]
23. Bakalowicz, M. Karst Groundwater: A Challenge for New Resources. *Hydrogeol. J.* **2005**, *13*, 148–160. [CrossRef]
24. Bakalowicz, M. Le milieu karstique: Études et perspectives, identification et caractérisation de la ressource. In Proceedings of the CFH—Colloque Hydrogéologie et Karst au Travers des Travaux de Michel Lepiller 17 Mai 2008, Orléans, France, 16–17 May 2008.
25. Atkinson, T.C. Diffuse Flow and Conduit Flow in Limestone Terrain in the Mendip Hills, Somerset (Great Britain). *J. Hydrol.* **1977**, *35*, 93–110. [CrossRef]
26. Shuster, E.T.; White, W.B. Seasonal Fluctuations in the Chemistry of Lime-Stone Springs: A Possible Means for Characterizing Carbonate Aquifers. *J. Hydrol.* **1971**, *14*, 93–128. [CrossRef]
27. Clauser, C. Permeability of Crystalline Rocks. *Eos* **1992**, *73*, 233–238. [CrossRef]
28. Jeannin, P.-Y. Structure et Comportement Hydraulique des Aquifères Karstiques (Structure and Hydraulic Behavior of Karst Aquifers). Ph.D. Thesis, Université de Neuchâtel, Neuchâtel, Switzerland, 1996.
29. Delbart, C.; Valdés, D.; Barbecot, F.; Tognelli, A.; Couchoux, L. Spatial Organization of the Impulse Response in a Karst Aquifer. *J. Hydrol.* **2016**, *537*, 18–26. [CrossRef]
30. Chalikakis, K.; Plagnes, V.; Guerin, R.; Valois, R.; Bosch, F.P. Contribution of Geophysical Methods to Karst-System Exploration: An Overview. *Hydrogeol. J.* **2011**, *19*, 1169–1180. [CrossRef]
31. Chalikakis, K.; Nielsen, M.R.; Legchenko, A. MRS Applicability for a Study of Glacial Sedimentary Aquifers in Central Jutland, Denmark. *J. Appl. Geophys.* **2008**, *12*, 176–187. [CrossRef]
32. Legchenko, A.; Valla, P. A Review of the Basic Principles for Proton Magnetic Resonance Sounding Measurements. *J. Appl. Geophys.* **2002**, *50*, 3–19. [CrossRef]

33. Mazzilli, N.; Chalikakis, K.; Carrière, S.D. Surface Nuclear Magnetic Resonance Monitoring Reveals Karst Unsaturated Zone Recharge Dynamics during a Rain Event. *Water* **2020**, *12*, 3183. [CrossRef]
34. Scholz, E. *Synthèse Hydrogéologique des Calcaires du Barrois*; ANDRA: Bure, France, 2011; p. 97.
35. Jaillet, S. Un Karst de Bas Plateau: Le Barrois, Structure, Fonctionnement, Evolution (A Low Plateau Karst: The Barrois, Structure, Functioning, Evolution). Ph.D. Thesis, Université de Bordeaux, Bordeaux, France, 2000.
36. Decloux, J.-P. *Hydrologie et Hydrogeologie des Aquiferes de Surface sur les Bassins de la Saulx et de L'ornain—Rapport de Tâche 1 (RT1)*; ANDRA: Bure, France, 2018; p. 47.
37. Mangin, A. Contribution à L'étude Hydrodynamique des Aquifères Karstiques. Ph.D. Thesis, Université de Dijon, Dijon, France, 1975.
38. Cholet, C. Fonctionnement Hydrogéologique et Processus de Transport dans les Aquifères Karstiques du Massif du Jura. Ph.D. Thesis, Université Bourgogne Franche-Comté, Besançon, France, 2017.
39. Delbart, C. Variabilité Spatio-Temporelle du Fonctionnement d'un Aquifère Karstique du Dogger: Suivis Hydrodynamiques et Géochimiques Multifréquences; Traitement du Signal des Réponses Physiques et Géochimiques. Ph.D. Thesis, Université Paris-Sud—Paris XI, Paris, France, 2013.
40. Hvorslev, J. *Time Lag and Soil Permeabilty in Ground*; Waterways Experiment Station: Vicksburg, MS, USA, 1951; Volume 50.
41. *ISO 22282-2*; Reconnaissance et Essais Géotechniques—Essais Géohydrauliques—Partie 2: Essai de Perméabilité à L'eau Dans un Forage en Tube Ouvert. ISO: Geneva, Switzerland, 2013.
42. *NF P94-130 Standard*; Soils: Investigation and Testing—Pumping Test. AFNOR: Paris, France, 2002.
43. Moench, A.F. Flow to a Well of Finite Diameter in a Homogeneous, Anisotropic Water Table Aquifer. *Water Resour. Res.* **1997**, *33*, 1397–1407. [CrossRef]
44. Theis, C.V. The Relation between the Lowering of the Piezometric Surface and the Rate and Duration of Discharge of a Well Using Ground. *Eos Trans. AGU* **1935**, *16*, 519–524. [CrossRef]
45. Kruseman, G.P.; De Ridder, N.A. *Analysis and Evaluation of Pumping Test Data*; International Institute for Land Reclamation and Improvement: Wageningen, The Netherlands, 1991; Volume 47.
46. Vouillamoz, J.-M. La Caractérisation des Aquifères par une Méthode Non Invasive: Les Sondages par Resonance Magnetique Protonique. Ph.D. Thesis, Université de Paris XI, Paris, France, 2003.
47. Legchenko, A.; Baltassat, J.-M.; Beauce, A.; Bernard, J. Nuclear Magnetic Resonance as a Geophysical Tool for Hydrogeologists. *J. Appl. Geophys.* **2002**, *50*, 21–46. [CrossRef]
48. Legchenko, A.; Valla, P. Processing of Surface Proton Magnetic Resonance Signals Using Non-Linear Fitting. *J. Appl. Geophys.* **1998**, *39*, 77–83. [CrossRef]
49. Legchenko, A.; Valla, P. Removal of Power-Line Harmonics from Proton Magnetic Resonance Measurements. *J. Appl. Geophys.* **2003**, *53*, 103–120. [CrossRef]
50. Legchenko, A. MRS Measurements and Inversion in Presence of EM Noise. *Bol. Geol. Min.* **2007**, *118*, 489–508.
51. Mazzilli, N.; Boucher, M.; Chalikakis, K.; Legchenko, A.; Jourde, H.; Champollion, C. Contribution of Magnetic Resonance Soundings for Characterizing Water Storage in the Unsaturated Zone of Karst Aquifers. *Geophysics* **2016**, *81*, WB49–WB61. [CrossRef]
52. Legchenko, A. *Magnetic Resonance Imaging for Groundwater*; Wiley-ISTE: Hoboken, NJ, USA, 2013; ISBN 978-1-84821-568-9.
53. Legchenko, A.; Comte, J.-C.; Ofterdinger, U.; Vouillamoz, J.-M.; Lawson, F.M.A.; Walsh, J. Joint Use of Singular Value Decomposition and Monte-Carlo Simulation for Estimating Uncertainty in Surface NMR Inversion. *J. Appl. Geophys.* **2017**, *144*, 28–36. [CrossRef]

Disclaimer/Publisher's Note: The statements, opinions and data contained in all publications are solely those of the individual author(s) and contributor(s) and not of MDPI and/or the editor(s). MDPI and/or the editor(s) disclaim responsibility for any injury to people or property resulting from any ideas, methods, instructions or products referred to in the content.

water

MDPI

Article

Modelling Approach for Assessment of Groundwater Potential of the Moghra Aquifer, Egypt, for Extensive Rural Development

Ahmed Shalby [1], Bakenaz A. Zeidan [1], Katarzyna Pietrucha-Urbanik [2,*], Abdelazim M. Negm [3] and Asaad M. Armanuos [1]

[1] Irrigation and Hydraulics Engineering Department, Faculty of Engineering, Tanta University, Tanta 31733, Egypt; ahmed.shalby@f-eng.tanta.edu.eg (A.S.); b.zeidan@f-eng.tanta.edu.eg (B.A.Z.); asaad.matter@f-eng.tanta.edu.eg (A.M.A.)

[2] Department of Water Supply and Sewerage Systems, Faculty of Civil, Environmental Engineering and Architecture, Rzeszow University of Technology, Al. Powstańców Warszawy 6, 35-959 Rzeszow, Poland

[3] Department of Water and Water Structures Engineering, Faculty of Engineering, Zagazig University, Zagazig 44519, Egypt; amnegm85@yahoo.com

* Correspondence: kpiet@prz.edu.pl

Abstract: Groundwater-dependent cultivation is imperative to meet the ever-increasing food demands in Egypt. To explore the Moghra aquifer's potential, where a large-scale rural community is being established, a finite element groundwater flow (i.e., FEFLOW®) model was invoked. The developed model was calibrated against the observed water levels. GRACE-based groundwater storage was incorporated into the tuning procedure of the developed model. Eight abstraction rates from 1000 wells, changing from 800 to 1500 m^3/day/well, were simulated for a 100-year test period. The maximum resulting drawdown values, respectively, ranged from 59 to 112 m equating to about 20–40% of the aquifer's saturated thickness. The implications of the climate change from gradual sea level rise and an increase in crop consumptive water use were investigated. Extending seawater invasion into the aquifer caused a slight increase in the piezometric levels within a narrow strip along the seaside. Applying a chronologically increasing withdrawal rate to meet the projected increment in crop water requirements raised the maximum resulting drawdown by about 7.5%. The sustainable exploitation regime was defined as a time-increasing withdrawal rate adequate to reclaim 85,715 acres (34,688 ha). The recommended development scheme is compatible with the withdrawal rationing rule, aiming to maintain that the resulting drawdown does not exceed one meter a year.

Keywords: FEFLOW; agriculture; sustainable management; aquifer depletion; over-abstraction

1. Introduction

Globally, water and food shortage problems have aggravated during the last few decades. Intensifying groundwater withdrawal has taken place to satisfy freshwater demands for domestic purposes [1]. The malpractice of uncontrolled pumping is further exacerbated to meet increasing agricultural water requirements [2]. Even fossil (non-renewable) aquifers are highly exploited, particularly in semiarid and arid countries [3]. Overdraft resulting in aquifer depletion is an emerging issue owing to the development of such non-renewable aquifers [4]. Thus, it is widely urged to rationalize pumping and judiciously use non-renewable aquifers [5]. However, achieving sustainable management of such resources is a key challenge, particularly in regions plagued with water scarcity. Egypt is within an arid climate region featuring extinct precipitation, high temperatures, and elevated humidity, which leads to an increased rate of evapotranspiration [6,7]. Due to climate change (CC) and the damming construction at the Nile River upstream, Egypt would be unable to draw as much as its water quota [8,9]. Accordingly, Egypt shall witness an imminent challenge for the agriculture sector to cater to the demands of the exponentially growing human population [10]. Rural development is therefore crucial in

Egypt to meet the growing food needs [11,12]. Accordingly, the government has initiated an ambitious rural development strategy through a mega groundwater-dependent cultivation project [13].

A mega reclamation project is now being implemented in Egypt under the framework of moving towards horizontal expansion in barren lands distanced from the Nile River [14]. Thus, desert fossil aquifers have become the sole source of freshwater [11,15]. Currently, groundwater withdrawal is well underway in the newly cultivated areas, mainly for irrigation purposes [16]. The pumping of groundwater is projected to increase year in and year out [17]. A concentrated number of wells that are not spatially distributed over wide areas, are being established [18]. Mismanagement or lack of pumping management, with its consequent overconsumption of the underground reserve, restricts groundwater availability. It, therefore, endangers the exploited aquifer through depletion and water quality degradation. Additionally, the severe decline in groundwater level might result in adverse consequences, including land subsidence, diminished surface vegetation, etc. [19]. Deficient replenishment of arid-region aquifer systems poses additional intricacy in their management. Attainment of a sustainable yield from an aquifer is, therefore, a major constraint for groundwater-beholden agribusiness [20]. Thus, a management approach should be set to maintain the aquifer storage in terms of quantity and quality aspects.

Groundwater flow models are increasingly recognized as a supportive utility for a sustainable groundwater management approach [21]. Groundwater models provide an approximate solution for the partial differential equation that visualizes water flow through a porous medium [22]. Modelling is, therefore, an essential tool for assessing an aquifer's potentiality and exemplifying its stages under pumping stresses [23]. Several numerical simulation codes have been programmed based on finite difference and finite element approaches [24]. MODFLOW is the most commonly used finite difference-based code used in the field of groundwater modelling. The Finite Element subsurface FLOW (FEFLOW®) is a relatively new 3D groundwater simulation code [25]. However, it has become one of the simulators widely utilized for groundwater flow and transport problems. FEFLOW has a substantial geometrizing skill over alternative finite-difference models (e.g., MODFLOW) [26]. Many studies have employed the FEFLOW for assessing trade-offs among potential water pumping policies and accounting for the drivers that have resulted in aquifer depletion and deteriorating water quality [27–30].

The recently drilled wells into the Moghra aquifer (Egypt) may be a clear-cut cause for water table drawdown and quality degradation. Thus, groundwater managers urged defining the sustainable management scheme of the aquifer. Herein, a hydrogeological investigation of the subsurface Moghra aquifer system is provided through the robust development of a 3D conceptual numerical model. The groundwater flow mechanism of the Moghra aquifer and its behaviour under stressful pumping conditions were thoroughly simulated utilizing the FEFLOW® numerical model. The main goal is to provide an exploitation approach that sustains groundwater in the target development area. CC, the resulting SLR, and increases in crop water requirements were considered. The developed hydrologic model could provide additive support for decision-makers to maintain the sustainability of ongoing agribusiness activities.

2. Study Area

The availability of a huge amount of stored water, convenient climatic conditions, and favourable soil texture render the Moghra desert one of the most promising reclamation plots in Egypt [14,15]. Accordingly, the Moghra desert was incorporated into a mega-rural development project. Previously, the study area of the Moghra desert was almost barren, with no land cover feature that may hinder such proposed large-scale cultivation activities [14]. It is located within the Marmarican Homoclinal plateau, which covers the uninhabited desert region between the Mediterranean Sea and the Qattara depression. It is in an arid climate region featuring long, hot summers and short, warm, rainless winters. It occupies a non-perennial area of 150,000 acres (60,702 ha), extending between latitude

28°11′ and 31°38′ N and between longitude 28°14′ and 31°22′ E, as shown in Figure 1. It includes the proposed cultivation swaths suggested within the national strategic plan, where the fossil groundwater reserves would be the main water source. The wells field is located 75 km away from the Mediterranean shoreline and away from the coastal area that is highly susceptible to seawater intrusion [31]. It includes two conspicuous features, namely, the Qattara depression to the west and the Moghra swamp (locally called Moghra Lake), which is located at 38 m below the mean sea level (MSL), as shown in Figure 1. Recently, the region has been subject to significant land use changes since 2015, when intense agribusiness activities of the national rural development project were initiated. The cultivation project is well underway in the area. As deduced by the analysis of Gravity Recovery and Climate Experiment (GRACE) satellite mission-derived groundwater storage (GWS), the GWS within the development area is currently overexploited, a fact that bears adverse impacts on the whole aquifer extent [32]. The Moghra aquifer is the main water-bearing formation, covering the majority of the study area [33]. The Moghra aquifer occupies a surface area of approximately 5 million hectares (ha), stretching between the Qattara depression to the west and the Nile River to the east and between the El-Fayoum depression to the south and the Mediterranean Sea to the north [34].

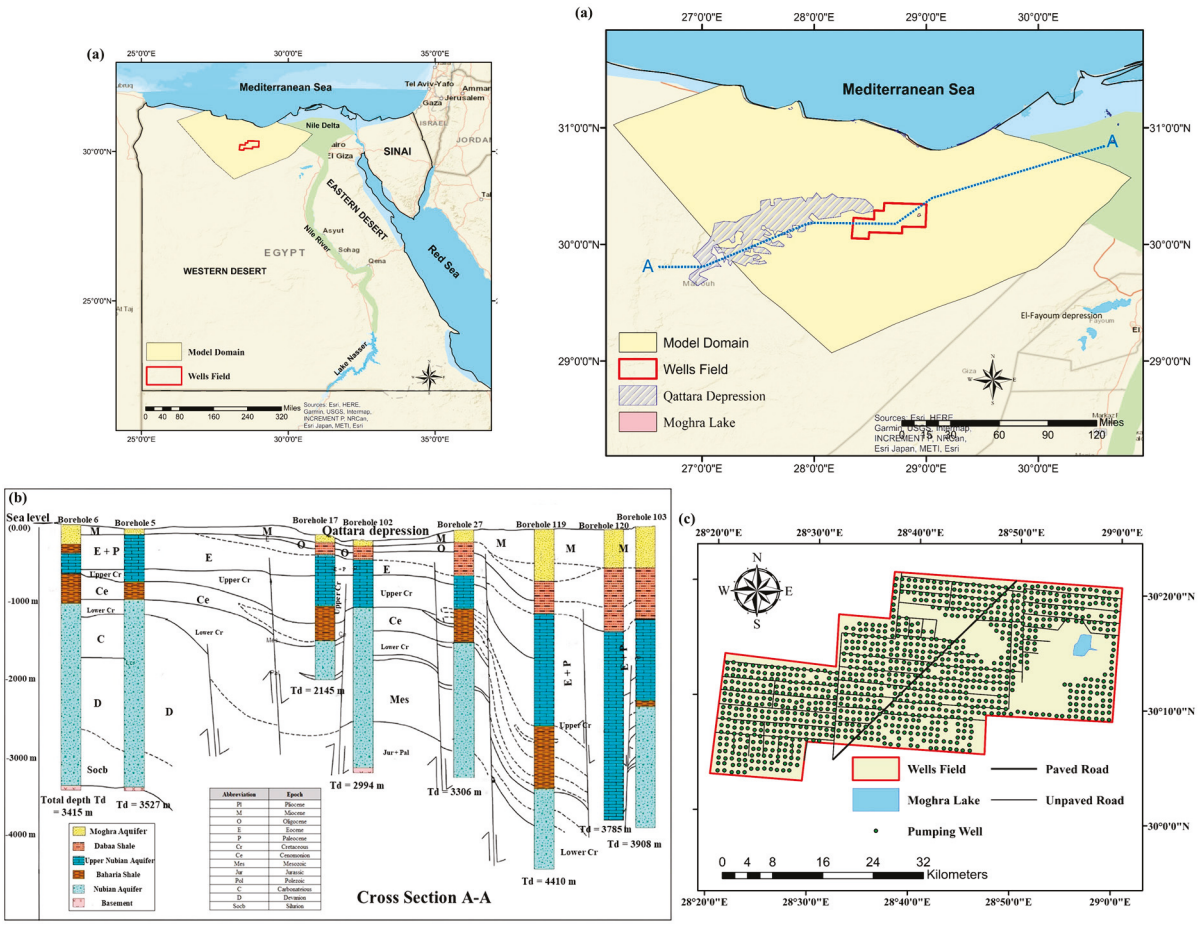

Figure 1. (**a**) Location and main features of the study area, (**b**) geological cross-section of the Moghra aquifer (adapted with permission from Ref. [35]. 2024, Elsevier), and (**c**) spatial distribution of the production wells within the development area.

The Moghra Formation is a well-identified geological unit composed of sand and sandstone that belongs to the Lower Miocene epoch [36]. The deposition is intercalated by clay and siltstone that increase in the northward direction [37]. The depth of the aquifer ranges from 0 to 500 m, underlain by Oligocene Dabaa shale and Eocene Baharia shale, as shown in Figure 1b [34]. The aquifer is almost phreatic, but it seems confined within the

narrow strip adjacent to the Nile delta aquifer [38]. Paleo (fossil) groundwater constitutes the main bulk of the aquifer storage [17]. However, the aquifer may be recharged by lateral seepage from the adjacent Nile Delta aquifer (Pleistocene formation) and the Nile River in the east [39]. The groundwater level varies from about −50 m at the Qattara depression in the west to −10 m in the eastern portions close to the Nile Delta. The main groundwater flow is from the north and northeast towards the Qattara depression in the southwest [36].

An area of 142,716 ha (about 352,659 acres) to the east of the Qattara depression was dedicated as a wells field within the reclamation project, as shown in Figure 1a. Installing the production wells was initiated by the end of 2015 with an ambitious plan to cultivate 135,000 acres (about 54,633 ha) [39]. Pumping and replacement experiments conducted on some existing pumping and test wells within the development area indicated high potentiality in terms of groundwater storage and productivity [37]. Moderate conductivity in a range between 5 and 25 m/d along with high storativity in a range between 0.1 and 0.001 were reported [40]. The transmissivity values range between 550 and 3500 m^2/d [31].

3. Conceptual Model Development

The conceptual model is the digital 3D hydro-geologic representation of the physical groundwater system that is organized in a computerized format. FEFLOW (version 7.5) numerical software is adopted for model compilation and development. FEFLOW is favourable for aquifers with complex geological structures [41]. FEFLOW facilitates local mesh refinements along the model domain borders; hence, the boundary conditions (BCs) are precisely defined. Further, the ability of mesh refinements within the area of interest (e.g., the wells fields) helps to avoid the creation of excessive element numbers [42]. Herein, the conceptual model assumes that the aquifer system comprises an unconfined, one-layered formation. A hydraulic connection with the underlying Nubian Sandstone Aquifer (NSA) through an aquitard was suggested [17]. However, the vertical leakage remains poorly defined. The exchange is hereby negligible due to a lack of precise data to quantify water exchange by the interlayer vertical flow.

3.1. Digital Hydro-Geologic Framework Model

To describe the modelled system geometry, ArcGIS was used to prepare the input files in a format accepted by FEFLOW. ArcGIS is vital to ensure all input parameters are properly projected into Zone 35 N of the Universal Transverse Mercator (UTM) coordinate system. Figure 1 shows the map that denotes the computational domain and embedded stress area (i.e., the wells field). The modelled system covers a total area of about 6 M ha, and it is 445 km in length and 224 km wide at its longest and widest parts, respectively, as shown in Figure 1. The location of the installed and proposed pumping wells was retrieved from the Egyptian Countryside Development Company (ECDC's website at http://elreefelmasry.com; accessed on 1 May 2023). During the first stage of the reclamation project, from 2016 to 2019, 450 wells were drilled [17]. As a development expansion, 550 wells are proposed to be added [43]. Worth mentioning is that the wells field was found within the most favourable areas for such a cultivation project according to environmental and economic criteria [14].

3.2. Hydro-Geologic Boundary Conditions

The accurate denotation of hydrogeologic conditions along the outer boundaries of the conceptual model area is essential. The BCs control fluid flows into or out of the modelled system during steady-state and time-dependent (transient state) simulations [44]. All boundaries were selected far enough from the effect of pumping wells to be regarded as constant head boundaries, as shown in Figure 2. Along the outer border of the modelled area, the first kind (Dirichlet) BC that specifies a time-constant or time-varying head value is applied. The northern and northeastern BCs were chosen to be natural boundaries (i.e., water bodies). The Mediterranean Sea completely controls the head along the northern boundary. The water level of 0.0 m was initially assigned as the head value for northern

BC. A wide main canal, locally called the "El-Nubariya" canal, appears on the right side of the studied area and extends for 127 km in length. It starts as a tributary of the "El-Rayah El-Beheiry" at the "Pollin" barrage area and cuts through the sandy soil, reaching the Mediterranean Sea. Its water levels are controlled by a few hydraulic structures (e.g., regulators) and temporally change according to the releasing discharges, with an average water level of 9.03 m at its mouth [45]. Accordingly, it acts as an influent stream and is considered a source for groundwater recharge. Dirichlet BC of head linearly change from 0.0 to 9.03 m was assumed along the line striking at almost N-E direction, as shown in Figure 2. Along other borders, no natural BC or fault (water divide) exists close to the boundary. Instead, head contour lines that represent the aquifer's water levels before initializing the development project were used [33]. The head values at each intersection of the model borders with the contour lines were assigned. Then, the interactive linear 1D interpolation tool was used to interpolate hydraulic head values along the BCs, as shown in Figure 2. Pumping wells were set as nodal BCs (i.e., the fourth kind of BC) within the development area, based on the wells map that depicts the original locations of pumping wells. Several pumping rates were assigned through a linked attribute table containing the pumping rate, radius, and screen's top and bottom elevation of each well. The well's diameter (outer/inner) was 420/280 mm (16.5/11″). The penetration depth reaches a maximum of 140 m into the Moghra geological formation. The screen depth was an average of 30 m.

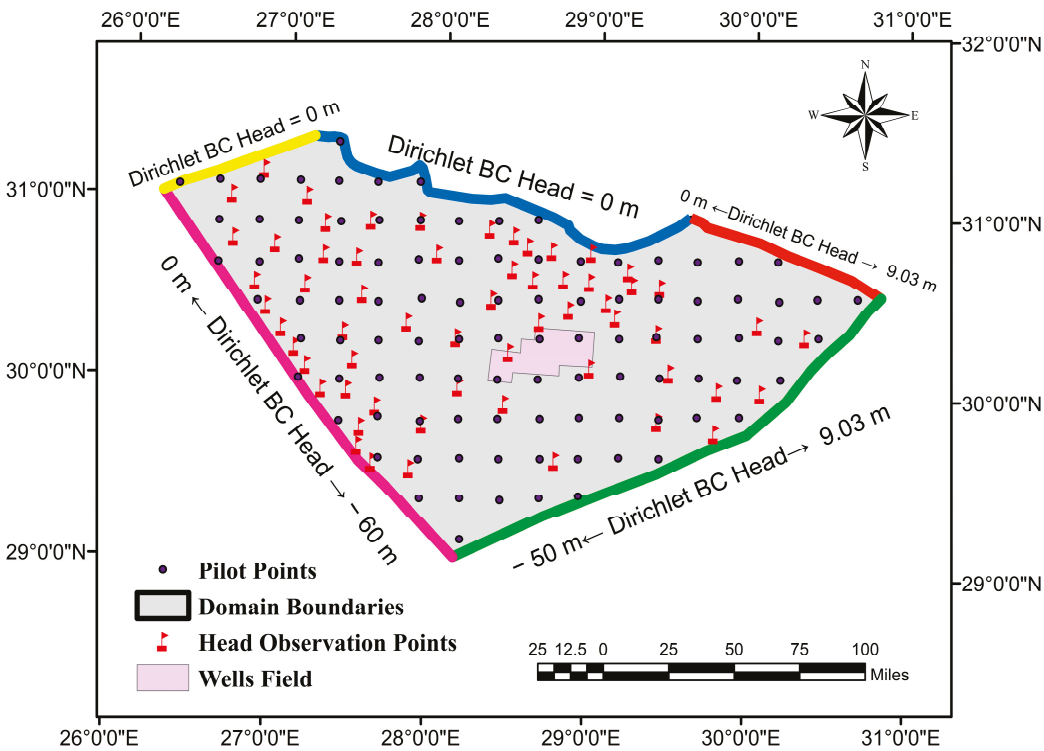

Figure 2. Applied boundary conditions for the modelled domain and distribution of observation heads and pilot points to define the aquifer's anisotropic conductivities.

Episodic recharge that may result from infrequent, low-intensity precipitation events in such arid climates was neglected [46,47]. Additionally, the water table throughout the aquifer extent is below the extinction depth of 0.5 m to include evaporation [48]. Thus, no evaporation of groundwater from such bare, sandy soil occurs.

3.3. Domain Discretization

Obtaining a proper spatial discretization of the model domain into well-shaped prisms that have no distorted elements reduces simulation difficulties and the risk of instabil-

ities [42,49]. So much attention was paid to discretizing the finite element mesh of the computational model domain. The available element types allow the selection of either quadrilateral or triangular elements, where the fluid flow is calculated over each element node [41]. The triangulation algorithm was selected to discretize the model domain into 2D-triangle meshes. This mesh generation algorithm is favourable for such a complex model domain, allowing a minimum angle to be determined for all accommodated complex configurations of finite elements [29]. Local mesh refinements with a maximum element size along the domain margins and within the area of production wells were carried out. Mesh smoothing was typically applied to generate better mesh quality. "The denser the mesh, the better the numerical accuracy, and the higher the computational effort" [41]. Satisfactory element numbers and geometrical criteria optimized with computational time have been obtained after many trials. Figure 3 depicts the super-element mesh that represents the basic structure of the model domain. The mesh area averaged 4.56 km^2, but with element concentration and refinements along the domain borders and throughout the wells field, as shown in Figure 3. The mesh configuration led to 13,064 elements and 7004 nodes on each slice (surface). Then, this mesh has been expanded in depth according to the lithology information, resulting in six-node finite elements.

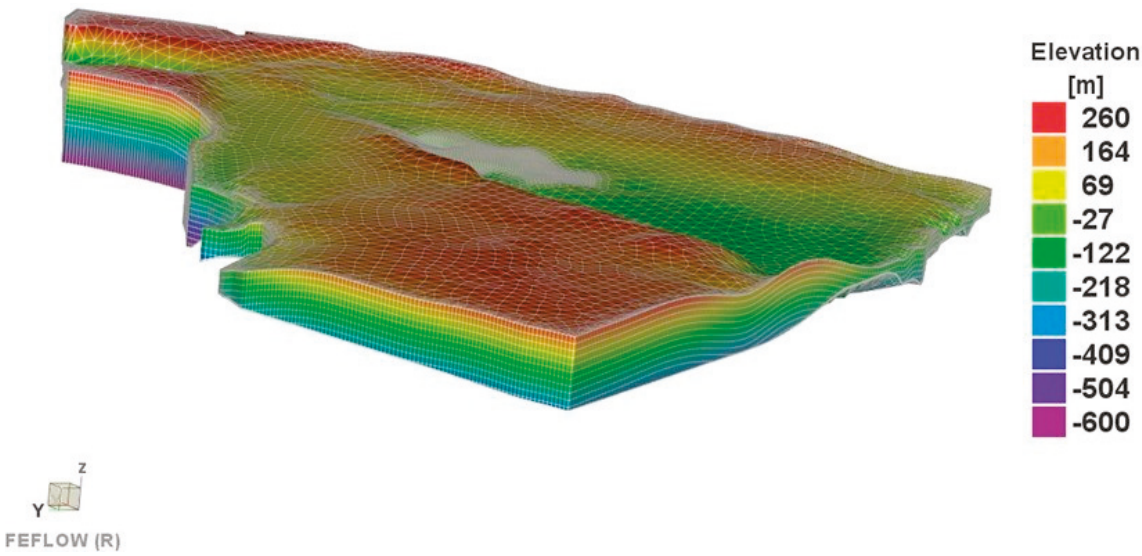

Figure 3. Configured unstructured meshes along with a 3D view of the constructed groundwater flow model (depth is scaled up by 30 times).

3.4. Subsurface Stratigraphy

The conceptualized hydrogeological system has a simplistic physiographic feature. It is vertically composed of one main Miocene formation resting on Oligocene basaltic sheets that create thick impervious base strata, as shown in Figure 1b [50]. The topography of the model domain was retrieved using the Digital Elevation Model (DEM) processed from the Shuttle Radar Topography Mission (SRTM) data. The ground surface elevation within the model domain ranges from −111 m below MSL to 269 m above MSL, as shown in Figure 3. Two data sources were employed to locate the depth down to the impervious shale base and construct the geological stratification of the modelled area: (1) fifty-four groundwater exploration wells were excavated by the Egyptian Ministry of Water Resources and Irrigation (MWRI) to locate groundwater supplies in the Western Desert of Egypt [51], and (2) forty-two deep boreholes were drilled by the national oil companies to explore for fossil fuels in the Western Desert [52]. The subsurface lithologic elevation information of the wells was utilized in combination with surface geologic data for the expansion of the modelled grid into three dimensions (3D). Akima's bivariate data regionalization method, along with the linear interpolation technique, was applied to assigning the elevation to a group of adjacent nodes. The aquifer's total depth ranges from 302 to 824 m. The aquifer was then

discretized into a few sublayers of varied depths with an average of 50 m. A 3D view of the constructed model domain, composed of 12 slices and 11 layers, is shown in Figure 3. A total of 143,704 elements and 84,048 nodes, which cover an area of about 5.9×10^4 km^2 and a volume of 2.4×10^4 km^3, were created. The flexible, unstructured discretization and local grid refinements appropriately fulfil the irregular geometry and topography of the model domain without nesting. Figure A1 in Appendix A depicts the super-element mesh that represents the basic structure of the model domain.

3.5. Hydrogeological and Pumping Data

Following the 3D mesh expansion, the properties of the depositing formation and pumping conditions were set up. The development progress in the Moghra region has been divided into three successive stages. The ECDC is technically and administratively supervising the project [43]. The first stage was initiated in early 2016 by drilling 450 pumping wells; each well is about 1 km away from the others. According to the wells' pumping test analysis, the clear separation distance between the adjacent wells is sufficient to prevent pumping interference. The pre-development static water levels within the installed wells field ranged from −35 to −49 m, and the depth down to the water level was about 55 m. A drip irrigation system, as a high-efficiency distribution technique, is adopted, and the average water duty is 14 m^3/acre/day (≈34.6 m^3/hectare/day). The developed lands in the first stage were distributed to small investors and young people [43]. Further, 550 wells are being established during the following phases, as shown in Figure 1c. The groundwater salinity (as measured by TDS measurements) reaches up to 8000 mg/L, rating it as brackish water. Thus, only salt-tolerant crops such as canola, barley, quinoa, olive, and jojoba are cultivated in the project area. Through a field survey report with the investors and farmers in the study area, a close picture of overall groundwater pumping was obtained. The pumping pattern for each well was difficult to retrieve due to irregular monitoring frequencies of pumped water. The pumping hydrograph shows a seasonal pattern that peaks in summers while troughs occur in winters. Solar energy, as a renewable energy resource, is used to pump water. The sunshine limits the well's daily operation time to eight hours and restricts the maximum pumping rate to 120 m^3/h.

The hydraulic parameters were compiled from diverse literature, field surveys, and recently executed pumping and recovery analysis tests. A wide range of hydrogeological parameters for the extended Moghra aquifer were reported in the literature [13]. In general, the values of hydraulic parameters are higher in the central portion of the model domain, where the wells field is. The horizontal hydraulic conductivity (K_x) of the entire Moghra aquifer ranges between 0.2 and 100 m/d. The transmissivity values vary from 760 m^2/d to 7600 m^2/d. The vertical conductivity (K_z) was found to be 10% of the horizontal conductivity (K_x). In such an unconfined aquifer, the specific yield "S_y" is used to represent the aquifer's storativity (S). Ten pumping tests that have been conducted in the Moghra aquifer demonstrated a relatively narrow range of specific storage (S_s) values varying from 5×10^{-4} to 1×10^{-4} m^{-1} with the majority ranging around 13×10^{-5} m^{-1} [37]. While the specific yield (S_y) varied from 0.005 to 0.13 [37]. The average storativity is about 0.15. The spatial distribution and the actual values of the initially assigned parameters were reviewed during the calibration process.

4. Numerical Model Set-Up

A saturated stratum, where Darcy's Law is applicable, was configured. By default, the whole model domain was initially kept as unconstrained heads. The upper slice was defined as the free surface of a movable slice. The simulation was initiated in a steady state and then run under transient conditions.

4.1. Steady-State Simulation

Accurate simulation of a flow problem through an aquifer requires achieving a reliable steady state. Up until late 2015, before initializing the rural development project, the

Moghra aquifer was almost untapped. Water levels within the aquifer system were near equilibrium, and the effect of wide-distributed private tube wells was negligible.

4.1.1. Model Calibration

The calibration is imperative to ensure a reliable simulation result by adjusting the input hydrogeological parameters [53]. The steady-state calibration was executed as a fully implicit simulation in which the pre-development water heads (by the year 2015) were used as a target condition. The system is regarded as steady when the overall balance for the entire domain is achieved. Due to the importance of the conductivity and the model's high sensitivity to its alteration, anisotropic conductivity was adopted, in which the conductivity is calibrated along the X, Y, and Z axes. Given their swiftness and ease, non-linear parameter estimation techniques (PEST) are now commonly used for the proper identification of adjustment parameters. FePEST® is the graphical user interface for the development of the FEFLOW model with the PEST utilities. In FePEST, two spatial characterization techniques (i.e., pilot points and constant zones) are used to represent heterogeneities of hydraulic properties within the modelled hydrogeological basin [26]. The pilot points approach was applied in this study as it provides an improved heterogeneity representation of the system. A uniform distribution of 101 pilot points was generated throughout the model domain, as shown in Figure 2. Exaggeration in the number of pilot points would require extensive modelling times and could result in over-parameterization and large variations in the parameter values over small distances [26]. Herein, the Moghra model was calibrated by adjusting conductivity values such that simulated groundwater tables matched the observed hydraulic heads. K_x was bounded between 0.1 and 200 m/day (minimum and maximum limits), according to prior information given in the literature. K_y and K_z values were tied to changes in K_x by applying an initial relationship: $K_x = K_y = 10\ K_z$. The calibration fit was assumed when a divergence of less than 1 m (about 10% of the difference between the maximum and minimum water levels) was achieved between the computed and observed heads.

The model's results were assessed by comparing simulated heads against observed heads at 60 points scattered throughout the model domain, as shown in Figure 2. The observed heads ranged from 0 to −80 m. The model demonstrated a normalized root mean square error (NRMSE) of 1.8% (1.6 m) and a correlation factor (r) of 0.9973. Figure 4 shows a scatter plot depicting the comparison conducted between the monitored water levels and the simulated results. The value of the obtained root mean square error (RMSE) was 1.94 m. The conductivities were largely consistent with values reported in the literature, varying between a maximum of 2.4×10^{-3} m/s and a minimum of 1.2×10^{-6} m/s. Model simulations thereby replicated flow patterns in terms of hydraulic gradients and flow directions. The estimated hydraulic head throughout the model domain under the steady-state condition is shown in Figure 5. Using the particle tracking technique, streamlines of regional groundwater flow were visualized, as shown in Figure A2 in Appendix A. The flow's main direction is from the north and northeast towards the south and then radially south-westward.

4.1.2. Model Sensitivity

It is essential to analyse the uncertainty and sensitivity related to the input hydrologic parameters. The sensitivity analysis identifies uncertainties in input parameters for the model. Additionally, this analysis addresses an overall understanding of the modelled system and enhances the calibration procedures [54]. In this context, FePEST, through the "SENSAN" utility, enables estimating sensitivities for a set of input parameters. The model's sensitivity was examined by multiplying calibrated conductivities throughout the model's interior nodes by factors of 3.0, 2.5, 2.0, 1.5, 1.2, 0.8, 0.4, and 0.2.

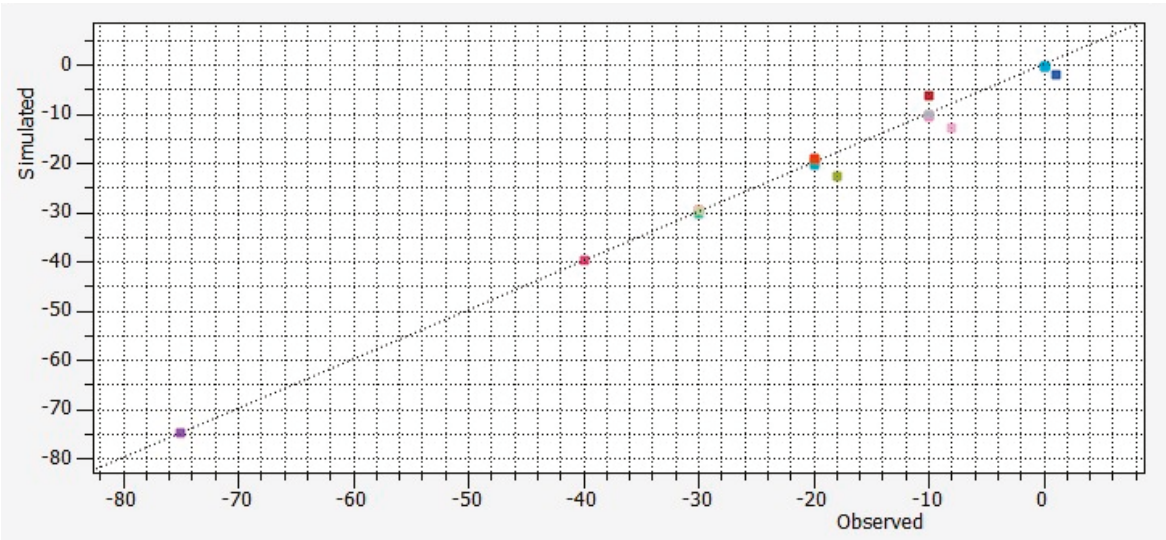

Figure 4. Comparison between observed and simulated water levels for steady-state calibration.

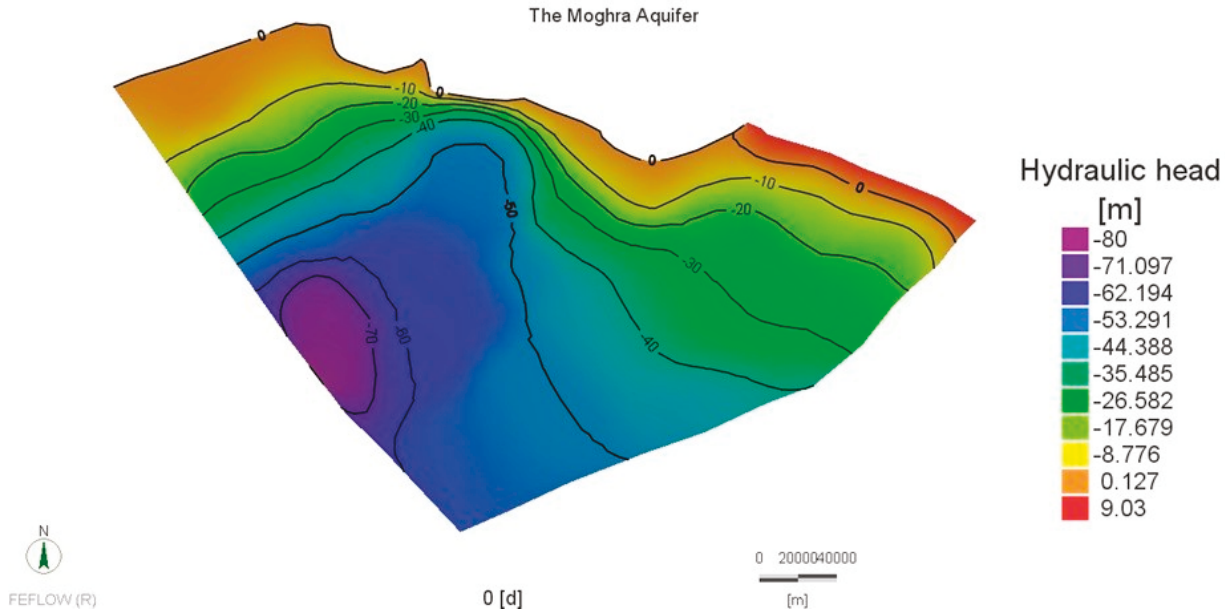

Figure 5. Steady state simulated hydraulic heads for the year 2015 over the modelled domain.

Table 1 summarizes the sensitivity analysis to changes in K of the steady-state model. The model is reasonably sensitive to alterations in hydraulic conductivity, referring to its importance in model adjustment. A change of 20% in conductivity values resulted in an average sensitivity value of 0.22. Applying a constant change factor for both longitudinal and transverse conductivities throughout the model domain maintained the general groundwater flow direction. But a high-water budget imbalance was indicated when applying higher and lower conductivity values.

Table 1. Percentage of groundwater head variations versus the changes in hydraulic conductivity.

Change Factor of Conductivity	% Change of Hydraulic Head
0.2	0.16
0.4	0.26
0.6	0.16
0.8	0.30
1.2	0.26
1.5	0.20
2.0	0.16
2.5	0.22
3.0	0.20

4.2. Time-Dependent Simulation

4.2.1. Transient Calibration Using Pumping Test Data

Adjusting the input properties under transient state conditions was performed by employing data from continuous pumping experiments conducted on 39 recently installed production wells [37]. The pumping analysis test is transient data commonly utilized for calibration of the groundwater flow model in cases of insufficient temporal variation in pumping records and water level [55]. The storativity was adjusted to fit the observed drawdown in response to pumping. As shown in Figure 6, the computed drawdown matches well with those observed during the pumping tests.

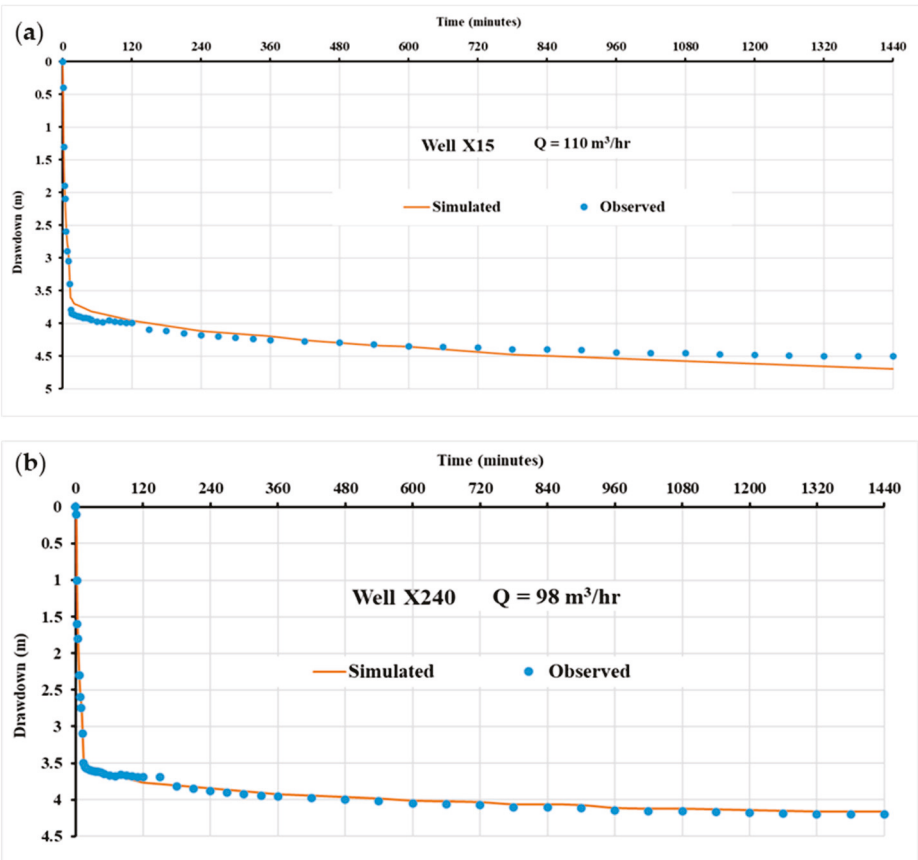

Figure 6. Transient calibration using (**a**) 24 h pumping test data of Well X15 @ (longitude 28.48° and latitude 30.12°) and (**b**) 48 h pumping test data of Well X136 @ (longitude 28.56° and latitude 30.27°).

4.2.2. Transient Verification Using GRACE-Retrieved Data

Motivated by the observed capacity of the GRACE mission for tracking changes in GWS, this study explores the use of GRACE-derived GWS changes for the transient

verification of the developed model [56]. GRACE-based GWS alterations were incorporated in the tuning procedure of groundwater flow models to overcome insufficient in situ measurements [57,58]. GRACE was also employed to estimate groundwater storage coefficients, including the storativity or specific yield (S_y), as appropriate [59,60]. The time series that represents the change in terrestrial water storage (ΔTWS) was extracted from the recently released gridded GRACE dataset provided by the three processing centres (i.e., GRACE's science data centres) [32]. This dataset consists of a temporal monthly TWS anomaly, a mass deviation from the baseline, which is expressed in terms of equivalent water height (EWH) and posted on a 1° grid resolution (PODAAC website at https://grace.jpl.nasa.gov/data/get-data/monthly-mass-grids-land; accessed on 1 March 2023). Within such a semiarid area with no perennial surface waters, groundwater, and soil moisture (SM) account for all inferred alterations in the TWS. Therefore, ΔGWS was estimated by subtracting the SM's contribution from GRACE-derived TWS [61]. The SM was estimated based on the outputs of the land surface model (GLDAS-NOAH) [62]. During the verification period (2016–2021), the water table had undergone an average decline of 0.96 m within the wells field. Minor alterations in groundwater tables were observed in the rest of the model domain.

The temporal pattern of GRACE-inferred GWS has been incorporated as an additional regularization dataset for verification of the developed model. The FEFLOW software allows the control of the simulation time via an integration scheme [41], while the simulation results can be depicted according to the recorded output time steps. An automatic time control scheme using the Adams-Bashforth/backward trapezoid (AB/TR) predictor-corrector scheme was adopted [30]. Using the "Period Budget" utility, the developed model can capture the inflows and outflows quantity during a simulation period, and thereby the corresponding storage loss/gain is estimated. The simulated annual mean storage anomaly from 2016 to 2021 was obtained as 16.27 Mm^3 (about 0.276 cm EWH), which is close to the GRACE-derived GWS anomaly (0.26 cm/year), as shown in Figure 7.

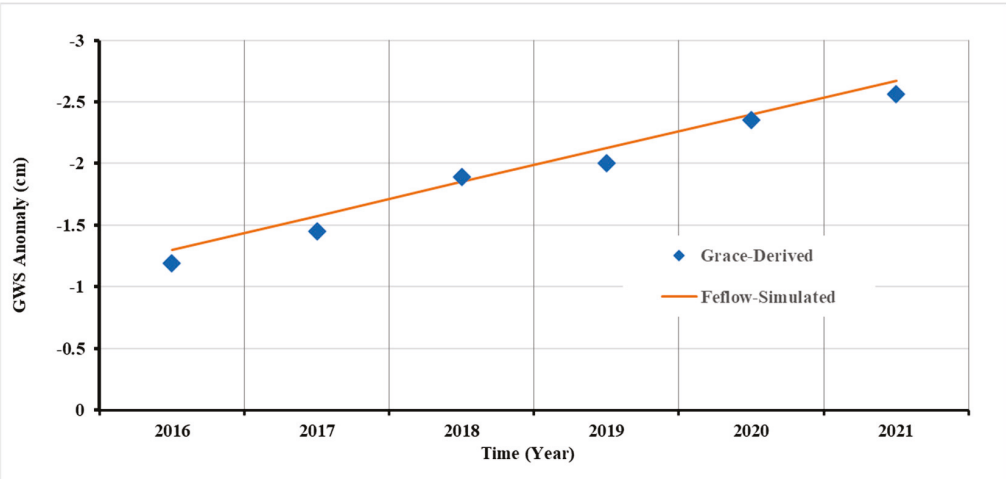

Figure 7. Comparison of GRACE-derived and simulated GWS changes from 2016 to 2021 over the model domain.

4.3. Management Schemes

The calibrated model was run afterwards for a 100-year test period as a predictive simulation. Estimated water levels during the steady-state simulation were regarded as the initial conditions for the transient simulation. The BCs and the material properties (e.g., hydraulic conductivity and storativity) were kept unchanged. The added input to the model was the pumping wells. To investigate the CC implications, time-varying boundary-condition data were applied.

The adjusted model was employed to mimic the aquifer's behaviour under variant exploitation strategies. The traditional safe yield concept, meant to mean discharge equals

recharge, does not apply to such a non-renewable aquifer [63]. The pumping-induced loss in aquifers' storage is not offset, and the resulting drawdown is inevitable. However, a rationing restriction is to be set to ensure the long-term water supply and, thereby, the sustainability of the dependent cultivation activities [37]. For the Moghra aquifer, the abstraction-regulating rule states the drawdown after 100 years should not exceed a third of the saturation depth. Hereby, the maximum allowable drawdown rate is one meter each year.

Sustainable management should consider CC and the resulting SLR. The Moghra model is employed to investigate the combined implications of SLR, and the water duty increment due to global warming. The Representative Concentration Pathways (RCPs) are a suite of scenarios addressed in the Fifth Assessment Report (AR5) that was released by the Intergovernmental Panel on Climate Change (IPCC) to project future climatic conditions [64]. RCP 85 is the CC worst-case scenario that involves a global average temperature increase of about 4.3 °C by this century's end [65]. The corresponding average SLR is projected in a range of 53 to 98 cm [66]. However, due to the distinct features of the Mediterranean Sea as a semienclosed basin connected with the ocean through the narrow Gibraltar Strait, its local level change will not exceed 0.5 m [67,68].

Crop consumptive use is often referenced to the evapotranspiration (ET) that can be estimated using different theoretical approaches (e.g., the Blaney–Criddle formula). Global warming causes an increase in crop water requirements that differ regionally. Regional climate models (RCMs) are therefore employed to project climate conditions on a regional scale and thus provide accurate estimates over general circulation models (GCMs) [7]. The outputs of "MPI-ESM-LR/RCA4, GCM/RCM" ensemble simulations, provided through the CORDEX project (CORDEX website at https://esg-dn1.nsc.liu.se/projects/esgf-liu/; accessed on 1 January 2024) were used to project the increase in potential evapotranspiration (PET) over the wells field [69]. Figure 8 shows the projected percentage change in PET during the upcoming 100 years. The average annual increase in PET is 0.0058 mm, which implies an annual increase in water duty by 0.019 m^3/acre/day (≈0.047 m^3/hectare/day).

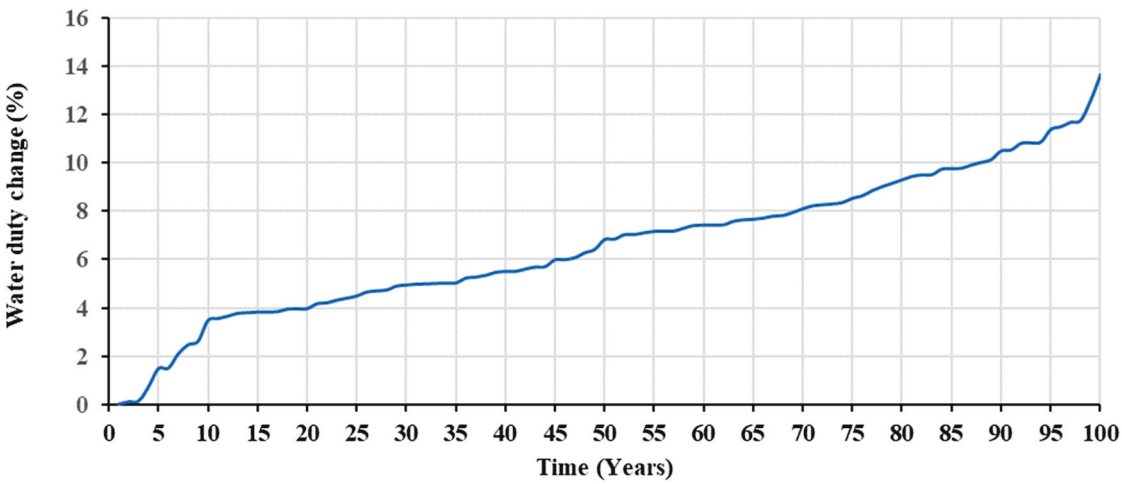

Figure 8. Percentage increment in crop water consumptive use under the climate change worst-case scenario.

5. Results and Discussions

5.1. Pumping Scenarios

Invoking the calibrated model, a set of alternative pumping policies was designed and reliably tested to identify the optimal water resources management scheme. Eight pumping regimes ranging from 0.8 to 1.5 Mm^3/day were simulated. The continuous pumping has resulted in decreasing groundwater levels throughout the model domain. The maximum drawdown was observed within the wells field. Table 2 summarizes the

resulting drawdown breakthrough under the applied pumping policies during a 100-year test period.

Table 2. Maximum drawdown (m) for different pumping rates along a 100-year test period.

Scenario	Total Pumping "Mm^3/Day"	Cultivated Area "Acres" *	Time (Years)									
			10	20	30	40	50	60	70	80	90	100
1	0.80	57,143	8.72	15.75	22.34	28.55	34.29	39.66	44.72	49.54	54.15	58.59
2	0.90	64,286	9.81	17.72	25.15	32.15	38.62	44.68	50.40	55.84	61.06	66.09
3	1.00	71,429	10.90	19.70	27.96	35.75	42.96	49.71	56.09	62.17	68.00	73.62
4	1.10	78,571	11.99	21.67	30.77	39.63	47.32	54.76	61.81	68.35	74.98	81.20
5	1.20	85,714	13.08	23.65	33.59	42.98	51.68	59.83	67.55	74.91	81.99	88.82
6	**1.30**	**92,857**	**14.17**	**25.63**	**36.41**	**46.6**	**56.05**	**64.91**	**73.31**	**81.33**	**89.04**	**96.49**
7	1.40	100,000	15.26	27.61	39.23	50.23	60.43	70.00	79.09	87.77	96.12	104.2
8	1.50	107,143	16.36	29.59	42.06	53.86	64.82	75.12	84.89	94.24	103.24	111.96

Notes: * 1 acre = 0.404686 hectares = 0.00404686 km^2. Bold font refers to recommended pumping scenario.

According to the obtained results, it is concluded that the optimum management pathway is to pump a total water quantity of 1.3 Mm^3/day through 1000 wells (i.e., Pumping Scheme No. 6). Considering a daily water duty of 14 m^3/acre (34.6 m^3/ha), the cultivated areas would reach up to 92,857 acres (37,578 ha). The resulting drawdown is up to about 96.49 m, which is compatible with the MWRI's regulations stating that the drawdown threshold should not exceed 1.0 m in a year, as shown in Table 2. Figure 9 shows the simulated hydraulic head and drawdown under this pumping regime after 100 years. Appendix B showcases detailed information on the recommended pumping scheme to be adopted in the Moghra region. Figure A3 depicts the maximum drawdown resulting through a 100-year test period from different investigated pumping rates, where the optimum one is marked. Figure A4 depicts the rate budget analysis of the groundwater system under this pumping scheme during the simulation period. The net storage was estimated as the difference between captured and released storage, which showed an average storage loss of 1.31 Mm^3/day. Figure A5 depicts the resulting drawdown every ten years on a cross-sectional view (Section A-A, Figure 1b) of the model domain.

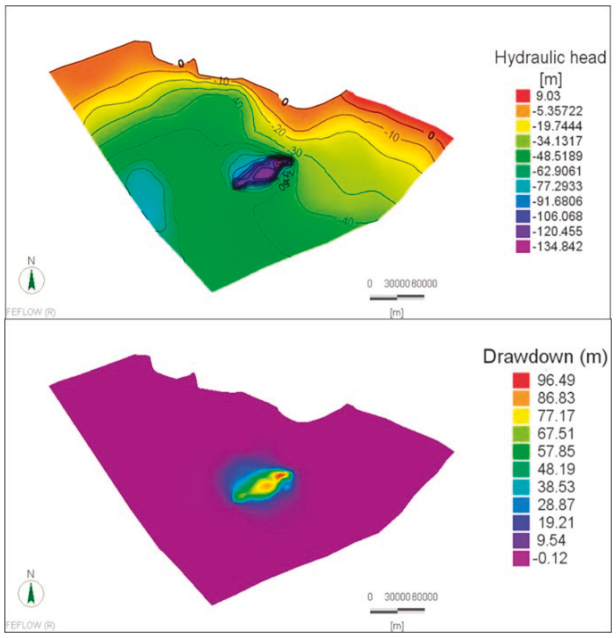

Figure 9. Simulated hydraulic heads (**Up**) and drawdowns (**Down**) for the recommended pumping scheme (1.3 Mm^3/day) after 100 years.

5.2. Climate Change Impacts

As mentioned, the maximum pumping rate is 1.3 Mm^3/day through 1000 wells, which is sufficient to irrigate about 92,850 acres (about 37,575 ha) with an average water duty of 14 m^3/acres/day, as shown in Table 2. However, CC would impose significant pressure on the aquifer to meet the anticipated increase in crop consumptive water use. To avoid the loss of a portion of the reclaimed areas in the future, a time-increasing abstraction rate should be applied. Accordingly, the developed model was utilized to investigate the combined effect of SLR and the increase in crop-consumptive water use. A time series representing a linear rise by 0.5 m in sea level during the upcoming 100 years was assigned for the northern BC along the Mediterranean Sea. Additionally, the daily pumping rate to maintain the cultivated area was defined as a time series considering the increase in PET under the worst-case CC scenario (i.e., RCP 85), as shown in Figure 8.

Figure 10 shows the resulting heads and drawdown after a 100-year simulation period under a constant pumping rate of 1300 m^3/day/well, considering a gradual SLR of up to 0.5 m after 100 years. The water levels within a narrow strip along the seaside were marginally raised, but they were not altered over the rest of the model domain. The low effect of SLR on water levels is attributed to the vast area of the model domain. Accordingly, the resulting drawdown within the wells field was almost unaffected, as shown in Figure 10. On the contrary, the resulting drawdown from assigning a time-increased withdrawal rate was 103.7 m, as shown in Figure 10, compared to 96.5 m when applying a fixed pumping rate of 1300 m^3/day/well. The simulation affirmed the exceeding of this management scenario under CC implications for the maximum rationalizing limit of drawdown. The combined effect of SLR and pumping increases in all management scenarios on the modelled domain is shown in Table 3. The exploitation scheme No. 5, which involves cultivating 85,714 acres, may be more consistent with the drawdown rationalizing limit. The resulting drawdown by the end of the simulation period under the combined effect of global warming and the resulting SLR is shown in Figure 11. The resulting drawdown is 95.4 m by the simulation period's end. This value is compatible with the MWRI's regulations, which state that the maximum annual drawdown should not exceed 1.0 m. Appendix C showcases more information about the implications of a variant pumping scheme considering climate change impacts. Figure A6 depicts the maximum drawdown resulting through a 100-year test period from different investigated pumping rates, where the optimum one is marked. Figure A7 depicts the average rate budget analysis of the groundwater system over 100 years of applying time-increasing abstraction rates under the combined effects of climate change. The net storage was estimated as the difference between captured and released storage, which showed an average storage loss of 1.362 Mm^3/day.

Table 3. Maximum drawdown (m) along a 100-year test period under a chronologically increasing abstraction rate corresponding to climate change implications on crop water requirements.

Scenario	Cultivated Area "Acres" *	Time (Years)									
		10	**20**	**30**	**40**	**50**	**60**	**70**	**80**	**90**	**100**
1	57,143	8.85	16.19	23.09	29.67	35.81	41.64	47.19	52.53	57.74	62.89
2	64,286	9.96	18.22	25.99	33.41	40.34	46.92	53.18	59.22	65.12	70.94
3	71,429	11.07	20.25	28.90	37.16	44.87	52.21	59.20	65.95	72.53	79.05
4	78,571	12.17	22.28	31.81	40.91	49.42	57.52	65.23	72.70	79.98	87.20
5	**85,714**	**13.28**	**24.31**	**34.73**	**44.67**	**53.98**	**62.84**	**71.30**	**79.48**	**87.48**	**95.40**
6	92,857	14.39	26.35	37.64	48.43	58.55	68.18	77.39	86.3	95.01	103.65
7	100,000	15.5	28.38	40.56	52.2	63.13	73.54	83.5	93.14	102.59	111.96
8	107,143	16.61	30.42	43.49	55.98	67.72	78.92	89.63	100.02	110.21	120.32

Notes: * 1 acre = 0.404686 hectares = 0.00404686 km^2. Bold font refers to recommended pumping scenario.

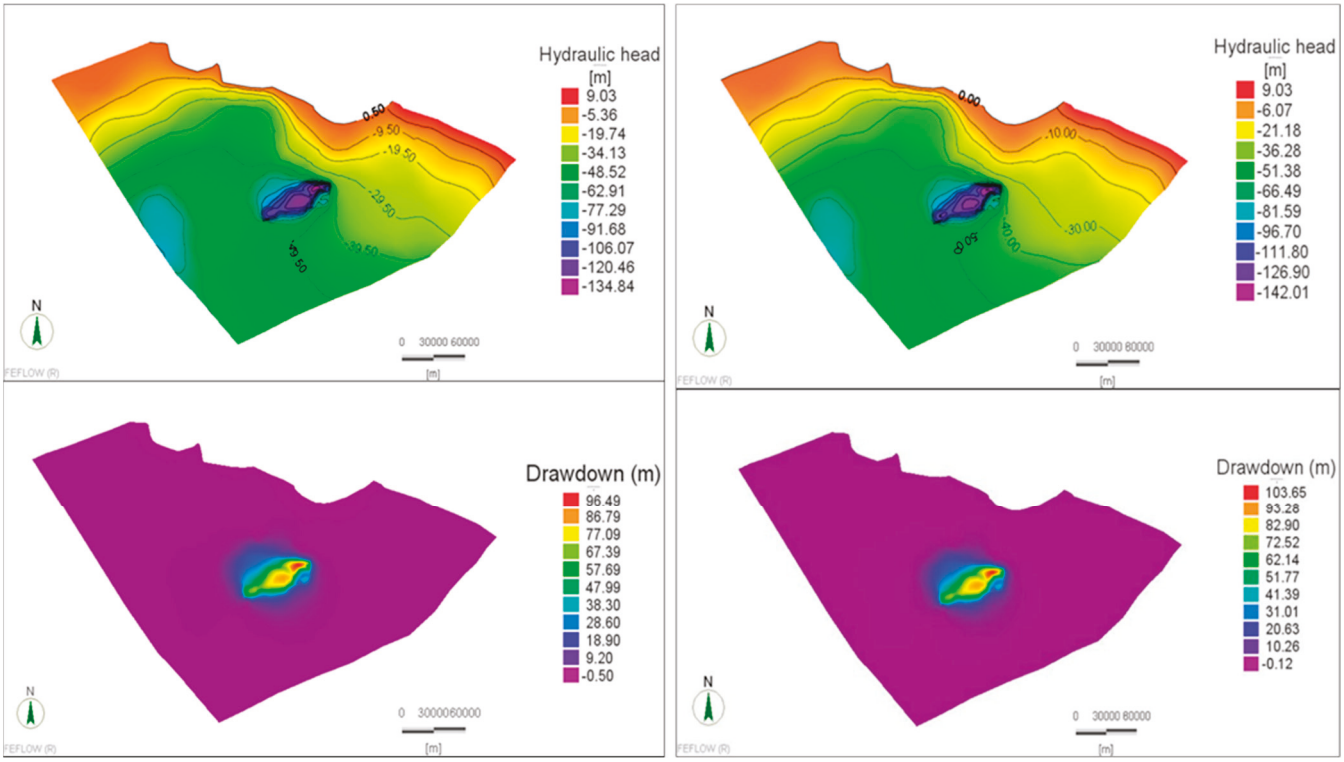

Figure 10. Simulated hydraulic heads (**Up**) and drawdown (**Down**) after 100 years under a constant pumping rate of 1.3 m^3/day/well considering (**Right**) a sea level rise of 0.5 m and (**Left**) an increase in crop water requirements.

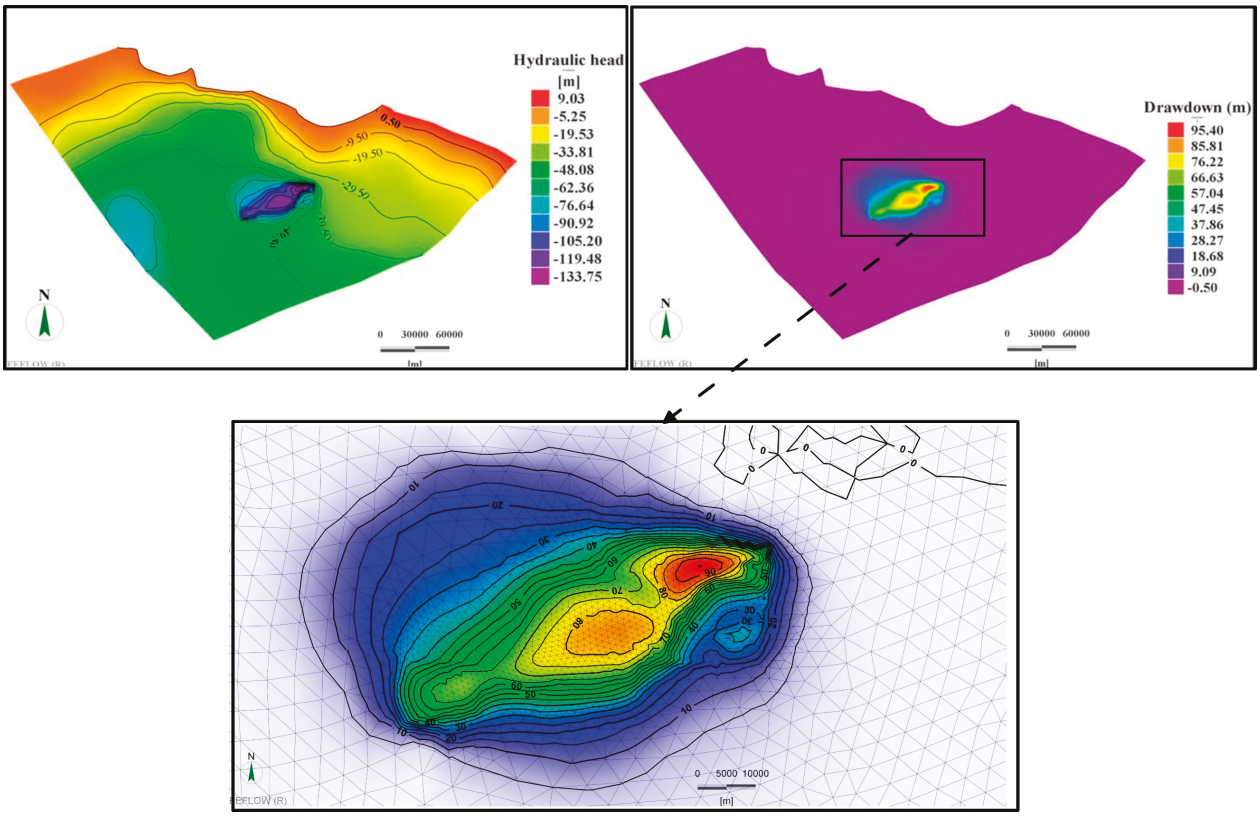

Figure 11. Simulated hydraulic heads (**Left**) and drawdowns (**Right**) after 100 years of applying the recommended development regime under the combined effects of climate change.

6. Conclusions

To cope with the rising food shortage issue in Egypt, there is a crucial need to expand cultivation swaths outside of the overpopulated Nile Delta and Valley. Thus, a groundwater-dependent reclamation project was advocated to reclaim the barren desert areas. The allocated aquifers for the proposed cultivation activities are almost non-renewable systems. Nevertheless, there is still substantial room for exploitation of this water resource, provided its pumping is regulated by principles of wisdom and rationality. Herein, a groundwater flow model was generated using the FEFLOW software to explore the Moghra aquifer's potential for extensive rural development. A simulation of reality is performed by representing the aquifer's boundary conditions, hydrogeological parameters, and groundwater extraction rates. The developed model was calibrated against the observed water levels in the archive and continuous pumping experiments. Simulated losses in groundwater storage (GWS) from 2016 to 2021 were compatible with the GRACE-derived GWS anomaly. Subsequently, the calibrated model was utilized to produce the groundwater equipotential surface and hydraulic head gradient under the influence of changing abstraction regimes. The persistently high abstraction rates play a significant role in lowering groundwater heads within the development area. To provide an integrated management approach, this study has also investigated the effects of global warming. SLR would increase the extent of saltwater encroachment into the aquifer, causing a slight increase in the piezometric levels within the coastal plain. It, therefore, has no effect on the heads within the well field. The projected increase in crop water requirement was estimated for climate change's worst-case scenario (i.e., RCP 85). The corresponding temporal-increasing abstraction rate to irrigate the cultivation area without any reduction was assigned. The maximum pumping regime that coincides with the regulation rule that was set by the MWRI for the next 100 years has been concluded. There is a potential for sustainable exploitation of this water resource to irrigate a total area of 85,715 acres (34,687 ha). The resulting drawdown is expected to reach 95.4 m.

This study addressed the first modelling of the Moghra aquifer using a finite-element-based code. The developed model can be invoked by decision-makers to beneficially use its outcomes to define sustainable management approaches. It is suggested to upgrade the model to evaluate the degree to which the production wells would intrude saltwater into the aquifer system.

Author Contributions: Conceptualization, A.S., B.A.Z. and A.M.A.; methodology, A.S., A.M.N. and A.M.A.; software, A.S. and A.M.A.; validation, A.S. and A.M.A.; formal analysis, A.M.A. and K.P.-U.; investigation, A.S., A.M.A. and K.P.-U.; resources, K.P.-U. and A.M.A.; data curation, A.S.; writing—original draft preparation, A.S.; writing—review and editing, A.S., A.M.A. and K.P.-U.; visualization, A.S. and A.M.A.; supervision, B.A.Z. and A.M.A. All authors have read and agreed to the published version of the manuscript.

Funding: Financial support received from the Science, Technology & Innovation Funding Authority STDF-Egypt (Grant number: 46278) has facilitated this collaborative research as a part of a project titled "Optimal Exploitation Strategies for Sustainable Utilization of Fossil Groundwater Reserves in Egypt".

Data Availability Statement: Research data are available from the corresponding author on request.

Acknowledgments: The authors would like to thank the STDF-Egypt for the financial support received under the framework of a project (ID#46278). The authors are beholden to the Egyptian Countryside Development Company ECDC's officials for providing in situ observation, reports, surveys, and hosting during the field campaign. Thanks must go to the DHI group for providing technical support for the FEFLOW software. All authors acknowledge the reviewers' time and efforts to revise and improve the manuscript.

Conflicts of Interest: The authors state no conflicts of interest that could influence the study reported in this paper. The funders had no role in the design of this study; in the collection, analyses, or interpretation of data; in the writing of the manuscript; or in the decision to publish the results.

Appendix A. Model Development and Calibration

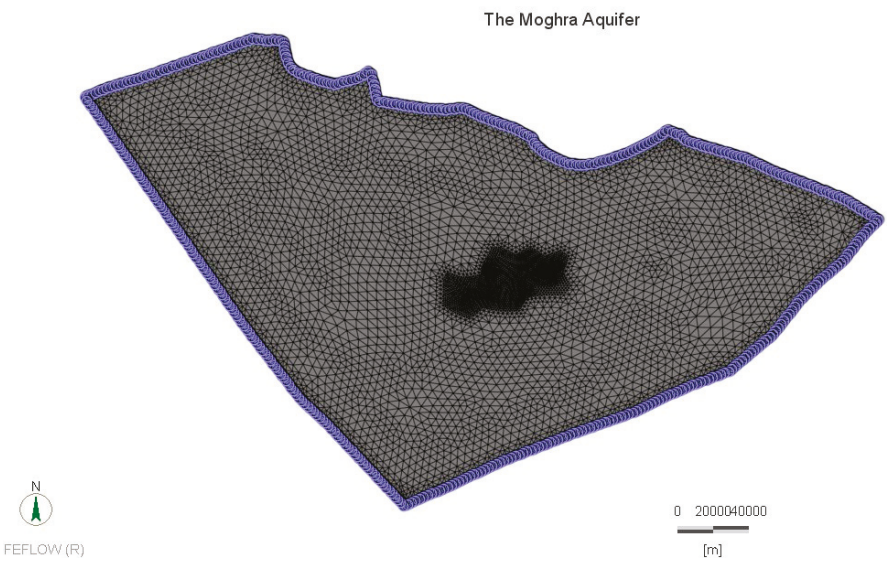

Figure A1. Configured mesh and boundary conditions of the modelled domain.

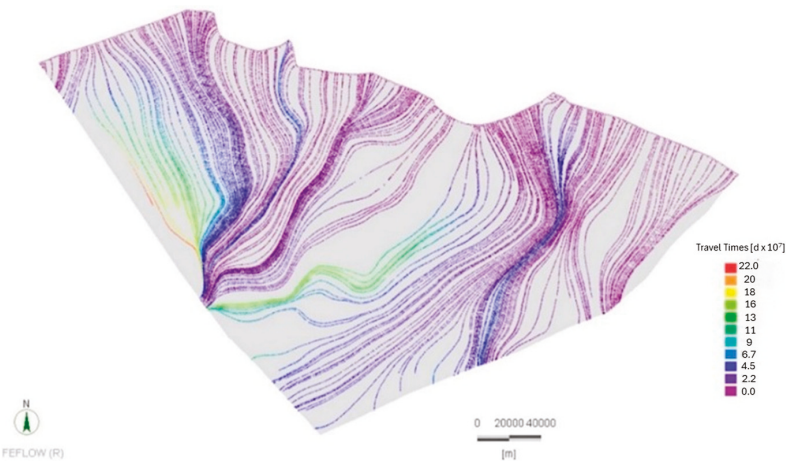

Figure A2. Visualization of paths and travel times of virtual particles released at the domain's boundaries.

Appendix B. Optimum Pumping Scheme without Considering Climate Change Impact

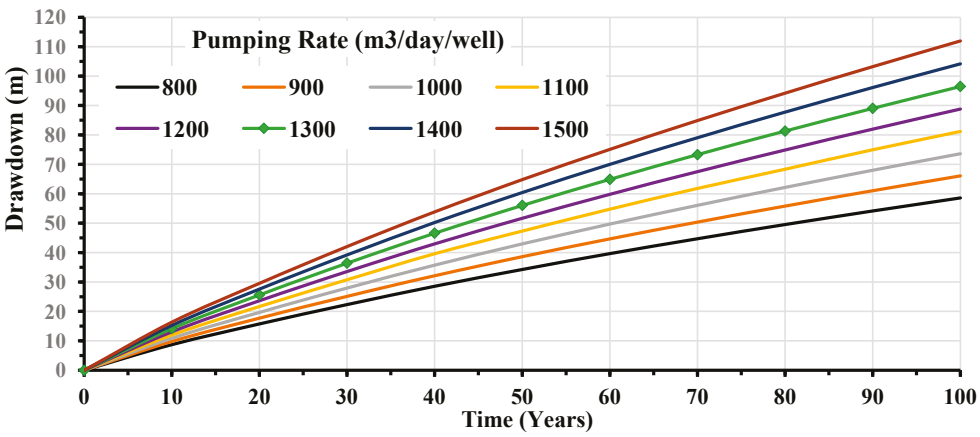

Figure A3. Predicted maximum drawdown resulting from different pumping rates through a 100-year test period.

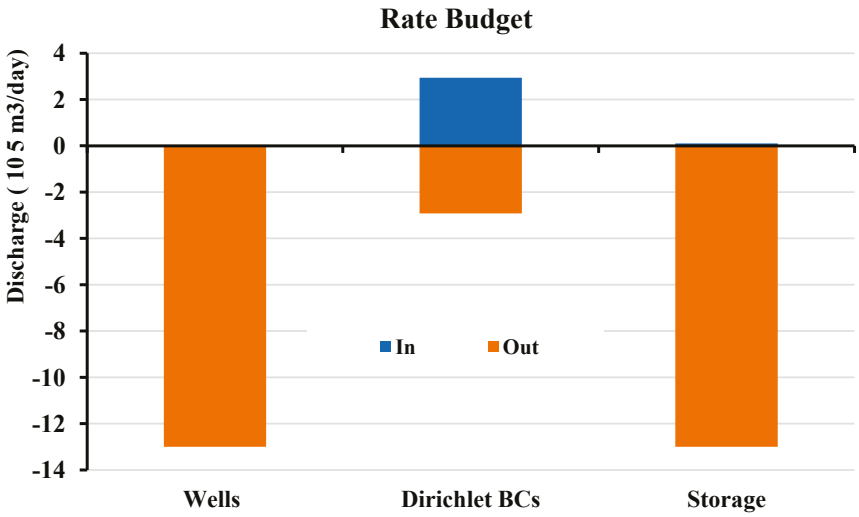

Figure A4. Components of the groundwater budget analysis (+) for inflow and (−) for outflow for the recommended pumping scheme (1.3 Mm^3/day) after 100 years.

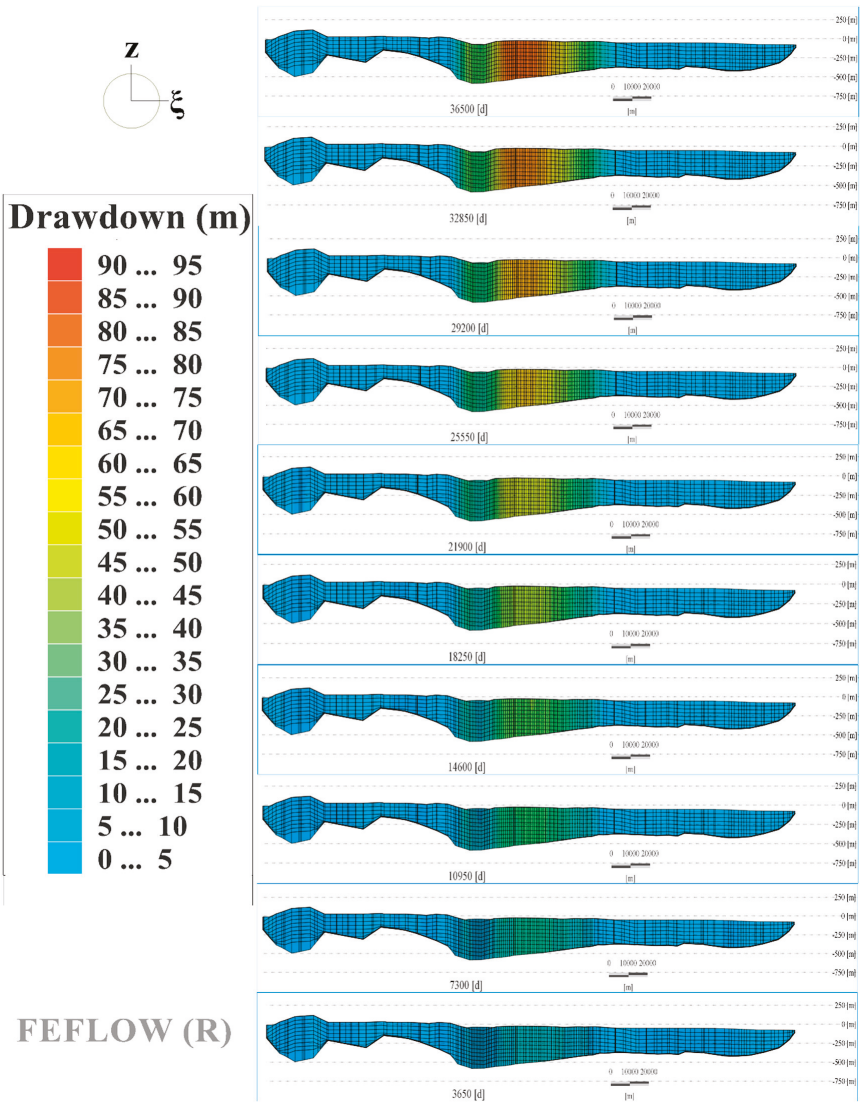

Figure A5. Cross-section (A-A) view showing the resulting drawdown from the recommended pumping scheme (1.3 Mm^3/day) (depth is scaled up by 30 times).

Appendix C. Optimum Pumping Scheme Considering Climate Change Impact

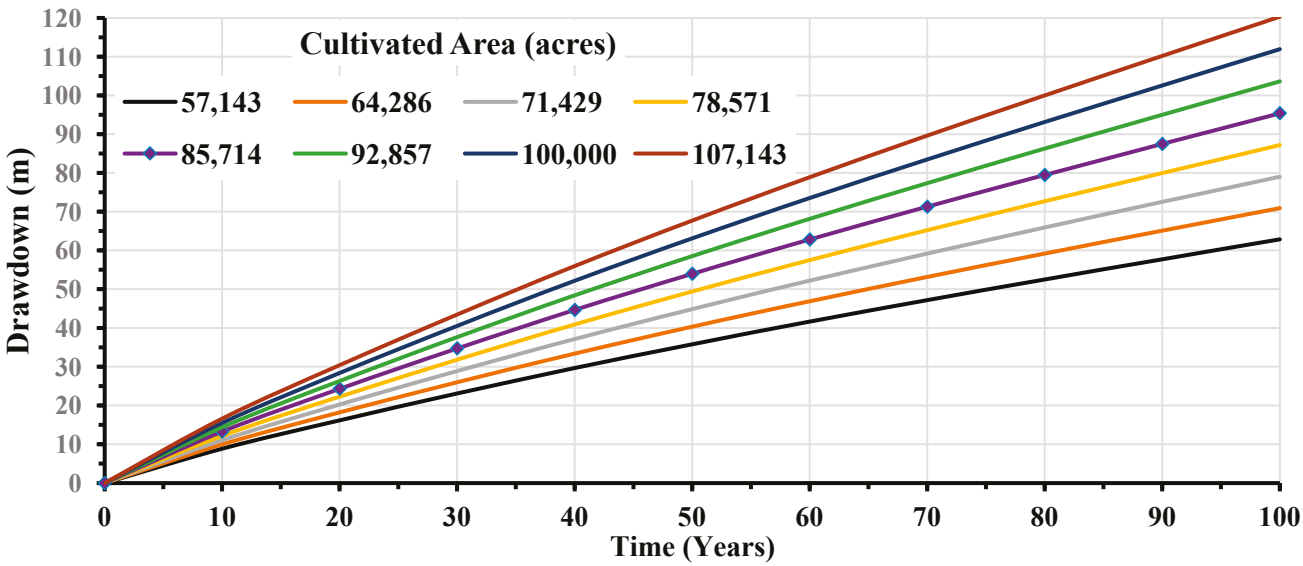

Figure A6. Maximum drawdown resulting from time-increasing abstraction rates through a 100-year test period.

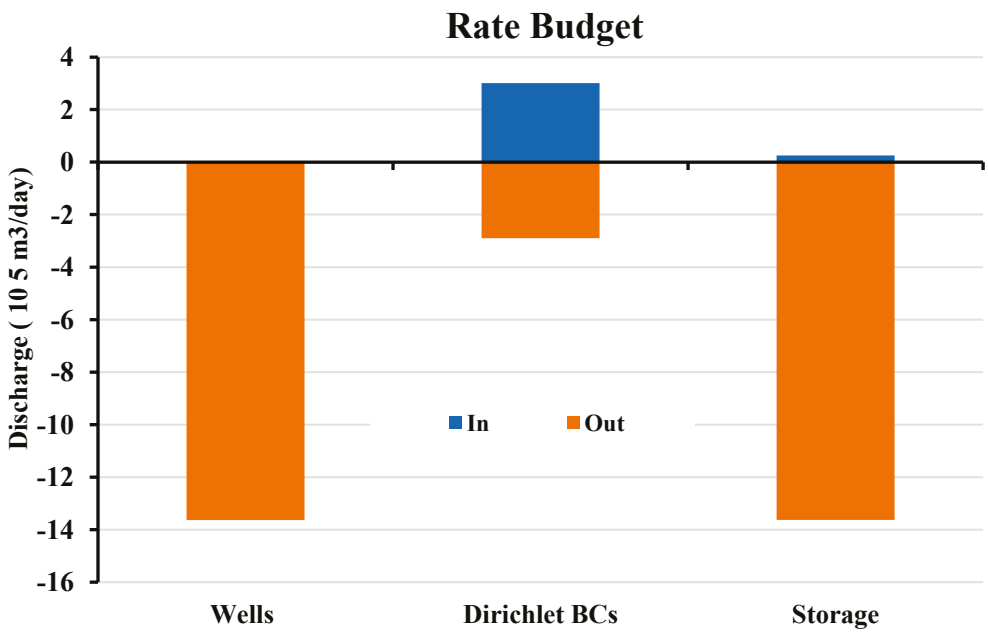

Figure A7. Components of the groundwater budget analysis (+) for inflow and (−) for outflow after 100 years of applying the recommended development regime (a growing pumping rate initiated by 1.3 m^3/day/well) under the combined effects of climate change.

References

1. Frappart, F.; Ramillien, G. Monitoring groundwater storage changes using the Gravity Recovery and Climate Experiment (GRACE) satellite mission: A review. *Remote Sens.* **2018**, *10*, 829. [CrossRef]
2. Closas, A.; Rap, E. Solar-based groundwater pumping for irrigation: Sustainability, policies, and limitations. *Energy Policy* **2017**, *104*, 33–37. [CrossRef]
3. Rubio-Aliaga, Á.; Sánchez-Lozano, J.M.; García-Cascales, M.S.; Benhamou, M.; Molina-García, A. GIS based solar resource analysis for irrigation purposes: Rural areas comparison under groundwater scarcity conditions. *Sol. Energy Mater. Sol. Cells* **2016**, *156*, 128–139. [CrossRef]
4. Zektser, S.; Loáiciga, H.A.; Wolf, J.T. Environmental impacts of groundwater overdraft: Selected case studies in the southwestern United States. *Environ. Geol.* **2005**, *47*, 396–404. [CrossRef]

5. Khater, A.R.; Water, N. Intensive groundwater use in Middle East and North Africa. In *Intensive Use of Groundwater: Challenges and Opportunities*; CRC Press: Boca Raton, FL, USA, 2019; pp. 355–386.
6. Gado, T.A.; El-Hagrsy, R.M.; Rashwan, I.M.H. Spatial and temporal rainfall changes in Egypt. *Environ. Sci. Pollut. Res.* **2019**, *26*, 28228–28242. [CrossRef]
7. Gado, T.A.; Mohameden, M.B.; Rashwan, I.M.H. Bias correction of regional climate model simulations for the impact assessment of the climate change in Egypt. *Environ. Sci. Pollut. Res.* **2022**, *29*, 20200–20220. [CrossRef]
8. Farrag, A.A. The hydraulic and hydrochemical impacts of the Nile system on the groundwater in upper Egypt. *Assuit Univ. Bull. Environ. Resour* **2005**, *8*, 87–102.
9. Aziz, S.A.; Zelenáková, M.; Mésároš, P.; Purcz, P.; Abd-Elhamid, H. Assessing the Potential Impacts of the Grand Ethiopian Renaissance Dam on Water Resources and Soil Salinity in the Nile Delta, Egypt. *Sustainability* **2019**, *11*, 7050. [CrossRef]
10. Shalaby, M.Y.; Al-Zahrani, K.H.; Baig, M.B.; Straquadine, G.S.; Aldosari, F. Threats and challenges to sustainable agriculture and rural development in Egypt: Implications for agricultural extension. *J. Anim. Plant Sci.* **2011**, *21*, 581–588.
11. Aly, M.M.; Elhamid, A.M.I.A.; Abu-Bakr, H.A.-A.; Shalby, A.; Fayad, S.A.K. Integrated Management and Environmental Impact Assessment of Sustainable Groundwater-Dependent Development in Toshka District, Egypt. *Water* **2023**, *15*, 2183. [CrossRef]
12. Aly, M.M.; Sakr, S.A.; Fayad, S.A.K. Evaluation of the impact of Lake Nasser on the groundwater system in Toshka under future development scenarios, Western Desert, Egypt. *Arab. J. Geosci.* **2019**, *12*, 553. [CrossRef]
13. El-Agha, D.E.; Molle, F.; Metwally, M.I.; Emara, S.R.; Shalby, A.; Armanuos, A.M.; Negm, A.; Gado, T.A. Review: Toward sustainable management of groundwater in the deserts of Egypt. *Hydrogeol. J.* **2023**. [CrossRef]
14. Shalby, A.; Emara, S.R.; Metwally, M.I.; Negm, A.M.; Gado, T.A.; Armanuos, A.M. Geospatial model for allocating favorable plots for groundwater-dependent cultivation activities in Egypt. *Egypt. J. Remote Sens. Sp. Sci.* **2023**, *26*, 777–788. [CrossRef]
15. Sayed, E.; Riad, P.; Elbeih, S.; Hagras, M.; Hassan, A.A. Multi criteria analysis for groundwater management using solar energy in Moghra Oasis, Egypt. *Egypt. J. Remote Sens. Sp. Sci.* **2019**, *22*, 227–235. [CrossRef]
16. Elmenshawy, M.R.; Shalaby, S.M.; Elshinnawy, A.I.; Gado, T.A. Groundwater desalination for agricultural purposes using reverse osmosis and nanofiltration technologies: Case study wadi El-natrun, Egypt. *Process Saf. Environ. Prot.* **2023**, *180*, 669–685. [CrossRef]
17. Gomaa, S.M.; Hassan, T.M.; Helal, E. Assessment of seawater intrusion under different pumping scenarios in Moghra aquifer, Egypt. *Sci. Total Environ.* **2021**, *781*, 146710. [CrossRef]
18. Elmansy, Y.; Mohamed, M.S.; Hassan, A.A.; Riad, P. Sustainable Agricultural Groundwater Management for New Reclaimed Areas in Farafra Oasis, Western Desert of Egypt. *Int. J. Eng. Adv. Technol.* **2020**, *9*, 118–127. [CrossRef]
19. Singh, A. Groundwater resources management through the applications of simulation modeling: A review. *Sci. Total Environ.* **2014**, *499*, 414–423. [CrossRef]
20. Alley, W.M.; Leake, S.A. The Journey from Safe Yield to Sustainability. *Ground Water* **2004**, *42*, 12–16. [CrossRef]
21. Janipella, R.; Pujari, P.R. Review on Groundwater Flow and Solute Transport Modelling in India: Recent Advances and Future Directions. *J. Geol. Soc. India* **2022**, *98*, 278–284. [CrossRef]
22. Dibaj, M.; Javadi, A.A.; Akrami, M.; Ke, K.Y.; Farmani, R.; Tan, Y.C.; Chen, A.S. Modelling seawater intrusion in the Pingtung coastal aquifer in Taiwan, under the influence of sea-level rise and changing abstraction regime. *Hydrogeol. J.* **2020**, *28*, 2085–2103. [CrossRef]
23. Zhou, Y.; Li, W. A review of regional groundwater flow modeling. *Geosci. Front.* **2011**, *2*, 205–214. [CrossRef]
24. Strack, O.D.L. Finite differences and finite elements. In *Analytical Groundwater Mechanics*; Cambridge University Press: Cambridge, UK, 2017; Volume 7, pp. 403–422. ISBN 9781316563144.
25. Koukidou, I.; Panagopoulos, A. Application of Feflow for the Simulation of Groundwater Flow at the Tirnavos (Central Greece). *Bull. Geol. Soc. Greece* **2010**, *43*, 1747–1757. [CrossRef]
26. Arenas, M.C.; Pescador, J.P.; Garzón, L.D.D.; Saavedra, E.Y.; Obando, P.F.A. Hydrogeological modeling in tropical regions via feflow. *Earth Sci. Res. J.* **2020**, *24*, 283–293. [CrossRef]
27. Dufour, R.; Aguirre, C.; Sanchez, M.; Maqueda, A.; Zwinger, J.; Renz, A.; Cho, J.; Evans, D. *Pit Dewatering Optimisation of a 3D Feflow Unstructured Groundwater Model at Geologically Complex Antamina Mine Site in Peru*; Australian Centre for Geomechanics: Perth, Australia, 2020; pp. 1329–1348. [CrossRef]
28. Normi Idris, A.; Zaharin Aris, A.; Sheikhy Narany, T.; Praveena Mangala, S.; Suratman, S.; Tawnie, I.; Khairul Nizar Shamsuddin, M.; Sefie, A. Simulation of Saltwater Intrusion in Coastal Aquifer of Kg. Salang, Tioman Island, Pahang, Malaysia. *MATEC Web Conf.* **2017**, *103*, 4024. [CrossRef]
29. Chu, J.; Liu, N.; Miao, Y.; Lin, X.; Tan, H.; Liu, F. Numerical simulation and pollution prediction of karst groundwater in water-conducting faults distribution area. *IOP Conf. Ser. Earth Environ. Sci.* **2020**, *585*, 012097. [CrossRef]
30. Sefelnasr, A.; Sherif, M. Impacts of Seawater Rise on Seawater Intrusion in the Nile Delta Aquifer, Egypt. *Groundwater* **2014**, *52*, 264–276. [CrossRef] [PubMed]
31. Emara, S.R.; Armanuos, A.M.; Shalby, A. Groundwater for Sustainable Development Appraisal seawater intrusion vulnerability for the Moghra coastal aquifer, Egypt—Application of the GALDIT index, sensitivity analysis, and hydro-chemical indicators. *Groundw. Sustain. Dev.* **2024**, *25*, 101166. [CrossRef]
32. Shalby, A.; Emara, S.R.; Metwally, M.I.; Armanuos, A.M.; El-Agha, D.E.; Negm, A.M.; Gado, T.A. Satellite-based Estimates of Groundwater Depletion over Egypt. *Environ. Monit. Assess.* **2023**, *105*, 594. [CrossRef]

33. Abdel Mogith, S.; Ibrahim, S.; Hafiez, R. Groundwater Potentials and Characteristics of El-Moghra Aquifer in the Vicinity of Qattara Depression. *Egypt. J. Desert Res.* **2013**, *63*, 1–20. [CrossRef]
34. Ahmed, M.; Chen, Y.; Khalil, M.M. Isotopic composition of groundwater resources in arid environments. *J. Hydrol.* **2022**, *609*, 127773. [CrossRef]
35. Sayed, E.; Riad, P.; Elbeih, S.F.; Hassan, A.A.; Hagras, M. Sustainable groundwater management in arid regions considering climate change impacts in Moghra region, Egypt. *Groundw. Sustain. Dev.* **2020**, *11*, 100385. [CrossRef]
36. Yousf, A.F.; El Fakharany, M.A.; Abu Risha, U.A.; Afifi, M.M.; Al Sayyad, M.A. Contributions to the geology of the New Valley area, Western Desert, Egypt. *J. Basic Environ. Sci.* **2018**, *5*, 1–19.
37. el-Aziz Abu-Bakr, H.A.; Abdelmoniem, M. Groundwater potentiality delineation in Moghra, Egypt. *Ain Shams Eng. J.* **2023**, 102337. [CrossRef]
38. Morad, N.A.; Masoud, M.H.; Abdel Moghith, S.M. Hydrologic factors controlling groundwater salinity in northwestern coastal zone, Egypt. *J. Earth Syst. Sci.* **2014**, *123*, 1567–1578. [CrossRef]
39. Selim, T.; Moghazy, N.H.; Elasbah, R.; Elkiki, M.; Eltarabily, M.G. Sustainable agricultural development under different climate change scenarios for El Moghra region, Western Desert of Egypt. *Environ. Dev. Sustain.* **2024**, *26*, 14957–14979. [CrossRef]
40. El Osta, M.; Masoud, M.; Alqarawy, A.; Badran, O. Utilizing of aquifer hydraulic parameters to assess the groundwater sustainability in the new reclamation area of Moghra Oasis: Western Desert—Egypt. *Appl. Water Sci.* **2023**, *13*, 238. [CrossRef]
41. Diersch, H.J.G. *FEFLOW: Finite Element Modeling of Flow, Mass and Heat Transport in Porous and Fractured Media*; Springer: Berlin/Heidelberg, Germany, 2014; ISBN 9783642387395.
42. Zheng, Y.; Chen, S.; Qin, H.; Jiao, J.J. Modeling the spatial and seasonal variations of groundwater head in an urbanized area under low impact development. *Water* **2018**, *10*, 803. [CrossRef]
43. ECDC "Egyptian Countryside Development Company" EGDC "Egyptian Countryside Development Company". Available online: http://elreefelmasry.com (accessed on 1 May 2023).
44. Sarwar, A.; Eggers, H. Development of a conjunctive use model to evaluate alternative management options for surface and groundwater resources. *Hydrogeol. J.* **2006**, *14*, 1676–1687. [CrossRef]
45. Sobeih, M.M.; El-Arabi, N.E.; Helal, E.E.D.Y.; Awad, B.S. Management of water resources to control groundwater levels in the southern area of the western Nile delta, Egypt. *Water Sci.* **2017**, *31*, 137–150. [CrossRef]
46. Gado, T.A.; Shalaby, B.A.; Guo, Y.; Rashwan, I.M.H. Assessment of Satellite-Based Precipitation Estimates over Egypt. *J. Hydrol. Eng.* **2024**, *29*, 05023027. [CrossRef]
47. Thomas, B.F.; Behrangi, A.; Famiglietti, J.S. Precipitation intensity effects on groundwater recharge in the southwestern United States. *Water* **2016**, *8*, 90. [CrossRef]
48. Shah, N.; Nachabe, M.; Ross, M. Extinction depth and evapotranspiration from ground water under selected land covers. *Ground Water* **2007**, *45*, 329–338. [CrossRef]
49. Campoli, D.; Crestaz, E.; Fehervari, M.; Patata, L.; Scipioni, P. 3D density-dependent groundwater modeling in assessing optimisation of a pumping strategy within a chemical plant. *Water Resour. Manag. III* **2005**, *80*, 131–141.
50. Wassef, R.; Schüttrumpf, H. Impact of sea-level rise on groundwater salinity at the development area western delta, Egypt. *Groundw. Sustain. Dev.* **2016**, *2–3*, 85–103. [CrossRef]
51. Abdel Azeem, H.; El-Didy, S.; Eizeldin, M.; Helmi, A. Hydrogeological Evaluation of Massive Salty Lagoons, (Case Study: Qattara Depression). *Al-Azhar Univ. Civ. Eng. Res. Mag.* **2017**, *39*, 277–291.
52. El Shazly, E.M.; Abdel Hady, M.A.; El Ghawaby, M.A.; Khawasik, S.M.; El Shazly, M.M. Landsat satellite imagery of the Qattara Depression area, Egypt. *Acta Astronaut.* **1978**, *5*, 947–957. [CrossRef]
53. Moharram, S.H.; Gad, M.I.; Saafan, T.A.; Allah, S.K. Optimal groundwater management using Genetic Algorithm in El-Farafra Oasis, Western Desert, Egypt. *Water Resour. Manag.* **2012**, *26*, 927–948. [CrossRef]
54. Al-Muqdadi, S.W.H.; Abo, R.; Khattab, M.O.; Abdulhussein, F.M. Groundwater flow-modeling and sensitivity analysis in a hyper arid region. *Water* **2020**, *12*, 2131. [CrossRef]
55. Sultan, M.; Yan, E.; Sturchio, N.; Wagdy, A.; Abdel Gelil, K.; Becker, R.; Manocha, N.; Milewski, A. Natural discharge: A key to sustainable utilization of fossil groundwater. *J. Hydrol.* **2007**, *335*, 25–36. [CrossRef]
56. Haddad, O.B.; Tabari, M.M.R.; Fallah-Mehdipour, E.; Mariño, M.A. Groundwater Model Calibration by Meta-Heuristic Algorithms. *Water Resour. Manag.* **2013**, *27*, 2515–2529. [CrossRef]
57. Hu, L.; Jiao, J.J. Calibration of a large-scale groundwater flow model using GRACE data: A case study in the Qaidam Basin, China. *Hydrogeol. J.* **2015**, *23*, 1305–1317. [CrossRef]
58. Sun, A.Y.; Green, R.; Swenson, S.; Rodell, M. Toward calibration of regional groundwater models using GRACE data. *J. Hydrol.* **2012**, *422–423*, 1–9. [CrossRef]
59. Lo, M.H.; Famiglietti, J.S.; Yeh, P.J.F.; Syed, T.H. Improving parameter estimation and water table depth simulation in a land surface model using GRACE water storage and estimated base flow data. *Water Resour. Res.* **2010**, *46*. [CrossRef]
60. Sun, A.Y.; Green, R.; Rodell, M.; Swenson, S. Inferring aquifer storage parameters using satellite and in situ measurements: Estimation under uncertainty. *Geophys. Res. Lett.* **2010**, *37*, 1–5. [CrossRef]
61. Richey, A.S.; Thomas, B.F.; Lo, M.H.; Reager, J.T.; Famiglietti, J.S.; Voss, K.; Swenson, S.; Rodell, M. Quantifying renewable groundwater stress with GRACE. *Water Resour. Res.* **2015**, *51*, 5217–5237. [CrossRef] [PubMed]

62. Rodell, M.; Chen, J.; Kato, H.; Famiglietti, J.S.; Nigro, J.; Wilson, C.R. Estimating groundwater storage changes in the Mississippi River basin (USA) using GRACE. *Hydrogeol. J.* **2007**, *15*, 159–166. [CrossRef]
63. Bierkens, M.F.P.; Wada, Y. Non-renewable groundwater use and groundwater depletion: A review. *Environ. Res. Lett.* **2019**, *14*, 43. [CrossRef]
64. Shalby, A.; Elshemy, M.; Zeidan, B.A. Assessment of climate change impacts on water quality parameters of Lake Burullus, Egypt. *Environ. Sci. Pollut. Res.* **2019**, *27*, 32157–32178. [CrossRef] [PubMed]
65. Moss, R.; Babiker, M.; Brinkman, S.; Calvo, E.; Carter, T.; Edmonds, J.; Elgizouli, I.; Emori, S.; Erda, L.; Hibbard, K.; et al. Towards New Scenarios for Analysis of Emissions, Climate Change, Impacts and Response Strategies. In Proceedings of the IPCC Expert Meeting Report, Noordwijkerhout, The Netherlands, 19–21 September 2008.
66. Gregory, J. *Projections of Sea Level Rise*; Climate Research: Cambridge, UK; New York, NY, USA, 2014.
67. Shaltout, M.; Tonbol, K.; Omstedt, A. Sea-level change and projected future flooding along the Egyptian Mediterranean coast. *Oceanologia* **2015**, *57*, 293–307. [CrossRef]
68. Shalby, A.; Elshemy, M.; Zeidan, B.A. Modeling of climate change impacts on Lake Burullus, coastal lagoon (Egypt). *Int. J. Sediment Res.* **2020**. [CrossRef]
69. Alkhawaga, A.; Zeidan, B.; Elshemy, M. Climate change impacts on water security elements of Kafr El-Sheikh governorate, Egypt. *Agric. Water Manag.* **2022**, *259*, 107217. [CrossRef]

Disclaimer/Publisher's Note: The statements, opinions and data contained in all publications are solely those of the individual author(s) and contributor(s) and not of MDPI and/or the editor(s). MDPI and/or the editor(s) disclaim responsibility for any injury to people or property resulting from any ideas, methods, instructions or products referred to in the content.

water

MDPI

Article

Identification of Microplastics Using μ-Raman Spectroscopy in Surface and Groundwater Bodies of SE Attica, Greece

Maria Perraki [1,*], Vasilios Skliros [1], Petros Mecaj [2,3], Eleni Vasileiou [1], Christos Salmas [2], Ioannis Papanikolaou [2] and Georgios Stamatis [2]

[1] School of Mining and Metallurgical Engineering, Division of Geo-Sciences, National Technical University of Athens, 15773 Zografou, Greece; sklirosbill@gmail.com (V.S.); elvas@metal.ntua.gr (E.V.)
[2] Mineralogy-Geology Laboratory, Department of Natural Resources and Agricultural Engineering, Agricultural University of Athens, 11855 Athens, Greece; petros.mecaj@univ-lyon1.fr (P.M.); c.salmas@aua.gr (C.S.); i.pap@aua.gr (I.P.); stamatis@aua.gr (G.S.)
[3] Université Claude Bernard Lyon 1, LEHNA UMR 5023, CNRS, ENTPE, F-69622 Villeurbanne, France
* Correspondence: maria@metal.ntua.gr

Abstract: Sixteen surface (5) and groundwater (11) samples were collected from the south-eastern part of Attica, Greece, and analysed for physico-chemical parameters and microplastics (MPs) by optical microscopy and Raman microspectroscopy (RS). A total of 3399 particles were optically identified in all sixteen samples, ranging from only 16 particles/L in a sample from a deeper borehole to 513 particles/L in a sample from a shallow water well. They were then visually classified into eight categories based on their color, texture, size, reflectivity, shape, and general morphological properties. Raman microspectroscopy was performed on the particles on the filters and revealed four different types of MPs, namely polyethylene (PE, 35%), polypropylene (PP, 30%), polystyrene (PS, 10%), and polyethylene terephthalate (PET, 25%). The samples from the shallow phreatic aquifer contained more MPs than the samples from the deeper borehole, which contained fewer MPs and categories. This is to be expected, since the phreatic aquifer (a) is generally more contaminated, as it is close to human activities that generate MPs and its infiltration depth is only a few metres, which means that many microplastics can infiltrate at such shallow depths, and (b) it is exposed to the atmosphere, so they can also be suspended in the air. On the other hand, it is interesting to note that MPs, especially PET and PE, were detected in the borehole sample, suggesting that MPs can migrate to greater depths through water infiltration. Chemical analyses of the groundwater samples revealed high values of E.C., Ca^{2+}, Mg^{2+}, Cl^{-}, and Na^{+}, which indicate that seawater intrusion is taking place in the coastal aquifer system of the Erasinos basin. The increased concentrations of NO_3^{-} and PO_4^{3-} also indicate the impact of agricultural activities.

Keywords: polyethylene; polypropylene; polystyrene; polyethylene terephthalate microplastics; groundwater; Attica; Raman spectroscopy

1. Introduction

Environmental geochemistry is an important application of Raman spectroscopy (RS) in the geosciences. From inorganic to organic and biological contaminants in soil, water and air, RS is an important tool for their characterization. In the last decade, RS has been successfully used to identify microplastics (MPs) [1,2]. "Microplastics" were defined as plastic particles smaller than 5 mm by the National Oceanic and Atmospheric Administration (NOAA) International Research Workshop on the occurrence, effects, and fate of microplastic marine debris (2009, [3]). Since then, MPs have been systematically detected in soils, sediments, and in marine and aquatic environments around the world, raising scientific interest and public health concerns [4]. The main types of polymers that can be detected in the environment are polyethylene (PE), polypropylene (PP), and polystyrene (PS). Microplastics are either primary MPs, which include production pellet nurdles and

microbeads, or secondary MPs, which are formed by the mechanical and chemical decomposition of larger plastic waste and fibers from synthetic textiles [5]. Although MPs are mostly colorless, colored MPs are also frequently found. This is due to the increasing trend of adding color pigments to plastics to obtain more attractive plastic products or to absorb part of the ultraviolet light as a light stabilizer to prevent or delay photodegradation and thus extend the life of plastic products [6].

From the Mediterranean [7] to the Pacific Ocean [8], Arctic Sea ice [9], and freshwater lakes [10], MPs are reported in an increasing number of studies worldwide.

The identification of MPs is of great significance and follows the process of separation, extraction, or concentration. The physicochemical properties of MPs, such as size, shape, and composition, are crucial for studying their pathways in soil, marine, and aquatic environments. Microscopic methods such as optical microscopy and scanning electron microscopy mainly provide information on the size, color, and shape of the MPs, whereas the vibrational spectroscopic analytical methods, Fourier Transform Infrared Spectroscopy (FT-IR) and RS, are employed to reveal the chemical composition of the MPs [11]. More advanced analytical methods such as Flow Cytometry (FCM), Dynamic Light Scattering (DLS), hyperspectral imaging (HIS), and Atomic Force Microscopy (AFM) have also been applied to the study of MPs [12–14] and others have yet to be adopted.

Capable of detecting MPs with particle sizes as small as 1 μm [15], RS spectroscopy combined with an RS microscope (μ-RS) offers rapid, generally non-destructive analysis and is becoming a conventional tool in MPs identification, as evidenced by the rapidly growing number of related publications. Raman imaging has also been applied in identifying MPs on filters [16].

Identifying the type of MPs found in soils and waters provides information on the origin of MPs, as well as the weathering/degradation processes that follow the original deposition/release. This may further contribute to monitoring and assessing the different types of MPs in the environment, setting up future prevention measures.

Even though MPs are considered a significant factor in groundwater pollution, a limited number of studies have linked them to other quality parameters such as electric conductivity (EC), pH, temperature (T), dissolved oxygen (DO), oxidation–reduction potential (ORP), total dissolved solids (TDS), turbidity, and salinity. Measuring and assessing these physical parameters in situ could improve the determination of the sources and behavior of MPs as a contaminant in aquifer systems [17]. However, the existing knowledge on how these parameters affect water or interact with MPs is still very limited. It is assumed that microplastics adsorb and transfer organic pollutants and ionic heavy metal pollutants (e.g., Cu, Pb, Hg, Cd, and Cr) in the aquatic environment [18]. The adsorption process of MPs is also controlled by various anions and cations [19]. It is believed that the physical parameters and chemical composition of groundwater are important factors influencing the occurrence of MPs in groundwater [17]. In the coming years, the big challenge for researchers will be the following: how do MPs interact with the chemical composition of groundwater and other contaminants?

There are only a limited number of published studies on the occurrence of MPs in Greek marine and aquatic ecosystems, mostly focussing on seawater samples and sediments. The analytical methods of SEM and ATR-FTIR have been mainly used to study the degradation of plastic materials in different marine environments in Greece [20], plastic pellets and fragments of polyethylene (PE) and expanded polystyrene (EPS) from two beaches of Salamina Island [21], and PE and PP as ingested microplastics in *Boops Boops* fish in the Southern Ionian Sea and Saronikos Gulf [22]. In addition, the temporal and spatial distribution of plastic pellets and fragments on nine sandy beaches along the coast of Northern Crete was investigated using Gas Chromatography—Ion Trap Mass Spectrometry (GC-ITMS) [23]. However, the possible presence of MPs in groundwater from wells and boreholes in Greece has yet to be explored, limiting our knowledge to the coastal and marine environment.

In this work, we conducted a thorough investigation of MPs detected in the surface water and groundwater of the Erasinos River basin in the southeastern part of Attica, Greece, using RS, after filtering and detailed visual presorting. In addition, chemical analyses of water samples were also carried out, in order to investigate the relationship between the chemical status of the groundwater and the occurrence of MPs in the Erasinos basin. The study area was selected because it is characterized by certain anthropogenic activities and land uses (Eleftherios Venizelos International Airport, with more than 25 million passengers annually, large shopping malls). In the Erasinos basin, there are also a variety of potential sources of MPs entering the groundwater system, such as surface runoff, agricultural activities (agrochemical products), atmospheric deposition, and wastewater, which can contribute to MP contamination. The aim was to determine the morphological characteristics and type(s) of MPs present, the impact of degradation, and the possible dependence on the depth of the aquifer. This will further contribute to build up a database of MPs present in Greek ecosystems, including underground aquifers of different types and depths.

2. Materials and Methods

2.1. Study Area

The study area of the Erasinos basin is located in the south-eastern part of Attica Prefecture, covering an area of approximately 204 km^2. The basin is bordered to the east by the coastline of Rafina–Artemis–Porto Rafti. The Erasinos River flows into the southern Gulf of Evoikos. The climate of the region is characterized by low precipitation and high summer temperatures. The average annual precipitation is estimated at 406 mm per year.

The Erasinos basin is part of the Attico-Cycladic Massif. The dominant geological formations in the basin are as follows [24,25] (Figure 1): (a) the crystalline basement of Paleozoic–Upper Cretaceous age (schists and carbonate rocks, mainly limestones and dolomite marbles), and (b) the clastic depositions of Neogene and Quaternary age (marl limestones, marls, clays, sandstones, conglomerates, and other unconsolidated materials).

A knowledge of the hydrogeological conditions of the basin is a crucial factor for the migration of MPs. In general, the groundwater flows towards the sea and discharges into Vavrona bay, while in some parts of the basin, it flows into the Erasinos River [26]. The groundwater flow is locally determined mainly by impermeable schists.

The main aquifer systems in the area are the following [27]:

- A karstic aquifer with a high capacity (discharge rate over 100 m^3/h) as it is also fractured. Along the coasts of Porto Rafti and Artemis, scattered underwater sources of this karst water have been identified, confirming the hydraulic connection with seawater.
- The alternation of permeable and impermeable layers favors the development of unconfined and confined aquifers in the Neogene deposits. The capacity of these systems is low (discharge rates up to 5 m^3/h). The shallow aquifer is overexploited by extensive pumping to meet irrigation and industrial needs in the region.
- A phreatic aquifer has developed in Quaternary deposits with low capacity (discharge rates of 15 up to 35 m^3/h). The phreatic aquifer is exploited by many wells, resulting in seawater intrusion in the coastal parts of the aquifer system. This fact is also reflected in the groundwater quality, as it is characterized as brackish.
- Fractured aquifers are mainly developed in the Rafina area, due to secondary porosity, created by metamorphic and tectonic processes and the weathering of impermeable formations.

The main recharge of the aquifer system, investigated here, originates from the following: (a) direct infiltration of precipitation and (b) infiltration of surface runoff, rivers, and streams, and (c) lateral recharge from other aquifer systems that are hydraulically connected.

Land uses are mainly as follows: (i) agriculture, (ii) industry, (iii) pastures, (iv) transportation (Eleftherios Venizelos International Airport), (v) residential, and (vi) commercial.

The area is intensively used for agriculture, resulting in aquifer degradation, with significant concentrations of inorganic pollutants such as NO_3^-, NO_2^-, and PO_4^{3-}. In addition, high concentrations of sodium (Na^+) and chlorine (Cl^-) are also traced due to seawater intrusion from excessive pumping [26,27]. The area is also exposed to significant pollution from plastic materials due to intensive agriculture and anthropogenic processes, such as the Eleftherios Venizelos International Airport and the neighbouring city of Koropi.

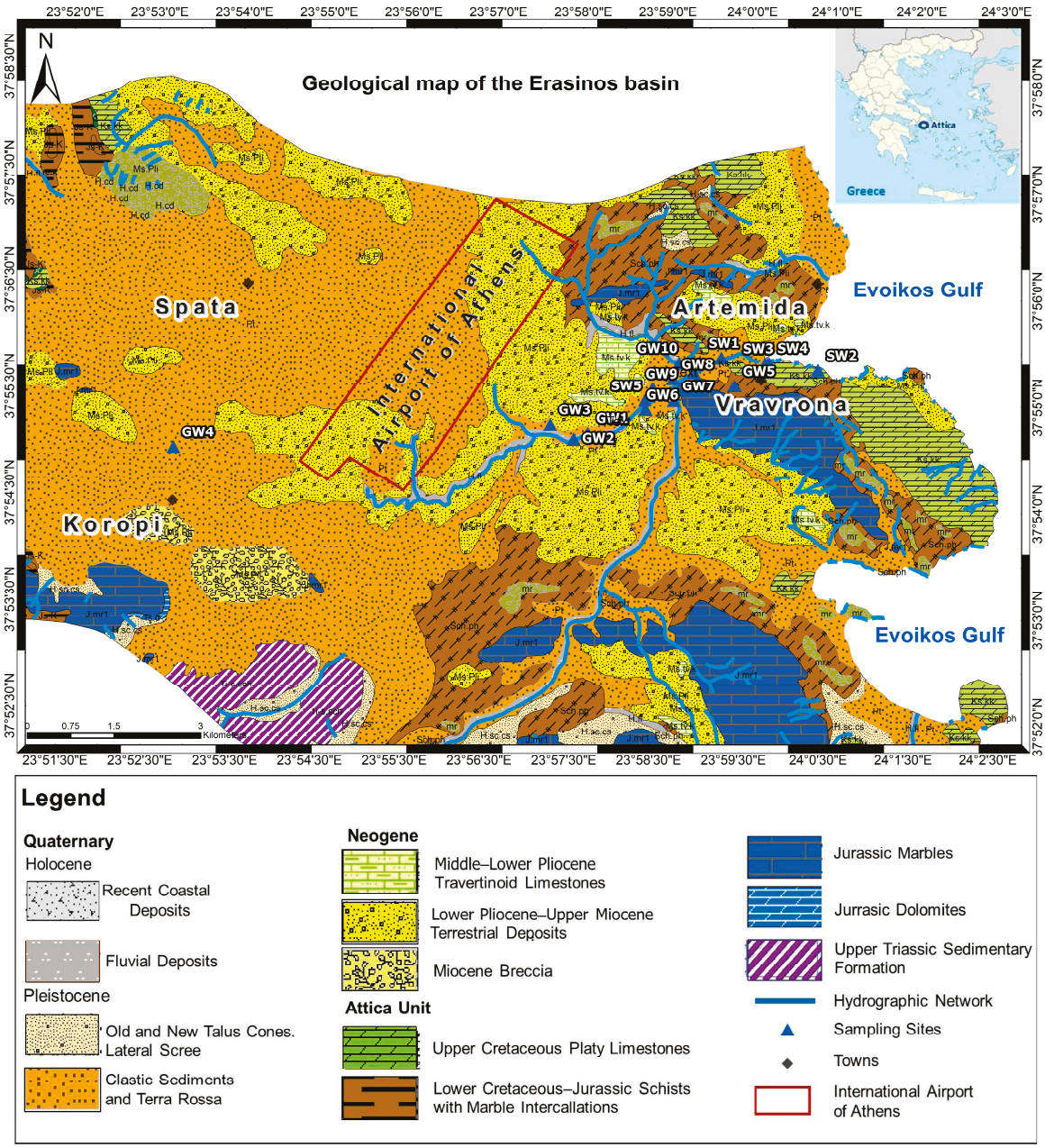

Figure 1. Geological map of the Erasinos basin, with the locations of the surface and groundwater samples studied here (modified from the 1:50,000 geological map published by the Institute of Geology and Mineral Exploration of Greece [28]).

2.2. Sampling

Sixteen (16) samples were collected in August 2020 from surface waters, groundwater wells, and a borehole from the catchment area of the Erasinos River in the area of Vravrona and Koropi; five (5) from surface waters (SW1, SW2, SW3, SW4, SW5), one (1) of which

(SW2) was from the river exit into the sea, ten (10) from wells (GW1, GW2, GW3, GW5, GW6, GW7, GW8, GW9, GW10, GW11), and one (1) from a water borehole (GW4) (Figure 2). All groundwater samples, except GW4, were collected from the phreatic water table (up to 8 m), and the surface water samples SW1, SW3, SW4, and SW5 were collected from the Erasinos River estuary. Borehole sample GW4 was taken from a deeper aquifer (70 m) within the Neogene sediments. In all cases, the water was used exclusively for irrigation purposes. The sampling sites are presented in Table 1. The water samples were collected in two 500 mL glass bottles for microplastic analysis and 1000 mL polyethylene bottles for chemical analysis. In each case, the bottles were pre-cleaned, acid-washed, and thoroughly rinsed first with distilled water and then with Milli-Q deionized water [29,30]. Before sampling, the polyethylene bottles were rinsed three times with the water to be sampled. In addition, each sample was stored immediately after sampling without being treated—apart from transport—prior to laboratory analysis [29]. The physical parameters temperature (T), pH, Eh, dissolved oxygen (DO), and electrical conductivity (EC) were measured in situ immediately after sampling, using the YSI Professional Digital Sampling System (ProDSS).

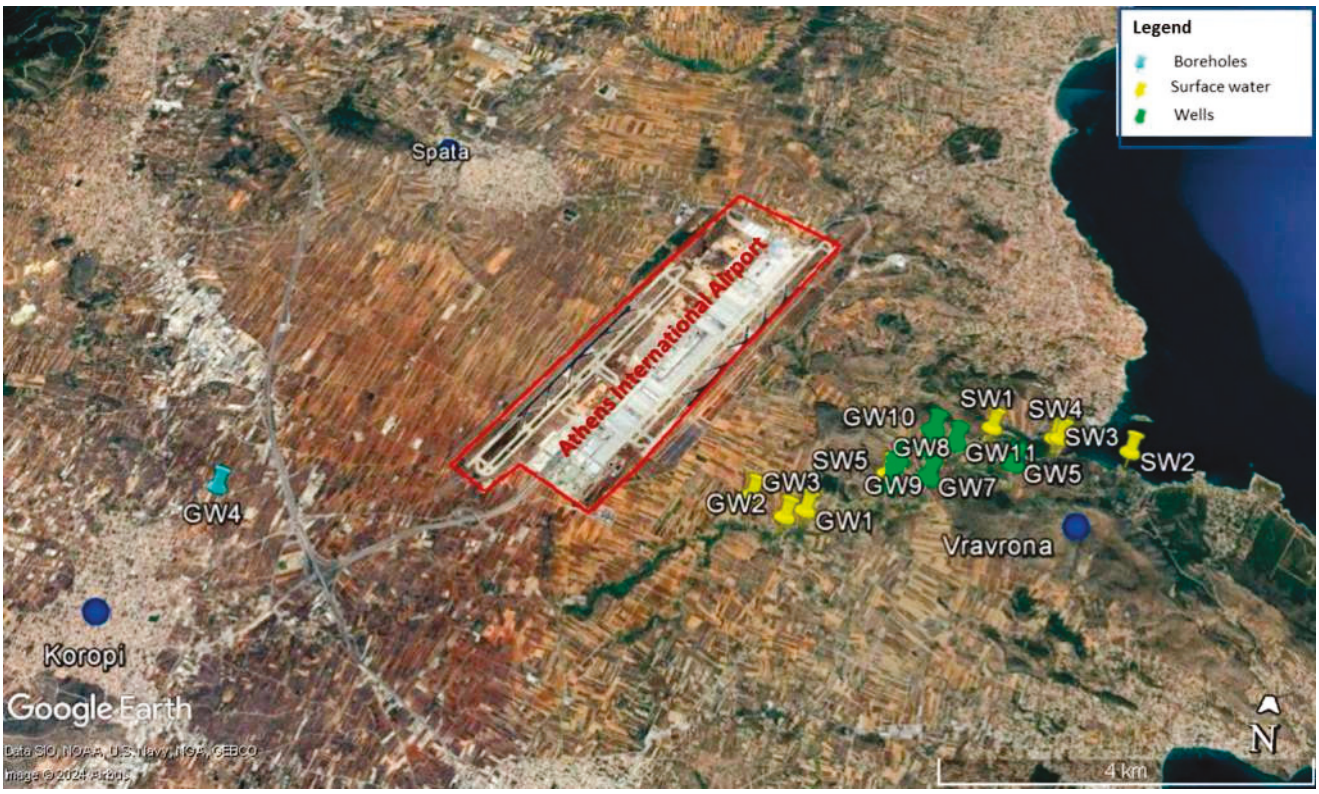

Figure 2. Sampling sites in the Erasinos basin (Google Earth).

Twelve selected water samples (SW1, GW5, SW2, SW3, SW4, SW5, GW6, GW7, GW8, GW9, GW10, and GW11) were analyzed to determine major cations (i.e., Ca^{2+}, Mg^{2+}, Na^{+}, and K^{+}) and anions (i.e., Cl^{-}, SO_4^{2-}, HCO_3^{-}, NO_3^{-}, and PO_4^{3-}). The saturation indices for calcite and dolomite were calculated, depending on the site and the prevailing hydrogeological conditions. The analyses of major ions were determined by atomic absorption spectrometry (Ca^{2+}, Mg^{2+}, Na^{+}, and K^{+}), by spectrophotometry (NO_3^{-}, NO_2^{-}, NH_4^{+}, and PO_4^{3-}), by titrimetry (Cl^{-r} and HCO_3^{-}), and by turbidimetry (SO_4^{2-}). The total dissolved solids (TDS) content was calculated directly from the sum of the major ions. All QC protocols were applied to the blank samples on site and in the laboratory, as well as to the duplicate analyses of the samples. The analytical accuracy of the ion measurement was determined by calculating the charge balance error in each sample and was less than ±10%.

Table 1. Sampling sites.

Sample ID	X Longitude	Y Latitude	Elevation (m.a.s.l.) *	Notes
GW1	23°57′57.77″ E	37°54′53.56″ N	25 m	Well—phreatic water table
GW2	23°57′43.44″ E	37°54′50.45″ N	33 m	Well—phreatic water table
GW3	23°57′27.13″ E	37°54′58.95″ N	41 m	Well—phreatic water table
GW4	23°52′59.76″ E	37°54′53.20″ N	103 m	Borehole
SW1	23°59′29.80″ E	37°55′33.56″ N	10 m	Surface water
GW5	23°59′38.50″ E	37°55′17.50″ N	9.5 m	Well—phreatic water table
SW2	24°0′37.90″ E	37°55′24.90″ N	0 m	Surface water—river mouth to the sea
SW3	24°0′0.85″ E	37°55′29.64″ N	8.5 m	Surface water
SW4	24°0′3.50″ E	37°55′29.85″ N	0 m	Surface water
SW5	23°58′33.4″ E	37°55′7.40″ N	19.5 m	Surface water
GW6	23°58′32.55″ E	37°55′5.16″ N	19.8 m	Well—phreatic water table
GW7	23°58′55.15″ E	37°55′10.10″ N	15.2 m	Well—phreatic water table
GW8	23°58′55.11″ E	37°55′22.59″ N	12 m	Well—phreatic water table
GW9	23°58′40.60″ E	37°55′17.65″ N	14 m	Well—phreatic water table
GW10	23°58′59.85″ E	37°55′31.39″ N	13.5 m	Well—phreatic water table
GW11	23°59′10.14″ E	37°55′25.90″ N	5.2 m	Well—phreatic water table

Note: * m.a.s.l.: meters above sea level.

2.3. Geochemical Modeling

The geochemical software PHREEQC version 3.1.2 was used to calculate the saturation indices (SIs) of the water samples. The mineral SIs for calcite, dolomite, and quartz were employed to define the mineral dissolution and precipitation processes in the water samples of the Erasinos basin.

A positive SI indicates that the mineral is oversaturated or supersaturated with respect to the solution [31]; thus, the mineral could precipitate. Conversely, a negative SI indicates that the solution is undersaturated with respect to the selected mineral, suggesting that the mineral is dissolved in the groundwater to reach equilibrium.

2.4. Sample Extraction

Each sample was filtered using a vacuum pump (−100 mbar pressure) to extract the MPs. Filtration was performed on GN–6 Metricel mixed cellulose ester membranes (47 mm diameter, Pore Size 0.45 μm, 152 μm thickness, gamma irradiated, gridded) at a constant flow rate. The samples were then dried at room temperature and the filters were covered with Petri glass dishes to prevent possible external contamination and the loss of particles. Samples were analyzed microscopically using a Dino X-light digital microscope with 200× optics (AM413MT, Dino-Lite, Almere, The Netherlands). The lowest resolution limit per particle size was set at 6μm. Bright field was used to visualize the samples, and color images were extracted to examine the results. The image analysis software DINOCAPTURE 2.0 was used. The size of the particles was estimated based on the Feret min diameter.

A protocol was applied to avoid contamination within the laboratory during the analysis. All work surfaces were disinfected with double-filtered 70% ethanol before handling the samples, and cotton gowns and nitrile gloves were used throughout the process. Samples were processed in a laminar flow cabinet (switched off) and plastic-free laboratory equipment was used whenever possible [30]. Considering the literature on microplastic sample preparation, three blanks (3) were used in each major analytical step [29]. All the blanks were open 50 mm Petri dishes [32] placed as follows: (1) in the room where the samples were stored for 24 h to dry, (2) under the laminar flow cabinet where the samples were processed while the process was running, and (3) next to the samples that were analyzed under the microscope at the time of analysis. The blanks were subjected to microscopic analysis, during which 1–5 fibers were removed. Blank #3 contained 5 fibers, which can be explained by the fact that the microscopy room and sample inspection as an action are associated with increased human movement [30]. All fibers that resulted from blanks were categorized but not included in our results.

Subsequently, a non-destructive Raman study was performed on 194 suspect particles of each of these MP categories directly on the filters, without further treatment, employing a Renishaw inVia Reflex micro-Raman (Renishaw, Gloucestershire, UK), at the School of Mining and Metallurgical Engineering of the Technical University of Athens, Greece. The spectra were excited at room temperature with the 785 nm (near-infrared) excitation wavelength of a diode laser, in the spectral range 100 cm^{-1}–4000 cm^{-1}. The light was scattered by a diffraction grating with 1800 lines/mm. The laser beam was focused on the samples by means of a ×100 short working distance objective under a Leica microscope. The laser spot on the surface had a diameter of ~1 μm and a power of 4 mW. Wavenumber calibration was checked periodically by measuring the LO phonon mode at 521 cm^{-1} of an internal silicon reference standard. An exposure time of 20 s and 2 accumulation cycles for each spectrum were applied. Attention should be paid to the laser power used to excite the Raman spectra of the MPs, as some of them are very temperature-sensitive, and a laser beam with high radiant energy can lead to their degradation during Raman analysis. The spectra were processed with the software WIRE 3.4. The peaks were assigned by comparing the Raman peaks with reference values from the literature.

3. Results

Table 2 shows the chemical analyses and the saturation indices of all water samples. All groundwater samples, with the exception of GW4, originate from the developed shallow unconfined aquifer system in Quaternary sediments. The water depth of this aquifer system is less than 8 m for all water wells. The borehole from which sample GW4 was taken also exploits this aquifer at a depth of 70 m.

Table 2. Analyzed physical and chemical parameters of the investigated water samples in the Erasinos basin.

Sample ID	pH	TDS	E.C.	Temp	Na^+	K^+	Ca^{2+}	Mg^{2+}	Cl^-	HCO_3^-	NO_3^-	Si	SO_4^{2-}	PO_4^{3-}
		mg/L	μS/cm	°C	mg/L	mg/L	mg/L	mg/L	mg/L	mg/L	mg/L	mg/L	mg/L	mg/L
SW1	7.4	1126	1732	21	99.3	4	136	39.4	212.8	366	31.7	10.7	120	0.034
GW5	7.4	1807	2780	22.6	346	3.4	208.8	74.2	531.9	317.2	72.2	6	470	0.14
SW2	8.1	35,750	55,000	20	10,300	420	435.2	1393.6	12,198.6	170.8	11	0.8	2640	0.055
SW3	7.8	1251	1925	22	206.6	5	147.2	81.4	425.5	396.5	31.2	10.3	162.5	0.145
SW4	7.8	11,440	17,600	21	208	70	227.2	506.6	6241.1	549	22	8.1	195.5	0.13
SW5	7.7	965	1485	24.8	93.3	3.2	116.8	43.7	248.2	329.4	36.1	9.8	43.8	0.069
GW6	7.4	1043	1605	22.5	95.1	4	142.4	47.7	283.7	347.7	40.5	10.5	115	0.11
GW7	7.3	1040	1600	22	101	3.8	123.2	69.1	319.2	427	16.7	8.9	72.5	0.07
GW8	7.9	917	1410	21.5	86.6	6.4	120	39.3	248.2	384.3	12.3	9.5	17.5	0.935
GW9	7.1	1339	2060	21.2	114	3.6	174.4	57.5	372.3	366	61.2	13.1	125	0.14
GW10	6.9	1411	2170	24	122	2.2	209.6	53.2	407.8	396.5	48	9.9	87.5	0.07
GW11	7.5	897	1380	25	91.6	4.2	123.2	66.7	319.2	372.1	36.5	8	50	0.155

As shown in Table 3, the pH values range from 6.9 to 8.1; the water samples are characterized as neutral to alkaline, and the electrical conductivity (E.C.) values range from 1380 to 55,000 μS/cm. The measurements of major ions show strong fluctuations in the Erasinos basin. The concentration of Ca^{2+} ranges from 116.8 to 435.2 mg/L, of Mg^{2+} from 39.3 to 1393.6 mg/L, of K^+ from 2.2 to 420 mg/L, of Na^+ from 91.6 to 10,300 mg/L, of Cl^- from 212.8 to 12,198 mg/L, and of NO^{3-} from 11 to 72.2 mg/L. All saturation indices are oversaturated except for the sample SW2, in which the SI for quartz is undersaturated.

Table 3. Calculated saturation indices of the investigated water samples in the Erasinos basin.

Sample ID	SI (Calcite)	SI (Dolomite)	SI (Quartz)
SW1	0.45	0.66	0.62
GW5	0.49	0.84	0.35
SW2	0.71	2.25	−0.42
SW3	0.87	1.8	0.59
SW4	0.94	2.55	0.52
SW5	0.7	1.32	0.52
GW6	0.46	0.77	0.59
GW7	0.39	0.85	0.53
GW8	0.93	1.68	0.56
GW9	0.19	0.2	0.71
GW10	0.13	0.01	0.55
GW11	0.6	1.28	0.44

Table 4 displays the number of particles identified in the sixteen samples. A total of 3399 particles were identified in all sixteen samples. The mean value is 212.5 particles per liter of water. The highest value (513 particles/L) was found in an uncapped well (GW5), while the lowest value (16 particles/L) was found in the borehole sample (GW4), indicating that potential airborne microplastic pollution should be considered and quantified in future work. Specifically, 2008 MPs particles were detected in the 11 groundwater samples, with a mean value of 182.5 MPs/L. On the other hand, the surface water samples showed a higher microplastic accumulation, with a mean value of 278.2 MPs/L. The closer we get to the banks of the Erasinos River (SW4), the more microplastics were detected, indicating that pollution is accumulating throughout the catchment area. The predominant visual category was F, with a total number of more than 2500 particles. The microplastic particles in the form of fibers and fragments were predominantly blue in color.

Table 4. Number of MPs particles/L per category identified in the investigated water samples in the Erasinos basin.

Category/Samples No of MPs Particles/L	A	B	C	D	E	F	G	H	Total
SW1 (MPs particles/L)	26	7	2	4	2	89	0	40	170
GW5 (MPs particles/L)	11	4	3	10	1	458	0	26	513
SW2 (MPs particles/L)	16	6	7	7	3	347	1	16	403
SW3 (MPs particles/L)	14	2	2	7	0	166	1	15	207
SW4 (MPs particles/L)	27	7	7	44	12	303	13	72	485
SW5 (MPs particles/L)	3	0	3	8	1	95	0	16	126
GW6 (MPs particles/L)	17	5	4	16	0	220	0	18	280
GW7 (MPs particles/L)	8	2	2	7	0	29	1	8	57
GW8 (MPs particles/L)	12	1	1	5	3	229	0	13	264
GW9 (MPs particles/L)	13	0	5	8	20	362	2	21	431
GW10 (MPs particles/L)	9	2	2	8	3	77	0	11	112
GW11 (MPs particles/L)	11	1	1	5	2	128	0	9	157
GW1 (MPs particles/L)	17	1	0	2	3	31	4	9	67
GW2 (MPs particles/L)	18	0	3	6	2	36	0	5	70
GW3 (MPs particles/L)	1	0	0	2	0	37	0	1	41
GW4 (MPs particles/L)	4	0	0	0	0	5	6	1	16
Total per category	207	38	42	139	52	2612	28	281	3399

3.1. Visual Presorting

Microplastics were classified into eight categories based on their color, texture, size, reflectivity, shape, and general morphological features (Figure 3). These categories are described below:

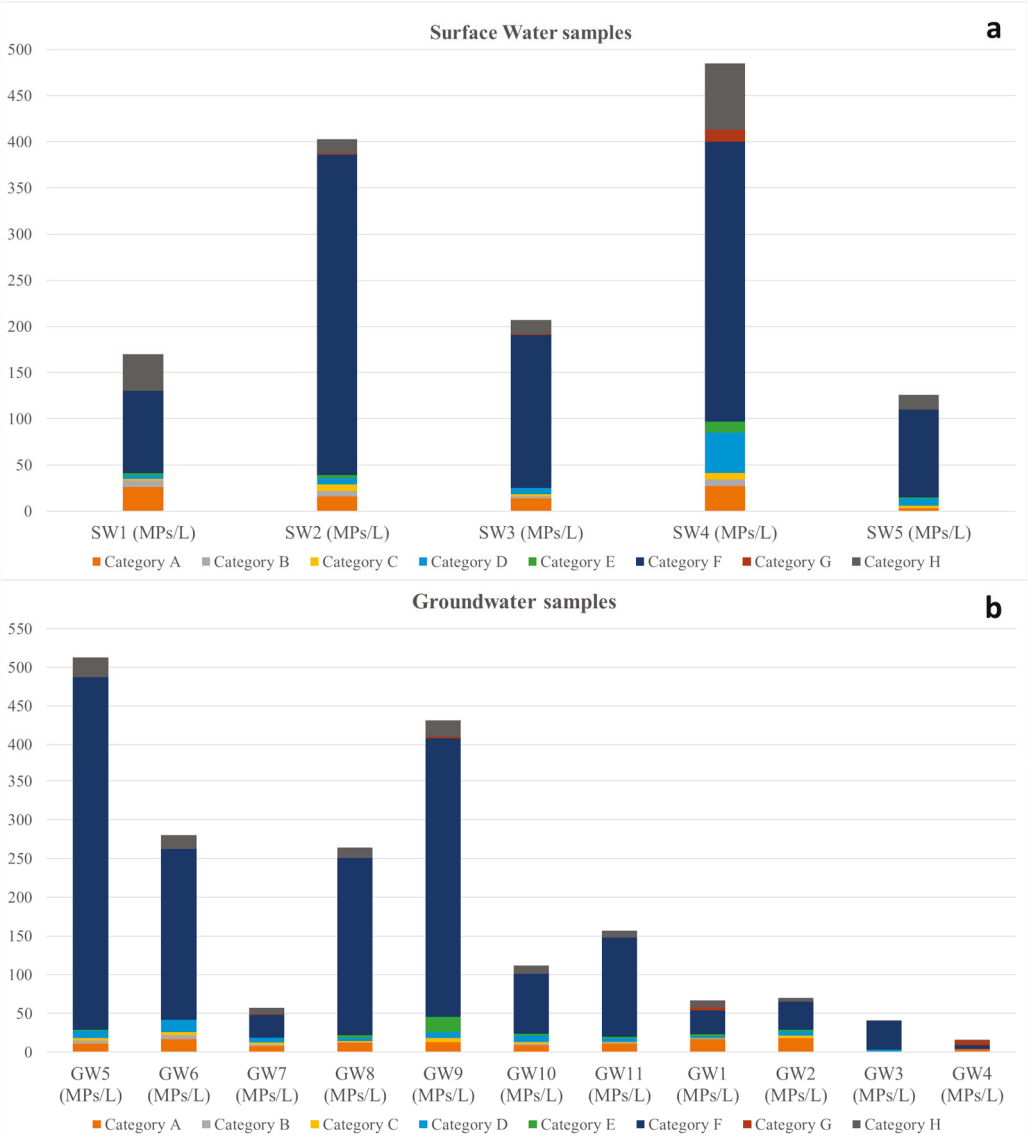

Figure 3. (**a**) MPs/L/Surface water, (**b**) MPs/L/Groundwater.

Category A: Blue–colored fibers with a length of >150 µm, characterized mostly by uniform coloring throughout their length and a fairly stable thickness (minor or no thickness differentiations along strike). Some of them may have scissor-tailed tips.

Category B: Light blue–/azure fibers. All other characteristics are similar to category A.

Category C: Reddish–colored fibers. All other characteristics are similar to category A.

Category D: Blue–colored particles. Their color ranges from light blue, turquoise, and cyan to dark blue. Their size >30 µm and their shape is characterized as angular, irregular, and in a few cases as needle-shaped. Their color is uniform throughout their length, except for some needle-shaped particles where local discoloration can be observed.

Category E: Red-to-orange particles and granules. Their color is uniform throughout their length, their size >25 µm and their shape ranges from irregular, angular to rounded.

Category F: White–/whitish-gray particles and granules. Their coloring ranges from pale yellow, beige, whitish, and white to gray and their size >20 µm. Their shape is characterized as irregular, angular up to medium/half-rounded. Gray-colored particles tend to be transparent.

Category G: Highly reflective particles. They are highly reflective in a vertical light source, but if the light source forms an angle with the particles, then they are either low- or non-reflective. Their size >40 μm, and their shape is characterized as irregular and angular.

Category H: Blue–colored fibers, but different from category A. Their color varies from light blue, blue, dark blue, up to black. Their size is mostly >140 μm. Their morphological features and texture differ significantly from category A fibers, since they are characterized by heterogeneity in shape, texture, and thickness.

3.2. Raman Spectroscopy

Considering that most of the samples contained particles of each visual category, four randomly selected samples (three well samples and one borehole sample) covering most of the Erasinos catchment were subjected to μ-Raman analysis.

The 194 microplastics from each sample and category were analyzed using RS; RS analysis showed that each visual category was indicative of microplastics. In total, four different types of MPs were identified in the four samples based on their characteristic Raman peaks, namely, polyethylene (PE), polypropylene (PP), polystyrene (PS), and polyethylene terephthalate (PET) (Table 5, Figures 4–7). In general, the peaks in the spectral range 2780–2980 cm^{-1} of the Raman spectra of MPs correspond to the stretching vibrations of $CH/CH_2/CH_3$ groups; in the spectral range 1580–1640 cm^{-1}, to the aromatic bending vibrations, and in the spectral range 709–759 cm^{-1}, to the symmetric stretching vibrations of CF_2 [15,33]. In total, four different types of MPs polymers can be identified by their Raman peaks in these three spectral regions. In detail:

Polyethylene (PE) was identified in three samples (GW1, GW2, GW4), mainly by the two intense peaks at ~2850 and 2885 cm^{-1} corresponding to CH_2 stretching vibrations. Moreover, the antisymmetric and symmetric stretching vibrations of C–C at ~1062 cm^{-1} and 1129 cm^{-1}, respectively, and the bending vibrations of CH_2 at 1296 and 1440 cm^{-1}, were clearly visible in the Raman spectra of PE. The weak peak at ~2725 cm^{-1} is an overtone of wavenumbers in the range 1400–1495 cm^{-1} ($–CH_2^-$ bonds). In the spectral region below 1000 cm^{-1}, stretching and bending vibrations of C–C are expected, possibly together with CH_2 twisting and rocking vibrations of methylene units in a Gauche relation. A typical spectrum of PE is shown in Figure 4a. In Figure 4b,c, in addition to the bands of PE (at ~1062, 1129, 1296, 1417, 1440, 1460, 2725, 2850, and 2885 cm^{-1}), bands appear at ~483, 678, 746, 955, 1145, and 1530 cm^{-1}. These bands are attributed to the blue pigment copper phthalocyanine (Pigment Blue 15, IRUG collection #ROD00126 [34]), which is often used to color plastics and is consistent with the blue color of these MPs. Polyethylene was identified in samples GW1, GW2, and GW4 (40% of the total Raman analyses) mainly in category A, followed by D, B, and E.

Isotactic polypropylene (iPP) was found in three samples (GW1, GW2, and GW3, 35%). It is characterized by intense peaks at 396 cm^{-1} attributed to CH_2 wagging and CH bending, at ~809 cm^{-1} corresponding to the rocking vibrations of CH_2 and stretching vibrations of C–C and C–CH_3, at 841 cm^{-1} due to the rocking of CH_2 and CH_3 and the stretching of C–C and C–CH_3, at 973 cm^{-1} assigned to CH_3 rocking and C–C stretching, at 1153 cm^{-1} resulting by stretching vibrations of C–C and C–CH_3, bending vibrations of CH, and rocking vibrations of CH, at 1330 cm^{-1} attributed to bending vibrations of CH, at 1360 cm^{-1} due to the symmetric bending of CH_3 and CH bending, and at 1460 cm^{-1} due to the asymmetric bending of CH_3 and CH_2 bending (Figure 5b,c). The peaks of CH_2 stretching vibrations between 2800 and 3000 cm^{-1} were relatively weak in some spectra, and a broad and strong band was also observed in the range of 2100–2200 cm^{-1}. In Figure 5b,c, additional peaks at ~682, 750, and 1532 cm^{-1} are assigned to the pigment copper phthalocyanine (Pigment Blue 15, IRUG collection #ROD00126 [34]); this is consistent with the blue color of these two microplastic particles.

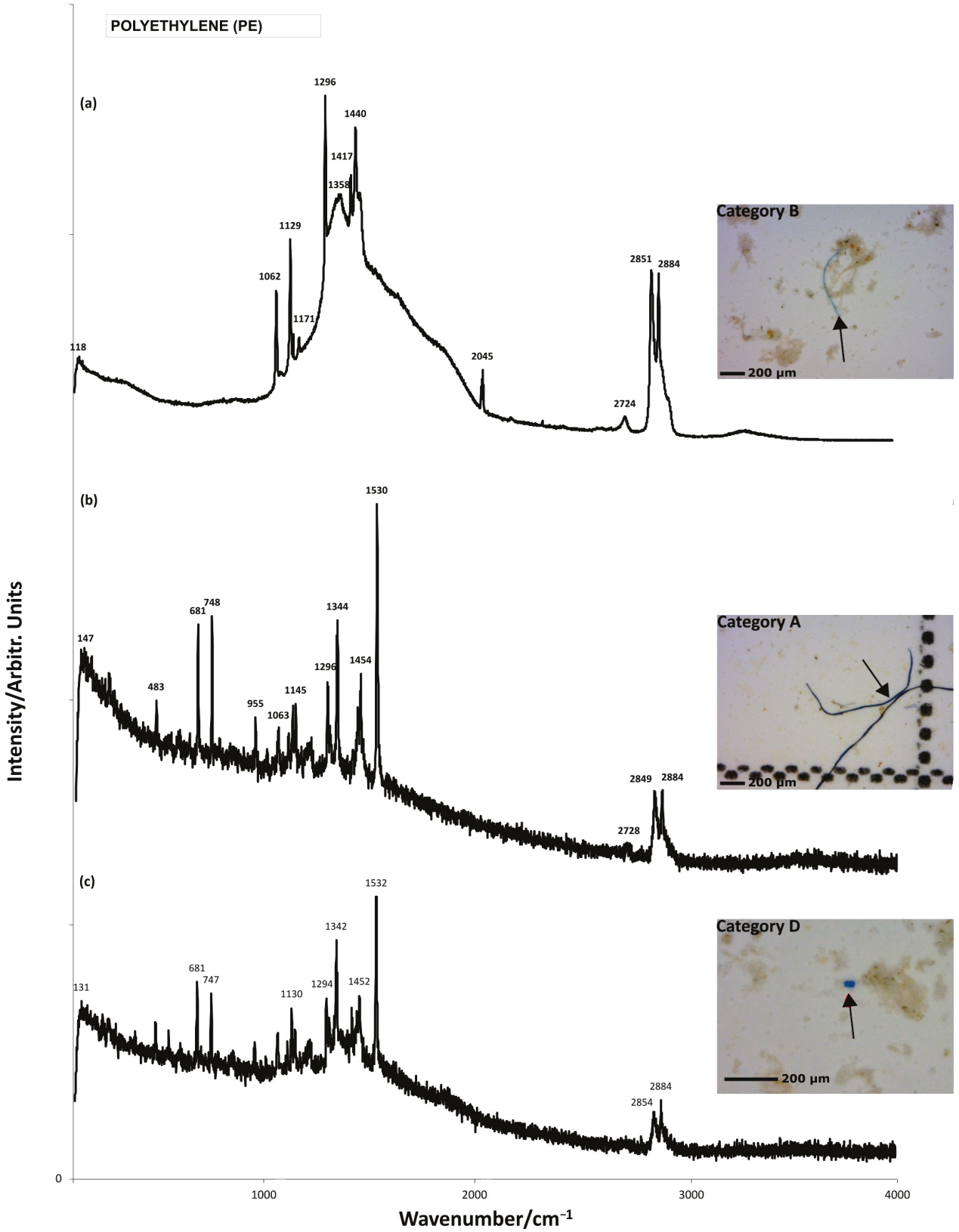

Figure 4. (**a**–**c**) Raman spectra of polyethylene-type MPs, found in the studied samples. The black arrow on the inset shows the analyzed MP. In (**b**,**c**) additional peaks at ~682, 750, and 1532 cm^{-1} are assigned to the pigment copper phthalocyanine (Pigment Blue 15, IRUG collection #ROD00126 [34]).

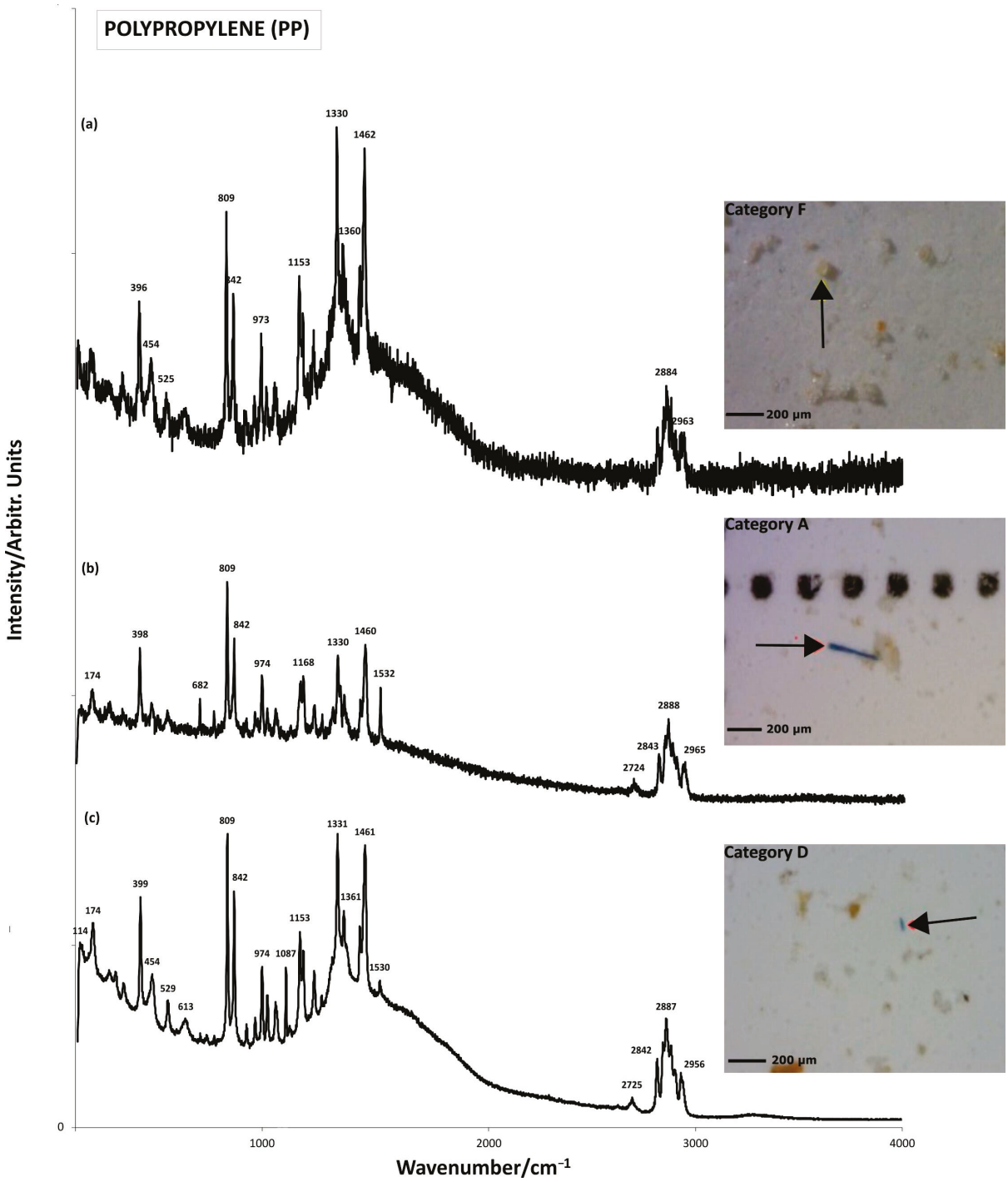

Figure 5. (**a**–**c**) Raman spectra of polypropylene-type MPs, found in the studied samples. The black arrow on the inset shows the analyzed MP.

Polyethylene terephthalate (PET) was identified in all samples studied (25%), mainly in category F, followed by D and G. The peak at approximately 1100 cm^{-1} corresponds to C–O and C–C stretching or C–O–C bending. A shoulder at about 1120 cm^{-1} indicates an amorphous phase. The peak at ~1615 cm^{-1} is due to the C-C ring of phenyl, and the peak at ~1730 cm^{-1} is assigned to the stretching vibrations of C=O. Between 2800 and 3000 cm^{-1}, the peaks of CH_2 stretching vibrations arise (Figure 6). The peak at 817 cm^{-1} in Figure 6b is attributed to C−H out-of-plane bending vibrations in para-xylene (p-xylene) [35,36].

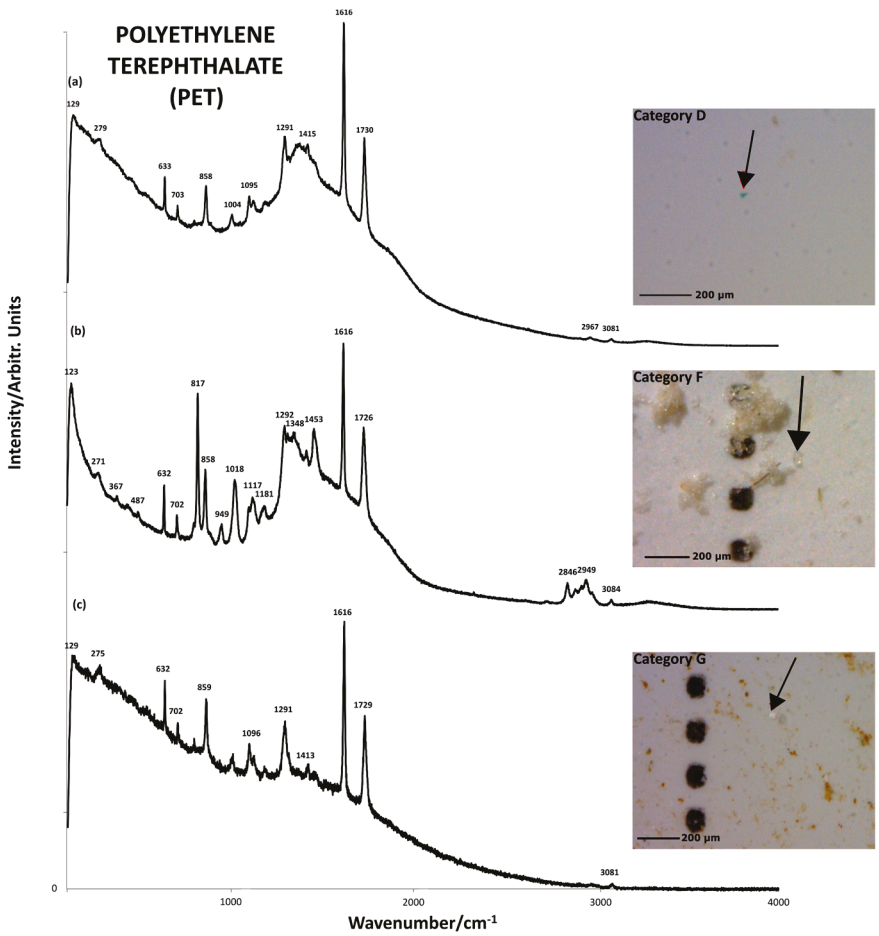

Figure 6. (**a**–**c**) Raman spectra of polyethylene terephthalate-type MPs, found in the studied samples. The black arrow on the inset shows the analyzed MP.

Polystyrene (PS), identified only in sample GW1 (10%), provided intense Raman peaks at 1002 cm^{-1}, corresponding to C–C symmetric stretching vibrations (Figure 7). Other characteristic PS bands were observed at ~621, 797, 1033, 1157, 1450, and 1604 cm^{-1}, corresponding to the ν_{6b} radial ring-stretching mode, ν_1 symmetric ring-stretching mode, ν_{18a} tangential C–H bending mode, ν_{15} mode, ν_{19b} stretching or CH_2 bending vibrations, and ν_{12} C–C stretching mode, respectively [37,38]. Overlapping bands at 3060 cm^{-1} appear due to the C–H bonds stretching on the benzene ring.

Finally, some blue fibers analyzed yielded the Raman spectrum of the pigment indigo blue (250, 545, 599, 1310, 1228, 1575, and 1584 cm^{-1} [39]. Due to the high background of these spectra, it was not possible to identify the substrate of the pigment.

Raman spectroscopy on microparticles in the groundwater samples investigated also revealed the presence of inorganic mineral phases, mainly carbonates (calcite, dolomite) and quartz.

By combining the results of virtual sorting and Raman microspectroscopy, we found the following:

Polyethylene (PE) was found mainly in the form of dark and light blue fibers >150 µm long (visual categories A and B). A limited number of blue angular, irregular, and in a few cases acicular particles with a size of >30 µm (visual category D), and very rare red-to-orange particles and granules with a size of >25 µm, were also identified as PE.

Polypropylene (PP) was found mainly in the form of blue fibers >150 µm long (visual category A). Angular, irregular particles of a blue (visual category D) and whitish-gray (visual category E) color sized >25 µm were also identified as PP.

Polyethylene terephthalate (PET) was found mainly as irregular, angular-to-medium/semi-rounded particles and granules of a color ranging from pale yellow, beige, whitish, and white to gray and of a size of >20 μm (visual category F). A few angular, irregular particles of a blue color (visual category D) and a limited number of highly reflective angular, irregular particles in vertical reflected light (visual category G) were also identified as PET.

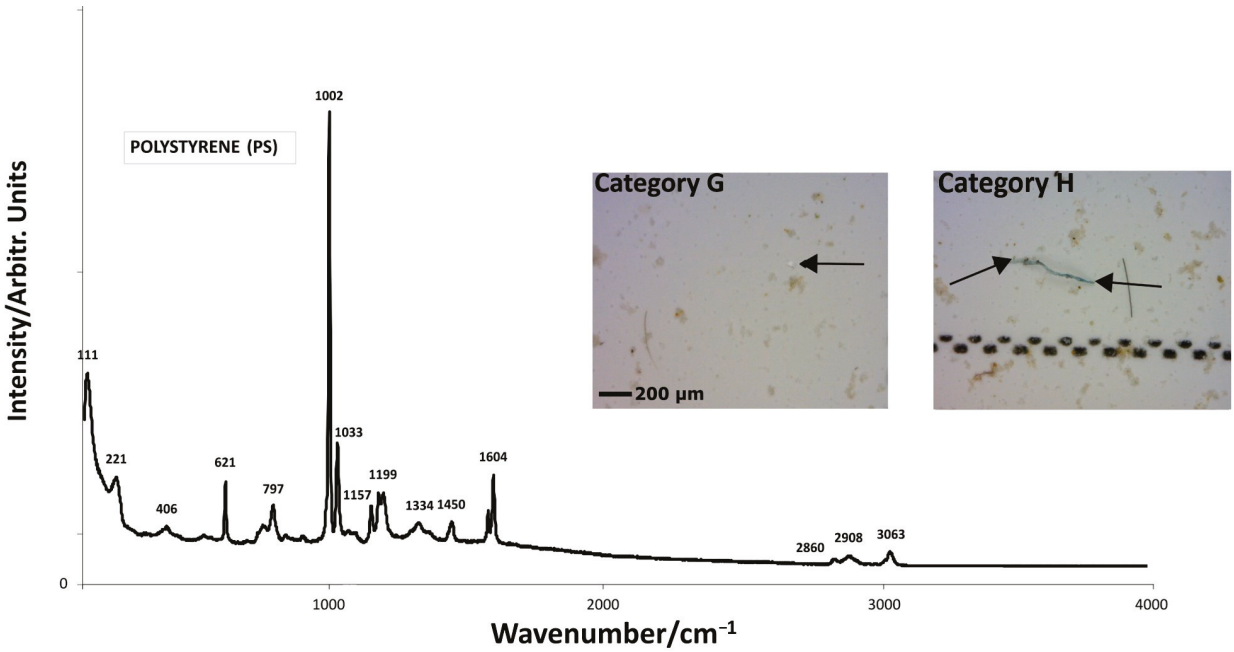

Figure 7. Raman spectra of polystyrene MPs, found in the studied samples. The black arrow on the inset shows the analyzed MP.

A very limited number of PS MPs were identified as highly reflective irregular, angular particles (visual category G) and blue–colored fibers characterized by a high heterogeneity in shape, texture, and thickness (visual category H).

Table 5. Identified polymer types in the studied samples based on their Raman peaks.

Polymer Types	Polymer Formula	Raman Peaks (cm^{-1})	Sample	Visual Categories
PE	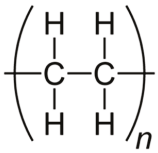 $(C_2H_4)_n$	1062_s (ν_{as}C–C) [40–42] ~1129_s (ν_sC–C) [40–42] 1296_s (τCH_2) [40–42] ~1417_m (ωCH_2) [42] ~1440_s (δCH_2) [40,41] 1512_w (δCH_2) [40,41] ~2850 ($\nu_s CH_2$) [43,44] ~2884_s ($\nu_{as} CH_2$) [43,44] 396_s (ωCH2,δCH) [45,46]	GW1, GW2, GW4	A,B,D,E
PP	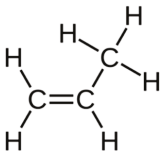 $(C_3H_6)_n$	809_{vs} (ρCH_2, vCC, vC–CH_3 [42,45,46] 841_s (pCH_2, vCC_b, vC–CH_3, pCH_3) [45,46] 973_m (ρCH_3 + vC–C chain) [45,46] 1153_s (vCC_b, vC–CH_3, δCH, pCH_3) [45,46] ~1330_s (δCH) [45,46] ~1460_s (δCH_3) [45,46] ~2842_m(νCH_2) [43,44] 2860_m(νCH_2) [43,44] ~2885_s ($\nu_s CH_3$) [43,44] 2954-2963_m ($\nu_a CH_3$) [43,44]	GW1, GW2, GW3	A,C,D,F

Table 5. *Cont.*

Polymer Types	Polymer Formula	Raman Peaks (cm^{-1})	Sample	Visual Categories
PS	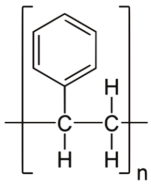 $(C_8H_8)_n$	621s (νC–C) [37,38] 797m ($ν_s$C–C) [37,38] 1002_s (νC–C) [45] 1033 (δC–H) [37] 1157_w (ν15 mode) [37] 1450_w [ν19b or δ(CH2)] [37] 1604_m ($ν_s$C–C) [37] 2860_w ($ν_s CH_2$) [42] 2908_w ($ν_{as} CH_2$) [42] 3063_w (νC–H) [42]	GW1	G,H
PET	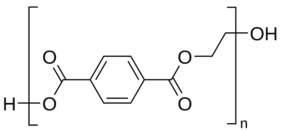 $(C_{10}H_8O_4)_n$	860_s ($ρCH_2$) 1097_m (νC–O, νC–C, δC–O–C) [47] $1612\text{-}1617_s$ (C–C ring of phenyl) [43,47] $1726\text{-}1730_s$ (νC=O) [47] 2850_w,m ($νCH_2$) [43,47] 2883_w,m ($νCH_2$) [43,47] 3081_w (C–H of phenyl) [43,47]	GW1, GW2, GW3, GW4	D,F,G

4. Discussion

In view of the above, visual presorting, while a very time-consuming method, does not provide an unambiguous identification of the type of MPs in a sample; the latter is only possible with the use of a microspectroscopy method such as RS. However, visual presorting is faster in quantifying the total number of MPs in a sample. Future challenges in this field include the use of Raman hyperspectral mapping on filters aiming not only the identification but also the quantification of MPs, and/or the in situ identification of MPs with portable Raman microspectrometers.

Polyethylene and PP were the most abundant MPs in the samples studied. This is consistent with the fact that these two plastic polymers are the most commonly produced in the world and are therefore frequently found in relevant studies, especially in the marine environment (e.g., [48]).

Although one might attribute the abundance of blue MPs in the studied samples to possibly biased visual presorting, this could be explained by the faster photoaging of blue plastics compared to red or yellow plastics. As stated by Zhao et al. [6] in the visible light region, red or yellow pigments with longer wavelengths may absorb short-wave light with higher energy, while blue pigments absorb long-wavelength light with lower energy. The corresponding light energy transmitted to the blue plastic is consequently higher than that transmitted to red or yellow plastics, which makes the photoaging more intense. Because blue plastics cannot absorb UV light effectively, they age faster when exposed to sunlight, and higher levels of bluish microplastics are often found in the environment, especially in the smallest sizes [49].

Copper phthalocyanine (Pigment Blue 15), a common blue pigment used for dyeing plastics (e.g., [50]), was identified in both PP and PE MPs. In general, the MPs in the form of blue-colored fibers mainly correspond to either PP or PE and, less frequently, PS. Overall, RS confirmed that all identified particles were indeed MPs. Even though MPs are visually similar and belong to the same optical categories, RS has shown that they can differ in nature. Nevertheless, there is a trend that separates PP and PE, in one visual group (A, B, D), from PS and PET, which are part of another visual group (G, H, E). This trend needs further research.

Samples SW2 and SW4 are the only samples that have MPs from all eight categories, while GW4 has the least number of MPs and fewer categories. This was to be expected, as samples SW2 and SW4 were collected from surface water which is (a) generally more contaminated due to its proximity to human activities that generate MPs and (b) exposed to the atmosphere, so that MPs can also be enriched by air. Furthermore, it is very important to mention that they were collected at the estuary of Erasinos (SW4) and at the sea, where

the river flows in and has accumulated MPs from the entire catchment area. This is also justified by the fact that more MPs were detected in samples SW1, GW5, SW2, SW3, SW4, SW5, GW6, GW7, GW8, GW9, GW10, and GW11, collected downstream, than in samples GW1, GW2, GW3, and GW4, which were collected further upstream of the catchment. Comparing the results in Figure 3, it can be assumed that surface water is generally more susceptible to MP contamination than groundwater, as on average, more MP particles/L of water samples were detected. On the other hand, it is interesting to note that MPs, and in particular PET and PE, were detected in the sample from the water borehole, suggesting that MPs can migrate to greater depths through water infiltration. Another alternative scenario for tracing MPs at greater water depths would be the possibility of waste injection through other boreholes.

The role of inorganic mineral phases such as carbonates and quartz in connection with microplastics needs further investigation in the future. Column experiments have shown that the presence of iron and manganese oxides, as well as calcite, not only changes the transport behavior of plastics, but can also shield plastics from UV light (e.g., [51,52]). In this context, it was investigated whether the groundwater tends to dissolve or precipitate the minerals calcite, dolomite, and quartz in particular. The positive SI value of these minerals indicates that the water is oversaturated in relation to the solution, which leads to the precipitation of these minerals. These mineral phases were also identified by Raman analyses, which confirmed their precipitation. Saturation-induced precipitation leads to the formation of small crystals on the surface of MPs.

A major challenge for researchers is the mechanism of how microplastics migrate through the vadose zone into the saturated zone and how they contaminate groundwater. The hydrogeological conditions of a region appear to play a key role in the transport of microplastics via different pathways. The most important hydrogeological factors that have recently been suggested to influence the distribution and migration of microplastics in groundwater are as follows [53–55]: (a) the permeability and porosity of an aquifer, which favor the size of microplastics that can migrate into groundwater, (b) the recharge of the aquifer by surface runoff, (c) the structure of the vadose zone, (d) the seasonal periods of recharge, (e) the hydraulic conductivity of an aquifer, (f) the water–soil interaction, (g) the groundwater velocity, (h) the lateral hydraulic connection between aquifers or the intrusion of seawater, and (i) the water depth. Another important factor for the migration of microplastics into groundwater is the type of sources, i.e, diffuse linear sources (torrents, rivers, streams) or point sources (spills, etc.), as well as the land cover of an area [56]. However, the extent to which these individual factors influence the migration of MPs and their interactions is an open field for future research.

The physico-chemical properties of the analyzed water samples (surface and groundwater) indicate the decisive role of anthropogenic activities in the area. According to Wang et al. [57], the pH of water could theoretically influence the sorption of ionic chemicals by MPs. The high values of E.C., Ca^{2+}, Mg^{2+}, Cl^{-}, and Na^{+} indicate the intrusion of seawater into the coastal area of the Erasinos basin due to the overexploitation of aquifers for irrigation. Agricultural activities are also a potential source of microplastics in surface and groundwater, mainly due to plastic bottles and the plastic in greenhouses. Agricultural activities in the study area were confirmed by the high NO_3^{-} and PO_4^{3-} concentrations depicted in Table 2. In addition, major anions and cations are abundant in the groundwater environment [19]. It is hypothesized that the increased concentrations of Ca^{2+} forms increase the number of adsorption sites and enhance the adsorption of microplastics in the media. In contrast, it is assumed that the influence of increased concentrations of HCO_3^{-} and SO_4^{2-}, in the water solution reduces the adsorption of MPs on the surface of the aquifers [19]. Monitoring the chemical properties of groundwater, in conjunction with the quantification and identification of MPs, will provide sufficient results when considering the correlation between chemical parameters and the presence of MPs. The latter may facilitate tracing the influence of different sources of MPs among the samples. This study

can contribute to future databases that may correlate the presence of certain MPs with specific sources and environments supported by the geochemical analyses.

In the Erasinos basin, groundwater recharge from seepage of the Erasinos River and other surface runoff (torrents, rivers, streams) could potentially enhance the migration of MPs to the saturated zone. As seawater infiltrates into the nearshore part of the basin, there is a hydraulic connection between the aquifer system and the sea, which could represent an additional source of MPs.

This study is the first systematic work on MPs in groundwater in Attica, Greece, and one of the few worldwide [58–60] that have recently investigated the presence and transport of microplastics in groundwater. The results indicate that the investigation of microplastics in other aquifers needs to be expanded in order to monitor the extent of contamination and trace the sources where possible. As groundwater is in many cases not only used for irrigation but also as drinking water, it is of great importance and relevant for public health to investigate the occurrence of microplastics more systematically.

The concentrations of MPs are not stable and standardized in a region and vary due to the geomorphological characteristics, hydrogeological conditions, atmospheric conditions, and land use of each area, since they define the MPs sources. For example, the amount of MPs in shallow aquifers close to industrial and agricultural activities can be as high as 6832 MP particles/L [61]. In contrast, an average of 6.4 particles/L [53] was observed in karstic aquifers with low anthropogenic activities. In our study area, the high amount of microplastics (3399 particles/ per 16 Liters) is related to the intensive anthropogenic activities (agricultural, industrial, and urban) in this area, combined with the shallow aquifer.

5. Conclusions

In this work, we have investigated and documented for the first time the occurrence of MPs in groundwater in shallow and deep aquifers in Attica, Greece. Based on our results, the following conclusions can be drawn:

- The characterization of MPs by Raman microspectroscopy revealed the presence of the following:
  a. PE and PP in the form of fibers and fragments;
  b. PET as angular irregular particles;
  c. PS as reflective irregular angular particles and blue-colored fibers.
- Microplastics are more prevalent in shallow aquifers, as expected, reaching up to 513 MPs/L. In the deeper aquifers (water table ~70 m), the abundance of MPs is lower (up to 16 MPs/L); however, this is no less significant, as it may indicate that MPs are able to migrate to greater depths through water infiltration.
- The types of MPs appear to vary due to different land use and the vulnerability of groundwater systems. A high amount of microplastics (3399 particles/ per 16 Liters) was found where intensive anthropogenic activities (agricultural, industrial, and urban) take place.
- The mechanism of MPs admission into the deep (water table ~70 m) aquifer needs further investigation. Seawater intrusion, which is reflected in the qualitative characteristics of groundwater, could potentially be a source of microplastics. The extent at which seawater MP contamination interacts with other potential sources such as agricultural activities requires further in-depth geochemical investigations, to document the correlation between MPs and key chemical parameters.

This study can contribute to future databases that, supported by geochemical analyses, will link the presence of MPs to specific sources and environments.

Author Contributions: Conceptualization, M.P., E.V. and I.P.; methodology, M.P., E.V. and I.P.; resources: P.M., E.V., C.S., I.P. and G.S.; investigation, all; data curation, P.M., V.S. and C.S.; writing—original draft preparation, M.P. and V.S.; writing—review and editing, all; supervision, M.P., E.V. and I.P. All authors have read and agreed to the published version of the manuscript.

Funding: This research received no external funding.

Data Availability Statement: Data are contained within the article.

Conflicts of Interest: The authors declare no conflicts of interest.

References

1. Cowger, W.; Gray, A.; Christiansen, S.H.; DeFrond, H.; Deshpande, A.D.; Hemabessiere, L.; Lee, E.; Mill, L.; Munno, K.; Ossmann, B.E.; et al. Critical Review of Processing and Classification Techniques for Images and Spectra in Microplastic Research. *Appl. Spectrosc.* **2020**, *74*, 989–1010. [CrossRef] [PubMed]
2. Silva, A.B.; Bastos, A.S.; Justino, C.I.L.; da Costa, J.P.; Duarte, A.C.; Rocha-Santos, T.A.P. Microplastics in the Environment: Challenges in Analytical Chemistry—A Review. *Anal. Chim. Acta* **2018**, *1017*, 1–19. [CrossRef] [PubMed]
3. Arthur, C.; Baker, J.E.; Bamford, H.A. NOAA Technical Memorandum NOS-OR&R-30. In Proceedings of the International Research Workshop on the Occurrence, Effects, and Fate of Microplastic Marine Debris, University of Washington Tacoma, Tacoma, WA, USA, 9–11 September 2008.
4. Ziani, K.; Ioniță-Mîndrican, C.-B.; Mititelu, M.; Neacșu, S.M.; Negrei, C.; Moroșan, E.; Drăgănescu, D.; Preda, O.-T. Microplastics: A Real Global Threat for Environment and Food Safety: A State of the Art Review. *Nutrients* **2023**, *15*, 617. [CrossRef]
5. An, L.; Liu, Q.; Deng, Y.; Wu, W.; Gao, Y.; Ling, W. Sources of Microplastic in the Environment. In *Microplastics in Terrestrial Environments: Emerging Contaminants and Major Challenges*; He, D., Luo, Y., Eds.; The Handbook of Environmental Chemistry; Springer International Publishing: Cham, Switzerland, 2020; pp. 143–159. [CrossRef]
6. Zhao, X.; Wang, J.; Yee Leung, K.M.; Wu, F. Color: An Important but Overlooked Factor for Plastic Photoaging and Microplastic Formation. *Environ. Sci. Technol.* **2022**, *56*, 9161–9163. [CrossRef]
7. Suaria, G.; Avio, C.G.; Mineo, A.; Lattin, G.L.; Magaldi, M.G.; Belmonte, G.; Moore, C.J.; Regoli, F.; Aliani, S. The Mediterranean Plastic Soup: Synthetic Polymers in Mediterranean Surface Waters. *Sci. Rep.* **2016**, *6*, 37551. [CrossRef]
8. Isobe, A.; Iwasaki, S.; Uchida, K.; Tokai, T. Abundance of Non-Conservative Microplastics in the Upper Ocean from 1957 to 2066. *Nat. Commun.* **2019**, *10*, 417. [CrossRef]
9. Peeken, I.; Primpke, S.; Beyer, B.; Gütermann, J.; Katlein, C.; Krumpen, T.; Bergmann, M.; Hehemann, L.; Gerdts, G. Arctic Sea Ice Is an Important Temporal Sink and Means of Transport for Microplastic. *Nat. Commun.* **2018**, *9*, 1505. [CrossRef]
10. González-Pleiter, M.; Velázquez, D.; Edo, C.; Carretero, O.; Gago, J.; Baron-Sola, Á.; Hernández, L.E.; Yousef, I.; Quesada, A.; Leganés, F.; et al. Fibers Spreading Worldwide: Microplastics and Other Anthropogenic Litter in an Arctic Freshwater Lake. *Sci. Total Environ.* **2020**, *722*, 137904. [CrossRef]
11. Nguyen, N.B.; Kim, M.-K.; Le, Q.T.; Ngo, D.N.; Zoh, K.-D.; Joo, S.-W. Spectroscopic Analysis of Microplastic Contaminants in an Urban Wastewater Treatment Plant from Seoul, South Korea. *Chemosphere* **2021**, *263*, 127812. [CrossRef]
12. Hidalgo-Ruz, V.; Gutow, L.; Thompson, R.C.; Thiel, M. Microplastics in the Marine Environment: A Review of the Methods Used for Identification and Quantification. *Environ. Sci. Technol.* **2012**, *46*, 3060–3075. [CrossRef] [PubMed]
13. Shan, J.; Zhao, J.; Liu, L.; Zhang, Y.; Wang, X.; Wu, F. A Novel Way to Rapidly Monitor Microplastics in Soil by Hyperspectral Imaging Technology and Chemometrics. *Environ. Pollut.* **2018**, *238*, 121–129. [CrossRef] [PubMed]
14. Fu, W.; Min, J.; Jiang, W.; Li, Y.; Zhang, W. Separation, Characterization and Identification of Microplastics and Nanoplastics in the Environment. *Sci. Total Environ.* **2020**, *721*, 137561. [CrossRef] [PubMed]
15. Käppler, A.; Fischer, D.; Oberbeckmann, S.; Schernewski, G.; Labrenz, M.; Eichhorn, K.-J.; Voit, B. Analysis of Environmental Microplastics by Vibrational Microspectroscopy: FTIR, Raman or Both? *Anal. Bioanal. Chem.* **2016**, *408*, 8377–8391. [CrossRef]
16. Käppler, A.; Windrich, F.; Löder, M.G.J.; Malanin, M.; Fischer, D.; Labrenz, M.; Eichhorn, K.-J.; Voit, B. Identification of Microplastics by FTIR and Raman Microscopy: A Novel Silicon Filter Substrate Opens the Important Spectral Range below 1300 Cm^{-1} for FTIR Transmission Measurements. *Anal. Bioanal. Chem.* **2015**, *407*, 6791–6801. [CrossRef]
17. Lee, J.-Y.; Cha, J.; Ha, K.; Viaroli, S. Microplastic Pollution in Groundwater: A Systematic Review. *Environ. Pollut. Bioavailab.* **2024**, *36*, 2299545. [CrossRef]
18. Ma, H.; Chao, L.; Wan, H.; Zhu, Q. Microplastic Pollution in Water Systems: Characteristics and Control Methods. *Diversity* **2024**, *16*, 70. [CrossRef]
19. Li, S.; Yang, M.; Wang, H.; Jiang, Y. Adsorption of Microplastics on Aquifer Media: Effects of the Action Time, Initial Concentration, Ionic Strength, Ionic Types and Dissolved Organic Matter. *Environ. Pollut.* **2022**, *308*, 119482. [CrossRef] [PubMed]
20. Ioakeimidis, C.; Fotopoulou, K.N.; Karapanagioti, H.K.; Geraga, M.; Zeri, C.; Papathanassiou, E.; Galgani, F.; Papatheodorou, G. The Degradation Potential of PET Bottles in the Marine Environment: An ATR-FTIR Based Approach. *Sci. Rep.* **2016**, *6*, 23501. [CrossRef]
21. Tziourrou, P.; Megalovasilis, P.; Tsounia, M.; Karapanagioti, H.K. Characteristics of Microplastics on Two Beaches Affected by Different Land Uses in Salamina Island in Saronikos Gulf, East Mediterranean. *Mar. Pollut. Bull.* **2019**, *149*, 110531. [CrossRef]
22. Tsangaris, C.; Digka, N.; Valente, T.; Aguilar, A.; Borrell, A.; de Lucia, G.A.; Gambaiani, D.; Garcia-Garin, O.; Kaberi, H.; Martin, J.; et al. Using *Boops Boops* (Osteichthyes) to Assess Microplastic Ingestion in the Mediterranean Sea. *Mar. Pollut. Bull.* **2020**, *158*, 111397. [CrossRef]

23. Karkanorachaki, K.; Kiparissis, S.; Kalogerakis, G.C.; Yiantzi, E.; Psillakis, E.; Kalogerakis, N. Plastic Pellets, Meso- and Microplastics on the Coastline of Northern Crete: Distribution and Organic Pollution. *Mar. Pollut. Bull.* **2018**, *133*, 578–589. [CrossRef] [PubMed]
24. Jacobshagen, V. Geologie von Griechenland. Available online: https://www.schweizerbart.de/publications/detail/isbn/9783443110192/Geologie_von_Griechenland (accessed on 27 January 2024).
25. Katsikatsos, G. *Geology of Greece*; University of Patras: Patras, Greece, 1992.
26. Champidi, P.; Stamatis, G.; Zagana, E. Groundwater Quality Assessment and Geogenic and Anthropogenic Effect Estimation in Erasinos Basin (E. Attica). *Eur. Water* **2011**, *33*, 11–27.
27. Stamatis, G.; Lambrakis, N.; Alexakis, D.; Zagana, E. Groundwater Quality in Mesogea Basin in Eastern Attica (Greece). *Hydrol. Process.* **2006**, *20*, 2803–2818. [CrossRef]
28. Latsoudas, X. *Geological Map "Koropi-Plaka", Scale 1:50.000*; Institute of Geology and Mineral Exploration: Athens, Greece, 2003.
29. Koelmans, A.A.; Mohamed Nor, N.H.; Hermsen, E.; Kooi, M.; Mintenig, S.M.; De France, J. Microplastics in Freshwaters and Drinking Water: Critical Review and Assessment of Data Quality. *Water Res.* **2019**, *155*, 410–422. [CrossRef]
30. Kutralam-Muniasamy, G.; Shruti, V.C.; Pérez-Guevara, F.; Roy, P.D.; Elizalde-Martínez, I. Common Laboratory Reagents: Are They a Double-Edged Sword in Microplastics Research? *Sci. Total Environ.* **2023**, *875*, 162610. [CrossRef] [PubMed]
31. Merkel, B.; Friedrich, B. *Groundwater Geochemistry: A Practical Guide to Modeling of Natural and Contaminated Aquatic Systems*; Nordstorm, D.K., Ed.; Springer: Berlin/Heidelberg, Germany, 2005. [CrossRef]
32. Shruti, V.C.; Kutralam-Muniasamy, G. Blanks and Bias in Microplastic Research: Implications for Future Quality Assurance. *Trends Environ. Anal. Chem.* **2023**, *38*, e00203. [CrossRef]
33. Jin, N.; Song, Y.; Ma, R.; Li, J.; Li, G.; Zhang, D. Characterization and Identification of Microplastics Using Raman Spectroscopy Coupled with Multivariate Analysis. *Anal. Chim. Acta* **2022**, *1197*, 339519. [CrossRef]
34. Scherrer, N.C.; Stefan, Z.; Francoise, D.; Annette, F.; Renate, K. Synthetic Organic Pigments of the 20th and 21st Century Relevant to Artist's Paints: Raman Spectra Reference Collection. *Spectrochim. Acta Part A Mol. Biomol. Spectrosc.* **2009**, *73*, 505–524. [CrossRef]
35. Vedad, J.; Reilly, L.; Desamero, R.Z.B.; Mojica, E.-R.E. Quantitative Analysis of Xylene Mixtures Using a Handheld Raman Spectrometer. In *Raman Spectroscopy in the Undergraduate Curriculum*; ACS Symposium Series; American Chemical Society: Washington, DC, USA, 2018; Volume 1305, pp. 129–152. [CrossRef]
36. Lapa, H.M.; Martins, L.M.D.R.S. P-Xylene Oxidation to Terephthalic Acid: New Trends. *Molecules* **2023**, *28*, 1922. [CrossRef]
37. Zhou, X.-X.; Liu, R.; Hao, L.-T.; Liu, J.-F. Identification of Polystyrene Nanoplastics Using Surface Enhanced Raman Spectroscopy. *Talanta* **2021**, *221*, 121552. [CrossRef]
38. Kellar, E.J.C.; Galiotis, C.; Andrews, E.H. Raman Vibrational Studies of Syndiotactic Polystyrene. 1. Assignments in a Conformational/Crystallinity Sensitive Spectral Region. *Macromolecules* **1996**, *29*, 3515–3520. [CrossRef]
39. Caggiani, M.C.; Cosentino, A.; Mangone, A. Pigments Checker Version 3.0, a Handy Set for Conservation Scientists: A Free Online Raman Spectra Database. *Microchem. J.* **2016**, *129*, 123–132. [CrossRef]
40. Gall, M.J.; Hendra, P.J.; Peacock, C.J.; Cudby, M.E.A.; Willis, H.A. Laser-Raman Spectrum of Polyethylene: Part 1. Structure and Analysis of the Polymer. *Polymer* **1972**, *13*, 104–108. [CrossRef]
41. Fischer, J.; Wallner, G.M.; Pieber, A. Spectroscopical Investigation of Ski Base Materials. *Macromol. Symp.* **2008**, *265*, 28–36. [CrossRef]
42. Nava, V.; Frezzotti, M.L.; Leoni, B. Raman Spectroscopy for the Analysis of Microplastics in Aquatic Systems. *Appl. Spectrosc.* **2021**, *75*, 1341–1357. [CrossRef] [PubMed]
43. Dong, M.; Zhang, Q.; Xing, X.; Chen, W.; She, Z.; Luo, Z. Raman Spectra and Surface Changes of Microplastics Weathered under Natural Environments. *Sci. Total Environ.* **2020**, *739*, 139990. [CrossRef] [PubMed]
44. Kniggendorf, A.-K.; Wetzel, C.; Roth, B. Microplastics Detection in Streaming Tap Water with Raman Spectroscopy. *Sensors* **2019**, *19*, 1839. [CrossRef] [PubMed]
45. De Baez, M.A.; Hendra, P.J.; Judkins, M. The Raman spectra of oriented isotactic polypropylene. *Spectrochim. Acta Part A Mol. Biomol. Spectrosc.* **1995**, *51*, 2117–2124. [CrossRef]
46. Andreassen, E. Infrared and Raman Spectroscopy of Polypropylene. In *Polypropylene*; Karger-Kocsis, J., Ed.; Polymer Science and Technology Series; Springer: Dordrecht, The Netherlands, 1999; Volume 2, pp. 320–328. [CrossRef]
47. Ciera, L.; Beladjal, L.; Almeras, X.; Gheysens, T.; Van Landuyt, L.; Mertens, J.; Nierstrasz, V.; Van Langenhove, L. Morphological and Material Properties of Polyethyleneterephthalate (PET) Fibres with Spores Incorporated. *Fibres Text. East. Eur.* **2014**, *22*, 29–36.
48. Prata, J.C.; da Costa, J.P.; Duarte, A.C.; Rocha-Santos, T. Methods for Sampling and Detection of Microplastics in Water and Sediment: A Critical Review. *TrAC Trends Anal. Chem.* **2019**, *110*, 150–159. [CrossRef]
49. Martí, E.; Martin, C.; Galli, M.; Echevarría, F.; Duarte, C.M.; Cózar, A. The Colors of the Ocean Plastics. *Environ. Sci. Technol.* **2020**, *54*, 6594–6601. [CrossRef]
50. Gregory, P. Industrial Applications of Phthalocyanines. *J. Porphyr. Phthalocyanines* **2000**, *4*, 432–437. [CrossRef]
51. Leiser, R.; Jongsma, R.; Bakenhus, I.; Möckel, R.; Philipp, B.; Neu, T.R.; Wendt-Potthoff, K. Interaction of Cyanobacteria with Calcium Facilitates the Sedimentation of Microplastics in a Eutrophic Reservoir. *Water Res.* **2021**, *189*, 116582. [CrossRef] [PubMed]

52. Dodhia, M.S.; Rogers, K.L.; Fernández-Juárez, V.; Carreres-Calabuig, J.A.; Löscher, C.R.; Tisserand, A.A.; Keulen, N.; Riemann, L.; Shashoua, Y.; Posth, N.R. Microbe-Mineral Interactions in the Plastisphere: Coastal Biogeochemistry and Consequences for Degradation of Plastics. *Front. Mar. Sci.* **2023**, *10*, 1134815. [CrossRef]
53. Panno, S.V.; Kelly, W.R.; Scott, J.; Zheng, W.; McNeish, R.E.; Holm, N.; Hoellein, T.J.; Baranski, E.L. Microplastic Contamination in Karst Groundwater Systems. *Groundwater* **2019**, *57*, 189–196. [CrossRef] [PubMed]
54. Severini, E.; Ducci, L.; Sutti, A.; Robottom, S.; Sutti, S.; Celico, F. River–Groundwater Interaction and Recharge Effects on Microplastics Contamination of Groundwater in Confined Alluvial Aquifers. *Water* **2022**, *14*, 1913. [CrossRef]
55. Gong, X.; Tian, L.; Wang, P.; Wang, Z.; Zeng, L.; Hu, J. Microplastic Pollution in the Groundwater under a Bedrock Island in the South China Sea. *Environ. Res.* **2023**, *239*, 117277. [CrossRef] [PubMed]
56. Ye, S.; Pei, D. Relationships between Microplastic Pollution and Land Use in the Chongqing Section of the Yangtze River. *Front. Ecol. Evol.* **2023**, *11*, 1202562. [CrossRef]
57. Wang, F.; Shih, K.M.; Li, X.Y. The Partition Behavior of Perfluorooctanesulfonate (PFOS) and Perfluorooctanesulfonamide (FOSA) on Microplastics. *Chemosphere* **2015**, *119*, 841–847. [CrossRef]
58. Shockley, D.J.; Lapworth, D.J. Microplastics in Groundwater: A Literature Review. Available online: https://nora.nerc.ac.uk/id/eprint/532669/ (accessed on 27 January 2024).
59. Alvarado-Zambrano, D.; Rivera-Hernández, J.R.; Green-Ruiz, C. First Insight into Microplastic Groundwater Pollution in Latin America: The Case of a Coastal Aquifer in Northwest Mexico. *Environ. Sci. Pollut. Res.* **2023**, *30*, 73600–73611. [CrossRef]
60. Sangkham, S.; Aminul Islam, M.d.; Adhikari, S.; Kumar, R.; Sharma, P.; Sakunkoo, P.; Bhattacharya, P.; Tiwari, A. Evidence of Microplastics in Groundwater: A Growing Risk for Human Health. *Groundw. Sustain. Dev.* **2023**, *23*, 100981. [CrossRef]
61. Mu, H.; Wang, Y.; Zhang, H.; Guo, F.; Li, A.; Zhang, S.; Liu, S.; Liu, T. High Abundance of Microplastics in Groundwater in Jiaodong Peninsula, China. *Sci. Total Environ.* **2022**, *839*, 156318. [CrossRef] [PubMed]

Disclaimer/Publisher's Note: The statements, opinions and data contained in all publications are solely those of the individual author(s) and contributor(s) and not of MDPI and/or the editor(s). MDPI and/or the editor(s) disclaim responsibility for any injury to people or property resulting from any ideas, methods, instructions or products referred to in the content.

water

MDPI

Article

Recharge Assessment in Greek Karst Systems: Methodological Considerations and Implications

Eleni-Anna Nanou *, Konstantinos Perdikaris, Panagiotis Tserolas and Eleni Zagana

Laboratory of Hydrogeology, Department of Geology, Faculty of Natural Sciences, University of Patras, Rion, 26504 Patras, Greece; zagana@upatras.gr (E.Z.)
* Correspondence: e.nanou@ac.upatras.gr

Abstract: The recharge of karst aquifers is significant for the effective management of groundwater resources, and its estimation should be tailored to accommodate their specific hydrogeological characteristics. This study provides a two-step methodological approach for the determination of karst aquifer recharge. Initially, mean annual recharge rates were estimated in the karst system of Ziria (Southern Greece) utilizing the APLIS and modified APLIS methods in order to decipher which was the most suitable version for recharge assessments. The results indicated similar mean recharge rate values at 42.7% and 41.4%, respectively, but significant differences in the spatial distribution. The modified methodology emerged as a more accurate and realistic approach, mainly due to the incorporation of permeability assessments. The final phase of the methodological approach involved the application of modified APLIS in two additional karst hydrosystems, Planitero and Xiromero, while a quantitative cross-comparison of the recharge rates was obtained for a deeper understanding of the factors controlling the groundwater recharge process. In Ziria, recharge rates exhibit a relatively uniform distribution throughout the area, with a median value of 46.7%. Conversely, in Planitero, High recharge rates (60–80%) occupy 56.8% of the surface, while in Xiromero, Moderate recharge rates (40–60%) dominate, representing 53.4% of the land coverage. These variations underscore the spatial heterogeneity of recharge within the karst systems, highlighting the importance of considering local geological and hydrological conditions in its assessments. The methodological approach of this study is flexible and can be adapted to different karst sites for the determination of recharge regimes, contributing to the alleviation of the groundwater depletion issue.

Keywords: karst; groundwater recharge; geographic information systems; APLIS method

1. Introduction

Groundwater resources play an immense role in today's society [1,2], since the universal demand for water supply is crucially increasing. The achievement of sustainable groundwater management is a pressing and often addressed issue due to its critical role in meeting basic human requirements [3]. The escalating need for freshwater, driven by global population growth and rapid urbanization, can cause groundwater reservoirs to face over-extraction and depletion, compromising their sustainability. Simultaneously, the issue of groundwater contamination has become extensive, with pollutants from agricultural runoff, industrial discharges, and improper waste disposal infiltrating aquifers.

Besides the ramifications that can arise from human activities, climatic causes may burden aquifers further, with dire impacts on their resources. In an era dominated by the pervasive effects of climate change, Earth's hydrological cycle faces unprecedented challenges with shifts in temperature regimes, alterations in precipitation patterns, and intensified extreme weather events. These climate-induced changes can cause direct and indirect repercussions on global reserves [4], disrupt traditional recharge mechanisms, and intensify water scarcity. The increasing occurrence of droughts may lead to changes in the water balance, while rising global temperatures contribute to heightened evaporation rates,

further amplifying water scarcity in vulnerable regions. The challenges facing groundwater resources have reached a critical juncture, potentially influencing their global distribution in the future. This underscores the imperative to address numerous water-related issues in a sustainable manner. Groundwater depletion constitutes a universal concern due to the unbalanced abstractions in comparison to the natural recharge. Obviously, the study of groundwater recharge is quite challenging, especially in karst aquifers.

At the forefront of hydrological environments, karst aquifers provide high-quality groundwater that is utilized either for drinking water supply or irrigation purposes. Climate-induced shifts can cause severe repercussions, leading to both a degradation in the availability and a compromise in the quality of water resources [5–8]. At the same time, with distinct characteristics and processes, karst aquifers are able to provide substantial amounts of groundwater, often resulting in their overexploitation [9,10], in order to meet the water demands of the constantly increasing population.

In Greece, there are numerous carbonate massifs distinguished by a diverse array of geological, geomorphological, and hydrogeological features, leading to a substantial variation in the degree of karstification across the country. Over the last decade, increasing research efforts have been directed towards the characterization, protection, and sustainable management of native karst aquifers, highlighting their significant value as water sources in Greece [11]. Up to 80% of the domestic karst systems are defined by good groundwater quality and quantity conditions, while qualitative issues are recorded mainly in coastal aquifers on islands, represented by a percentage of 5% [12].

The viable management of groundwater use requires the aversion of resource depletion. Recharge is one of the most significant parameters to be assessed in order to sustain the overall effective function of an exploited aquifer. Its approximation is essential to evaluating the maximum volume of water obtainable and to avoid overutilization [13]. Stable isotopes [14–17], lump and spatial models (e.g., Karstmod, VarKarst, Modflow-CFP), as well as index-based methods (e.g., APLIS, KARSTLOP), are widely used in order to determine the recharge process in karst environments [11,18–24]. Due to the heterogeneity of porosity and permeability that transcends karst aquifers [25,26] and significantly affects many of their qualities, the quantification of recharge constitutes a challenging task. The APLIS method was developed by Andreo et al. [27] and later modified by Marin [28] for the estimation of the recharge rate, expressed as a percentage of precipitation. Its parametric methodology is based on a geographic information system (GIS) and was developed specifically for carbonate aquifers under Mediterranean climatic conditions. APLIS has been implemented as well as compared to several other methods by numerous researchers [29–32], while many modifications have been made since to accommodate varying circumstances [33–35].

In this research, we applied a two-step-based methodological approach. Initially, the efficiency of APLIS and its modified version were compared in the karst system of Ziria in Southern Greece. The quantitative comparison of the two methods showed that modified APLIS is more suitable for Greek karst systems. The next step was the application of modified APLIS at two additional karst sites, Planitero and Xiromero, located in Southern and Western Greece, respectively. A comprehensive examination of the method's performance was provided across distinct hydrogeological settings. The outcomes from all three study sites underwent statistical analysis in order to decipher the hydrogeological factors that influence the recharge process. To the best of our knowledge, this methodological approach was initially applied within this manuscript. Considering that groundwater recharge constitutes the most important parameter in the fight against groundwater depletion, this study contributes to the quantification and deeper understanding of the infiltration regime in karst hydrosystems.

2. Materials and Methods

2.1. Background Information and Geological Overview of the Study Sites

In the frame of this research, the recharge rate was estimated at three Greek karst sites. Similarities and differences are both present between the study areas in regards to the geological-topographical setting and the precipitation regime. From east to west, the aforementioned sites are: (a) Ziria, (b) Planitero, and (c) Xiromero.

The karst groundwater system of Ziria (EL0200220) was delineated in the framework of River Basin Management Plans [36] that were drafted according to the requirements of the 2000/60/EC Directive [37]. It is located in Northern Peloponnese, Southern Greece, approximately 45 km west of the city of Corinth, and covers an area of roughly 200 km^2. The aquifers of the system are formed within a large mountainous area of an almost circular extension known as Mount Killini or Ziria (2368 m.a.s.l.). A large karstic polje with an orientation of almost E-W is situated in the southern part of the study area, within which Stymphalia Lake was developed. The topography is rough, with often steep slopes, since the mountain occupies a considerable extent of the hydrological system. Ziria is primarily composed of Upper Triassic–Cretaceous and undifferentiated limestones and dolomites (Tripolis Zone) along with Cretaceous limestones (Olonos–Pindos nappe) that were thrust over the latter (Figure 1) [38,39]. The metamorphic bedrock of the area consists of quartzites, phyllites, and schists that mainly surface in the SW and NW regions. A substantial part of the karst system is covered by Quaternary deposits, including the polje, which, according to geoelectrical investigations [40], is mostly filled by impermeable clays.

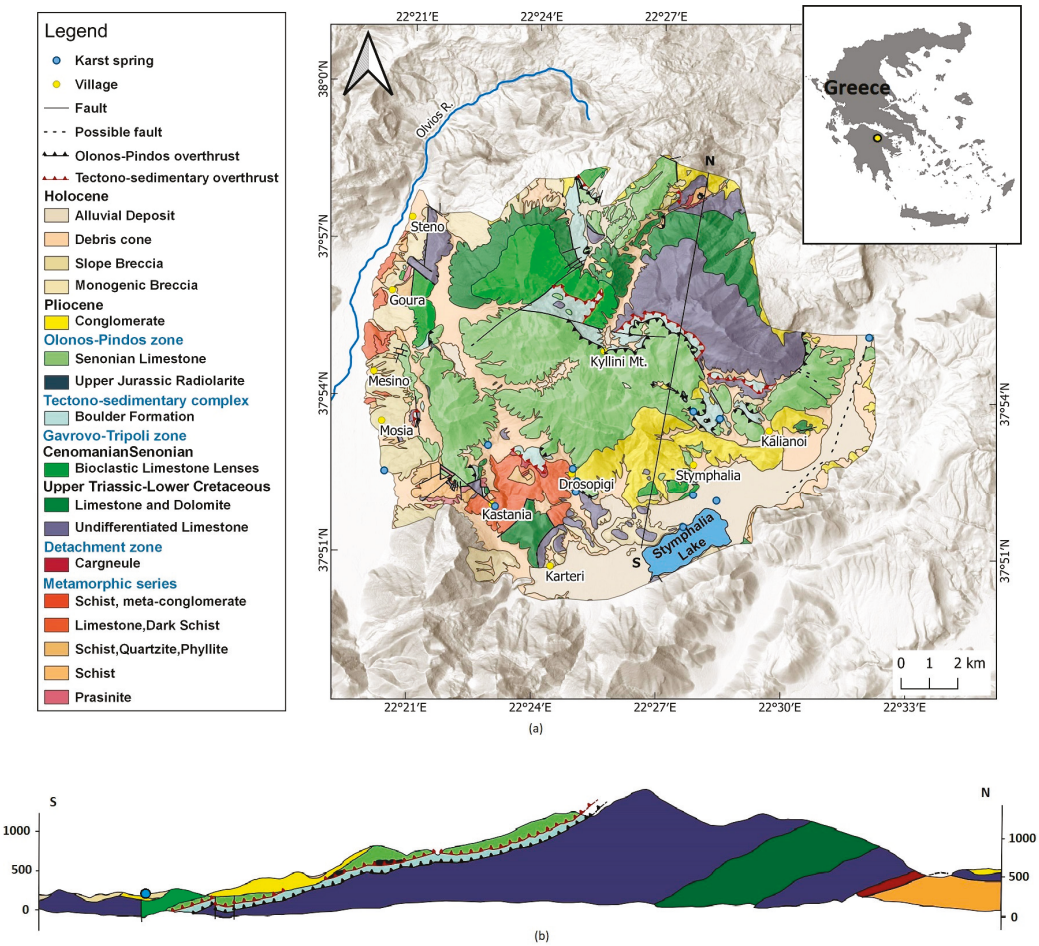

Figure 1. (**a**) Geological setting of the karst groundwater system of Ziria (modified by [38,39]), (**b**) Geological cross section (modified by [38]).

The karstification degree is prominent with the presence of many karstic landforms, such as dolines, swallow holes, and caves, while the recharge of the aquifers occurs in both diffuse and concentrated forms. The front of Stymphalia springs discharges one of the largest aquifers in the area and provides the drinking water supply for the cities of Corinth and Kiato. The groundwater of the system is also heavily used for irrigation purposes since large sections of the polje and the adjacent areas are being cultivated.

The aquifers of Planitero manifest within the Aroania (Chelmos) Mountains, which are located approximately 20 km west of Mount Ziria, so, due to their close proximity, the geological setting is very similar. This site constitutes a part of the much larger Ladon system (EL0100030), severed in order to include the recharge area of Planitero springs. It occupies 112 km^2 of land, and it is mainly composed of karstified carbonate rocks (Tripolis and Pindos zones) (Figure 2A) [38,41,42]. A considerable segment of the site is covered by Quaternary deposits, while there are outcrops of flysch and metamorphic bedrock. The aquifers discharge from a front of springs that supplement the Aroanios River. The presence of multiple faults and overthrusts makes the tectonic stress of the region indisputable. The resemblance between Ziria and Planitero is also evident in the steep terrain, with abrupt altitudinal inclinations and high elevations over 2300 m.a.s.l.

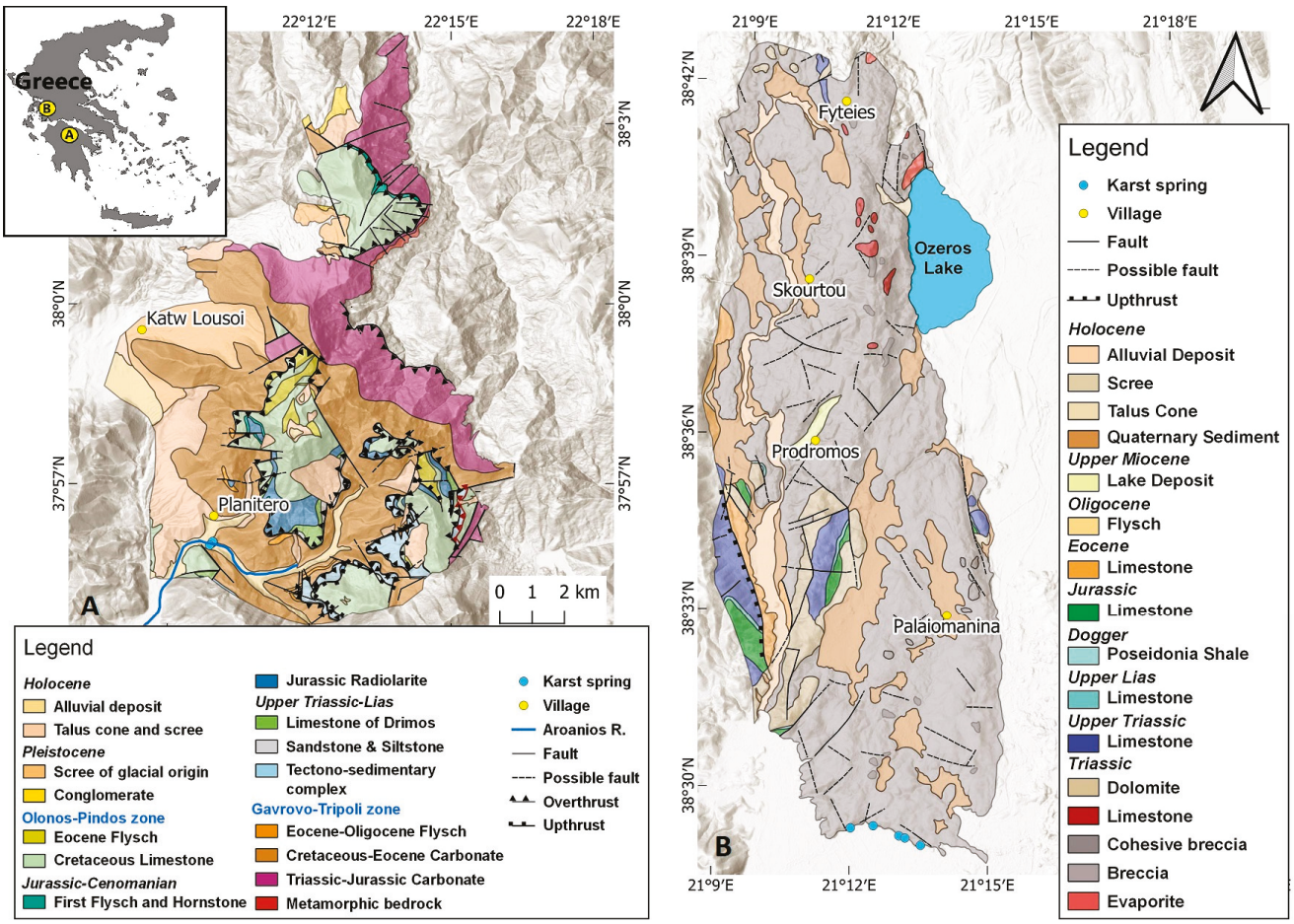

Figure 2. Geological setting of (**A**) Planitero (modified by [38,41,42]) and (**B**) Xiromero (modified by [43,44]).

Xiromero (approximately 170 km^2) is located in Western Greece and presents many dissimilarities compared to the other study sites. Like Planitero, it is also a delimited section of the Katouna–Lesini system (EL0400050), due to the emersion of evaporites in the northern part of the area, near Fyteies, functioning as a hydrological barrier. The aquifers are formed within the karstified Triassic breccia that prevail in the area and were developed by the fragmentation of adjacent Triassic limestones and dolomites (Figure 2B). They discharge from the Lambra–Agios Dimitrios front of springs, providing groundwater to accommodate the needs of adjacent villages. Quaternary deposits consisting mainly of clays and sandy materials, along with small outcrops of various limestones, complete the geological setting of the area [43,44]. Compared to the other study sites, the topography is much gentler, with altitudes not exceeding 510 m.a.s.l. Due to its location, Xiromero is also defined by greater rainfall amounts, since the precipitation pattern in Greece shows a general latitudinal decrease from west to east [45].

2.2. Application of the APLIS Method

The initial APLIS method [27] was applied in the karst system of Ziria, followed by the implementation of its modified version [28] in order to obtain a cross-comparison between the two adaptations. Modified APLIS was subsequently applied in the Planitero system, while in Xiromero the method was updated from Zagana et al. [29], with karst landforms emerging from remote sensing techniques derived from a more recent study [46].

In order to express recharge in mm/year, the percentage (%) maps resulting from modified APLIS were multiplied with the spatial distribution of precipitation in each study site. Precipitation data corresponding to time series spanning 30 years were collected from meteorological stations in the vicinity of the sites. The methodology employed for the spatial analysis considered the variation in precipitation according to elevation.

2.2.1. Assessing Recharge with APLIS and Modified APLIS in the Karst System of Ziria

APLIS estimates the mean annual recharge rate of carbonate aquifers. The assessed recharge originates solely from precipitation, and it is expressed as its percentage. The methodology behind APLIS also enables the acquisition of maps with the spatial distribution of the estimated recharge rates. To achieve that, the method proposes the combination of individual intrinsic variables that can potentially influence recharge in karst aquifers, such as Altitude (A), Slope (P), Lithology (L), Infiltration landforms (I), and Soil type (S) [27]. The APLIS method was later modified by Marín [28], who introduced refinements such as the reclassification of slopes, adjustments to infiltration scorings, and the incorporation of a correction factor (Fh) that is associated with the permeability of the formation outcropping on the surface. To apply the method, the prior variables were developed as information layers within a Geographic Information System (GIS). Scoring values, ranging from 1 (minimum) to 10 (maximum), were then assigned according to the influence on recharge. All the map layers that were developed for the application of APLIS and modified APLIS in Ziria are depicted in Figures 3 and 4.

The altitude map (A) was derived from a Digital Elevation Model (DEM) of the country, which in turn originated the slope map (P) in percent rise as required by the method. The elevation in the study area ranges from 600 to 2368 m.a.s.l., and the altitude was classified in 6 sequences of 300 m intervals. The slopes span from 0%, mainly in the polje of Stymphalia, to over 100% on the steep inclinations of Mount Ziria. The scoring of the first two variables was attributed so that the higher the altitude, the greater the recharge due to the increase in precipitation, and the greater the slope, the lower the recharge into the aquifer [27] (Table 1). In both scenarios, the altitude map and its corresponding values remain consistent. However, the classification and scoring of the slopes differ in APLIS and its modified version, with the latter presenting an additional class.

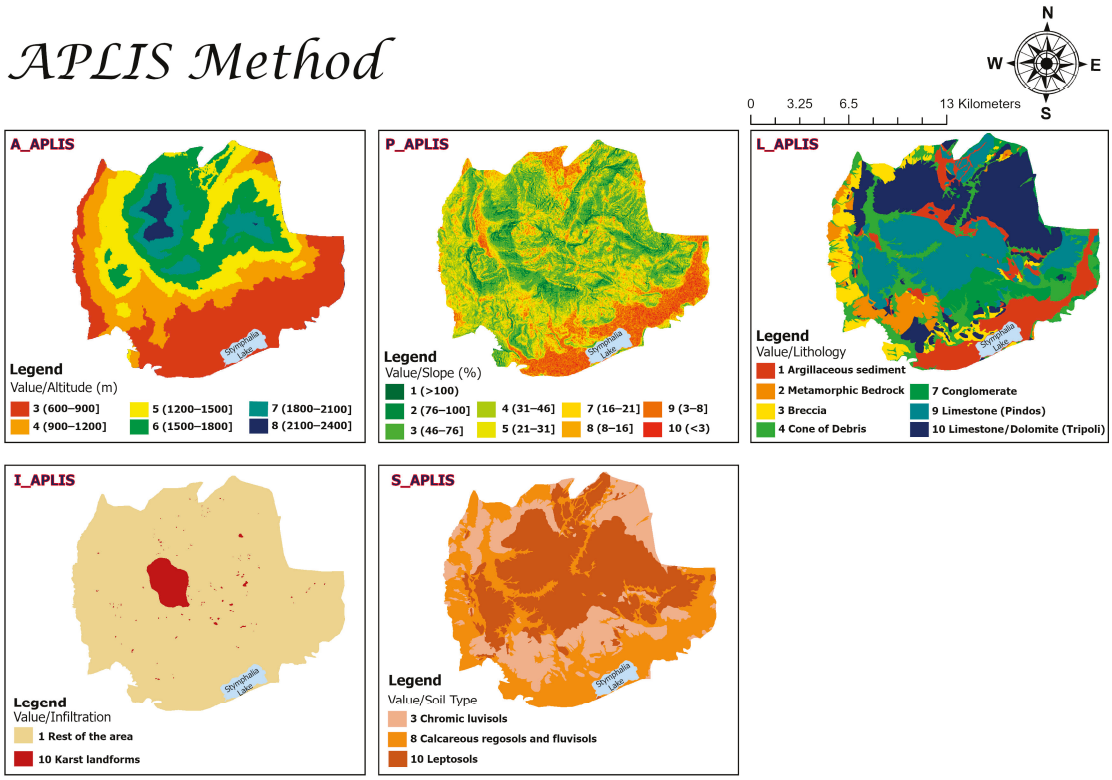

Figure 3. Maps of all the variables developed for the application of the APLIS method.

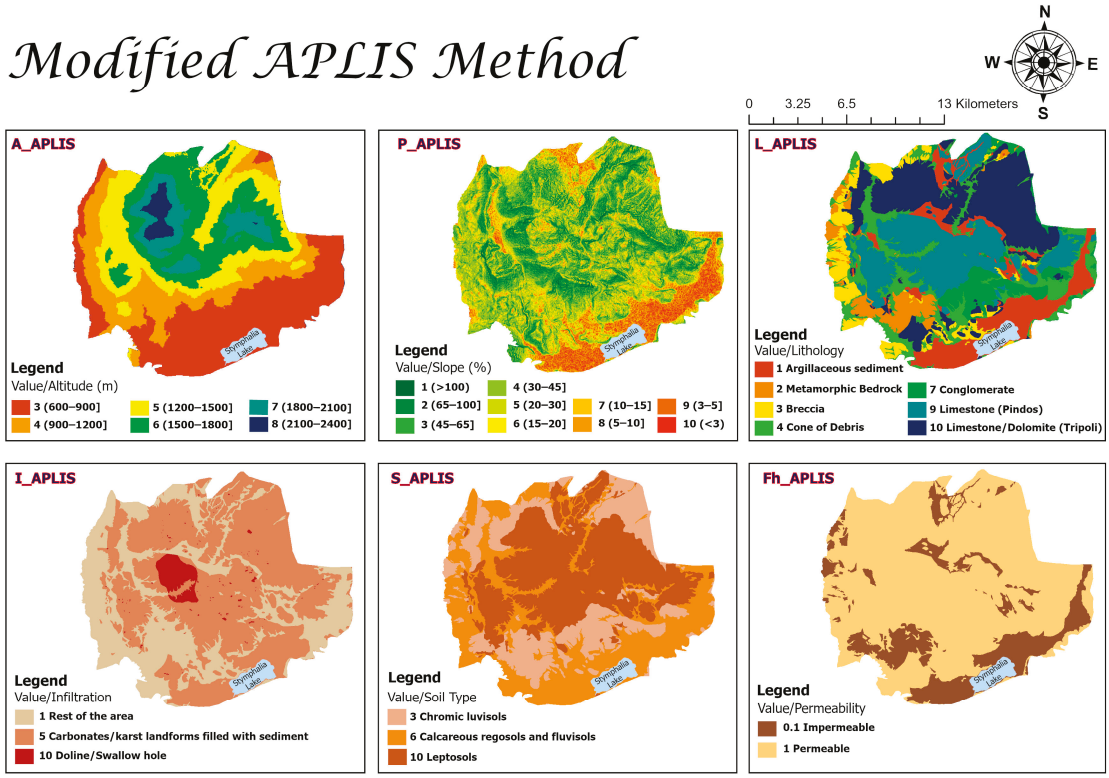

Figure 4. Maps of all the variables developed for the application of modified APLIS.

Table 1. Scoring of the Altitude (A) and Slope (P) variables for the karst system of Ziria.

Scoring	1	2	3	4	5	6	7	8	9	10
Altitude (m)	-	-	(600–900]	(900–1200]	(1200–1500]	(1500–1800]	(1800–2100]	(2100–2400]	-	-
Slope (%)										
APLIS	>100	(76–100]	(46–76]	(31–46]	(21–31]	-	(16–21]	(8–16]	(3–8]	<3
Modified APLIS	>100	(65–100]	(45–65]	(30–45]	(20–30]	(15–20]	(10–15]	(5–10]	(3–5]	<3

Considering the lithological aspect (L), there are seven major units dominating the site that all received scoring based on imputes from previous studies [47,48] and field observations. All the carbonates received high scores due to their karstification degree and tectonic stress. The limestones of Tripolis are considered to be more karstified than the Cretaceous limestones of Pindos because the latter often intervene with thin layers of radiolarite [48], therefore they were attributed the values 10 and 9, respectively. The Quaternary formations exhibit fluctuations due to changes in grain size and composition, along with the presence of argillaceous materials. The alluvial deposits in the polje, along with the outcrop at the north-eastern part of the area, received lower values than the rest. Finally, the conglomerates were attributed a significantly higher score than what is proposed by APLIS since they are considered to be karstic [49].

The areas of preferential infiltration (I) were located with remote sensing techniques, using aerial photographs and stereo pairs in Erdas Imagine 2010 software that enabled the three-dimensional representation of the system. Predominantly, these landforms were observed on the limestones of the Mountain, where the dominance of bare rocks and the absence of vegetation facilitated the clear delineation of such topographic depressions. On the Cretaceous limestones of Pindos, fields of dolines can be visually distinguished through satellite images and photographs, with no further assistance from remote sensing software. These landforms were collectively grouped rather than individually digitized, occupying, in such a way, a significant section of the limestones. Regarding this variable, APLIS provides only two rankings: a score of 10, which was attributed to the preferential infiltration landforms, and a score of 1, which was assigned to the rest of the system. Karst landforms that are filled with Quaternary sediments were assigned the lowest value (1), due to the method's limited scoring options. In modified APLIS, an additional intermediate value of 5 was introduced. It was received by the polje and other karstic features that are covered by various materials, as well as attributed to all the carbonate outcrops, in order to be distinguished from the non-carbonate formations.

Due to the lack of specific soil data, the evaluation of the soil types (S) was based on the combination of information provided by different Soil maps [50–52]. A substantial section of the Mountain is characterized by exposed rock, devoid of soil and vegetation. Leptosols, assigned the highest value of 10, were designated as the soil type for limestone areas exhibiting minimal to no vegetation. Chromic luvisols were attributed to formations with denser vegetation, while calcareous regosols and fluvisols were predominantly assigned to Quaternary sediments. There are minimum scoring differences between the two methods.

For the estimation of the correction factor in modified APLIS, permeable formations such as carbonates, conglomerates, and most of the Quaternary deposits were identified with aquifer potential and were assigned the correction coefficient (Fh) 1. Impermeable formations like the metamorphic series and argillaceous sediments were assigned the value 0.1.

The reliability of the used data for the application of the methods is provided in the Supplementary Materials.

The scorings that were attributed to the rest of the variables for the application of modified APLIS are displayed in Table 2. For the estimation of the annual recharge rate

and the creation of maps with its spatial distribution in both scenarios, the expressions of the original (1) and modified method (2) were utilized in ArcGIS 10.8 software:

$$R = (A + P + 3 \times L + 2 \times I + S)/0.9 \quad (1)$$

$$R = [(A + P + 3 \times L + 2 \times I + S)/0.9] \times Fh. \quad (2)$$

Table 2. Scoring values of the variables L, I, and S for the application of modified APLIS in Ziria.

Lithology (L)	*Scoring*	**Infiltration Landforms (I)**	*Scoring*
Argillaceous sediment	1	Rest of the area	1
Metamorphic bedrock	2	Carbonates/karstic landforms filled with sediment	5
Breccia	3	Doline/Swallow hole	10
Cone of Debris	4	**Soil Type (S)**	*Scoring*
Conglomerate	7	Chromic luvisols	3
Cretaceous Limestone (Pindos)	9	Calcareous regosols and fluvisols	6
Limestone/Dolomite (Tripoli)	10	Leptosols	10

2.2.2. Application of Modified APLIS to Planitero and Xiromero

The neighboring Planitero system presents many similarities to Ziria, and the values that were assigned to each variable are depicted in Table 3, while the scoring of the first two parameters (A and P) corresponds to Table 1.

Table 3. Assigned values to the variables of the modified APLIS for Planitero.

Lithology (L)	**Scoring**	**Infiltration Landforms (I)**	**Scoring**
Flysch/Argillaceous sediment	1	Rest of the area	1
Metamorphic bedrock	2	Carbonates/karstic landforms filled with sediment	5
Quaternary deposits	3	Doline	10
Talus Cone/Scree	4	**Soil Type (S)**	**Scoring**
		Chromic luvisols	3
Carbonates (Pindos Zone)	9	Calcareous regosols and fluvisols	6
Carbonates (Tripolis Zone)	10	Leptosols	10

The application of modified APLIS in Xiromero is thoroughly described in [29], while Table 4 presents the updated values that were attributed to each variable.

Table 4. Assigned values to the variables of modified APLIS for Xiromero—modified from [29].

Lithology (L)	**Scoring**	**Infiltration Landforms (I)**	**Scoring**
Quaternary Sediment	1	Rest of the area	1
Evaporites/non karstified limestones	2	Karstified Limestone/Breccia	5
Talus Cone/Scree	3	Doline	10
Alluvial Deposit	4	**Soil Type (S)**	**Scoring**
		Fluvisols	6
Dolomite	7	Calcareous Lithosols	6
Triassic Limestone/Breccia	9	Leptosols	10

3. Results and Discussion

3.1. Comparison of the Results That Each Version of the APLIS Method Provided in the Karst System of Ziria

The spatial distribution of recharge rates in Ziria reveals significant disparities when assessed by the original and modified methodologies. Considering the first case (Figure 5a), the recharge rates in the area are predominantly Low (20–40%) and Moderate (40–60%), while those identified as High (60–80%) and Very High (>80%) are in correlation with preferential infiltration zones or the presence of flattened slopes in carbonates. The annual recharge rate estimated by APLIS ranges from 16.6% to 85.5%, with a mean annual value of 42.7%.

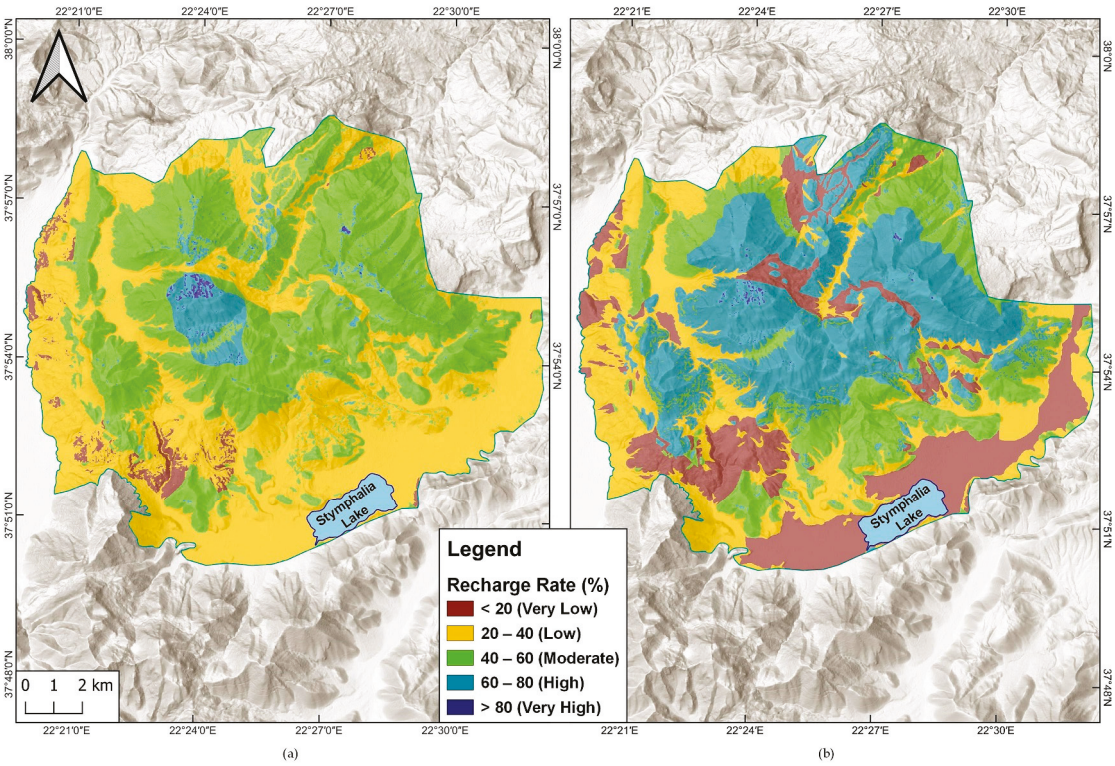

Figure 5. Spatial distribution of the annual recharge rate (%) in the karst system of Ziria utilizing (**a**) the APLIS method and (**b**) modified APLIS.

In modified APLIS (Figure 5b), the spatial distribution of recharge has been significantly impacted by the introduction of the correction factor (Fh). Notably, the recharge rates in a substantial portion of the area, encompassing the polje and other outcrops of low-permeability materials, have been categorized as Very Low (<20%). Furthermore, there is a noteworthy shift in the recharge classification for carbonate outcrops in Mount Ziria, elevating them from the previous Moderate class (40–60%) to High recharge rates (60–80%) due to the additional value (5) in the preferential infiltration parameter that was attributed to all the carbonates. A similar upgrading is observed for conglomerates, transitioning from Low (20–40%) to Moderate (40–60%) recharge rates. Despite the significant divergence in spatial distribution compared to APLIS, the simultaneous expansion of formations with Very Low (<20%) and High (60–80%) recharge rates has resulted in a marginal alteration of the mean annual recharge rate, which has slightly decreased to 41.4%. With the modified version of APLIS, the recharge rate in the study area ranges from 1.6% to 85.5%.

The spatial distribution of the recharge rate resulting from both methods seems to be in unison for a significant part of the system classified as Low and Moderate, mainly referring to some of the Quaternary deposits and sections of the carbonates.

In a hydrological balance study carried out in the area, the infiltration coefficient was estimated at 51% for the carbonates of Mount Ziria, 35% for the conglomerates, 15% for the Quaternary deposits, and 2% for the tectono-sedimentary complex [53]. According to Röckel and Hötzl [49], on the other hand, the infiltration was roughly estimated at 50% for limestones and conglomerates since both of them are considered karstified, 20% for Quaternary gravels, and 4% for clays and marls. It is also suggested that, especially for the carbonate outcrops on Mount Ziria, 60% of infiltration can be expected because of the dominance of bare karst on vast areas.

The inputs of these prior studies align more closely with the outcomes derived from modified APLIS, where, first and foremost, due to the correction factor (Fh), the areas of very low permeability and recharge below 8% can be recognized, contrary to the original methodology. In the alluvial deposits of the polje, along with the tectono-sedimentary complex, the recharge rates span between 1.6% and 3.5%. The percentages that are essentially identified in the conglomerates are in the range of 44–52%, while for the carbonates of Mount Ziria, they are 51–70%. In contrast, APLIS indicates different recharge rates for the same formations: approximately 16–28% for the alluvial deposits in the polje, 24–33% for the tectono-sedimentary complex, 35–42% for the conglomerates, and 44–64% for the limestones and dolomites. The highest percentage of recharge in both methods is 85%, but the range of 70% to 85% primarily refers to specific karstic landforms.

Data distribution and statistics contributed to the comparison between the two outcomes (Figure 6). In APLIS, the median recharge value is 38.9%, with 25% of the data falling below the threshold of 31.1% (representing the first quartile), while 75% of the data falls below the rate of 53.3% (corresponding to the third quartile). In modified APLIS, the median and first quartile values are 46.7% and 27.8%, respectively, while the third quartile stands at 62.2% (Figure 6a). The distribution of data within each recharge class appears to be more evenly distributed in the modified methodology. Conversely, in the original APLIS method, there is a noticeable deviation between the classes (Figure 6b). Low (20–40%) and Moderate (4060%) recharge rates dominate the area, collectively covering nearly 94% of the karstic system.

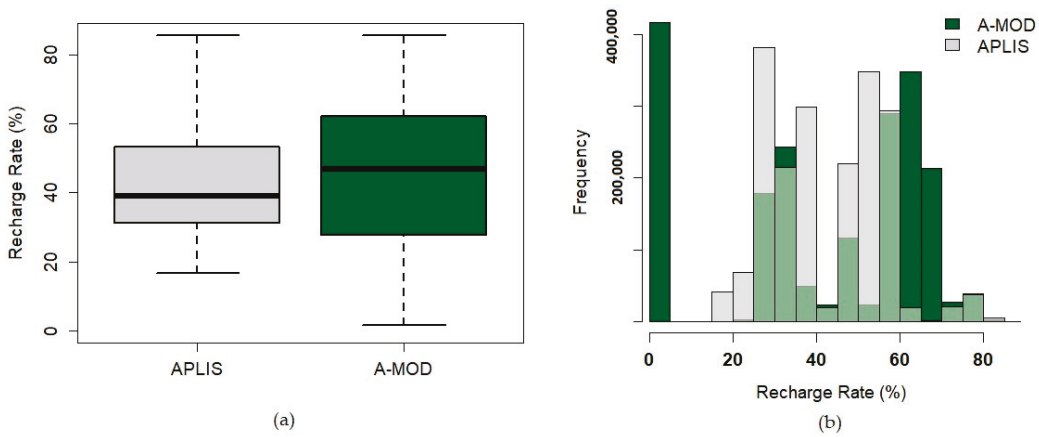

Figure 6. (**a**) Data visualization and comparison with boxplots; (**b**) Histogram with data distribution and range of values (A-MOD represents modified APLISand the light green color portrays areas of overlap).

In the modified methodology, High recharge rates (60–80%) appear to be the most prevalent, occupying 63 km^2 of carbonate sediments. There is a substantial difference between the methods regarding the Very Low (<20%) recharge class, where the variation in the two data volumes translates to 2.1% (APLIS) and 21% (modified) with respect to area coverage. In both methods, Very High (>80%) recharge rates are the least widespread, taking up an area of 0.5 and 0.25 km^2, respectively. Since the scoring of each variable corresponding to the karstic landforms of the mountain that primarily exhibit such a

recharge class is exactly the same, the differentiation of the occupied surface between the methods is most likely due to the diverse classification of the slope factor (P).

To conclude, the modifications made to the APLIS method have significantly enhanced the accuracy of recharge rate estimations, leading many researchers to adopt the adapted methodology for their assessments. The attribution of additional values and the reclassification of specific variables have proven to be pivotal in shaping the final outcome. Modified APLIS distinguishes the infiltration landforms in three categories (1, 5, and 10), in contrast to the initial method, which has only two categories (1 and 10). Consequently, the category with a score of 5 is more representative for many formations of the studied hydrosystem compared to the initial score of 1. The greater extent of the lowest recharge rates is due to the correction factor (Fh) that was introduced in the modified methodology and empowers users to provide a more precise permeability assessment for the geological formations. Inevitably, in the final map, extreme values of recharge rates (e.g., <20% and 60–80%) cover a greater area. Consequently, the mean annual value of the recharge rate estimated by the modified APLIS is lower than the initial method. The permeability factor has notably addressed the limitation of the original method, which could not estimate recharge rates below 8%. In non-permeable formations, APLIS estimated recharge rates between 16% and 33%, as it relied solely on the minimum attributed values of the lithological parameter. High elevations, flattened slopes, and thin soil coverage, however, can increase the recharge rate of an impermeable formation that receives high scores in all three categories.

Other researchers have also compared the two adaptations of the method. Espinoza et al. [34] applied APLIS and its modified version to a fractured karst aquifer in Peru, estimating the mean annual recharge rates at 48% and 24%, respectively, and emphasizing the key role of the correction factor in this differentiation. In another study, AHP, APLIS, and modified APLIS were implemented to evaluate the infiltration potential of the Roein Esfarayen Basin in Iran [54], with modified APLIS demonstrating the highest correlation coefficient (0.85) among the three methods, underscoring its efficacy in capturing and describing the complexities of recharge dynamics. Overall, the methodology behind modified APLIS consistently produces a more coherent and realistic portrayal of the recharge rate.

3.2. Statistical and Spatial Comparison of the Annual Recharge Rates in All Three Karst Sites Utilizing Modified APLIS

The estimation of the annual recharge rate was conducted using modified APLIS in both Planitero and Xiromero, resulting in maps illustrating its spatial distribution (as shown in Figure 7a,b).

In Planitero, recharge rates exhibit a broad range, spanning from 1.3% to 86.6%, with a mean value of 48.6%. Notably, the site is primarily composed of carbonate formations, which accounts for the prevalence of High recharge rates (60–80%) covering 62.7 km^2 of the total area (Figure 8a). A very small percentage, approximately 0.007%, is classified as Very High (>80%), mainly associated with infiltration landforms. Very Low (<20%) and Moderate (40–60%) recharge rates are nearly equally represented, encompassing 14.3 km^2 and 13.4 km^2 of the system, respectively.

The annual recharge rate in Xiromero ranges from 1.4% to 76.6%, with a mean annual value of 46.9%. It stands as the only site among the three that does not exhibit recharge rates that exceed 80% (Figure 7b). This differentiation can be attributed to the significantly lower elevations in the area, along with the absence of the highest lithological scoring (10). The dominant recharge class in Xiromero is Moderate (40–60%), occupying more than half of the entire surface (Figure 8a), and it is primarily associated with karstified breccia and limestone outcrops. High recharge rates (60–80%) correspond to 21.9% of the system, with a higher prevalence of this recharge class observed in both Ziria and Planitero.

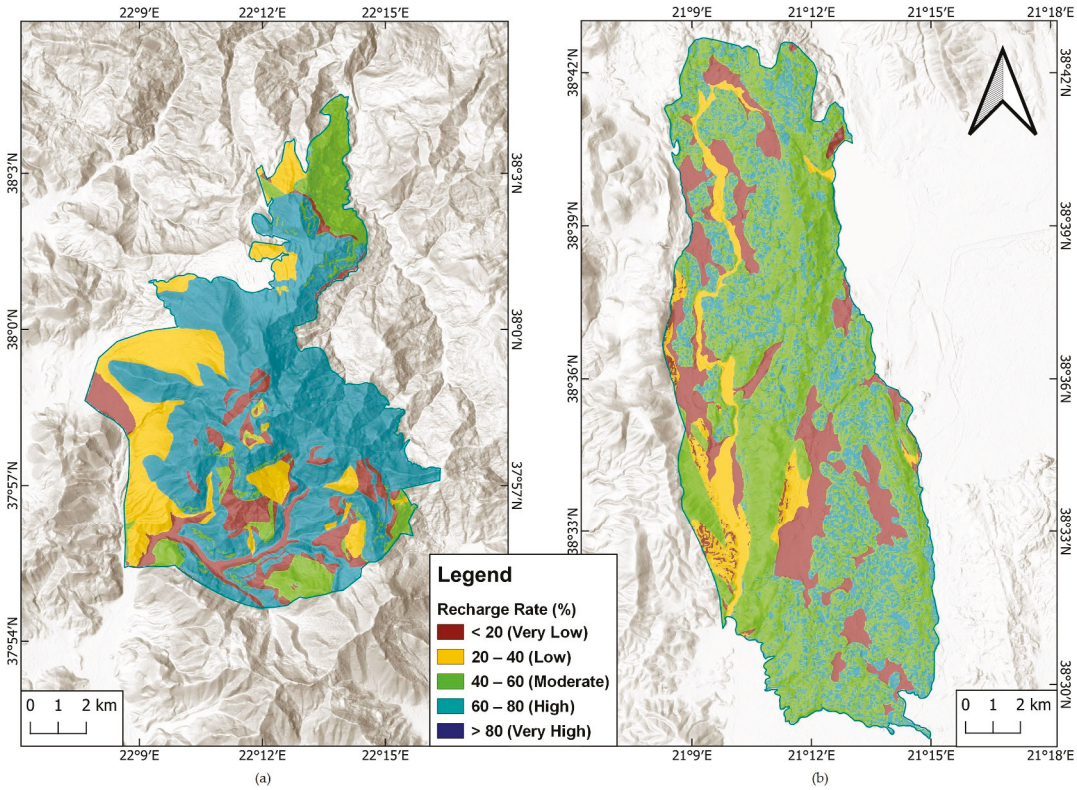

Figure 7. Annual recharge rate estimated with modified APLIS (**a**) in Planitero, Northern Peloponnese, and (**b**) in Xiromero, Western Greece.

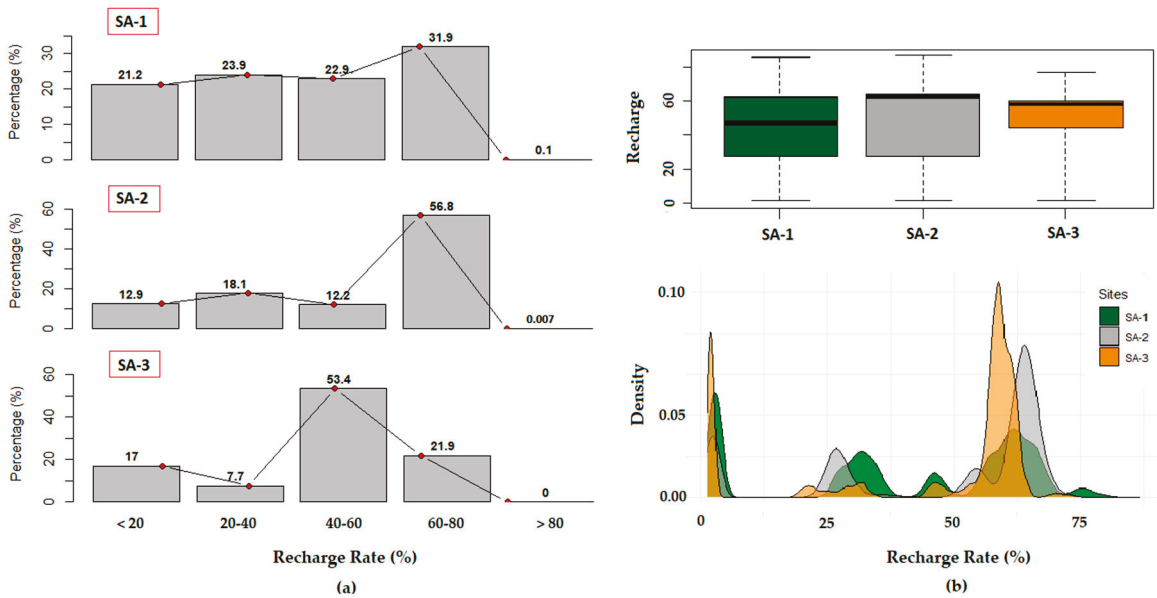

Figure 8. (**a**) Surface coverage of each recharge class in Ziria (SA-1), Planitero (SA-2), and Xiromero (SA-3), and (**b**) Boxplots illustrating the distribution of the annual recharge rate data in SA-1, SA-2, and SA-3 (**top**) and a density plot (**bottom**) showing its allocation between the sites.

A comparative analysis of all three sites (Figure 8a,b) reveals noteworthy distinctions in the annual recharge rates. In Ziria, apart from the Very High Class (>80%), recharge rates are much more evenly distributed throughout the area (median value 46.7%), since it is the only site that is not dominated by a specific geological formation. While Ziria and Planitero share several similarities, the range of recharge values in the latter is broader. The

median and third quartile values are 62.2% and 64.4%, respectively, suggesting a tendency towards higher recharge values (Figure 8b). In contrast, the range of recharge rates in Xiromero is comparatively narrower, with the median value being 57.8% and the third quartile being 60%. These variations underscore the unique hydrogeological characteristics and geological formations of each system, which influence the distribution of recharge rates.

The quantification of recharge in mm/year was accomplished by multiplying the spatial distribution of the assessed recharge rates (%) with precipitation (mm/year). Due to the close proximity of Ziria and Planitero, the same equation was utilized in order to convert contours into isohyets lines. In Ziria, recharge ranges from 13.7 to 1423.4 mm/year with a mean annual value of 498 mm/year, while in Planitero, due to the dominance of limestones and dolomites, the mean annual recharge is 618 mm/year. Xiromero does not exhibit Very High recharge rates (>80%), and the elevations in the area are considerably lower than in the other systems. However, due to the different precipitation regime in Western Greece, recharge in Xiromero spans from 13 to 852.5 mm/year, and the mean annual value is 439 mm/year.

Several methods and models have been developed over the years for the determination of aquifer recharge. The methodology behind APLIS provides reasonable results with an easy GIS-based application without requiring data that is difficult to acquire or not available, unlike many other approaches. It also enables the determination of the spatial distribution of recharge, something that separates it from many other methods. Its methodology has been widely used, so if it is necessary to have the spatial distribution of mean annual recharge rates, APLIS constitutes the most suitable method.

3.3. Implications/Limitations and Future Works

The estimation of recharge is a very intricate subject for karst environments due to their hydrogeological uniqueness. APLIS has yielded valuable insights, but it is essential to acknowledge the implications of this approach. The accuracy of the method heavily depends on the quality of input data and the attribution of scoring values, while it is not difficult to generate unreliable results. One major challenge arose from the assignment of values to the Soil types (S) within the study sites. The problem stems from the reliance on global and continental-scale soil maps that often provide generic and generalized data. This can introduce a level of uncertainty into the method, as local variations in soil characteristics may not be adequately represented. Consequently, the accuracy and reliability of the recharge assessment may be compromised, necessitating caution in interpreting the results and highlighting the need for higher-resolution local soil data for more precise assessments.

Another important consideration pertains to the variables Lithology and Preferential infiltration, which are of paramount importance in the expression of recharge assessment. The values assigned in Lithology in particular entail a degree of subjectivity, as they are left to the discretion of the user. This introduces a degree of user-dependent variability into the method, leading to variations in the outcomes based on individual judgment. It is crucial to communicate this inherent subjectivity, emphasizing that the accuracy of the recharge assessment is inherently linked to the quality and appropriateness of the values selected.

While the APLIS method is effective in mapping the spatial distribution of annual recharge within a given area, it exhibits a limitation in its capacity to estimate its temporal variability. This limitation stems from the inherent nature of the method, which predominantly focuses on spatial aspects, neglecting the intricate temporal dynamics of recharge processes and providing averaged annual values of recharge rates. Recharge in karst aquifers is not a constant phenomenon but can vary significantly over time, influenced by factors such as seasonal variations in precipitation, land use changes, and climate fluctuations. Kirn et al. [55] extended the spatial dimension of the method to include the aspect of time variance and concluded that APLIS tends to overestimate recharge in dry years and underestimate it in wet years.

APLIS is a promising method for assessing the mean annual recharge that has been applied to several karst aquifers under Mediterranean climatic conditions, yielding satisfactory results. Given the intricate nature of karst systems and the challenges associated with verifying recharge assessments, the adoption of a multi-method approach is essential. In the future, further research will be conducted in order to strengthen the premise of this ongoing project. A comparison of APLIS' results with lump simulation models is strongly suggested. The implementation of advanced modeling at the study sites will provide a more holistic view of recharge, aid in error reduction, and enhance the reliability of findings associated with APLIS as an individual technique. Sensitivity analyses and robustness testing will be conducted in order to assess the potential impact of varying the parameters on the method's results, and tectonic lineaments will be introduced as possible infiltration landforms. Discharge measurements and hydrograph analysis from the front of springs in the karst system of Ziria will contribute to the verification of the results. The determination of recharge rates on a hydrogeological basin scale is valuable for the understanding of karst aquifer functions. Nevertheless, we strongly suggest comparing the results with the hydrological component of infiltration at the hydrological basin scale [56]. This approach could better determine underground runoff, which is critically important in the groundwater extraction process for the sustainable water supply of the community. Future research will incorporate hydro-chemical data, high-frequency discharge measurements, and isotopic data from groundwater and rain.

4. Conclusions

The two-step methodological approach that was applied in this study revealed that the geological structure influences the recharge rates of a karst aquifer. The conclusions are summarized below:

- The discretization of formation permeability increases the reliability of recharge rate determinations.
- Modified APLIS, compared to the initial method, provided extended zones with Very Low (<20%) and High (60–80%) recharge rates.
- The modified APLIS method estimated a relatively lower recharge rate (41.4%) compared to the initial method (42.7%) in Ziria, mainly due to the imported parameter of permeability.
- The cross-comparison of the results between the different karst systems revealed that the coverage of karst aquifers determines the recharge rate.
- The highest mean recharge rate was estimated in the Planitero karst system (48.6%) due to the absence of coverage of the karstified rocks.

This study revealed that modified APLIS constitutes a flexible method for the estimation of karst aquifer recharge rates in the Mediterranean region. The quantification and spatial distribution of mean annual recharge rates can increase the accuracy of water balance estimations, which is a fundamental step for sustainable groundwater resource management.

Supplementary Materials: The following supporting information can be downloaded at: https://www.mdpi.com/article/10.3390/w16040568/s1, Reliability of used data.

Author Contributions: Conceptualization, E.-A.N. and E.Z.; data curation and processing, E.-A.N., P.T. and K.P.; software, E.-A.N., P.T. and K.P.; writing-original draft preparation, E.-A.N.; writing–review and editing, E.-A.N. and E.Z.; supervision, E.Z.; funding acquisition, E.-A.N. All authors have read and agreed to the published version of the manuscript.

Funding: Part of the research work was supported by the Hellenic Foundation for Research and Innovation (HFRI) under the HFRI PhD Fellowship grant (Fellowship Number: 684).

Data Availability Statement: The presented data are available on request from the corresponding author.

Acknowledgments: A section of this study has been presented at the 12th International Hydrogeological Conference held in Nicosia, Cyprus, in 2022.

Conflicts of Interest: The authors declare no conflict of interest.

References

1. Wada, Y.; Van Beek, L.P.H.; Van Kempen, C.M.; Reckman, J.W.T.M.; Vasak, S.; Bierkens, M.F.P. Global depletion of groundwater resources. *Geophys. Res. Lett.* **2010**, *37*, L20402. [CrossRef]
2. Scanlon, B.R.; Fakhreddine, S.; Rateb, A.; de Graaf, I.; Famiglietti, J.; Gleeson, T.; Grafton, R.Q.; Jobbagy, E.; Kebede, S.; Kolusu, S.R.; et al. Global water resources and the role of groundwater in a resilient water future. *Nat. Rev. Earth Environ.* **2023**, *4*, 87–101. [CrossRef]
3. Mishra, B.K.; Kumar, P.; Saraswat, C.; Chakraborty, S.; Gautam, A. Water Security in a Changing Environment: Concept, Challenges and Solutions. *Water* **2021**, *13*, 490. [CrossRef]
4. Taylor, R.G.; Scanlon, B.; Döll, P.; Rodell, M.; Van Beek, R.; Wada, Y.; Longuevergne, L.; Leblanc, M.; Famiglietti, J.S.; Edmunds, M.; et al. Ground water and climate change. *Nat. Clim. Chang.* **2012**, *3*, 322–329. [CrossRef]
5. Jia, Z.; Zang, H.; Zheng, X.; Xu, Y. Climate Change and Its Influence on the Karst Groundwater Recharge in the Jinci Spring Region, Northern China. *Water* **2017**, *9*, 267. [CrossRef]
6. Lukač Reberski, J.; Rubinić, J.; Terzić, J.; Radišić, M. Climate Change Impacts on Groundwater Resources in the Coastal Karstic Adriatic Area: A Case Study from the Dinaric Karst. *Nat. Resour. Res.* **2020**, *29*, 1975–1988. [CrossRef]
7. Klaas, D.K.S.Y.; Imteaz, M.A.; Sudiayem, I.; Klaas, E.M.E.; Klaas, E.C.M. Assessing climate changes impacts on tropical karst catchment: Implications on groundwater resource sustainability and management strategies. *J. Hydrol.* **2020**, *582*, 124426. [CrossRef]
8. Sivelle, V.; Jourde, H.; Bittner, D.; Mazzilli, N.; Tramblay, Y. Assessment of the relative impacts of climate changes and anthropogenic forcing on spring discharge of a Mediterranean karst system. *J. Hydrol.* **2021**, *598*, 126396. [CrossRef]
9. Taheri, K.; Taheri, M.; Parise, M. Impact of intensive groundwater exploitation on an unprotected covered karst aquifer: A case study in Kermanshah Province, western Iran. *Environ. Earth Sci.* **2016**, *75*, 1221. [CrossRef]
10. Zhang, Z.; Xu, Y.; Zhang, Y.; Guo, L.; Wang, Z.; Zheng, Q. Impact of groundwater overexploitation on karst aquifer and delineation of the critical zones: Case study of Jinci spring in Shanxi, China. *Carbonates Evaporites* **2022**, *37*, 68. [CrossRef]
11. Kazakis, N.; Chalikakis, K.; Mazzilli, N.; Ollivier, C.; Manakos, A.; Voudouris, K. Management and research strategies of karst aquifers in Greece: Literature overview and exemplification based on hydrodynamic modelling and vulnerability assessment of a strategic karst aquifer. *Sci. Total Environ.* **2018**, *643*, 592–609. [CrossRef]
12. Voudouris, K.S. Status and codification of karst aquifer systems in Greece. *Bull. Geol. Soc. Greece* **2021**, *57*, 23–51. [CrossRef]
13. Seiler, K.P.; Gat, J.R. *Groundwater Recharge from Run-Off, Infiltration and Percolation*; Springer: Dordrecht, The Netherlands, 2007.
14. Sappa, G.; Vitale, S.; Ferranti, F. Identifying Karst Aquifer Recharge Areas using Environmental Isotopes: A Case Study in Central Italy. *Geosciences* **2018**, *8*, 351. [CrossRef]
15. Dar, F.A.; Jeelani, G.; Perrin, J.; Ahmed, S. Groundwater recharge in semi-arid karst context using chloride and stable water isotopes. *Groundw. Sustain. Dev.* **2021**, *14*, 100634. [CrossRef]
16. Iacurto, S.; Grelle, G.; De Filippi, F.M.; Sappa, G. Karst Recharge Areas Identified by Combined Application of Isotopes and Hydrogeological Budget. *Water* **2021**, *13*, 1965. [CrossRef]
17. Petitta, M.; Banzato, F.; Lorenzi, V.; Matani, E.; Sbarbati, C. Determining recharge distribution in fractured carbonate aquifers in central Italy using environmental isotopes: Snowpack cover as an indicator for future availability of groundwater resources. *Hydrogeol. J.* **2022**, *30*, 1619–1636. [CrossRef]
18. Radulovic, M.; Stevanovic, Z.; Radulovic, M. A new approach in assessing recharge of highly karstified terrains-Montenegro case studies. *Environ. Earth Sci.* **2012**, *65*, 2221–22230. [CrossRef]
19. Hartmann, A.; Barbera, J.A.; Lange, J.; Andreo, B.; Weiler, M. Progress in the hydrologic simulation of time variant recharge areas of karst systems—Exemplified at a karst spring in Southern Spain. *Adv. Water Resour.* **2013**, *54*, 149–160. [CrossRef]
20. Malard, A.; Sinreich, M.; Jeannin, P.-Y. A novel approach for estimating karst groundwater recharge in mountainous regions and its application in Switzerland. *Hydrol. Process.* **2016**, *30*, 2153–2166. [CrossRef]
21. Hosseini, S.M.; Ataie-Ashtiani, B.; Simmons, C.T. Spring hydrograph simulation of karstic aquifers: Impacts of variable recharge area, intermediate storage and memory effects. *J. Hydrol.* **2017**, *552*, 225–240. [CrossRef]
22. Jukić, D.; Denić-Jukić, V.; Lozić, A. An alternative method for groundwater recharge estimation in karst. *J. Hydrol.* **2021**, *600*, 126671. [CrossRef]
23. Messerschmid, C.; Aliewi, A. Spatial distribution of groundwater recharge, based on regionalised soil moisture models in Wadi Natuf karst aquifers, Palestine. *Hydrol. Earth Syst. Sci.* **2022**, *26*, 1043–1061. [CrossRef]
24. Berthelin, R.; Olarinoye, T.; Rinderer, M.; Mudarra, M.; Demand, D.; Scheller, M.; Hartmann, A. Estimating karst groundwater recharge from soil moisture observations—A new method tested at the Swabian Alb, southwest Germany. *Hydrol. Earth Syst. Sci.* **2023**, *27*, 385–400. [CrossRef]
25. White, W.B. Conceptual models for karstic aquifers. In *Karst Modeling*; Palmer, A.N., Palmer, M.V., Sasowsky, I.D., Eds.; The Karst Waters Institute: Charles Town, WV, USA, 1999; pp. 11–16.
26. Bakalowicz, M. Karst groundwater: A challenge for a new resources. *Hydrogeol. J.* **2005**, *13*, 148–160. [CrossRef]
27. Andreo, B.; Vías, J.; Durán, J.J.; Jiménez, P.; López-Geta, J.A.; Carrasco, F. Methodology for groundwater recharge assessment in carbonate aquifers: Application to pilot sites in southern Spain. *Hydrogeol. J.* **2008**, *16*, 911–925. [CrossRef]

28. Marín, A.I. Los Sistemas de Información Geográfica Aplicados a la Evaluación de Recursos Hídricos y a la Vulnerabilidad a la Contaminación de Acuíferos Carbonatados: Caso de la Alta Cadena (Provincia de Málaga). Ph.D. Thesis, University of Malaga, Malaga, Spain, 2009.
29. Zagana, E.; Tserolas, P.; Floros, G.; Katsanou, K.; Andreo, B. First outcomes from groundwater recharge estimation in evaporate aquifer in Greece with the use of APLIS method. In *Advances in the Research of Aquatic Environment*; Lambrakis, N., Stournaras, G., Katsanou, K., Eds.; Springer: Berlin/Heidelberg, Germany, 2011; Volume 2, pp. 89–96.
30. Martos-Rosillo, S.; Rodriguez-Rodriguez, M.; Pedrera, A.; Cruz- SanJulian, J.J.; Rubio, J.C. Groundwater recharge in semi-arid carbonate aquifers under intensive use: The Estepa Range aquifers (Seville, southern Spain). *Environ. Earth Sci.* **2013**, *70*, 2453–2468. [CrossRef]
31. Hartmann, A.; Mudarra, M.; Andreo, B.; Marín, A.; Wagener, T.; Lange, J. Modeling spatiotemporal impacts of hydroclimatic extremes on groundwater recharge at a Mediterranean karst aquifer. *Water Resour. Res.* **2014**, *50*, 6507–6521. [CrossRef]
32. Mudarra, M.; Hartmann, A.; Andreo, B. Combining Experimental Methods and Modeling to Quantify the Complex Recharge Behavior of Karst Aquifers. *Water Resour. Res.* **2019**, *55*, 1384–1404. [CrossRef]
33. Farfán, H.; Corvea, J.L.; De Bustamante, I. Sensitivity Analysis of ALPIS Method to Compute Spatial Variability of Karst Aquifers Recharge at the national Park of Viñales (Cuba). In *Advances in Research in Karst Media*; Andreo, B., Carrasco, F., Durán, J.J., LaMoreaux, J.W., Eds.; Springer: Berlin/Heidelberg, Germany, 2010; pp. 19–24.
34. Espinoza, K.; Marina, M.; Fortuna, J.H.; Altamirano, F. Comparison of the APLIS and Modified-APLIS methods to estimate the recharge in fractured karst aquifer, Amazonas, Peru. In *Hydrogeological and Environmental Investigations in Karst Systems*; Andreo, B., Carrasco, F., Durán, J.J., Jiménez, P., LaMoreaux, J.W., Eds.; Springer: Berlin/Heidelberg, Germany, 2015; Volume 1, pp. 83–90.
35. Alem, H.; Soudejani, A.E.; Farmanieh, S.N. Ground water recharge assessment in the karst aquifers of North Khorasan, Iran using APLIS method. *Acta Carsologica* **2017**, *46*, 283–294. [CrossRef]
36. Special Secretariat for Water. *Management Plans of Northern Peloponnese River Basin District*; Ministry of Environment and Energy: Athens, Greece, April 2013.
37. WFD. Directive 2000/60/EC of the European Parliament and of the Council of 23 October 2000 establishing a framework for Community action in the field of water policy. *Off. J. Eur. Communities* **2000**, *L 327*, 1–72.
38. De Wever, P.; Dercourt, J.; Fleury, J.J. *Kandhila Sheet. 1:50.000*; Institute of Geology and Mineral Exploration: Athens, Greece, 1982.
39. Tataris, A.; Maragoudakis, N.; Kounis, G.; Christodoulou, G.; Tsaila-Monopoli, S. *Nemea Sheet. 1:50.000*; Institute for Geology and Subsurface Research: Athens, Greece, 1970.
40. Hötzl, H.; Merkler, G.; Reichert, B.; Röckel, T.; Watzel, R. Interpretation of geophysical measurements in the poljes of Alea-Scotini and Stymfalia. In *Karst Hydrogeology of the Central and Eastern Peloponnesus (Greece), Proceedings of the 5th International Symposium on Underground Water Tracing, Athens, Greece, 22–27 September 1986*; Steirische Beiträge zur Hydrogeologie; Morfis, A., Zojer, H., Eds.; Springer: Cham, Switzerland, 1986; Volumes 37/38, pp. 44–54.
41. Meilliez, F.; Flament, J.M.; De Wever, P.; Dercourt, J.; Fleury, J.J. *Dhafni Sheet. 1:50.000*; Institute of Geology and Mineral Exploration: Athens, Greece, 1978.
42. Psonis, K.; Skourtsi-Koroneou, V.; Carras, N.; Varti-Mataragha, M. *Aeghion Sheet. 1:50.000*; Institute of Geology and Mineral Exploration: Athens, Greece, 2013.
43. Psonis, K.; Tsapralis, V.; Skourtsi-Koroneou, V. *Astakos Sheet. 1:50.000*; Institute of Geology and Mineral Exploration: Athens, Greece, 1986.
44. Kouris, C.; Tsaila-Monopolis, S. *Echinades Sheet. 1:50.000*; Institute of Geology and Mineral Exploration: Athens, Greece, 1989.
45. Gofa, F.; Mamara, A.; Anadranistakis, M.; Flocas, H. Developing gridded climate data sets of precipitation for Greece based on homogenized time series. *Climate* **2019**, *7*, 68. [CrossRef]
46. Kakavas, M.; Nikolakopoulos, K.G.; Kyriou, A.; Zagana, H. Assessment of freely available DSMs for automatic karst feature detection. *Arab. J. Geosci.* **2018**, *11*, 388. [CrossRef]
47. Morfis, A.; Zojer, H. (Eds.) *Karst Hydrogeology of the Central and Eastern Peloponnesus (Greece), Proceedings of the 5th International Symposium on Underground Water Tracing, Athens, Greece, 22–27 September 1986*; Steirische Beiträge zur Hydrogeologie; Springer: Cham, Switzerland, 1986; Volumes 37/38, pp. 1–301.
48. Zervogiannis, G. *Final Hydrogeological Study for the Reformation of the Stymphalian Springs in the Prefecture of Corinth*; Ministry of Agriculture: Athens, Greece, 1991. (In Greek)
49. Röckel, T.; Hötzl, H. Polje of Stymfalia. In *Karst Hydrogeology of the Central and Eastern Peloponnesus (Greece), Proceedings of the 5th International Symposium on Underground Water Tracing, Athens, Greece, 22–27 September 1986*; Steirische Beiträge zur Hydrogeologie; Morfis, A., Zojer, H., Eds.; Springer: Cham, Switzerland, 1986; Volumes 37/38, pp. 127–152.
50. Katakouzinos, D.S. *Soil Map of Greece. 1:1.000.000*; Ministry of Agriculture: Athens, Greece, 1967.
51. FAO; UNESCO. *Soil Map of the World. 1:5.000.000*; UNESCO: Paris, France, 1978.
52. European Soil Bureau Network. *Soil Atlas of Europe*; European Commission: Luxembourg, 2005; p. 128.
53. Voudouris, K.; Panagopoulos, A.; Markantonis, K. Hydrological balance and possibilities of sustainable water resources management in Stimfalia basin (prefecture of Korinthos). In Proceedings of the 6th Pan-Hellenic Geographical Conference of the Hellenic Geographical Society, Thessaloniki, Greece, 3–6 October 2002; Volume 2, pp. 327–334.
54. Rad, M.M.; Mokhtari, L.G.; Bahrami, S.; Asadi, M.Z. Assessment of infiltration potential using the AHP, APLIS and modified APLIS models (Case study: Esfarayen Basin). *Quant. Geomorphol. Res.* **2018**, *7*, 117–139.

55. Kirn, L.; Mudarra, M.; Marín, A.; Andreo, B.; Hartmann, A. Improved assessment of groundwater recharge in a Mediterranean karst region: Andalusia, Spain. In *EuroKarst 2016, Neuchâtel*; Renard, P., Bertrand, C., Eds.; Springer: Cham, Switzerland, 2017; pp. 117–125.
56. Malov, A.I. Groundwater resources of the White Sea Basin (NW Russia). In *The Arctic: Current Issues and Challenges*; Malov, A.I., Pokrovsky, O.S., Kirpotin, S.N., Eds.; Nova Science Publishers: New York, NY, USA, 2020; pp. 239–266.

Disclaimer/Publisher's Note: The statements, opinions and data contained in all publications are solely those of the individual author(s) and contributor(s) and not of MDPI and/or the editor(s). MDPI and/or the editor(s) disclaim responsibility for any injury to people or property resulting from any ideas, methods, instructions or products referred to in the content.

water

MDPI

Article

Nature-Based Solutions for the Restoration of Groundwater Level and Groundwater-Dependent Ecosystems in a Typical Inland Region in China

Min Liu [1,2], Zhenlong Nie [1,2,*], Le Cao [1,2,*], Lifang Wang [1,2] and Huixiong Lu [3]

[1] Institute of Hydrogeology and Environmental Geology, Chinese Academy of Geological Sciences, 268 Zhonghua North Street, Shijiazhuang 050061, China; agnes0505@163.com (M.L.); wanglifang@mail.cgs.gov.cn (L.W.)
[2] Key Laboratory of Groundwater Sciences and Engineering, Ministry of Natural Resources, 268 Zhonghua North Street, Shijiazhuang 050061, China
[3] Airborne Survey and Remote Sensing Center of Nuclear Industry, Shijiazhuang 050002, China; 13933164939@163.com
* Correspondence: nzlngj@163.com (Z.N.); caole@mail.cgs.gov.cn (L.C.)

Abstract: The rapid drop in groundwater level and the degradation of groundwater-dependent ecosystems (GDEs) has led to serious imbalances in the development of the socio-ecological system (SES) in Minqin Oasis, northwest China. In this study, the interactions between the elements of the SES were analyzed, and the effects of the implementation of nature-based solutions (NbS) and the resilience of the SES were assessed using the methods of linear trend analysis, correlation, and fuzzy comprehensive evaluation. The results showed that: (i) the most important contributing factor to the increase in groundwater depth (GLD) and the degradation of GDEs was the continuous groundwater extraction for the irrigation of farmland; and (ii) the natural vegetation began to be degraded when the GLD surpassed 5 m; (iii) the initial goal of NbS was achieved, the increase in GLD has been curbed, and the vegetation and the wetland area of Qingtu lake have begun to be restored. The SES resilience index increased by a factor of 1.82 from 2009 to 2017; however, it was still below 0.6, and thus the NbS should be continued in the future. This study provides a reference for the sustainable development of the SES in other similar areas under various environmental challenges.

Keywords: groundwater depth; vegetation ecology; wetland ecology; resilience of socio-ecological system; Minqin Oasis

1. Introduction

The crises currently facing the world are constantly escalating, and the interactions between humans and the environment continue to deteriorate, suggesting that humans and other life on Earth may be approaching a catastrophic tipping point [1]. Global issues such as climate change, food shortages, groundwater depletion, and loss of biodiversity pose significant challenges to social and ecological systems on which humans rely for survival. In response, human beings urgently need innovative solutions to these problems, and to reconsider the relationship between humans and nature. It is time to shift from the disorderly utilization of natural resources to respecting nature, cooperating with nature, and maximizing the power of nature. Thus, the concepts and methods of Nature-based Solutions (NbS) are emerging [2–8].

NbS is a new concept that has arisen during the past two decades, and there are currently multiple definitions and interpretations of the term [9,10]. In the fifth session of the United Nations Environment Assembly of the United Nations Environment Programme, NbS was defined as "actions to protect, conserve, restore, sustainably use and manage natural or modified terrestrial, freshwater, coastal and marine ecosystems, which

address social, economic, and environmental challenges effectively and adaptively, while simultaneously providing human well-being, ecosystem services and resilience and biodiversity benefits" [11]. Many such NbS initiatives, including ecological restoration and protection, holistic management, groundwater recharge, and blue-green infrastructure practices, involve multiple methods of cooperating with nature to achieve social benefits. These methods are being implemented globally, especially in rural communities and among people in low- and middle-income countries [12,13]. Although NbS may provide more productive and cost-effective remedies than conventional techniques, monitoring and assessment methods for implementing these solutions are not documented across multiple scales and resources; how NbS practices can be transformed into the direct application of management activities remains an open question.

The Shiyang River Basin (SRB) is a typical inland arid basin in northwest China. Minqin Oasis, located downstream of the SRB, was once one of the seventeen poverty-stricken counties in Gansu Province that accounted for 40% of the "Silk Road Economic Belt" in China. The area has a dry climate with scarce water resources. Groundwater is the main water source for maintaining local socio-economic development, agriculture, and the oasis environment. Since 1970, continuous groundwater exploitation in the SRB has led to the transformation of the downstream Minqin Oasis into a pure pumping-well irrigation area, and there has been a rapid decline in the groundwater level [14,15]. By 2007, the groundwater depth (GLD) in Minqin Oasis was generally between 20 and 40 m, far lower than the ecologically suitable GLD for surface vegetation [16,17]. Thus, the vegetation ecology in the oasis–desert ecotone (ODE) was severely degraded. Sandstorms were frequent, and the wetland area of the terminal lake (Qingtu Lake) was significantly reduced. Due to the intrusion of sandstorms from the northwest Badain Jaran Desert, there has been extensive sand intrusion and human retreat in the oasis. Faced with the serious imbalance of the socio-ecological system (SES) in Minqin Oasis, the Chinese government proposed a series of NbS, called the Comprehensive Administration Project of the SRB (CASRB). This program aimed to restore the groundwater level (GL) and vegetation of the Minqin Oasis in the lower SRB, and in the meantime lift the county out of poverty by increasing the per-capita income of the residents, ultimately achieving sustainable development of the SES. With regard to the effect of the CASRB, the recovery of the GL [16,18] and the ecological functions of the groundwater [17,19] have been investigated by some researchers. However, there are few reports on the evaluation of this NbS from the perspective of the sustainable development of regional SES.

Therefore, the objectives of this study were: (1) to analyze the changes in hydro-climatic elements, land use and land cover, and the normalized difference vegetation index (NDVI) in the oasis–desert ecotone (ODE) during the past several decades; (2) to investigate the close interactions among the elements of the SES both in agroecological area and natural ecological area; (3) to reveal the effects of the CASRB on the restoration of the groundwater and groundwater-dependent ecosystems (GDEs) by primary indicators; and (4) to assess the changes in the resilience of the SES in the post-CASRB period by using the fuzzy comprehensive evaluation method based on the above interaction analysis and the selected indicators. This study can enrich the theory and practice of NbS in combination of irrigation oasis and natural oasis in arid regions, and provide decision-making references for the sustainable development, planning, and management of the SES in the SRB under various environmental challenges.

2. Materials and Methods

2.1. Study Area

The SRB is located in the central part of Gansu Province and the eastern edge of the Hexi Corridor; it forms one of the three arid inland basins in China. The upper reaches of the SRB are in the Qilian Mountain, and the middle reaches comprise the Wuwei sub-basin, with Liangzhou County as the capital. The main study area of Minqin Oasis is in the downstream area of the SRB (Figure 1). In its natural state, runoff flows into Minqin after

being consumed in the middle sub-basin, then flows through the Caiqi section located upstream of Hongyashan Reservoir. Minqin Oasis is located between longitude 101°49′41″ E–104°12′10″ E and latitude 38°3′45″ N–39°27′37″ N [20]. Due to being sandwiched between the northwest Badain Jaran Desert and the southeast Tengger Desert, the ecology of Minqin Oasis is a vital natural barrier that prevents the two deserts from converging. It has a typical continental arid desert climate, with an average annual temperature of 7.8 °C, an average annual precipitation of 116.5 mm, and an average annual evaporation of 2308 mm during 1971–2010 [21]. The irrigation areas in Minqin Oasis mainly consist of the Dam, Quanshan, and Lake irrigation areas (Figure 1). In 2017, the GLD in Minqin Oasis was generally between 20 and 30 m in the irrigation area and was generally less than 10 m in the Qingtu Lake area [17]. The natural vegetation in the oasis–desert ecotone (ODE) of Minqin Oasis is largely temperate desert (arid desert) vegetation dominated by arid and super-arid shrubs and semi-shrubs. The main shrub species include *Tamarix* spp., *Nitraria* spp., *Kalidium foliatum*, *Haloxylon ammodendron*, *Artemisia arenaria* and *Reaumuria soongorica*. Arbors include *Populus gansuensis*, *Populus euphratica*, *Angustifolia elaeagnus* and *Salix matsudana*. Herbs include *Achnatherum splendens*, *Phragmites australis*, *Bassia dasyphylla*, *Sophora alopecuroides*, and *Agriophyllum squarrosum* [16,17,22,23].

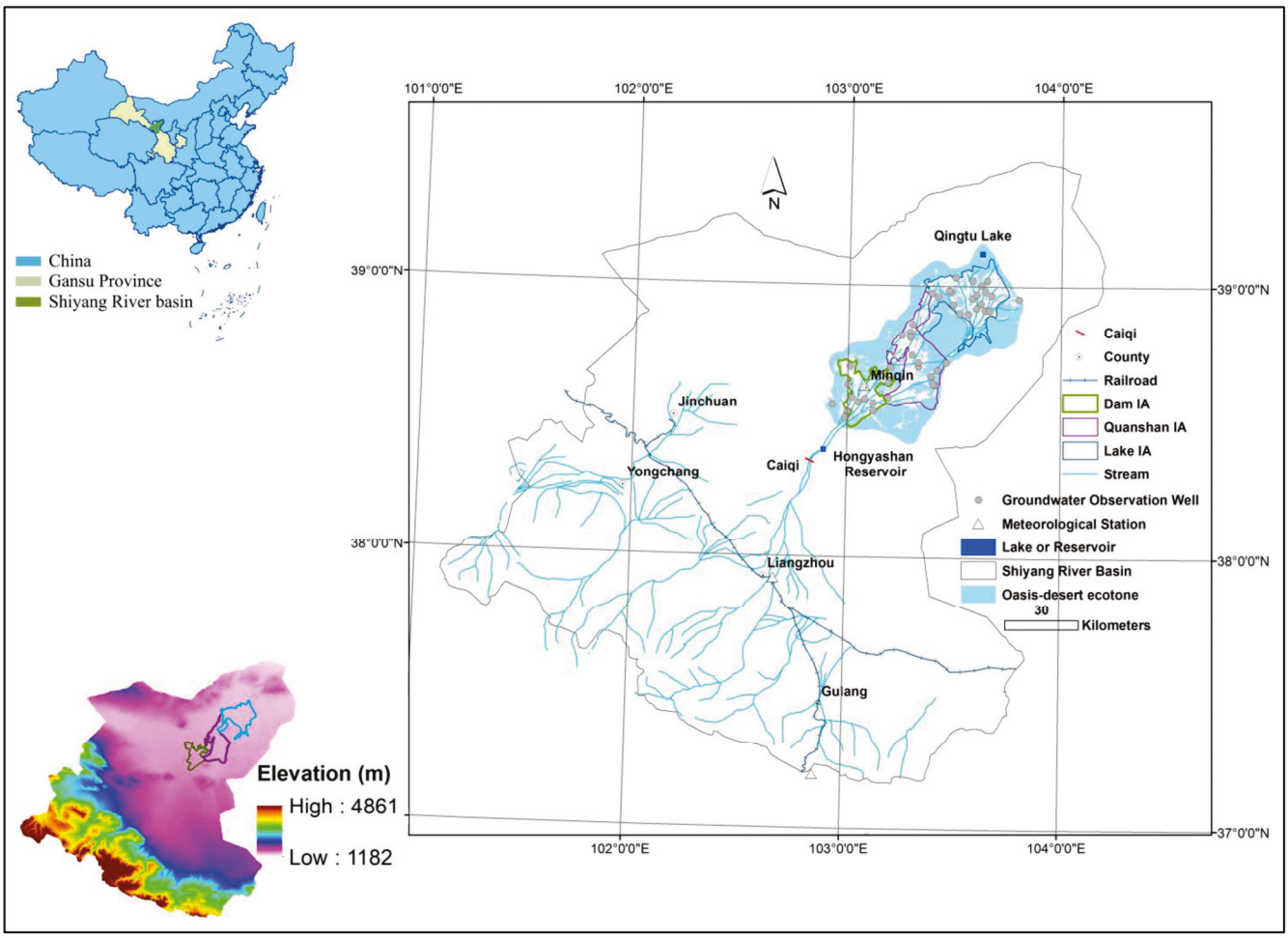

Figure 1. Study area (IA: irrigation area).

2.2. Data

In this study, the meteorological data were collected from the National Meteorological Administration, and the runoff and water supply data were collected from the Wuwei Water Affairs Authority. The GLD data were collected from the Institute of Hydrogeological Engineering Geology, Gansu Provincial Bureau of Geology and Mineral Exploration and

Development. There were 46 observation wells for phreatic aquifers. The wells were mostly distributed in irrigation areas (Figure 1). The time series for these data were monthly during 1980–2017. The land-use and land-cover data of 1985, 2008, and 2017 were derived from the thematic mapper (TM), enhanced thematic mapper (ETM), and operational land imager (OLI) data obtained by the US Landsat satellite-5, the US Landsat satellite-7, and the US Landsat satellite-8. The annual mean normalized difference vegetation index (NDVI) for 2000–2017 were also obtained from the Landsat satellites. The area of the Qingtu Lake wetland for 2009–2017 was obtained from both the Landsat satellites and the China Gaofen-1 satellite and Gaofen-2 satellite due to that the high resolution of Gaofen satellites has great advantage in the interpretation of small areas. The image map data were derived by atmospheric correction, geometric correction, image fusion, image stitching, and band calculation [24]. The species richness data and corresponding GLD were from the natural vegetation quadrat survey, in which the species richness is defined as the number of species within a quadrat. The per-capita income data of Minqin County during 2009–2017 were obtained from the Statistical Yearbook of Wuwei City.

2.3. Methods

2.3.1. Mathematical Statistics Method

The mathematical statistics method studies the regularity of the inter-relationships between the sample and the population, as well as the regularity of the inter-relationships among various related factors. A linear trend analysis and a correlation analysis was applied in this study.

1. Linear trend analysis

Linear trend analysis is a highly general and therefore very flexible data-analytic system that can be used for studying specific quantitative relationships between variables [25]. It is normally used to establish mathematical models that reflect the specific quantitative relationships between geographic elements, namely regression models [26]. The form of the relationship is not constrained; it may be univariate or multivariate. In this study, a univariate linear regression model was used to examine the variation rates of the air temperature, precipitation, runoff, the GLD of each observation well, and the wetland area of Qingtu lake. The least squares estimation was used for the parameter estimation [26].

2. Correlation analysis

Correlation analysis is a statistical analysis method that investigates the relationship between two or more random variables of equal status. The general meaning of the concept is that knowledge with regard to one of the variables carries information about the other variable [27]. It is the process of describing the degree of closeness between objective things and expressing it with appropriate statistical indicators [26]. A correlation analysis was used to analyze the relationships between the elements of the SES in this study.

2.3.2. GLD—Natural Vegetation Quadrat Joint Survey

The GLD—natural vegetation ecology quadrat joint survey was adapted from previously published guidelines [28] while considering the actual distribution of the groundwater-dependent vegetation communities in the SRB. Therefore, this survey added GLD measurements near each vegetation quadrat. If no groundwater observation well was available near the vegetation quadrat, the investigators would dig a simple groundwater measuring well on site, and GLD was measured once the groundwater level had stabilized. The survey was conducted in August and September 2018. The procedure used in the joint survey is described in Liu et al. [17].

2.3.3. Fuzzy Comprehensive Evaluation Method

The fuzzy comprehensive evaluation method was used to assess the resilience of the SES during the post-CASRB period of Minqin Oasis. The theory was introduced as follows [26,29].

For two finite sets, $U = \{U_1, U_2, \ldots\ldots, U_m\}$ and $V = \{V_1, V_2, \ldots\ldots, V_m\}$, where U represents a set of indicators based on which comprehensive evaluation is performed and V is a set of judgments, a fuzzy comprehensive evaluation is a fuzzy transformation process as follows:

$$B = A \circ R \tag{1}$$

In Equation (1), A is a fuzzy subset of U, and the evaluation result B is a fuzzy subset of V. $A = \{a_1, a_2, \ldots\ldots, a_m\}$, $0 \leq b_j \leq 1$, where a_i is the degree of membership of U to A. a_i represents the relative importance (weight) of the indicator U_i among all of the evaluation indicators, and also represents the ability of U_i to determine the grade, satisfying $\sum_{i=1}^{m} a_i = 1$. b_j is the degree of membership of grade V_j to B, representing a comprehensive evaluation result.

The fuzzy transformation matrix is:

$$R = \begin{bmatrix} r_{11}, & r_{12}, & \ldots & r_{1n} \\ r_{21}, & r_{22}, & \ldots & r_{2n} \\ \ldots & \ldots & & \ldots \\ r_{m1}, & r_{m2}, & \ldots & r_{mn} \end{bmatrix}, \tag{2}$$

where r_{ij} is the degree of membership of grade V_j for U_i, and thus, the ith row $R_i = (r_{i1}, r_{i2}, \ldots\ldots, r_{in})$ in the matrix R represents the evaluation results of U_i.

In this study, the indicators used for comprehensive evaluation were determined based on the factors influencing the sustainable development of SES in Minqin. The evaluation procedure involved the following steps: (1) selection of the resilience indicators of the SES, (2) determination of grading values and the corresponding rating scores, (3) determination of the weight for each resilience indicator, and (4) composite evaluation index calculation of the resilience of SES.

3. Results

3.1. Changes in Elements of Climate, Water Resources, and Ecology

3.1.1. Variations in Natural Hydro-Climatic Elements

Annual air temperature in Minqin showed a significant upward trend under global warming. The rate of increase was 0.4 °C/10a during 1956–2017 (Figure 2a). Temporally, the air temperature increased slowly during 1956–1986, then rose significantly after 1987, and the rising trend reached a new level in 1998. Annual precipitation showed a nonsignificant increase rate of 2.8 mm/10a (Figure 2b). Temporally, precipitation decreased in the 1960s, then increased in the 1970s, and then decreased again from the 1980s, finally increasing since 1994. Pan evaporation (E601) showed a nonsignificant increase rate of 9.8 mm/10a (Figure 2c). The runoff at the mountain pass in the upper SRB showed no clear trend. However, the runoff had a high flow rate before 1970, then entered a normal flow period during the next two decades before experiencing a low flow period in the 1990s. The runoff has increased since 2003 (Figure 2d). This was in accordance with the conclusion that the largest tributary of the Shiyang River entered a wet period in 2003 by Song et al. [30]. The natural runoff at the Caiqi section would eventually flow into the Minqin sub-basin after being consumed in the middle SRB. There was a significant decreasing trend with the rate of 81 million cubic meters of water per decade (Figure 2d).

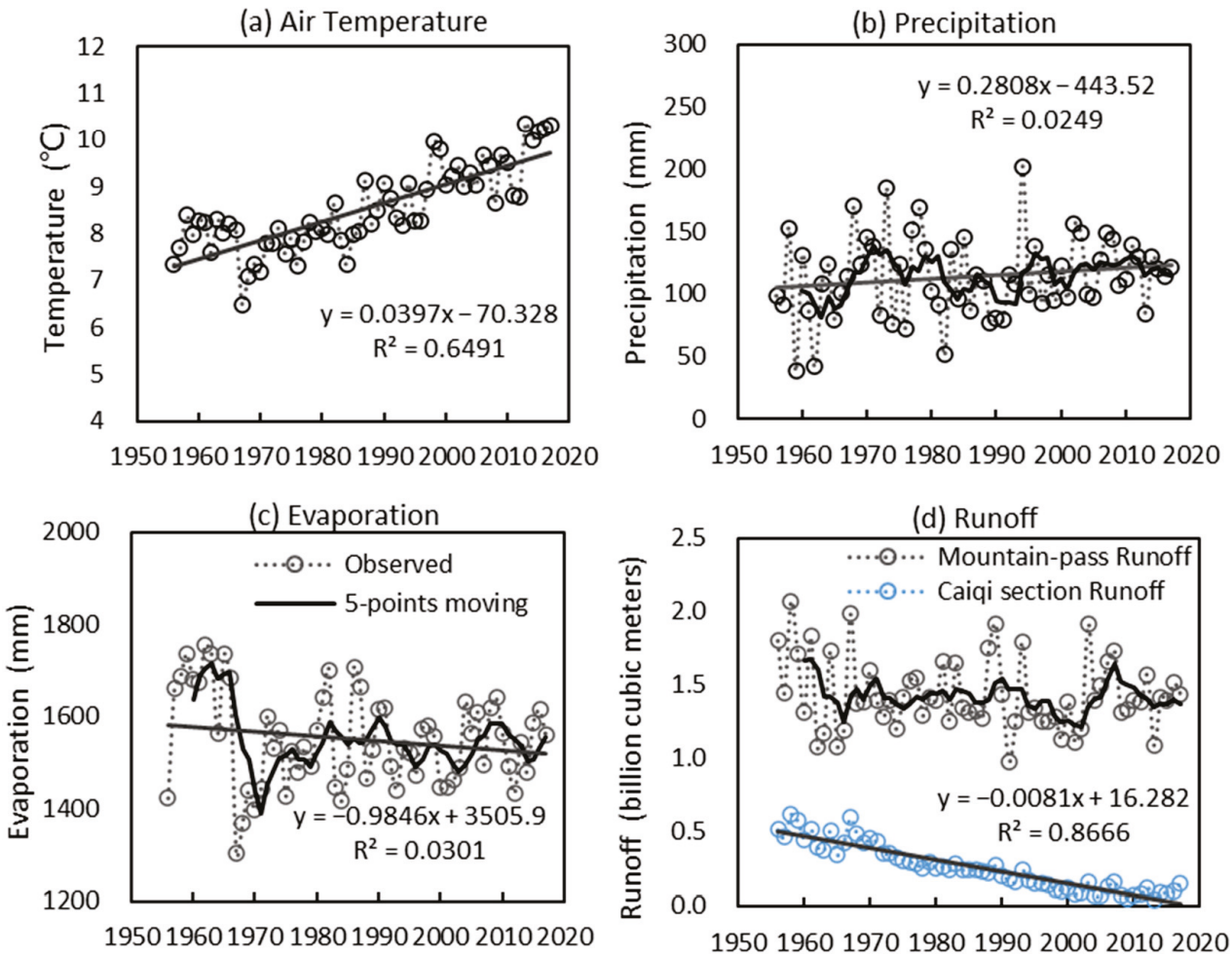

Figure 2. Variations in climatic elements in Minqin and runoff at the mountain-pass. (The dotted line represented 'Observed'; the grey solid line represented the linear trend; the black solid line represented 5-points moving).

3.1.2. Changes in Groundwater Depth

GLD increased dramatically during 1980–2017 (Figure 3). The trend of the GLD at all of the observation wells was significant at the 0.05 level. The increase rates of the GLD of the wells were mostly between 4 m/10a and 6 m/10a, and the rates were greater in the center of the irrigation areas, while becoming less in the lake irrigation area and the eastern peripheral areas of Minqin Oasis (Figure 3a). On the irrigation area scale, the increase rate was larger in the Dam and Quanshan irrigation areas, while being relatively smaller in the lake irrigation area (Figure 3b). Temporally, the change in the GLD experienced two periods (Figure 3b); i.e., the rapid increasing period before the implementation of the CASRB, and a stable or recovery trend from then on, was due to the initial effect of the implementation of CASRB.

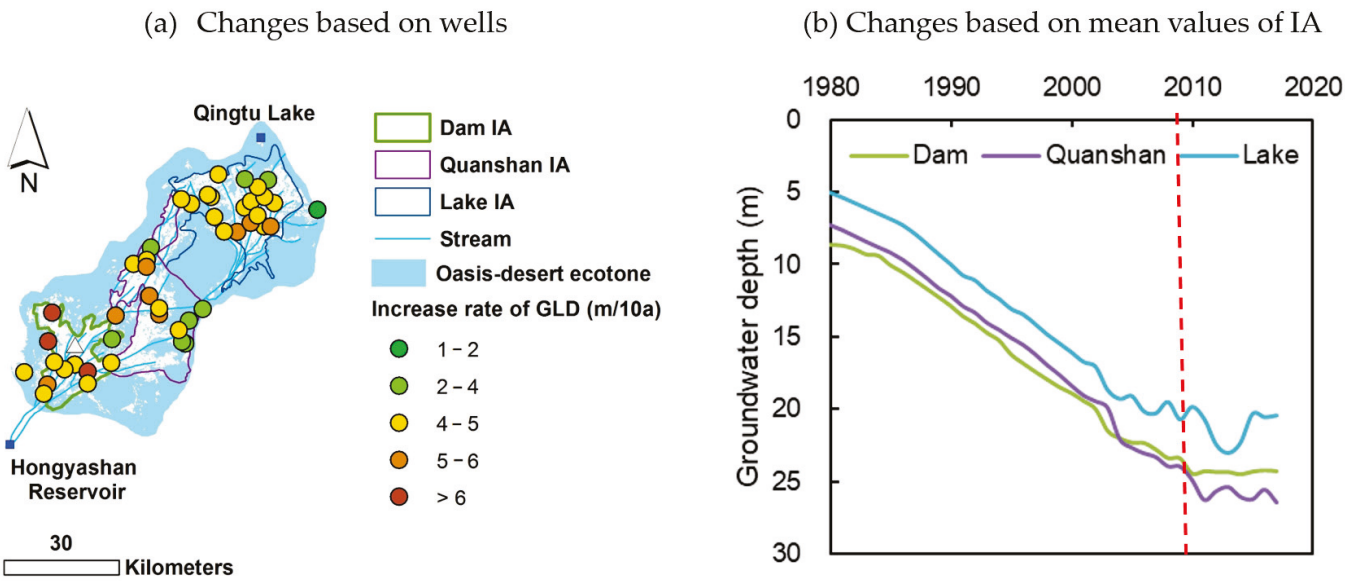

Figure 3. Changes in the groundwater depth in the irrigation areas of Minqin Oasis during 1980–2017 (GLD: groundwater depth; IA: irrigation area; the red dotted line represented the turning point year).

3.1.3. Changes in Land Use and Land Cover (LULC)

The area of the natural oasis and the natural wetland showed decreasing trends from 1985 to 2017. The area of the natural oasis in 2017 was just 78% of that in 1985, and the area of the natural wetland in 2017 was just 18.5% of that in 2017 (Figure 4). Temporally, the decreasing trend became milder after 2008. In the meantime, the area of the artificial oasis, including the farmland and the artificial wetland, increased dramatically until 2008, when the trend leveled off (Figure 4). The farmland expanded by a factor of 1.25 from 1985 to 2008; after which the area was stable from 2008 to the present. The area of the artificial wetland was 5.8 times that in 1985. Furthermore, the area of planted forest (including arbors, shrubs, and grasses) showed an initial decreasing trend before 2008, and then an increasing trend from 2008 (Figure 4). There was also a turning-point year in the land-use type at around 2008, the year after the implementation of the CASRB. The construction land has always shown an increasing trend (Figure 4).

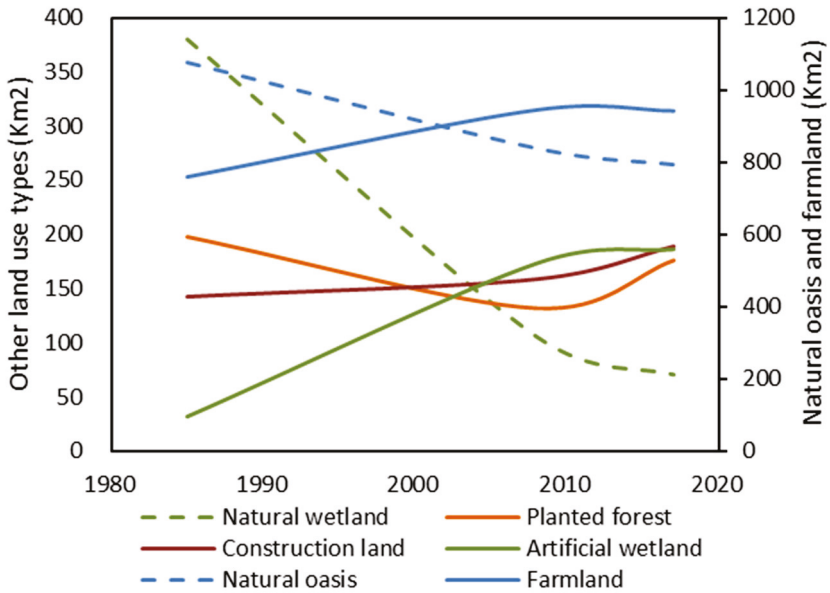

Figure 4. Changes in land-use types in Minqin Oasis (other land use types represent planted forest, construction land, artificial wetland, natural wetland, and farmland).

3.1.4. Changes in NDVI in Oasis–Desert Ecotone

The annual regional mean value of NDVI was between 0.07 and 0.10 during 2000–2011 (Figure 5). This indicated that there was almost no vegetation growth in large areas of the oasis–desert ecotone, and most of the area experienced desertification. From 2011 to 2017, the annual mean NDVI of natural vegetation increased from 0.09 to 0.21, reflecting an improvement in vegetation growth. This was due to the artificial afforestation implemented by the CASRB to prevent the desertification [16] and the restoration of the groundwater ecological function in the areas with a shallow groundwater depth [17].

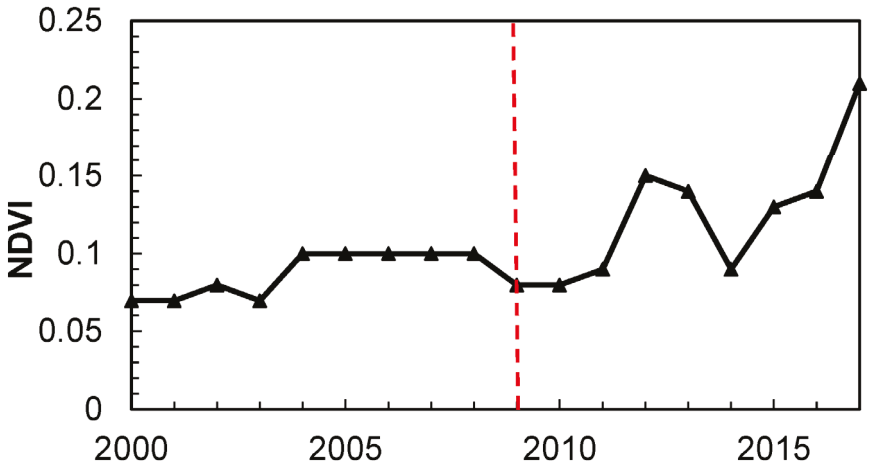

Figure 5. Annual regional mean NDVI value in the Minqin Oasis–desert ecotone [16] (the red dotted line represented the turning point year).

3.2. Interactions among the Elements of Social and Ecological Systems

3.2.1. Farmland–Groundwater Abstraction–Groundwater Depth–Natural Oasis

With the dry climate and the shortage of surface water, the SRB is a region whose socio-economic development, especially regarding agricultural production, was primarily supported by groundwater irrigation. Therefore, the interactions between the land-use type and the groundwater extraction in Minqin Oasis were analyzed based on the data before 2008, when the CASRB had not been fully implemented. The results showed that the area of farmland had a high positive correlation with the groundwater extraction; when the area of the farmland increased, the groundwater abstraction increased (Figure 6b). This finding indicated that groundwater was extracted primarily for agricultural irrigation. Furthermore, the GLD had a strong correlation with the accumulated groundwater extracted during the period of overexploitation. Every increase of 10 million cubic meters of water extracted from the aquifer would lead to a 3 cm decline in the GL (Figure 6d). Eventually, the GL declined beyond the level where most of the surface vegetation could reach, thereby leading to a shrinkage of the natural oasis (Figure 6c). Every increase of 1000 square kilometers of farmland would lead to a decrease of 957 square kilometers of natural oasis (Figure 6a). This indicated that the expansion of the irrigated farmland was the dominant factor to the significant decline in GL and the degradation of the groundwater-dependent vegetation in Minqin Oasis.

The accumulated groundwater extraction instead of annual groundwater extraction was adopted when analyzing the interactions with the GLD. The reasons were as follows. When the groundwater is over-extracted for a long period, this has a direct and accumulated impact on the GL due to the low rate of the aquifer recharge. In other words, the gap between the extraction and the input continuously increased, and thus the GL declined.

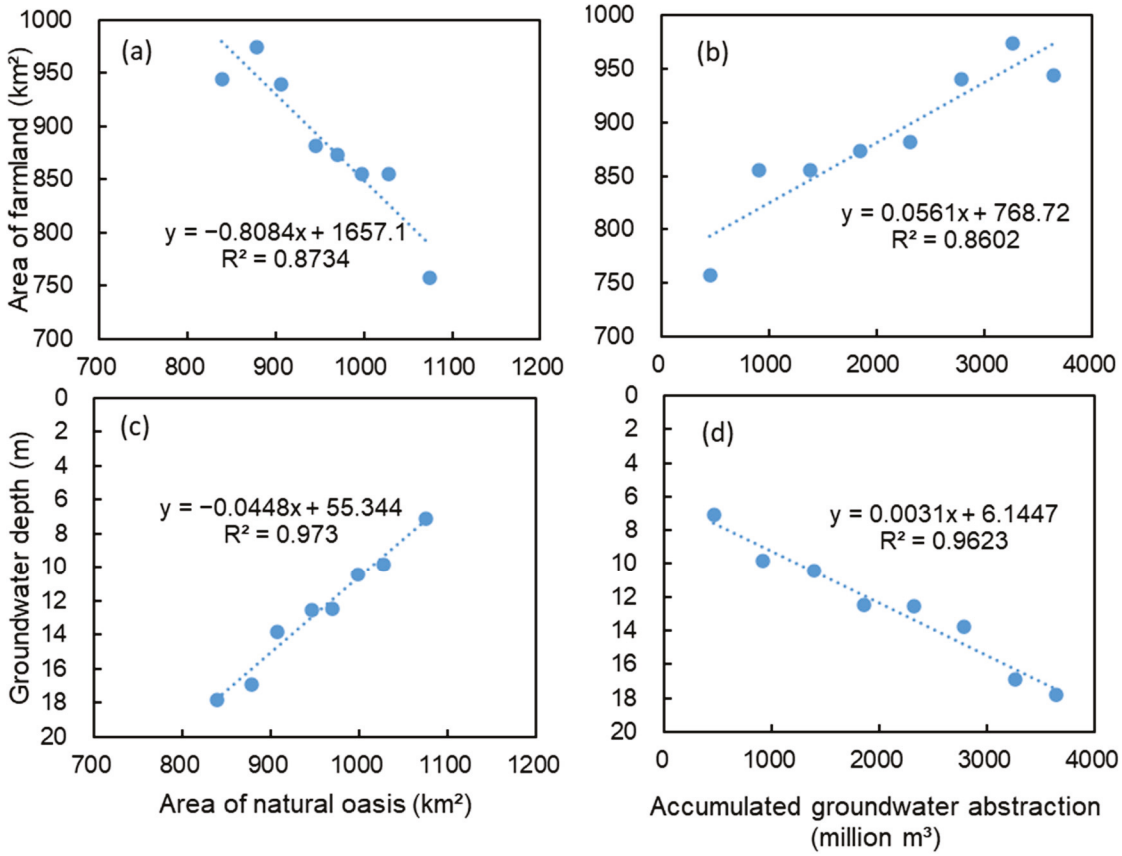

Figure 6. Interactions among the farmland–groundwater abstraction–groundwater depth–natural oasis. ((**a**): represented the correlation between areas of farmland and natural oasis; (**b**): represented that of farmland area and the groundwater abstraction; (**c**): represented that of groundwater depth and area of natural oasis; (**d**): represented that of groundwater depth and groundwater abstraction).

3.2.2. The Relationship of Groundwater to the Main Vegetation Indicators

An ecologically suitable GLD was estimated by analyzing the relationship between GLD with the NDVI of the natural vegetation in the ODE during 2000–2017. The results showed that in 94% of the years considered, the GLD corresponding to the maximum value of NDVI ranged from 2.2 to 3.7 m, and the mean GLD corresponding to the peak value of NDVI was 3.0 m (Figure 7a). After the GLD had increased more than 5.0 m, the value of NDVI was generally less than 0.1 (except for several years the vegetation was planted since 2012), and there was no significant correlation between the GLD and NDVI. When the GLD was less than 5 m, the two indicators were significantly negatively correlated, with a correlation coefficient (r) reaching 0.85 (Figure 7c) [17]. This was in agreement with the results of Cao et al. [16]. Furthermore, an ecological survey of vegetation quadrats and groundwater was conducted, and the results indicated that the species richness reached a maximum at a GLD of about 3 m. That is to say, with the GLD increased from 1 m to 3 m, species richness increased, peaking at approximately 3 m at 10 species; and then slowly become less as the GLD increased greater than 3 m (Figure 7b) [17]. Due to the sparse vegetation in the northwest desert area, vegetation development was only considered when the NDVI value of vegetation is greater than a certain value, such as in Ejina Banner Oasis, where the index was bounded by 0.08 [31]. Therefore, when the GLD exceeded 10 m, there was almost no vegetation, and the transient vegetation growth was influenced more by individual rainfall events and shallow soil moisture [16,17]. In addition, the close relationship between the GLD and vegetation was only observed for soil salinity below 5 g/kg. Our research work demonstrated that soil salinity may also be a restrictive factor for the growth and development of vegetation. The vegetation coverage began to

decrease when the soil salinity was greater than 5 g/kg, and when this reached 20 g/kg, the vegetation nearly disappeared and desertification occurred [32].

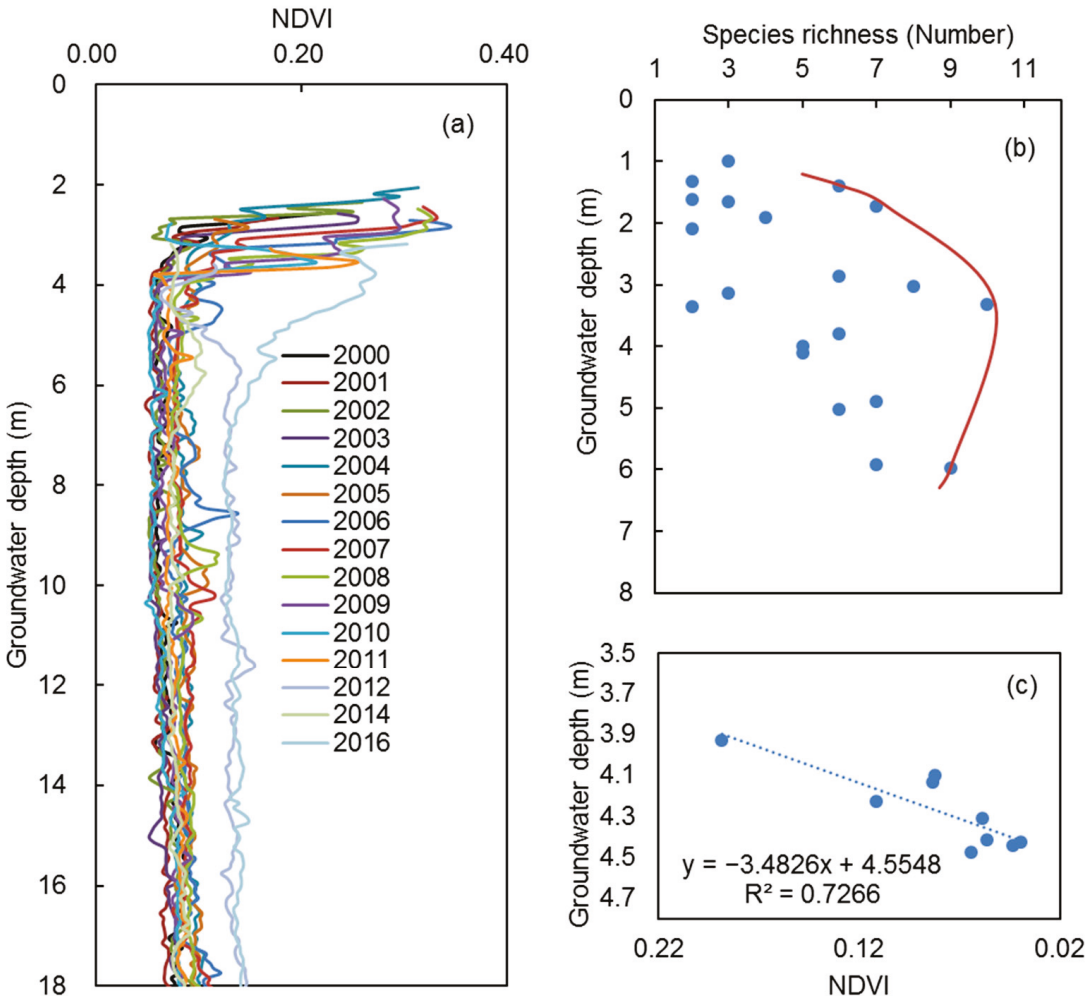

Figure 7. The relationship of groundwater depth with NDVI and species richness in the Minqin Oasis–desert ecotone [17]. ((**a**): the annual relationship between groundwater depth and NDVI based on grid; (**b**): the relationship between groundwater depth and species richness based on survey of vegetation quadrats; (**c**): the relationship between annual regional mean groundwater depth and NDVI in Qingtu Lake area).

All in all, under arid climate conditions and without irrigation, there can be no agriculture. The rapid increases in the population, farmland area, and intense agricultural irrigation activities have led to the excessive use of groundwater resources. These disorganized ways of utilizing water and land resources were the direct cause of the significant increase in GLD and the main reason for the degradation and shrinkage of natural vegetation in the ODE. This seriously restricted the sustainable development of SES in SRB. The ODE plays an important role in the stability of the oasis and the control of desertification, despite it being a key ecological sensitivity zone. Therefore, it is extremely important to protect and restore the ecosystem in ODE.

4. Discussion

4.1. The Effects of the Nature-Based Solutions

Based on the concept of NbS, the local government adopted a series of measures to protect and restore the groundwater resources and the GDEs in Minqin Oasis. This effort was called the CASRB and was launched in 2007. The concrete measures primarily

consisted of increasing the surface water supply through water transfer projects, decreasing groundwater mining by locking the pumping wells, and formation of water user associations, planting natural vegetation instead of crops, enhancing industrial water-saving technologies, and the adjustment of the agricultural planting structure by planting low-water-consuming crops [18,33]. These measures, combining the recovery of GLD with the afforestation project, aim to gradually restore the natural ecological function of the groundwater resources and eventually promote the resilience of the SES.

1. The proportions of surface water and groundwater to total water supply amounts

Water transfer projects have greatly increased the amount of surface water entering Minqin Oasis. The effort primarily involved two water transfer projects [18,34]. The first was the Jingdian Project Phase II that diverted water from the Yellow River starting in 2001; the second was diverting water from the Xiying River—a tributary of the Shiyang River—that began in 2006. With the additional water supply from the two water diversion projects, the amount of water diverted continued to increase, and the cross-sectional flow at Caiqi station showed a significant increasing trend [34]. In 2019, the cross-sectional flow reached 401 million m^3, almost the same as that in the 1970s (Figure 2b), of which 208 million m^3 was the amount of diverted water.

In addition to the measures for reducing groundwater extraction, the consumption of groundwater for agriculture continued to decrease. The proportion of the water supply used for agriculture gradually became less than 90% [34]. The groundwater exploitation has gradually decreased and stabilized. Since 2009, the groundwater extraction has been constantly below 110 million m^3. Analysis on the statistical data from the Wuwei Water Authority illustrated that the water supply composition of Minqin has been transformed from primarily emphasizing on groundwater before 2009 to emphasizing on both surface water and groundwater (Figure 8).

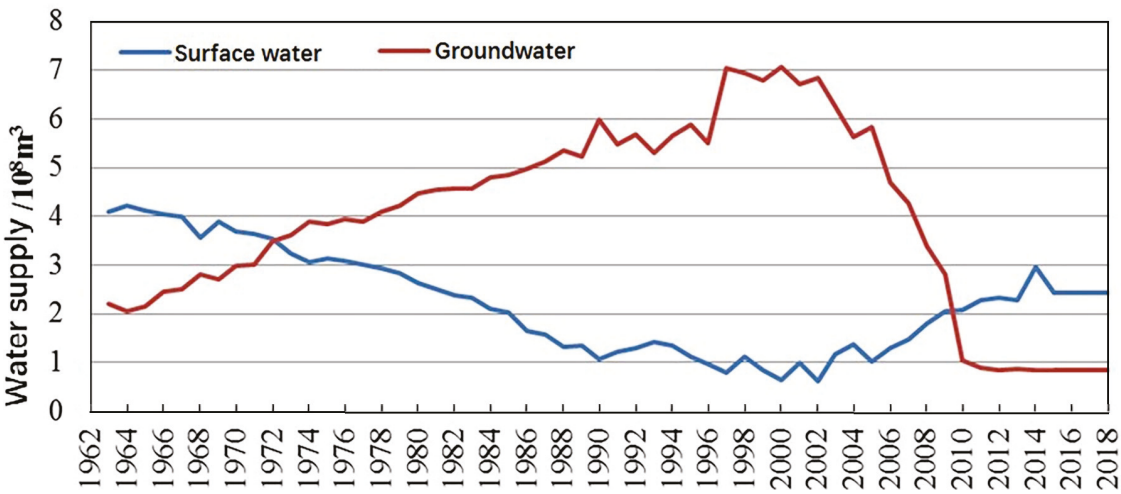

Figure 8. Changes in proportions of water supply amounts in Minqin Oasis.

2. Groundwater level recovery

By increasing the surface water supply and reducing groundwater exploitation, as well as implementing other water-saving policies and technologies, the GL has shown a recovery trend since 2009 compared to the previous period (Figures 3 and 9). The increasing rate of the GLD became less, from mostly between 4 m/10a and 6 m/10a (Figure 3a) to less than 4 m/10a (Figure 9), especially in the lake irrigation area, where the GLD of parts of the observation wells began to show a negative change trend. The CASRB thus has had a remarkable effect on the prevention of increased GLD.

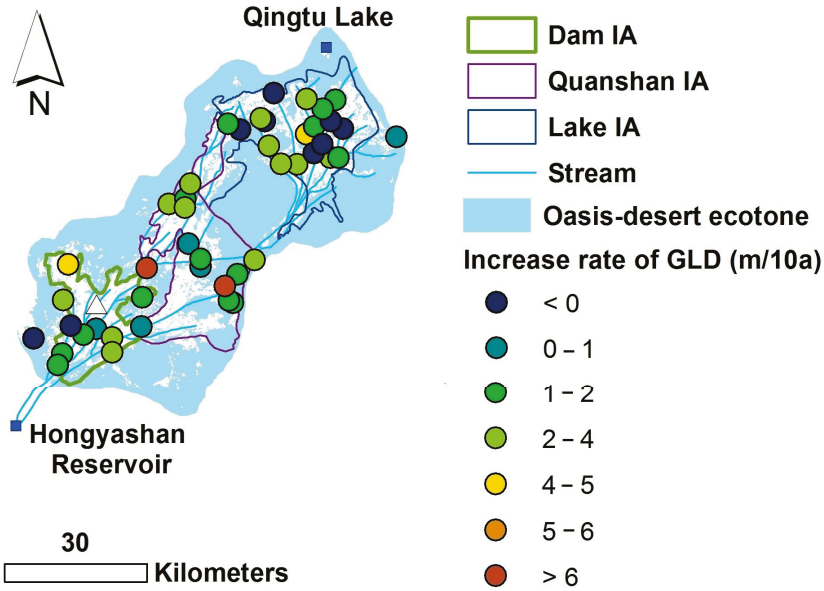

Figure 9. Change rate of the groundwater depth during 2009–2017.

3. Wetland area of Qingtu Lake

In addition to carrying out the above solutions, 280 million cubic meters of water was directly added to the Qingtu Lake from the Hongyashan Reservoir from 2010 to 2019 [34]; this greatly increased the area of Qingtu Lake (Figure 10) and the surrounding vegetation. The increasing rate of the Qingtu Lake was about 2.48 km^2 per year (Figure 10). The addition also played a role in the rise of the GL around Qingtu Lake in the downstream area [19,35].

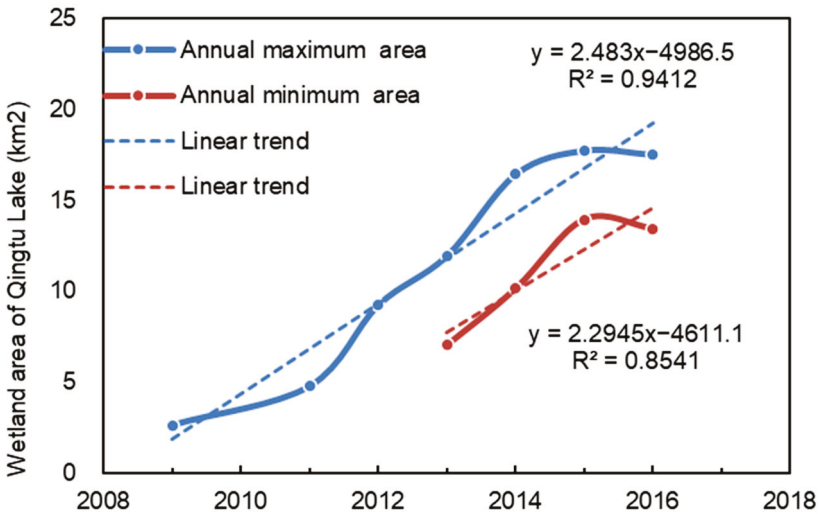

Figure 10. Changes in the wetland area of Qingtu Lake.

4. Vegetation ecology in the oasis–desert ecotone

From 2009 to 2017, the annual mean NDVI of natural vegetation gradually increased from 0.09 to 0.21 [34]. This demonstrated the effects of the implementation of the CRSRB on the improvement in vegetation ecology of the ODE. Currently, the areas with increasing NDVI are distributed in the eastern and southeastern peripheral areas of Minqin Oasis, the western part of Minqin Oasis, and the areas around Qingtu Lake. The increasing rate of the annual mean NDVI in these areas reached 0.1–0.3/10a [16]. Combined with the GLD of these areas and the correlation between the GLD and NDVI, we also found that the improvement of the vegetation in the western part of Minqin Oasis where the GLD was still

about 20–30 m, was largely attributed to the afforestation project; the improvement of the vegetation in the lake irrigation area and the peripheral areas of the oasis were attributed to both the recovery of the GLD and the afforestation project. Under these interventions, the ecological function of the groundwater was gradually restored.

5. Lifting residents out of poverty

Based on the NbS of the CASRB, and in accordance with the requirements of high efficiency, new modes, new varieties, and new technologies, the Minqin County government continued to adjust the agricultural structure and resolutely prohibited the planting of high-water-consuming crops such as onions and corn. The county has vigorously developed efficient water-saving agriculture, agricultural practices, green organic agriculture, and ecological circular agriculture as well as the creation of a variety of characteristic vegetable- and fruit-based products. The agricultural water production has increased from 2.66 yuan/m^3 in 2005 to 21.7 yuan/m^3 in 2020, and the per capita disposable income of farmers in the rural area has increased from 3869 yuan in 2007 to 15,466 yuan in 2020. These measures have successfully eliminated the farmers' poverty and achieved solutions for the sustainable utilization of water resources, ecological protection, and increased income for farmers.

4.2. Comprehensive Evaluation of the Resilience of the Socio-Ecological System

The composite evaluation index of the SES resilience during 2009–2017 was calculated by the fuzzy comprehensive assessment method. The steps were as follows.

1. Selection of the resilience indicators of the SES

There are various resilience indicators of the SES. Since the main issues regarding the sustainable development of the SES in Minqin were the drop in GL, the degradation of GDEs, and the poverty of the residents, the NDVI, the wetland area of the Qingtu, the per-capita income, the GLD, and its change rate were selected as the indicators to assess the resilience of the SES (Table 1). The units of the indicators are shown in Table 1.

Table 1. Rating criteria of the resilience indicators of socio-ecological system.

Indicators	V1	V2	V3
NDVI	0.50	0.15	0.08
Area of the Qingtu wetland (km^2)	17.73	11.46	2.63
Per-capita income (Yuan/person)	31,128	19,110	9160
GLD (m)	3.0	5.0	10.0
Change rate of GLD (%)	−5.0	0.0	5.0
Rating score	0.95	0.50	0.05

2. Determination of grading values and the corresponding rating score

According to the theory of fuzzy mathematics, the values of the above-selected indicators were divided into three levels of rating score, i.e., V1, V2, and V3. Among these, V1 indicates that the resilience of the SES is relatively strong; V3 indicates that the resilience of the SES is close to the minimum value. V2 is between V1 and V3, indicating a medium level of resilience. To quantitatively reflect the resilience of the SES, V1, V2, and V3 were scored between 0 and 1 (Table 1). The composite index (CI) of the SES was calculated using the Equation (1), in which a is the CI; b is the weight of each indicator, and α is the rating score. The thresholds of indicators corresponding to V1, V2, and V3 were determined by the following method. That of NDVI was determined based on the analysis of changes detailed above and by previous studies on the desert vegetation [17,31,32]. The thresholds of the wetland area were determined by the maximum, mean, and minimum values during the evaluation period. The thresholds of per-capita income were determined according to the maximum, mean, and minimum values for Wuwei City. The thresholds of GLD were determined according to the interactions between the GLD and vegetation, as in

Liu et al. [17]. The thresholds for the change rate were determined by the increasing or decreasing trends of the GLD due to the fact that a decreasing trend is favorable for the restoration of groundwater and its dependent ecology.

$$\sum_{j=1}^{3} b_j^k \cdot \alpha_j / \sum_{j=1}^{3} b_j^k \tag{3}$$

3. Determination of the weight for each resilience indicator

The indicators were classified into three categories, i.e., the ecology, the socio-economy, and the groundwater resources (Table 2). Combining the principles of analytic hierarchy processes and expert scoring methods, the relative weights of NDVI, wetland area, per-capita income, GLD, and the change rate of GLD were finally adjusted to 0.198, 0.132, 0.340, 0.198, and 0.132.

Table 2. Weights of the indicators.

Classification	Weights	Indicators	Weights
Ecology	0.33	NDVI Area of the Qingtu wetland (km^2)	0.6 0.4
Socio-economy	0.33	Per-capita income (yuan/person)	1.0
Groundwater	0.34	GLD (m) Relative rate of GLD (%)	0.6 0.4

4. Composite evaluation index of the resilience of SES

Changes in the composite index of the SES (*Vc*) during 2009–2017 were shown in Figure 11. The results illustrated that *Vc* in most of the years was below 0.6, indicating a relatively low resilience of the SES. However, the *Vc* showed an increasing trend, especially increasing significantly from 2011 to 2017, the second stage of the CASRB. The value in 2017 was 1.73 times that in 2011. In the meantime, *V*3 showed a decreasing tendency, while *V*1 had an increasing tendency. This illustrated the dramatic effects of the CASRB. Temporally, the increase in the CI was initially attributed more to the increase in *V*2, and in turn to more to *V*1. This process suggested that the resilience of SES was gradually stronger after the implementation of the CASRB. Among the three rating levels, *V*2 still accounted for most of the current state, being almost twice that of *V*1. Therefore, the resilience of the SES in Minqin Oasis could still be enhanced.

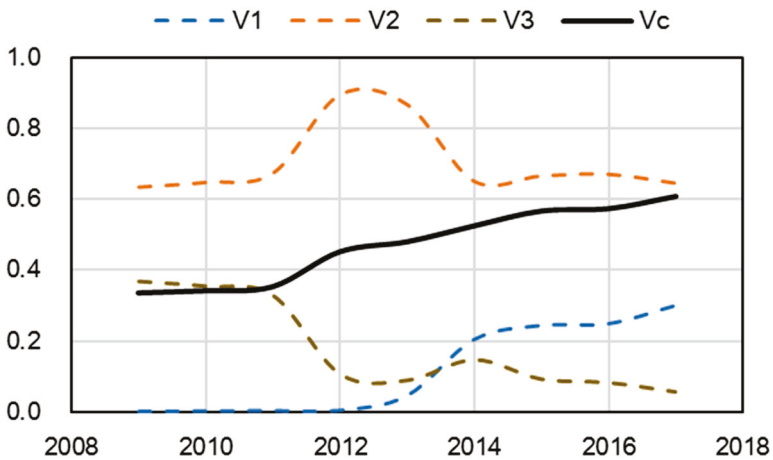

Figure 11. Changes in the composite index of the resilience of the socio-ecological system.

4.3. Recommendations and Measures

Based on the above analysis, we conclude that the implementation of the CASRB has had a positive effect on the resilience of the SES of Minqin Oasis. The GLD reached a relatively balanced status, the ecological environment has been on a path of restoration, and residents of Minqin County have been comprehensively lifted out of poverty. However, the overall GLD in the Minqin Oasis is still very large, especially in the western part of Minqin, where the current GLD is 20–40 m. The artificially planted *Haloxylon ammodendron* grows poorly in dry years and is still insufficient to withstand the intrusion of the Badain Jilin Desert. Therefore, it is necessary to continue to strengthen this comprehensive governance. Furthermore, the authors recommended that in the later stages of the CASRB, different measures need to be taken for different regions within the oasis.

(1) The ODE is a natural vegetation protection region. The critical GLD of soil salinization (2 m) and the critical vegetation-degradation value of groundwater ecological function (5 m) are recommended as GLD thresholds [17,34]. In the near future (i.e., by the year 2035), the main goal is to restore the ecological functioning of groundwater and prohibit its overexploitation. In the long term (after 2035), attention should be paid to controlling the GLD less than 2 m to avoid salt desertification. Artificial afforestation should be suited to local conditions, and shrub and grass planting projects should conform to the local climate and environment, selecting drought- and salt-tolerant plant species.
(2) In agroecosystem regions, groundwater should be extracted rationally. Multiple factors such as the amount of groundwater recharge, the soil salinization threshold of the GLD, and the influence of groundwater mining on the surrounding natural ecology should be comprehensively considered. The GLD values of 2 m and 10 m are recommended as the minimum and maximum thresholds, and the amount of groundwater extraction could be determined according to these GLD thresholds. Therefore, the near future goal of the agroecosystem region is food security. The local government should reasonably determine the scale of agricultural land and irrigate the farmland by the joint regulation of surface water and groundwater. In the long term, attention should be paid to controlling the GLD greater than 2 m to avoid causing secondary salinization of the soil and affecting the quality and yield of crop.
(3) In the urban ecological security guarantee region, the safety guarantee of underground buildings is the primary task. The local government should reasonably determine the maximum GLD threshold and appropriately extract groundwater by holistically coordinating regional water level changes. The authors recommend the minimum and maximum thresholds as 10 m and 15–20 m, respectively, due to the conclusion that a high GL would lead to the instability of underground buildings.

5. Conclusions

(1) The natural runoff flowing into Minqin Oasis decreased significantly at a rate of 81 million cubic meters per decade. Combined with the expansion of irrigated farmland in Minqin Oasis, GLD increased dramatically, and the natural vegetation ecology of the ODE was seriously degraded. There was a strong correlation between each couple factor among the four factors on the causal chain; i.e., expansion of farmland–increase in groundwater abstraction amount–increase in GLD–degradation of natural ecosystem.
(2) Since the implementation of the NbS in 2007, the dropping trend of GL has been curbed, the natural vegetation of the ODE has been partially restored, the wetland area of Qingtu Lake has increased, and people's income has also increased. The SES resilience index has increased by a factor of 1.82 from 2009 to 2017, but it was still below 0.6, and the GLD has not reached the ecologically suitable depth.
(3) To continually improve the resilience of the SES of Minqin Oasis, the idea of harmonious coexistence between humans and nature should continue to be adhered to in the later comprehensive treatment of the SRB, and the implementation of the CASRB

should focus on comprehensive management, systematic management, and zoning management to promote the integrated protection and restoration of mountains, rivers, forests, fields, lakes, grass, and sand.

Author Contributions: Conceptualization, Z.N. and M.L.; methodology, M.L., Z.N. and L.C.; software, M.L., L.W. and H.L.; validation, L.W. and L.C.; formal analysis, M.L.; investigation, M.L., L.C. and L.W.; resources, M.L., L.W., L.C. and H.L.; data curation, L.W. and L.C.; writing—original draft preparation, M.L.; writing—review and editing, Z.N. and L.C.; supervision, Z.N.; project administration, Z.N.; funding acquisition, M.L. and Z.N. All authors have read and agreed to the published version of the manuscript.

Funding: This research was funded by the National Natural Science Foundation of China [No. 41902262]; the Innovation Capability Enhancement Plan of Hebei Province [No. 225A4204D], and the Geological Survey Project of China [No. DD20230432].

Data Availability Statement: The data presented in this study are available on request from the corresponding author.

Acknowledgments: We thank Wang Jinzhe, Wang Qian, Cui Haohao, et al. in our team for their help in the joint investigation of groundwater and ecological quadrat. We also thank the three anonymous reviewers for spending time on reviewing our manuscript and providing us with a list of constructive comments.

Conflicts of Interest: The authors declare no conflict of interest.

References

1. Intergovernmental Panel on Climate Change. *Global Warming of 1.5 °C*; Cambridge University Press: Cambridge, UK; New York, NY, USA, 2018.
2. World Bank. *Biodiversity, Climate Change, and Adaptation: Nature-Based Solutions from the World Bank Portfolio*; World Bank: Washington, DC, USA, 2008.
3. Cohen-Shacham, E.; Walters, G.; Maginnis, S.; Janzen, C. *Nature-Based Solutions to Address Global Societal Challenges*; IUCN: Gland, Switzerland, 2016.
4. Cohen-Shacham, E.; Andrade, A.; Dalton, J.; Dudley, N.; Jones, M.; Kumar, C.; Maginnis, S.; Maynard, S.; Nelson, C.; Renaud, F.; et al. Core principles for successfully implementing and upscaling Nature-based Solutions. *Environ. Sci. Policy* **2019**, *98*, 20–29. [CrossRef]
5. United Nations Development Programme. *Human Development and Planetary Health: The Role of Nature-Based Solutions*; United Nations: San Francisco, CA, USA, 2019. Available online: https://hdr.undp.org/content/human-development-and-planetary-healththe-role-nature-based-solutions (accessed on 16 September 2023).
6. International Union for Conservation of Nature. *Guidance for Using the IUCN Global Standard for Nature-Based Solutions: A User-friendly Framework for the Verification, Design and Scaling up of Nature-Based Solutions*, 1st ed.; International Union for Conservation of Nature: Gland, Switzerland, 2020.
7. European Environment Agency; Castellari, S.; Zandersen, M.; Davis, M.; Veerkamp, C.; Förster, J.; Marttunen, M.; Mysiak, J.; Vandewalle, M.; Medri, S.; et al. *Nature-Based Solutions in Europe Policy, Knowledge and Practice For Climate Change Adaptation and Disaster Risk Reduction*; Publications Office of the European Union, LU: Luxembourg, 2021.
8. Pérez-Cirera, V.; Cornelius, S.; Zapata, J. *Powering Nature: Creating the Conditions to Enable Nature-Based Solutions*; WWF: Gland, Switzerland, 2021. Available online: https://lp.panda.org/powering-nature-report (accessed on 16 September 2023).
9. European Union. Towards an EU Research and Innovation Policy Agenda for Nature-based Solutions & Renaturing Cities. 2015. Available online: https://publications.europa.eu/en/publication-detail/-/publication/fb117980-d5aa-46df-8edc-af367cddc202 (accessed on 16 September 2023).
10. International Union for Conservation of Nature. Call for Wetland Decade under the UN Decade on Ecosystem Restoration (2021–2030). 2019. Available online: https://www.iucn.org/news/water/201903/call-wetland-decade-under-un-decade-ecosystem-restoration-2021--2030 (accessed on 16 September 2023).
11. United Nations. Nature-based Solutions for Supporting Sustainable Development, Resolution 5 of United Nations Environment Assembly Adopted on 2 March 2022, 2022 Retrieved on 5 June 2022. Available online: https://wedocs.unep.org/bitstream/handle/20.500.11822/39864/NATURE-BASED%20SOLUTIONS%20FOR%20SUPPORTING%20SUSTAINABLE%20DEVELOPMENT.%20English.pdf?sequence=1&isAllowed=y (accessed on 16 September 2023).
12. Mehta, D.; Pandey, R.; Gupta, A.K.; Juhola, S. Nature-based Solutions in Hindu Kush Himalayas: IUCN Global Standard Based Synthesis. *Ecol. Indic.* **2023**, *154*, 110875. [CrossRef]
13. Yu, R.; Mu, Q. Implementation progress of NbS in China: A Global Comparative Review. *NbS* **2023**, *4*, 100075.

14. Fan, X. The Characteristics of Groundwater Resources and the Environmental Problems Caused by Development of Water Resource, the Arid Area in the Northwest of China. *Hydrol. Eng. Geol.* **1990**, *1*, 3–7, 12–16. (In Chinese)
15. Ding, H.; Wang, G.; Huang, X. Runoff Reduction into Hongyashan Reservoir and Analysis on Water Resources Crisis of Minqin Oasis. *J. Des. Res.* **2003**, *23*, 84–89.
16. Cao, L.; Nie, Z.; Liu, M.; Wang, L.; Wang, J.; Wang, Q. Changes in Natural Vegetation Growth and Groundwater Depth and Their Relationship in the Minqin Oasis in the Shiyang River Basin. *Hydro. Eng. Geol.* **2020**, *47*, 25–33. (In Chinese)
17. Liu, M.; Nie, Z.; Cao, L.; Wang, L.; Lu, H.; Wang, Z.; Zhu, P. Comprehensive Evaluation on the Ecological Function of Groundwater in the Shiyang River Watershed. *J. Ground. Sci. Eng.* **2021**, *9*, 326–340. [CrossRef]
18. Hao, Y.; Xie, Y.; Ma, J.; Zhang, W. The Critical Role of Local Policy Effects in Arid Watershed Groundwater Resources Sustainability: A Case Study in the Minqin Oasis, China. *Sci. Total Environ.* **2017**, *601–602*, 1084–1096. [CrossRef]
19. Huang, F.; Chunyu, X.; Zhang, D.; Chen, X.; Ochoa, C.G. A Framework to Assess the Impact of Ecological Water Conveyance on Groundwater-Dependent Terrestrial Ecosystems in Arid Inland River Basins. *Sci. Total Environ.* **2020**, *709*, 136155. [CrossRef]
20. Zhang, Z.; Yang, X.; Li, H.; Li, W.; Yan, H.; Shi, F. Application of A Novel Hybrid Method for Spatiotemporal Data Imputation: A Case Study of the Minqin County Groundwater Level. *J. Hydrol.* **2017**, *553*, 384–397. [CrossRef]
21. Wang, X.; Chen, X.; Ding, Q.; Zhao, X.; Wang, X.; Ma, Z.; Lian, J. Vegetation and Soil Environmental Factor Characteristics, and Their Relationship at Different Desertification Stages: A Case Study in the Minqin Desert-Oasis Ecotone. *Acta Ecolo Sinica* **2018**, *38*, 1569–1580, (In Chinese with English abstract).
22. Zhang, Y.; Chang, Z. Study on the Dynamic Vegetation Degeneration in the Minqin Desert Area. *Arid Zone Res.* **2008**, *25*, 16–21, (In Chinese with English abstract). [CrossRef]
23. Liu, H.; Liu, S.; Li, Y.; Yang, Z.; Li, Y.; Zhang, Y.; Guo, C.; Liu, S. Response of Riparian Vegetation to the Change of Groundwater Level at Middle and Lower Reaches of the Shiyang River. *Arid Zone Res.* **2012**, *29*, 335–341, (In Chinese with English abstract).
24. Lu, H.; Nie, Z.; Liu, M.; Feng, B.; Cheng, X.; Wang, J.; Wang, Q.; Cui, H.; Fan, F. Research on Land Cover Changes in Shiyang River Basin in Recent 50 Years Based on RS and GIS. *Geogr. Res.* **2020**, *29*, 8, (In Chinese with English abstract).
25. Hess, A.; Iyer, H.; Malm, W. Linear Trend Analysis: A Comparison of Methods. *Atmos. Environ.* **2001**, *35*, 5211–5222. [CrossRef]
26. Xu, J. *Mathematical Methods in Modern Geography*, 2nd ed.; Higher Education Press: Beijing, China, 2002; pp. 305–335.
27. Cohen, P.; Cohen, P.; West, S.G.; Aiken, L.S. *Applied Multiple Regression/Correlation Analysis for the Behavioral Sciences*, 2nd ed.; Psychology Press: London, UK, 1983. [CrossRef]
28. Fang, J.; Wang, X.; Shen, Z.; Tang, Z.; He, J.; Yu, D.; Jiang, Y. Methods and Protocols for Plant Community Inventory. *Biodi. Sci.* **2009**, *17*, 533–548. (In Chinese)
29. Lou, S. *Fuzzy Mathematics*; Science Press: Beijing, China, 1983.
30. Song, S.; Nie, Z.; Geng, X.; Shen, X.; Wang, Z.; Zhu, P. Response of Runoff to Climate Change in the Area of Runoff Yield in Upstream Shiyang River Basin, Northwest China: A Case Study of the Xiying River. *J. Groundw. Sci. Eng.* **2023**, *11*, 89–96. [CrossRef]
31. Jin, X. Quantitative Relationship Between the Desert Vegetation and Groundwater Depth in Ejina Oasis, the Heihe River Basin. *Earth Sci. Front.* **2010**, *17*, 181–186, (In Chinese with English abstract).
32. Cao, L.; Nie, Z.; Liu, M.; Wang, L.; Wang, Q. The Ecological Relationship of Groundwater–Soil–Vegetation in the Oasis–Desert Transition Zone of the Shiyang River Basin. *Water* **2021**, *13*, 1642. [CrossRef]
33. Chen, L.; Feng, Q. Geostatistical Analysis of Temporal and Spatial Variations in Groundwater Levels and Quality in the Minqin Oasis, Northwest China. *Environ. Earth Sci.* **2013**, *70*, 1367–1378. [CrossRef]
34. Nie, Z.; Liu, M.; Liu, P. *Acceptance Report of the Research and Demonstration of Rational Exploitation and Utilization of Groundwater Resources and the Protection of Its Ecological Function in the Shiyang River Basin*; Ministry of Science and Technology of the People's Republic of China: Beijing, China, 2021.
35. Gu, J.; Guo, P.; Huang, G. Achieving the Objective of Ecological Planning for Arid Inland River Basin Under Uncertainty Based on Ecological Risk Assessment. *Stoch. Environ. Res. Risk Assess.* **2016**, *30*, 1485–1501. [CrossRef]

Disclaimer/Publisher's Note: The statements, opinions and data contained in all publications are solely those of the individual author(s) and contributor(s) and not of MDPI and/or the editor(s). MDPI and/or the editor(s) disclaim responsibility for any injury to people or property resulting from any ideas, methods, instructions or products referred to in the content.

water

MDPI

Article

A Participatory Approach to Exploring Nexus Challenges: A Case Study on the Pinios River Basin, Greece

Dimitrios Malamataris [1], Anna Chatzi [1], Konstantinos Babakos [1], Vassilios Pisinaras [1], Evangelos Hatzigiannakis [1], Barbara A. Willaarts [2], Manuel Bea [2], Alessandro Pagano [3] and Andreas Panagopoulos [1,*]

[1] Soil and Water Resources Institute, Hellenic Agricultural Organization "DEMETER", 57400 Thessaloniki, Greece; d.malamataris@swri.gr (D.M.); a.chatzi@swri.gr (A.C.); k.babakos@swri.gr (K.B.); v.pisinaras@swri.gr (V.P.); e.hatzigiannakis@swri.gr (E.H.)

[2] ICATALIST S.L., Las Rozas de Madrid, 28232 Madrid, Spain; bwillaarts@icatalist.eu (B.A.W.); mbea@icatalist.eu (M.B.)

[3] Consiglio Nazionale delle Ricerche, Istituto di Ricerca Sulle Acque (IRSA-CNR), 70132 Bari, Italy; alessandro.pagano@ba.irsa.cnr.it

* Correspondence: a.panagopoulos@swri.gr; Tel.: +30-2310798790 (ext. 205)

Abstract: The conservation of natural resources is indispensable for supporting sustainable development. Water–Energy–Food–Ecosystem (WEFE) nexus management is widely acknowledged as the utmost priority of our time. Considering the specificities of the different nexus sectors, conflicting views of sustainability may arise from different stakeholders. This paper presents and analyses an effective stakeholders' participation strategy aiming at identifying WEFE challenges in the Pinios River Basin (PRB), the most agriculturally productive and natural resource-stressed basin of Greece. The presented methodology was developed in the context of a Learning and Action Alliance (LAA) scheme adopted by the H2020 REXUS project, intended to support resilient nexus system management with the engagement of stakeholders. The proposed comprehensive methodology comprises multiple phases, including "framing", "mapping", "involvement", "co-production", and "sharing" phases. The involvement phase is the most interactive one, including the organisation and outputs of efficient crowdsourcing theme sessions organised in the framework of the first REXUS PRB stakeholders' workshop. This paper illustrates and analyses stakeholders' perceptions regarding nexus status in the PRB and reveals the most critical challenges in the pilot basin, along with their interdependencies and correlations. The determination of nexus challenges insights by stakeholders could significantly contribute to redefining policies so that they align with sustainable development aims. This methodology is proposed to form the baseline strategy in stakeholders' engagement for future nexus management studies.

Keywords: WEFE nexus; Pinios River Basin; stakeholder engagement; sustainability; Thessaly; Mediterranean area; natural resource management; crowdsourcing; expert knowledge

1. Introduction

1.1. Natural Resource Security and Nexus

Human activities have currently reached a threshold that could damage the Earth's systems [1]. Worldwide, the agricultural sector accounts for about 70% of freshwater abstractions, the energy sector accounts for about 60% of total greenhouse gas emissions [2], and land use changes have affected 32% of the globe's land area since 1960 [3–5]. The global population is projected to grow to 8.5 and 9.7 billion in 2030 and 2050, respectively, according to the latest projections [2]; thus, we are expected to need 55% more water, 80% more energy, and 60% more food by 2050 [6,7].

Resolving natural resource scarcity, particularly in arid and semi-arid regions, including the Mediterranean region, constitutes a critical challenge for supporting human lives

and improving well-being in the context of sustainable development [8–10]. These regions face common natural pressures, such as increasing temperature, decreasing precipitation, and spatiotemporal imbalances between natural resource supply and demand [11], apart from the management challenges related to stakeholders' involvement in the decision and policy making processes [12,13]. Primarily, water, energy, food/agriculture, and ecosystems/climate are the most precious and essential sectors for sustaining healthy ecosystem functioning to facilitate improved human well-being, stable economic development, and strengthened social cohesion [14–18]. Improved natural resource management constitutes a prerequisite for achieving sustainability in accordance with the Sustainable Development Goals [19]. In this direction, a coordinated and integrated management of resources across sectors, supporting the cost-effective, efficient, and sustainable resources use, is being increasingly promoted [20–22].

Integrated approaches emphasising effective governance [23,24] and the promotion of innovative solutions, such as Nature-based Solutions (NbS) [25], have recently emerged as crucial factors to guarantee natural resource security. The characteristics of governance have also shifted from a state-centric to a decentralised and more transparent approach characterised by the broad participation of stakeholders [26,27]. Increasing attention is being given to cross-sectoral stakeholder collaboration, since impacts of sectoral decisions and policies could easily affect other domains and may result in resource shortages and conflicts among users [28–31].

In 2011, the concept of the Water–Energy–Food (WEF) nexus was conceived and put forward for the first time; water is the core element of this nexus system [32]. In the same year, the Global Risks Report [4] recognised the complex relationships among WEF nexus sectors, characterising their risks as one of the three most important global risks. The WEF link relationship was then further explained by the Asian Development Bank [33] and the Food and Agriculture Organization of the United Nations [5]. Since then, nexus approaches have become widely recognised by academic communities [34–42]. The essence of the nexus is the interconnections between different sectors, and the nexus is inextricably connected to the concept of resource security. Achieving the UN's Sustainable Development Goals (SDGs), including those regarding food (SDG 2), water (SDG 6), and energy (SDG 7), will require substantial, if not transformative, efforts across many sectors and landscapes. Nexus thinking advocates for water, energy, and food systems to be viewed collectively and holistically in order to achieve water, energy, and food (WEF) security. The nexus concept has been also broadened to include other factors, such as ecosystems, land, climate, or emissions [39].

1.2. Stakeholders' Engagement in Nexus Studies

An effective natural resource management of complex nexus systems requires the participation of stakeholders [43–46]. Despite the challenges and potential conflicts related to stakeholder involvement, consultation among stakeholders is fundamental in order to guarantee that existing interlinkages regarding the management of natural resources are highlighted and in order for a line to be drawn between the use and protection of certain limited natural resources [47,48]. Stakeholder participation can be understood as a means through which authorities of different levels and sectors, including end users, local managers, policy and decision makers, academics, organised citizens, and every single user, try to contribute to improving the understanding and management of natural resources [13,49].

Successful stakeholder participation is centred around incorporating, amongst other things, a broad spectrum of heterogeneous backgrounds and knowledge levels of participants, as well as possibly conflicting interests regarding resource allocation to create a "common sense" consensus [50–52]. There is evidence that transparent and democratic stakeholder engagement may result in more well-founded decisions [53], potentially leading to less social resistance, easier implementation [54], and higher efficiency [55]. Stakeholder engagement forms and tools can vary, ranging from questionnaires to forums

and other means of participation [56]. However, whatever the form of engagement is, a participatory approach that involves both qualitative and quantitative methods is thought to be the most appropriate for addressing uncertainties and enhancing the understanding of nexus systems [39,57].

A number of studies involving engaging stakeholders in nexus systems analysis have been carried out. Howarth and Monasterolo investigated the interactions between water, energy, and food in the United Kingdom through the organisation of five themed workshops, recognising the added value of an interdisciplinary approach focused on facilitating a constructive dialogue and more efficient decision making [47,58]. Johnson and Karlberg proposed a participatory scenario building process involving stakeholders with different levels of knowledge and experience and priorities to address water, energy, and food nexus challenges in Ethiopia and Rwanda [59]. Hoolohan et al. collected insights from stakeholders through interviews, case studies, and workshops to examine the value of stakeholder engagement in terms of addressing water, energy, and food nexus challenges [60]. Brethaut et al. analysed results obtained from interviews and workshops to better understand water, food, and energy nexus conflicts in the WWF Conservation Mekong Flooded Forest Landscape in Cambodia, Asia [61]. Kropf et al. conducted semi-structured interviews and a workshop to elicit sectoral stakeholders' perceptions on water, ecosystems, food, and climate nexus sectors' relationships in the Seewinkel agricultural region, Austria [62]. Through stakeholder workshops, Karutz et al. integrated local stakeholder perspectives into a coherent framework for food, water, and energy analysis in Bhima basin, India [63]. Vinca et al. [64] adopted a co-production approach through a series of workshops to identify nexus challenges in the Indus Basin and stakeholders' perspectives on these challenges, and they used this information to co-develop a number of quantitative future scenarios. De Vito et al. [65] used System Dynamics tools to facilitate a dialogue among stakeholders, particularly focusing on water resource management for agriculture, trying to understand the impact of policies and decisions across multiple nexus sectors.

1.3. Literature Gaps and Objective Focus

One of the major obstacles to achieving WEFE nexus sustainability is involving multiple stakeholders with various interests into all of the resource planning and implementation processes [66]. Nonetheless, most of the publications in the literature on stakeholders' engagement in the context of nexus sustainability frameworks focus either on nexus challenges and identifying their interrelations or on the determination of measures. Focusing on the Pinios River Basin (PRB), a highly stressed basin in Greece, the current study investigates and presents an effective stakeholder engagement strategy that can be adapted for any other nexus system. For this study, the perceptions and interpretations of stakeholders in terms of the main PRB WEFE challenges and their interconnections were investigated. Particular attention was given to (i) the collaborative identification of the main challenges for the area in terms of the conservation of natural resources, (ii) and the identification and analysis of the main cross-sectoral interconnections and dependencies related to resource use (and security), (iii) and the collaborative identification of potential sustainability pathways for the study area.

The proposed stakeholder engagement strategy aims to bridge the gap between science and implementation, facilitating the active involvement of stakeholders on the whole roadmap towards achieving nexus sustainability, i.e., from the identification of nexus challenges related to the security of natural resources to the identification and selection of potential measures. To the authors' knowledge, the design and development of a holistic and integrated WEFE nexus system regarding the PRB and shifting from "Nexus Thinking to Nexus Doing" within the context of the climate crisis and based on different stakeholders' viewpoints has not been described in the literature previously.

The remainder of this article is structured as follows: Section 2 presents the WEFE characteristics of the Pinios River Basin and the strategy developed for effective stakeholder participation. Section 3 is divided into five sub-sections dedicated to illustrating and

analysing the stakeholder engagement strategy, including framing, mapping, involvement, co-production, and sharing phases. Emphasis is placed on the presentation of the first REXUS PRB stakeholder workshop organisation and the challenges identified in the study area and the interrelations between them.

2. Materials and Methods

2.1. Study Area

The Pinios River Basin (Figure 1) is situated in Thessaly, Central Greece, covering an area of ca 11,000 km^2. It is characterised by rugged terrain, predominantly along the northern and western–southwestern margins of the basin, with two main plains gently sloping to the southeast and a considerable topographic elevation range spanning from 0 to 2810 m a.s.l. The hydrologic basin is mainly drained by the Pinios River, which has a length of 213 km, constituting the third longest river in Greece. The Pinios River course starts at the northwestern part of the Thessaly plain, crosses a large part of Central Greece, and discharges into the Aegean Sea, forming a NATURA convention-protected delta area. The major tributaries of the Pinios River are the Malakasiotiko, Portaikos, Pamisos, Enippeas, Ion, Lithaios, Neochoritis, and Titarisios rivers, which all drain extensive and heterogenous areas. Agricultural areas predominate, comprising 50.90% of the total area in the PRB, followed by forest and seminatural areas (45.32%), artificial surfaces (2.80%), water bodies (0.82%), and wetlands (0.15%). In-depth information on PRB water balance and detailed analyses of the hydrodynamic mechanisms in the region can be provided and supported, respectively, by the Pinios Hydrologic Observatory (PHO), which was established in the PRB in 2015, belonging to the International Long-Term Ecological Research Network, which aims to promote sustainable ecosystems and natural resource management [67]. However, several studies have been elaborated utilising hydrologic and climatic monitoring data series of the past 5 decades maintained by several public bodies.

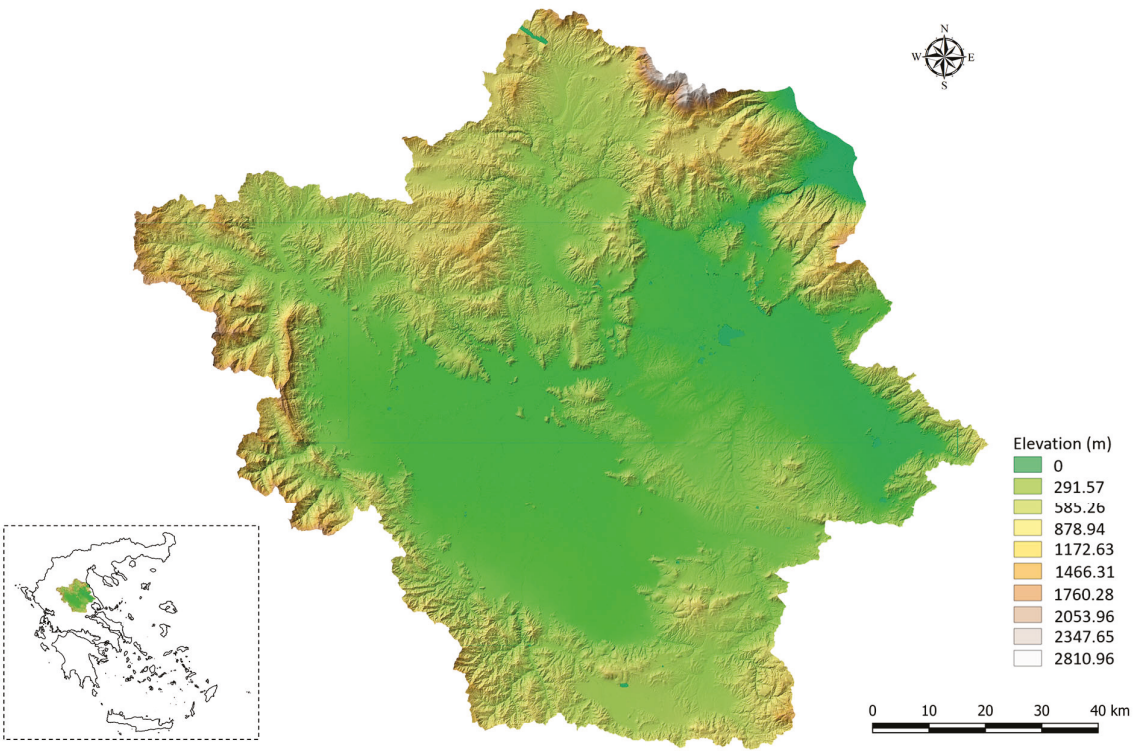

Figure 1. Pinios River Basin pilot area—DEM generated by the Hellenic Cadastre S.A at 5 m spatial resolution.

The PRB presents highly diversified climatic, geological, and hydrogeological conditions [68], supporting developed economic activities that, in turn, create several pressures,

thus shaping a regional nexus scheme that is rather complex to comprehend, analyse, and manage. Climatic conditions vary considerably eastwards, following the dominant topographic discretisation in the eastern central and western parts. In particular, at the western and central parts, the continental climate type is dominant, while at the eastern part of the basin, the typical Mediterranean climate type is apparent. According to Pisinaras et al. [68], long-term average precipitation between 1971 and 2000 was 770 mm/year, ranging between 500 mm/year in the eastern Thessaly plain around the city of Larissa and 1800 mm/year in the western boundary of the basin. Most of the PRB's area is covered by permeable geological formations (44%), followed by impermeable formations (40%), and karstified marbles (16%). The aquifer systems of the plains are rich in the thick alluvial deposits that fill the eastern and western basins and are characterised by high groundwater potential that largely covers the regional water demands. The karstic marbles mostly crop out at the margins of the plains and give rise to high-potential aquifers that play a key role in the hydrodynamic evolution of the alluvial aquifers [69] (Figure 2, in GGRS87 coordinate system).

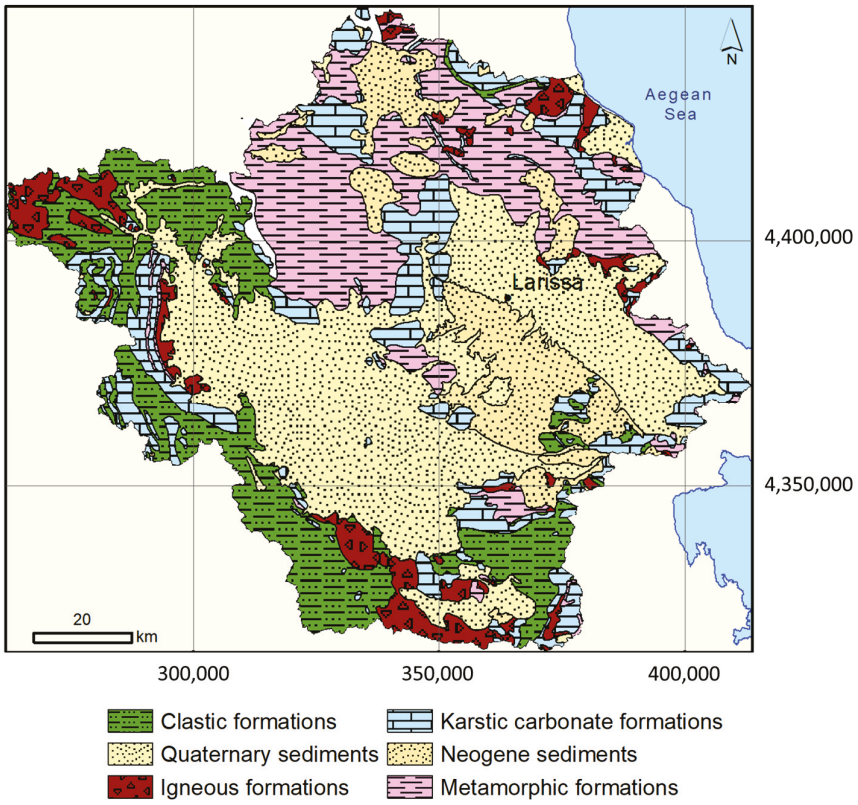

Figure 2. Hydrolithology of the Pinios River Basin.

The Pinios River Basin is considered one of the most characteristic examples of non-sustainable WEFE resource management in Greece, with contradicting opinions regarding the appropriate solutions amongst those involved in the relevant sectors, often leading to many disputes and confrontation, as well as maintaining the long-standing tradition of stakeholder inactivity and disengagement. Intensive agricultural activities have led to the over-exploitation of natural resources and increased environmental and energy pressures, while a notable water deficit for more than the last four decades has been established [70,71]. The identification of the main challenges in the PRB by stakeholders varies significantly, since they present different views and priorities according to differing criteria, including their area(s) of interest, main economic activity, and even social perception, adding to the complexity of the situation. As such, the process of identifying the main PRB challenges becomes a fairly complicated process.

The PRB Water sector: The PRB covers almost 85% of the spatial extent of the Thessaly water district (EL08). In the framework of the 1st Revision of River Basin Management Plans of Thessaly Water District (implemented in accordance with the European Union Water Framework Directive), 64 rivers, 2 natural lakes, 1 artificial lake, 2 coastal water systems, and 40 groundwater systems have been identified in the PRB (Figure 3a, in WGS84 coordinate system). Regarding water allocation, agricultural use constitutes the major reason for water consumption in the PRB, accounting for about 93% of total water consumption (1292 hm^3), followed by domestic (5.5%), livestock (1%), and industrial (0.5%) uses [69]. The systematic over-exploitation of the area's groundwater resources, as well as its surface water resources, was initiated in the PRB in the late 1980s. The highly intensified agricultural activity, in conjunction with irrational irrigation practices, has resulted in a remarkable need for an increase in irrigation water, and attempts to address this need have mainly involved the over-exploitation of groundwater resources. The exploitation of non-renewable groundwater resources, along with nitrate contamination, constitute the most critical threats to groundwater sustainability [72]. The concentration of nitrates in the regional aquifers is expected to increase in the future, mainly due to the decrease in groundwater recharge and increase in water abstraction for several uses [73]. In the past decade, signs of reductions in documented groundwater heads, leading to declining trends and small-scale reversal trends, have been noticed as a result of the rationalisation of the practiced irrigation, the reduction in irrigated land, and the shift to less water-demanding crops [74]. The persistent groundwater deficit underscores the urgent need to develop collective irrigation networks to reduce the excessive reliance on private wells and promote sustainable groundwater resource management [75].

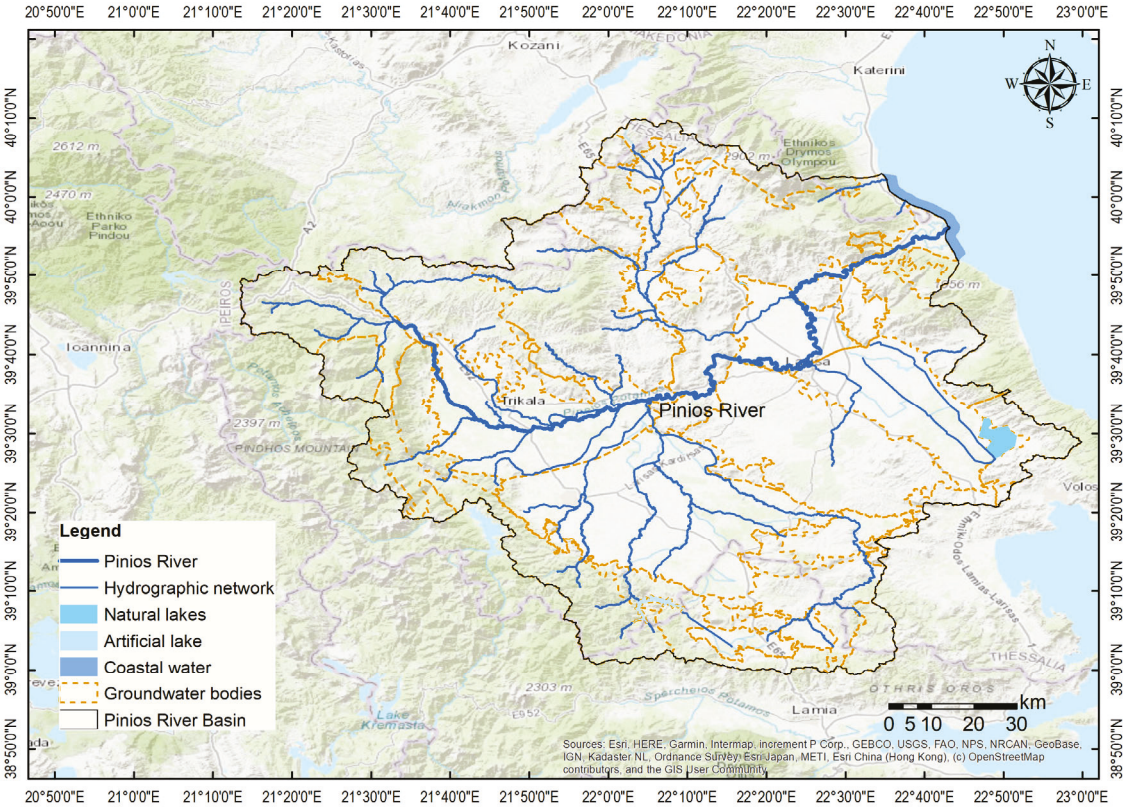

(**a**)

Figure 3. *Cont.*

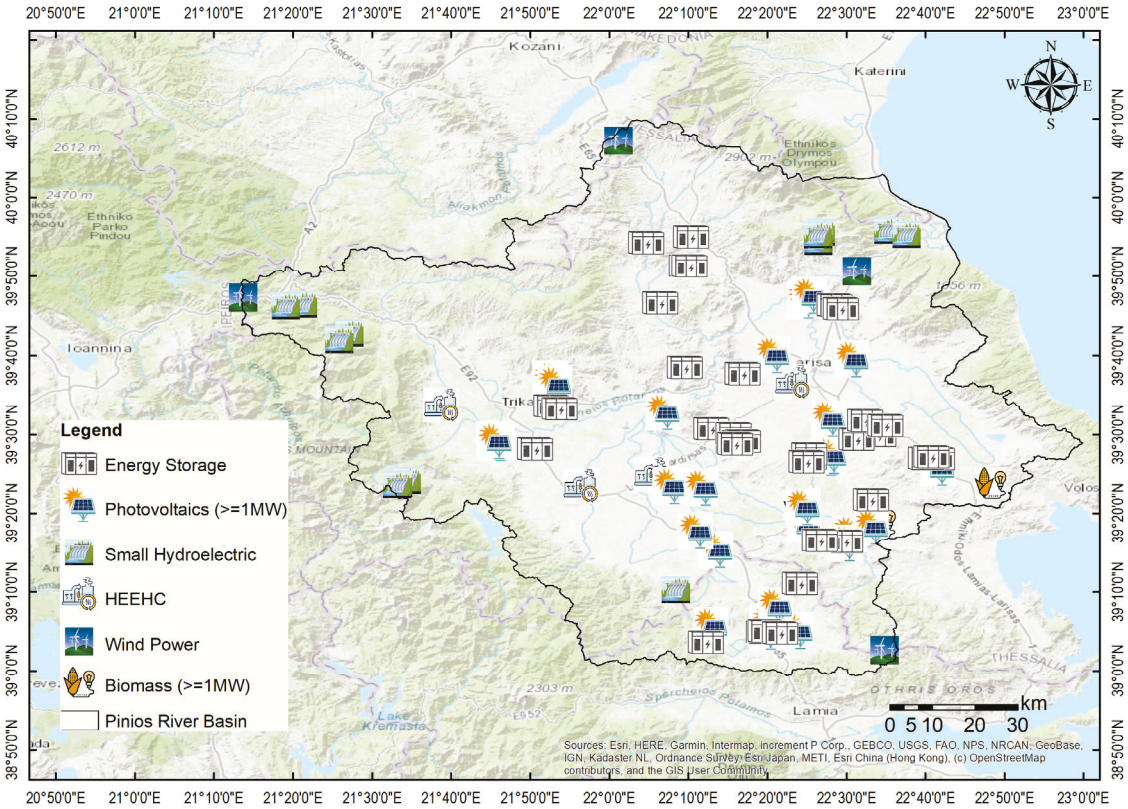

(**b**)

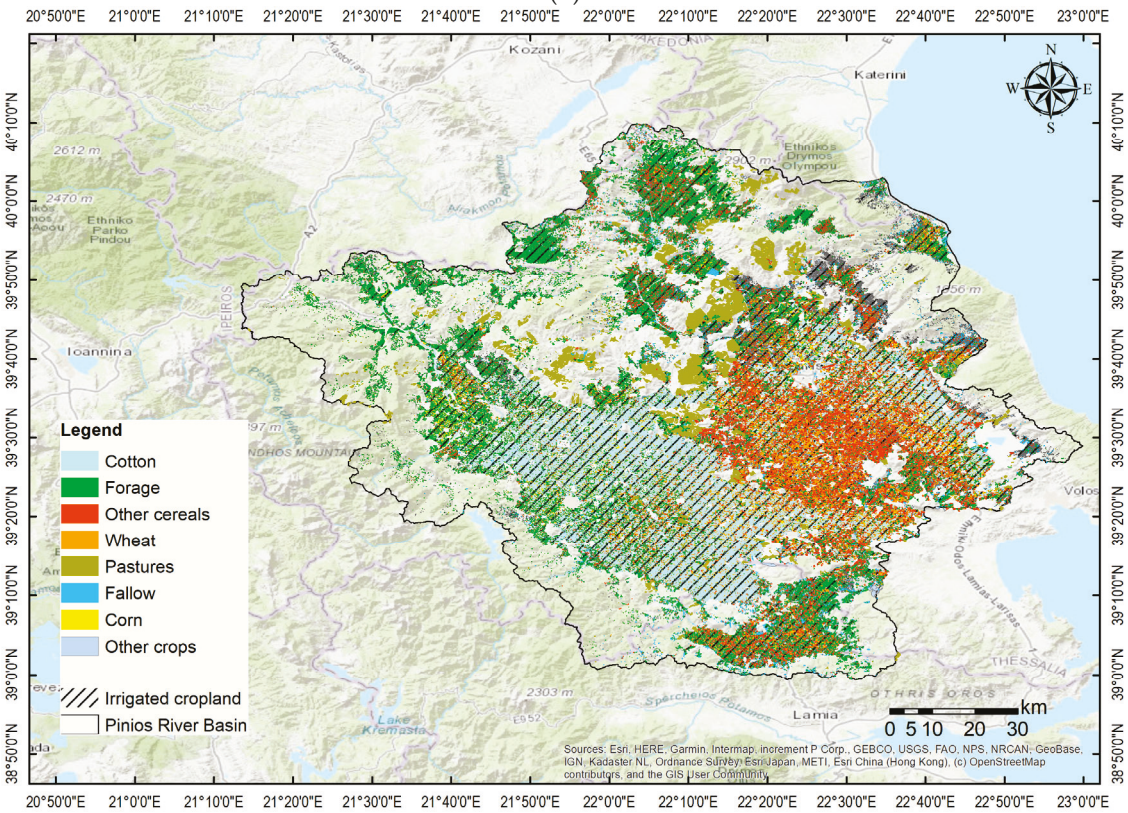

(**c**)

Figure 3. *Cont.*

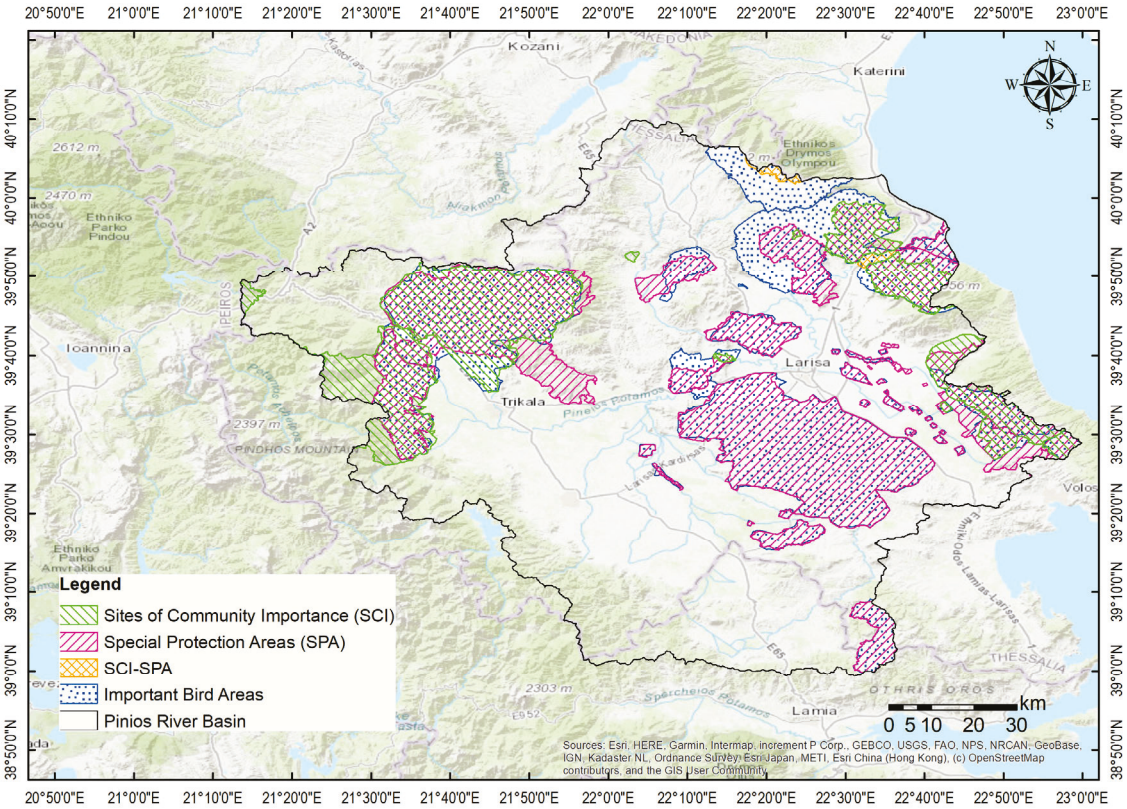

(**d**)

Figure 3. (**a**) Water sector in the Pinios River Basin. (**b**) Energy sector in the Pinios River Basin. (**c**) Food/Agriculture sector in the Pinios River Basin. (**d**) Ecosystems/Climate sector in the Pinios River Basin.

The PRB Energy sector: The water-intensive agricultural sector in the PRB has led to an increase in energy consumption for irrigation purposes, especially considering that most needs are covered by groundwater at declining levels, i.e., greater abstraction depths. This, in turn, results in a significant increase in agricultural production costs, magnified in recent years by the energy crisis. To this end, a wide expansion of installed Renewable Energy Sources (RES) is thought to be imperative for Greece, among other countries, in view of meeting the European Union RES expansion targets in the framework of the post-lignite era developments. However, the availability of suitable sites, land use competitiveness (mainly with agriculture), and the limited capacity of the national power grid pose additional constraining factors in the complex PRB nexus framework. Based on the latest available data provided by the Geospatial Map of the Hellenic Regulatory Authority for Energy [76], the currently installed and licensed RES units that operate in the PRB include 36 energy storage units, 33 photovoltaic stations (each with a power capacity of over 1 MW), 15 small hydroelectric stations, 5 high-efficiency electricity–heat cogeneration (HEEHC) stations, 4 wind power stations, and 3 biomass stations (each with a power capacity of more than 1 MW) (Figure 3b, in WGS84 coordinate system).

The PRB Food/Agriculture sector: The PRB constitutes the most productive and intensively cultivated agricultural basin in Greece [77]. The plains cover almost 45% of the PRB's spatial extent and are divided through a low-lying hill split into two parts: (a) a western part, including the cities of Trikala and Karditsa, and (b) an eastern part, including the city of Larisa. Cotton is the dominant crop in the PRB (19.81%), followed by forage (17.29%), other cereals (15.80%), wheat (13.52%), pastures (7.72%), fallow (4.63%), corn (4.20%), nuts (3.04%), energy crops (2.00%), olives (1.77%), legumes (1.70%), seeds for sowing (1.08%), other forest crops (1.01%), and other crops (6.43%), according to data from

2021 from the records of the Payment and Control Agency for Guidance and Guarantee Community Aid (Figure 3c, in WGS84 coordinate system). Almost 55% of the cropland area is under irrigation, of which almost 35–40% is dedicated to collective irrigation networks, while the rest is dedicated to private irrigation networks [78].

The PRB Ecosystems/Climate sector: The PRB is considered one of the most important hydro-ecosystems in Central Greece, with 34% of its total area, i.e., 3762 km^2, included in the EU Natura2000 protected areas and Important Bird Areas. In particular, in the PRB, there are 10 Sites of Community Importance (SCI), which amount to a total area of 1516 km^2, 13 Special Protection Areas (SPA), covering a total area of 2947 km^2, 2 SCI-SPA areas, covering a total are of 288 km^2, and 11 Important Bird Areas (IBA), spanning a total area of 3170 km^2 (Figure 3d, in WGS84 coordinate system).

2.2. Stakeholders' Participation

Based on the presented analysis of the basin, the PRB is characterised by critical issues that need to be resolved in a coordinated way to ensure that it has a long-lasting future. Complex nexus interdependencies need to be analysed in-depth in order to address the challenges it faces in a comprehensive and efficient manner. To this end, ideally, a broad spectrum of stakeholders covering all 4 identified key sectors of the WEFE nexus, all levels of hierarchy, and the entire productive web of the basin needs to be recruited into an actively participating group that collaborate to unravel the challenges of the basin and shape appropriate measures for their alleviation.

The stakeholders' participatory activities developed in the PRB have followed backbone guidelines proposed in the REXUS project. These guidelines provide overall strategy clustering as core (common in all pilots) and additional (pilot-specific) activities for efficient stakeholder engagement from the perspectives of both conceptual and practical implementation. This means that the developed strategy, from its onset, is meant to be replicable and flexible enough to be customised to different contexts, even beyond the scope of the European Union's goals.

Stakeholders' sampling and approaching processes are dictated by the resources and time available, although the inclusion of multiple different views and opinions is important. Participatory workshops, forums, surveys, or other methods are useful for capturing stakeholders' perceptions, depending also on the level of desired detail concerning the collected information.

Background information on the stakeholders could be helpful if external factors are thought to be influencing their perceptions and priorities, limiting discussions and negotiations among stakeholders, and, in turn, inhibiting them from establishing a common ground of understanding.

3. Results and Discussion

The proposed stakeholder engagement strategy comprises both individual and group activities. The use of individual activities (in the form of semi-structured interviews) primarily allowed us to directly take into account individual viewpoints regarding the 'sectoral' perspective each stakeholder could provide. This analysis included a preliminary investigation of the main needs and challenges (related to resources security) each stakeholder typically faced (including, e.g., conflicting uses of resources and the impacts of climate change on resource availability and state). Participants were initially offered the option to express themselves freely in private in their own environment, without the pressure of time and/or potential challenges in the form of refusal, opposition, or provocation by other members of the group, all of which could have been limiting factors. Subsequently, the analysts worked on developing a 'summary' of the main issues that emerged from the interviews, asking either the stakeholders or the leaders of the study for specific clarifications on potential inconsistencies or conflicting views. Lastly, a summary of the outcomes of the individual interviews was presented and discussed—without any reference to individual stakeholders—in group exercises during a stakeholder workshop.

During the workshop, some results of modelling activities were also presented in order to supplement the discussion with scientific evidence. The support of facilitators during the workshop was crucial to building a consensus while discussing potentially contrasting viewpoints and keeping track of the differences in perspectives.

Throughout the whole stakeholder engagement process, key principles have to be followed to optimise the results. In particular, creating a friendly environment allows everyone to become invested and join in, limiting the possibility of anyone feeling excluded from the participatory process. Transparency in every decision taken and methodological step followed has to be ensured, thus avoiding the feeling of lobbying in decision making. The viewpoints and perceptions of participants have to be respected and valued, disregarding the level of appeal they may have to wider society. The time devoted by the participants and their privacy have to be respected to encourage free and goal-oriented discussions. The adoption of a neutral position among all of the facilitators also supports the freedom of the discussions. In addition, iterative processes that allow for the building of knowledge and progressive shaping of actions have to be followed to develop sound and acceptable pathways to safety. Regarding all the Learning and Action Alliances (LAAs) actions, the "co-" prefix constitutes the key synthetic in terms of working with the stakeholders, for the stakeholders, and their working and living ecosystem. The needs of the stakeholders have to be identified and addressed to the best possible degree, as these may relate to expressing their viewpoints, their complaints, their ideas, and their proposals, in a context shaped to ensure an amicable, equitable, and respectful environment. In light of this, the "mere" data provision process has to be distinguished from stakeholder engagement, and in no case should stakeholders get the impression that they have been approached or recruited to simply act as data providers. Furthermore, patience and time availability always have to be considered, since stakeholders need time to warm and open up and feel like they are in a non-hostile, inviting environment wherein their voice is respected and taken into consideration beyond formalities, thus building a sphere of trust and a sense of belonging among the project's scientific team and the stakeholders. Stakeholders' specificities have to be respected, but boundaries must be set, and stakeholders should not order others around or impose their ideas on the group, regardless of their level of expertise of influence.

The developed strategy comprises five main steps, consisting of framing, mapping, involvement, co-production, and sharing processes (Figure 4).

The following sub-sections contain more in-depth discussions on the proposed approach and the key points that should be considered when applying the methodology.

3.1. Framing

Initial Study of Challenges: Firstly, the key challenges to be addressed were identified. A baseline investigation of the study area, which helped to identify the key problems faced across the PRB, was carried out through conducting research in the study area and utilising the research team's expertise and key consultancy skills. The identification of the PRB's challenges not only enabled the research team to pinpoint the key sectors to focus efforts on but also allowed for an initial characterisation of the basin and the identification of sub-basins for more specific discussions. The preliminary identification of challenges was also supported by the information provided by stakeholders in the round of individual interviews. Indeed, part of the questions focused on the selection of their main needs related to the use of natural resources and potential barriers to fulfilling these needs (including biophysical and governance aspects). Subsequently, the key approaches and methodological frameworks to be tested were proposed. This process was accompanied by the definition of a wish list of data requirements. Key sectoral challenges, cross-sectoral interrelations, data requirements and availability, potential levels of intervention, and the spatial distribution of issues were preliminarily determined. This step also involved the preliminary selection of which stakeholders should be invited to participate in the LAA.

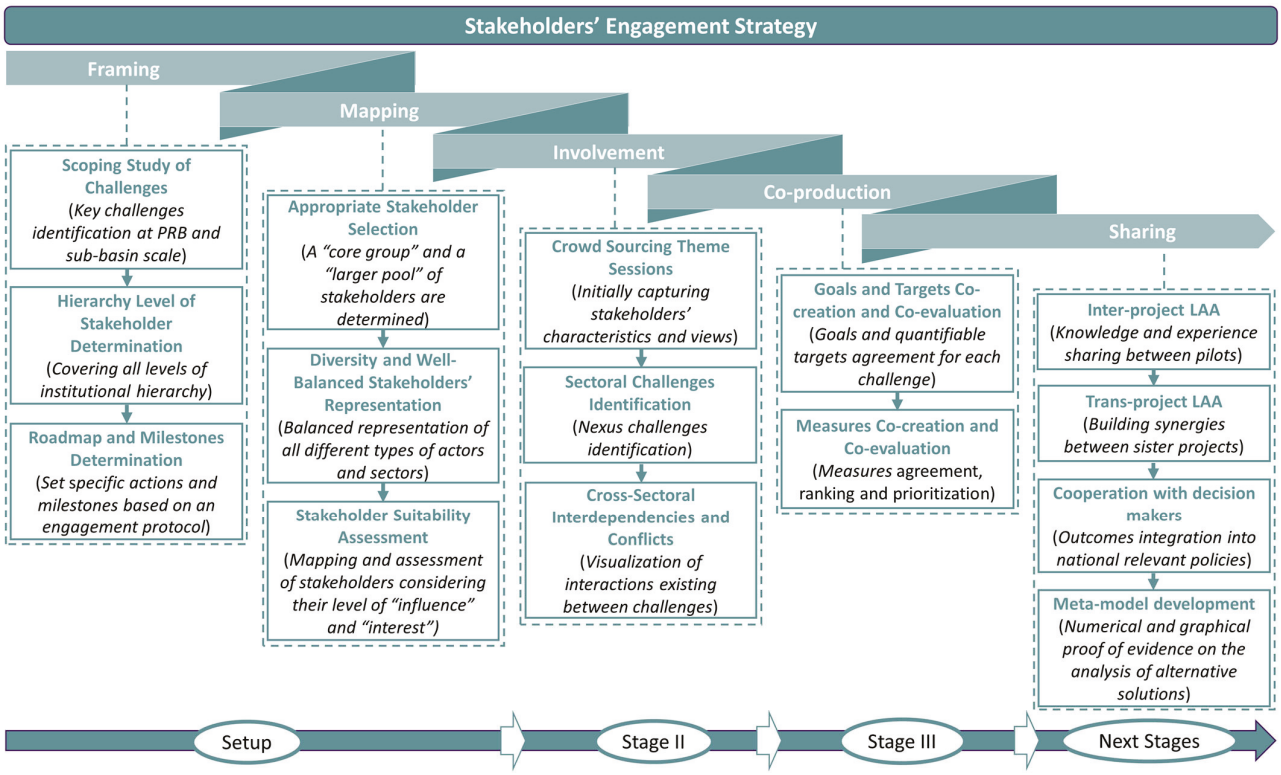

Figure 4. Stakeholder engagement strategy as part of the PRB LAA development process.

Determination of the Hierarchy Levels of Stakeholders: Identifying the hierarchy levels that need to be covered and the institutional profiles that need to be included in the pool of stakeholders greatly depends upon the size of the study area, the nature of the identified issues, the envisaged problems' resolution plans, the need to perform in depth analyses at small scales, and the need to consider potential institutional changes, awareness raising, and capacity building initiatives. Evidently, the more comprehensive and wide the pool of key stakeholders is, the more representative it is, lowering the possibility of omitting/missing criticalities in the construction of a holistic management plan. On the other hand, the wider the pool of stakeholders, the greater the likelihood of conflicts arising and the consultation concluding without a consensus being reached. In the case of the PRB, in view of the multitude of complex issues that need to be tackled, an expanded stakeholders' panel was set up. Therefore, the adopted approach aimed to cover all levels of institutional hierarchy, such as end users, decision makers, strategic planning/policy makers, non-governmental organisations, experts, research institutions, and private companies, to the best possible degree, thus potentially facilitating interaction throughout the entire pyramid (i.e., from the bottom to the top and from the top to the bottom).

Roadmap and Milestone Construction: A roadmap and milestones for the stakeholder engagement strategy were then constructed. Starting from when the stakeholders were initially approached, a specific engagement protocol was drawn up and followed to ensure the highest possible engagement level and a low incidence of stakeholders declining to participate. This protocol was based on systematic and frequent follow-up contact on a personalised level, starting with phone calls and also involving regular e-mail communication, followed, in due time, by individual in-person interviews and small group meetings. Achieving high success rates in recruitment necessitates making use of existing personal contacts, gaining new personal contacts, and developing relationships in a continuous effort to build and maintain/confirm trust. Stakeholders' individual characteristics and profiles, along with the profiles of the body they represent, were studied prior to approaching them and collaborating with them.

The stakeholder engagement strategy has been strategically shaped to address the demands of the project whilst taking into account stakeholders' characteristics, the key features of the study area, the institutional capacity and structure surrounding the project, and the level of knowledge among the stakeholders about the nexus approach and nexus concepts. Based on the tasks to be accomplished by the project and the focus developed for the study, a roadmap mapping the whole trajectory of the project and specific actions and milestones was established in collaboration with the involved partners. Hence, a series of meetings, workshops, and desk work sessions have been defined to be elaborated with specific content and target and a precise timeline to reach the required result. In every step of the process, it has to be clearly understood that successful stakeholder engagement is an elaborate and long investment that needs to be developed on the basis of mutual understanding and respect.

3.2. Mapping

Appropriate Stakeholder Selection: An initial list of potential stakeholders was drafted, based largely on the work experience of the REXUS research team regarding the region of Thessaly, and augmented by the personal relations that were developed among them. In parallel, a wide search for additional stakeholders was performed; this search for stakeholders was carried out through using the snowball technique, partially ensuring their high level of interest, and an online search for potential stakeholders who represent significant actors in the study area; however, the a priori assurance of their willingness to actively participate in the project was not part of this search. An initial list of more than 150 stakeholders was compiled.

Starting with this list, specific criteria were used to reduce the final number of stakeholders; these criteria were as follows: representativeness of all sectors, coverage of all hierarchy levels, participation of key actors, wide geographical coverage, presence of critical policy and decision making as well as implementation bodies, representation of all key socio-economic activities, pluralism in stated viewpoints (including the academic literature, consultancy, production, society, technocrats, etc.). Subsequently, the list of preselected stakeholders comprised approximately 50 people, all of which were invited to participate in the REXUS project. This number was assumed to be realistic in helping the research team achieve effective and representative results. Invitations were extended on a personalised level through telephone calls, e-mails, and in-person visits when requested to communicate the targets of the project and explain the role of the stakeholders and their engagement in the active participatory approach towards developing holistic management solutions. Approximately 35 people responded positively to the invitation, forming the initial group of stakeholders for the project. This number was increased to 44 following the suggestions offered by the participating stakeholders, as some nominated their contemporaries to ensure a higher degree of representativeness.

Orientation criteria and hints for the selection of appropriate stakeholders were employed, resulting in the construction of a list of two distinct groups of stakeholders. The "core group" consisted of stakeholders who mainly focused on most of the feedback in the co-mapping of the challenges, the co-identification of the constraints and criticalities, and the co-design and redefinition of a potential set of solutions in the holistic management strategy. These are the people that presented the highest interest, influential capacity, and decision making power while possessing the deepest knowledge of the study area. The "larger pool" incorporated the aforementioned group but also included a large number of stakeholders that essentially formed a conclusive list of existing representatives of all sectors and levels with variable degrees of knowledge and scholarly education, involvement, abilities to influence and/or motivate, and decision capacities, but every one still had a vast knowledge of the study area and/or the sectoral issues.

Both groups were dynamically altered as the project progressed to adjust to its needs and ensure alignment with the responses of the stakeholders. To this end, the opinions and suggestions of the stakeholders were seriously considered to inform their inclusion in either

group. Overall, the key criteria considered for stakeholders' inclusion in the core group included "representativeness", "coverage", "performance", "experience", "influence", "collaboration", and "satisfaction/preference". Adequate representativeness of the nexus sectors and societal groups at regional and local scales under all the identified institutional levels has to be ensured. Both a holistic coverage of sectors and topics that ensures no critical challenge, impacted system, or activity is left unconsidered and a trans-sectoral coverage enabling improved and more efficient designs of acceptable and applicable "working" holistic solutions have to be achieved. Also, the entire spectrum of performance (from poor to excellent) has to be covered with regard to resource management at the regional level, as long as stakeholders directly or indirectly become involved in problem solving for the study area. The adoption of best practices by stakeholders and their responses to troublesome, inadequate, or mismanaged resources and occurrences in their respective sectors, along with everything in between, are of great interest. Obviously, well-performing stakeholders were prioritised, as they are normally aware of issues, needs, and problems and capable of actively assisting in shaping best practices for holistic management with the aim of increasing resilience and enhancing sectoral security. However, it is strongly believed that considering the viewpoints and analyses of poorly performing stakeholders may help considerably in mapping problems and perhaps even more so in understanding the reasons behind their poor performance. In the end, these are the stakeholders that need to participate in the co-decision process on the development of solutions that merit social consent, inclusivity, justice, and acceptability in order to ensure full-scale implementation. In addition, having a wealth of collective experiences to share and diffuse amongst the core group of stakeholders is of the utmost importance to achieve a deep and conclusive understanding of the current conditions of the study area and improve the likelihood of the designed solutions being applied successfully. The potential influence of stakeholders should be considered to improve the feasibility of the co-designed solutions and ensure they are efficiently communicated, as increasing the probability their actual implementation is of great interest, as is the ability of stakeholders to collaborate with other stakeholders and scientific teams, ensuring a healthy, fruitful, and overall amicable collaboration with the highest possible degree of efficiency. Moreover, sometimes, the appointed representative of the stakeholders' board of directors does not necessarily choose with the most appropriate or obvious choice amongst the available options, but ensuring that a consensus is met is critical in finding and, more importantly, implementing solutions.

The group of engaged "core stakeholders" comprised 44 members and was synthesised as presented synoptically in Figure 5 and detailed in Appendix A (Table A1). A unique code was provided to each different stakeholder based on their main related nexus sector (i.e., the prefixes W, EN, F, and EC refer to the water, energy, food, and ecosystem sectors, respectively). Overall, the water, energy, food, and ecosystem sectors were represented by 11, 3, 23, and 7 stakeholders, respectively (Figure 5a). In addition, stakeholders were categorised according to their type; i.e., there were 15 decision makers and policy-makers (POL), 11 representatives of end users and individual end users (USER), 2 citizens and NGOs (CIT), 3 individual experts (EXP), 3 representatives of private companies (COM), and 10 research and academia representatives (RES) (Figure 5b). Levels of influence and interest were also assigned to each stakeholder, as presented in Table A1.

Diversity and Well-Balanced Stakeholders Representation: Diversity and a well-balanced representation of all WEFE nexus sectors and institutional/governance levels and types constitutes a prerequisite for a nexus approach and therefore has to be ensured. The higher number of stakeholders representing the food and water nexus components is attributed to the dominance of the agricultural and water-related sectors in the PRB; however, these sectors were not treated favourably compared to the other sectors since the engaged stakeholders were asked to express their views on all of the nexus components. This is illustrated in Figure 5, where it is clear to see that the water and food sectors outnumber the others, especially the energy sector. Still, as energy is strongly interrelated to the water and food sectors, especially due to the financial aspects escalating from contemporary

critical issues, the energy sector was indirectly but responsibly covered in equal terms by the group of stakeholders. Interestingly enough, the assessments and categorisations made by our research team for each stakeholder with regard to the key sector each one represents best on the basis of their profiles shifted towards the water sector, as proved by the self-determination exercise practiced in the very first meeting that was held, as explained in Section 3.3.

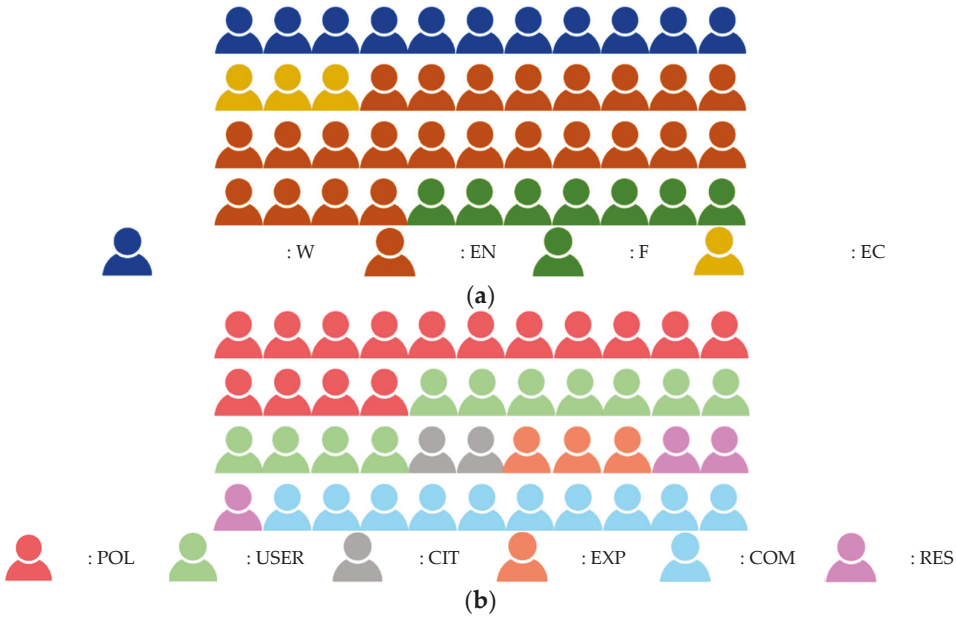

Figure 5. Characteristics of engaged stakeholders based on (**a**) their related nexus sector and (**b**) their type.

Stakeholders' Suitability Assessment: Once the list of selected stakeholders was created, stakeholders were characterised and mapped in terms of their influence and interest criteria. The idea of developing a stakeholder power grid to visualise the influence and interest of stakeholders was conceived by Mendelow in 1991 [79]. Stakeholders differ in how much influence they have and in how much they are interested in a particular topic. The term "influence" refers to the capacity/power of stakeholders to solve or exacerbate a problem, while the term "interest" refers to the importance of a problem in the eyes of stakeholders regarding the level of relevance it has to their business. Our research team's approach involved the stakeholders being categorised into four classes: "promoters", "defenders", "latents", and "apathetics" [80]. Promoters are those who usually have both great interest in an issue and the power to help resolve it successfully, defenders are stakeholders who have a vested interest and can voice their support in the community but may have little actual power to influence the issue in any way, latents are those who have no particular interest or involvement in an issue but have the power to influence it greatly if they become interested, and apathetics include stakeholders who have little interest, little power, and may not even be aware of an issue. The stakeholders were mapped on a four-quadrant plot based on their levels of influence and interest, and this plot is depicted in Figure 6.

The distribution of stakeholders in the four quadrants reflects the perception of the analysts. However, in our case, to facilitate LAA activities through the active engagement of the different groups of stakeholders, the selection procedure involved assessing each individual's level of influence and interest. Hence, members of the group that were assigned to the bottom two quadrants (apathetics and latents) were filtered out and not considered further. All the engaged stakeholders were therefore distributed in the upper two quadrants of the mapping diagram, meaning that they were characterised as promoters and defenders and that they were all interested in the nexus issues. The filtering out of

the latents and apathetics in the developed PRB LAA activities was carried out to avoid the negative effect they may have on the implementation of a project and its outcomes. About a third of engaged stakeholders (15) were characterised as promoters (those with high levels of influence and interest), with the remaining 29 being classed as "defenders". Interestingly, the distribution between the two categories is rather balanced for three of the four sectors too. As already stated, the mapping described herein is the result of filtering the initially compiled stakeholders' pool to ensure a group of stakeholders with the potential to leverage decision making on nexus management throughout the whole project. However, stakeholder characterisation and mapping can dynamically change as a result of several factors, including potential erroneous assessments by the scientific team members, changes in the prioritisation and obligations of the stakeholders, failing to the attract attention of the stakeholders to the scope of the project/process, a lack of genuine interest in the process among participants, and disproportionate requirements for investing time in the process.

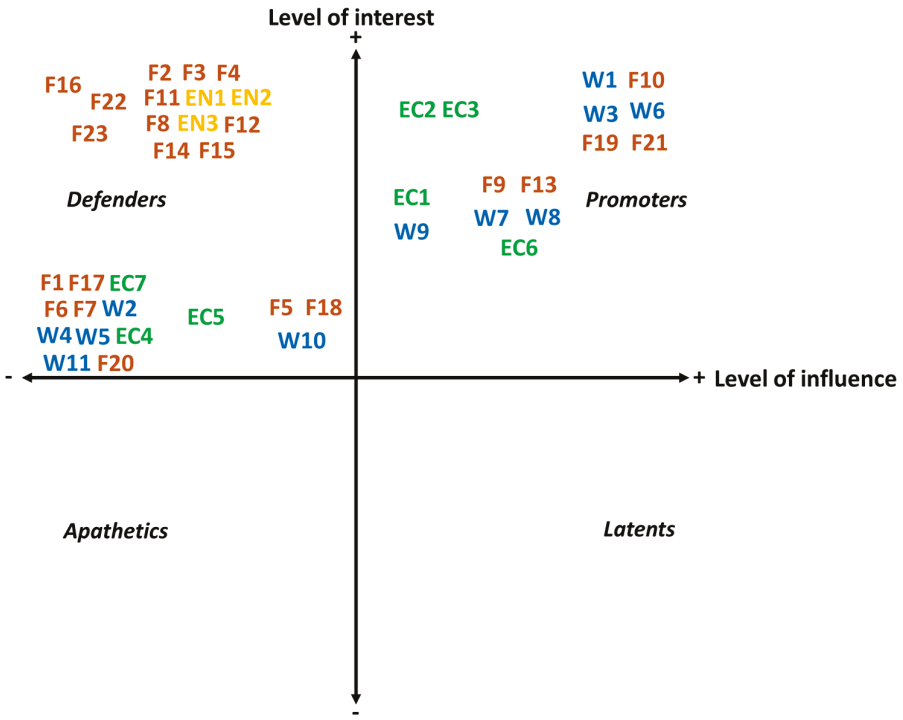

Figure 6. Selected stakeholders' classification based on influence and interest criteria.

3.3. Involvement

This phase is central for the stakeholder engagement, as it centres around enabling the active participation of relevant stakeholders through a series of participatory activities, details of which are provided in the following sub-sections. This phase is centred on the 'diagnosis' of PRB conditions and is carried out to both select relevant sectoral challenges for the area and to better understand cross-sectoral interdependencies.

Crowd Sourcing Theme Sessions: The next step consisted of the preparation and realisation of the first meeting of the REXUS PRB stakeholders, which took place online on 30 November 2021. The meeting consisted of three crowd sourcing theme sessions to initially capture stakeholders' characteristics and views and two virtual roundtable discussions to involve all the stakeholders in a common virtual discussion.

In particular, 15 online questions were included in the framework of the three crowd sourcing theme sessions of the REXUS PRB Learning and Action Alliance kick-off meeting, allowing for immediate feedback on the overall status of the stakeholders' perceptions. The questions, along with an analysis of the stakeholders' responses, are presented synoptically below and in-depth in Appendix B. Each session involved asking five questions to stoke

the interest of the audience regarding the nexus system issues and register their viewpoints on the fly. The Mentimeter online platform was employed for this purpose.

In fact, the first session acted as an ice breaking session for the stakeholders, elucidating their linkages to the PRB, perceptions of the nexus approach, and their expectations for the REXUS project. Almost 80% of the participated stakeholders have ties to the water and food/agriculture sectors, revealing the agricultural nature of the PRB. The vast majority of them are familiar with the PRB nexus system, and they could decisively contribute to the analysis of cross-sectoral challenges, while half of them are mainly ministers and academics who could influence the decision making process. A high level of nexus principle understanding was also revealed by the fact that most stakeholders acknowledged the need for each WEFE sector to be approached equally, while this perspective did not seem to be clear enough among stakeholders related to the food/agriculture sector, highlighting the complexity of the agricultural sector in the PRB. The main reasons for stakeholders' involvement were related to their intentions to express their interest in and concerns about the challenges associated with the PRB, along with their desire to co-design a sustainable future.

The second session was developed to capture stakeholders' viewpoints on the PRB's conditions. The management framework of the PRB nexus system was characterised as very complex or complex among the vast majority of stakeholders, exposing the limited effectiveness of already implemented measures. The water sector of the PRB faces the most crucial challenges, a fact that was recognised by stakeholders from all the different nexus sectors. In addition, the water and food/agriculture sectors appeared to have the highest importance and were the most thoroughly investigated PRB sectors.

The third session was conducted to capture the perception of stakeholders on the implemented management practices. The efficiency of the already implemented measures was characterised as moderate, with a selection of these measures mainly being affected by the influential capacity of some stakeholders. The water and food/agriculture sectors present the strongest interaction and are either already being significantly affected or expected to be affected by the climate crisis.

The Identification of Sectoral Challenges: In the framework of the first REXUS meeting of the PRB stakeholders, a roundtable discussion was organised and conducted to select the most critical nexus challenges. As mentioned before, a series of individual semi-structured interviews were conducted, either in-person or virtually, with each different stakeholder, and this resulted in an extensive list of challenges that should be addressed to ensure the sustainability of the study area (Figure 7). As highlighted in the figure below, the focus was firstly on the nexus sectors in isolation. Interestingly enough, governance issues were identified as central issues in all sectors. The process was not influenced by any direct or indirect indications on the challenges to consider. As a result, the identification of the most important ones was based on the stakeholders' own critical judgment only through a specific session organised during the stakeholders' workshop.

A set of critical challenges was thus identified for each sector, in addition to the major issue of governance. Governance is a multidimensional concept that refers to the political, social, economic, and administrative systems in place that influence the development and management of resources such as water, land, or energy. In the water sector, several frameworks have been developed to diagnose water governance and support the development of action planning [81–84]. Despite the different focuses of governance assessments and target groups, diagnosis focuses on analysing formal structures (i.e., the existence, adequacy, and coherence of the policy and regulatory framework and the roles and responsibilities of the different institutions managing the resources and financing) and how well processes work in practice (i.e., level of coordination, cooperation, implementation, and performance). As the Organisation for Economic Co-operation and Development [85] describes, it is about exploring the effectiveness and efficiency of formal and procedural aspects, as well as trust and engagement (Figure 8).

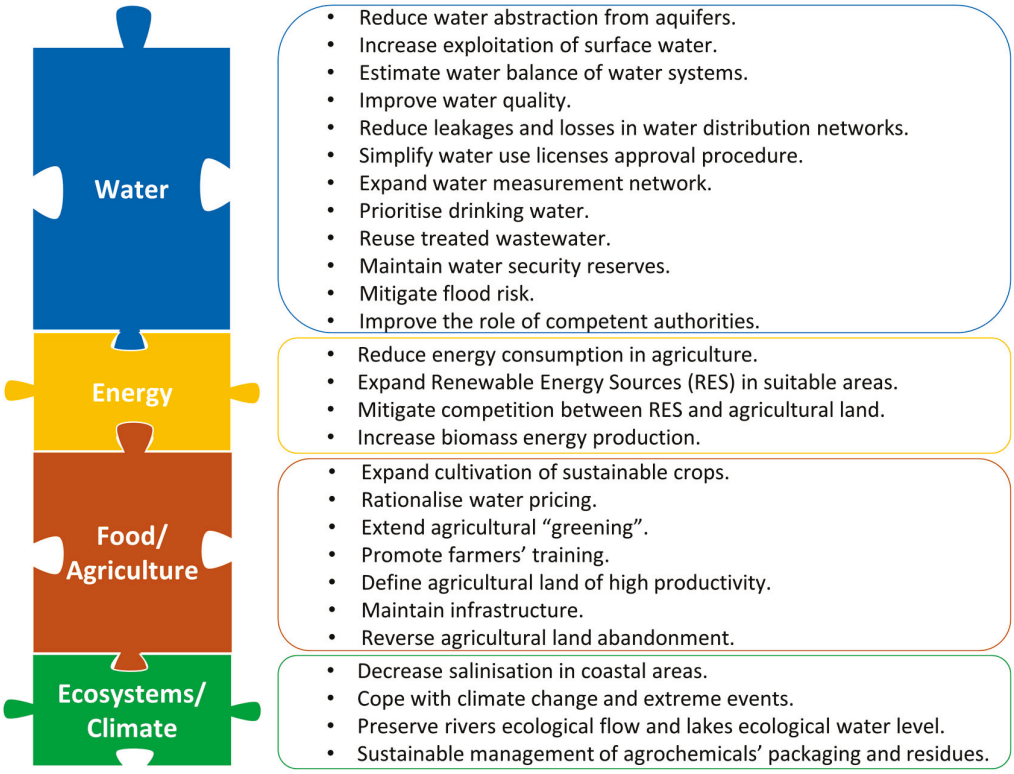

Figure 7. Critical nexus challenges with respect to the Pinios River Basin.

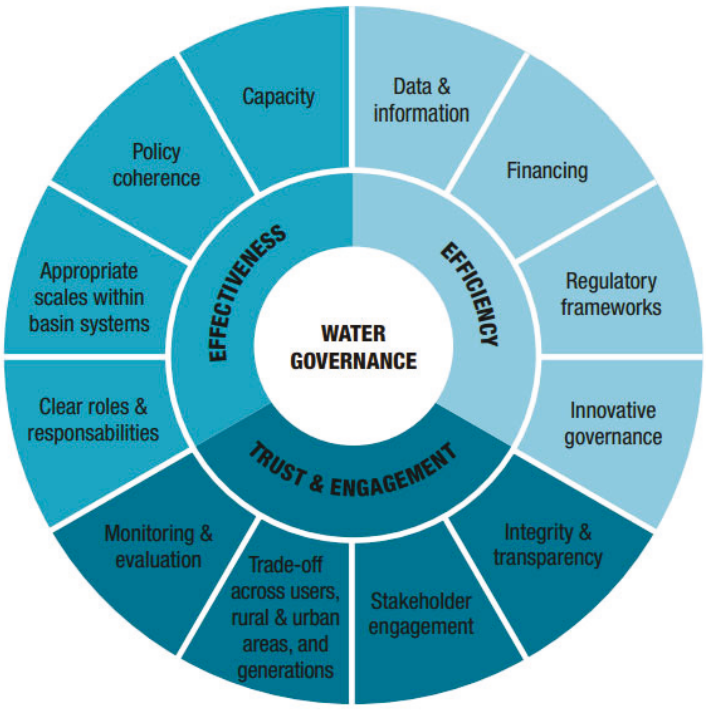

Figure 8. OECD principles regarding water governance [85].

Effective administration and governance in the PRB is of paramount importance and directly or indirectly reflected in all four sectors as a challenge. Its importance lies in the fact that none of the measures defined and proposed for implementation in order to address the identified challenges may be successful and meaningfully impact the system unless the governance structure is well developed and supplemented by efficient administrative units.

Complex legislation framework and scattered responsibilities among competent authorities were identified as the most critical barriers in the PRB, hindering effective administration and governance.

The water-associated challenges primarily relate to ensuring sufficiency in terms of fair spatiotemporal distribution to ensure the coverage of all socio-economic activities without disregarding quality, especially in specific parts of the basin and with respect to agriculture-related pollutants. In parallel, as part of the management practices proposed to address the water-related challenges, flood risk mitigation, resilience to shortages due to droughts, and the utilisation of treated domestic effluents are high on the agenda. The food-related challenges pertain to the development of viable and sustainable agriculture, towards which production cost rationalisation and greening are thought to be of paramount importance, as are the productive utilisation of agricultural land and the training of farmers. The rehabilitation and preservation of ecosystems and their functions are the key challenges relating to the environment and, along with the sustainable management of agrochemical' residues and the preservation of ecological river flows and minimum lake levels. High use efficiency lies at the essence of the identified energy-related challenges; the energy sector's challenges include the expansion of renewable and biomass energy production to resolve issues such as the antagonistic use of high-productivity land and reducing energy consumption in the agricultural sector.

The PRB challenges were also critically analysed through reviewing previous studies. Groundwater overexploitation and water quality deterioration are triggered mainly by non-sustainable agricultural management practices which have been carried out since the mid-1980s [67]. Mean annual precipitation in the PRB is projected to decrease, while temperature and evaporation are projected to increase until 2100, resulting in a significant decrease in water availability, which is strongly related to the projected declining groundwater recharge trend and increasing trend in relation to irrigation water demand. Ecological flow is difficult to preserve in some rivers in the PRB, presenting low to zero discharge during the summer months in recent years [78], while the total runoff in the PRB is projected to decrease further from 22% to 66% until 2080 compared to the 1980–2000 period [14,71]. Flood occurrences increased between 1990–2010 and 1979–1989 in the PRB, with most flood events being recorded in the southern part of the PRB and most of the damage occurring in rural areas [86]. The PRB has also experienced severe, extreme, and persistent droughts that have affected large areas since the late 1970s and became more evident and frequent during the last three decades, especially over the past 5–7 years.

Cross-Sectoral Interdependencies and Conflicts: During one stakeholders' meeting, a second roundtable discussion was conducted to explore the transectoral relations between the identified challenges in order to facilitate a holistic approach. The identified interrelations were then finalised, and further details on them were obtained from personal interviews with stakeholders. The final interrelations were drawn up and visualised (Figure 9). The colour selected for each connecting line refers to the nexus sector of the related driving challenge (i.e., the blue, yellow, brown, and green lines refer to water-, energy-, food/agriculture- and ecosystems/climate-related challenges, respectively).

Cross-sectoral interdependencies provide a comprehensive understanding of the bonds between nexus sectors, helping to identify how and where exactly each sector interacts and depends on another. Unless these dependencies are fully mapped, understood, and taken into account, any attempt to design and successfully implement management measures will inevitably be of limited efficiency and impact. Successful holistic approaches involve a global overview and examination of the sectors that form the nexus of a system and require a common understanding of the identified issues, challenges, and interdependencies in order to reach a wide consensus on ways to improve progress towards sustainable management.

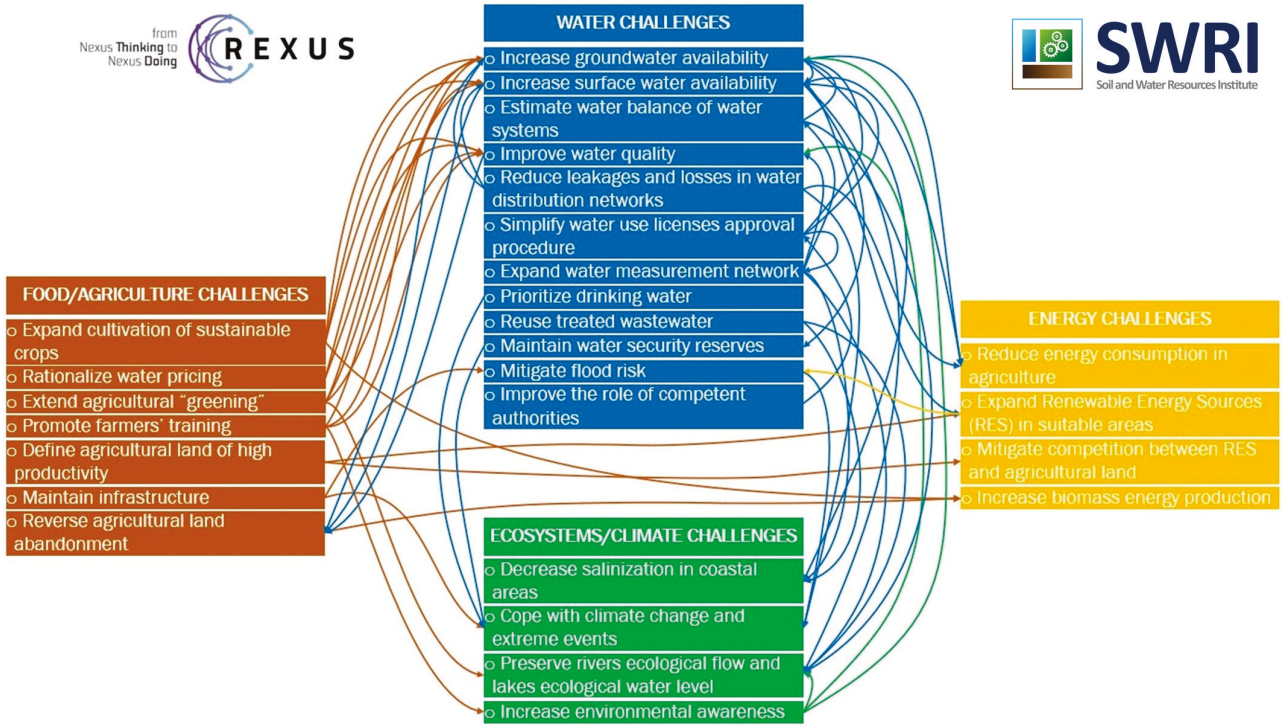

Figure 9. Interrelations of critical challenges in the Pinios River Basin.

The canvas illustrated in Figure 9, which summarises the feedback from participants, clearly shows the complexity of the studied nexus and the tight bonds amongst its sectors. Especially between the water and food/agriculture sectors, multiple and multi-level dependencies are denoted for the PRB, clearly suggesting that managing an element of one sector would inevitably influence the other. Interestingly enough, a very strong dependency was identified between the former two sectors and the ecosystems/climate sector, which mainly reflects concerns surrounding the current management conditions and perceived sustainability status. Evidently, the stakeholders acknowledge that there are less interdependencies for the energy sector. This can be attributed to the limited knowledge on the local relevance of the sector, considering the challenges that are faced worldwide.

3.4. Co-Production

The Co-creation and Co-evaluation of Goals and Targets: The challenges that emerged from the involvement phase helped in setting the goals for achieving nexus sustainability. Clear goal setting could help policy and decision makers to improve their performance in terms of sustainable development [87]. In addition, quantifiable targets have to be determined to measure the satisfaction level of defined goals and thus promote WEFE security.

To promote their applicability and effectiveness, targets should be in compliance with international and national WEFE legislative regimes. The Sustainable Development Goals (SDGs) included in the 2030 Agenda for Sustainable Development [19] were established in compliance with the rights and commitments of the United Nations, and they are considered political goals, not legal rules. The SDGs and associated targets serve as inspirational statements that constitute crucial parts of international legislative instruments and aim to trigger action that will yield results in critical areas for the well-being of humans and the planet by 2030. The SDGs attempt to orchestrate the wide variety and diversity of targets already embedded in various international agreements.

Regarding the PRB, proposed goals and targets should be in accordance with European and national policies. European Union (EU) legislation pervades the national policies of all member states while regulating most of aspects of the WEFE nexus. In terms of the water sector, the Water Framework Directive (2000/60/EC) sets out rules to prevent water

status deterioration and achieve a good status for all deteriorated surface and groundwater bodies [88]. Regarding the energy sector, the recent Revision of the Renewable Energy Directive (COM/2022/230) proposes to further increase the target of renewable energy sources in the EU to 45% by 2030 [89]. In the field of agriculture and rural development, the Common Agricultural Policy (CAP) 2023–27, implemented on 1 January 2023, aims to ensure stable food supply, ensure farmers' incomes, and keep rural areas vibrant within the context of environmental sustainability [90]. In terms of EU climate action, initiatives include engaging all parts of society in climate-benefitting actions, further reducing emissions by 2030, and making Europe the world's first climate-neutral continent by 2050 [91].

The proposed goals and targets may interact among each other, mirroring the interrelations and critical trade-offs among the WEFE challenges. In particular, some goals and targets seem to be independent of each other, while others may reinforce or impose constraints on others due to the competition for scarce natural resources. However, effective stakeholder engagement and involving stakeholders in common discussions could mitigate potential policy conflicts, resulting in the development of a coherent set of goals and targets and a complete consensus, ultimately shifting goals and targets from being centred around achieving acceptable trade-offs to achieving win–win scenarios.

The Co-creation and Co-evaluation of Measures: Defined goals and targets call for both sustained and sustainable development through the compilation and implementation of specific measures. Policy makers and decision makers need to elaborate on how to integrate goals and targets into management policies to address nexus challenges. A wide range of sustainable measures could be implemented, including supply-side and demand-side options, across all nexus sectors. Supply measures are mainly related to infrastructure and treatment technologies, while demand management measures include resource efficiency promotion, changes in resource allocation mechanisms, and improvements in resource productivity and availability. However, each measure presents specific strengths and weaknesses which have to be properly considered. Efforts should be made to analyse, rank, and prioritise measures using as wide a range of objective criteria as possible, covering technical, social, and other characteristics. The creation of effective measures may secure reliable supplies of natural resources to meet future demands.

There is an increasing awareness of Nature-based Solutions (NbS), which have the potential to address both climate mitigation and adaptation challenges at a quite low cost while promoting human and nature benefits. NbS promote the sustainable use and management of natural resources while tackling economic and environmental challenges and sustaining human well-being. In addition, NbS emerge as an integrated approach that mitigate trade-offs and promotes synergy among the SDGs. The importance of promoting NbS is even greater considering that some SDGs, including those centred around stabilisation and adaptation to climate change (SDG13) and biodiversity protection (SDGs 14 and 15), are unlikely to be met by 2030 [92]. The importance of NbS was recognised by their endorsement in the Climate Change and Land Report of the Intergovernmental Panel on Climate Change (IPCC) [93] and the fact that they were included in a COP cover policy for the first time during the 27th Conference of the Parties to the United Nations Framework Convention on Climate Change (COP27).

3.5. Sharing

Inter- and trans-project approaches can significantly advance nexus management towards resilient WEFE systems and drive sustainability transitions.

Inter-project LAA: Horizontal knowledge is expected to be enhanced through the development of an inter-project LAA centred around knowledge sharing between pilot areas of the project. Dialogue on policy integration needs and gears across pilot areas is promoted. In addition, cross-fertilisation amongst the project's pilots is being practiced to improve the developed strategies for nexus management, rectifying what has been found to not yield results and strengthening the efficient parts of the existing strategies.

Trans-project LAA: The produced experience will be further disseminated across other projects under the nexus scheme through the development of a trans-project LAA. This way, alignment with similar projects and building synergy among them will be achieved. The role of the trans-project LAA can prove crucial in a much broader context since integrating the lessons learnt from engagement strategies in areas with different particularities provide give a significant boost to align agendas and policies in a trans-sectoral perspective.

Cooperation with Decision Makers: Experience and information sharing may be practiced among influential decision making bodies and authorities, again aiming to improve the decisions to be made and perfect the outcomes of the nexus management project. To this end, within the framework of the REXUS project, the research team has initiated a twofold external collaboration (a) through creating a focal group of the Water Resources Management Plan (WRMP) of the Thessaly district that PRB belongs to and (b) establishing a focal group with the official consultancy for the implementation of the WRMPs on a nationwide level. Focal group (a) consists of high-ranking specialist executives of the Ministry of the Environment and Energy and specialist consultants of the consortium responsible for the second revision of the WRMP at the PRB. The objective of this collaboration is to strengthen and promote the holistic approach towards the effective and sustainable management of the PRB by exchanging viewpoints and aligning information and data that enhances pluralism and integration. The ultimate aim of this collaboration is to establish a revised plan that has a higher chance of being successfully implemented and yielding results. Focal group (b) consists of highly experienced executive technocrats that are responsible for guiding and consulting the ministerial and regional services towards aligned efforts for the efficient implementation of the WRMPs at national level through the consultancy work carried out by several consortia and the regional authorities' scientific staff. They share the vision of holistic nexus management, and the target of this collaboration is to disseminate the virtues and needs for holistic nexus management nationwide through the systematic, active engagement of stakeholders whilst offering help in efforts towards training scientists involved in this activity.

Meta-Model Development: A meta-modelling approach can be employed to visualise and more easily present the main information and outcomes of a project or task. A meta-model transforms produced implicit knowledge into straightforward results, supporting the analysis of information and thus the accumulation of knowledge. The meta-model's layout and component selection could be based on users' opinions, including the indicators, scenarios, and measures that a meta-model could present and the type of visualisations that a meta-model could offer. Specific answers to these generic questions mainly depend on the target audience; thus, meta-model co-development constitutes an inextricably linked component of the whole stakeholder engagement process. An efficient meta-model design could allow users to easily gain insights into the complex nexus systems, supporting decision making processes within a holistic point of view. Its development for the PRB is largely shaped on the needs and requirements of the stakeholders, who we envisage to be amongst the key users of it.

4. Conclusions

The main objective of the present work was to present an effective strategy for incorporating different stakeholders' views and priorities through their active engagement in group discussions to define the critical challenges of WEFE nexus components in the Pinios River Basin. Defining critical challenges and their interconnections in WEFE-stressed areas could help in redefining policies and seeking solutions within an integrated sustainable development context. The findings of the present work are summarized below:

- The identification of key challenges, along with their interconnections and interdependencies, is crucial to supporting policy makers in enhancing the resilience of the study area.

- Despite the scientific team's extensive experience regarding the study area, the responses of the stakeholders offered new viewpoints and challenges that had not been realised in previous activities.
- The use of a holistic approach as a basis for the engagement process revealed impressive interdependencies amongst the key nexus sectors. More importantly, governance emerged as a hotspot challenge by itself, having been indicated in several ways and shapes as such in all four examined sectors.
- The involvement of a broad spectrum of stakeholders not only improves the representativeness of the identified challenges but also renders the participatory process more transparent. As a consequence, the identified solutions are expected to have wider social acceptance and an increased chance of being successfully and efficiently implemented.

In conclusion, the proposed methodology shows a clear and detailed path of actions that need to be taken to support stakeholder engagement in nexus studies. In the methodology, particular attention is given to the process of stakeholder selection and analysis, as well as to their involvement both in individual activities (interviews) and group exercises. The purpose of this is to have information related to each sector in isolation (e.g., sectoral challenges) but also, even more importantly, on cross-sectoral interdependencies and potential conflicts. The whole approach comprises multiple phases and steps and is flexible enough to be adapted to the specificities of other case studies.

Future research could include the analysis of changes in stakeholders' viewpoints after their most intensive engagement in the actions of the REXUS project, also in view of assessing the effectiveness of the engagement roadmap.

Author Contributions: Conceptualisation, A.P. (Andreas Panagopoulos) and V.P.; methodology, A.P. (Andreas Panagopoulos), V.P., E.H., B.A.W., M.B. and A.P. (Alessandro Pagano); resources, D.M., A.C. and K.B.; data curation, D.M.; writing—original draft preparation, D.M., A.P. (Andreas Panagopoulos) and V.P.; writing—review and editing, A.P. (Andreas Panagopoulos), V.P., B.A.W., and A.P. (Alessandro Pagano); visualisation, D.M.; supervision, A.P. (Andreas Panagopoulos); project administration, A.P. (Andreas Panagopoulos) and V.P.; funding acquisition, A.P. (Andreas Panagopoulos) and V.P. All authors have read and agreed to the published version of the manuscript.

Funding: This research article was funded by the European Union's Horizon 2020 research and innovation program under grant agreement No. 101003632, project REXUS.

Data Availability Statement: Data is contained within the article.

Acknowledgments: Then: authors would like to thank the Pinios stakeholders for participating in the stakeholders' meeting.

Conflicts of Interest: The authors declare no conflict of interest.

Appendix A

Table A1. Characteristics of the participating stakeholders, as assessed by the research team.

Code	Stakeholder's (Body) Description	Type	Level of Influence	Level of Interest
F1	Legal advisor, collective irrigation organisations	EXP	- - -	+
F2	Irrigation Organisation A	USER	- -	+ + +
F3	Irrigation Organisation B	USER	- -	+ + +
W1	National-level authority, water services planning and management	POL	+ + +	+ + +
EC1	International NGO related to environment protection	CIT	+	+ +
F4	Agricultural interprofessional organisation, Irrigation Organisation C	USER	- -	+ + +
EC2	Local environmental protection authority	CIT	+	+ + +

Table A1. *Cont.*

Code	Stakeholder's (Body) Description	Type	Level of Influence	Level of Interest
F5	Former representative of relevant chamber and currently involved in several actions for the improvement of water resource management in the basin	EXP	-	+
F6	Professor, expert in crop production and rural environment	RES	- - -	+
F7	Professor, expert in irrigation and water resource management	RES	- - -	+
W2	Professor, expert in water resource management and representative of international organisation for sustainable development	RES	- - -	+
EC3	Professor, expert in ecology and ecosystems	POL	+	+ + +
F8	Farmers' Cooperative of Thessaly	USER	- -	+ + +
F9	Regional authority related to agricultural development	POL	+ +	+ +
EC4	Former member of NGOs related to environmental protection	EXP	- - -	+
EN1	Wind farm development and installation company	COM	- -	+ + +
F10	National-level authority, cultivation systems and crop production	POL	+ + +	+ + +
F11	Agricultural Association A	USER	- -	+ + +
F12	Agricultural Association B	USER	- -	+ + +
W3	National-level authority, water environment protection and management	POL	+ + +	+ + +
F13	Regional-level authority related to agricultural economy and veterinary services	POL	+ +	+ +
W4	Professor, expert in water resource management	RES	- - -	+
F14	Irrigation Organisation D	USER	- -	+ + +
F15	National-scale authority related to irrigation water management	USER	- -	+ + +
EN2	National-scale corporation related to electricity supply	COM	- -	+ + +
W5	Professor specialising in water resource management	RES	- - -	+
F16	Food production and distribution company	COM	- - -	+ + +
W6	National-level authority, water services costing and pricing	POL	+ + +	+ + +
F17	Research organisation related to crop quality control, classification, and standardisation	RES	- - -	+
F18	Regional division of chamber related to geotechnical professionals	POL	-	+
W7	Regional authority responsible for water resource management	POL	+ +	+ +
F19	National authority related to land reclamation and mechanisation	POL	+ + +	+ + +
W8	Regional authority related to hydro-economy	POL	+ +	+ +
W9	Consortium of private companies involved in the development of water resource management studies in the basin	POL	+	+ +
EC5	Research organisation related to groundwater exploitation	RES	- -	+
EN3	Operator of hydroelectric plant	USER	- -	+ + +
F20	Organisation related to agricultural education and training	RES	- - -	+
F21	National authority related to land reclamation, soil, and water	POL	+ + +	+ + +
F22	Young farmer	USER	- - -	+ + +
EC6	Regional authority related to environment and spatial planning	POL	+ +	+ +
W10	Regional department of chamber related to geotechnical professionals	POL	-	+
EC7	National research organisation related to biodiversity and ecosystems	RES	- - -	+
W11	Professor, expert in water resource management and environment protection	RES	- - -	+
F23	Agricultural Cooperative	USER	- - -	+ + +

Appendix B

Appendix B.1 Session A: Ice Breaking

Q1: Which of the following sectors are you mostly associated with? (select 1 out of 4 predefined answers).

A1: More than half (54%) of the stakeholders who participated in the first meeting of the PRB pilot area self-identified as having ties to the water sector, and 25% had ties to the food/agriculture sector; a fact that reveals the importance of these sectors in the PRB. Representatives of the ecosystems/climate and energy sectors accounted for almost 21% of the participants.

Q2: What is your relation with the Pinios River Basin (work-residence-knowledge of PRB's nexus system)? (select 1 out of 4 predefined answers).

A2: The vast majority (90%) of the stakeholders who participated declared that they were familiar with the PRB nexus system, and therefore, they could play a significant role in the framework of the identification of management problems and solutions. Half (50%) of the participants did not reside or work in the basin, and these participants were mainly high-level stakeholders, including ministers and academics. The highest proportion of the stakeholders who were not familiar with the PRB nexus system were the stakeholders related to the energy sector (33%); a fact that is attributed to both the early development stage and the multivariate complexity of this specific sector in the study area.

Q3: How can problems of the Pinios River Basin be resolved to achieve resilience and sustainability? (select 1 out of 3 predefined answers).

A3: Most of the stakeholders (85%) acknowledged the need for equally approaching WEFE sectors to achieve resilience and sustainability; a fact that reveals a high level of understanding of the necessity for a holistic approach in resource management. Only a small proportion of stakeholders (4%) were pessimistic and believed that the problems in the PRB cannot be resolved. More than half (57%) of the stakeholders related to the food/agriculture sector appeared not to have a clear view regarding the pathway to achieve sustainability in the PRB. This is mainly attributed to the complexity of the agricultural sector in the study area, the viability of which presents probably the highest interdependency to the other sectors, and this sector has already suffered the impacts of economic and energy crises and climate change.

Q4: What do you expect to gain from being involved as a stakeholder in the REXUS project? (select maximum 3 out of 4 predefined answers).

A4: Almost 40% of the stakeholders were involved in a project centred around co-developing solutions in the context of a holistic management framework; a fact that demonstrates their high levels of motivation and strong desire for a sustainable future for the PRB, along with a strong belief and a demand for participating in shaping their future by directly affecting the sustainability of the basin or contributing their expertise to shape the future, even if they do not reside in the PRB.

Q5: What do you expect to gain from your participation in the current meeting? (select maximum 2 out of 4 predefined answers).

A5: None of the involved stakeholders considered their participation in the first PRB stakeholders' meeting as a chore. In particular, more than 40% of the stakeholders participated in the meeting in order to become more informed about the ways that they can be actively involved in the tasks and activities of the project. Almost 58% of the stakeholders participated in the meeting to express their interest/concerns regarding the PRB's challenges and also to become informed about the other stakeholders' perceptions.

The answers of stakeholders to Q1-Q5 are presented in Figure A1, where questions 1–5 correspond to responses a–e, respectively.

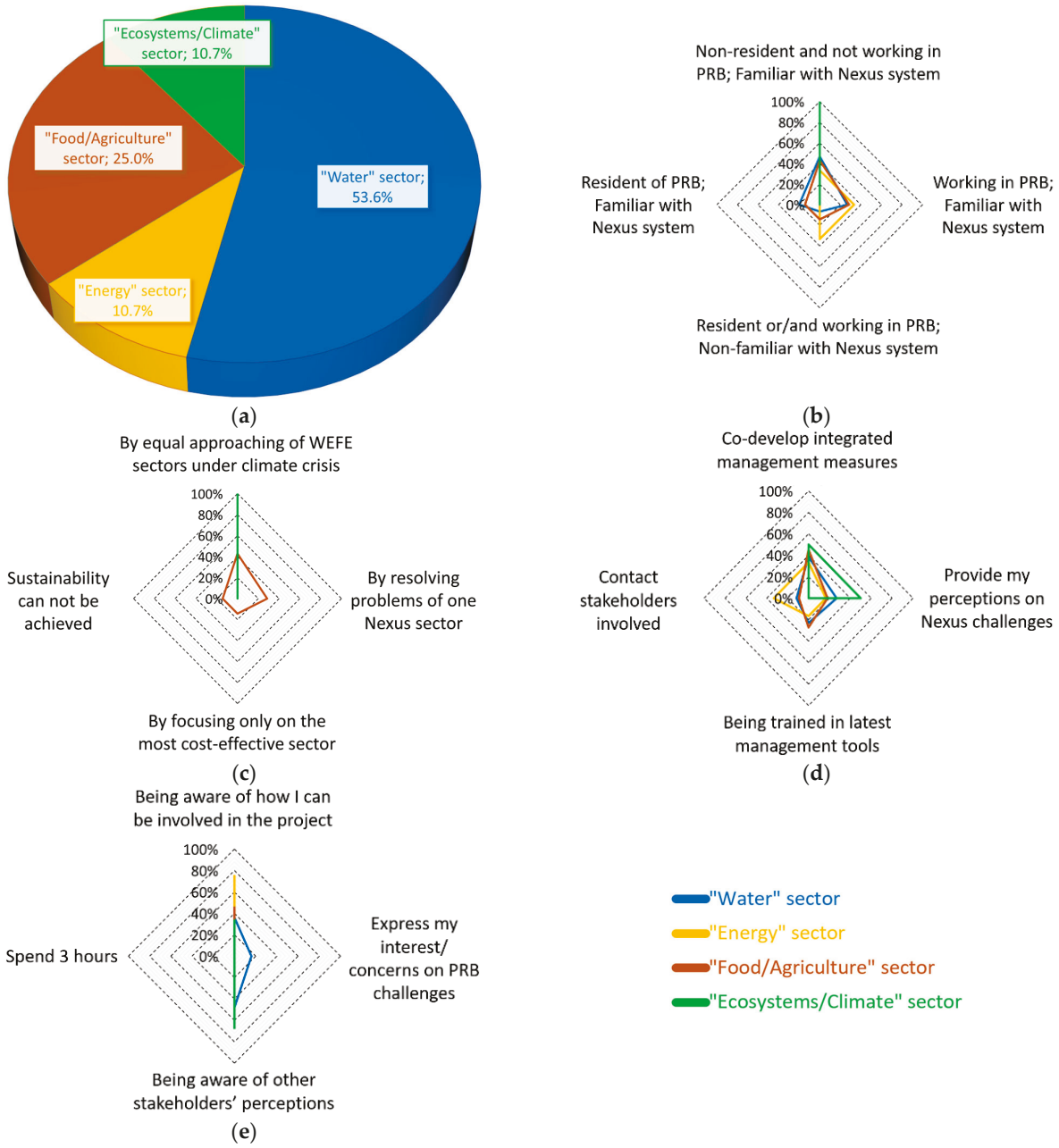

Figure A1. Responses of Pinios River Basin stakeholders to (**a**) Q1, (**b**) Q2, (**c**) Q3, (**d**), Q4 and (**e**) Q5 of the first crowd sourcing theme session.

Appendix B.2 Session B: Pinios River Basin Current Conditions

Q6: How can the management framework of the nexus system of Pinios River Basin be characterised? (select 1 out of 4 predefined answers).

A6: The vast majority of the stakeholders (90%) position the management framework of the PRB nexus system as a very complex spectrum, while only 10% of the stakeholders characterise it as moderately complex or simple. This fact reveals the limited effectiveness of previously implemented policies and poses higher expectations on the ongoing project. Only a small percentage (14%) of the food/agriculture-related stakeholders characterised the PRB's management framework as a simple one, believing that the promotion of new water transfer projects can simply address the relevant challenges.

Q7: Which sector of the nexus system faces the most crucial challenges? (select maximum 2 out of 4 predefined answers).

A7: Almost half (49%) of the participants consider the water sector as the PRB nexus sector that faces the most crucial challenges, followed by the ecosystems/climate (30%), food/agriculture (18%), and energy (3%) sectors. It should be highlighted that the water-related challenges are recognised as the most crucial ones by the stakeholders of all of the nexus sectors. The energy-related challenges are mostly recognised by the stakeholders related to the food/agriculture sector and are associated with the increased required energy amount and cost and thus agricultural production cost. Although the recognition of the high importance of the energy sector, the water, ecosystems/climate, and food/agriculture sectors seem to face most crucial challenges in the agricultural areas of the PRB in terms of the promotion of its socio-economic stability and development. The impulse response of the stakeholders may have been stimulated by the research teams' perception on the current challenges of the PRB, as expressed in a presentation that preceded the crowd sourcing meeting.

Q8: Which sector of the nexus system presents the highest complexity? (select maximum 2 out of 4 predefined answers).

A8: The water and ecosystems/climate sectors were suggested to present the highest level of complexity, according to the beliefs of 87% of the participating stakeholders.

Q9: How are the nexus sectors ranked according to their importance? (1-low to 4-high).

A9: The water sector (3.6 out of 4) was perceived as the most important sector in the PRB, followed by the food/agriculture (2.8 out of 4), ecosystems/climate (2.3 out of 4), and energy (1.5 out of 4) sectors. The water sector's high importance was unanimously recognised by stakeholders related to all PRB nexus sectors.

Q10: Which sector has already been investigated more thoroughly? (select maximum 2 out of 5 predefined answers).

A10: The food/agriculture sector (58%) was identified as the sector that has been the most extensively investigated, according to the perceptions of the participants, followed by the water (38%) and energy (4%) sectors, while none of the participants recognised the ecosystems/climate sector as the most studied one. This fact reveals that previous efforts and policies have mainly focused on the food/agriculture and water sectors, thus reflecting their importance for the PRB. Apparently, this approach denotes the "traditional" tendency to disregard, at least to an extent, the roles of the ecosystems/climate and energy sectors in sustaining the nexus system of a basin, despite the fact that large portions of the PRB's area have been included in one or more lists of environmental protection areas.

Appendix B.3 Session C: Management Practices

Q11: How do you characterise the efficiency of the management framework related to the challenges of your sector? (select 1 out of 5 predefined answers).

A11: Most (63%) of the stakeholders characterised the management framework efficiency of the sector they are involved in as moderate, followed by those who believe that the management context is low (25%), high (1%), or very low (1%). The moderate characterisation was found to be the most popular answer among the stakeholders from all the different nexus sectors. This fact reflects the efficiency of the previously implemented management policies in the PRB, which were deemed to have moderate impacts.

Q12: Which pairs of nexus sectors present the strongest interaction? (select maximum 2 out of 6 predefined answers).

A12: Half (50%) of the participants believe that the water–food/agriculture pair present the highest inter-dependency in the PRB, followed by the water–ecosystems/climate (30%), water–energy (7%), energy–ecosystems/climate (7%), food–ecosystems/climate (3%), and energy–food/agriculture (3%) pairs. It should be highlighted that the top three pairs with the strongest interaction in the PRB include the water nexus component, which denotes the importance attributed to the sector by all the different groups of stakeholders.

Q13: To what extent do the existing management practices consider more than one sectors? (select 1 out of 5 predefined answers).

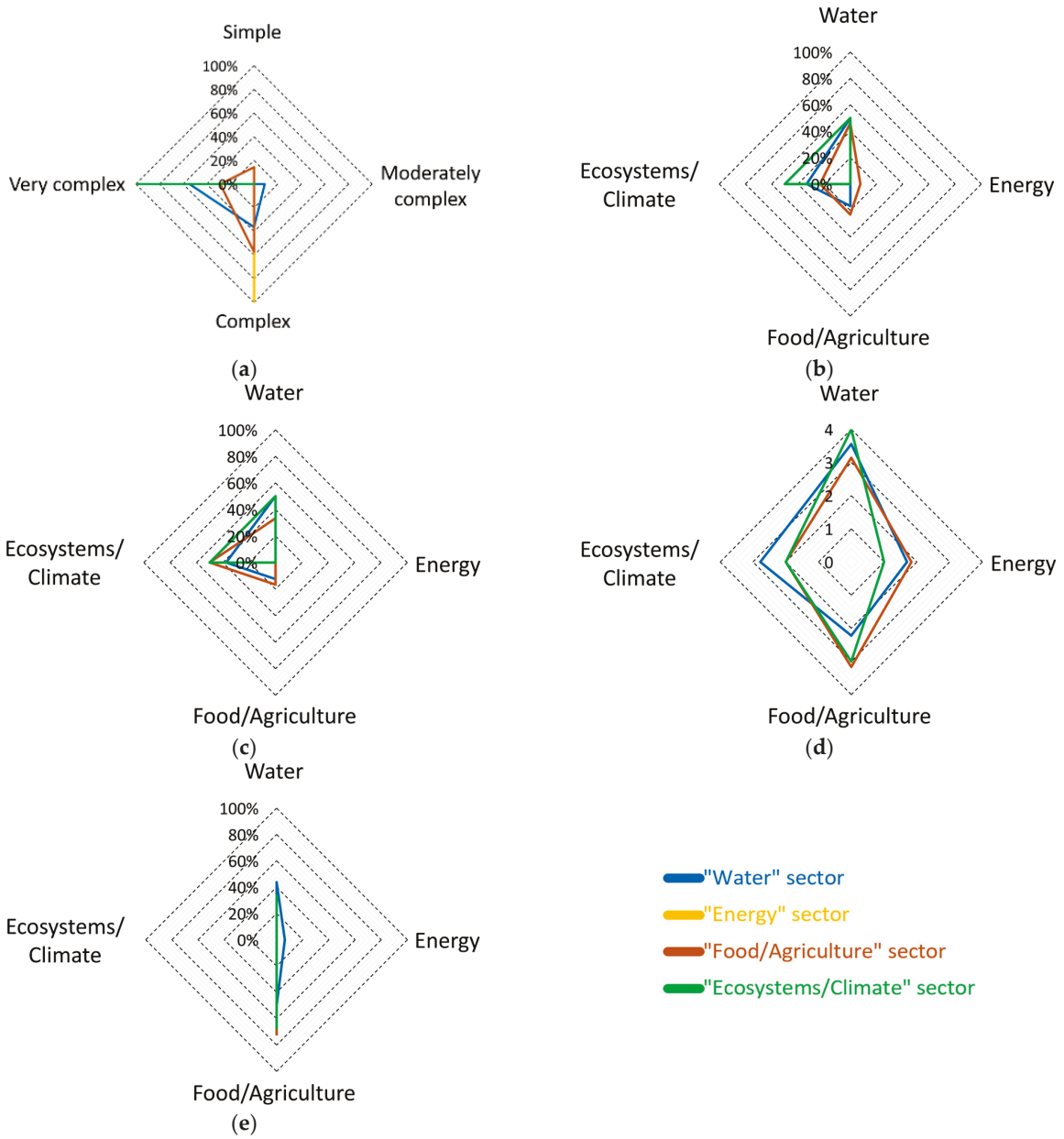

Figure A2. Responses of Pinios River Basin stakeholders to (**a**) Q6, (**b**) Q7, (**c**) Q8, (**d**) Q9, and (**e**) Q10 of the second crowd sourcing theme session.

A13: The vast majority (88%) of the stakeholders believe that the existing practices consider the other nexus sectors in the PRB to a moderate or low degree, followed by those who believe that other sectors are considered to a very low (6%) or high (6%) degree.

Q14: Which is/are the main basis/-es of management practices' selection? (select maximum 2 out of 5 predefined answers).

A14: The influential capacity of some stakeholders was recognised as the major factor affecting the selection of management practices by almost half of the stakeholders (44%), followed by the active stakeholder engagement (22%), non-active stakeholder engagement (15%), acceptance by local society (11%), and scientific evidence and sustainable development (8%), according to the perceptions of the participating stakeholders. The influential capacity of some stakeholders was found to be the most popular answer by the participants across all nexus sectors.

Q15: How is your sector affected or will be affected due to climate change? (select 1 out of 5 predefined answers).

A15: The vast majority (93%) of stakeholders believed their associated sector is already or will be highly or immensely affected by the climate crisis. Only 7% of the stakeholders believed that their sector is or will be moderately affected by climate change, while none of them assumed that climate change will not affect their related sector at all or minimally. It is also worth mentioning that most of the stakeholders related to the water and food/agriculture sectors believed that climate change is already having or expected to have a very high impact on their sectors. This perception is probably influenced by the intense and prolonged drought periods and the extreme precipitation events that recently occurred in the PRB, including the tropical-like cyclone named Ianos, which impacted the wider area in September 2020. The Ianos cyclone was the most intense medicane ever recorded in the Mediterranean region [94], causing casualties, severe floods, extensive infrastructure destruction, and heavy agricultural damage.

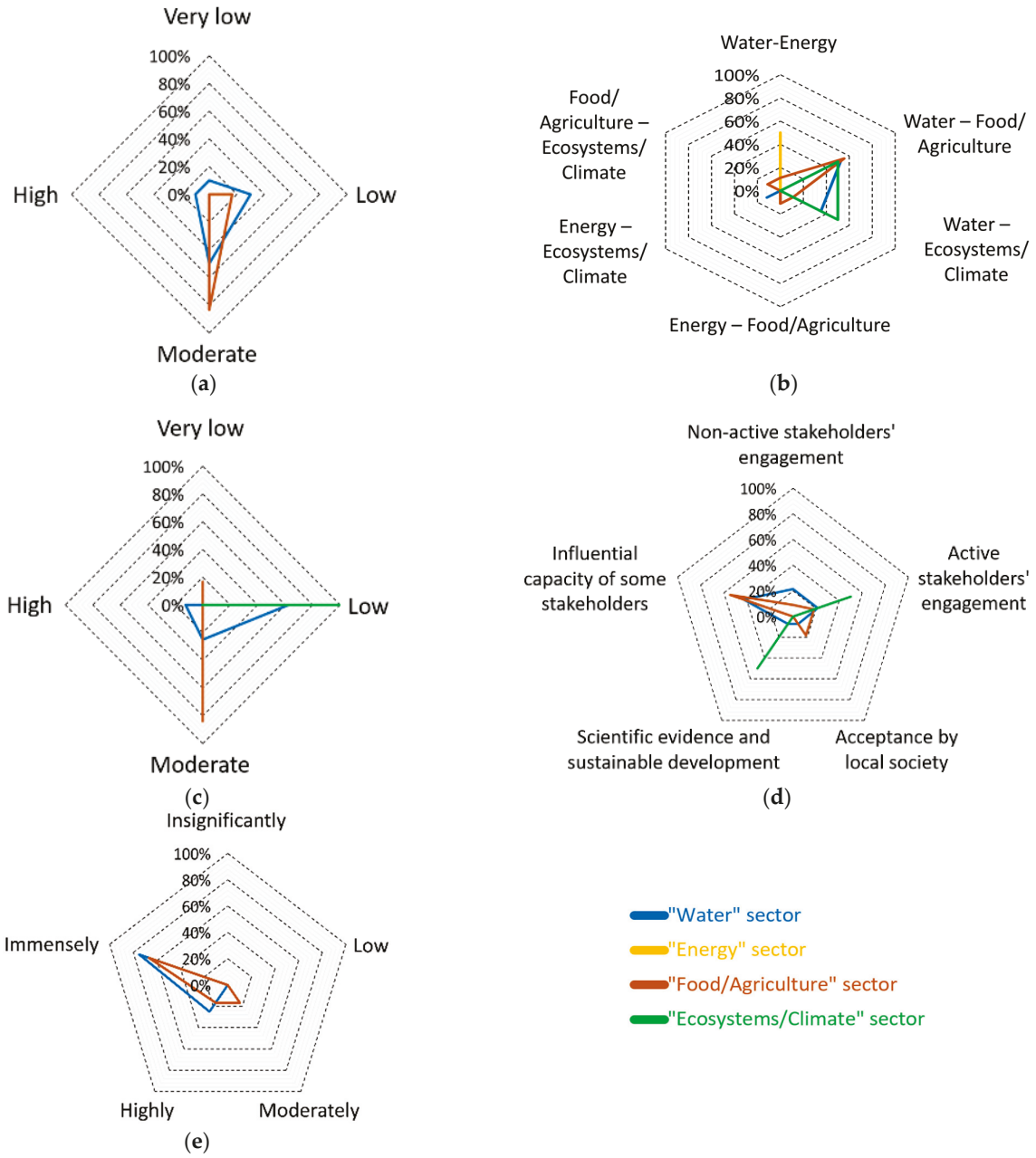

Figure A3. Responses of Pinios River Basin stakeholders to (**a**) Q11, (**b**) Q12, (**c**) Q13, (**d**) Q14, and (**e**) Q15 of the third crowd sourcing theme session.

References

1. Persson, L.; Carney Almroth, B.M.; Collins, C.D.; Cornell, S.; De Wit, C.A.; Diamond, M.L.; Fantke, P.; Hassellöv, M.; Macleod, M.; Ryberg, M.W.; et al. Outside the Safe Operating Space of the Planetary Boundary for Novel Entities. *Environ. Sci. Technol.* **2022**, *56*, 1510–1521. [CrossRef] [PubMed]
2. United Nations (UN) Sustainable Development Goals. Available online: https://www.un.org/sustainabledevelopment/ (accessed on 16 September 2022).
3. Winkler, K.; Fuchs, R.; Rounsevell, M.; Herold, M. Global Land Use Changes Are Four Times Greater than Previously Estimated. *Nat. Commun.* **2021**, *12*, 2501. [CrossRef] [PubMed]
4. World Economic Forum. *Global Risks: An Initiative of the Risk Response Network*; World Economic Forum: Cologny, Switzerland, 2011; ISBN 9295044479.
5. Food and Agriculture Organization of the United Nations (FAO). *The Water-Energy-Food Nexus A New Approach in Support of Food Security and Sustainable Agriculture*; FAO: Rome, Italy, 2014.
6. International Renewable Energy Agency (IRENA). *Renewable Energy in the Water, Energy and Food Nexus*; International Renewable Energy Agency: Abu Dhabi, United Arab Emirates, 2015.
7. Organisation for Economic Co-operation and Development (OECD); Food and Agriculture Organization of the United Nations (FAO). *OECD-FAO Agricultural Outlook 2021–2030*; OECD Publishing: Paris, France, 2021.
8. Pisinaras, V.; Paraskevas, C.; Panagopoulos, A. Investigating the Effects of Agricultural Water Management in a Mediterranean Coastal Aquifer under Current and Projected Climate Conditions. *Water* **2021**, *13*, 108. [CrossRef]
9. Sánchez, J.M.; Simón, L.; González-Piqueras, J.; Montoya, F.; López-Urrea, R. Monitoring Crop Evapotranspiration and Transpiration/Evaporation Partitioning in a Drip-Irrigated Young Almond Orchard Applying a Two-Source Surface Energy Balance Model. *Water* **2021**, *13*, 2073. [CrossRef]
10. Arampatzis, G.; Hatzigiannakis, E.; Pisinaras, V.; Kourgialas, N.; Psarras, G.; Kinigopoulou, V.; Panagopoulos, A.; Koubouris, G. Soil Water Content and Olive Tree Yield Responses to Soil Management, Irrigation, and Precipitation in a Hilly Mediterranean Area. *J. Water Clim. Chang.* **2018**, *9*, 672–678. [CrossRef]
11. Willaarts, B.A.; Lechón, Y.; Mayor, B.; de la Rúa, C.; Garrido, A. Cross-Sectoral Implications of the Implementation of Irrigation Water Use Efficiency Policies in Spain: A Nexus Footprint Approach. *Ecol. Indic.* **2020**, *109*, 105795. [CrossRef]
12. Chitsaz, N.; Azarnivand, A. Water Scarcity Management in Arid Regions Based on an Extended Multiple Criteria Technique. *Water Resour. Manag.* **2017**, *31*, 233–250. [CrossRef]
13. Villada-Canela, M.; Muñoz-Pizza, D.M.; García-Searcy, V.; Camacho-López, R.; Daesslé, L.W.; Mendoza-Espinosa, L. Public Participation for Integrated Groundwater Management: The Case of Maneadero Valley, Baja California, Mexico. *Water* **2021**, *13*, 2326. [CrossRef]
14. Panagopoulos, A.; Arampatzis, G.; Tziritis, E.; Pisinaras, V.; Herrmann, F.; Kunkel, R.; Wendland, F. Assessment of Climate Change Impact in the Hydrological Regime of River Pinios Basin, Central Greece. *Desalin. Water Treat.* **2016**, *57*, 2256–2267. [CrossRef]
15. Osann, A.; Nino, P.; Zajicek, A.; Evangelou, E. Evaluation of Environmental and Economic Sustainability of Different Nutrient Management Strategies. In Proceedings of the 6th Congress on Soil and Water Resources, Izmir, Turkey, 12–14 November 2019.
16. Malamataris, D.; Kolokytha, E.; Loukas, A. Integrated Hydrological Modelling of Surface Water and Groundwater under Climate Change: The Case of the Mygdonia Basin in Greece. *J. Water Clim. Chang.* **2020**, *11*, 1429–1454. [CrossRef]
17. Li, J.; Ma, J.; Yu, L.; Zuo, Q. Analysis and Regulation of the Harmonious Relationship among Water, Energy, and Food in Nine Provinces along the Yellow River. *Water* **2022**, *14*, 1042. [CrossRef]
18. Bazilian, M.; Rogner, H.; Howells, M.; Hermann, S.; Arent, D.; Gielen, D.; Steduto, P.; Mueller, A.; Komor, P.; Tol, R.S.J.; et al. Considering the Energy, Water and Food Nexus: Towards an Integrated Modelling Approach. *Energy Policy* **2011**, *39*, 7896–7906. [CrossRef]
19. United Nations (UN). *Transforming Our World: The 2030 Agenda for Sustainable Development*; United Nations (UN): New York, NY, USA, 2015.
20. Winters, Z.S.; Crisman, T.L.; Dumke, D.T. Sustainability of the Water-Energy-Food Nexus in Caribbean Small Island Developing States. *Water* **2022**, *14*, 322. [CrossRef]
21. Fjäder, C. Developing Partnerships for Building Resilience. In *Handbook of Disaster Risk Reduction for Resilience*; Eslamian, S., Eslamian, F., Eds.; Springer: Cham, Switzerland, 2021; pp. 261–278.
22. Global Commission on Adaptation. Adapt Now: A Global Call for Leadership on Climate Resilience. Available online: https://gca.org/wp-content/uploads/2019/09/GlobalCommission_Report_FINAL.pdf (accessed on 5 September 2022).
23. Jiménez, A.; Saikia, P.; Giné, R.; Avello, P.; Leten, J.; Lymer, B.L.; Schneider, K.; Ward, R. Unpacking Water Governance: A Framework for Practitioners. *Water* **2020**, *12*, 827. [CrossRef]
24. Loukas, A.; Garrote, L. Feature Papers of Water Resources Management, Policy and Governance. *Water* **2022**, *14*, 2191. [CrossRef]
25. Penning, E. Using Nature-Based Solutions to Address Water Security Changes. *Hydrolink* **2022**, *2*, 45–47.
26. Graham, J.; Amos, B.; Plumptre, T. *Principles for Good Governance in the 21st Century. Policy Brief No. 15*; Institute on Governance: Ottawa, ON, Canada, 2003.
27. Blühdorn, I.; Deflorian, M. The Collaborative Management of Sustained Unsustainability: On the Performance of Participatory Forms of Environmental Governance. *Sustainability* **2019**, *11*, 1189. [CrossRef]

28. Villholth, K.G.; Sharma, B.R. Creating Synergy Between Groundwater Research and Management in South and South East Asia. In Proceedings of the IWMI-ITP-NIH International Workshop, Roorkee, India, 8–9 February 2005.
29. Kolokytha, E.; Malamataris, D. Integrated Water Management Approach for Adaptation to Climate Change in Highly Water Stressed Basins. *Water Resour. Manag.* **2020**, *34*, 1173–1197. [CrossRef]
30. Aldaya, M.M.; Sesma-Martín, D.; Schyns, J.F. Advances and Challenges in the Water Footprint Assessment Research Field: Towards a More Integrated Understanding of the Water-Energy-Food-Land Nexus in a Changing Climate. *Water* **2022**, *14*, 1488. [CrossRef]
31. Liu, J.; Bao, Z.; Wang, G.; Zhou, X.; Liu, L. The Spatial and Temporal Assessment of the Water-Land Nexus in a Changing Environment: The Huang-Huai-Hai River Basin (China). *Water* **2022**, *14*, 1905. [CrossRef]
32. Hoff, H. Understanding the Nexus. In Proceedings of the Water, Energy and Food Security Nexus Solutions for the Green Economy, Stockholm, Sweden, 16–18 November 2011.
33. Asian Development Bank. *Thinking about Water Differently: Managing the Water–Food–Energy Nexus*; Asian Development Bank: Metro Manila, Philippines, 2013.
34. Hamidov, A.; Helming, K. Sustainability Considerations in Water–Energy–Food Nexus Research in Irrigated Agriculture. *Sustainability* **2020**, *12*, 6274. [CrossRef]
35. Higgins, C.W.; Najm, M.A. An Organizing Principle for the Water-Energy-Food Nexus. *Sustainability* **2020**, *12*, 8135. [CrossRef]
36. Purwanto, A.; Sušnik, J.; Suryadi, F.X.; de Fraiture, C. Water-Energy-Food Nexus: Critical Review, Practical Applications, and Prospects for Future Research. *Sustainability* **2021**, *13*, 1919. [CrossRef]
37. Taghdisian, A.; Bukkens, S.G.F.; Giampietro, M. A Societal Metabolism Approach to Effectively Analyze the Water-Energy-Food Nexus in an Agricultural Transboundary River Basin. *Sustainability* **2022**, *14*, 9110. [CrossRef]
38. Wang, J.; Ju, K.; Wei, X. Where Will Water-Energy-Food Research Go Next? —*Visualisation Review and Prospect. Sustainability* **2022**, *14*, 7751. [CrossRef]
39. González-Rosell, A.; Blanco, M.; Arfa, I. Integrating Stakeholder Views and System Dynamics to Assess the Water–Energy–Food Nexus in Andalusia. *Water* **2020**, *12*, 3172. [CrossRef]
40. Kurian, M. The Water-Energy-Food Nexus: Trade-Offs, Thresholds and Transdisciplinary Approaches to Sustainable Development. *Environ. Sci. Policy* **2017**, *68*, 97–106. [CrossRef]
41. Liu, J.; Hull, V.; Godfray, H.C.J.; Tilman, D.; Gleick, P.; Hoff, H.; Pahl-Wostl, C.; Xu, Z.; Chung, M.G.; Sun, J.; et al. Nexus Approaches to Global Sustainable Development. *Nat. Sustain.* **2018**, *1*, 466–476. [CrossRef]
42. Albrecht, T.R.; Crootof, A.; Scott, C.A. The Water-Energy-Food Nexus: A Systematic Review of Methods for Nexus Assessment. *Environ. Res. Lett.* **2018**, *13*, 043002. [CrossRef]
43. van Buuren, A.; van Meerkerk, I.; Tortajada, C. Understanding Emergent Participation Practices in Water Governance. *Int. J. Water Resour. Dev.* **2019**, *35*, 367–382. [CrossRef]
44. Goodspeed, R.; Babbitt, C.; Briones, A.L.G.; Pfleiderer, E.; Lizundia, C.; Seifert, C.M. Learning to Manage Common Resources: Stakeholders Playing a Serious Game See Increased Interdependence in Groundwater Basin Management. *Water* **2020**, *12*, 1966. [CrossRef]
45. King, H.; Guehlstorf, N. Assessing the Variances of Citizen Stakeholder Justice in Watershed Governance: Is Action More Effective with Reactive or Proactive Administrations. *Water* **2022**, *14*, 878. [CrossRef]
46. Yuan, M.H.; Lo, S.L. Principles of Food-Energy-Water Nexus Governance. *Renew. Sust. Energ. Rev.* **2022**, *155*, 111937. [CrossRef]
47. Howarth, C.; Monasterolo, I. Understanding Barriers to Decision Making in the UK Energy-Food-Water Nexus: The Added Value of Interdisciplinary Approaches. *Environ. Sci. Policy* **2016**, *61*, 53–60. [CrossRef]
48. Vogler, D.; Macey, S.; Sigouin, A. *Stakeholder Analysis in Environmental and Conservation Planning*; Network of Conservation Educators and Practitioners, Center for Biodiversity and Conservation: New York, NY, USA, 2017; Volume 7, pp. 5–16.
49. Geaves, L.H.; Penning-Rowsell, E.C. Flood Risk Management as a Public or a Private Good, and the Implications for Stakeholder Engagement. *Environ. Sci. Policy* **2016**, *55*, 281–291. [CrossRef]
50. Ferraro, F.; Beunza, D. Creating Common Ground: A Communicative Action Model of Dialogue in Shareholder Engagement. *Organ. Sci.* **2018**, *29*, 1187–1207. [CrossRef]
51. Kapetas, L.; Kazakis, N.; Voudouris, K.; McNicholl, D. Water Allocation and Governance in Multi-Stakeholder Environments: Insight from Axios Delta, Greece. *Sci. Total Environ.* **2019**, *695*, 133831. [CrossRef]
52. Pagano, A.; Pluchinotta, I.; Pengal, P.; Cokan, B.; Giordano, R. Engaging Stakeholders in the Assessment of NBS Effectiveness in Flood Risk Reduction: A Participatory System Dynamics Model for Benefits and Co-Benefits Evaluation. *Sci. Total Environ.* **2019**, *690*, 543–555. [CrossRef]
53. Elster, J. *Deliberative Democracy*; Cambridge University Press: Cambridge, UK, 1998.
54. Bjerregaard, R. Getting Europe's Waters Cleaner: Getting the Citizens Involved. *Water Policy* **1998**, *1*, 73–80. [CrossRef]
55. Giatti, L.L.; Urbinatti, A.M.; De Carvalho, C.M.; Bedran-Martins, A.M.; De Oliveira Santos, I.P.; Honda, S.O.; Fracalanza, A.P.; Jacobi, P.R. Nexus of Exclusion and Challenges for Sustainability and Health in an Urban Periphery in Brazil. *Cad. Saude Publica* **2019**, *35*, 1–12. [CrossRef]
56. Endo, A.; Tsurita, I.; Burnett, K.; Orencio, P.M. A Review of the Current State of Research on the Water, Energy, and Food Nexus. *J. Hydrol. Reg. Stud.* **2017**, *11*, 20–30. [CrossRef]

57. Röckmann, C.; Ulrich, C.; Dreyer, M.; Bell, E.; Borodzicz, E.; Haapasaari, P.; Hauge, K.H.; Howell, D.; Mäntyniemi, S.; Miller, D.; et al. The Added Value of Participatory Modelling in Fisheries Management—What Has Been Learnt? *Mar. Policy* **2012**, *36*, 1072–1085. [CrossRef]
58. Howarth, C.; Monasterolo, I. Opportunities for Knowledge Co-Production across the Energy-Food-Water Nexus: Making Interdisciplinary Approaches Work for Better Climate Decision Making. *Environ. Sci. Policy* **2017**, *75*, 103–110. [CrossRef]
59. Johnson, O.W.; Karlberg, L. Co-Exploring the Water-Energy-Food Nexus: Facilitating Dialogue through Participatory Scenario Building. *Front. Environ. Sci.* **2017**, *5*, 24. [CrossRef]
60. Hoolohan, C.; Larkin, A.; McLachlan, C.; Falconer, R.; Soutar, I.; Suckling, J.; Varga, L.; Haltas, I.; Druckman, A.; Lumbroso, D.; et al. Engaging Stakeholders in Research to Address Water–Energy–Food (WEF) Nexus Challenges. *Sustain. Sci.* **2018**, *13*, 1415–1426. [CrossRef] [PubMed]
61. Bréthaut, C.; Gallagher, L.; Dalton, J.; Allouche, J. Power Dynamics and Integration in the Water-Energy-Food Nexus: Learning Lessons for Transdisciplinary Research in Cambodia. *Environ. Sci. Policy* **2019**, *94*, 153–162. [CrossRef]
62. Kropf, B.; Schmid, E.; Mitter, H. Multi-Step Cognitive Mapping of Perceived Nexus Relationships in the Seewinkel Region in Austria. *Environ. Sci. Policy* **2021**, *124*, 604–615. [CrossRef]
63. Karutz, R.; Omann, I.; Gorelick, S.M.; Klassert, C.J.A.; Zozmann, H.; Zhu, Y.; Kabisch, S.; Kindler, A.; Figueroa, A.J.; Wang, A.; et al. Capturing Stakeholders' Challenges of the Food–Water–Energy Nexus—A Participatory Approach for Pune and the Bhima Basin, India. *Sustainability* **2022**, *14*, 5323. [CrossRef]
64. Vinca, A.; Parkinson, S.; Riahi, K.; Byers, E.; Siddiqi, A.; Muhammad, A.; Ilyas, A.; Yogeswaran, N.; Willaarts, B.; Magnuszewski, P.; et al. Transboundary Cooperation a Potential Route to Sustainable Development in the Indus Basin. *Nat. Sustain.* **2021**, *4*, 331–339. [CrossRef]
65. de Vito, R.; Pagano, A.; Portoghese, I.; Giordano, R.; Vurro, M.; Fratino, U. Integrated Approach for Supporting Sustainable Water Resources Management of Irrigation Based on the WEFN Framework. *Water Resour. Manag.* **2019**, *33*, 1281–1295. [CrossRef]
66. Cansino-Loeza, B.; Ponce-Ortega, J.M. Sustainable Assessment of Water-Energy-Food Nexus at Regional Level through a Multi-Stakeholder Optimization Approach. *J. Clean. Prod.* **2021**, *290*, 125194. [CrossRef]
67. Pisinaras, V.; Panagopoulos, A.; Herrmann, F.; Bogena, H.R.; Doulgeris, C.; Ilias, A.; Tziritis, E.; Wendland, F. Hydrologic and Geochemical Research at Pinios Hydrologic Observatory: Initial Results. *Vadose Zone J.* **2018**, *17*, 180102. [CrossRef]
68. Pisinaras, V.; Herrmann, F.; Panagopoulos, A.; Tziritis, E.; McNamara, I.; Wendland, F. Fully Distributed Water Balance Modelling in Large Agricultural Areas—The Pinios River Basin (Greece) Case Study. *Sustainability* **2023**, *15*, 4343. [CrossRef]
69. Arampatzis, G.; Panagopoulos, A.; Pisinaras, V.; Tziritis, E.; Wendland, F. Identifying Potential Effects of Climate Change on the Development of Water Resources in Pinios River Basin, Central Greece. *Appl. Water Sci.* **2018**, *8*, 51. [CrossRef]
70. Vasiliades, L.; Loukas, A.; Liberis, N. A Water Balance Derived Drought Index for Pinios River Basin, Greece. *Water Resour. Manag.* **2011**, *25*, 1087–1101. [CrossRef]
71. Panagopoulos, A.; Herrmann, F.; Pisinaras, V.; Wendland, F. Impact of Climate Change on Irrigation Need and Groundwater Resources in Pinios Basin. *Proceedings* **2018**, *2*, 659. [CrossRef]
72. Sidiropoulos, P.; Mylopoulos, N.; Vasiliades, L.; Loukas, A. Stochastic Nitrate Simulation under Hydraulic Conductivity Uncertainty of an Agricultural Basin Aquifer at Eastern Thessaly, Greece. *Environ. Sci. Pollut. Res.* **2021**, *28*, 65700–65715. [CrossRef]
73. Sidiropoulos, P.; Tziatzios, G.; Vasiliades, L.; Mylopoulos, N.; Loukas, A. Groundwater Nitrate Contamination Integrated Modeling for Climate and Water Resources Scenarios: The Case of Lake Karla over-Exploited Aquifer. *Water* **2019**, *11*, 1201. [CrossRef]
74. Vrouhakis, I. Hydrogeological Research Using Modern Management Tools in the Framework of Qualitative and Quantitative Monitoring of the Groundwater System of Tirnavos Sub-Basin (Thessaly). Ph.D. Thesis, Agricultural University of Athens, Athens, Greece, 2022.
75. Tziatzios, G.; Sidiropoulos, P.; Vasiliades, L.; Lyra, A.; Mylopoulos, N.; Loukas, A. The Use of the Pilot Points Method on Groundwater Modelling for a Degraded Aquifer with Limited Field Data: The Case of Lake Karla Aquifer. *Water Supply* **2021**, *21*, 2633–2645. [CrossRef]
76. Hellenic Regulatory Authority for Energy. Geospatial Map for Energy Units & Requests. Available online: https://geo.rae.gr/ (accessed on 10 September 2022).
77. Loukas, A. Surface Water Quantity and Quality Assessment in Pinios River, Thessaly, Greece. *Desalination* **2010**, *250*, 266–273. [CrossRef]
78. Hatzigiannakis, E.; Filintas, A.; Ilias, A.; Panagopoulos, A.; Arampatzis, G.; Hatzispiroglou, I. Hydrological and Rating Curve Modelling of Pinios River Water Flows in Central Greece, for Environmental and Agricultural Water Resources Management. *Desalin. Water Treat.* **2015**, *57*, 11639–11659. [CrossRef]
79. Mendelow, A. Stakeholder Mapping. In Proceedings of the 2nd International Conference on Information Systems, Cambridge, MA, USA, 16–18 December 1991.
80. Winter, S. Organizational Perspective on Leadership Strategies for the Success of Cross-Disciplinary Science Teams. In *Strategies for Team Science Success. Handbook of Evidence-Based Principles for Cross-Disciplinary Science and Practical Lessons Learned from Health Researchers*; Hall, K.L., Vogel, A.L., Croyle, R.T., Eds.; Springer Nature: Cham, Switzerland, 2019; pp. 329–345.

81. Hermann-Friede, J.; Kropac, M.; Achermann, S.; Heeb, J.; Feuerstein, L.; Integrity Management Toolbox for Water Service Providers. Manual for Facilitators. Available online: https://sswm.info/sites/default/files/reference_attachments/WSP-Toolbox-Manual_WEB2.pdf (accessed on 25 August 2022).
82. Anon Global Water Partnership. GWP Integrated Water Resources Management Toolbox. Available online: https://www.gwp.org/en/learn/iwrm-toolbox/About_IWRM_ToolBox (accessed on 11 October 2023).
83. OECD. *Implementing the OECD Principles on Water Governance: Indicator Framework and Evolving Practices*; OECD Publishing: Paris, France, 2018.
84. Stein, U.; Bueb, B.; Knieper, C.; Tröltzsch, J.; Vidaurre, R.; Favero, F. The Diagnostic Water Governance Tool–Supporting Cross-Sectoral Cooperation and Coordination in Water Resources Management. *Environ. Sci. Policy* **2023**, *140*, 111–121. [CrossRef]
85. OECD. OECD Principles on Water Governance. Available online: www.oecd.org/governance/oecd-principles-on-water-governance.htm (accessed on 5 October 2023).
86. Bathrellos, G.D.; Skilodimou, H.D.; Soukis, K.; Koskeridou, E. Temporal and Spatial Analysis of Flood Occurrences in the Drainage Basin of Pinios River (Thessaly, Central Greece). *Land* **2018**, *7*, 106. [CrossRef]
87. Kim, R.E. The Nexus between International Law and the Sustainable Development Goals. *Rev. Eur. Comp. Int. Environ. Law.* **2016**, *25*, 15–26. [CrossRef]
88. European Parliament and Council. *Directive 2000/60/EC on Establishing a Framework for Community Action in the Field of Water Policy*; European Parliament and Council: Strasbourg, France, 2000; pp. L 327/1–L 327/72.
89. European Commission. *REPowerEU Plan: Communication from the Commission to the European Parliament, the European Council, the Council, the European Economic and Social Committee and the Committee of the Regions*; COM(2022) 230 Final; European Commission: Brussels, Belgium, 2022.
90. European Commission. The New Common Agricultural Policy: 2023–2027. Available online: https://agriculture.ec.europa.eu/common-agricultural-policy/cap-overview/cap-2023-27_en (accessed on 22 May 2023).
91. European Commission Climate Action. Available online: https://climate.ec.europa.eu/index_en (accessed on 11 June 2023).
92. Seddon, N.; Chausson, A.; Berry, P.; Girardin, C.A.J.; Smith, A.; Turner, B. Understanding the Value and Limits of Nature-Based Solutions to Climate Change and Other Global Challenges. *Philos. Trans. R. Soc. B Biol. Sci.* **2020**, *375*, 20190120. [CrossRef]
93. IPCC. *Climate Change and Land: An IPCC Special Report on Climate Change, Desertification, Land Degradation, Sustainable Land Management, Food Security, and Greenhouse Gas Fluxes in Terrestrial Ecosystems*; Shukla, P.R., Skea, J., Calvo Buendia, E., Masson-Delmotte, V., Portner, H.O., Roberts, D.C., Zhai, P., Slade, R., Connors, S., van Diemen, R., et al., Eds.; IPCC: Geneva, Switzerland, 2019.
94. Lagouvardos, K.; Karagiannidis, A.; Dafis, S.; Kalimeris, A.; Kotroni, V. Ianos—A Hurricane in the Mediterranean. *Bull. Am. Meteorol. Soc.* **2021**, *103*, E1621–E1636. [CrossRef]

Disclaimer/Publisher's Note: The statements, opinions and data contained in all publications are solely those of the individual author(s) and contributor(s) and not of MDPI and/or the editor(s). MDPI and/or the editor(s) disclaim responsibility for any injury to people or property resulting from any ideas, methods, instructions or products referred to in the content.

water

MDPI

Article

Hydrogeological Hazards in Open Pit Coal Mines–Investigating Triggering Mechanisms by Validating the European Ground Motion Service Product with Ground Truth Data

Ploutarchos Tzampoglou [1,2,*] and Constantinos Loupasakis [1]

[1] Laboratory of Engineering Geology and Hydrogeology, Department of Geological Sciences, School of Mining and Metallurgical Engineering, National Technical University of Athens, 15780 Athens, Greece; cloupasakis@metal.ntua.gr
[2] Department of Civil & Environmental Engineering, University of Cyprus, Nicosia 1678, Cyprus
* Correspondence: tzampoglou.ploutarchos@ucy.ac.cy

Abstract: This research focuses on the investigation of hydrogeological hazards in open pit coal mines. The study area is the Amyntaio sub-basin area, located in West Macedonia prefecture, Greece. A major part of the SE of this area is occupied by the Amyntaio open pit coal mine. In recent decades, the Amyntaio basin's aquifer has been overexploited both by dewatering wells of the open pit coal mine and irrigation wells, triggering extensive land subsidence in an area that extends 3 km around the mine. Additionally, one of the biggest mining landslides worldwide occurred on the South-West slopes of the open pit on 10 June 2017. The current study investigates the land subsidence phenomenon and the landslide, highlighting the influence and the interaction of their causal factors which were strongly affected by the groundwater management. To estimate ground surface movement, Earth Observation data from the European Ground Motion Service, of the Copernicus European Union's Earth observation program, were used for the period 1 January 2016–31 December 2020. The geologic, geotechnical and hydrogeologic data coming from the extensive ground truth survey have been incorporated with the Earth Observation data, highlighting the opposing mechanisms of the interacting geohazards.

Keywords: mining landslide; land subsidence; amyntaio basin; mining geohazards; ground water management; Copernicus; land monitoring

1. Introduction

Anthropogenic activities, such as mining, significantly affect the natural environment [1], causing various types of hazards. The most common geohazards are land subsidence and landslides; these catastrophic events can occur during mining as well as in the post-mining period (in cases where appropriate mitigation measures are not taken) and can be triggered by a range of hydrologic, geologic, and tectonic factors. Specifically, 132 different cases of slope failures have been documented worldwide since 1960 [2], causing hundreds of deaths and massive economic damage. Key examples include the Bingham Canyon Mine landslide in Utah, USA, in which two landslides displaced around 145 million tons of geomaterial on 10 Arpil 2013 [3–6], and the Jade Mine landslide in the northern state of Kachin, Myanmar, in which over 170 people were killed [7]. In contrast, land subsidence slowly affects extensive areas around mines, causing mainly significant economic damage [8–12].

To date, many studies have been conducted to investigate the failure mechanisms triggering natural hazards such as landslides [13], land subsidence [14,15], floods [16,17], and seasonal ground movement due to swelling formations [18] using state of the art Earth Observation technologies. The use of Synthetic Aperture Radar Interferometry satellite data (InSAR) combined with the geotechnical research helps to obtain new insights into

the failure mechanisms of the geohazards. Furthermore, it can contribute significantly to estimating the main causal factors that play an active role in the occurrence of the geohazard. Thus, it can give the opportunity to take all the necessary measures for the mitigation of the catastrophic events.

The study area in this work is the Amyntaio sub-basin, which is located in the West Macedonia prefecture of Greece. A major part of the southeast of this area is occupied by the Amyntaio open pit coal mine. A 220 m deep coal mine that operated between 1989 and 2020, with 179 million tons of lignite production and 1595 million m^3 of total excavations.

There are four lakes and ten villages within the Amyntaio basin, and the basin's agricultural area exceeds 200 km^2. In recent decades, an extensive groundwater level drop has been recorded due to the overpumping of the aquifer, both for protecting the open pit coal mine's slopes (i.e., draining wells) and providing for the irrigation needs of the area's agricultural activity. Specifically, the groundwater level drawdown between May 1992 and May 2015 reaches 70 m near the mine, extending northwest to the village of Valtonera and west to Anargiroi village [19–23]. The drop in the groundwater level, combined with the area's general geotectonic setting, triggered extensive land subsidence in an area extending up to 2 km around the mine, causing damage to villages and infrastructure since 2002. Additionally, one of the world's largest mining landslides took place on the South-West slopes of the open pit mine on 10 June 2017. Based on previous studies, the landslide mass involved in this event was 80 million m^3 [24]. A timely prediction of this event allowed precautionary measures (such as stopping work inside the mine) to be taken and, therefore, loss of human life was avoided.

Aiming to further study the mechanisms of the catastrophic events that took place at the perimeter of the Amyntaio open pit coal mine, this study employs InSAR data from the European Ground Motion Service (EGMS) product covering the period 2016–2021. The EGMS provides reliable information regarding natural and anthropogenic ground motion over the Copernicus Participating States and across national borders, with millimeter accuracy [25–29].

The motivation of this study is to combine the ground truth datasets acquired for the study of the mining geohazards, namely land subsidence and landslide, with the EGMS InSAR data set, aiming to cross-verify their outcomes. The main objectives of the study are to (a) estimate the spatial distribution of the vertical deformation due to land subsidence and landslide by evaluating the EGMS InSAR datasets; (b) correlate the above data with the data obtain thought the geotechnical research highlighting opposite driving failures mechanisms and main causal factors and (c) estimate the interaction between these two catastrophic events.

The comparison of the ground truth survey data (that have been acquired for more than 15 years since 2005) with the INSAR datasets, provides an excellent case study to demonstrate the reliability and value of the EGMS product. The understanding of the failure mechanism of land subsidence and landslide as well the estimation of their interaction can help local and regional authorities to understand the arising risks. This knowledge will enable them to take appropriate mitigation measures to ensure the future safe landplaning development.

2. Study Area

2.1. Geologic, and Geotechnical Setting

The study area forms part of the Kozani–Amyntaio–Ptolemaida–Florina basin and belongs to the Pelagonian geotectonic zone. The area consists of a Paleozoic and Mesozoic crystalline schist bedrock covered by Neogene and Quaternary deposits. Based on previous geotechnical studies [23,30–32], some useful insights can be gained relating to the geotechnical behavior of the formations developed in the study area. In detail, the study area's geological formations are as follows (Figure 1).

Recent alluvial deposits: including lacustrine and peat deposits. They obtain high to extremely high compressibility index (Cc) values of up to 0.187 and 1.707, respectively.

Despite their high compressibility index, these units occur superficially and, therefore, are unlikely to be significantly affected by changes in groundwater levels; thus, they likely do not play a major role in driving land subsidence due to overexploitation of the aquifer. However, these units exhibit land subsidence driven by oxidation as a result of their high organic content levels.

Anargiroi Formation: Quaternary formation comprising of silty–clayey sands and red clays with coarse-grained intercalations. This unit has high strength values, consistent with its soil grain distribution; its Cc value, which reaches 0.133 for the clay intercalations, is likely due to the presence of small amounts of swelling clay minerals. This formation occurs in hilly areas of the study region's lowlands, at heights above the aquifers' phreatic head. Thus, it is not directly affected by groundwater head variations and does not contribute to or interact with land subsidence phenomena.

Perdikas formation: Quaternary formation divided into sandy silty clay (65–75%), organic silty clay (10–20%), and coarse-grained (10–20%) layers with some organic silty–clayey intercalations in the upper part. This unit mainly occurs under the recent deposits across the majority of the basin. In terms of its geotechnical data, the Perdikas formation shows high Cc values due to the significant montmorillonite content, which reach 0.16 for the silty–clayey sand, 0.27 for the sandy silty clay, and 0.99 for the organic silty clay horizons. Therefore, this formation, as a result of its composition (around 65–75% clayey horizons) and its geotechnical setting, is prone to vertical deformation in areas where fluctuation of the aquifer occurs.

Proastio Formation: lower Quaternary formation consisting of sandy coarse-grained horizons with red silty–clayey sands, clays, and organic layers [33]. It can be separated into two distinct parts; the upper part consists of more than 80% coarse-grained material and the lower part contains over 30% silty clay layers. The average Cc values are 0.16 for the silty–clayey sands, 0.18 for the organic layers, and 0.16 for the sandy silty clay layers. Due to the minor contribution of the fine-grained layers in the stratigraphy of the Proastio formation, their impact on the overall land subsidence is considered insignificant.

The Neogene formations underlie the Proastio formation. They are separated into two series: (a) the lignite-bearing Ptolemaida formation (Amyntaio and Ptolemaida lignite deposits), which consists mainly of gray silty clays and clayey marls [34,35], and (b) the lignite-bearing Komnina formation (Vegora and Komnina lignite deposits), which consists of sand and clay layers with intercalations of xylite [35] and sandstones. These formations are over-consolidated and impermeable, occurring beneath the base of the aquifer. Thus, they are not considered prone to consolidation, even if the active stresses change. However, it should be stressed that throughout this formation, bedding-parallel shear zones with reduced shear strength values occur [36]. These zones are highly likely to contribute to the formation of failure planes along the working slopes. Therefore, although this formation is not susceptible to land subsidence, it is susceptible to landslide failures.

Alpine–pre-Alpine formations: these formations are divided into: (a) Paleozoic metamorphic rocks (gneiss and schists) and (b) Triassic–Lower Jurassic carbonate rocks (crystalline limestones and marbles) [37,38]. They mainly occur in the west of the basin.

The faults in the Amyntaio sub-basin can be separated into two groups [39–42]. The first, trending NW–SE, affects only the Alpine–pre-Alpine formations, and the second, trending NE–SW, extends up to the Quaternary deposits. Three active tectonic structures with NE-SW directions [43] occur in the Amyntaio basin (Figure 1): (a) the Petron–Xino Nero–Aetos fault (Fpxa) in the northwest; (b) the Anargiroi fault (Fang) in the south, and (c) the Vegoritida fault (Fveg) on the east to northeast side of the basin.

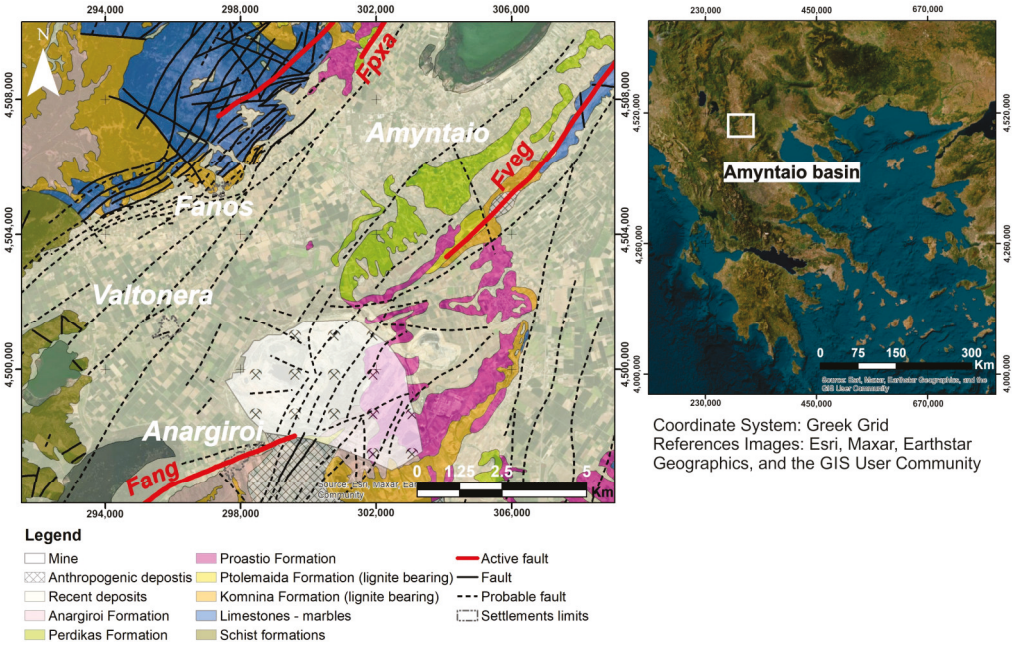

Figure 1. Geological map of the Amyntaio basin. The three active tectonic lines identified in the Amyntaio basin are clearly indicated.

2.2. Hydrogeologic Setting

Two aquifer systems can be identified in the Amyntaio sub-basin. The first one constitutes a karstic aquifer system within the Alpine–pre-Alpine bedrock formations, while the second one is developed in the Quaternary formations.

The piezometric head of the karstic aquifer system exceeds 100 m above the open pit bottom floor. Given that high piezometric loads were transferred on the slopes of the open pit mine in addition to the existence of bedding-parallel shear zones, negative slope stability conditions are expected [24]. Note that this aquifer does not affect the land subsidence phenomenon as it is not subjected to any kind of exploitation along its entire plane due to its depth, considering that it is completely isolated underneath the Neogene formations. The shallow semiconfined aquifer is recharged by both karstic water overflow, along the boundaries of the basin, and by filtration of surface water; its total depth does not exceed 120 m [44].

During recent decades, a significant level drop in this aquifer has been identified as a result of systematic overpumping both for protecting the open pit coal mine's slopes (i.e., draining wells) and providing for the irrigation needs of the area's agricultural activity. Considering the results of extensive field investigation measurement campaigns [20,45,46], some key conclusions concerning changes in the piezometric level are as follows (Figure 2A–E): according to the results of groundwater level measurements that were carried out at the end of the dry season (October 2014 and October 2015), the groundwater flow appears to occur toward the open pit mine, forming an extensive depression cone (Figure 2B,D). In addition, local dynamic depression cones of minor importance were observed in areas of agricultural activity. A similar groundwater flow trend was identified in data that were obtained from water level measurement campaigns during May 2015 and May 2016 (i.e., the end of the wet period). Therefore, currently the open pit along with the surrounding draining wells operate as an oversized (4 km wide) well, continuously draining a big part of the Amyntaio basin.

The evolution of the groundwater flow over time can be easily estimated by comparing equal-drawdown contour lines between May 1992–May 2015 [23] and May 1992–May 2016 [47]. Note that the data from May 1992 relate to the period before the operation of the open pit coal mine [48]. As shown in Figure 3A,B, the drawdown reaches 70 m near the working slopes of the mine and decreases with increasing distance away from the mine.

The depression cone extends to the west reaching to the villages of Valtonera and Anargiroi. On the contrary, as indicated in Figure 2A, before the operation of the mine, only a gentle groundwater flow from the west towards the east of the basin can be identified. It is clear that during the last three decades the operation of the mine and, secondarily, the increase of the agricultural activities radically changed the groundwater dynamics of the basin.

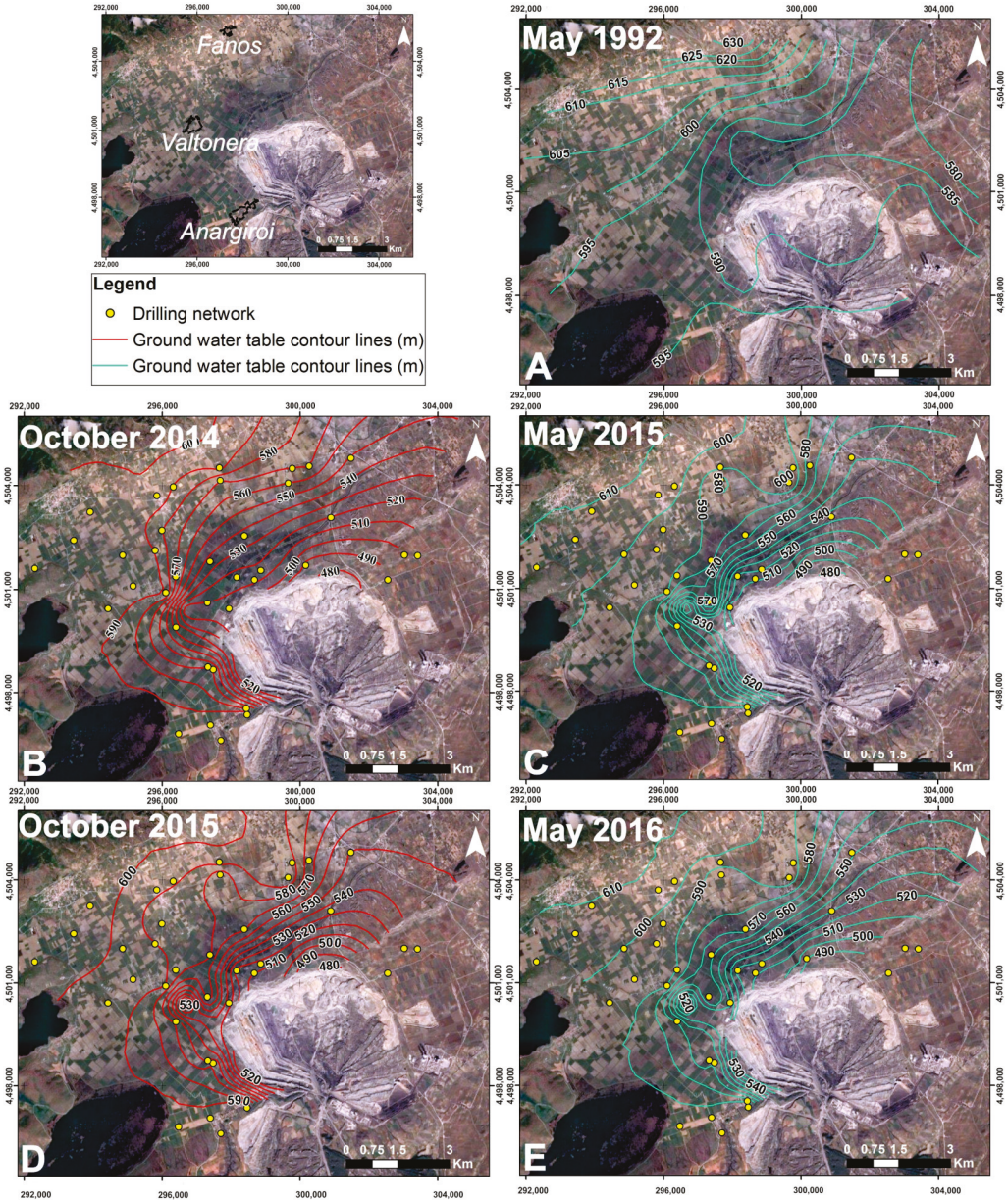

Figure 2. Ground water table contour lines based on the measurements carried out on: (**A**) May 1992 [48], (**B**) October 2014; (**C**) May 2015, (**D**) October 2016, and (**E**) May 2016.

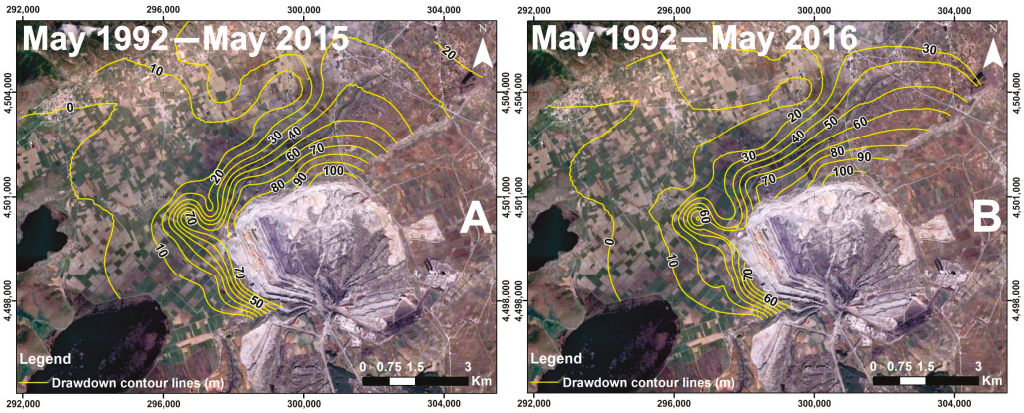

Figure 3. Equal drawdown contour lines between: (**A**) May 1992–May 2015 and (**B**) May 1992–May 2016.

3. Methodology for the Determination of the Catastrophic Events Driving Mechanism

Initially, all geological [34], tectonic [28,34,35,37,43], geotechnical [32] and hydrogeological [42] data, from previous studies, were collected and reevaluated during the 15 years long study, conducted by the authors of the current paper. New data sets have been added to the existing knowledge, including: (a) engineering geological mapping of the study area, (b) geotechnical laboratory tests' results from over 60 samples; (b) four ground water level measurements' campaigns (October 2014, May 2015, October 2015, May 2016) on a newly established network of over 40 wells and (c) detailed surface rapture mapping and infrastructure damage recording. All data sources taken into account are presented in the Supplementary Material (Table S1).

Aiming to validate the ground truth datasets as well as to identify the spatial distribution of deformation occurring in the villages surrounding the mine, data from the EGMS product were cross-validated with the above-described ground truth data sets. The EGMS is based on the multi-temporal interferometric analysis of Sentinel-1 radar images at full resolution. This technique allows for identifying reliable measurement points for which ground motion velocity values and time series of deformation are extracted [47]. The EGMS Ortho product provides purely vertical and purely east-west displacements over time with 100 m × 100 m output resolution cells. The data available for the studied site range from 5 January 2016 to 31 December 2021 [26], which includes the period of the landslide event that occurred on 10 June 2017.

The cross-validation of the Earth Observation data with the ground truth data sets provided a clear view on the driving mechanism of the land subsidence and landslide phenomena, highlighting their opposing triggering factors.

3.1. The Land Subsidence Mechanism

In 2001, Anargiroi village was affected by land subsidence. Until 2006, vertical deformation was recorded across the entire study area. To investigate the spatial distribution of surface ruptures in the Amyntaio basin, observations from previous studies were initially compiled [23,49–52]. Then, six field work campaigns were carried out, in which 15.5 km of surface ruptures were recorded (Figure 4). Most of these ruptures are oriented NW–SE and NE–SW, following the trends of the area's main fault lines. Thus, the tectonic faults acted as a pre-existing structural fabric that has controlled the orientation of later ruptures.

Three villages have been significantly affected by surface deformation (Anargiroi (Figure S1), Valtonera (Figure S2), and Fanos (Figure S3)) [23]. All these settlements share some common characteristics, namely (a) they are located in areas affected by groundwater level drawdown, (b) they are crossed by faults, and (c) they are underlain by the Perdikas formation.

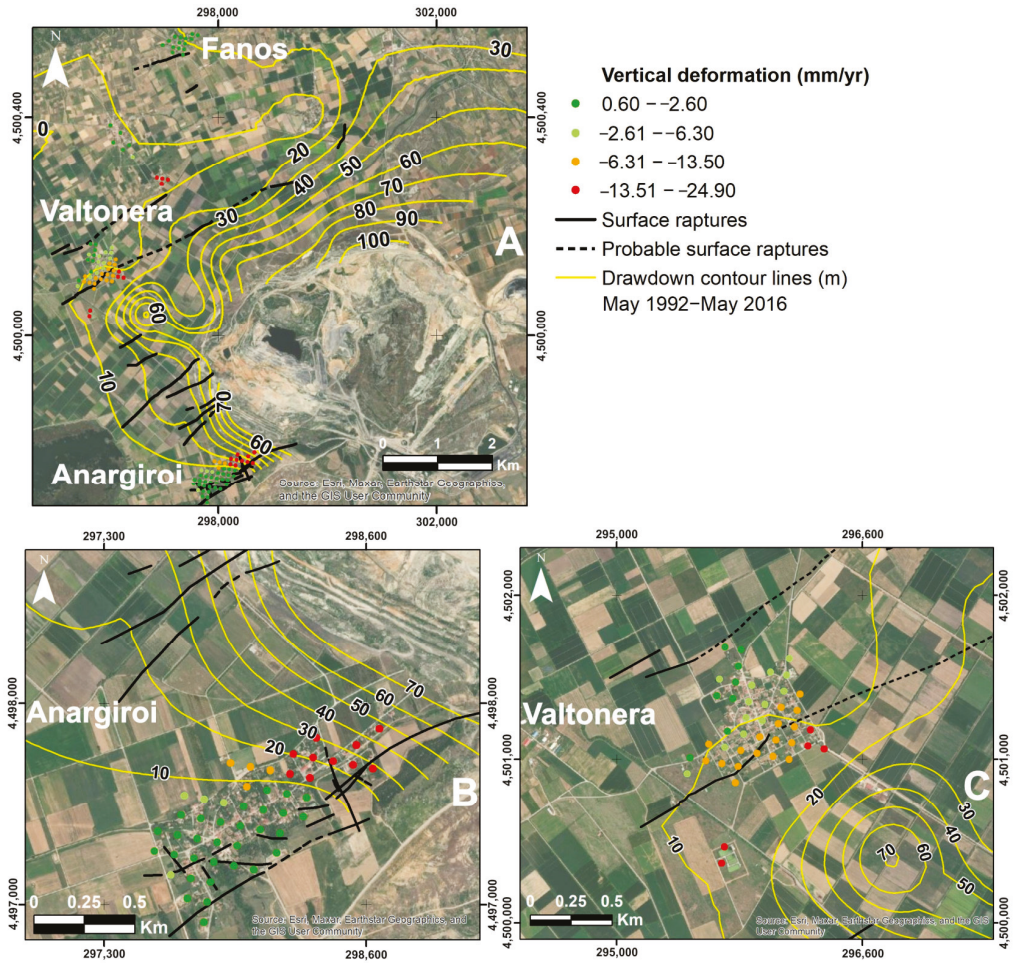

Figure 4. (**A**) Vertical deformations (mm/year) between 5 January 2016 and 31 December 2020 according to the InSAR data provided by Copernicus Land Monitoring Service [26] along with the recorded surfaces ruptures and the drawdown contour lines. (**B**,**C**) scale up view of the Anargiroi and Valtonera villages.

The vertical displacements of the surface ruptures appear to be proportional to the groundwater table drop and the distance from the mine. Specifically, the largest offsets (0.5 m to 1 m) are observed in areas near the mine where the groundwater withdrawal reaches 70 m. The differential displacements decrease with increasing distance from the mine and do not occur in areas where no water table level drop is recorded.

The correlation of the persistent scatterer (PS) point data obtained from the EGMS datasets (for the period between 5 January 2016 and 31 December 2020) with the recorded surface ruptures and drawdown contour lines for the period between May 1992 and May 2016 can be shown in Figure 4. Although the datasets do not refer to the exact same period, their correlation is applicable as the general hydrogeological conditions remain practically unchanged since 1992. The open pit keeps on operating as the main draining source while no extra irrigation wells have been drilled at the wider area. Evaluating the EGMS datasets, it is clear that the largest vertical displacement amplitudes, exceeding −20 mm/year, are observed to the northwest of Anargiroi village; the vertical deformation then decreases southeast of the village. This observation correlates closely with the recorded surface ruptures and drawdown contour lines, highlighting that land subsidence is still occurring in the study area.

Similar conclusions can be drawn from the PS points at Valtonera village. The observed water level drop in this area of around 10 to 20 m can trigger high-amplitude vertical displacements.

3.2. The Landslide Mechanism

On 10 June 2017, the largest recorded Greek mining landslide took place on the mining slopes of the Amyntaio open pit coal mine (Figure 5). According to estimates, the collapse mass reached 80 million m^3, extending over an area of 2 km in width and 2.2 km in length, while the foot of the landslide coincided with the lower point of the open pit mine at a depth of 210 m.

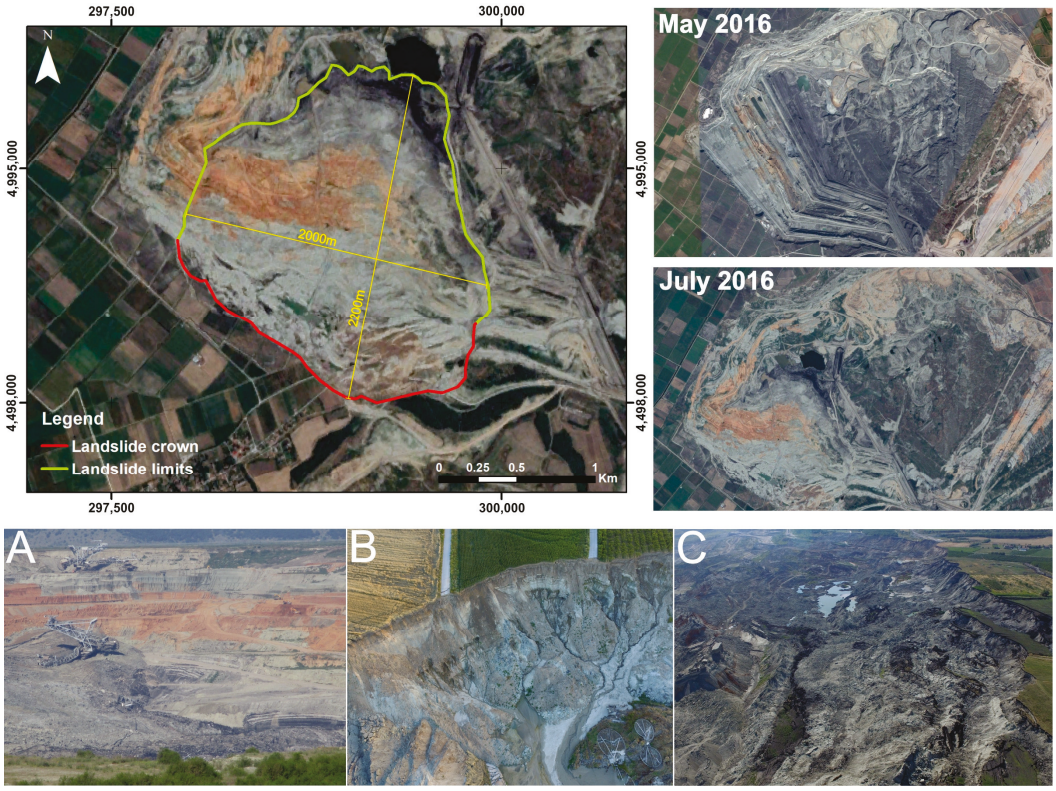

Figure 5. The spatial extent of the 10 June 2017 landslide at the Amyntaio mine, as shown by satellite imagery. Images obtained by Google Earth. (**A**–**C**) show oblique views of the landslide area. (**A**) one of the bucket wheel excavators buried inside the sliding mass; (**B**) panoramic view of the landslide scarp in front of the Anargyroi village; and (**C**) panoramic view of the landslide head looking towards East West.

The first signs of this failure were recorded some months before it occurred. In detail, eight months before the failure (November 2016), archaeological excavations, which were being carried out on the plain above the northwest side of the mine, were interrupted due to the occurrence of rapidly formed surface raptures caused by the increasing vertical deformation. In addition, five months before the failure (February 2017), deformation along the surface ruptures in the wider area of Anargiroi village began to increase. The timely recognition and prediction of the phenomenon allowed the evacuation of the open pit coal mine eight days before the failure, which contributed to avoiding the loss of lives.

Furthermore, the financial impacts of this landslide, which affected infrastructure both inside the mine and in the nearby area, were extremely large. Specifically, four bucket wheel excavators (weighing 500 to 1500 tons each), many small excavators, and several kilometers of conveyor were significantly damaged or buried inside the mine (Figure 5A). Additionally, 25 million tons of lignite were buried under the sliding mass, leading to further losses. Outside the open pit coal mine, the landslide caused enormous damage to the village of Anargiroi (Figure S4). In particular, the northwest part of Anargiroi village was severely damaged and permanently evacuated, the wastewater treatment plant collapsed into the pit (Figure 5B,C), and hundreds of meters of road network and

electricity and water supply infrastructure were destroyed (Figure 6A–E). Furthermore, an archaeological settlement of lacustrine Neolithic age, which was located at the western perimeter of the mine, disappeared as it collapsed into the open cast pit.

Figure 6. Spatial distribution of surface ruptures identified behind the crown of the 10 June 2017 landslide. (**A**,**B**) surface ruptures within the basin between Anargiroi and Valtonera village (the height of the scarp is approximately 1 m), (**C**,**D**) pre-existing surface ruptures caused by the land subsidence phenomenon that were intensified by the landslide event in the NW part of Anargiroi village, and (**E**) damage along the Anargyroi village road network.

To constrain the potential failure mechanism for this event, the three main triggering factors, tectonic activity, groundwater pore pressure, and slope geometry, were investigated. In terms of tectonic activity, according to the National Observatory of Greece's earthquake database [53], no earthquakes of magnitude 2.5 or above were recorded in the area surrounding the open pit in the five-month period preceding the landslides. Therefore, the area's tectonic activity is deemed to have not played a major active role in activating this particular landslide or in the associated pre-failure vertical deformation. Nonetheless, it should be stressed that the faults crossing the mine affected the formations occupying the working slopes of the mine, creating zones with reduced shear strength. In particular, the Vegoritida fault (F_{Veg}) defines the western boundary of the landslide while the Anargiri fault (F_{Ang}) crosses the crown and eastern boundary of the landslide. In addition, secondary parallel faults cross the site, affecting the geometry of the landslide mass. Thus, the tectonic structure of the study area can be characterized as a preparatory factor, but not a triggering causal factor, of the landslide on 10 June 2017.

In regard to the groundwater pore pressure, two aquifer systems occur in the study area. The aquifer system developed in the Quaternary formations has been systematically overexploited during recent decades, aiming to protect the mining slopes from failure. The volume of water pumped out from the aquifers, via the mine protection wells, was reduced over time as the subsurface consolidation resulted in compaction of the aquifers and a gradual reduction of their hydraulic conductivity. In detail, the protection wells

around the mine extracted 13×10^6 m^3/year of water in 2002, 9×10^6 m^3/year in 2009, and 3×10^6 m^3/year in 2016 [51]. Furthermore, the pumping activities directly adjacent to Anargiroi village, according to PPC [51], were essentially stopped in 2016, aiming to eliminate the deformation caused by overpumping at the nearby village. These two factors led to a steady increase in the water table between Anargiroi village and the mine, thereby significantly degrading the mechanical properties of the Quaternary deposits. This increase became visible after the occurrence of the landslide when water from the aquifer began gushing from the main scarp of the landslides (Figure 5B). In contrast, this did not occur along the northwestern parts of the main scarp where pumping activities were active at least since the slope failure (Figure 5C). Additionally, the karstic aquifer system created negative slope stability conditions by transferring piezometric load to the lower Neogene formations at the bottom of the mine.

The geometry of the working slopes was uneven and steep, negatively impacting their stability. The evaluation of all available satellite images of the mine illustrates that the two upper benches were excavated first in order to unload the slope. Subsequently, the excavation of the lower benches of the coal seams was prioritized to meet production needs. As a result, the excavation of the middle benches, occupied by the upper Neogene and lower Quaternary formations, was systematically neglected. Accordingly, the geometry of the working slopes was uneven, as the upper parts were more gently sloped and the lower parts steeper. This configuration, with a steeper base of the working slopes, raises significant issues concerning the overall safety factor.

Overall, the stratigraphy of the Neogene formations, including shear zones, the tectonic structure of the plain with faults crossing the mine, and the hydrogeologic setting with two aquifer systems interacting with the mine are considered to be the main preparatory factors for the studied landslide event. Respectively, the main triggering factors of this failure were: (a) the increase in the water table in the Quaternary formation aquifer due to selective reduction of pumping and (b) the steep geometry of the working slopes.

4. Results and Discussion

Based on the vertical and east-west displacement time series from PS points at the villages of Anargiroi, Valtonera, and Fanos, various insights can be gained into the spatial distribution of land subsidence and the impact of the landslide.

In regard to the Anargiroi village, the maximum vertical displacements occur in areas closer to the mine (Figures 4 and S1). This area is underlain by the highly compressible Perdikas Formation; in addition, the maximum groundwater dropdown values of the mine's depression cone occur in this area. As anticipated, the vertical displacement decreases (from NE to SW) in proportion to the groundwater level drop (Figures 4 and S1). In contrast, at the southwestern end of the village, only slight seasonal groundwater fluctuations appear to affect the displacements (A7).

Considering the vertical displacement time series, the village appears to be affected by a steadily decreasing deformation trend (i.e., decreasing land subsidence) during the period January 2016 to December 2020. This observation is directly linked with changes in pumping activities, which have practically stopped since 2016 (Figure 7), allowing partial recovery of the unconfined aquifer.

The abrupt fluctuations of PS points in both the vertical and east/west displacements that can be observed in the period around 10 June 2017, especially in the NE part of the village (i.e., A1, A2, A3, and A6), highlights the significant impact of the landslide. Furthermore, as clearly shown from the east–west horizontal displacement time series (Figure 7), the majority of the PSs around the NE part of the village display a steady eastward displacement trend, towards the open pit, after the landslide. The westward displacement trend identified at two PS points (A2 and A3) can be attributed to rotational movements of the structures that operated as reflectors for those two PSs. Thus, the present trends suggest that the studied site is slowly moving toward the abandoned 220 m deep open pit located only 180 m from the first houses of the village. Physical evidence of the

ongoing activity of the landslide can be obtained by the continuous deformations recorded at the damaged buildings located close to the open pit (Figure S7).

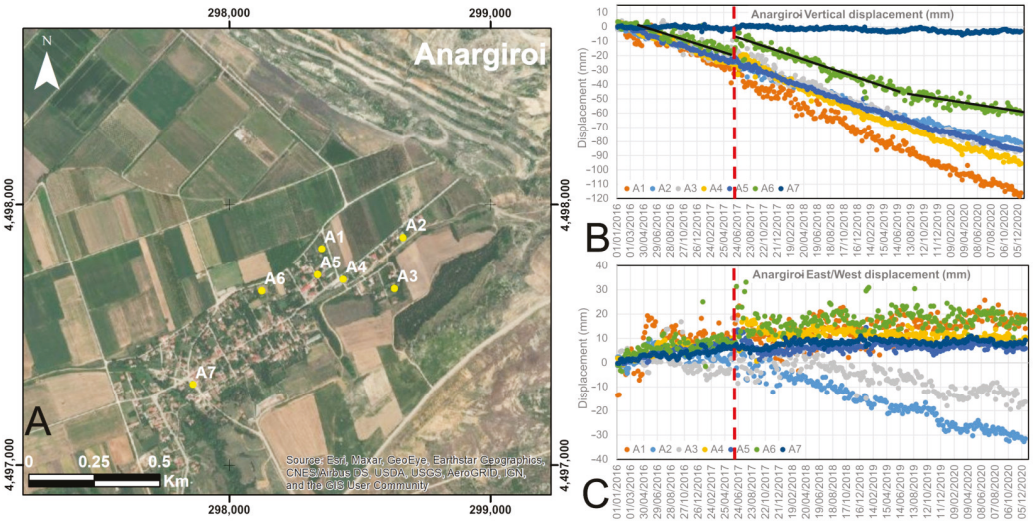

Figure 7. Spatial distribution of examined PS points (**A**) along with their displacement time series (**B**,**C**) at the village of Anargiroi. The dashed red line indicates the date of the mining landslide event. The trend lines added to the time series of point A6 indicate the variations of the land subsiding trend due to the draining activities before and after the occurrence of the landslide, as well as after the 2016 cessation of pumping from the wells located between the village and the open pit. Point A6 was selected as it clearly presents the disturbance caused by the landslide as well as the slight reduction of the deformations after the end of the end of the draining activities.

Consistent with the vertical displacement distribution identified at Anargiroi village, the deformation at Valtonera village increases toward the east, i.e., in areas closer to the mine (Figure 4). Similar to Anargiroi village, this area is also underlain by the highly compressible Perdikas formation and the depression cone of the mine is present. The vertical displacements clearly decreased in the western part of the village with increasing distance from the mine.

The vertical displacement time series in the village of Valtonera shows a steadily decreasing trend with pronounced annual fluctuations. This observation is highly consistent with the water table time series at Valtonera village, which shows a steady downward trend with seasonal fluctuations. The observed trend of a continuous groundwater level drop can be attributed to the draining of the aquifer toward the mines, whereas the seasonal fluctuation likely results from exploitation of the aquifers for irrigation purposes followed by a partial rebound of the groundwater head during the winter [47]. As shown in Figure 8, the vertical displacements each year exhibit a decreasing trend until October (end of the dry period) followed by an increasing trend until May (end of the rainy period). Note that as this village was unaffected by the landslide (Figure S5), no abrupt scatter in the vertical and east–west displacement time series can be identified during the landslide period (Figure 8).

Considering the east–west horizontal displacement time series (Figure 7), most of the PSs around the village indicate a steady eastward displacement trend toward the open pit. These movements cannot be attributed to any landslide activity due to the great distance of the village from the mine (1800 m) relative to the height of the slopes (220 m). Thus, this deformation can only be attributed to ongoing land subsidence-driven deformation. It should be noted that the village is crossed by the Vegoritida fault (Fveg) dipping to the SE and that the fault acted as a pre-existing structural fabric that controls the orientation of the later ruptures generating slight horizontal movements.

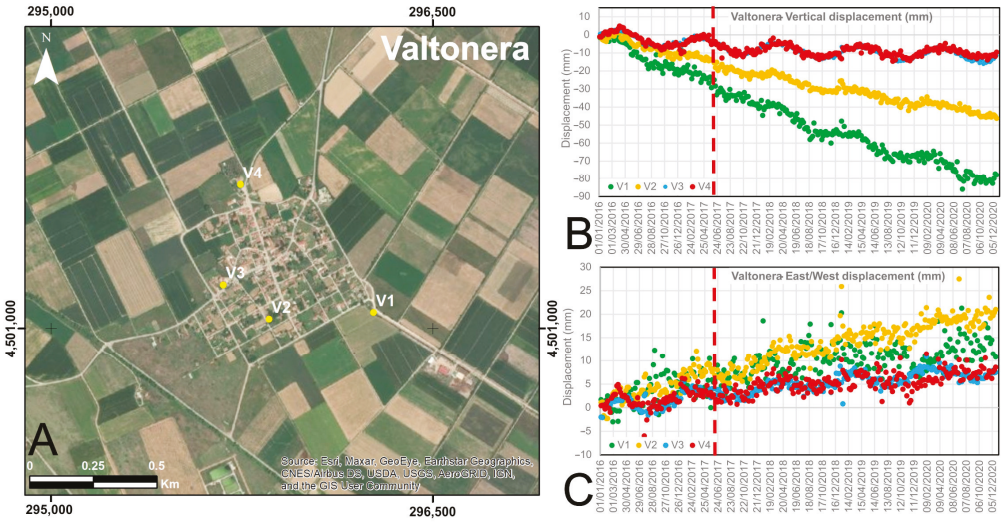

Figure 8. Spatial distribution of examined PS points (**A**) along with their displacement time series (**B**,**C**) at the village of Valtonera. The dashed line indicates the date of the mining landslide event.

The vertical displacements identified at the Fanos village are significantly less intense than those at the Valtonera and Anargiroi villages; nonetheless, this village also suffers from the occurrence of surface ruptures and differential deformation. These deformation types can be attributed to the pronounced stiffness and compressibility differences of the area's underlying formations, as the northern part of the village overlies Neogene rocks, and the western part overlies Quaternary formations.

Considering the vertical displacement time series (Figure 9), although annual fluctuations can be observed, there is no evidence of a gradually evolving long-term land subsidence trend. This implies that groundwater exploitation of the aquifer for irrigation needs is the main factor triggering the deformation that more strongly affects the softer and more compressible Quaternary formations. As shown in the deformation time series, no disturbance is recorded that can be attributed to the 10 June 2017 landslide (Figures 9 and S6); in addition, there are no clear trends observed in the east–west displacement values.

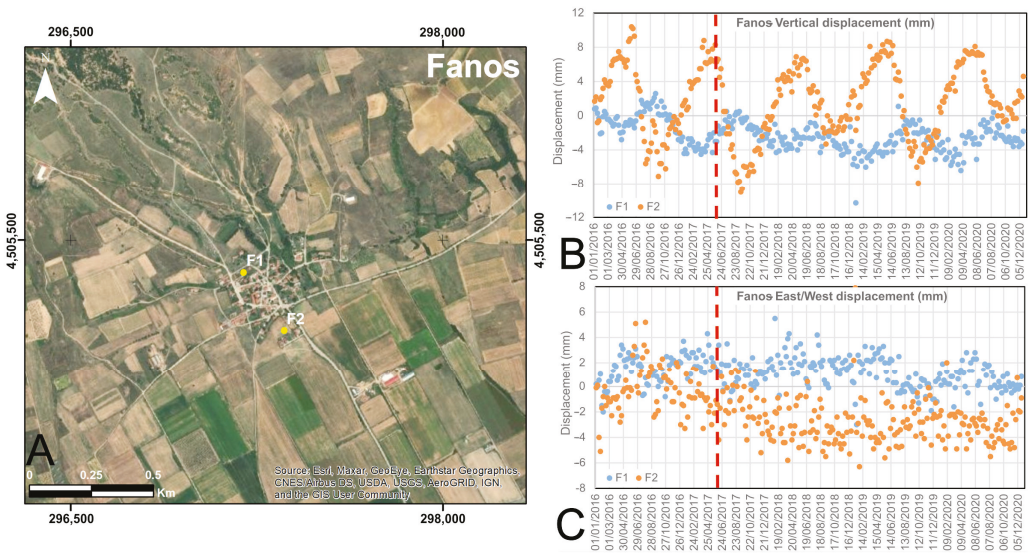

Figure 9. Spatial distribution of examined PS points (**A**) along with their displacement time series (**B**,**C**) at the village of Fanos. The dashed line indicates the date of the mining landslide event. The points were selected from both sides of the fault crossing the village, pointing to the displacements taking place on the stiff Neogene, point F1, and the soft Quaternary, point F2, formations.

5. Conclusions

In conclusion, the combination of ground truth data and information from EGMS datasets provides important insights into the mechanisms and interactions of geocatastrophic events taking place at the Amyntaio coal mine.

In particular, Anargiroi village is clearly affected by aquifer overexploitation via the mine's protection wells. The seasonal fluctuations in vertical deformation identified at Valtonera and Fanos villages, due to the operation of irrigation wells, are not visible in the vertical displacement time series acquired for Anargiroi village. Accordingly, farming activity is interpreted as not contributing significantly to land subsidence in the vicinity of Anargiroi village. This conclusion was largely expected as most of the farms in the village are irrigated from irrigation canals rather than from wells. In addition, the coincidence between the observed decreasing subsidence trends and the termination of pumping activities in 2016 between the open cast mine and the village also strongly supports the interpretation that the subsidence phenomenon is mainly caused by dewatering activities performed at the perimeter of the open cast mine. Regarding the effect of the 10 June 2017, landslide, the InSAR data set demonstrates that the failure affected and continues to affect at least the NE part of the village; in addition, slow horizontal movements toward the open pit are still taking place.

In terms of the deformation occurring at Valtonera village, the 10 June 2017, landslide did not affect the settlement due to the large distance between the village and the open cast mine. Subsidence in this area can be attributed to overpumping caused by both the mine's dewatering activity and farming activity. The mining activity appears to be responsible for the ongoing steady subsidence trend affecting the village, causing substantial damage. In contrast, farming activities in this area appear to cause gentle fluctuating deformations of a minor scale compared to those caused by mining activities.

The deformations at Fanos village are affected only by farming activity, as evidenced by the lack of any observed cross-seasonal or long-term deformation trend and the exclusive occurrence of seasonal deformation in this area. In addition, as expected, the fluctuating deformations appear to be more intense in areas of soft Quaternary formations rather than those of the stiff Neogene.

As a final conclusion, it should be stressed that EGMS datasets are a powerful resource for deciphering the different causal factors of deformations affecting the study area for more than two decades, highlighting the important role of the groundwater management. Because these datasets are provided by an independent and reliable international source, their conclusions are highly robust. Overall, InSAR techniques represent a highly important approach for the study of geohazards.

Supplementary Materials: The following supporting information can be downloaded at: https://www.mdpi.com/article/10.3390/w15081474/s1, Figure S1: The impact of land subsidence at the Anarigoi village. The photos were capture in May 2016 (before the landslide event that occurred on 10 June 2017); Figure S2: The impact of land subsidence at the Valtonera village. The photos were capture in May 2016 (before the landslide event that occurred on 10 June 2017); Figure S3: The impact of land subsidence at the Fanos village. The photos were capture in May 2016 (before the landslide event that occurred on 10 June 2017); Figure S4: The impact of landslide event in areas previously affected by land subsidence, at the Anarigoi village. The expansion of the surface raptures and the intensification of the damages on the constructions is clearly precented; Figure S5: Images taken at the Valtonera village before and after the occurrence of the major landslide event, that took place on 10 June 2017. It is clear that, as expected due to the large distance of the village from the open pit, the landslide did not cause any further damages to the already damaged, by the land subsidence, constructions of the village; Figure S6: Images taken at the Fanos village before and after the occurrence of the major landslide event, that took place on 10 June 2017. It is clear that, as expected due to the large distance of the village from the open pit, the landslide did not cause any further damages to the already damaged, by the land subsidence, constructions of the village; Figure S7: Images taken at the Anargyroi village after the occurrence of the major landslide event, that took place on 10 June 2017. The deformations taking place due to the continuous landslide and

land subsidence movements since the occurrence of the landslide are clearly presented; Table S1: Ground truth dataset.

Author Contributions: Methodology, P.T. and C.L.; Validation, P.T. and C.L.; Formal analysis, P.T.; Investigation, P.T.; Writing—original draft, P.T.; Writing—review & editing, C.L.; Supervision, C.L. All authors have read and agreed to the published version of the manuscript.

Funding: This research received no external funding.

Data Availability Statement: The datasets used and/or analyzed during the current study are available from the authors upon request.

Acknowledgments: The authors would like to acknowledge the European Land Monitoring Service of the European Environment Agency for freely providing the INSAR data.

Conflicts of Interest: The authors declare no conflict of interest.

References

1. Passariello, B.; Giuliano, V.; Quaresima, S.; Barbaro, M.; Caroli, S.; Forte, G.; Carelli, G.; Iavicoli, I. Evaluation of the environmental contamination at an abandoned mining site. *Microchem. J.* **2002**, *73*, 245–250. [CrossRef]
2. WISE_Uranium_Project. Chronology of Major Tailings Dam Failures. Available online: https://www.wise-uranium.org/mdaf.html (accessed on 30 August 2022).
3. Williams, C.; Ross, B.; Zebker, M.; Leighton, J.; Gaida, M.; Morkeh, J.; Robotham, M. Assessment of the available historic RADARSAT-2 synthetic aperture radar data prior to the manefay slide at the bingham canyon mine using modern InSAR techniques. *Rock Mech. Rock Eng.* **2021**, *54*, 3469–3489. [CrossRef]
4. Moore, J.R.; Pankow, K.L.; Ford, S.R.; Koper, K.D.; Hale, J.M.; Aaron, J.; Larsen, C.F. Dynamics of the Bingham Canyon rock avalanches (Utah, USA) resolved from topographic, seismic, and infrasound data. *J. Geophys. Res. Earth Surf.* **2017**, *122*, 615–640. [CrossRef]
5. Hibert, C.; Ekström, G.; Stark, C.P. Dynamics of the Bingham Canyon Mine landslides from seismic signal analysis. *Geophys. Res. Lett.* **2014**, *41*, 4535–4541. [CrossRef]
6. Pankow, K.L.; Moore, J.R.; Hale, J.M.; Koper, K.D.; Kubacki, T.; Whidden, K.M.; McCarter, M.K. Massive landslide at Utah copper mine generates wealth of geophysical data. *GSA Today* **2014**, *24*, 4–9. [CrossRef]
7. Lin, Y.N.; Park, E.; Wang, Y.; Quek, Y.P.; Lim, J.; Alcantara, E.; Loc, H.H. The 2020 Hpakant Jade Mine Disaster, Myanmar: A multi-sensor investigation for slope failure. *ISPRS J. Photogramm. Remote Sens.* **2021**, *177*, 291–305. [CrossRef]
8. Sun, Y.; Zhang, X.; Mao, W.; Xu, L. Mechanism and stability evaluation of goaf ground subsidence in the third mining area in Gong Changling District, China. *Arab. J. Geosci.* **2015**, *8*, 639–646. [CrossRef]
9. Carnec, C.; Delacourt, C. Three years of mining subsidence monitored by SAR interferometry, near Gardanne, France. *J. Appl. Geophys.* **2000**, *43*, 43–54. [CrossRef]
10. Wolkersdorfer, C.; Thiem, G. Ground water withdrawal and land subsidence in northeastern Saxony (Germany). *Mine Water Environ.* **1999**, *18*, 81–92. [CrossRef]
11. Tang, W.; Motagh, M.; Zhan, W. Monitoring active open-pit mine stability in the Rhenish coalfields of Germany using a coherence-based SBAS method. *Int. J. Appl. Earth Obs. Geoinf.* **2020**, *93*, 102217. [CrossRef]
12. Mohammady, M.; Pourghasemi, H.R.; Amiri, M. Assessment of land subsidence susceptibility in Semnan plain (Iran): A comparison of support vector machine and weights of evidence data mining algorithms. *Nat. Hazards* **2019**, *99*, 951–971. [CrossRef]
13. Hong, H.; Tsangaratos, P.; Ilia, I.; Loupasakis, C.; Wang, Y. Introducing a novel multi-layer perceptron network based on stochastic gradient descent optimized by a meta-heuristic algorithm for landslide susceptibility mapping. *Sci. Total Environ.* **2020**, *742*, 140549. [CrossRef]
14. Kaitantzian, A.; Loupasakis, C.; Tzampoglou, P.; Parcharidis, I. Ground Subsidence Triggered by the Overexploitation of Aquifers Affecting Urban Sites: The Case of Athens Coastal Zone along Faliro Bay (Greece). *Geofluids* **2020**, *2020*, 8896907. [CrossRef]
15. Svigkas, N.; Loupasakis, C.; Papoutsis, I.; Kontoes, C.; Alatza, S.; Tzampoglou, P.; Tolomei, C.; Spachos, T. InSAR Campaign Reveals Ongoing Displacement Trends at High Impact Sites of Thessaloniki and Chalkidiki, Greece. *Remote Sens.* **2020**, *12*, 2396. [CrossRef]
16. Nhu, V.-H.; Thi Ngo, P.-T.; Pham, T.D.; Dou, J.; Song, X.; Hoang, N.-D.; Tran, D.A.; Cao, D.P.; Aydilek, İ.B.; Amiri, M. A new hybrid firefly–PSO optimized random subspace tree intelligence for torrential rainfall-induced flash flood susceptible mapping. *Remote Sens.* **2020**, *12*, 2688. [CrossRef]
17. Ilia, I.; Tsangaratos, P.; Tzampoglou, P.; Chen, W.; Hong, H. Flash flood susceptibility mapping using stacking ensemble machine learning models. *Geocarto Int.* **2022**, *37*, 1–27. [CrossRef]
18. Tzampoglou, P.; Loukidis, D.; Koulermou, N. Seasonal Ground Movement Due to Swelling/Shrinkage of Nicosia Marl. *Remote Sens.* **2022**, *14*, 1440. [CrossRef]

19. Loupasakis, C. *Study of the Geotechnical Conditions of the Amintaio Coalmine Slopes Close to the Anargiri Village, Aetos Municipality, Florina Prefecture, Greece*; IGME: Athens, Greece, 2006; p. 48.
20. Tzampoglou, P.; Loupasakis, C. Updated ground water piezometry data of the Amyntaio sub-basin and their effect to the manifestation of the land subsidence phenomena. In Proceedings of the 11th International Hydorgeological Congress of Greece, Athens, Greece, 4–6 October 2017.
21. Loupasakis, C.; Angelitsa, V.; Rozos, D.; Spanou, N. Mining geohazards—Land subsidence caused by the dewatering of opencast coal mines: The case study of the Amyntaio coal mine, Florina, Greece. *Nat. Hazards* **2014**, *70*, 675–691. [CrossRef]
22. Tzampoglou, P.; Loupasakis, C. Mining geohazards susceptibility and risk mapping: The case of the Amyntaio open-pit coal mine, West Macedonia, Greece. *Environ. Earth Sci.* **2017**, *76*, 542. [CrossRef]
23. Tzampoglou, P.; Loupasakis, C. Evaluating geological and geotechnical data for the study of land subsidence phenomena at the perimeter of the Amyntaio coalmine, Greece. *Int. J. Min. Sci. Technol.* **2018**, *28*, 601–612. [CrossRef]
24. Loupasakis, C. Contradictive mining–Induced geocatastrophic events at open pit coal mines: The case of Amintaio coal mine, West Macedonia, Greece. *Arab. J. Geosci.* **2020**, *13*, 1–12. [CrossRef]
25. European Ground Motion Service. End-to-end Implementation and Operation of the European Ground Motion Service (EGMS). In *Product User Manual*; European Environment Agency (EEA): Copenhagen, Denmark, 2022.
26. European Union; European Environment Agency (EEA). Copernicus Land Monitoring Service. 2022. Available online: https://egms.land.copernicus.eu/ (accessed on 21 September 2022).
27. Crosetto, M.; Solari, L.; Mróz, M.; Balasis-Levinsen, J.; Casagli, N.; Frei, M.; Oyen, A.; Moldestad, D.A.; Bateson, L.; Guerrieri, L. The evolution of wide-area DInSAR: From regional and national services to the European Ground Motion Service. *Remote Sens.* **2020**, *12*, 2043. [CrossRef]
28. Crosetto, M.; Solari, L.; Balasis-Levinsen, J.; Bateson, L.; Casagli, N.; Frei, M.; Oyen, A.; Moldestad, D.; Mróz, M. Deformation monitoring at european scale: The copernicus ground motion service. *Int. Arch. Photogramm. Remote Sens. Spat. Inf. Sci.* **2021**, *XLIII-B3-2*, 141–146. [CrossRef]
29. Costantini, M.; Minati, F.; Trillo, F.; Ferretti, A.; Novali, F.; Passera, E.; Dehls, J.; Larsen, Y.; Marinkovic, P.; Eineder, M. European Ground Motion Service (EGMS). In Proceedings of the 2021 IEEE International Geoscience and Remote Sensing Symposium IGARSS, Brussels, Belgium, 11–16 July 2021; pp. 3293–3296.
30. Doukissa, K. *Geotechnical Study of the Bridge in the Central Trench of Aanargiroi Area*; Municipality of Aetos: Thessaloniki, Greece, 2010; p. 24.
31. Dhmaras, K.; Georgiadhs, M. *Lifting and Waterproofing Study of the Existing Embankment of Lake Cheimaditida Florina*; Geognosi Public Limited Company: Thessaloniki, Greece, 2002.
32. Tzampoglou, P. Mining geohazards in Greece. The case of the Amyntai open-pit coal mine. Ph.D. Thesis, National Technical University of Athens, Athens, Greece, 2017.
33. Koukouzas, C.; Kotis, T.; Ploumidis, M.; Metaxas, A. *Coal Exploration of Anargiri-Amynteon Area, Mineral Deposit Research*; Institution of Geology and Mineral Exploration: Athens, Greece, 1979; Volume 9.
34. Institution of Geology and Mineral Exploration. *Geological Map of Greece, Scale 1:50,000, Ptolemaida Sheet*; Institution of Geology and Mineral Exploration: Athens, Greece, 1997.
35. Metaxas, A.; Karageorgiou, D.; Varvarousis, G.; Kotis, T.; Ploumidis, M.; Papanikolaou, G. Geological evolution-stratigraphy of Florina, Ptolemaida, Kozani and Saradaporo graben. *Bull. Geol. Soc. Greece* **2007**, *40*, 161–172. [CrossRef]
36. Leonardos, M.; Terezopoulos, N. Rim slope failure mechanism in the Greek deep lignite mines–A case study. *Min. Technol.* **2003**, *112*, 197–204. [CrossRef]
37. Mountrakis, D. *Geology of Greece*; University Studio Press: Thessaloniki, Greece, 1985.
38. Spyropoulos, N. The geological structure of Pelagonian zone in the Mount of Askio D. Macedonia. Ph.D. Thesis, Aristotle University of Thessaloniki, Thessaloniki, Greece, 1992.
39. Pavlides, S.; Mountrakis, D. Neotectonics of the Florina-Vegoritis-Ptolemais Neogene Basin (NW Greece): An example of extensional tectonics of the greater Aegean area. *Ann. Géol. Pays Hell.* **1985**, *33*, 311–327.
40. Pavlides, S. Neotectonic evolution of the Florina-Vegoritis-Ptolemais basin (W. Macedonia, Greece). Ph.D. Thesis, Aristotle University of Thessaloniki, Thessaloniki, Greece, 1985.
41. Pavlides, S.; Mountrakis, D. Extensional tectonics of northwestern Macedonia, Greece, since the late Miocene. *J. Struct. Geol.* **1987**, *9*, 385–392. [CrossRef]
42. Koukouzas, C.; Kotis, T.; Ploumidis, M.; Metaxas, A.; Dimitriou, D. *Coal Exploration of Komninon-Ptolemaidas Area. Mineral Deposit Research*; Institution of Geology and Mineral Exploration: Athens, Greece, 1983; Volume 2.
43. Ganas, A.; Oikonomou, I.; Tsimi, A. NOAfaults: A digital database for active faults in Greece. *Bull. Geol. Soc. Greece* **2015**, *47*, 518–530. [CrossRef]
44. Stamos, A.; Giannoulopoulos, P. *Hydrogeological Report, Geotechnical Work to the Anargiri Village, Aetos Municipality, Florina Prefecture, Greece*; Institution of Geology and Mineral Exploration: Athens, Greece, 2010; p. 34.
45. Tzampoglou, P.; Loupasakis, C. New data regarding the ground water level changes at the Amyntaio basin-Florina Prefecture, Greece. *Bull. Geol. Soc. Greece* **2016**, *50*, 1006–1015. [CrossRef]
46. Tzampoglou, P.; Loupasakis, C. Land subsidence due to the overexploitation of the aquifer at the Valtonera village. *Bull. Geol. Soc. Greece* **2017**, *50*, 1006. [CrossRef]

47. Tzampoglou, P.; Loupasakis, C. Numerical simulation of the factors causing land subsidence due to overexploitation of the aquifer in the Amyntaio open coal mine, Greece. *HydroResearch* **2019**, *1*, 8–24. [CrossRef]
48. Dimitrakopoulos, D. Hydrogeological conditioning at the Amyndeon mine. Problems occuring during the exploitation and their mitigation actions. Ph.D. Thesis, NTUA, Athens, Greece, 2001.
49. Tsourlos, P. *Research for the Appearance of Surface Cracks in the Valtonera Village, Amyntaio Municipality, Florina Region*; School of Geology of the Aristotle University of Thessaloniki Aristotelian University of Thessaloniki: Thessaloniki, Greece, 2015; p. 17.
50. Soulios, G.; Tsapanos, T.; Voudouris, K.; Kaklis, T.; Mattas, C.; Sotiriadis, M. Ruptures on surface and buildings due to land subsidence in Anargyri village (Florina Prefecture, Macedonia). *Environ. Earth Sci.* **2011**, *5*, 505–512.
51. Dimitrakopoulos, D.; Koumantakis, I. Hydrodynamic regime of Amynteon basin. Influence of open lignite mines. In Proceedings of the 11th International Hydrogeological Congress of Greece, Athens, Greece, 4–6 October 2017; pp. 101–112.
52. Tzampoglou, P.; Loupasakis, C. Land subsidence susceptibility and hazard mapping: The case of Amyntaio Basin, Greece. In Proceedings of the Fifth International Conference on Remote Sensing and Geoinformation of the Environment (RSCy2017), Paphos, Cyprus, 20–23 March 2017; p. 104441L.
53. NOA. Earthquake Database Search. Available online: https://www.gein.noa.gr/en/services-products/database-search/ (accessed on 25 September 2022).

Disclaimer/Publisher's Note: The statements, opinions and data contained in all publications are solely those of the individual author(s) and contributor(s) and not of MDPI and/or the editor(s). MDPI and/or the editor(s) disclaim responsibility for any injury to people or property resulting from any ideas, methods, instructions or products referred to in the content.

water

MDPI

Article

Repurposing of a Closed Surface Coal Mine with Respect to Pit Lake Development

Georgios Louloudis [1,*], Christos Roumpos [1,*], Emmanouil Louloudis [2], Eleni Mertiri [1] and Georgios Kasfikis [1]

[1] Public Power Corporation of Greece, Department of Mining Engineering and Closure Planning, 10432 Athens, Greece
[2] Department of Statistics, Athens University of Economics and Business, 10434 Athens, Greece
* Correspondence: g.louloudis@dei.gr (G.L.); c.roumpos@dei.gr (C.R.); Tel.: +30-697-000-5090 (G.L.); +30-697-979-9291 (C.R.)

Abstract: In the coal phase-out era, achieving sustainable mine closure is significant and prioritizes targets for the mining industry. In this study, the already closed lignite mine of Kardia, North Greece, is investigated, where the mine void left is naturally filled with water. The viability of different repurposing land uses is evaluated, and the natural water level development inside the mine pit is investigated concerning its future uses. The potential for solar photovoltaic (PV) panels developed on mining land and its surrounding area is evaluated in combination with the application of pumped hydro storage (PHS) technology, utilizing pit lake water. Except for electricity system planning, other end-uses that offer multiple, mutually reinforcing and lasting benefits are investigated, such as recreation parks, terrestrial wildlife, aquaculture and agriculture. All repurposing scenarios are evaluated with regard to the spatiotemporal evolution of the lake, by generating forecasts of the dependent variables (rainfall and temperature) via linear (autoregressive integrated moving average) and non-linear (artificial neural network) models. The prediction of pit lake natural development redefines the new land use layout and the land repurposing decisions. This is essential for strategic planning, considering the Greek lignite mining industry's priority regarding transitioning from the current coal-based electricity to renewable energy sources (RES) technology.

Keywords: mine closure; autoregressive integrated moving average (ARIMA); artificial neural network (ANN); post-mining; land use; energy; sustainability; spatiotemporal development; economic transition

1. Introduction

In the region of the South Ptolemais lignite-bearing basin, in Macedonia, N.W.(northwest) Greece (Figure 1), the Public Power Corporation (PPC) of Greece had developed extensive mining activity in order to provide adequate lignite quantities for 3000 MW power plants. However, Greece's commitment to the European Commission's long-term strategic vision to achieve net-zero greenhouse-gas emissions [1,2] has provided motivations for sustainable economic growth and spurred the modernization of the economy. The PPC operates within the framework of corporate environmental responsibility [3] and has established an environmental policy that reflects its commitment to comply with all applicable national and international laws and support continuous environmental improvement.

Over the last decade, particular policy attention has been paid to the transition from coal energy to clean energy technologies to reduce the risks of climate change impacts and contribute to climate-resilient pathways [4] for sustainable development. The goal is to integrate renewable sources and energy efficiency while simultaneously providing the lowest possible cost. As a result, multi-level planning is critical to designing and implementing effective strategies, exploring repurposing options, and making decisions about a post-mining future and economic transitions, considering regional and policy contexts [5].

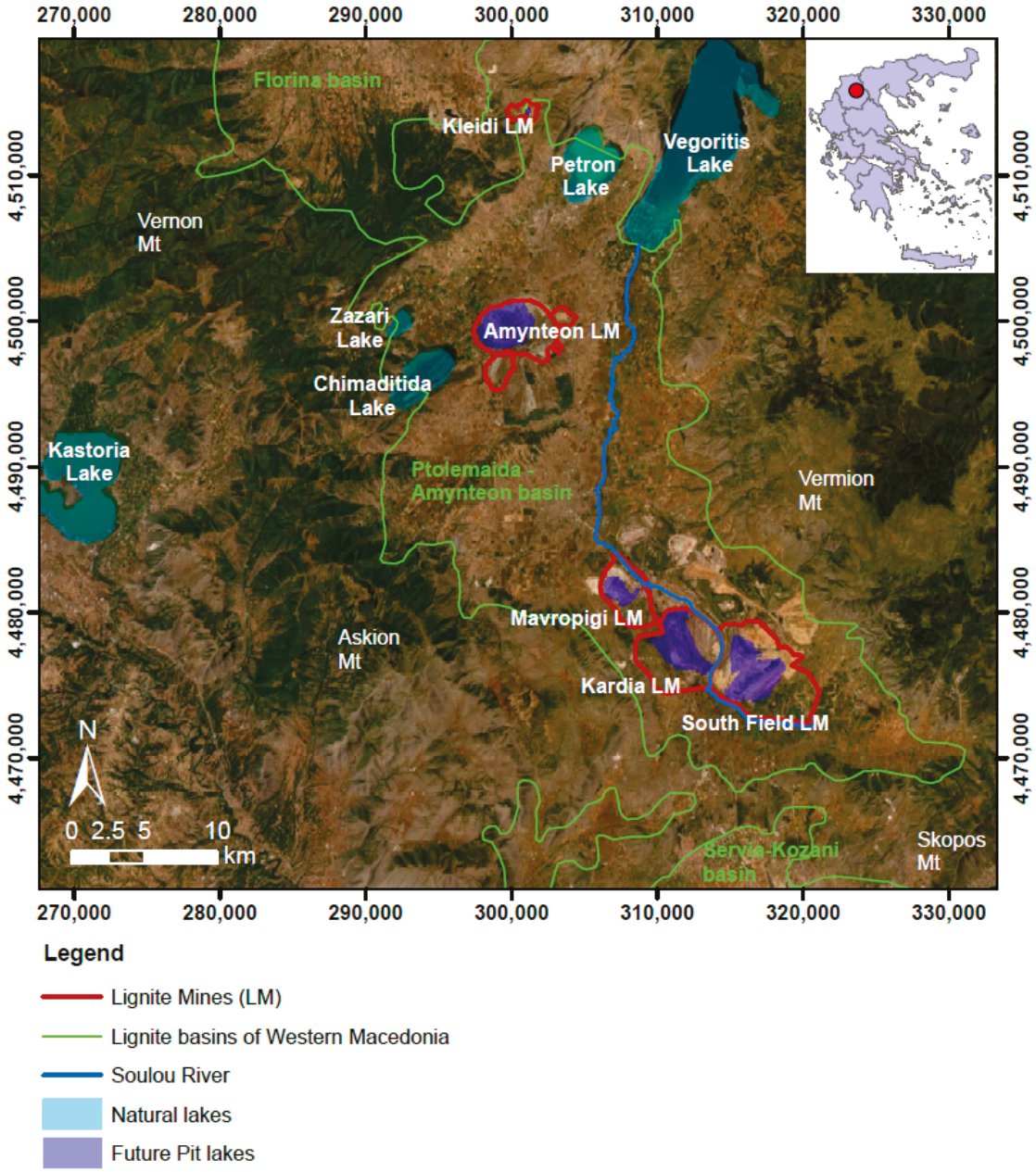

Figure 1. Research area and location of the Kardia Lignite Mine (LM), Greece. Basemap obtained from https://www.esri.com/en-us/home accessed on 30 March 2022 (Coordinate Reference System GGRS87/Greek Grid).

Recently, the PPC has investigated and evaluated alternative repurposing options to produce energy using renewable energy sources (RES) and has planned post-mining land uses to be sustainable [6] in the long term. In this context, the PPC is planning to transition from coal-based electricity to renewable energy. Specifically, the PPC's research is focused on the sustainable post-mining development of different RES plant types in the remaining post-mining landscapes and consequently evaluating whether implementing such technology could fulfill the electricity demand.

Regarding RES technology application, it is essential to consider the intermittent power outcome. In such a case, integrating energy storage technology with renewable energy production could be an effective solution. Therefore, the PPC uses a holistic approach to mine transition planning by examining energy storage technology, such as pumped hydro storage (PHS) technology.

A considerable volume of literature has been published on applying PHS technology in closed mines in combination with renewable energy sources, such as photovoltaic (PV) parks. According to Bódis et al. [7] the post-mining available landscape area for installing PV systems is abundant in the coal regions of the European Union. In addition, solar PV systems could replace the current coal-fired power plants, provided storage-flexible units with sufficient capacities are added. The first innovative project of a hybrid energy system, which combines PHS technology with multi-stage solar and wind renewable energy units in an abandoned mine, is the Kidston Clean Energy Hub Project [8] in Kidston, Far-North Queensland in Australia, which is expected to be in operation by 2024. According to Holcombe, pit voids in abandoned mines could become an asset underpinning RES development at mining sites and creatively reusing them [9]. Regarding economic feasibility, Wessel et al. reported that hybrid PHS–RES projects could be developed and operated at reasonably low costs [10].

Except for the production of electricity using RES, there is also a growing body of literature on other post-mining transitions and repurposing land-use scenarios [3,11,12], such as wildlife habitat, parks for recreation, eco-tourism and rehabilitation practices concerning pit lakes, i.e., development of fishing farms, recreational sport fisheries, angling, diving, hiking around the lake and even using pits for water storage and flood protection.

Therefore, water quality is an important parameter that could enable new beneficial end uses. Poor water quality could be significantly improved by rehabilitation practices, such as permanent flushing with river water, diverting seasonal floods into the pit lake [13,14], or even permanent river flow-through [15], which can mitigate the risk of eutrophication. Other rehabilitation practices have been reported in post-mining areas, such as appropriate landscaping of the pit lake banks with gentle sloping to emulate natural lakes if possible, filling the bottom of the open pit with alkaline substances such as re-excavated waste lime materials and application of riparian zone vegetation [14,16,17]. These rehabilitation practices could help the development of crucial aquatic biodiversity. Thus, a closure monitoring program is a prerequisite in post-mining areas to ensure long-term pit lake quality, since improving long-term environmental outcomes [18] could enhance pit lake ecosystem development and mitigate environmental damage.

Open pits include large areas that could also be used for waste disposal. Woodlawn is another innovative hybrid electric power project and an example of a circular economy, where the abandoned open pit was repurposed and is now converted into a bio-reactor landfill [12]. In this example, municipal wastes are disposed into the pit, and bio-gas power is produced, feeding the electricity grid. At the same time, other land repurposing is also applied in the surrounding area of the mine. It includes the development of RES technology using wind and solar farms to generate electricity, agricultural operations for farming practices, aquaculture and horticulture operations utilizing captured waste heat in hydroponic horticulture and to cultivate fish, and also the operation of a biological treatment facility to extract the organic content from waste and select recyclable materials or produce compost [19].

Another post-mining land-use transition is transforming mining landscapes into memorial pathways and places of remembrance, demonstrating historical artifacts to memorialize the local mining legacy [12]. In addition, these landmarks could become symbols of the region and thus help the development of tourism and recreation in the area [20].

This study aims to provide a case analysis to examine and evaluate land use repurposing scenarios in a mined-out pit of a closed mine. For this purpose, the mined-out pit of the already closed lignite mine of Kardia, northern Greece, was used as the case study. According to the planning studies for the closure of the lignite mines of western Macedonia [6], rehabilitation includes the development of lakes inside the open pits, photovoltaic (PV) parks developed in the surrounding area, areas used for agriculture or recreational activities and forest areas. In the Kardia mine, the construction of a PHS facility is proposed to work as an energy storage unit due to the major setback in the performance of PV

panels, i.e., the difficulty in adjusting to power demands at all times [7,12,21,22]. More specifically, the pit lake is repurposed as a PHS plant. It is used as an energy storage unit to supplement variable renewable capacity and enhance the proposed photovoltaic panels' performance, increasing the PV park's capacity factor. The conceptual idea is to utilize the pit lake that will start to develop after the end of mining activities, ensure the cessation of dewatering measures (dewatering wells and pumping stations) and create another or use an existing upper reservoir at higher altitudes. Then, taking advantage of the head difference between the pit lake (lower reservoir) and upper reservoir, the whole system could be used as a storage battery, releasing power when needed to compensate for renewable energy fluctuations.

In this framework, the feasibility of applying PHS technology is examined concerning the prediction of the natural development lake inside the open pit. In addition, considering the lake's potential growth, the application of different land repurposing scenarios in the Kardia mine is evaluated. Finally, all potential repurposing land uses are evaluated regarding the energy transition potential in the specific region, long-term socio-economic viability and successful adaptation. The intent of this paper is to recommend strategies for improving post-mining land use transition and transforming abandoned surface lignite mines—including pit lakes—into post-mining assets for the communities. In addition, our intent is to contribute to further advancing successful pit lake end uses, as pit lakes could become assets to the clean energy sector.

2. Materials and Methods

2.1. Research Area—Morphology of the Basin

The Ptolemais Lignite Field is located in Kozani Prefecture in north Greece, surrounded by the mountains Vermion, Askion and Skopos (Figure 1). The northern side of the basin is bounded by Komanos horst. The Public Power Corporation of Greece has exploited three lignite reserves in this area: Mavropigi, Kardia, and South Field. The Kardia deposit lies in the middle, with exploitable reserves of 273 million tons (since January 2020) that hosted a 1250 MW lignite-fired power plant for almost 40 years. Inside dumping was conducted mainly with spreaders (continuous surface mining) and, in some cases, with trucks and loaders (non-continuous surface mining). The internal waste dumps are estimated in the order of ≈1.0 billion m^3. Currently, the region's economy depends on agriculture and energy fuel reserves.

The deepest part of the Kardia mine excavation was +450 m a.s.l. when lignite exploitation activities terminated in 2021. By the end of 2022, backfilling of the bottom of the mine pit is planned to achieve slope stability conditions, and thus, the bathymetry of the Kardia excavation will alter, with the deepest part forming at approximately +523 m a.s.l. (Figure 2). The range of ground elevations in the pit is between ≈+523 m and +670 m a.s.l.

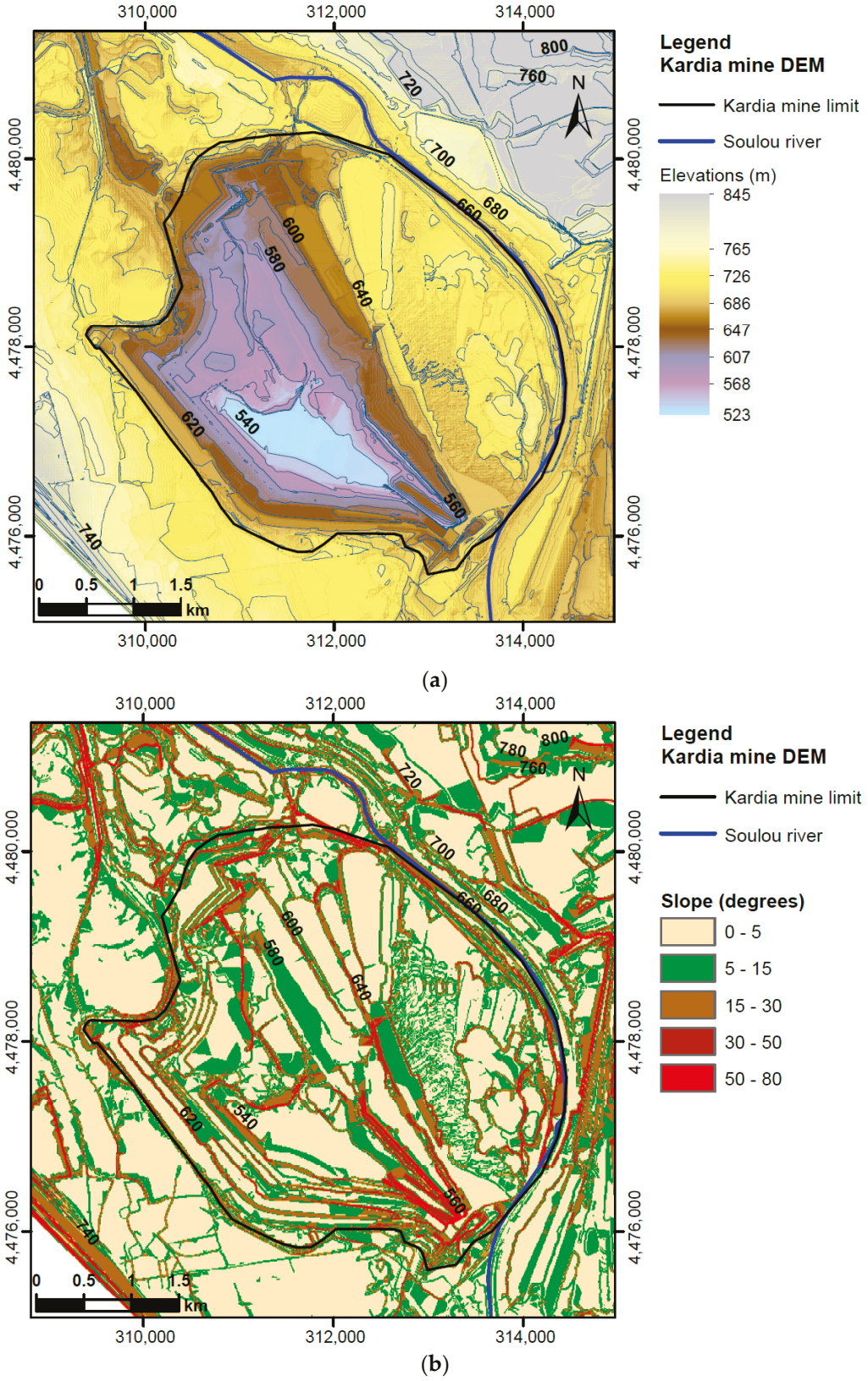

Figure 2. Kardia lignite mine geomorphology, Greece (Coordinate Reference System GGRS87/Greek Grid): (**a**) digital elevation model (DEM) of the open pit; (**b**) slope model (in degrees).

2.2. Hydrological and Hydrogeological Setting

The broader research area is part of larger lignite basins of western Macedonia, formed during the Pliocene. The region has a complex of natural lakes (Chimaditida, Zazari, Petron and Vegoritis) (Figure 1). Vegoritis Lake is located in the homonymous closed hydrological basin in western Macedonia, Greece, and is the final receiving body of the basin runoff, with a total area of 2000 km^2. Vegoritis Lake is also the surficial feature of a major karstic aquifer [23]. Therefore, any alteration in the surface or groundwater conditions within this area would affect the level of the lake. The primary water discharge into the lake is achieved via the Soulou River [24,25]. Therefore, the main priority of the PPC is not only the protection of the natural lakes but also the monitoring of the artificial lake evolution developed in the open voids of the closed lignite mines, as well as the evaluation of the chemical properties of lake water and of the new aquatic ecosystem that is formed.

Kardia open pit is an exhausted mine located on the western margins of the South Ptolemais lignite-bearing basin (Sarigiol basin) in the foothills of Askion Mountain. Quaternary sediments are met on the broader area, which consists mainly of intercalations of sands, clays, sandy marls and conglomerates. These formations overlie Paleozoic schists, ophiolites and granite formations. In addition, Mesozoic dolomitic limestones, volcanic sediments and flysch overlay the Paleozoic formations [6,26]. The lignite sequence underlies the Quaternary sediments and consists of impermeable Pliocene formations of marls and lignite. Lignite sequence formation is significant for the South Field Lignite Mine (LM) and Kardia LM operations due to the potential slope instabilities associated with sliding along a sub-horizontal lignite-to-clay/marl interface, mainly caused by the groundwater pressures [27].

Regarding the hydrolithological conditions in the area of the Kardia mine, two aquifers are generally recognized, the upper (Sarigiol aquifer) and the lower (Komanos aquifer). These aquifers are separated via the impermeable lignite sequence. The upper unconfined aquifer consists of high permeability layers (sands, conglomerates) with intercalations of low permeability layers (clayey interlayers, fluvial deposits). This unit consists of a unique hydraulically connected network that behaves as one aquifer [24].

The hydrogeological basin of Ptolemais South Field (Sarigiol basin) is surrounded by the Vermion (east side), Askion (west side) and Skopos (south side) mountains. The northern part of the basin is bounded by the Komanos tectonic horst. Most of the streams originate from the surrounding mountains, where the general water flow direction is towards the Soulou River. Part of the surface run-off is discharged into the Soulou River via the consolidated sediment channels formed on the ground surface, while part of the water is infiltrated inside the sediment formations. The stream network and the Soulou River are presented in Figure 3. The recharge area of the Sarigiol aquifer is mainly the Vermion and Askion foothills conglomerates and talus cones, whereas the Soulou River is the main outflow channel of the basin, which directs the water flow into Vegoritis Lake, north of the Kardia lignite mine (Figure 1).

Regarding the Sarigiol aquifer, the piezometric surface is conducted by considering the water levels measured in the boreholes. Based on the piezometry in the area of interest, the piezometric level is met at elevations between ≈+640 m and +660 m a.s.l. (Figure 3). The predominant direction of groundwater flow in the Sarigiol aquifer body south of the Kardia mine is generally NW to SE, while locally, next to the open pit Kardia mine location, the direction that prevails is S to N. It is noted that in the same area, the lignite sequence is met at elevations between ≈+350 m and +500 m a.s.l., while during excavations inside the Kardia open pit, the bottom of the lignite sequence was not revealed. Thus, in the conceptual model of Kardia pit lake formation, the simulation was oriented only in the aquifer above the lignite sequence, i.e., the Sarigiol aquifer.

In Figure 4, the methodological approach is presented briefly illustrating the modeled processes.

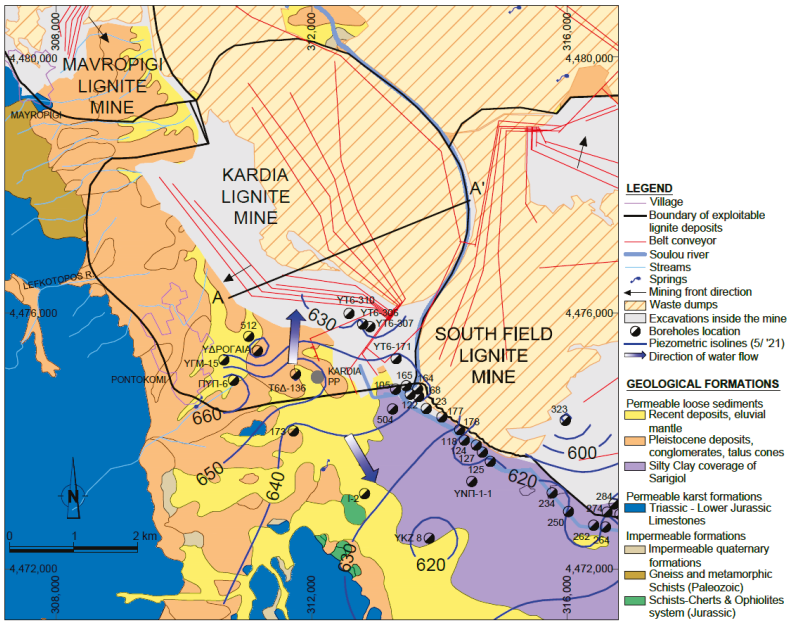

Figure 3. Geological and hydro-lithological map in the Ptolemais lignite field, northern Greece (Coordinate Reference System GGRS87/Greek Grid).

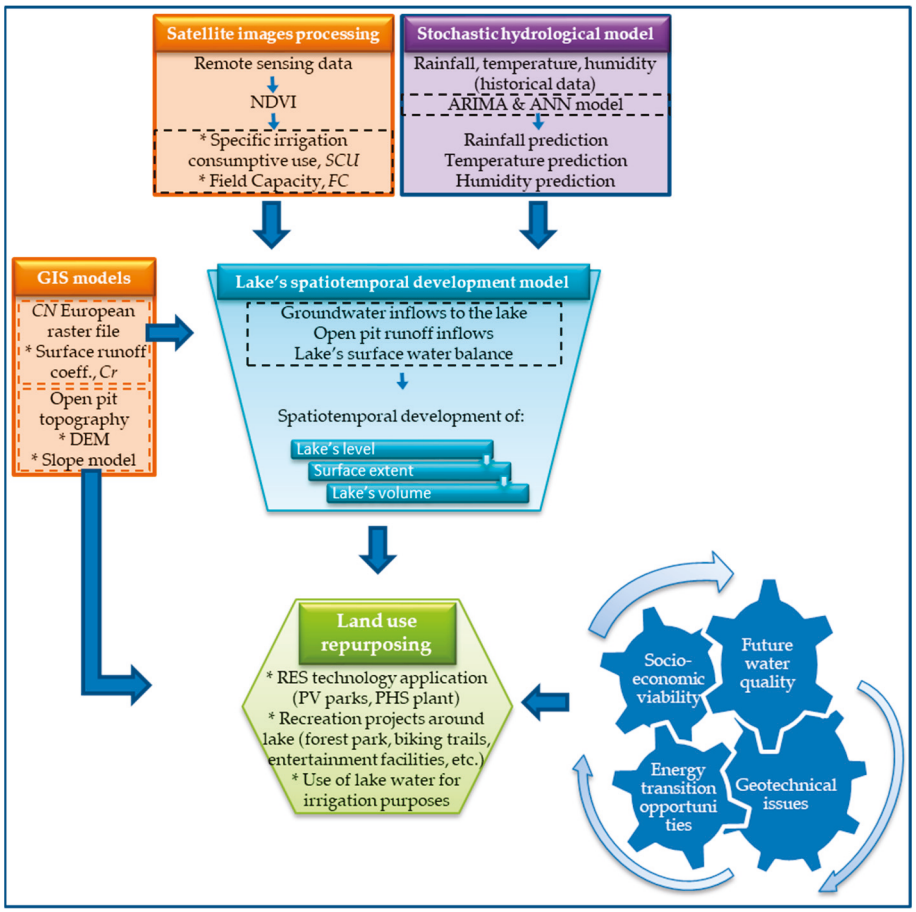

Figure 4. Flowchart of the methodological approach.

The renewable resource of the aquifer is the rainfall infiltration through the Quaternary sediments. Meteorological data (temperature, rainfall) were obtained from Kozani WMO No 16 632 weather station, recorded by the Hellenic National Meteorological Service, and

spanning a period of 44 years, from 1970–1997 and 2006–2021 (Figure 5). This station is approximately at the same elevation as the Ptolemais lignite field, located 14 km south of the Kardia LM. Meteorological data were also obtained from Ptolemaida LG26 weather station, recorded by the National Observatory of Athens (NOA), and spanning a period of 15 years, from 2006–2021.

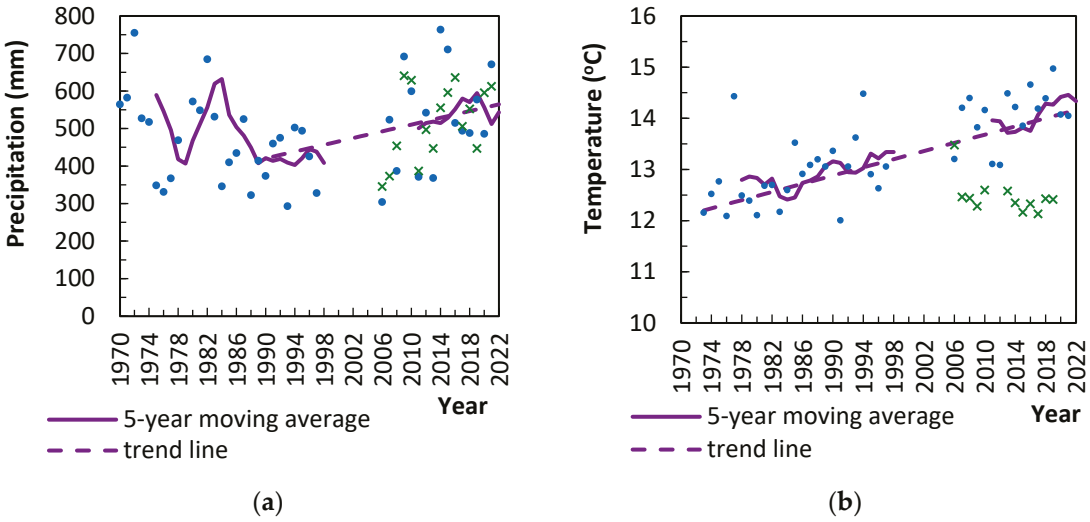

Figure 5. Mean annual: (**a**) rainfall and (**b**) temperature from the Kozani weather station (blue color) and Ptolemaida weather station (green color), northern Greece.

According to the meteorological stations' data, the study location in the Kardia lignite mine, in Ptolemais, had a Köppen climate classification of Cfa (moist with mild winters, wet all seasons with a hot summer), which is consistent with the updated 1-km resolution global maps of the Köppen–Geiger climate classification [28]. The average annual rainfalls at Ptolemais were 498.1 mm (±132.1 mm s.d.), and November was the wettest month with average monthly precipitation of 56.7 mm, while August was the driest month with an average monthly precipitation of 31.7 mm. The average annual temperature was 13.3 °C (±0.8 °C s.d.), with January being the coldest month, with an average temperature of 2.4 °C and the highest temperature of 6.1 °C. According to the meteorological data, there is a visible trend of long-term increase in temperature, presenting an average increase of approximately 2.2 °C over the last 50 years. Regarding precipitation, there seems to be an increasing trend during the period of the last 30 years.

Thornthwaite's water balance method [29,30] was used to predict the mean annual runoff for the unsaturated zone in the pit's catchment area and the Sarigiol hydrological basin. This method can provide mean annual estimates in close agreement with measured values [31]. The unsaturated zone's water balance during the time interval $(t,\ t+dt)$ is described through the moisture content B. The moisture content $B(t+dt)$ at the end of time dt is described by the following equation [30]:

$$B(t+dt) = B(t) + (N - V - R - SL\ )\ dt \tag{1}$$

where all quantities are expressed to the unit area, and $B\ (t)$ is the water content stored inside the unsaturated zone at the time t (mm), N is the precipitation rate (mm/month), V is the real evaporation (mm/month), R is the surface runoff outflow (mm/month), SL is the percolation rate (mm/month).

In the calculations, it was considered that deep percolation takes place when soil moisture reaches 70% of the field capacity (FC) [32], where FC is the amount of water

remaining when downward drainage has markedly decreased. Therefore, the following equations were applied for the different cases [30]:

$$B(t) + (N - V - R)dt \ \leq \ 0.7\ FC \text{ then } (SL)dt = 0 \tag{2}$$

$$F \leq B(t) + (N - V - R)dt \geq 0.7\ FC \quad \text{then } (SL)dt = 0.1\ (N - V - R)dt \tag{3}$$

$$B(t) + (N - V - R)dt \geq FC \qquad \text{then } (SL)dt = B(t) + (N - V - R)dt - FC \tag{4}$$

The real evaporation V was estimated as a portion of Thornwaite potential evaporation P. It was assumed that real evaporation takes place when soil moisture reaches 70% of the field capacity, and thus, the following equations were applied for the different cases:

$$B(t + dt) \ \geq \ 0.7\ FC \text{ then } V = P \tag{5}$$

$$B(t + dt) \ \leq 0.7\ FC \text{ then } V = P\left[0.188 + 2\ (B/FC) - 1.2\ (B/FC)^2\right] \tag{6}$$

The potential evaporation P is derived by the following equation:

$$P = 1.6\ (10\ t_n/I)^a \tag{7}$$

where t_n is the mean temperature of month n, I is a temperature coefficient of monthly temperature coefficients i_n summation ($I = \sum_{n=1}^{12} i_n$), where $i_n = (t_n/5)^{1.514}$ and a value can be determined as a polynominal function of the temperature coefficient I, where $a = 0.49239 + \left(1792 \times 10^{(-5)}\ I\right) - \left(771 \times 10^{(-2)}\ I^2\right) + \left(675 \times 10^{(-9)}\ I^3\right)$.

In addition, in the hydrological model it was assumed that real evaporation cannot exceed the available water derived from precipitation and soil moisture and thus, $(V)dt \leq (N - R)dt + B(t)$.

Considering the climate conditions in Greece, for the specific area, it is expected that soil moisture content reaches FC in April and thus, regarding the initial conditions of the unsaturated water balance at the time $t = 0$, then $B(0) = FC$ for April.

Sensitivity analysis performed towards field capacity FC for the unsuturated zone water balance Thornwaite model revealed the following linear relation between FC and percolation coefficient as SL percentage (%) of rainfall, which is taken as a percentage of precipitation, presenting a coefficient of determination $R^2 = 0.964$ (Figure 6):

$$SL = 32.429 - 0.0903\ FC \tag{8}$$

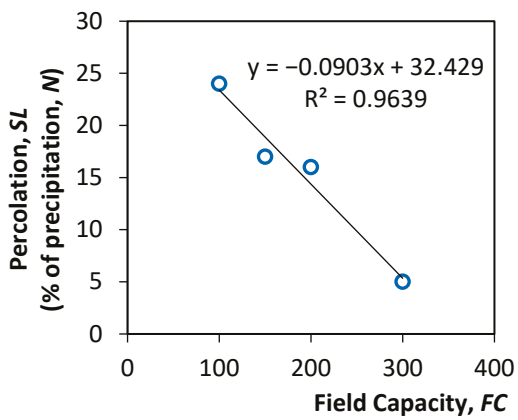

Figure 6. Sensitivity analysis of percolation rate SL, as a percentage of precipitation N, towards field capacity FC at the wider area of Ptolemais lignite field, northern Greece.

This relation helped in transforming FC values (deduced from $NDVI$ values) into percolation rate values SL.

According to the results (Table 1), for the hydrological cycle in the Sarigiol basin (2006–2021), the mean annual precipitation that the loose sediment basin receives is approximately 584 mm, while the real annual evaporation is estimated to be approximately 425 mm. Also, based on the 15-hydrological year annual water balance output, only 86 mm per year percolates down and recharges the unsaturated zone, which constitutes the long-term renewable recharge of the aquifer. Therefore, there is only one discharge from the Sarigiol basin, i.e., the surface runoff that occurs through the outflow of the Soulou River. In different historical time periods, either the Sarigiol aquifer discharges into the Soulou River or the Soulou River recharges the Sarigiol aquifer, depending on the groundwater level.

Table 1. Mean annual water balance for the unsaturated zone of the Sarigiol loose sediment basin.

Hydrological Cycle in Sarigiol Basin (2006–2021)	mm/yr	10^6 m^3/yr	Precipitation (%)
Mean annual precipitation	584	123	100
Mean annual real evaporation	425	90	73
Mean annual percolation	86	18	15
Mean annual runoff	72	15	12

2.3. Conceptual Model for the Pit Lake Long-Term Water Balance

In order to calculate the spatiotemporal evolution of the lake inside the Kardia open pit, a simplified conceptual hydrogeological model was developed (Figure 7), following the hydrogeological conceptual model of Louloudis et al. [33], in which the different origins of water inflows into the pit lake's body are presented. The inflows include (a) the groundwater inflows from the slope seepage face, (b) the surface runoff into the open pit, considering the open pit as a catchment area, and (c) water losses from the lake surface that occur due to direct evaporation processes which result in reducing the net recharge over the lake surface area (i.e., the hydrological processes of precipitation minus evaporative losses over the lake surface area).

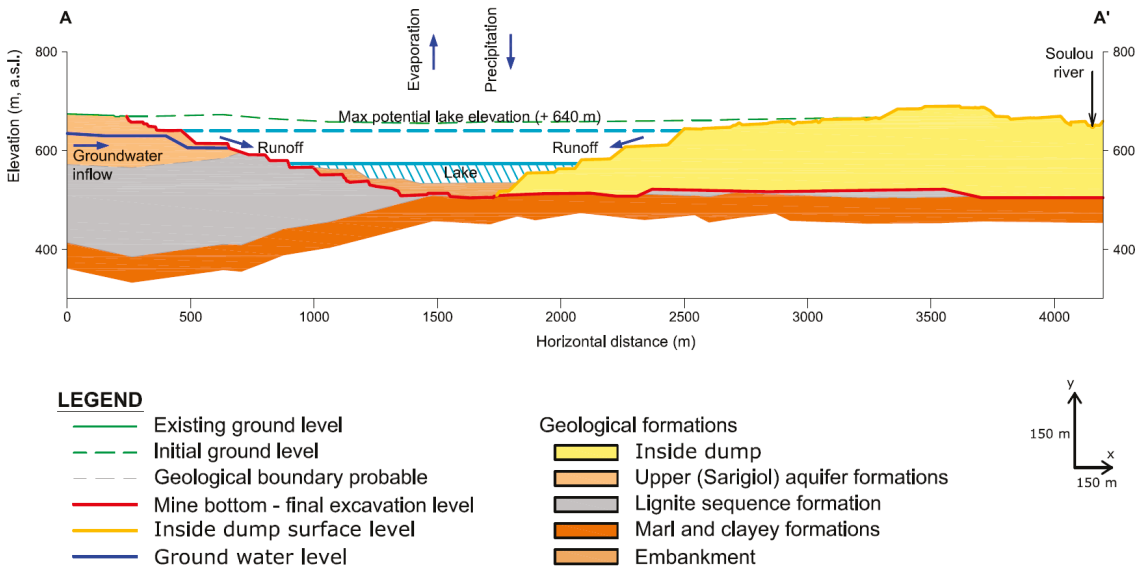

Figure 7. Hydrogeological conceptual model for Kardia pit lake, Greece (the location of the cross section A-A' is shown in Figure 3).

2.3.1. Groundwater Inflows

Since the dewatering measures adopted for mine protection will cease after the mine closure by the end of the year 2022, the inflowing groundwater will then begin to increase.

As a result, the open pit will fill with groundwater rebound, and the groundwater level will rise. The discharging water derives from the upper aquifer (i.e., above lignite stratification) and the confined aquifers inside the recently developed internal dumps.

For the initial conditions of the model in the year 2022 ($q_{(2022)}$) the groundwater inflow was calculated by Darcy's law [34] to be around 1.7×10^6 m^3. This quantity was cross-validated by the records of the water sump pumped quantities during the summer period in 2020, considered as baseflow of surficial hydraulic protection. Specifically, approximately 1.2×10^6 m^3 of groundwater inflow is pumped from the sumps, and 0.5×10^6 m^3 is pumped from the dewatering wells during the summer period. In addition, the seepage face of groundwater inflow into the excavation is also subjected to an evaporation procedure at mine's benches. For the Kardia mine, it is estimated that 70% of this quantity is evaporated; thus, only 30% of the groundwater inflow finally reaches and recharges at the pit lake's water body (i.e., around 0.6×10^6 m^3).

For each year i of the prediction period, the groundwater inflow $q(i)$ was estimated with respect to the surface lake water level h increase. More specifically, the groundwater inflow rate Q per unit face length A is calculated according to the following equation [35]:

$$q(i) = Q/A = K\left(H^2 - h^2\right)/2L \tag{9}$$

where K is the hydraulic conductivity, H is the aquifer's thickness, L is the influence radius of the open pit and h is the height of the lake water level calculated from the surface of the lignite sequence (considered as impermeable formation).

Hydraulic conductivity K ranges from 1.03 to 25.92 m/day, according to pumping tests analysis [36], with an average value of 13.48 m/day. The upper aquifer's thickness H is estimated in the order of 100 m [24,36] and thus, transmissivity T presents an average value in the order of 50 m^2/day on the west side of Kardia excavation and a range of 200–1200 m^2/day in the south region, while the average hydraulic gradient towards the excavation is approximately 2%, as depicted in Figure 3.

To delineate the groundwater inflow rate in the future, groundwater attenuation is considered due to the excessive irrigation consumptive use in the area. In the methodology followed for estimating the aquifer's depletion, the groundwater recharge of the Sarigiol aquifer around Kardia excavation was considered and the specific consumptive use SCU of irrigation water. The renewable recharge of the aquifer was estimated via Thornthwaite's water balance method (Table 1), while the SCU was derived from the evapotranspiration ET.

For the calculation of the crop water needs P_C, i.e., the water amount needed to meet the water loss through evapotranspiration, the following general relationship between the reference crop and the crop actually grown was used:

$$P_C = Kc \times ETo \tag{10}$$

where ETo is the reference crop evapotranspiration calculated by using the Blaney–Criddle method (mm/month) [37], while Kc is the crop factor derived from the normalized difference vegetation index ($NDVI$) [38] which was estimated equal to $Kc = 0.58$:

$$ETo = 30\ p\ (0.46\ T_{mean} + 8) \tag{11}$$

$$Kc = 1.18\ NDVI + 0.04 \tag{12}$$

$$NDVI = (NIR - RED)/(NIR + RED) \tag{13}$$

where T_{mean} is the mean daily temperature (°C), and p is the mean daily percentage of annual daytime hours depending on the latitude of the area. In addition, satellite-based $NDVI$ is computed from the red and near-infrared bands of the satellite by processing a satellite image acquired in 2018, as presented in Figure 8.

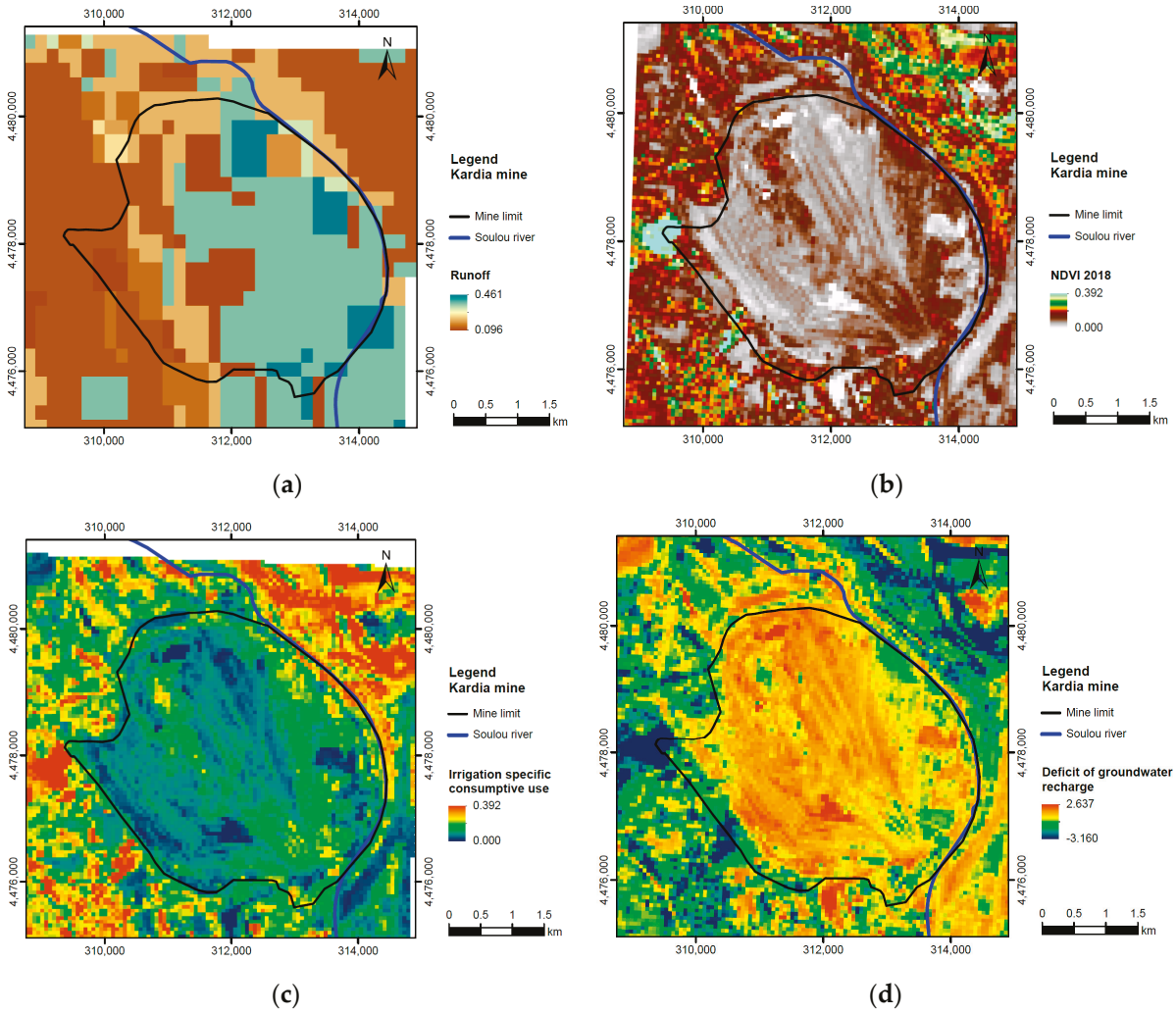

Figure 8. Spatial distribution of: (**a**) runoff coefficient by processing CN European raster; (**b**) spectra indices of $NDVI$ using Landsat-8 (image acquired in July 2018); (**c**) irrigation-specific consumptive use SCU (m^3/m^2); (**d**) annual drawdown in m, corresponding to the deficit of groundwater recharge due to excessive irrigation consumptive use of groundwater in Kardia lignite field, northern Greece (Coordinate Reference System GGRS87/Greek Grid).

The crop water need P_C is supplied to the crops by a combination of irrigation and rainfall. Therefore, the irrigation water need (IN, mm of water column/month) is the difference between the crop water need P_C and the effective rainfall Ne, i.e., the part of the rainfall effectively used by the plants:

$$IN = P_C - Ne \tag{14}$$

where Ne is estimated based on an empirical relationship presented by the Greek Land Reclamation Service of the Ministry of Agriculture [39] for the irrigation period from May to October:

$$Ne = N - (12 + 0.125\,N) \tag{15}$$

where N is the precipitation rate (mm/month).

Subsequently, the specific consumptive use SCU (m^3/m^2) was derived from the irrigation water need IN (mm/ month), using the methodology used by Louloudis and Stathopoulos [40]. A statistically significant correlation between irrigation water SCU (m^3/m^2) and $NDVI$ is shown in the Figure 9, presenting a coefficient of determination $R^2 = 0.781$. The linear regression analysis was performed by using the electric power

consumption of irrigation pumps in the area of the Sarigiol basin for 2018 and also by using a Landsat image acquired in July 2018 (Landsat-8: 15 July 2018). Based on the results, the following relationship between the irrigation water SCU (m^3/m^2) and $NDVI$ was used for the calculation of the SCU spatial distribution (Figure 8) for the Sarigiol basin area:

$$SCU = 1.539\ NDVI - 0.150 \tag{16}$$

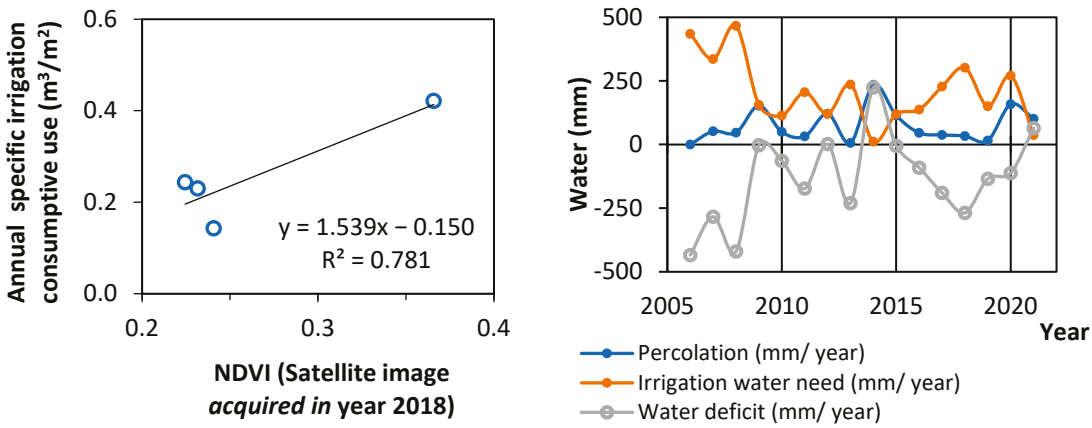

(**a**) (**b**)

Figure 9. (**a**) Irrigation-specific consumptive use (m^3/m^2) versus $NDVI$ using Landsat-8 (image acquired in July 2018) and (**b**) Percolation, irrigation and groundwater deficit time series during the period 2006–2021 in Sarigiol basin, Greece.

In addition, the deficit of groundwater recharge due to excessive irrigation consumptive use of groundwater near Kardia lignite field is presented in Figure 9, and its spatial distribution for the Sarigiol basin area is shown in Figure 8. The aquifer's annual drawdown due to the irrigation for the period from July to September was calculated as a difference between annual percolation and irrigation water need, divided by the storage coefficient considered equal to 0.1.

2.3.2. Surface Runoff

Surface runoff is the most essential inflow to the lake's body. Surface runoff also appears to be the more sensitive parameter in the lake's filling model so there is a need for precision in surface runoff coefficients introduced to the model. In order to achieve a reliable estimation of the surface runoff coefficient, Cr, in the hydrologically ungauged Kardia area, CN European raster file [41] was processed and the following equations were used [42,43]:

$$Cr = \left(P_{vol} - 0.2\left(\frac{25,400}{CN} - 254\right)\right)^2 / P_{vol}\left(P_{vol} + 0.8\left(\frac{25,400}{CN} - 254\right)\right) \tag{17}$$

$$P_{vol} = I_{TC}\ \ T_C \tag{18}$$

where P_{vol} is the volume of rainfall in mm, CN is the curve number, I_{TC} is the mean rainfall intensity (mm/h) for the time of the concentration T_C (h) which is described by Giandotti equation [44].

In Figure 8 spatial distribution of the runoff coefficient using CN European raster file is presented. Based on the results, inside the active mine area, high values of the runoff coefficient are calculated, in the order of 30% to 40%, whereas outside the perimeter of the excavation, in the zone of the loose sediments between Kardia excavations and Askion Mountain the calculated values hardly exceed 15%. In the western area on the consolidated sediments of Askion Mountain, a runoff coefficient of 20% in magnitude is calculated, while northern of this area near Mavropigi village insignificant values in the order of 5%

are revealed. Also, Lefkotopos and Lagorema streams in the region of Skopos Mountain consolidate carbonate sediments with a considerable runoff coefficient of 10% up to 20% in magnitude.

2.3.3. Water Losses from the Lake's Surface

There are many expressions to evaluate evaporation from the lake's water surface. The well-known, and highly accurate, Penman–Monteith approach involves many variables (air temperature, solar radiation, relative humidity, wind speed) [45–47] which in some cases may not be available. In these cases, adjusted equations with fewer weather parameters are used. Eagleman proposed a simple correlation between these parameters [48]:

$$E_A = 0.035\, e_S\ \ (100 - RH)^{1/2} \tag{19}$$

where E_A is the adjusted pan evaporation in inches per month (free surface evaporation), e_S is the saturation vapour pressure [49] corresponding to the mean monthly temperature in millibars (mb), and RH is the mean monthly percent relative humidity:

$$RH = (e_S\ /e) \times 100 \tag{20}$$

$$e_S\ = 6.11\, exp\ [17.269\ T/(273 + T - 36)] \tag{21}$$

$$e = 6.11\, exp\ [17.269\ T/(273 + T - 36)]\ (RH/100) \tag{22}$$

In the case of the Kardia mine, mean values are used, i.e., the mean monthly temperature (°C), the mean monthly rainfall (mm) and the mean monthly relative humidity (%).

2.3.4. Spatiotemporal Development of the Pit Lake

A crucial research question that arises from this study is whether the pit lake can be naturally filled in a reasonable time frame or is there a need for artificial recharge by flooding with river water. Thus, the spatiotemporal development of the water level inside the Kardia pit void was assessed by generating forecasts of the dependent variables (rainfall and temperature) via linear (autoregressive integrated moving average—ARIMA) and non-linear (artificial neural network—ANN) models, following the same methodology described by Louloudis et al., for the Amynteon mine pit lake [33].

2.4. Energy Transition Strategies in the Post-Mining Era

In the Kardia mine, the PPC energy transition strategy is based on the PV parks that will be developed in the surrounding area, inside and outside the mining exploitation area. Thus, energy storage units are required to supplement the variable renewable capacity. In this mine, the best conditions prevail for a PHS facility installation thanks to its morphology, high exploitation depth of approximately 150 m, and sizable pit lake volume. Therefore, a PHS facility could be used as a storage battery and would provide sufficient storage capacity to compensate for renewable energy fluctuations.

Analyzing the electricity demand is a prerequisite for optimal planning of a hybrid PHS system. Figure 10 presents a representative scheme for the hybrid pumped hydro storage (HPHS) plant operational schedule during daytime hours for the case study area of the Kardia mine. This scheme presents the integration of RES electricity production and the utilization of a hybrid plant. A linear programming optimization model using the simplex method [50] has been developed, where the objective function value addressed to the capacity factor [51] of the PV park is maximized. The main restriction is that the sum of the PV power produced, the energy released in PHS and the grid supplementary power should meet load demands. Another restriction concerns the water balance in the PHS system, where the quantity of the water pumped into the upper reservoir equals the quantity of the water released downstream into the lower reservoir.

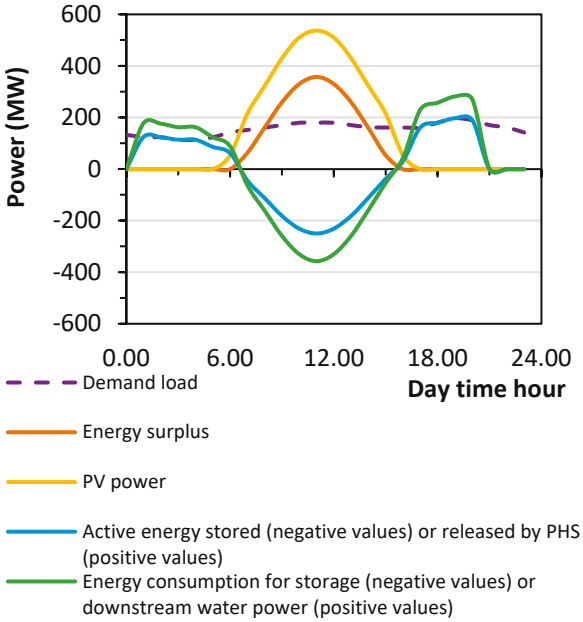

Figure 10. Representative scheme for the hybrid pumped hydro storage (HPHS) plant operational schedule during daytime hours and photovoltaic (PV) integration, considering the installation of a 270 MW PV plant in the Kardia mine.

In this idealized model, no legislative restrictions are taken into account regarding the deployment of energy storage by the PHS plant. According to the National Law provision (Law 3468, Government Gazette 129/A/27 June 2006) the total amount of electricity taken in from the network on an annual basis does not exceed 30 percent of the total amount of energy consumed for the filling of the storage system in that station. Thus only 30% of the energy produced by the PV plant is allowed to be stored using the PHS plant by utilizing the potential energy of water. Another assumption considered in the optimization problem is that the load demand distribution during daytime is set directly proportional to the electrical power distribution network flow [52]. In addition, the distribution system performance of the PV park during the daytime is set directly proportional to the distribution of the solar radiation production [53] during the daytime.

As depicted in Figure 10, the operation of the HPHS system dictates a pumping procedure between 7:00 and 16:00 and energy production in the rest of the 24 h cycle. The designed energy system for the PHS plant must be credible to cover the demand load of electricity during the whole day, providing efficient energy generation and a guaranteed rate. Consequently, when the energy system supplies more power than that required by the users (i.e., the total load produced is higher than the demand load), then this additional load is used to supply the PHS plant, and thus, some additional water can be stored in the upper reservoir of the plant. However, the "real" PHS storage load is lower due to energy losses.

For this purpose, representative synthetic time series, including load prediction data, must be generated during the design phase for the optimal planning of the HPHS system, aiming at the prediction of the potential energy storage. The potential energy storage P_e in a PHS complex required to supplement the PV park can be estimated by calculating the pumping energy consumption via the following formula, which is an expansion of Bernoulli's equation [54,55]:

$$P_e = (Q\,H)/(102\,n) \tag{23}$$

where P_e is the total power required (kW), Q is the flow rate (lt/s), H is the total head, i.e., the pressure head and elevation head (m), n is the combined effect of pumping efficiency and derating, and 102 is a unit conversion factor value. Pumping efficiency and derating

account for the operating efficiency of pumps, and efficiency losses between the energy required at the pump shaft and the total energy required [54].

The total power required to be stored in order to return it to the electric grid when needed can be obtained using two alternatives: (a) either by having a great hydraulic difference between the upper and lower reservoir, with a relatively small quantity of water per daily cycle uplift, (b) or by having a smaller hydraulic difference between the reservoirs, though with a larger quantity of pumped water. In addition, the head difference influences the efficiency of pumps and turbines [56]. The selection between the two options is mainly a financial decision since the magnitude of the project (mainly the number of units of pumps and generators, excavation volume of both reservoirs and area covered for PHS facilities to be mounted) is proportional to the required quantity of stored water. Thus, it affects the total cost. So, the option of a significant head difference could have the advantage of minimum fixed cost.

The required quantity of stored water and the head difference set the limits for the pit lake level variation LLV, which is a critical component in the design [10]. Based on this acknowledgment, a diagram that can help to select the appropriate altitude of the PHS upper reservoir water level can be the total power required P_e per unit m of water level daily fluctuation LLV in relation to the pit lake's level, as presented in the Section 3. This approach could help in the decision-making process and achieving a PHS plant's economic viability.

2.5. Economic Value

The prediction of the spatiotemporal evolution of the lake is crucial for achieving the financial efficiency of the HPHS project, by evaluating different levels of the lake's filling. The financial efficiency of each water level in the pit lake can be determined via performance indicators, i.e., net present value (NPV) and net cash recovery (NCR) of a cash flow series.

In the case of the Kardia pit lake, initial calculations of the economic feasibility of a PHS plant were performed with the help of the NPV method, where the values of alternative scenarios were evaluated. The NPV value indicates whether the overall lifetime costs of the project (benefits and costs of different scenarios), i.e., the investment, is less or more than the income generated. For example, for an investment project with a minimum design operational lifetime of up to 50 years, the following equation was used to estimate NPV [10]:

$$NPV_{real} = -I_o + \sum_{t=1}^{50} \left\{ (R_t - C_t)/q_r^t \right\} \tag{24}$$

where NPV_{real} is the NPV in real terms, considering also the inflation rate r and the interest rate i, C_t; R_t are costs and revenues at different points in time t, I_o is the initial investment at time $t = 0$ and q_r^t is the discounting factor which reflects the value of money in time t:

$$q_r^t = \{(1+i)/(1+r)\}^t \tag{25}$$

The component q_r^t in the equation above helps make the different cash flows in time comparable [10].

2.6. Geotechnical Issues to Be Considered in the Post-Mining Design

Several studies have sought to determine successful and unsuccessful cases of pit lakes in the post-closure mine phase. It has been documented that stability is improved as water levels increase inside the pit lake. Kavvadas et al. investigated the stability conditions that prevailed in decommissioning surface lignite mines in Greece [57], using the Amyntaion mine as a case study, where the pit is gradually filled with water. According to this report, it is shown that stability conditions are reinstated when the depth of water (critical depth) reaches approximately 15–35% of the final equilibrium condition, whereas, at higher lake levels, the safety factor is expected to increase significantly due to the beneficial effect of

the lake water pressure acting on the slope. Table 2 presents preliminary predictions in slope stability for different scenarios of lake water development inside the open pit [57].

Table 2. Variation in slope stability conditions related to the pit lake development in decommissioning surface lignite mines in Greece, used for preliminary prediction.

Lake Water Depth (Hw)/Height of the Slope (H)	FS/FSo*
0	1.0
0.1	<1.0
0.2	1.0
0.4	1.075
0.6	1.25
0.8	1.6

Note(s): * FS = Safety factor, FSo = initial FS when water depth Hw = 0. Source: [57].

In addition, in the early stages of the lake's development, more favorable slope stability conditions are expected to be achieved in only a few years. This result is associated with the fact that the surface area of the pit is smaller at deeper levels; thus, the depth of the water inside the pit increases rapidly in the early stages of the lake development.

Regarding the operation of the HPHS complex facility, in the daily cyclic process in the lower reservoir (i.e., the pit lake), excessive weathering and corrosion of the lake banks could appear, caused by the daily fluctuation of the head difference between the lower and the upper reservoir. Furthermore, the daily fluctuation induces an increase in water pressure at the pit lake banks; thus, slope instabilities could appear due to the fatigue effect. Consequently, adopting protection measures at the pit lake banks is a prerequisite, which could also affect the excavation volume and, as a result, the magnitude of the PHS complex facility.

3. Results and Discussion

3.1. Water Flux Trends and Forecast of Lake's Spatiotemporal Development

Predictive models to forecast rainfall in the near future, as well as surface runoff, evaporation, percolation rates and consumptive irrigation rates are generated for the next decade, from which the water balance of the lake's surface is derived. The results from the implementation of the NNAR model (neural network autoregression) with no seasonal participation are presented in Figure 11.

According to the NNAR predictions for the next decade, the maximum expected groundwater attenuation of the Sarigiol aquifer is estimated at 10 m (i.e., approximately one meter per year on average). This drawdown is due to excessive irrigation water demands [40], which allows the expectation that the groundwater level will be successively lowered below the elevation +635 m during our conceptual model of the lake filling time interval. Time series forecasts of annual drawdown for the next two decades are computed. This groundwater level attenuation was incorporated into the mathematical model for predicting the lake's water balance, where a 20% reduction in groundwater influxes to the lake's water body was introduced.

In addition, the lake's surface balance is displayed in Figure 11, as a result of the difference between evaporation and precipitation over the lake's surface. The results showed an increasing trend of yearly water losses in the lake's surface water balance due to a gradual increase in the water surface, as evaporation also increases.

Figure 12 displays the lake's spatiotemporal development based on the model developed in this study and the results from implementing the NNAR model. To highlight the influence of the time variable datasets, the different water inflows into the pit lake's body have been plotted together and are associated with the time component. The results indicate that, the filling of the lake model is very sensitive to surface runoff, which is described by an average value of 0.3 for the area inside the open pit (Figure 8). There is a clear decreasing trend of annual surface runoff due to the gradual decrease in the watershed area.

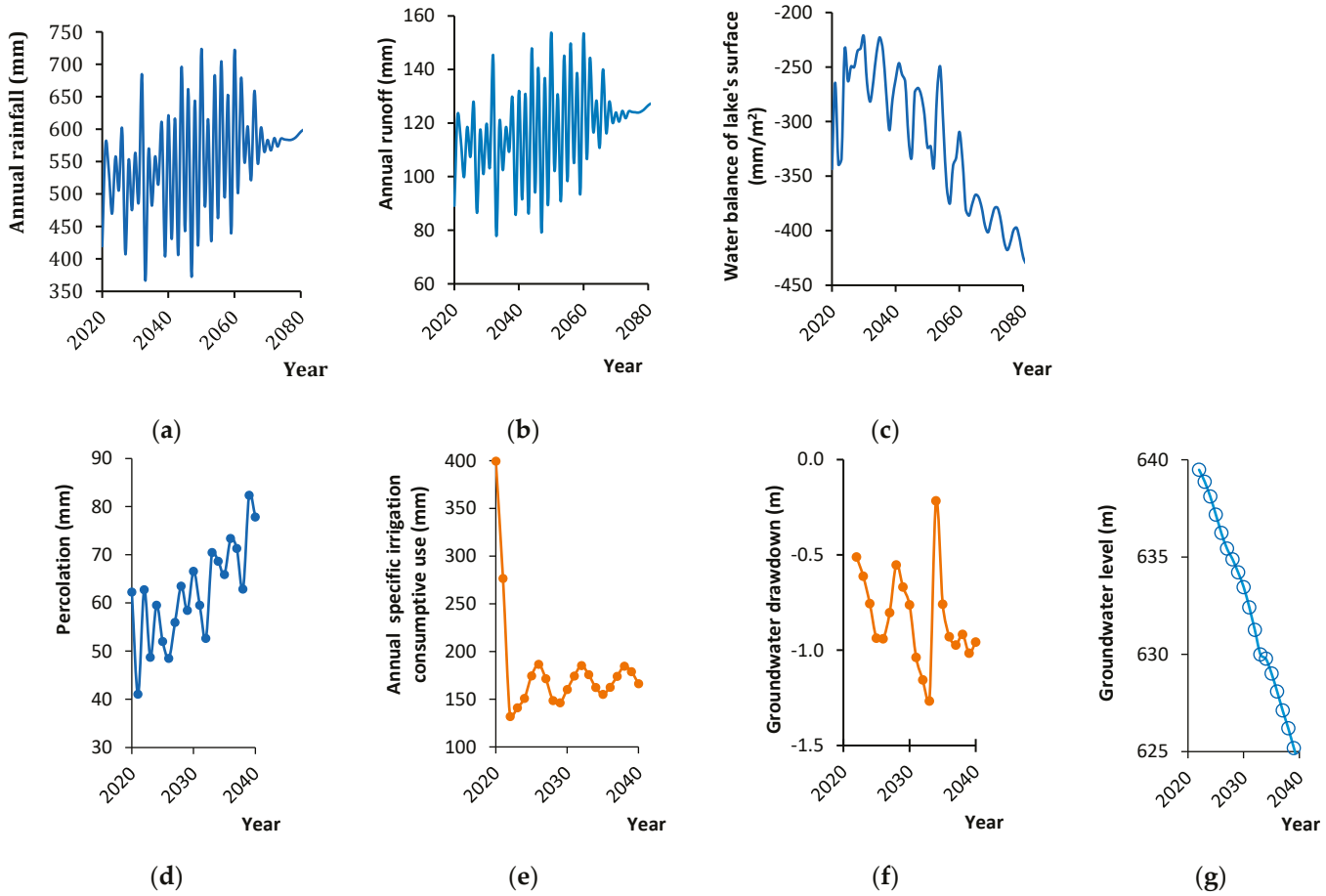

Figure 11. Artificial neural network prediction (NNAR) implemented for the Kardia lignite field area, northern Greece. NNAR results of the annual: (**a**) rainfall; (**b**) runoff; (**c**) water balance of lake's surface (precipitation minus evaporation on lake's surface); (**d**) percolation rate; (**e**) specific consumptive irrigation use; (**f**) drawdown (percolation minus groundwater attenuation as a result of irrigation consumption); (**g**) groundwater level in the Sarigiol aquifer (i.e., above the lignite sequence).

As the pit lake level and volume increase with time, the surface area of the pit decreases and thus, the surface runoff decreases. It is interesting, though, that, during the last phase of the lake's development, surface runoff still exceeds the lake's surface losses (water balance of lake's surface, i.e., precipitation minus evaporation on lake's surface). Despite the large water losses (in mm/m^2 of lake's surface) compared to surface runoff (in mm/m^2 of watershed surface) (Figure 11), the total annual surface runoff quantities exceed the water losses in the early stages of the lake's development (Figure 12).

The results of the lake's development displayed in Figure 12 indicate that the natural recharging of the lake is feasible. In the early stages, the lake expands rapidly, while in the last phase it does so very slowly. On the contrary, the lake's water body volume increases almost steadily. As a result, the maximum natural lake growth inside the pit can potentially cover almost 50% of the pit's total surface (Figure 2) in approximately 80 years, with a depth of approximately 117 m.

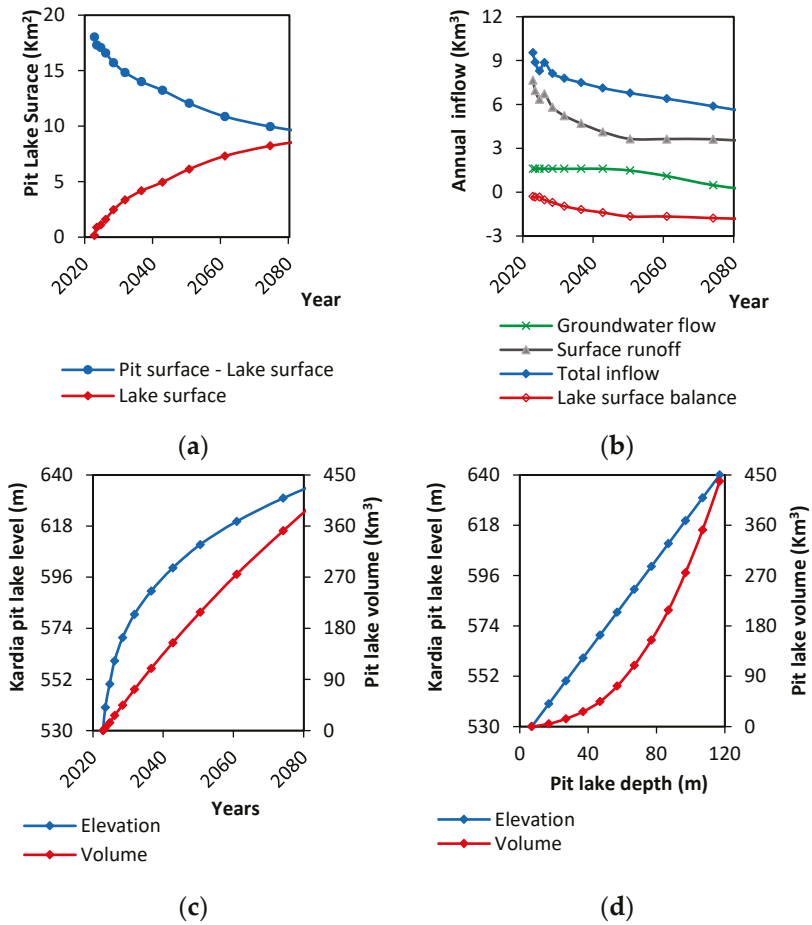

Figure 12. Forecast of the spatiotemporal development of the Kardia pit lake: (**a**) lake surface vs surface runoff decrease; (**b**) annual inflows and outflows; (**c**) the absolute elevations and gradual increase in stored water volume vs. time; (**d**) the absolute elevations and gradual increase in stored water volume vs. lake depth.

3.2. Evaluation of Potential Land Use Repurposing Scenarios

For the already closed lignite mine of Kardia, a preliminary evaluation was conducted for potential land use repurposing scenarios, by evaluating the landscape formed after the lignite exploitation activities terminated. Generally, in abandoned open pits, the pit void will eventually be filled with water at a specific time period. Thus, the viability of any repurposing land use scenarios should be evaluated concerning the spatiotemporal lake level development and the water coverage area compared to the pit's total surface.

In evaluating different land use scenarios, the energy transition potential in the specific region is of primary importance. It is considered with respect to long-term socioeconomic viability in the area. At the same time, the transition should be in line with the holistic policy framework developed by Greece to further develop renewable technology in the electricity sector and eventually achieve net-zero greenhouse-gas emissions. Consequently, repurposing land uses includes RES technology application in the remaining post-mining landscapes. Moreover, "Smart Post-mining" has to be developed in concert with "Green and Climate Smart Mining" [58], in a holistic approach so that the climate-driven clean energy transition is managed responsibly and sustainably.

Based on topographical criteria, from the digital elevation model (DEM) and the slope model implemented (Figure 2), it can be seen that the area between elevations +650 m and +680 m could be characterized as relatively flat. The flatness of this area makes it ideal for installing PV parks. Consequently, lake growth should not exceed the elevation of +650 m. Also, based on preliminary predictions as described in Table 2, stability conditions are

expected to be reinstated when the depth of lake water reaches approximately 22 m to 29 m, i.e., for pit lake elevations +545 m up to 552 m. Thus, adopting lower lake levels increases the risk of failure.

From the model developed in this study and the results from the implementation of the NNAR model, the maximum lake water level cannot exceed elevations +640 m ~ +650 m, as it is presented in Figure 12. This condition is due to hydraulic reasons, as this level is related to the groundwater level in the loose sediment aquifer overlying the lignite sequence. Considering the lake growth limitation, the flat area between elevations +650 m and +680 m could be examined for installing PV parks (Figure 13). This area is approximately 5 km^2, with an average inclination of approximately 3.5%.

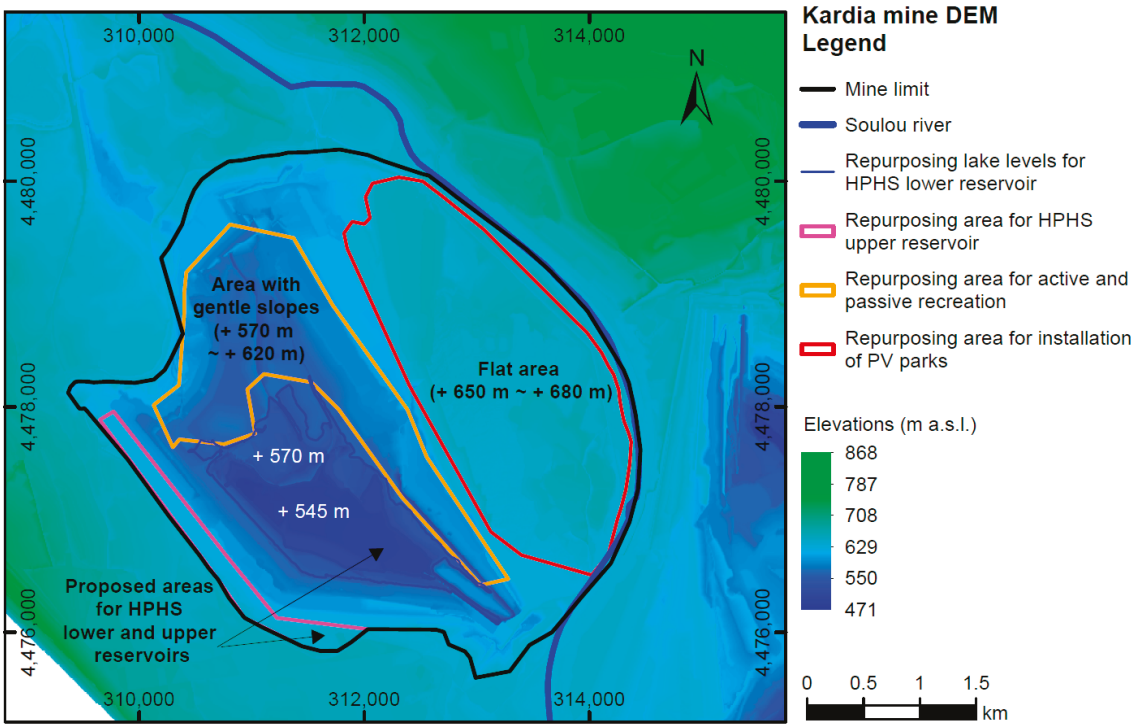

Figure 13. Land use repurposing inside the Kardia mine, Greece (Project Coordinate Reference System GGRS87/Greek Grid).

In addition, the area between elevations +570 m and +620 m on the lake's northeast side could be repurposed for active (such as swimming, diving, etc.) and passive recreation (such as biking trails, recreation forest park, road access network to the lake, entertainment facilities, etc.). This area appears to have gentle slopes presenting average inclinations in the order of 12~17% and covers approximately 3 km^2 of the surface.

An important issue emerging from these findings is that repurposing a PHS dam at the elevation of +545 m is feasible and can be achieved by naturally filling the pit lake for approximately three (3) years. Artificial recharging is also feasible if a fast filling is required to implement the PHS Project. More specifically, pumped water from Mavropigi and South field sumps could be diverted inside Kardia pit lake and, thus, fill the pit lake within a year.

Another alternative could be forming the lake water surface level at +570 m to implement the PHS and PV project. The findings from the implementation of the NNAR model suggest that this could be realized by naturally filling the pit lake in approximately seven (7) years. In the case of fast filling of the pit lake, this could be achieved in approximately three (3) years, i.e., four (4) years earlier.

The area on the southwest side of the lake is proposed for the upper reservoir installation of the PHS project. This area could be ideal for the location of the upper reservoir due to the proximity to both the lake (lower reservoir) and the Soulou River,

where, after the PHS operational start, the required discharge of overflow is prospected to be rejected. This area covers approximately 0.5 km^2 of the surface, with an average inclination of approximately 3%.

Based on these results, our findings indicate that the level + 570 m could cover the needs of a hybrid PHS plant (HPHS) and PV park while providing enough space for recreation projects on the lake banks and simultaneously ensuring slope stability. The stabilizing effect of the lake water pressure ensures more favorable slope stability conditions at higher lake levels. In addition, the stability conditions are further improved in case the PHS upper reservoir is mounted outside the mine exploitation area, at a safe distance from the excavations' slopes.

However, water pumping is required in such cases to maintain the level of the pit lake at a certain elevation. Thus, the pit lake water quality is an important parameter that could enable new beneficial end uses, such as exploiting the overflow of the pit lake water for irrigation purposes. For example, Figure 14 shows that the pit lake water is expected to have good quality and thus could be suitable for irrigation purposes. Moreover, waters are marked by salinization risk (measured on the x-axis by conductivity) rather than alkalinization risk (measured on the y-axis by sodium).

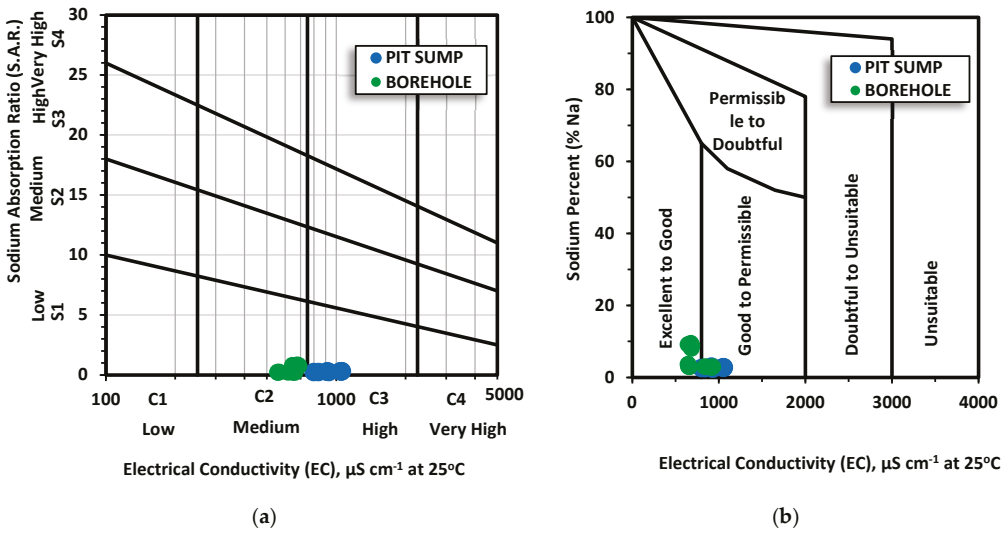

(**a**) (**b**)

Figure 14. Classification of groundwater and the mine's internal sump water for irrigation purposes: (**a**) diagram of sodium hazard (sodium adsorption ration) and salinity hazard (electrical conductivity) [59,60]; (**b**) suitability of water for irrigation use, according to Wilcox diagram [61].

3.3. PHS Plant Efficiency Potential

Figure 15 displays the potential energy storage P_e per unit m of the daily water level fluctuation (MW/ m of water fluctuation) in relation to the pit lake's elevation and volume, considering two different scenarios: a) in the case of the upper reservoir mounted inside the mine at the elevation +640 m a.s.l. and b) in the case of the upper reservoir mounted outside the mine exploitation area (i.e., +670 m a.s.l.). The graph shows that in the case of the Kardia mine and for a specific pit water level at + 570 m a.s.l., the estimated potential energy storage P_e is 40% higher in the case of a 30 m increase in the total head (H). In this example, lake level variation (LLV) at the pit lake was considered 1.0 m.

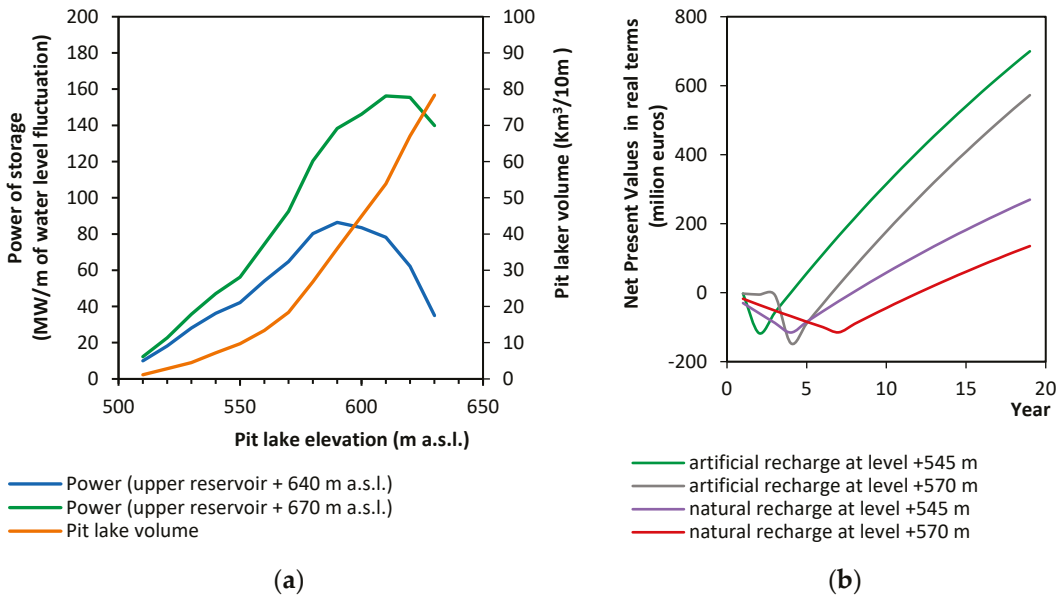

Figure 15. (**a**) Potential power of storage provision (MW/ m of water fluctuation) in relation to pit lake volume and water level, considering 1.0 m for the pit lake level variation (LLV), in the case of the upper reservoir mounted inside the mine (+ 640 m a.s.l.) and outside the mine exploitation area (+ 670 m a.s.l.) and, (**b**) indicative net present value in real terms (NPV_{real}) in alternative scenarios of the pit lake's elevation and filling procedure, inside the Kardia mine, Greece.

In a cash flow of revenues and expenses, net present values in real terms are evaluated for the next 20 years, as presented in Figure 15. Specifically, in the case of natural recharging of the pit lake, it is evident that an increase in the net present value in the order of 34% is estimated for the pit lake elevation +545 m, compared to the scenario where the pit lake elevation is formed at +570 m. In addition, in the case of artificial recharging of the pit lake, an increase in the net present value in the order of 18% is estimated for the pit lake elevation +545 m, compared to the scenario where the pit lake elevation is formed at +570 m, due to the late recovery of investment capital. In this initial economic feasibility evaluation, constant values of inflation $r = 0.07$ and rate of interest $i = 0.10$ were considered, whereas the same value of the investment I_o was considered in all scenarios.

4. Conclusions

In the abandoned Kardia lignite mine, the evaluation of land potential and resources is assessed regarding the lake water development inside the open pit area. Thus, the natural development of the lake is predicted, and different repurposing land uses are considered, concerning the energy transition potential in this specific region.

Initially, the spatiotemporal development of the lake in the final pit is calculated, and subsequently, land use repurposing is evaluated with regard to lake growth. Considering the energy transition strategies at this specific mine, it is concluded that on the east side of the lake, there is a relatively flat area of approximately 5 km^2, with an average inclination of approximately 3.5%. Therefore, this area is considered ideal for the installation of PV parks.

In addition, a hybrid PHS plant and PV park are examined to make provision for the energy surplus produced by the photovoltaic parks, aiming to meet electricity demand 24 h a day. Concentrating the solar power surplus with a PHS storage unit can provide flexible, renewable energy. This study has shown that repurposing a PHS dam at the elevation of + 545 m is feasible by naturally filling the pit lake for approximately three (3) years. Another scenario considering the elevation of +570 m could be achieved by recharging the pit within seven (7) years. Artificial recharging is also feasible in case fast filling is required due to the proximity of the Kardia lignite mine to two (2) other mines, the Mavropigi and

South field lignite mines. Therefore, a fast filling could be achieved in less than one (1) year for a lake elevation of +545 m and less than three (3) years for an elevation of +570 m.

From an engineering point of view, forming the lake at the level of +570 m is considered a better option for implementing the HPHS plant, as the stabilizing effect of the lake water pressure ensures more favorable slope stability conditions at higher lake levels. Moreover, the slope stability conditions are further improved in case the PHS upper reservoir is mounted outside the mine exploitation area, at a safe distance from the excavations' slopes.

Based on these results, our findings indicate that the surface lignite mine under investigation could cover both the needs of a hybrid PHS plant and PV park and, at the same time, provide enough space for activities (such as swimming, diving, etc.) and passive recreation (such as biking trails, recreation forest park, road access network to the lake, entertainment facilities, etc.) on the lake banks.

Forecasting the spatiotemporal development of a pit lake could help plan post-mining land repurposing, evaluate different scenarios, and find the optimum water level of the lake surface. The aim is to optimize land use repurposing in terms of economical design, efficiency and sustainability. In addition, the proximity of the Kardia lignite mine to the Mavropigi and South Field lignite mines is a crucial component to consider in the final design of the hybrid electric power project to make this project more economical, efficient and effective.

However, further studies need to be conducted to evaluate land repurposing, such as forecasting future water quality problems. In addition, different land repurposing projects are prospected to be developed under unfavorable geological settings of an abandoned open pit. This implies the need for detailed geotechnical (slope stability, bank erosion, corrosion, etc.) studies with the implementation of appropriate stability measures, in combination with a careful geotechnical monitoring application. To this end, continuous monitoring of ground movements is imperative. Therefore, this research question is an issue for further investigation and future model calibration when designing different repurposing land uses.

The whole system—pit lakes and alternative land repurposing scenarios—should be incorporated into a rational resources management program to optimize benefits to the land, water and electricity demands.

Author Contributions: Conceptualization, C.R. and G.L.; methodology, G.L., C.R., E.L. and E.M.; software, G.L. and E.M; validation, G.L., C.R., E.L., E.M. and G.K.; formal analysis, G.L., C.R., E.L, E.M. and G.K.; investigation, G.L., C.R., E.M. and G.K.; data curation, G.L., C.R., E.L., E.M. and G.K.; writing—original draft preparation, G.L. and E.L.; writing—review and editing, G.L., C.R. and E.M.; visualization, G.L., C.R., E.L., E.M. and G.K.; supervision G.L. and C.R.; project administration, C.R and G.L. All authors have read and agreed to the published version of the manuscript.

Funding: This research received no external funding.

Data Availability Statement: Data will be made available by the authors upon request.

Conflicts of Interest: The authors declare no conflict of interest.

References

1. European Commission. *A Clean Planet for All a European Strategic Long-Term Vision for a Prosperous, Modern, Competitive and Climate Neutral Economy*; Document EUR-Lex-52018DC0773. COM(2018) 773 Final; Publications Office of the European Union: Brussels, Belgium, 2018. Available online: https://eur-lex.europa.eu/legal-content/EN/TXT/?uri=CELEX:52018DC0773 (accessed on 11 January 2021).
2. European Commission. *The European Green Deal*; Document EUR-Lex-52019DC0640. COM(2019) 640 Final; Publications Office of the European Union: Brussels, Belgium, 2019. Available online: https://eur-lex.europa.eu/legal-content/EN/TXT/PDF/?uri=CELEX:52019DC0640&from=EN (accessed on 11 January 2021).
3. Sokratidou, A.; Gkouvatsou, E.; Roumpos, C.; Perdiou, A.; Tsagkarakis, G.; Kaimaki, S. Innovative Approaches to Coal Surface Mine Sites Rehabilitation: A Case Study of Megalopolis Lignite Fields. In Proceedings of the 14th International Symposium of Continuous Surface Mining, Thesaloniki, Greece, 24 September 2018; Sideri, D., Paraskevis, N., Eds.; pp. 437–452.

4. Pachauri, R.K.; Mayer, L.; Intergovernmental Panel on Climate Change (Eds.) *Climate Change 2014: Synthesis Report*; IPCC: Geneva, Switzerland, 2015; ISBN 978-92-9169-143-2. Available online: https://climate-adapt.eea.europa.eu/countries-regions/countries/greece (accessed on 11 January 2021).
5. Bistline, J.E.T.; Blanford, G.J. Value of Technology in the U.S. Electric Power Sector: Impacts of Full Portfolios and Technological Change on the Costs of Meeting Decarbonization Goals. *Energy Econ.* **2020**, *86*, 104694. [CrossRef]
6. Pavloudakis, F.; Roumpos, C.; Karlopoulos, E.; Koukouzas, N. Sustainable Rehabilitation of Surface Coal Mining Areas: The Case of Greek Lignite Mines. *Energies* **2020**, *13*, 3995. [CrossRef]
7. Bódis, K.; Kougias, I.; Taylor, N.; Jäger-Waldau, A. Solar Photovoltaic Electricity Generation: A Lifeline for the European Coal Regions in Transition. *Sustainability* **2019**, *11*, 3703. [CrossRef]
8. Nikolić, Z.; Nikolić, D. Practical Example of Solar and Hydro Energy Hybrid System—The Need for a Reversible Power Plant. In Proceedings of the International Conference on Renewable Electrical Power Sources, Belgrade, Serbia, 2 October 2018; Volume 6, pp. 165–171.
9. Keenan, J.; Holcombe, S. Mining as a Temporary Land Use: A Global Stocktake of Post-Mining Transitions and Repurposing. *Extr. Ind. Soc.* **2021**, *8*, 100924. [CrossRef]
10. Wessel, M.; Madlener, R.; Hilgers, C. Economic Feasibility of Semi-Underground Pumped Storage Hydropower Plants in Open-Pit Mines. *Energies* **2020**, *13*, 4178. [CrossRef]
11. McCullough, C.; Schultze, M.; Vandenberg, J. Realizing Beneficial End Uses from Abandoned Pit Lakes. *Miner* **2020**, *10*, 133. [CrossRef]
12. Holcombe, S.; Keenan, J. *Mining as a Temporary Land Use Scoping Project: Transitions and Repurposing*; The Social Aspects of Mine Closure Research Consortium; Centre for Social Responsibility in Mining, Sustainable Minerals Institute: Brisbane, Australia, 2020. Available online: https://www.mineclosure.net/elibrary/mining-as-a-temporary-land-use-industry-led-transitions-and-repurposing (accessed on 13 January 2021).
13. Gammons, C.H.; Harris, L.N.; Castro, J.M.; Cott, P.A.; Hanna, B.W. Creating Lakes from Open Pit Mines: Processes and Considerations, Emphasis on Northern Environments. *Can. Tech. Rep. Fish. Aquat. Sci. 2826* **2009**, 106.
14. Schultze, M. The Filling and Remediation of Pit Lakes in Former Open Cast Lignite Mines. Ph.D. Dissertation, Tech Univ Braunschweig Fac Archit Constr Eng Environ Sci, Braunschweig, Germany, 2012.
15. McCullough, C.D. Rehabilitation of Lake Kepwari: A Previously Acidic Mine Lake in Western Australia. In Proceedings of the IMWA—Mine Water Management for Future Generations; Stanley, P., Wolkersdorfer, C., Wolkersdorfer, K., Eds.; Cardiff University: Cardiff, Wales, UK, 2021; pp. 346–351. Available online: https://www.imwa.info/imwaconferencesandcongresses/proceedings/325-proceedings-2021.html (accessed on 20 January 2022).
16. Lund, M.; van Etten, E.; Polifka, J.; Vasquez, M.Q.; Ramessur, R.; Yangzom, D.; Blanchette, M.L. The Importance of Catchments to Mine-Pit Lakes: Implications for Closure. *Mine Water Environ.* **2020**, *39*, 572–588. [CrossRef]
17. Lund, M.A.; Blanchette, M. Can Saline Pit Lakes Offer Biodiversity Values at Closure? In Proceedings of the IMWA—Mine Water Management for Future Generations; Stanley, P., Wolkersdorfer, C., Wolkersdorfer, K., Eds.; Cardiff University: Cardiff, Wales, UK, 2021; pp. 300–306. Available online: https://www.imwa.info/imwaconferencesandcongresses/proceedings/325-proceedings-2021.html (accessed on 20 January 2022).
18. Blanchette, M.L.; Lund, M.A. Pit Lakes Are a Global Legacy of Mining: An Integrated Approach to Achieving Sustainable Ecosystems and Value for Communities. *Curr. Opin. Environ. Sustain.* **2016**, *23*, 28–34. [CrossRef]
19. Snashall, D.; Cox, K. Woodlawn Advanced Energy Recovery Centre Scoping Report; Australia. Available online: https://majorprojects.planningportal.nsw.gov.au (accessed on 11 May 2021).
20. Pytel, S.; Sitek, S.; Chmielewska, M.; Zuzańska-Żyśko, E.; Runge, A.; Markiewicz-Patkowska, J. Transformation Directions of Brownfields: The Case of the Górnośląsko-Zagłębiowska Metropolis. *Sustainability* **2021**, *13*, 2075. [CrossRef]
21. Ma, T.; Yang, H.; Lu, L.; Peng, J. Technical Feasibility Study on a Standalone Hybrid Solar-Wind System with Pumped Hydro Storage for a Remote Island in Hong Kong. *Renew. Energy* **2014**, *69*, 7–15. [CrossRef]
22. Matos, C.R.; Carneiro, J.F.; Silva, P.P. Overview of Large-Scale Underground Energy Storage Technologies for Integration of Renewable Energies and Criteria for Reservoir Identification. *J. Energy Storage* **2019**, *21*, 241–258. [CrossRef]
23. Kavvadas, M.J.; Marinos, P.G. Prediction of Groundwater Table Lowering for Lignite Open-Cast Mining in a Karstic Terrain in Western Macedonia, Greece. *Q. J. Eng. Geol. Hydrogeol.* **1994**, *27*, S41–S55. [CrossRef]
24. Louloudis, G. Hydrogeological conditions of South Lignite Bearing Field of Ptolemais region. Confrontation of groundwater problems during the exploitation. Ph.D. Dissertation, Natl Tech University Athen Sch Min Metall Eng, Athens, Greece, 1991. (In Greek)
25. Dimitrakopoulos, D.; Grigorakou, E. Aquatic Balance of Vegoritis Lake, West Macedonia, Greece, Ralated to Mining Activity. In *Proceedings of the Mine Water 2004—International Mine Water Association Symposium 1*; Jarvis, A.P., Dudgeon, B.A., Younger, P.L., Eds.; University of Newcastle: Newcastle upon Tyne, UK, 2004; pp. 201–207. Available online: https://www.imwa.info/imwaconferencesandcongresses/proceedings/189-proceedings-2004.html (accessed on 20 January 2022).
26. Koukouzas, N.; Ward, C.R.; Li, Z. Mineralogy of Lignites and Associated Strata in the Mavropigi Field of the Ptolemais Basin, Northern Greece. *Int. J. Coal Geol.* **2010**, *81*, 182–190. [CrossRef]
27. Kavvadas, M.; Roumpos, C.; Schilizzi, P. Stability of Deep Excavation Slopes in Continuous Surface Lignite Mining Systems. *Geotech. Geol. Eng.* **2020**, *38*, 791–812. [CrossRef]

28. Beck, H.E.; Zimmermann, N.E.; McVicar, T.R.; Vergopolan, N.; Berg, A.; Wood, E.F. Present and Future Köppen-Geiger Climate Classification Maps at 1-Km Resolution. *Sci. Data* **2018**, *5*, 180214. [CrossRef] [PubMed]
29. Thornthwaite, C.W.; Mather, J.R. *The Water Balance*; Drexel Institute of Technology, Laboratory of Climatology, N.J. Publications in Climatology, 1955; Volume VIII, p. 104. Available online: https://www.jstor.org/stable/210739?origin=crossref (accessed on 20 January 2022).
30. Kinzelbach, W. *Groundwater Modelling: An Introduction with Sample Programs in BASIC*; Developments in water science; Elsevier: Amsterdam, The Netherlands; Oxford, UK; New York, NY, USA; Tokyo, Japan, 1986; ISBN 978-0-444-42582-9.
31. Calvo, J.C. An Evaluation of Thornthwaite's Water Balance Technique in Predicting Stream Runoff in Costa Rica. *Hydrol. Sci. J.* **1986**, *31*, 51–60. [CrossRef]
32. Blau, R.V.; Hoehn, P.; Hufschmied, P.; Werner, A. Ermittlung Der Grundwasserneubildung Aus Niederschlägen. *Gas Wasser Abwasser Schweiz. Ver. Des Gas- Und Wasserfaches* **1983**, *63*, 45–54.
33. Louloudis, G.; Louloudis, E.; Roumpos, C.; Mertiri, E.; Kasfikis, G.; Chatzopoulos, K. Forecasting Development of Mine Pit Lake Water Surface Levels Based on Time Series Analysis and Neural Networks. *Mine Water Environ.* **2021**, *41*, 458–474. [CrossRef]
34. Manning, J.C. *Applied Principles of Hydrology*, 3rd ed.; Prentice Hall: Hoboken, NJ, USA, 1997.
35. Dupuit, J. *Theoretical and Practical Studies on the Movement of Water in Open Channels and through Permeable Soils*; Dunod: Paris, Frence, 1863. (In French)
36. Krassakis, P.; Pyrgaki, K.; Gemeni, V.; Roumpos, C.; Louloudis, G.; Koukouzas, N. GIS-Based Subsurface Analysis and 3D Geological Modeling as a Tool for Combined Conventional Mining and In-Situ Coal Conversion: The Case of Kardia Lignite Mine, Western Greece. *Mining* **2022**, *2*, 297–314. [CrossRef]
37. Zhan, G.; Lin Shelp, M. *Modified Blaney-Criddle Method—An Empirical Approach to Estimate Potential Evaporation Using Air Temperature*; The University of Western Australia: Perth, Australia, 2009; pp. 461–471.
38. Tasumi, M.; Allen, R.G.; Trezza, R. Calibrating Satellite-Based Vegetation Indices to Estimate Evapotranspiration and Crop Coefficients. In *Proceedings of the USCID Water Management Conference*; Wichelns, D., Anderson, S.S., Eds.; U.S. Committee on Irrigation and Drainage: Denver, CO, USA, 2006; pp. 103–112.
39. Memmos, N. *Soil Survey Report of the Drained Giannitsa Lake*; Ministry of Agriculture, Sector of Land Reclamation Service (YEB, Acronym in Greek): Thessaloniki, Greece, 1973; *unpublished*. (In Greek)
40. Louloudis, G.; Stathopoulos, N. Irrigation Water Consumptive Use Changes in South Ptolemais Lignite Bearing Hydrogeological Basin (Greece) Using NDVI Remotely Sensed Data. In *Proceedings of the 15th Internat ional Congress of the Geological Society of Greece*; Kranis, H., Ed.; Bulletin of the Geological Society of Greece; Harokopio University of Athens: Athens, Greece, 2019; Volume 7, pp. 611–612. Available online: https://ejournals.epublishing.ekt.gr/index.php/geosociety/issue/view/1265 (accessed on 20 January 2022).
41. Panagos, P.; Van Liedekerke, M.; Jones, A.; Montanarella, L. European Soil Data Centre: Response to European Policy Support and Public Data Requirements. *Land Use Policy* **2012**, *29*, 329–338. [CrossRef]
42. McCuen, R.H.; Bondelid, T.R. Relation Between Curve Number and Runoff Coefficient. *J. Irrig. Drain. Div.* **1981**, *107*, 395–400. [CrossRef]
43. Kim, N.; Shin, M.-J. Estimation of Peak Flow in Ungauged Catchments Using the Relationship between Runoff Coefficient and Curve Number. *Water* **2018**, *10*, 1669. [CrossRef]
44. Giandotti, M. Previsione delle piene e delle magre dei corsi d'acqua. In *Memorie e Studi Idrografici*; Ministero dei LL.PP., Servizio Idrografico Italiano: Rome, Italy, 1934; Volume 8, pp. 107–117.
45. Penman, H.L. Natural Evaporation from Open Water, Bare Soil and Grass. *Proc. R. Soc. Lond. A* **1948**, *193*, 120–145. [CrossRef]
46. Sellers, W.D. *Physical Climatology*; The University of Chicago Press: Chicago, IL, USA, 1965.
47. Tetens, O. About some meteorological terms. *J. Geophys.* **1930**, *6*, 297–309. (In German)
48. Eagleman, J.R. Pan Evaporation, Potential and Actual Evapotranspiration. *J. Appl. Meteorol. Climatol.* **1967**, *6*, 482–488. [CrossRef]
49. Monteith, J.; Unsworth, M. *Principles of Environmental Physics: Plants, Animals, and the Atmosphere*; Academic Press: Warszawa, Poland, 2013; Volume 4, ISBN 978-0-12-386910-4.
50. Gass, S.I. Linear Programming. In *Encyclopedia of Statistical Sciences*; Kotz, S., Read, C.B., Balakrishnan, N., Vidakovic, B., Johnson, N.L., Eds.; John Wiley & Sons, Inc.: Hoboken, NJ, USA, 2006; p. ess1466.pub2. ISBN 978-0-471-66719-3.
51. Boretti, A.; Castelletto, S.; Al-Kouz, W.; Nayfeh, J. Capacity Factors of Solar Photovoltaic Energy Facilities in California, Annual Mean and Variability. *E3S Web Conf.* **2020**, *181*, 02004. [CrossRef]
52. Tyralis, H.; Karakatsanis, G.; Tzouka, K.; Mamassis, N. Data and Code for the Exploratory Data Analysis of the Electrical Energy Demand in the Time Domain in Greece. *Data Brief* **2017**, *13*, 700–702. [CrossRef]
53. Koudouris, G.; Dimitriadis, P.; Iliopoulou, T.; Mamassis, N.; Koutsoyiannis, D. Investigation on the Stochastic Nature of the Solar Radiation Process. *Energy Procedia* **2017**, *125*, 398–404. [CrossRef]
54. Faour, K. *Farm Budget Handbook, Southern NSW-Irrigated Winter Crops 2001*; NSW Agriculture, 2001. Available online: https://lib.k-state.edu/gracroplands/cite.php?CiteID=3758 (accessed on 20 January 2022).
55. Gemitzi, A.; Lakshmi, V. Estimating Groundwater Abstractions at the Aquifer Scale Using GRACE Observations. *Geosciences* **2018**, *8*, 419. [CrossRef]

56. Pujades, E.; Orban, P.; Bodeux, S.; Archambeau, P.; Erpicum, S.; Dassargues, A. Underground Pumped Storage Hydropower Plants Using Open Pit Mines: How Do Groundwater Exchanges Influence the Efficiency? *Appl. Energy* **2017**, *190*, 135–146. [CrossRef]
57. Kavvadas, M.; Roumpos, C.; Servou, A.; Paraskevis, N. Geotechnical Issues in Decommissioning Surface Lignite Mines—The Case of Amyntaion Mine in Greece. *Mining* **2022**, *2*, 278–296. [CrossRef]
58. Jiskani, I.M.; Cai, Q.; Zhou, W.; Ali Shah, S.A. Green and Climate-Smart Mining: A Framework to Analyze Open-Pit Mines for Cleaner Mineral Production. *Resour. Policy* **2021**, *71*, 102007. [CrossRef]
59. Richards, L.A.; Allison, L.E.; Brown, J.W.; Hayward, H.E.; Richards, L.A.; Bernstein, L.; Fireman, M.; Pearson, G.A.; Wilcox, L.V.; Bower, C.A.; et al. *Diagnosis and Improvement of Saline and Alkali Soils*; Agricultural Handbook No. 60; Salinity Laboratory, Soil and Water Conservation Research Branch, Agricultural Research Service, US Department of Agriculture: Washington, DC, USA, 1954; pp. 69–82.
60. Wilcox, L.V. *Classification and Use of Irrigation Waters*; Salinity Laboratory, US Department of Agriculture: Washington, DC, USA, 1955; Circular No. 969; pp. 1–19.
61. Wilcox, L.V. *The Quality of Water for Irrigation Use*; Salinity Laboratory, US Department of Agriculture: Washington, DC, USA, 1948; Technical Bulletin No. 962; pp. 1–40. [CrossRef]

water

MDPI

Article

Spatiotemporal Analysis of Groundwater Storage Changes, Controlling Factors, and Management Options over the Transboundary Indus Basin

Kashif Mehmood [1,2,*], Bernhard Tischbein [1], Martina Flörke [3] and Muhammad Usman [4]

[1] Center for Development Research (ZEF), University of Bonn, Genscherallee 3, 53113 Bonn, Germany
[2] Department of Irrigation & Drainage, University of Agriculture, Faisalabad 38040, Pakistan
[3] Engineering Hydrology and Water Resources Management, Ruhr-Universität Bochum, 44801 Bochum, Germany
[4] Department of Geoecology, Institute of Geosciences and Geography, Martin Luther University, 06099 Halle, Germany
* Correspondence: kashif.mehmood@uni-bonn.de

Abstract: Intensive groundwater abstraction has augmented socio-economic development worldwide but threatens the sustainability of groundwater resources. Spatiotemporal analysis of groundwater storage changes is a prerequisite to sustainable water resource management over river basins. To estimate the groundwater storage changes/anomalies (GWCs) in the Indus River Basin (IRB), where observation wells are sparse, Gravity Recovery and Climate Experiment, the Global Land Data Assimilation System, and the WaterGAP Hydrological Model data were employed. The groundwater storage changes and controlling factors were investigated at three tier levels (TTLs), i.e., the basin, river reach, and region, to explore their implications on regional water resource management and provide management options at each level. Overall, the IRB groundwater declined from January 2003 to December 2016, with a relatively higher rate during 2003–2009 than during 2010–2016. Spatially, according to a reach-specific analysis, 24%, 14%, and 2% of the upper, middle, and lower reaches of the IRB, respectively, were indicated by a 'severe groundwater decline' over the entire period (i.e., 2003–2016). The GRACE-based GWCs were validated with in situ data of two heterogeneous regions, i.e., Kabul River Basin (KRB) and Lower Bari Doab Canal (LBDC). The analysis showed a correlation (R^2) of 0.77 for LBDC and 0.29 for KRB. This study's results reveal that climatic variations (increase in evapotranspiration); anthropogenic activities, i.e., pumping for irrigation; and water allocations in these regions mainly drive the groundwater storage changes across the Indus Basin.

Keywords: Kabul River Basin; groundwater dynamics; GRACE; WGHM; GLDAS; anthropogenic activities

1. Introduction

According to global estimates, approximately 43,000 km^3 of renewable freshwater resources are being fed to rivers, lakes, and aquifers annually, among which 70% is consumed by agriculture, 19% by industry, and 11% by households [1,2]. Presently, 38% of the global irrigated area (i.e., 307 million hectares) is contingent on groundwater [3]. In the Indus River Basin (IRB), where canal water supplies are unreliable and insufficient, groundwater is used independently or in conjunction with surface water. As irrigation in this region is sourced mainly from groundwater [4,5], the IRB aquifer is on the brink of an alarming water crisis due to large-scale groundwater extraction [6]. Therefore, the basin's sustainability requires proper water governance, management, and usage, especially given the complex, diversified hydrology and geopolitical nature of IRB. The key drivers of the basin's economy are agriculture and industry. Competition among the

primary users (agriculture, industry, domestic, and the environment) is spiraling as agriculture intensifies, the population grows, and people migrate to the cities [7]. Over the past several years, the continuously varying climate conditions and expansion of agricultural lands have altered the crop irrigation requirements, placing new demands on surface and groundwater resources [8,9]. Consequently, the groundwater resources in IRB have been overexploited [10].

In the Indus Basin, the overall water supply from groundwater has increased by 60% since 1960 as fresh aquifer systems are continuously pumped to meet the growing domestic and agricultural water demands [6,11]. Therefore, the groundwater aquifer system must be carefully assessed through critical long-term analysis of the groundwater storage changes (GWCs). Such an assessment builds a baseline for sustainable water use and its management. Ground-based measurement could provide a best estimate of changes in groundwater storage. However, ground-based observations are expensive and limited on spatial and temporal scales, especially in IRB, so groundwaters cannot be thoroughly monitored at different levels (regions and reaches). In particular, the limited network of observation wells reduces the understanding of the water cycle [12,13]. Policymakers and researchers believe that because there is a lack of in situ observations, groundwater regulation and the adoption of area-specific management strategies are severely compromised, especially under the effects of climate change [14]. To address these issues, many researchers are observing groundwater storage variations in real time by remote sensing observations supported by land-hydrological models at global and regional scales [5,15,16]. For example, Cheema et al. [5] employed satellite-based evapotranspiration (ET) and precipitation (P) data in the process-based Soil and Water Assessment Tool and estimated the groundwater depletion in the irrigated Indus Basin. Since the launch of the Gravity Recovery and Climate Experiment (GRACE) satellite, groundwater storage variations have been observed at different spatial and temporal scales [17] and the WaterGAP v2.2d Hydrological Model (WGHM) has emerged as a robust and qualitatively high-performing dataset of groundwater variations. The temporal changes in gravity observed by twin satellites reflect the changes in terrestrial water storage (TWS) [18]. TWS, obtained by summing the groundwater, snow water equivalent (SWE), soil moisture (SM), and surface water storage, represents the water stored above and underneath the Earth's surface [19]. Therefore, to isolate GWCs from TWS estimated by GRACE, water storage components must be subtracted from other auxiliary datasets of hydrological models. Many researchers have already combined GRACE data with land-hydro models to study the inter-annual changes in TWS and GWCs over the Indus Basin [20–22] and other aquifer systems around the globe [23–29]. However, most of these studies analyzed TWS and GWC variations on the catchment scale; a comprehensive evaluation of GWCs over the Indus Basin is lacking at different tier levels, i.e., the basin, river reach, and region. Normally, TWS and GWC variations are mainly caused by the combined effect of climate variability and human interventions [30]. Climatic parameters, i.e., precipitation (P), runoff (R), evapotranspiration (ET), and glacier recession, are influential factors of the changes in TWS and GWC [31]. Anthropogenic activities, i.e., groundwater abstraction, land use, and irrigation, also impact TWS and GWCs in populated areas [32]. Hence, it is important to investigate GWC and its controlling factors in IRB to ensure sustainable development of the basin as a whole. The water management in IRB is administered under the Indus Water Treaty 1960 at the international level [33], and administrative regulations are implemented province-wide under the Water Apportionment Accord 1991 at the national level [34]. Therefore, in addition to basin-scale studies, it is imperative to investigate the spatiotemporal dynamics of groundwater and its controlling factors at the regional (provincial) level to provide management options for each management unit. Due to the heterogeneity that exists among different reaches of IRB in terms of topography, land use, climate and agroecological conditions, and surface water distribution quotas, IRB was divided into three reaches (i.e., upper, middle, and lower). Due to these heterogeneities, there is considerable variability in the socio-economic conditions of the above-mentioned reaches. Therefore, hypothetically, human and natural controlling factors do vary among these reaches. In this regard, it is imperative to examine the groundwater changes both in space and time at the reach level in IRB.

Considering the limitations of previous studies in the Indus Basin [5,17,20,21,35–39], the novelty being captured in this study includes the following: (i) investigation of the groundwater dynamics at three tier levels (TTLs), i.e., the basin, river reach, and region, using GRACE and GLDAS for the period 2003–2016 to explore their implications on regional water resources management; (ii) assessment of the controlling factors (climatic and anthropogenic) at three tier levels to mitigate the vulnerability of groundwater resources; and (iii) identification of the hotspots of groundwater change patterns by decomposing and analyzing time series of the GRACE-extracted GWC, the Potential Groundwater Use (PGWUSE), and the Potential Groundwater Withdrawal (PGWWW) to explore groundwater management options.

2. Materials and Methods

2.1. Study Area

The area coverage of IRB is approximately 1.12 million km^2. It is shared among Pakistan (47%) and India (39%), followed by China (8%) and Afghanistan (6%) [2] and is situated between 66.3–82.47° E longitude and 24.63–37.05° N latitude (Figure 1). The Indus River (approximately 3000 km long) originates in the Tibetan Plateau near Mount Kailash (altitude 5500 m) and traverses towards the Arabian Sea [40]. The tributaries of IRB are the Indus, Jhelum, Chenab, Ravi, Sutlej, and Bias Rivers. The eastward-flowing tributary is the Chitral River, which originates in Pakistan, flows towards Afghanistan, and then drains into the Indus River in Pakistan [41]. The basin's climate ranges from subtropical arid and semiarid to temperate sub-humid on the plains of the Sindh and Punjab provinces to alpine in the northern mountainous highlands [2]. The average annual precipitation varies from 100 to 500 mm in the lowlands to approximately 2000 mm in the mountainous ranges. Moreover, the snowfall at higher altitudes (>2500 m) accounts for a significant part of the river flows in IRB. Although the higher peaks in the Upper Indus Basin (UIB) restrict the intrusion of monsoons, the low-lying areas in the northwest of the basin are subjected to monsoon rainfall, influencing GWCs over the basin.

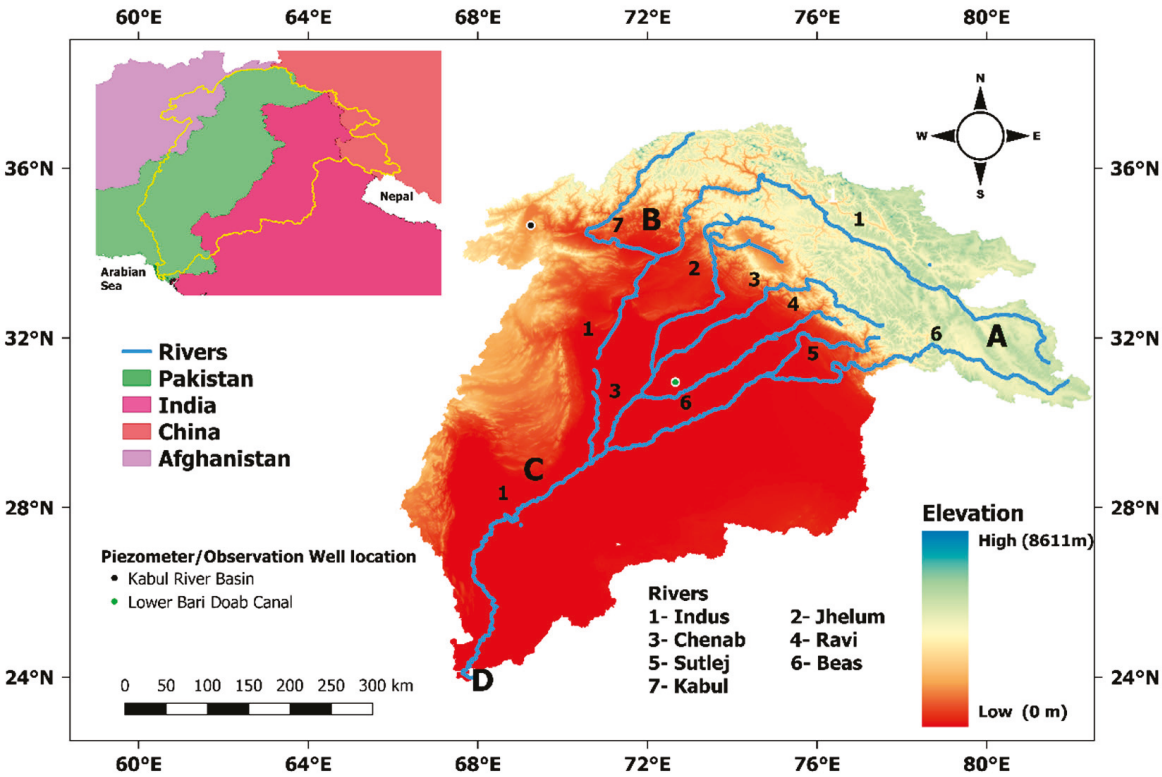

Figure 1. Transboundary Indus Basin with its tributaries and digital elevation model.

IRB is divided into upper, middle, and lower reaches based on its topography and climate. The upper reach includes Kashmir, Gilgit Baltistan, and Himachal Pradesh, which constitute the major watershed of IRB (points A to B). The middle reach (points B to C) comprises the major portions of Pakistani Punjab and Indian Punjab (the food basket of Pakistan and India), which produces most agricultural products and secures the region's food supply. The lowest part of the reach consists of Sindh (points C to Arabian sea), as shown in Figure 1. Agricultural production is influenced by waterlogged and saline agricultural lands in Sindh and some portions of Baluchistan.

Geologically, IRB is dominated by thick quaternary sediments. These sediments are mainly alluvial and deltaic deposits of fine- to medium-grained silt, sand, and clay. Coarser sands and gravels are present on the plain's upland margins while sand deposits can be found at the east of the Indus Plain (i.e., Thar and Cholistan). Cenozoic and Mesozoic sedimentary rocks can be found in a north–south region located at the west of the Indus Plain, which stretches from Peshawar to Karachi. Older sediments (Paleozoic) and crystalline base rocks (e.g., granites and metamorphic) are mainly found in the north, including Khyber Pakhtunkhwa, Jammu and Kashmir, and Gilgit regions. Groundwater yields from these sediments are typically in the range of 50–300 m^3/h down to a depth of 150 m.

2.2. Data Sources

We extracted the monthly TWS data of GRACE RL-06 released by the National Aeronautics and Space Administration (NASA) from 2003 to 2016, covering the globe with a spatial resolution of $1^\circ \times 1^\circ$. The GRACE landmass datasets of three laboratories, namely, the Centre for Space Research (CSR), Jet Propulsion Laboratory (JPL), and Geo Forschungs Zentrum Potsdam (GFZ), were obtained from the NASA website (www.jpl.nasa.gov accessed on 17 December 2019) supported by the NASA MEASUREs Programme [42–45]. The gridded surface-mass anomalies were derived from GRACE mission measurements and estimated the Earth's mean gravity at the specified time. For the JPL datasets, scaling factors were applied to convert the 3-degree gaussian filter resolution to 1-degree spherical harmonics solutions. These grids represent the storage of the terrestrial water cycle and ice magnitudes over the entire land. Furthermore, the non-captured atmospheric and oceanic processes are included in the corresponding GRACE component. The SM, SWE, and canopy water storage (CWS) were collected from GLDAS_NOAH10_M_001 at a $1^\circ \times 1^\circ$ spatial resolution [46]. The data from WGHM by the Institut für Physische Geographie, University of Frankfurt, accurately simulates the changes in all forms of terrestrial water storage and GWC except glaciers [47] to observe the agreement with GRACE-based GWC. The outputs of this model have been widely used in recent years [31,48]. The present study used the recent GWC, PGWUSE, and PGWWW data collected from 2003 to 2016, with a monthly temporal resolution and a spatial resolution of $0.5^\circ \times 0.5^\circ$ [47]. To explore the controlling factors of TWS and GWC, we extracted the data of three hydrological fluxes (P, ET, and runoff (R)) from different sources. The precipitation data of the Tropical Rainfall Measuring Mission (TRMM, version TRMM-3B43 Level-3) with a temporal resolution of 1 month and a spatial resolution of $0.25^\circ \times 0.25^\circ$ were obtained from NASA [49]. The monthly ET, P, and R data, output of WGHM with a spatial resolution of $0.5^\circ \times 0.5^\circ$, were taken from data published on the Earth and environmental science website [47].

2.3. Methods

The TWS data of IRB was obtained from the three laboratories using a specialized program written in R and averaged to compute GWC. To calculate the monthly GWC, SM, SWE, and SWS were excluded from the average gridded TWS values of the JPL, CSR, and GFZ laboratories. The groundwater storage change/groundwater anomaly ΔGWC was calculated as given in Equation (1) [50,51]:

$$\Delta GWC = TWS - \Delta SM - \Delta SWE - \Delta CWS \quad (1)$$

where ΔSM, ΔSWE, and ΔCWS are the anomalies for soil moisture, snow water equivalent, and total canopy water, respectively. All variables in Equation (1) (downloaded on a rectangular grid) were imported into a geographic information system (GIS) to mask the irregular boundaries of the Indus River Basin. The centroids of the rectangular grids were obtained as the grid coordinates, and the variables of Equation (1) extracted by the R-code quantified the spatiotemporal groundwater dynamics at various levels. The TWS values for missing months were determined by a linear interpolation technique [52], and statistical analyses were performed by Mann–Kendall tests, regression, and Spearman's rho correlation.

2.3.1. Time-Series Decomposition

A filtering procedure that decomposes a time series into its seasonal (S), trend (T), and residual (R) components using locally weighted scatterplot smoothing is commonly known as the STL method [53]. Numerous hydrological studies [54,55] have used STL to clarify, refine, and obtain the detailed characteristics of variations in timing data. STL decomposition based on LOESS at the time i in a time series Yi is given as:

$$Yi = Si + Ti + Ri \qquad \text{where } i = (1, 2, 3 \ldots, N). \tag{2}$$

In this study, the time series of GRACE-based GWC, PGWUSE, and PGWWW were decomposed, and the characteristics of each decomposed component were analyzed to extract valuable information. Figure 2 summarizes the datasets and research methodology as a flowchart.

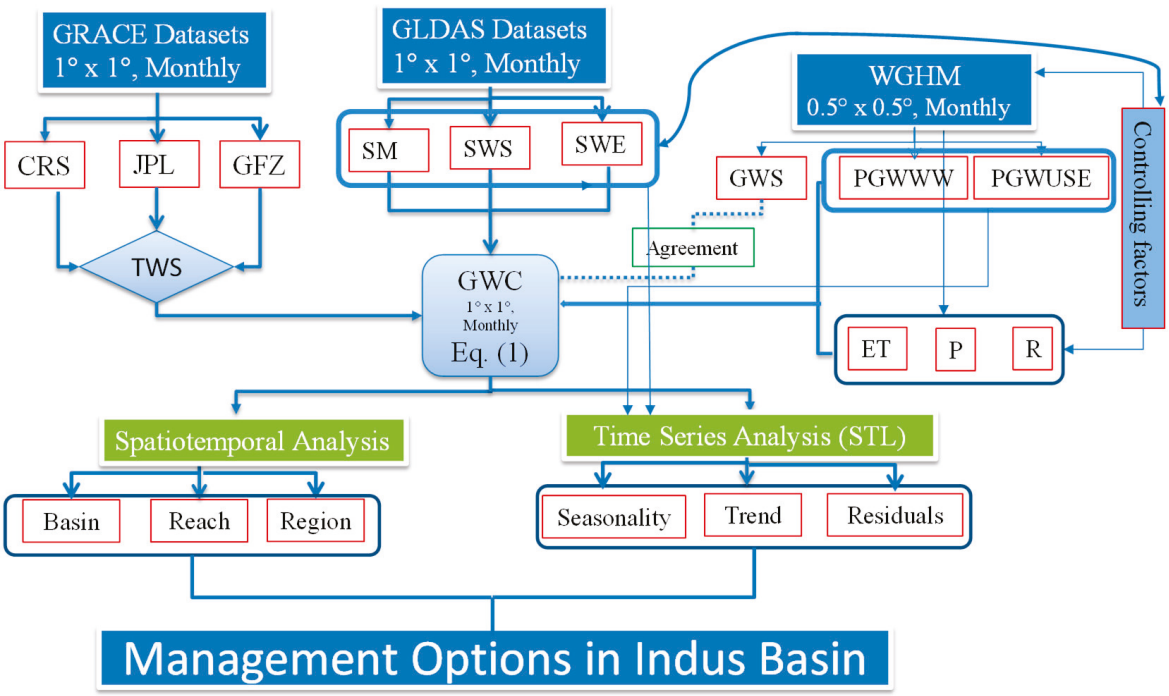

Figure 2. Flowchart of the datasets used and analyses performed.

2.3.2. Spatial and Temporal Analysis

Spatiotemporal analysis was performed to understand the groundwater dynamics of the basin using the available datasets. The 112 grids of the GRACE and GLDAS datasets covering the entire IRB were extracted using the GIS tool. The GRACE-based groundwater anomaly was averaged from January 2003 to December 2016 in each grid cell in the spatial analysis. The temporally averaged GWC values were then categorized into five classes based on GWC threshold values, providing more direct information for groundwater resource management options and planning [12]. The groundwater thresholds were identi-

fied by observing the range of GWC values over the IRB grids. The anomaly categorization is given in Table 1.

Table 1. Groundwater change categories in the Indus River Basin.

Sr. No	Groundwater Changes (mm)	Indication of Groundwater Change
1	<−100	Severe decline
2	−100 to −50	Minor decline
3	−50 to 0	Normal variation
4	0 to 50	Minor rise
5	>50	Abnormal rise

2.4. Performance Assessment of the Groundwater Storage Changes

GWCs estimated in this study across the wider IRB were evaluated at two random pixels both at the very extreme northwestern part (KRB) and at the downstream LBDC. The piezometric data of KRB was obtained from Taher et al. [56], which are monthly records and available for a period of 2005–2013 while for that of LBDC's, there are only two records available per year (i.e., pre and post monsoon) available from 2003 to 2015. The observation wells' data for LBDC was obtained from the Punjab Irrigation Department (Pakistan).

3. Results

The estimated spatial and temporal changes in GWC revealed a groundwater decline over the study period. The fluctuations in GWC were higher before 2010 compared to the later period (2010–2016), i.e., reflecting a substantial decrease in the GRACE-based groundwater storage anomaly in the earlier period (Figure 3a,c).

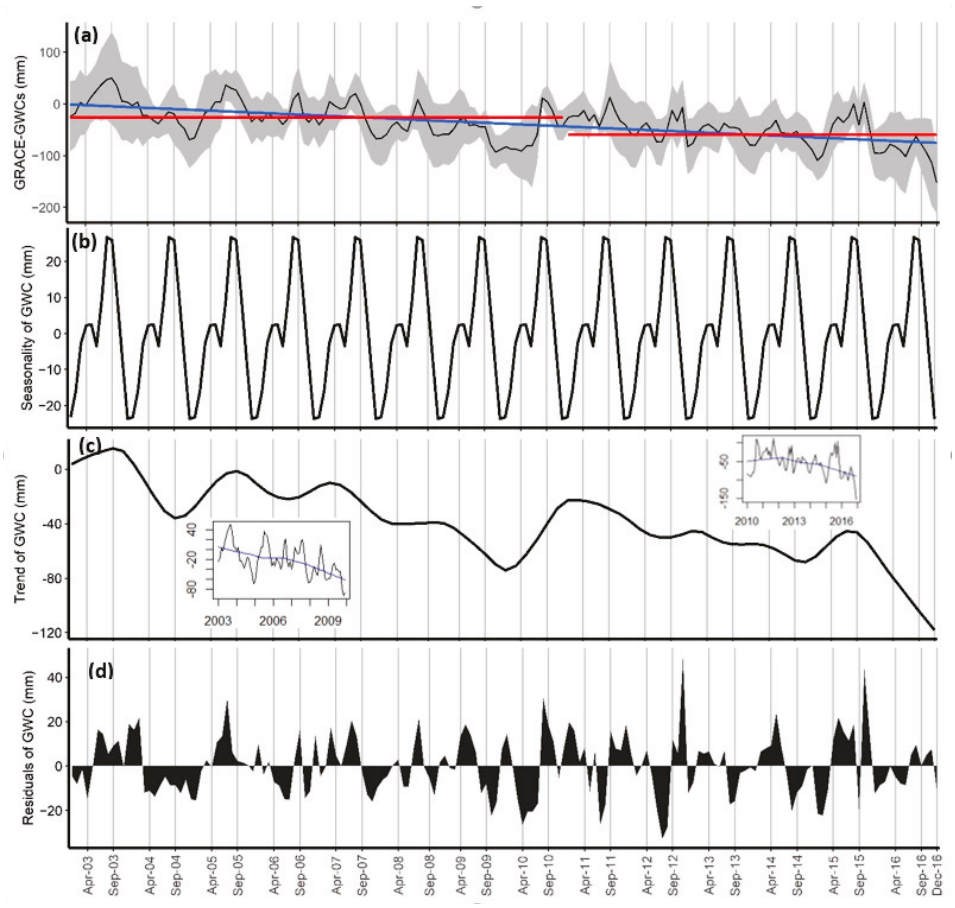

Figure 3. (**a**) GRACE-derived GWC time series, (**b**) seasonality, (**c**) trend, and (**d**) residuals of the decomposed GWC signals.

3.1. Spatiotemporal Groundwater Dynamics and Controlling Factors at the Basin Level

Figure 3a shows the temporal changes in the groundwater resources at the basin level. During the study period (January 2003 to December 2016), GWC decreased ($p = 2.2 \times 10^{-16}$; *t*-test) over the entire IRB. The mean GWC was −25.67 mm for the period of January 2003–December 2009 and −54.33 mm for January 2010–December 2016 (red lines in Figure 3a), confirming both a decline and shift in the mean GWC over the study period, and the fitted regression line (blue line in Figure 3a) showed an overall decreasing trend of 0.44 mm per month.

For the whole study period 2003–2016, the GWC trend declined at −0.44 mm/month in the GRACE model and −0.64 mm/month in WGHM. To identify the hotspots and understand the characteristics of GWC, the GRACE-based GWC time series was decomposed to observe its seasonality, trend, and abnormalities (see Figure 3). Across the entire IRB, the decomposed GWC signal showed a strong seasonality, with annual losses in the pre-monsoon period (around April) and annual gains in the post-monsoon period (around September) (Figure 3a,b). In each year, the seasonality curve dipped after April (Figure 3b) as excessive pumping for rice cultivation began. No significant changes were observed within the years in the seasonal component. The decomposed trend component (Figure 3c) of the GWC signal significantly declined until the end of the drought year (2009). Accordingly, groundwater changes (Figure 3c) were steeper in the first half of the study period, indicating an alarming decline in groundwater resources during this period as evident from the Mann–Kendall trend analysis, which indicated that the mean GWC was highly significant during the study period from January 2003 to December 2009 ($p = 1.65 \times 10^{-7}$) compared to January 2010–December 2016 ($p = 1.99 \times 10^{-4}$).

The groundwater level maximally declined in 2009, when the weak monsoon created drought conditions in the basin before the flood years [57]. Subsequently, it rose in the flood years, indicating the changes in groundwater mainly depend on the trend component. The residual component (a powerful indicator of abnormalities such as flood and drought events in the region) displayed abnormal signals in the winters of 2012 and 2015 (Figure 3d). In the Federal Flood Commission report [58], the years 2010–2016 were identified as flood years. Indeed, the groundwater levels showed a significant rise during these years, indicated by a wet period (Figure 3a) in the present analysis.

The spatial analysis revealed an overall decrease in groundwater resources throughout the basin. As shown in Figure 4, GWC declined from south to north and from west to east. A strip of severe GWCs was observed in Gilgit Baltistan, Kashmir, Himachal Pradesh, and Indian Punjab. In UIB, GWCs dominated in the range from −131 to −81 mm, indicating high groundwater storage variations with higher standard deviations. In the southwest part of IRB, the groundwater storages are minimum and with low variance. In general, the regions where the standard deviation of groundwater storage was high showed greater groundwater decline.

Groundwater storage changes were further explored using the SM, SWS, and SWE data from the GLDAS Noah model. Groundwater changes showed a declining trend in the study area (Figure 5a), and SWS contributed little to GWCs and their tendency (Figure 5b,c). The snow changes remained around zero because snow and ice concentrate in the mountainous part of the basin (upper IRB) and only cover parts of the Indus Basin. The SWE, which significantly affected the changes in groundwater storage, trended downward, particularly after 2005 (Figure 5c). The main contributor to GWC was SM, which is necessary for the growth and survival of flora. The occurrence of drought depends on when the current soil moisture cannot meet the plant's requirements. As shown in Figure 5c, SM and GWC exhibited the same declining trend patterns after the winter of 2007, indicating that GWC and SM are heavily dependent on each other in IRB.

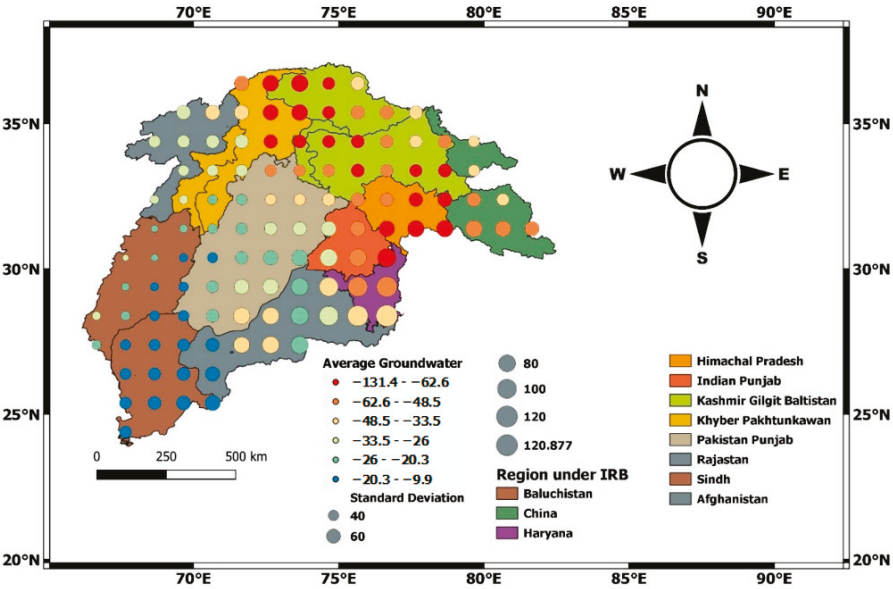

Figure 4. Spatial analysis of the time-averaged GWCs in IRB.

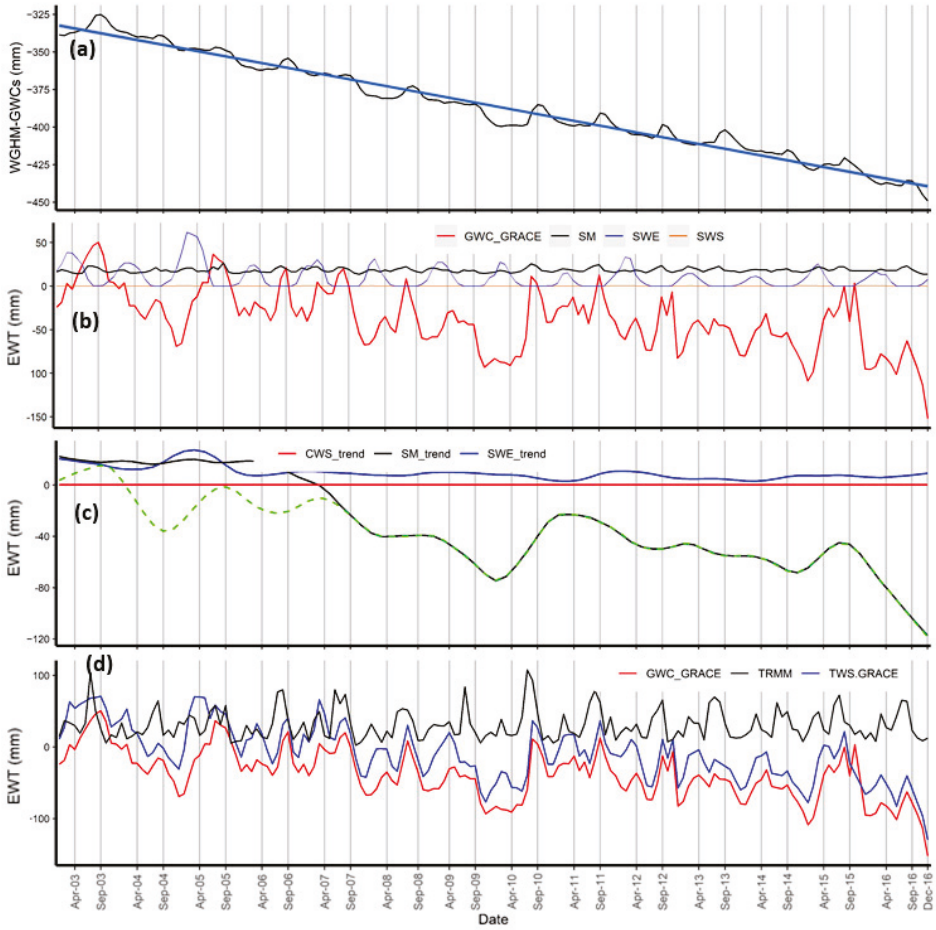

Figure 5. (**a**) Groundwater storage changes in WGHM (black line indicates the groundwater storage of WGHM and blue line indicates the fitted regression line); (**b**) changes and (**c**) trends of GWC, soil moisture (SM), canopy water storage (SWS), and snow water equivalent (SWE); (**d**) comparison of monthly time series of the GRACE-based GWC and TWS values and TRMM precipitation data in IRB.

The spatial differences in TWS and GWC were analyzed from the variabilities in ET, P, and R. We mainly analyzed the entire IRB, UIB, Middle Indus Basin (MIB), and Lower Indus Basin (LIB). In the Indus Basin, TWS and GWC declined at a rate of −0.545 and −0.640 mm/month, respectively; and ET, P, and R varied by a rate of 0.0417, 0.0659, and 0.034 mm/month, respectively (Figure 6a). The positive variability rates of ET, P, and R indicated that all these variables were sensitive to TWS and GWC. However, R is generated by precipitation and snowmelt in the study area, and contributed a minor amount to TWS and GWCs. Thus, we inferred that the ET increase was the main controlling factor of the groundwater and total water storage dynamics across IRB during the study period.

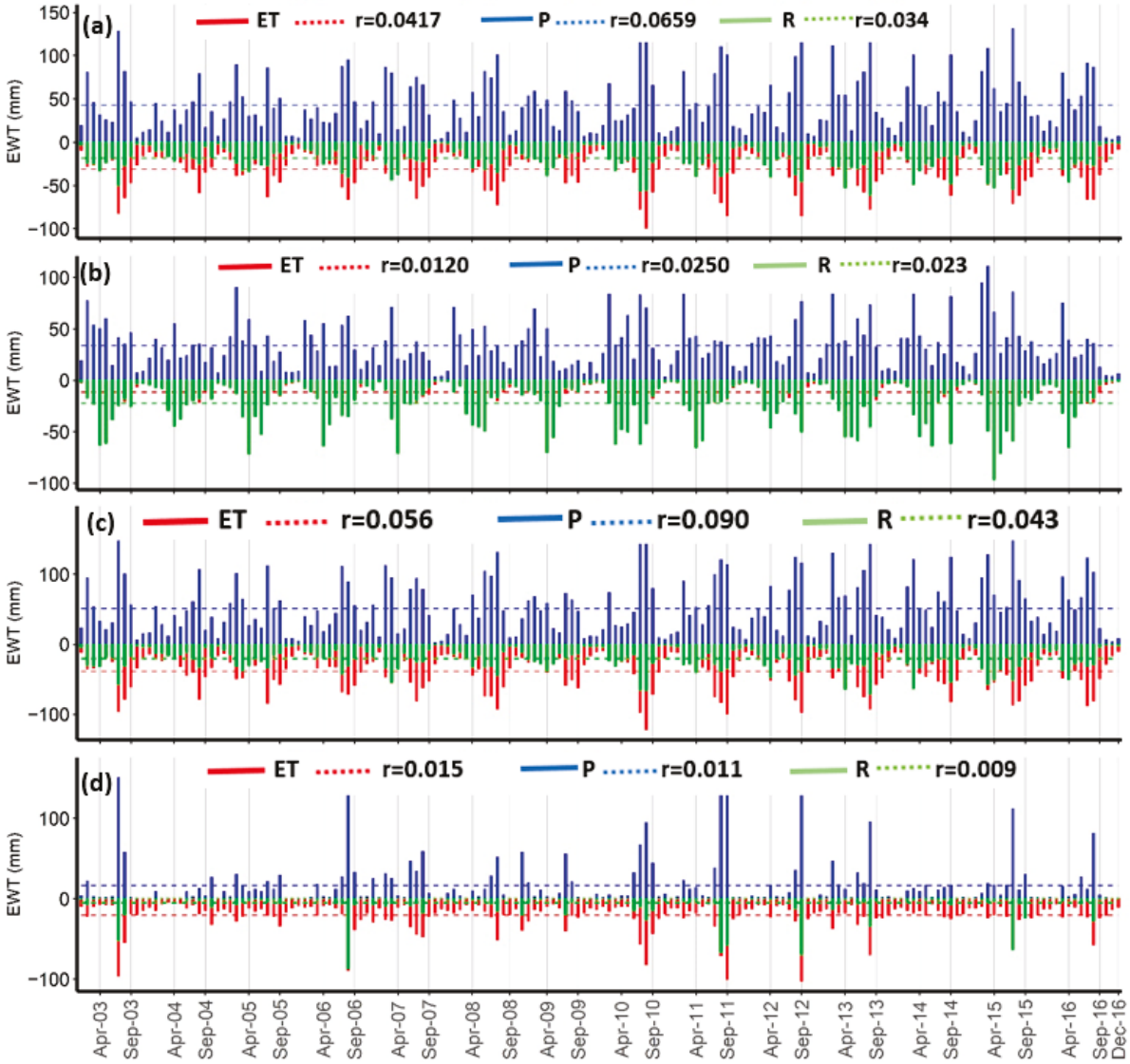

Figure 6. Time series analysis of P, ET, and R in (**a**) the entire Indus Basin, (**b**) Upper Indus Basin (UIB), (**c**) Middle Indus Basin (MIB), and (**d**) Lower Indus Basin (LIB). Here, 'r' (mm/month) denotes the rate of change from 2003 to 2016.

In UIB, TWS trended upward at an amount of 0.018 mm/month, whereas GWC declined at an amount of 0.22 mm/month. Both P and R showed a positive tendency with higher variability than ET (Figure 6b). P increased at an amount of 0.025 mm/month, whereas ET increased at an amount of 0.012 mm/month, indicating that the P increase mainly caused the TWS increase. The increasing trend of regional R was not consistent with the P variation (Figure 6b), suggesting that there is an additive water supply from snowmelt and glacier recession. Muhammad et al. [59] reported a negative mass balance

in upper IRB, with the most negative values ranging from -0.34 ± 0.31 to 0.44 ± 0.27 m w.e., with -1 in the Jhelum, Chenab, and Ravi sub-basins of the Himalaya. SWE in UIB changed by -1.02 mm/year (the glacier area was 115,675 km^2 in 2016). Therefore, our analysis suggests that glacier recession (not ET) is an important controlling factor of TWS and GWC variations in UIB.

In MIB, TWS and GWC significantly declined at an amount of -0.89 and -0.9604 mm/month, respectively. P and ET showed a positive tendency over time and higher variations in MIB than in the Indus Basin as a whole (Figure 6c). The rising ET trend accounts for most of the TWS loss. Meanwhile, the increasing trend in regional R (Figure 6c) is consistent with the P variation. Therefore, ET, groundwater usages and withdrawal were inferred to be the main factors that increase the TWS deficit and reduce the groundwater in MIB.

In LIB, TWS increased at a rate of 0.17 mm/month, whereas GWC declined at a rate of -0.138 mm/month. The variations in P, R, and ET were small and inconsistent with the TWS changes (Figure 6d), suggesting that precipitation and evapotranspiration are not the main factors leading to changes in the total water storage and GWC in this region. Instead, the surface water supply in terms of high water allowances to the canals provided by the Water Apportionment Accord (WAA) 1991 might explain the small groundwater and total water storage changes. The century-old irrigation system of IRB has allowed a variable allocation of surface water by its design [60]. The provincial bodies reviewed surface water allocations (WAs) at many stages to establish water rights and distribute the water of IRB among the four provinces of Pakistan, and these reviews led to a mutual consensus policy document: the Water Apportionment Accord (WAA) 1991 [60].

Precipitation markedly affects the spatial pattern of TWS and GWC and accelerates the spatial variation signal in the north–south direction. Figure 5d compares the mean monthly precipitation data from TRMM and the mean monthly TWS and GWC. The precipitation generated by TRMM varied from 2.28 (October 2007) to 107 mm/month (July 2010), whereas GWC ranged from -152.43 (December 2016) to 50.46 mm (September 2003).

As shown in Table 2, the TRMM, TWS, GWC, and SM data were positively correlated, indicating that the GWC values are affected not only by precipitation but also by parameters associated with anthropogenic activities, such as pumping. As shown in Figure 7a,b, the groundwater use in each year was lowest in February and highest in October. The PGWUSE started to increase after April as the rising temperature accelerated ET and rice cultivation activities in the basin. The decomposed trend components of PGWUSE and PGWWW showed highly reciprocal correlations with the trend of GWC (when PGWUSE was maximum, GWC was minimum; see Figure 7c). The monthly potential total water withdrawals from the groundwater resources were highly seasonal, minimal in April, and highest in November each year (Figure 7d,e). These results imply that much of the groundwater is withdrawn during cropping seasons and consumptive use. The trend component of the decomposed time series of PGWWW increased as the area became more dependent on groundwater (Figure 7f).

Table 2. Correlations between TRMM precipitation, TWS, and GWC.

		Correlations			
		TRMM	TWS	GWC	SM
Spearmen's Rho	TRMM	1.000	0.214 *	0.188 *	0.743 *
	TWS	0.214 *	1.000	0.907 *	0.299 *
	GWC	0.188 *	0.907 *	1.000	0.241 *
	SM	0.743 *	0.299 *	0.241 *	1.000

* Correlation is significant at the 0.01 level (two-tailed).

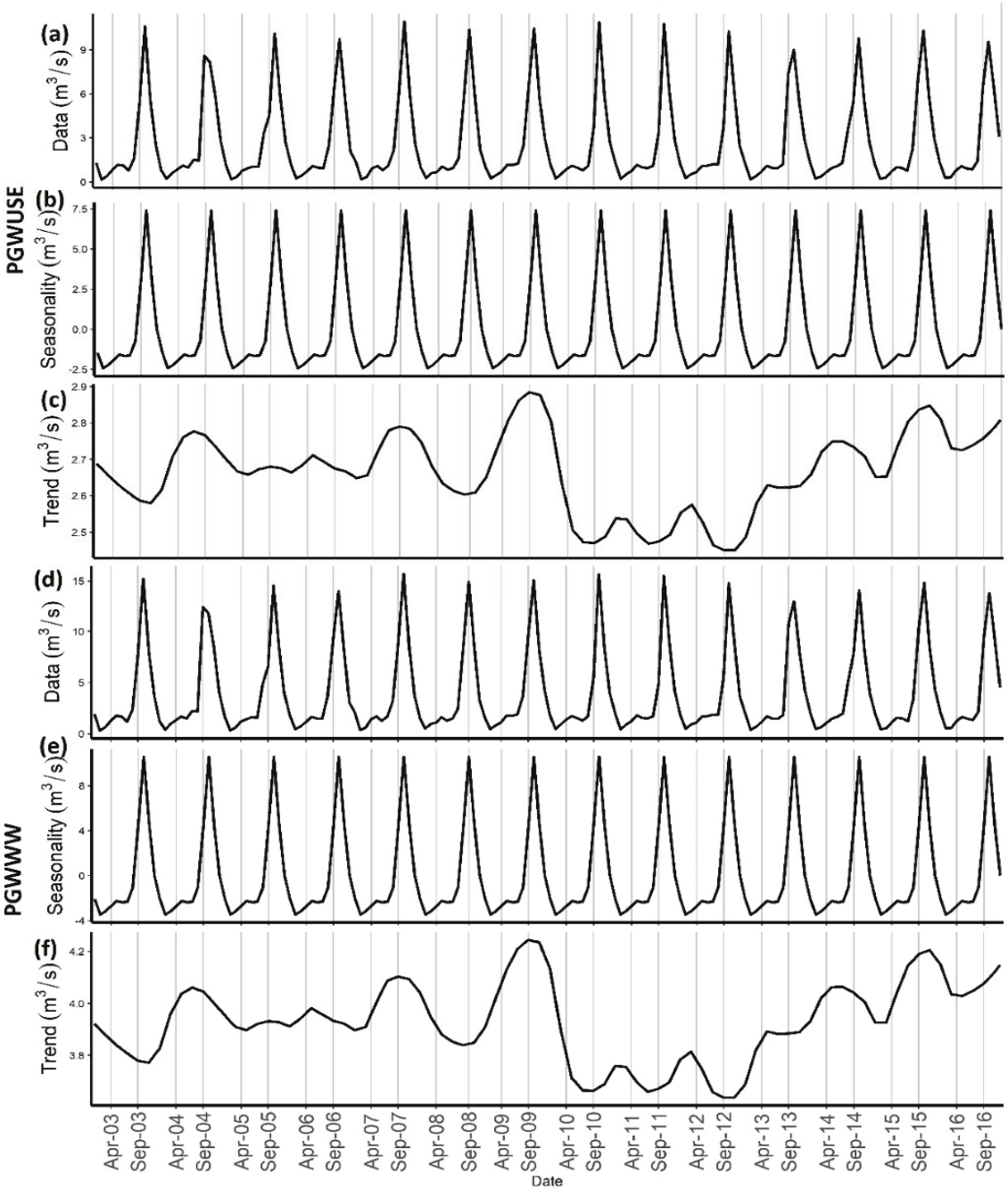

Figure 7. Time series: (**a**) data—PGWUSE; (**b**) seasonality—PGWUSE; (**c**) trend—PGWUSE; (**d**) data—PGWWW; (**e**) seasonality—PGWWW; and (**f**) trend—PGWWW over IRB during the 2003–2016 period.

3.2. Spatiotemporal Groundwater Dynamics in Different Reaches

Reach-wise groundwater storage analysis revealed that changes in groundwater storage were diverse among the three reaches of IRB (Figure 8a) during the study period. The lower reach showed relatively higher groundwater storage than the middle reach while GWC in the upper reach was much smaller than in the middle reach (Figure 8a). These differences can be explained by variations in ET, R, P, and groundwater withdrawals as described above. GWCs in the upper and middle reaches declined more rapidly in later years than in previous years. Moreover, after 2009, GWC was higher in the middle reach than in the other reaches. Contrarily, GWC as determined for each of the reaches showed monotonous behavior during the study period. In the lower reach, the minor increases

during 2007 and 2011 were contributed by groundwater recharge from flooding periods in previous years, explaining the smaller declining trend than the other reaches (Figure 8a).

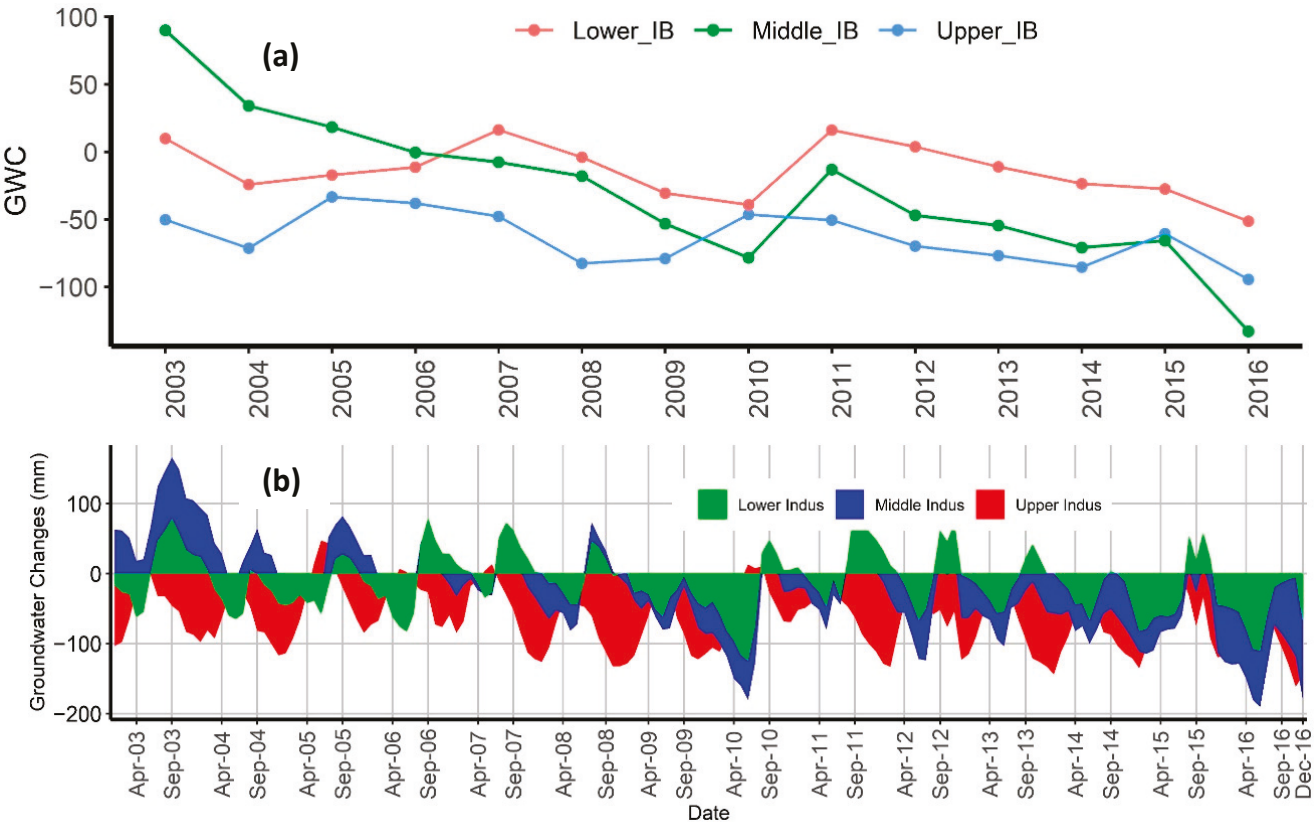

Figure 8. (**a**) Annual time series of the mean spatial groundwater storage changes in the three reaches of IRB. (**b**) Mean monthly GWC (mm/month) at different reaches in IRB.

Looking at the monthly scale groundwater changes (Figure 8b), we found no consistency in groundwater storage fluctuations among the three reaches during 2003–2009. However, the upper and lower reaches showed some consistency in their fluctuations during 2010–2016 (Figure 8b). In the upper reach, groundwater storage remained low in winter (~December) throughout the study period except for rising trends during the summer of 2005–2007 and 2010. The groundwater storage changes remained high during 2003–2008, and low in the rest of the study periods. The lower reach depicted high groundwater storage in the summer (~September). After the year 2009 (tipping year), groundwater storage values were continuously negative in the upper and middle reaches, indicating that the groundwater storage continuously remained lower when compared with the base period (2004–2009). Prior to 2010, all the reaches showed groundwater storage fluctuation in the range of −150–150 mm. After 2010, there was a less declining trend of the groundwater storage due to floods, and the annual minimum values were recorded during the study duration.

The most recent study year (2016) showed severe signs of depletion in groundwater storage, especially in the middle reach, as shown in Figure 9b. The upper reach showed surprisingly strong groundwater declines (<−100 mm) in all years except 2006, whereas the middle reach showed strong declines in groundwater storage from 2010 to 2016 onwards (Figure 9a,b). In general, the upper reach had the highest number of months that experienced severe groundwater declines compared with the other reaches during the study duration (Figure 9d). At the same time, there were no months with an abnormal rise (>50 mm) in the upper reach. The reach-specific analysis revealed that more rapid fluctuations in the upper reach make its ecosystem vulnerable, which may require further

attention. Groundwater depletion in the upper reach should be mitigated with climate mitigation strategies.

Figure 9. (**a**) Upper reach groundwater changes, (**b**) middle reach groundwater changes, (**c**) lower reach groundwater changes, and (**d**) annual severity of GWCs in the different reaches of IRB.

In the reach-specific analysis, 24%, 14%, and 2% of the time span of the groundwaters in the upper, middle, and lower reaches, respectively, were severely depleted over the entire period. These findings indicate the vulnerability of groundwater resources in the upper Indus reach (Figure 9d). During the same period, GWC rose abnormally in the middle reach. The reach-wise analysis revealed more rapid fluctuations in the upper reach, which may require further attention. In particular, groundwater depletion in the upper reach should be mitigated with climate mitigation strategies.

3.3. Spatiotemporal Groundwater Dynamics at the Regional Level

To study GWCs in a spatially explicit way, the study area was subdivided into eight regions: Kashmir and Gilgit Baltistan, Tibet–China, Khyber Pakhtunkhwa, Afghanistan, Punjab, Sindh, Baluchistan, and Indian Punjab–Himachal Pradesh–Haryana (hereafter referred to as the Indian part), along the Indus River from upstream to downstream. All eight regions of IRB exhibited irregular annual patterns of continuous decline in GWC after 2003 (Figure 10). China, Afghanistan, KP, and Sindh showed consistent groundwater storage changes within the range from 0 to −50 mm except in 2016. Before 2009, groundwater changes were within −50–100 mm for all the regions while after 2010, all the regions showed a rise in groundwater storage in 2011 and then a continuous decline. In the Indian part, the groundwater storage declined until 2010, but in the years beyond 2010, GWCs were in the range of −150 mm. The low GWC values in the Tibet–China and Indian part of IRB in the second phase and particularly in the final year of the study period (2016) indicate

a severe groundwater decline in these regions (see Figure 10). In the province of Sindh, the groundwater rose abnormally in 2011 and, after that, continuously declined at a lesser rate than in the other regions.

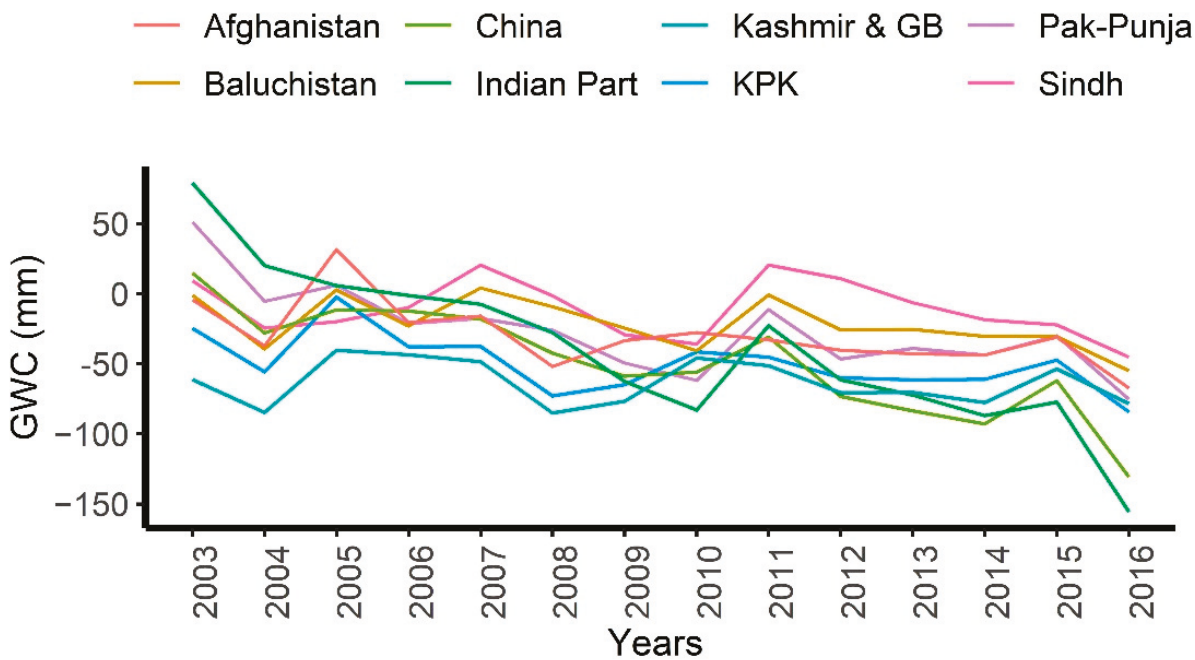

Figure 10. The annual time series of spatially averaged changes in groundwater storage in different regions.

The GRACE-based estimates of groundwater storage changes were compared to in situ measurements (1 piezometer data for KRB and 1 observation well for LBDC). In situ measurements for KRB and LBDC were available from 2003 to 2015 and 2005 to 2013, respectively. When the GWC and in situ measurements were compared, the correlation coefficients for LBDC and KRB were 0.78 and 0.35, respectively (Figure 11).

(**a**) Lower Bari Doab Canal (LBDC)

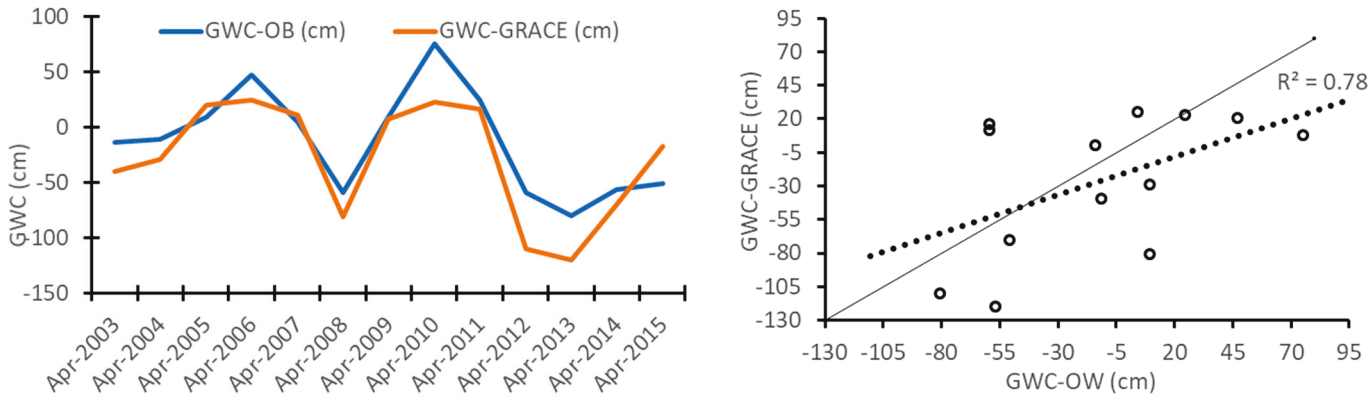

Figure 11. *Cont.*

(**b**) Kabul River Basin (KRB)

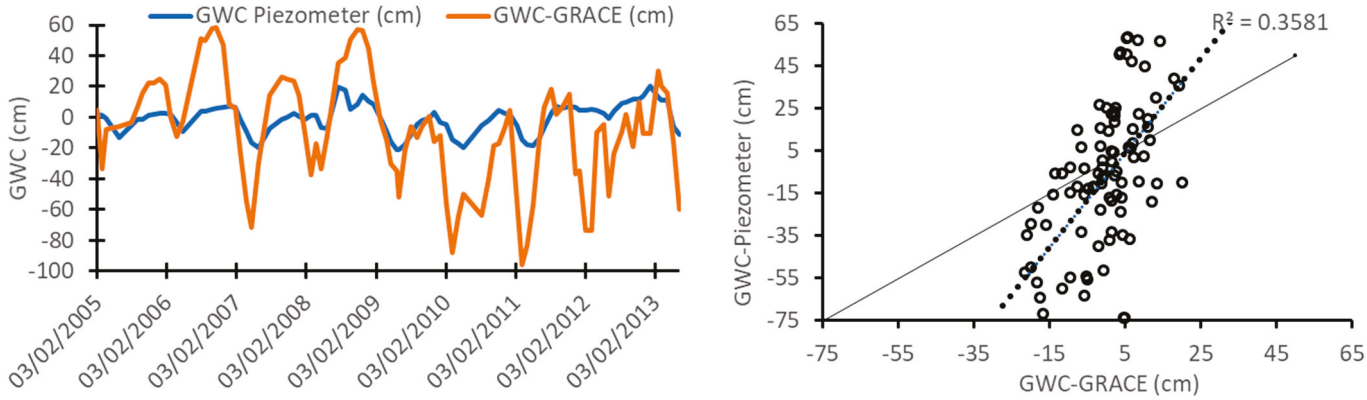

Figure 11. (**a**) Correlation of the observed (observation well data) and estimated (GRACE-based) groundwater storage anomalies in LBDC. (**b**) Correlation of the observed (piezometric data) and GRACE-based groundwater storage changes in the Kabul River Basin.

4. Discussion

Overall, our analysis revealed that regional GWCs in time and space could be derived from remote sensing data (GRACE) and data assimilation models (GLDAS). In the temporal analysis, a significant decline in GWC ($p = 2.2 \times 10^{-16}$) was observed over the entire study period (January 2003 to December 2016). The observed decreasing trend and fluctuations were larger before 2010 than in the second half of the study period, which is driven by the higher values in 2003 and very low numbers in 2010. The second phase of the time series is characterized by lower levels and extreme lower levels of GWC in 2016.

In the spatial analysis, a significantly declining trend in GWC was observed in the upper Indus reach, indicating a dominant snow receding effect [61]. On the regional scale, the aquifer storage showed a declining trend in upper Punjab (especially in Gujranwala, Sialkot, and Hafizabad) because the pumping rate was high in these regions. Similar results were reported by Qureshi et al. [62], Shoaib et al. [37], Arshad et al. [39], and Iqbal et al. [20], who mentioned that water is over-pumped at an alarming rate in areas where high delta crops (i.e., rice) are grown at a high tube well density. The groundwater depletion was moderate in the districts (Faisalabad, Vehari, Pakpattan, and Khanewal) of Pakistani Punjab because groundwater is overexploited to meet the crop water requirements (Iqbal et al. (2017)**)**. Qureshi [63] reported that groundwater is declining to below 6 m in more than 50% of the irrigated area of Punjab, causing groundwater quality deterioration and increased pumping costs.

Groundwater storage changes were severe in the Indian part of IRB, reaching a maximum in 2016. Dominant changes in groundwater were observed in the south-eastern regions of the IRB, covering Himachal Pradesh, Indian Punjab, Haryana, and Rajasthan (the northern Indian states, which account for 95% of groundwater use in the region). High groundwater-based irrigation can explain these large changes, which has expanded to meet the wheat and rice demands of Indian government policy [64]. Other causes of groundwater decline are exponential population growth and rapid economic development [65], which have increased the pumping of groundwater [5,66], in addition to the provision of subsidies on electricity and diesel for groundwater abstraction, an increased number and density of tube wells (>30/km^2 in different districts), augmented groundwater draft, expansion of rice and wheat areas [39], and spikes in cropping intensity [67,68]. Similarly, Rodell et al. [17] detected a significant groundwater depletion in the north-western part of India based on the GRACE datasets. They calculated a mean depletion rate of 40 ± 10 mm/year equivalent height of water, whereas Asoka et al. [69] estimated a 20 mm/year groundwater decline rate in the same region. Singh and Bhakar [70] reflected upon the alarming groundwater situation in Rajasthan and concluded that there is an uncertain future for this commodity.

Steenbergen et al. [71] attributed groundwater exhaustion in the Baluchistan province of Pakistan to the intensive use of water for agricultural purposes. The Sindh province of Pakistan, the southwest part of IRB, showed lower GWC fluctuations than the other parts of the basin and similar results were revealed by Arshad et al. [39]. Basharat and Azhar [60] attributed the lower GWCs to the higher water allowance of canals under WAA 1991. Therefore, the authority responsible for the WAA 1991 should rationalize water allowances over IRB to counteract waterlogging and salinity in the lower reach (i.e., the Sindh province of Pakistan) and over-abstraction of groundwater in the upper part of the basin. The observed in situ groundwater anomalies were compared with the estimated GRACE-based groundwater storage anomalies (Figure 11). The results were consistent with the study conducted by Akhtar et al. [38] and Ali et al. [37].

Due to drought conditions, the groundwater declined maximally in 2009 while during flood periods, groundwater storages were improved. Chen et al. [18] reported in Songhua River Basin that flood and drought conditions characterize the fluctuation in groundwater storage. GWS recovery was attributed to an increase in precipitation [72] in the Tasmania region, Australia, after 2010. However, Indus Basin exhibited a decline in groundwater storage that was inconsistent with the precipitation variation till 2010 (Figure 5c). Afterwards, it showed a continuous decline due to the significant impact of anthropogenic activities, i.e., mainly pumping in agriculture (Figure 7c,f). In addition, Feng et al. [73] also reported that the pumping of groundwater for irrigation and coal mining activities was a major contributing factor in North China.

The spatiotemporal patterns of groundwater behavior extracted from the GLDAS and GRACE data might assist the implementation of sustainable groundwater management by policymakers and managers. Admittedly, the spatial resolution of the GRACE mission is too coarse to monitor the finer surface mass changes in large water bodies such as dams and lakes. Although the applied datasets are the best current data sources for determining GWCs in this area, they are insufficient for understanding groundwaters in canal command areas. Moreover, the mission ended in 2017, necessitating a new perspective of groundwater dynamics. To this end, statistical modeling of the GRACE time series and downscaling of GRACE to the local scale of groundwater dynamics are required. By connecting the data of GRACE, the latest launched GRACE-FO, and statistical modeling, we can ensure the continuity of the groundwater dynamics for prediction, especially when data are missing during the operation period of GRACE-FO. Issues such as sea water intrusion, how surface water bodies affect groundwater quality and quality, and land subsidence are not addressed by GRACE [74]. The uncertainties in hydrological models, i.e., GRACE and GLDAS, could be considered in the perspective studies.

5. Conclusions

The GRACE and GLDAS datasets were combined into a novel algorithm that estimates the spatial and temporal changes in groundwater, thereby providing water-resource management options at the basin, reach, and regional levels. Groundwater resources in the whole basin have declined over time but exhibited a spatially heterogeneous change pattern. The main conclusions of this study and outlooks for future research and policy intervention are summarized as follows:

- When analyzed over time, almost all GWC values were negative, with an overall decreasing trend from January 2003 to December 2016. The fluctuations in GWCs were stronger before 2010 than in the second half of the study period. An increase in evapotranspiration was found to be the main controlling factor for the groundwater and total water storage changes across IRB.
- In the spatial analysis, GWC trended downward over the whole Indus Basin. The decline was severe (−131 to −108 mm) in UIB, highlighting a need for sub-basin analysis. We recommend the development of quantitative groundwater aquifer-related maps to visualize water withdrawals, groundwater recharge, groundwater storage changes, groundwater levels, aquifer thickness and yields, and tube well density over the whole

IRB. These maps provide useful support to develop area-specific groundwater management strategies.

- The reach-specific analysis showed that the upper reach is more vulnerable to groundwater decline compared to the other reaches due to glacier recession. We recommend the adaption of climate mitigation strategies to cater for the climate change impact on glacier recession. This study concludes that groundwater abstraction and groundwater consumption are the most significant driving factors in the middle reach. These results highlight the need for a robust mechanism to monitor the quantity and quality of groundwater abstractions in the middle reach. The outcomes for the lower reach reveal that the high water allowances provided to the canals under WAA 1991 are the main driver of lower groundwater storage change. So, surface water allowances in Pakistan should be allocated based on a detailed understanding of groundwater withdrawals and depletion.
- On the regional scale, the groundwater decline was severe in Himachal Pradesh, Indian Punjab, Haryana, upper Punjab of Pakistan, and China. Due to these regional differences, it is evident that a region-specific groundwater strategic framework is necessary. Hence, a comprehensive mechanism for monitoring and establishing regulatory and permitting arrangements and pricing structures should be developed to envisage sustainable management of the land area and water resources. Because the number and density of tube wells and boreholes have largely increased in recent years, we propose the construction of a database containing georeferenced locations of all existing and new tube wells and boreholes in the regions. Such a database would not only support but also improve management decisions.
- The correlation between the observed and estimated GWC both at KRB (i.e., $R^2 = 0.35$) and LBDC (i.e., $R^2 = 0.78$) shows that there are spatial heterogeneities across IRB, which needs to be considered during planning initiatives.

In a nutshell, basin-wide groundwater monitoring infrastructures must be established using the latest technologies (GIS, remote sensing, and Heliborne technology). Such infrastructures are essential for the development of a sound database and maps for groundwater regulation and sustainable management. These will also enable robust monitoring of the quantity and quality of groundwater resources and their use.

Author Contributions: Conceptualization, K.M. and B.T.; methodology, K.M.; software, K.M.; validation, K.M; formal analysis, K.M.; investigation, K.M.; data curation, K.M.; writing—original draft preparation, K.M.; writing—review and editing, M.F. and M.U.; visualization, M.U.; supervision, M.F. All authors have read and agreed to the published version of the manuscript.

Funding: This research received no external funding.

Data Availability Statement: Not applicable.

Acknowledgments: The first author is thankful to the Higher Education Commission, Pakistan, and the German Academic Exchange Service (DAAD), Germany, for funding this study under the Overseas Scholarship Program. The first author is also thankful to the University of Agriculture-Faisalabad for granting study leave to pursue Ph.D. studies. The authors also thank Hannes Müller Schmied, affiliated with the University of Frankfurt, Germany, for providing access to the data. Thanks to the Center for Development Research (ZEF) and the University of Bonn for facilitation and support.

Conflicts of Interest: The authors declare no conflict of interest.

References

1. Kinzelbach, W.; Bauer, P.; Siegfried, T.; Brunner, P. Sustainable Groundwater Management—Problems and Scientific Tools. *Episodes* **2003**, *26*, 279–284. [CrossRef] [PubMed]
2. Food and Agriculture Organization, Faoa. *Irrigation in Southern and Eastern Asia in Figures—AQUASTAT Survey—2011: Indus River Basin*; Food and Agriculture Organization: Rome, Italy, 2011; pp. 1–14.
3. Siebert, S.; Faures, J.M.; Frenken, K.; Hoogeveen, J. Groundwater Use for Irrigation—A Global Inventory. *Hydrol. Earth Syst. Sci.* **2010**, *14*, 1863–1880. [CrossRef]

4. Usman, M.; Qamar, M.U.; Becker, R.; Zaman, M.; Conrad, C.; Salim, S. Numerical Modelling and Remote Sensing Based Approaches for Investigating Groundwater Dynamics under Changing Land-Use and Climate in the Agricultural Region of Pakistan. *J. Hydrol.* **2020**, *581*, 124408. [CrossRef]
5. Cheema, M.J.M.; Immerzeel, W.W.; Bastiaanssen, W.G.M. Spatial Quantification of Groundwater Abstraction in the Irrigated Indus Basin. *Groundwater* **2014**, *52*, 25–36. [CrossRef] [PubMed]
6. Lytton, L.; Ali, A.; Garthwaite, B.; Punthakey, J.F.; Basharat, S. Groundwater in Pakistan's Indus Basin: Present and Future Prospects. 2021, p. 164. Available online: http://hdl.handle.net/10986/35065 (accessed on 16 April 2021).
7. Cheema, M.J.M.; Qamar, M.U. *Transboundary Indus River Basin: Potential Threats to Its Integrity*; Elsevier Inc.: Amsterdam, The Netherlands, 2019; ISBN 9780128127827.
8. Arfan, A.; Zhang, Z.; Zhang, W.; Gujree, I. Long-Term Perspective Changes in Crop Irrigation Requirement Caused by Climate and Agriculture Land Use Changes in Rechna Doab, Pakistan. *Water* **2019**, *11*, 1567. [CrossRef]
9. Sun, S.; Zhou, T.; Wu, P.; Wang, Y.; Zhao, X.; Yin, Y. Impacts of Future Climate and Agricultural Land-Use Changes on Regional Agricultural Water Use in a Large Irrigation District of Northwest China. *L. Degrad. Dev.* **2019**, *30*, 1158–1171. [CrossRef]
10. Watto, M.A. The Economics of Groundwater Irrigation in the Indus Basin, Pakistan: Tube-Well Adoption, Technical and Irrigation Water Efficiency and Optimal Allocation. Ph.D. Thesis, University of Western Australia, Crawley WA, Australia, 2015; pp. 1–218.
11. Qureshi, A.S.; Gill, M.A.; Sarwar, A. Sustainable Groundwater Management in Pakistan: Challenges and Pportunities. *Irrig. Drain.* **2010**, *59*, 107–116. [CrossRef]
12. Lin, M.; Biswas, A.; Bennett, E.M. Spatio-Temporal Dynamics of Groundwater Storage Changes in the Yellow River Basin. *J. Environ. Manage.* **2019**, *235*, 84–95. [CrossRef] [PubMed]
13. Mahmood, R.; JIA, S.; Lv, A.; Zhu, W. A Preliminary Assessment of Environmental Flow in the Three Rivers' Source Region, Qinghai Tibetan Plateau, China and Suggestions. *Ecol. Eng.* **2020**, *144*, 105709. [CrossRef]
14. Young, W.J.; Arif, A.; Bhatti, T.; Borgomeo, E.; Davies, S.; Garthwaite, W.R., III; Gilmont, E.M.; Leb, C.; Lytton, L.; Makin, I.; et al. *Pakistan: Getting More from Water*; World Bank: Washington, DC, USA, 2019; p. 163.
15. Yin, W.; Han, S.C.; Zheng, W.; Yeo, I.Y.; Hu, L.; Tangdamrongsub, N.; Ghobadi-Far, K. Improved Water Storage Estimates within the North China Plain by Assimilating GRACE Data into the CABLE Model. *J. Hydrol.* **2020**, *590*, 125348. [CrossRef]
16. Liu, F.; Kang, P.; Zhu, H.; Han, J.; Huang, Y. Analysis of Spatiotemporal Groundwater-Storage Variations in China from Grace. *Water* **2021**, *13*, 2378. [CrossRef]
17. Rodell, M.; Velicogna, I.; Famiglietti, J.S. Satellite-Based Estimates of Groundwater Depletion in India. *Nature* **2009**, *460*, 999–1002. [CrossRef] [PubMed]
18. Chen, H.; Zhang, W.; Nie, N.; Guo, Y. Long-Term Groundwater Storage Variations Estimated in the Songhua River Basin by Using GRACE Products, Land Surface Models, and in-Situ Observations. *Sci. Total Environ.* **2019**, *649*, 372–387. [CrossRef]
19. Tapley, B.D.; Bettadpur, S.; Watkins, M.; Reigber, C. The Gravity Recovery and Climate Experiment: Mission Overview and Early Results. *Geophys. Res. Lett.* **2004**, *31*, L09607. [CrossRef]
20. Iqbal, N.; Hossain, F.; Lee, H.; Akhter, G. Integrated Groundwater Resource Management in Indus Basin Using Satellite Gravimetry and Physical Modeling Tools. *Environ. Monit. Assess.* **2017**, *189*, 128. [CrossRef] [PubMed]
21. Iqbal, N.; Hossain, F.; Lee, H.; Akhter, G. Satellite Gravimetric Estimation of Groundwater Storage Variations over Indus Basin in Pakistan. *IEEE J. Sel. Top. Appl. Earth Obs. Remote Sens.* **2016**, *9*, 3524–3534. [CrossRef]
22. Tang, Y.; Hooshyar, M.; Zhu, T.; Ringler, C.; Sun, A.Y.; Long, D.; Wang, D. Reconstructing Annual Groundwater Storage Changes in a Large-Scale Irrigation Region Using GRACE Data and Budyko Model. *J. Hydrol.* **2017**, *551*, 397–406. [CrossRef]
23. Fallatah, O.A.; Ahmed, M.; Save, H.; Akanda, A.S. Quantifying Temporal Variations in Water Resources of a Vulnerable Middle Eastern Transboundary Aquifer System. *Hydrol. Process.* **2017**, *31*, 4081–4091. [CrossRef]
24. Ghebreyesus, D.; Temimi, M.; Fares, A.; Bayabil, H. A Multi-Satellite Approach for Water Storage Monitoring in an Arid Watershed. *Geosciences* **2016**, *6*, 33. [CrossRef]
25. Huang, X.; Gao, L.; Crosbie, R.S.; Zhang, N.; Fu, G.; Doble, R. Groundwater Recharge Prediction Using Linear Regression, Multi-Layer Perception Network, and Deep Learning. *Water* **2019**, *11*, 1879. [CrossRef]
26. Verma, K.; Katpatal, Y.B. Groundwater Monitoring Using GRACE and GLDAS Data after Downscaling Within Basaltic Aquifer System. *Ground Water* **2019**, *58*, 143–151. [CrossRef]
27. Srivastava, S.; Dikshit, O. Seasonal and Trend Analysis of TWS for the Indo-Gangetic Plain Using GRACE Data. *Geocarto Int.* **2020**, *35*, 1343–1359. [CrossRef]
28. Papa, F.; Frappart, F.; Malbeteau, Y.; Shamsudduha, M.; Vuruputur, V.; Sekhar, M.; Ramillien, G.; Prigent, C.; Aires, F.; Pandey, R.K.; et al. Satellite-Derived Surface and Sub-Surface Water Storage in the Ganges-Brahmaputra River Basin. *J. Hydrol. Reg. Stud.* **2015**, *4*, 15–35. [CrossRef]
29. Moghim, S. Assessment of Water Storage Changes Using GRACE and GLDAS. *Water Resour. Manag.* **2020**, *34*, 685–697. [CrossRef]
30. Li, H.; Lu, Y.; Zheng, C.; Zhang, X.; Zhou, B.; Wu, J. Seasonal and Inter-Annual Variability of Groundwater and Their Responses to Climate Change and Human Activities in Arid and Desert Areas: A Case Study in Yaoba Oasis, Northwest China. *Water* **2020**, *12*, 303. [CrossRef]
31. Zhu, Y.; Liu, S.; Yi, Y.; Qi, M.; Li, W.; Saifullah, M.; Zhang, S.; Wu, K. Spatio-Temporal Variations in Terrestrial Water Storage and Its Controlling Factors in the Eastern Qinghai-Tibet Plateau. *Hydrol. Res.* **2021**, *52*, 323–338. [CrossRef]

32. Huang, Y.; Salama, M.S.; Krol, M.S.; Su, Z.; Hoekstra, A.Y.; Zeng, Y.; Zhou, Y. Estimation of Human-Induced Changes in Terrestrial Water Storage through Integration of GRACE Satellite Detection and Hydrological Modeling: A Case Study of the Yangtze River Basin. *Water Resour. Res.* **2015**, *51*, 8494–8516. [CrossRef]
33. World Bank The Indus Waters Treaty 1960 (with Annexes). Signed at Karachi, on 19 September 1960. *United Nations—Treaty Ser.* **1962**, *6032*, 1–85.
34. IRSA Apportionment of Waters of Indus River System between the Provinces of Pakistan. *Indus River Syst. Auth. Gov. Pak.* **1992**, 1–47.
35. Ali, S.; Liu, D.; Fu, Q.; Cheema, M.J.M.; Pham, Q.B.; Rahaman, M.M.; Dang, T.D.; Anh, D.T. Improving the Resolution of Grace Data for Spatio-Temporal Groundwater Storage Assessment. *Remote Sens.* **2021**, *13*, 3513. [CrossRef]
36. Shekhar, S.; Mao, R.S.K.; Imchen, E.B. Groundwater Management Options in North District of Delhi, India: A Groundwater Surplus Region in over-Exploited Aquifers. *J. Hydrol. Reg. Stud.* **2015**, *4*, 212–226. [CrossRef]
37. Ali, S.; Wang, Q.; Liu, D.; Fu, Q.; Mafuzur Rahaman, M.; Abrar Faiz, M.; Jehanzeb Masud Cheema, M. Estimation of Spatio-Temporal Groundwater Storage Variations in the Lower Transboundary Indus Basin Using GRACE Satellite. *J. Hydrol.* **2022**, *605*, 127315. [CrossRef]
38. Akhtar, F.; Nawaz, R.A.; Hafeez, M.; Awan, U.K.; Borgemeister, C.; Tischbein, B. Evaluation of GRACE Derived Groundwater Storage Changes in Different Agro-Ecological Zones of the Indus Basin. *J. Hydrol.* **2022**, *605*, 127369. [CrossRef]
39. Arshad, A.; Mirchi, A.; Samimi, M.; Ahmad, B. Combining Downscaled-GRACE Data with SWAT to Improve the Estimation of Groundwater Storage and Depletion Variations in the Irrigated Indus Basin (IIB). *Sci. Total Environ.* **2022**, *838*, 156044. [CrossRef] [PubMed]
40. Archer, D.R.; Forsythe, N.; Fowler, H.J.; Shah, S.M. Sustainability of Water Resources Management in the Indus Basin under Changing Climatic and Socio Economic Conditions. *Hydrol. Earth Syst. Sci.* **2010**, *14*, 1669–1680. [CrossRef]
41. Iqbal Abdul Rauf Environmental Issues of Indus River Basin: An Analysis. *ISSRA Pap. Inst. Strateg. Stud. Res. Anal. (ISSRA) Natl. Def. Univ. Islam. Pak.* **2013**, *5*, 91–112.
42. Landerer, F.W.; Swenson, S.C. Accuracy of Scaled GRACE Terrestrial Water Storage Estimates. *Water Resour. Res.* **2012**, *48*, 1–11. [CrossRef]
43. Landerer, F. GFZ TELLUS GRACE Level-3 Monthly LAND Water-Equivalent-Thickness Surface-Mass Anomaly Release 6.0 in NetCDF/ASCII/GeoTIFF Formats. Ver. 6.0. PO.DAAC, CA, USA. Available online: Https://Doi.Org/10.5067/TELND-3AG06 (accessed on 17 December 2019).
44. Landerer, F. CSR TELLUS GRACE Level-3 Monthly LAND Water-Equivalent-Thickness Surface-Mass Anomaly Release 6.0 in NetCDF/ASCII/GeoTIFF Formats. Ver. 6.0. PO.DAAC, CA, USA. Available online: Https://Doi.Org/10.5067/TELND-3AC06 (accessed on 17 December 2019).
45. Landerer, F. JPL TELLUS GRACE Level-3 Monthly LAND Water-Equivalent-Thickness Surface-Mass Anomaly Release 6.0 in NetCDF/ASCII/GeoTIFF Formats. Ver. 6.0. PO.DAAC, CA, USA. Available online: Https://Doi.Org/10.5067/TELND-3AJ06 (accessed on 4 December 2019).
46. Rodell, M.; Beaudoing, H. *GLDAS CLM Land Surface Model L4 Monthly 1.0 × 1.0 Degree V001*; Goddard Earth Sciences Data and Information Services Center: Greenbelt, MD, USA, 2007.
47. Müller Schmied, H.; Cáceres, D.; Eisner, S.; Flörke, M.; Herbert, C.; Niemann, C.; Peiris, T.A.; Popat, E.; Portmann, F.T.; Reinecke, R.; et al. The Global Water Resources and Use Model WaterGAP v2.2d: Model Description and Evaluation. *Geosci. Model Dev. Discuss.* **2021**, *14*, 1037–1079. [CrossRef]
48. Feng, W.; Shum, C.K.; Zhong, M.; Pan, Y. Remote Sensing Groundwater Storage Changes in China from Satellite Gravity: An Overview. *Remote Sens.* **2018**, *10*, 674. [CrossRef]
49. Huffman, G.J.; Bolvin, D.T.; Nelkin, E.J. Integrated Multi-SatellitE Retrievals for GPM (IMERG), Version 4.4. NASA's Precipitation Processing Center. Available online: https://gpm.nasa.gov/data/policy (accessed on 6 February 2021).
50. Voss, K.A.; Famiglietti, J.S.; Lo, M.; De Linage, C.; Rodell, M.; Swenson, S.C. Groundwater Depletion in the Middle East from GRACE with Implications for Transboundary Water Management in the Tigris-Euphrates-Western Iran Region. *Water Resour. Res.* **2013**, *49*, 904–914. [CrossRef]
51. Frappart, F.; Ramillien, G. Monitoring Groundwater Storage Changes Using the Gravity Recovery and Climate Experiment (GRACE) Satellite Mission: A Review. *Remote Sens.* **2018**, *10*, 829. [CrossRef]
52. Yin, W.; Hu, L.; Jiao, J.J. Evaluation of Groundwater Storage Variations in Northern China Using GRACE Data. *Geofluids* **2017**, *2017*, 8254824. [CrossRef]
53. Cleveland, R.B.; William, S.; Cleveland, J.E.; McRAe, I.T. STL: A Seasonal-Trend Decomposition Procedure Based on Loess. *J. Off. Stat.* **1990**, *6*, 3–73.
54. Shamsudduha, M.; Chandler, R.E.; Taylor, R.G.; Ahmed, K.M. Recent Trends in Groundwater Levels in a Highly Seasonal Hydrological System: The Ganges-Brahmaputra-Meghna Delta. *Hydrol. Earth Syst. Sci.* **2009**, *13*, 2373–2385. [CrossRef]
55. Buma, W.G.; Lee, S.I.; Seo, J.Y. Hydrological Evaluation of Lake Chad Basin Using Space Borne and Hydrological Model Observations. *Water* **2016**, *8*, 205. [CrossRef]
56. Taher, M.R.; Chornack, M.P.; Mack, T.J. *Groundwater Levels in the Kabul Basin, Afghanistan, 2004–2013*; U.S. Department of the Interior, U.S. Geological Survey: Reston, VA, USA, 2014.

57. Yu, W.; Yang, Y.-C.; Savitsky, A.; Alford, D.; Brown, C.; Wescoat, J.; Debowicz, D.; Robinson, S. *The Indus Basin of Pakistan*; The World Bank: Washington, DC, USA, 2013.
58. Federal Flood Commission, Ministry of Water Resources. Annual Flood Report 2017. 2017. Available online: https://mowr.gov.pk/SiteImage/Misc/files/2017%20Annual%20Flood%20Report%20of%20FFC.pdf (accessed on 20 February 2020).
59. Muhammad, S.; Tian, L.; Khan, A. Early Twenty-First Century Glacier Mass Losses in the Indus Basin Constrained by Density Assumptions. *J. Hydrol.* **2019**, *574*, 467–475. [CrossRef]
60. Basharat, M.; Ali, S.U.; Azhar, A.H. Spatial Variation in Irrigation Demand and Supply across Canal Commands in Punjab: A Real Integrated Water Resources Management Challenge. *Water Policy* **2014**, *16*, 397–421. [CrossRef]
61. Ali, S.; Cheema, M.J.M.; Waqas, M.M.; Waseem, M.; Awan, U.K.; Khaliq, T. Changes in Snow Cover Dynamics over the Indus Basin: Evidences from 2008 to 2018 MODIS NDSI Trends Analysis. *Remote Sens.* **2020**, *12*, 2782. [CrossRef]
62. Qureshi, A.S.; Shah, T.; Akhtar, M. *The Groundwater Economy of Pakistan*; IWMI: Colombo, Sri Lanka, 2003; p. 31.
63. Qureshi, A.S. Groundwater Governance in Pakistan: From Colossal Development to Neglected Management. *Water* **2020**, *12*, 3017. [CrossRef]
64. Mishra, V.; Asoka, A.; Vatta, K.; Lall, U. Groundwater Depletion and Associated CO_2 Emissions in India. *Earth's Futur.* **2018**, *6*, 1672–1681. [CrossRef]
65. NASA NASA Satellites Unlock Secret to Northern India's Vanishing Water. Available online: https://www.nasa.gov/topics/earth/features/india_water.html (accessed on 3 February 2021).
66. Chen, J.; Famigliett, J.S.; Scanlon, B.R.; Rodell, M. Groundwater Storage Changes: Present Status from GRACE Observations. *Surv. Geophys.* **2016**, *37*, 397–417. [CrossRef]
67. Baweja, S.; Aggarwal, R.; Brar, M. Groundwater Depletion in Punjab, India. *Encycl. Soil Sci. Third Ed.* **2017**, 1–5. [CrossRef]
68. Shah, T.; Roy, A.D.; Qureshi, A.S.; Wang, J. Sustaining Asia's Groundwater Boom: An Overview of Issues and Evidence. *Nat. Resour. Forum* **2003**, *27*, 130–141. [CrossRef]
69. Asoka, A.; Gleeson, T.; Wada, Y.; Mishra, V. Relative Contribution of Monsoon Precipitation and Pumping to Changes in Groundwater Storage in India. *Nat. Geosci.* **2017**, *10*, 109–117. [CrossRef]
70. Singh, A.P.; Bhakar, P. Development of Groundwater Sustainability Index: A Case Study of Western Arid Region of Rajasthan, India. *Environ. Dev. Sustain.* **2020**, *23*, 1844–1868. [CrossRef]
71. van Steenbergen, F.; Kaisarani, A.B.; Khan, N.U.; Gohar, M.S. A Case of Groundwater Depletion in Balochistan, Pakistan: Enter into the Void. *J. Hydrol. Reg. Stud.* **2015**, *4*, 36–47. [CrossRef]
72. Yin, W.; Li, T.; Zheng, W.; Hu, L.; Han, S.C.; Tangdamrongsub, N.; Šprlák, M.; Huang, Z. Improving Regional Groundwater Storage Estimates from GRACE and Global Hydrological Models over Tasmania, Australia. *Hydrogeol. J.* **2020**, *28*, 1809–1825. [CrossRef]
73. Feng, T.; Shen, Y.; Chen, Q.; Wang, F.; Zhang, X. Groundwater Storage Change and Driving Factor Analysis in North China Using Independent Component Decomposition. *J. Hydrol.* **2022**, *609*, 127708. [CrossRef]
74. Alley, W.M.; Konikow, L.F. Bringing GRACE Down to Earth. *Groundwater* **2015**, *53*, 826–829. [CrossRef]

water

MDPI

Article

Impact of Boundary Conditions Dynamics on Groundwater Budget in the Campania Region (Italy)

Mattia Gaiolini [1], Nicolò Colombani [1,*], Gianluigi Busico [2], Fabrizio Rama [3] and Micòl Mastrocicco [2]

[1] Department of Material, Environmental Sciences and Urban Planning, Polytechnic University of Marche, Via Brecce Bianche 12, 60131 Ancona, Italy
[2] Department of Environmental, Biological and Pharmaceutical Sciences and Technologies, Second University of Naples, Via Vivaldi 43, 81100 Caserta, Italy
[3] Jealott's Hill International Research Centre, Syngenta Ltd., Warfield, Bracknell RG42 6EY, UK
* Correspondence: n.colombani@univpm.it; Tel.: +39-071-220-4710

Abstract: Groundwater budgets and fluxes are affected by human activities and climate change. Numerical models are cost-effective tools to investigate the different components of the hydrologic cycle. In this study, a groundwater flow model of the unconfined aquifers of the Campania region (Italy) has been developed and calibrated in Processing Modflow 11, resulting in an accurate assessment of groundwater fluxes and their trends over fifteen years (2000–2015). The model was implemented using a high-resolution grid to capture small hydrogeological features such as wells and rivers and informed by time variable datasets used as boundary conditions (i.e., river and sea levels, aquifer recharge, evapotranspiration, and discharge from adjacent systems). Good calibration and validation performances were achieved for piezometric heads (R^2 = 0.958). A set of scenarios was developed using constant boundary conditions (i.e., constant sea-level BC, uniform extinction depth BC), and the outputs were compared, quantitively assessing differences in groundwater fluxes. Simulations pointed out that using time series to inform boundary conditions in the model does not always result in a significant change in the computed fluxes. Overall, non-uniform extinction depth was the most influential condition, while both rivers and sea level conditions barely affected groundwater budgets. In addition, results highlighted the need for an accurate estimation of spatiotemporal variations of both recharge and evapotranspiration, due to their strong seasonal variability and their massive contribution to the hydrogeological cycle. Finally, a marked increase of evapotranspiration fluxes controlled by interannual variability of precipitation and atmospheric temperatures has been quantified over the modelled period.

Keywords: flow model; groundwater budget; remote sensing; recharge; evapotranspiration

1. Introduction

The Mediterranean region, where exceptional levels of biodiversity occur [1], has been identified as one of the most prominent "Hot-Spots" in actual and future climate change (CC) projections [2]. Climatic disturbance in terms of increasing temperatures [3,4], global hydrological cycle disturbance [5], and sea-level rise [6–8] could greatly affect both groundwater systems and groundwater-dependent ecosystems. Indeed, groundwater inputs support or compensate for surface water inputs and play a vital role in maintaining healthy ecosystems [9]. Since CC has a significant effect on the hydrological cycle [10], is mandatory for water managers to plan appropriate measures to avoid negative potential impacts on water resources [11]. Most of the studies, published so far focused on the above-ground components of the hydrological cycle, analysing both historical and projected changes, while the scientific knowledge on the subsurface components, such as recharge, groundwater levels, aquifer fluxes, and groundwater quality have been only recently emerging in literature [12–14]. The main tools that the research community has developed to face these issues are observation networks, which allow to record the hydraulic

parameters, and mathematical/physical models which simulate their evolution in time and space. Indeed, the implementation of numerical groundwater flow models is crucial to investigating groundwater-related issues by evaluating the trends of groundwater fluxes over a simulation time and thus quantifying the ongoing CC effects on the subsurface hydrological cycle [15]. Since its release in 1988, MODFLOW has become the worldwide standard for groundwater modelling because of its flexible modular structure, complete coverage of hydrogeological processes, and free availability [16]. MODFLOW can also be integrated with a geographic information system (GIS) to provide a visual environment for groundwater resources evaluation and management [17]. Application of groundwater flow models to large domains started a long time ago, in 1978, with the Regional Aquifer System Analysis (RASA) program of the U.S. Geological Survey [18], but only a few studies, so far, aimed to numerically evaluate changes in model outputs derived from constant or variable boundary conditions (BCs).

Coelho et al. [19] developed a study focusing on the influence of different BCs on numerical simulations of an unconfined aquifer in Brazil to define the most suitable BC, without considering scenarios with constant or variable BCs. Bastani and Harter [20] developed a three-dimensional transient flow and nitrate-transport model, comparing reference results to temporally upscaled models and considering annual-averaged flow and steady-state stresses across different scenarios. However, that study only focused on the concentrations of the nitrate discharging points without quantitively addressing changes in the groundwater budget. Moreover, employing proper spatial and temporal scales for both flow and transport simulations remains one of the most important challenges in numerical modelling [21–23]. One of the main tasks in transient groundwater modelling is the need for large amounts of hydrogeological data for both model implementation and calibration/validation; those constraints have often limited the use of transient numerical flow models to well-characterized field sites, while transient large-scale models are still rare [24]. Despite this, transient groundwater flow modelling has been recognized as one of the hydrological research fields extremely relevant for scientific progress [25]. In recent years, open datasets on hydrology and hydrogeology have been released by many research groups and international organizations, but their widespread use in numerical models still faces problems such as the lack of universally accepted guidelines or insufficient resolution [26]. To explore the new opportunities (and limitations) offered by open datasets to represent variable BCs in large-scale groundwater modelling, the unconfined aquifers of the Campania region (Italy) were selected as representative of potentially vulnerable to CC groundwater bodies. In fact, newly released open datasets on hydrology and hydrogeology can theoretically increase the model's capability to quantify the variations of groundwater fluxes induced by spatially and temporally variable BCs. Over the last few years, several studies have focused on developing conceptual and numerical models of the Campania region (Italy) to tackle a series of groundwater-related issues [27–30], but without investigating the impact of BCs variability on the model outputs. This study aimed to fill this gap, assessing the influence of different implementation of BCs (e.g., constant versus variable sea-level BC, uniform versus variable extinction depth BC, etc.) over the computed groundwater flow budget from 2000 to 2015. This kind of numerical analysis would also help in reducing both human and computational efforts in similar settings, by inferring what datasets are worth being simplified (e.g., averaged over time and space) and which need to be treated as spatially variable and transient over time.

2. Materials and Methods

2.1. The Study Area

The Campania region, located in the southern part of the Italian Peninsula, covers an area of about km^2. The region embraces a wide part of the Apennines chain, including composite geological and geomorphological units. The western slope of the Apennines is characterized by graben-like coastal depressions [31] and the plains alongside the coastal strip result from the aggradation of such structural depressions, whose bed is several

thousand meters lower than the Apennine massifs [32]. The lithological and structural complexity of the region controls the hydrogeological fluxes.

The domain extends from the Tyrrhenian Sea to approximately 50 km inland, delimited in the South by the Cilento mountain range (Figure 1). The study area includes different alluvial plains (e.g., Garigliano, Volturno, Sarno, and Sele plains), characterized by debris and alluvial deposits. An important part is also occupied by limestone (e.g., M. Massico and Lattari Mts.) and volcanic units caused by the aggregation of volcanic material released during historical eruptions in the area (i.e., Vesuvio, Phlegraean Fields, and Roccamonfina volcanos are located within the model domain). In addition, the Volturno plain is characterized by a vast lowland area, subjected to land reclamation since the seventeenth century, which promoted the development of agriculture and farming along with strong coastal urbanization [33]. For toponyms used in the text refer to Figure S1.

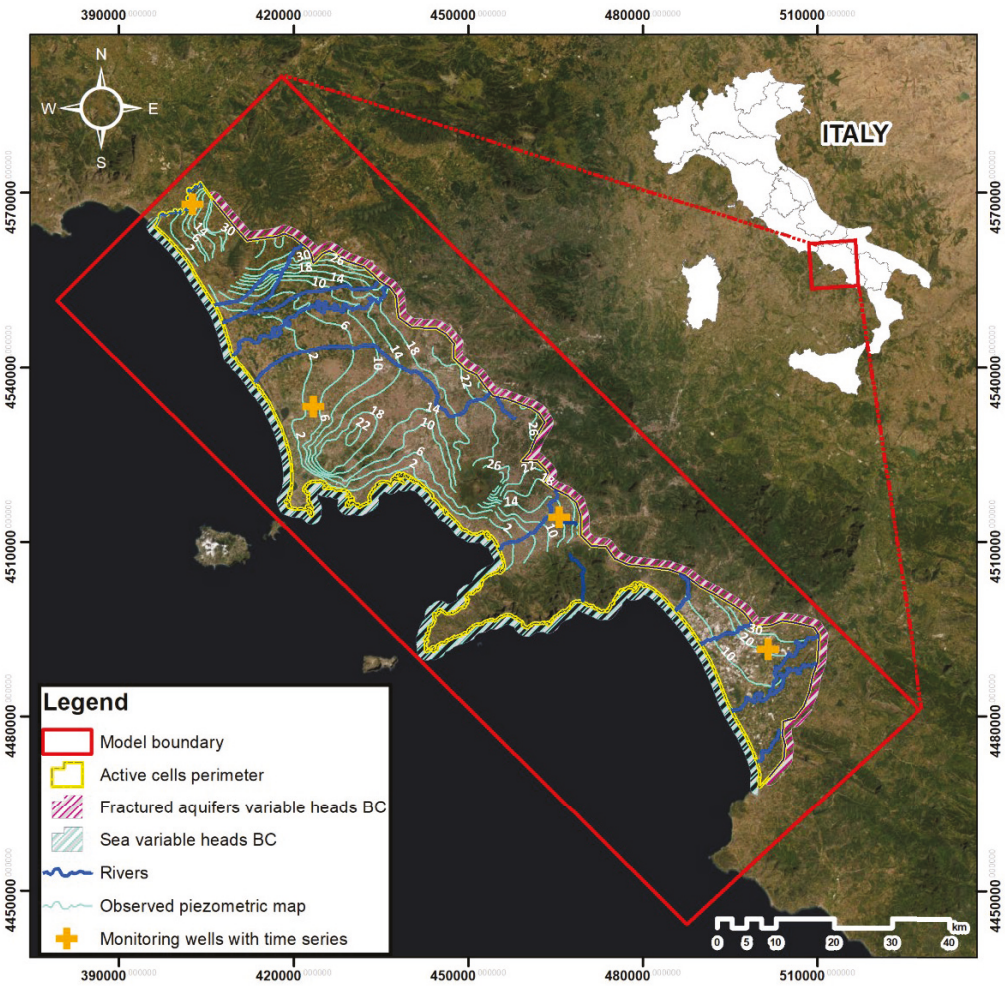

Figure 1. Model location with initial heads and boundary conditions (BCs).

2.2. Field Characterization and Boundary Conditions

Before the implementation of the groundwater flow model, all available datasets have been collected to define the conceptual model of the study area and the BCs (Table 1).

Table 1. National and worldwide open online datasets used to set up the model.

Dataset	Parameter	Repository	URL
Soil	Grain size distribution	ISRIC	https://maps.isric.org/ accessed on 17 July 2022
Geology	Aquifer thickness	ISPRA	http://sgi2.isprambiente.it/viewersgi2 accessed on 17 July 2022
Hydrogeology	Hydraulic conductivity	ISPRA	http://sgi2.isprambiente.it/viewersgi2 accessed on 17 July 2022
CORINE Land Cover	Land use	COPERNICUS	https://land.copernicus.eu/pan-european/corine-land-cover accessed on 17 July 2022
SEALEVELEURP HYL4MY008068	Sea levels	CMEMS	https://doi.org/10.48670/moi-00141 accessed on 13 June 2022
Hydrometric station dependent	Rivers stages	CFM	http://centrofunzionale.regione.campania.it/#/pages/sensori/archivio-idrometrici accessed on 17 July 2022
MYD16A3GF	Evapotranspiration	MODIS	https://doi.org/10.5067/MODIS/MOD16A2GF.006 accessed on 10 May 2022
PCRGLOBWB 2	Recharge	UU-HYDRO	https://github.com/UU-Hydro/PCR-GLOBWB_model accessed on 12 June 2022
BIGBANG40	Evapotranspiration	ISPRA	https://groupware.sinanet.isprambiente.it/bigbang-data/library/bigbang40/grids/it_evapotraspirazione_ae accessed on 17 July 2022
BIGBANG40	Recharge	ISPRA	https://groupware.sinanet.isprambiente.it/bigbang-data/library/bigbang40/grids/it_ricarica_degli_acquiferi_gr accessed on 17 July 2022

The regional SRTM Digital Terrain Model with a spatial resolution of 20 × 20 m cells was used to retrieve topographic information and represent morphology. The data files contain the elevation in a digital format, averaged on the model grid. Vegetation, buildings, and other cultural features were removed digitally, resulting in a proper terrain model.

The hydraulic conductivity of lithological units was obtained from permeability tests, by mining data from 91 borehole reports available on the online database of Instituto Superiore per la Protezione e Ricerca Ambientale [34]. All the data about pumping well rates, effective radius, screen length, and groundwater drawdown were retrieved from the same reports. The depth of the unconfined aquifer for each borehole was collected along with locations (latitude, longitude, and UTM coordinates). Other information on the aquifer's depth has been retrieved from previous studies carried out in the Campania region, such as logs on the Volturno river plain [35] or aquifer information in Cuma [36,37], Bagnoli, Giuliano, and San Valentino Torio.

Measurments on sea levels were downloaded from the open dataset Servizio Mareografico Nazionale (SMN). SMN exploits a network of 36 measuring stations uniformly distributed over the national territory and located mainly inside the port facilities. The hydrometric level is monitored since 2010 using a new microwave (radar) level meter with millimetric precision, coupled with a second level meter with a floater. Each level is referred to the absolute altimetric network of Istituto Geografico Militare (IGM). To gain a better understanding of the sea level behaviour across the entire region, Napoli, Salerno, Gaeta, and Palinuro stations were considered. However, since SMN open dataset does not cover the entire period of simulation, the datasets of the Copernicus Marine Environment Monitoring Service (CMEMS) were also exploited for sea-level trends at the same locations. CMEMS altimetric satellite data were elaborated together with the SMN ones allowing to cover the entire period of study.

The Moderate Resolution Imaging Spectroradiometer (MODIS) products have been deployed to obtain the trends of evapotranspiration in the study area for the period 2000–2015. Data were downloaded using the AppEEARS [38] interface and the MYD16A3GF model [39] to obtain spatially interpolated values. The algorithm used in MODIS is based on the Penman-Monteith equation, which includes daily meteorological data along with remotely sensed variables, such as vegetation dynamics, albedo, and land cover [40]. Land use and

soil texture maps (Table 1) were overlapped via GIS to derive a two-dimensional matrix representing the evapotranspiration extinction depth [41].

Time series of groundwater recharge has been extracted from the outputs of PCR-GLOBWB v2.0 (Utrecht University, Utrecht, The Netherland) [42], a grid-based global hydrology and water resources model. Global hydrological models (GHMs) are tools able to quantify the global terrestrial water cycle, simulating the distributed hydrological response to weather and climate variations at high resolution.

Hydrometric levels were downloaded from the Centro Funzionale Multirischi (CFM), a Civil Protection Agency of the Campania region, to represent the variation of the river stage over the simulation period. CFM provides a list of all hydrometric stations of the region recording data with a daily frequency. The closest stations to the model's boundaries were considered representative of the baseflow entering the domain from the fractured aquifers. Hydraulic head fluctuation in the fractured aquifers was modified according to the average baseflow variations over the simulation time.

2.3. Numerical Modelling

To estimate the groundwater flow budget at a regional scale, assessing the influence of variable BCs, all the data were elaborated in a GIS environment and processed via Processing Modflow 11. The flow simulation was carried out using the MODFLOW-2005 code [43]. The equation that stands at the base of MODFLOW-2005 is the partial-differential equation that describes the three-dimensional movement of groundwater of constant density through a porous matrix:

$$\frac{\partial}{\partial x}\left(K_{xx}\frac{\partial h}{\partial x}\right)+\frac{\partial}{\partial y}\left(K_{yy}\frac{\partial h}{\partial y}\right)+\frac{\partial}{\partial z}\left(K_{zz}\frac{\partial h}{\partial z}\right)+W=S_s\frac{\partial h}{\partial t} \quad (1)$$

where K_{xx}, K_{yy} and K_{zz} are values of hydraulic conductivity along x, y and z coordinate axes (LT^{-1}); h is the potentiometric head (L); W is a volumetric flux per unit volume representing sources and/or sinks of water (T^{-1}); S_s is the specific storage of the porous material (L^{-1}); and t is time (T). The standard version of MODFLOW-2005 treating the fractured units as equivalent porous media and not complex ones such as the Conduit Flow Package [44] was used given the lack of information on the location and dimensions of such zones. Thus, for the principle of parsimony in numerical modelling, a simpler representation was here adopted [45].

The model domain consisted of 656 rows, 335 columns, and 3 layers with variable width and thickness. The top of the grid represents the local ground surface, ranging from −3.49 m to 1642 m above sea level (a.s.l.). The bottom of the grid represents the bottom of the unconfined aquifers and ranges from −83 m below sea level (b.s.l.) to 144 m a.s.l.

Initially, a steady-state simulation has been run and the model has been calibrated via PEST [46] against an observed piezometric map of the Campania region for the year 2000 [47]. Given that the piezometric map was available only as a vector map, it was sampled along the contour lines to create 500 observation points that were compared versus calculated ones with an estimated error of ±1.0 m. Tyrrhenian Sea levels have been initially set to 0 m as constant head cells. Values of hydraulic conductivity, corresponding to boreholes in the same cluster, have been averaged to get an average value for each geological formation in the study area. In this way, the model domain was subdivided into polygons whose extension corresponds to the extension of the different geological formations reported in the geological map. Figure 2 highlights the heterogeneity of the Campania region, where the horizontal hydraulic conductivity values range from 1×10^{-6} m/s in the coastal part of the Volturno plain, where clay layers are present, to 6.6×10^{-4} m/s in the Vesuvio area, where highly fractured volcanic rocks are present. The value of the vertical hydraulic conductivity was set equal to the value of the horizontal hydraulic conductivity assigned to that cell in fractured units, while it was set as a tenth of the horizontal hydraulic conductivity in sedimentary units, to account for internal layering. It must be stressed,

however, that local scale heterogeneities such as intensively faulted zones, small lenses, etc. have not been explicitly incorporated in this large-scale model.

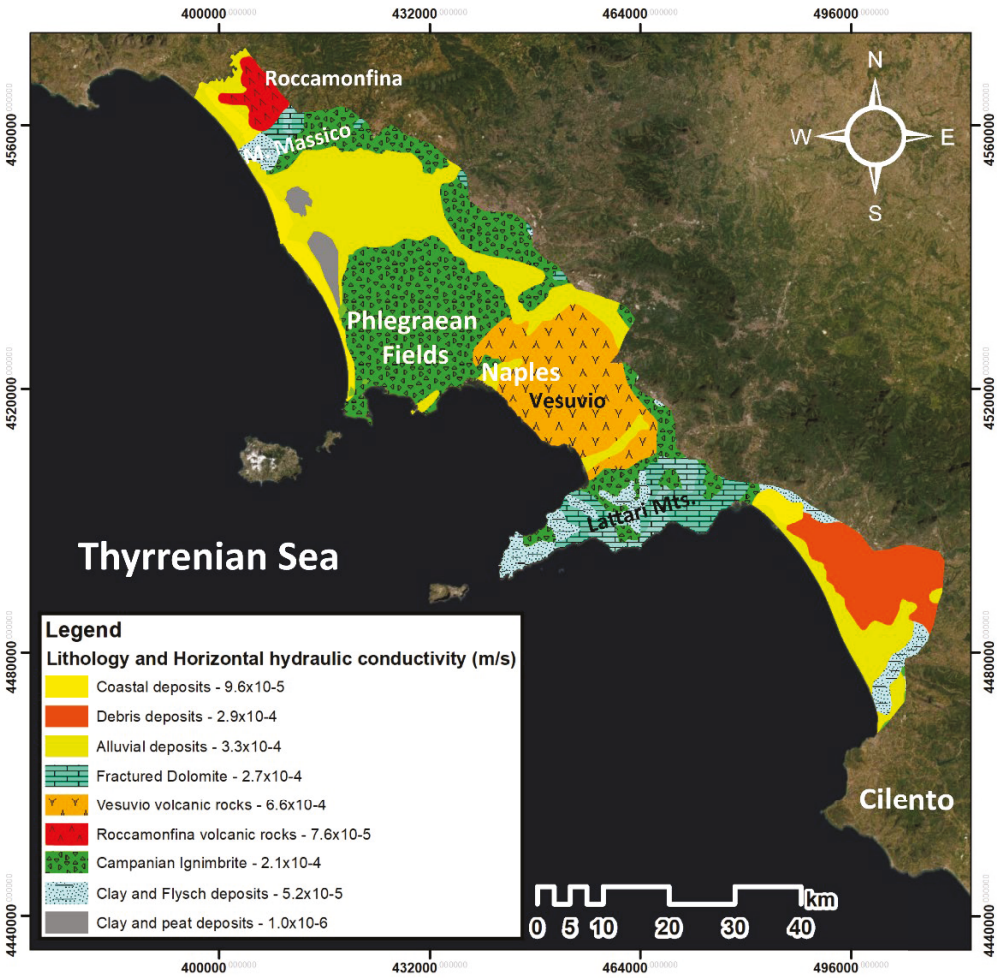

Figure 2. Distribution of the lithological units and their horizontal hydraulic conductivity values in layer 1 of the model domain.

For the steady-state simulation, evapotranspiration rates for the year 2000 were averaged from the MODIS dataset and interpolated on the numerical grid; while the recharge rates were averaged from the PCR-GLOBWB v2.0 for the same period and interpolated on the numerical grid. The Processing Modflow polyline input method in the River Package was employed to simulate, from North to South, Garigliano, Savone, Agnena, Volturno, Regi Lagni, Sarno, Picentino, Tusciano, Sele, and Calore rivers, drawing their actual pathways and defining river parameters. The riverbed conductance per unit length C_{rivl} (LT^{-1}), the river stage h_{riv} (L), and the elevation of the riverbed bottom B_{riv} (L) have been assigned to the most upstream and downstream vertices of each river polyline and then applied to the model cells employing a linear interpolation. River stages were assumed close to the assigned starting head value and kept constant for the entire steady-state simulation. The flow rate Q_{riv} (L^3T^{-1}) between each river reach and the model cell is calculated by the following equations:

$$Q_{riv} = \begin{cases} C_{riv} \cdot (h_{riv} - h), & \text{if } h > B_{riv} \\ C_{riv} \cdot (h_{riv} - B_{riv}), & \text{if } h < B_{riv} \end{cases} \quad (2)$$

where h (L) is the calculated hydraulic head in the cell containing the reach.

The wells analysed from the online ISPRA database were entered into the model through the Well Package. Industrial wells were set with continuous pumping rates, while

the agricultural wells were set with discontinuous pumping rates, active only during the spring and summer seasons. Since the specified wells penetrate more than one model layer, the total pumping rate has not been distributed over the penetrated layers, but it has been assigned to the lowest cell of the well, belonging to the third model layer. The Drain Package was used to simulate the reclamation channels in the Marina di Licola area and also to simulate the effect of the underground metro lines in Naples, the mean height of each feature a.s.l. was derived from the topographical online database, while the cell conductance C_d (L^2T^{-1}) was set to a very high value (0.01) to ensure optimal groundwater withdrawal from the aquifer. The location of the depth of the different metro lines was sourced from Russo et al. [48]. The discharge rate Q_d (L^3T^{-1}) from the model cell to the drain is calculated by:

$$Q_d = \begin{cases} C_d \cdot (h - h_d), & \text{if } h > h_d \\ 0, & \text{if } h \leq h_d \end{cases} \tag{3}$$

The horizontal hydraulic conductivity was estimated by inverse modelling using the numerical code PEST, assigning a parameter number to it. PEST searches optimum parameter values for which the sum of squared deviations between model-calculated and observed values from the piezometric map of the region is reduced to a minimum. Such comparison has been performed using a scatter diagram of the simulated and observed data (Figure 3).

To investigate possible changes in the groundwater system associated with temporal variations of evapotranspiration and recharge patterns, a transient simulation was carried out. Sixty-four stress periods of seasonal length (3 months), subdivided into three time steps of 1 month each, were used. As recommended by Harbaugh [43], the starting hydraulic heads for the transient simulation have been set equal to the head values calculated at the end of the steady-state simulation. Table 2 shows the specific storage (S_s) and specific yield (S_y) values, depending on the geologic material, together with the riverbed conductance (C_{riv}) gained after the calibration procedure.

Table 2. S_s and S_y depending on the geologic material (upper panel), and C_{riv} gained after the calibration procedure (lower panel).

Material	S_s (m^{-1})	S_y (-)
Clayey and calcareous clayey units	0.001	0.2
Debris, alluvial, fluviolacusters and fluvioglacial deposits	1×10^{-4}	0.33
Lavas, ignibrites, pyroclastics	1×10^{-5}	0.21
Organogenic, neritic, and platform limestone	1×10^{-5}	0.14
River	**C_{riv} (m^2/s)**	
Garigliano	from 0.021 to 0.235	
Savone	from 0.017 to 0.058	
Agnena	from 0.001 to 0.033	
Volturno	from 0.009 to 0.044	
Regi Lagni	from 0.007 to 0.072	
Sarno	from 0.007 to 0.040	
Picentino	from 0.009 to 0.011	
Tusciano	from 0.011 to 0.019	
Sele	from 0.014 to 0.116	
Calore	from 0.060 to 0.086	

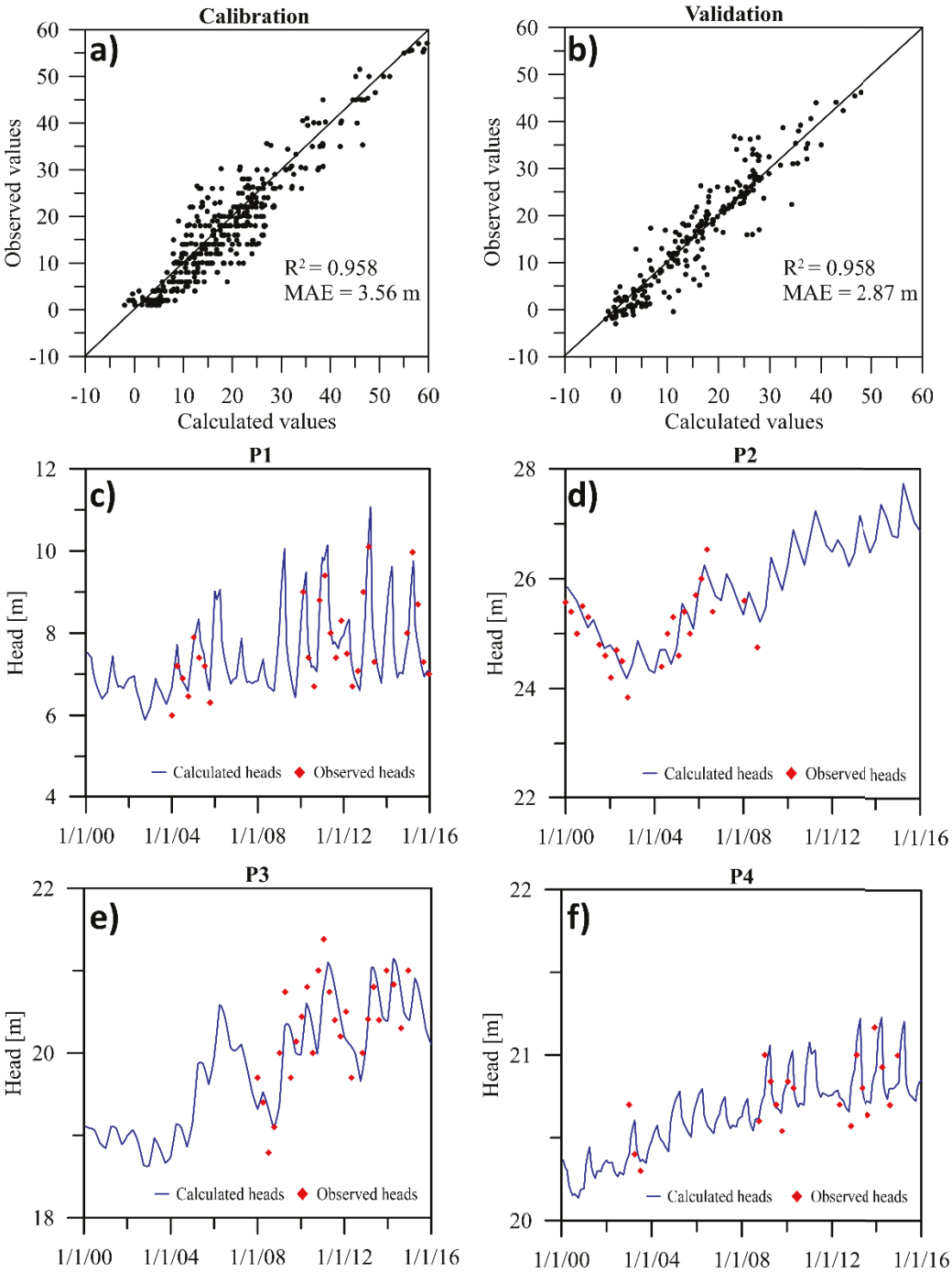

Figure 3. Head Scatter Diagrams of the calibration (**a panel**) and validation processes (**b panel**), and comparison between calculated and observed heads at piezometers P1, P2, P3 and P4 (**c–f panels**), represented in Figure 1.

To consider the variability of the evapotranspiration over time, the MODIS data have been spatialized using the kriging technique and inserted into the model with seasonal frequency. The values of recharge rate from the global numerical hydrologic model published by de Graaf et al. [49] have been processed in python to obtain spatially interpolated values for the period 2000–2015, which have been assigned to the model with seasonal frequency. The calibrated model was implemented with the before-mentioned transient datasets accounting for the seasonal changes in hydrometric levels, Tyrrhenian Sea levels, and fractured aquifer seasonal head fluctuations as variable BCs. The Evapotranspiration

Package was also integrated with spatially variable extinction depths dependent on the land use and soil texture maps.

The validation of the transient state model was performed by exploiting a piezometric map of the Campania region for the year 2013, which was derived from a secondary elaboration of the global groundwater depth dataset [50] to match modelled and measured hydraulic heads. Besides, selected monitoring wells (Figure 1) with piezometric trend data were compared versus model results.

Both the model calibration and validation were assessed by calculating and comparing the value of the coefficient of determination (R^2) and the mean absolute error (MAE).

The Processing Modflow ZoneBudget routine [43] can produce water budgets for user-defined zones within the model domain. Zones are defined by assigning zone numbers to model cells, allowing for to calculation of the volumetric water budget in a different part of the domain, accounting for evapotranspiration, fractured aquifers, rivers, and the Tyrrhenian Sea component separately. Each trend calculated by the model, considering all the transient input datasets as variable BCs (transient model), was compared with the respective trend calculated by an upscaled model considering a uniform extinction depth, a constant head at the fractured aquifers, and constant sea and river levels (basic model). Moreover, to investigate which datasets are worth being averaged, a set of scenarios have been developed applying to the transient model each of the averaged BCs individually:

- constant head at the fractured aquifers BC (scenario S1);
- uniform extinction depth BC (scenario S2);
- constant Tyrrhenian Sea level BC (scenario S3);
- constant river levels BC (scenario S4).

In addition, to numerically quantify the impact of the averaged conditions, the 15-year average flux of each groundwater budget component has been estimated and differences between basic, transient, S1, S2, S3, and S4 simulations were graphically compared.

Finally, since the pivotal contribution to the groundwater budget of both recharge and evapotranspiration, an additional recharge and evapotranspiration rates dataset has been investigated. Alternatively, to the PCR-GLOBWB v.2.0 published by Sutanudjaja et al. and the MODIS products, the BIGBANG (*Bilancio Idrogeologico GIS BAsed a scala Nazionale su Griglia regolare*) [51] distributed model was employed, and results compared.

3. Results and Discussion

3.1. Flow Model Performance

Given the extremely challenging regional scale of the domain (3672 km^2), reasonably good calibration and validation were achieved for hydraulic heads, resulting in an R^2 of 0.958 (Figure 3). MAE values of 3.56 m for calibration and 2.87 m for validation, were judged acceptable in the wide range of the simulated piezometric levels (>100 m). Observations of groundwater levels from selected monitoring wells were used to verify the ability of the model to describe water table fluctuations in the unconfined aquifers (Figure 3). Unfortunately, a widespread monitoring network of wells is not available in the region, and this is a limitation for the model performance. Indeed, monitoring groundwater levels at regional scale may enable a better assessment of groundwater depletion, as well as inferring changes in flow directions over time, as recently pointed out by Brakkee et al. [52]. Moreover, piezometric data are missing in some karst and fractured areas of the domain (Massico mountain, Vesuvio volcano, and Monti Lattari) consequently model reliability is lower on those areas than in alluvial zones. By means of the Processing Modflow ZoneBudget routine [43] a defined zone number was assigned to those areas and their importance in relation to the overall model domain was assessed in terms of water budget component percentages. As expected, groundwater recharge played a very important role in karst environments, representing 12.7% of the overall domain, while evapotranspiration was just 1.5% with respect to the total, given that in mountain areas the groundwater depth from the surface is higher than the extinction depth. The storage capacity turns out to be consistent, whereas all the other budget components resulted to be negligible. The

general high permeability grade due to fracturing leads to a high groundwater recharge rate [53] that varies between 48% and 78% of the mean annual effective precipitation [54,55], depending on the relative abundance of limestone and dolomites lithologies.

The validated transient model allowed analysing and quantifying relevant stresses in different portions of the domain at different times. Figure 4 shows an example of both the three-dimensional and planar view of the calculated hydraulic heads map at the end of the simulation. It pointed out regions of the domain characterized by high hydraulic gradient, especially the northern part in correspondence of the Roccamonfina Volcano, which acted as a groundwater mounding area, as well as the Vesuvio, Phlegraean Fields, and Monti Lattari. Hydraulic heads resulted to be very low in the Volturno river plain, following the topographic gradient. Near the coast, the water level was very shallow, due to reclamation channels located in the Marina di Licola area (lower Volturno plain).

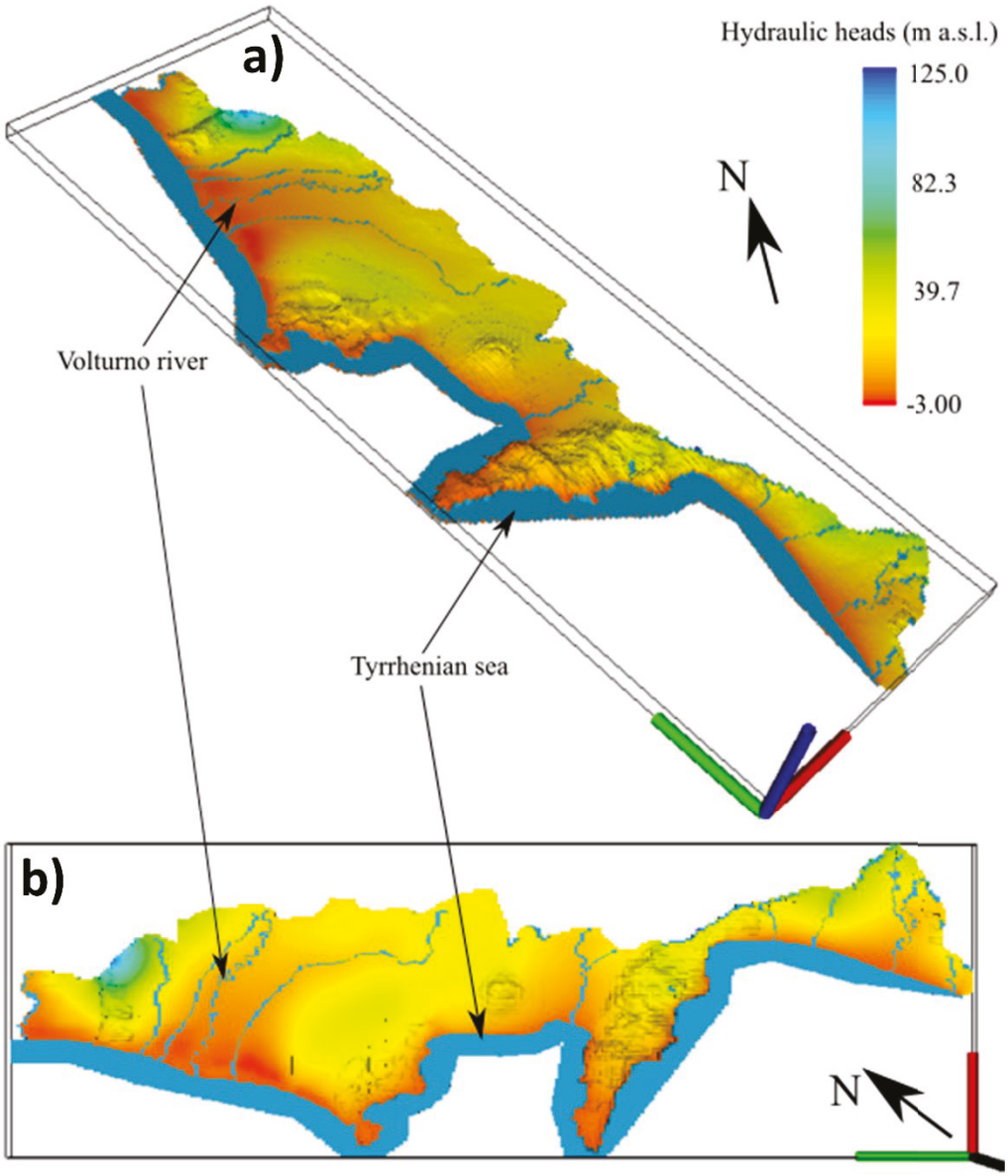

Figure 4. Three-dimensional sketch (**a panel**) and plan view (**b panel**) of the model calculated hydraulic heads map at the end of the simulation time.

In addition, the model produced accurate estimates of the groundwater budget with a mean error of less than 0.3% among in and out components. This allowed focusing on the single water budget components, whose fluxes are difficult to estimate without

a physically based model even though they are crucial for better management of the hydrogeological basins.

3.2. Water Fluxes Trends and Comparative Analysis

The fluxes trends have been estimated accounting for the inflow from the fractured aquifers, the evapotranspiration, the river-groundwater interactions, and the Tyrrhenian Sea component, separately. To highlight the influence of the time variable datasets, the basic model calculated trends (red line), the transient model calculated trends (blue line), and the scenarios (S1, S2, etc.) calculated trends (dashed green line) associated with the budget component have been plotted together.

Figure 5a displays the inflow component from the fractured aquifers. The transient model calculated trend shows a quite higher flux with a wider seasonal variation throughout the simulation time, with respect to the basic and S1 model.

The evapotranspiration component represents the most important outflow contribution. Figure 5b clearly shows its seasonal variability with increasing fluxes over the warm seasons, reaching values up to 20 m^3/s. Moreover, since the extinction depth affects the evapotranspiration fluxes, the S2 trend perfectly reflects the basic model, underlying the importance of considering a non-uniform extinction depth over the domain to account for different land cover and different soil types that directly drive the extinction depth [41].

The seawater intrusion component (Figure 5c) is characterized by a very low flux and can be considered negligible with respect to submarine groundwater discharge. However, importing a transient sea-level dataset leads the seawater intrusion flux of the transient model to display positive peaks due to the seasonal oscillation of the Tyrrhenian Sea. This could be further investigated at the local scale by performing a variable-density flow and transport simulation. There are no evident changes between the basic, transient, and S3 scenarios in submarine groundwater discharge, which shows a mean flux over the simulation time between 5 and 6 m^3/s (Figure 5d).

Both river inflow and outflow (Figure 5e,f), which represent the losing and gaining flow rate from and to the river, show no significant changes between basic, transient, and S4 simulations. Therefore, considering the effort to import all required data in the models, a constant river level dataset averaged over the simulation time should be considered for large-scale simulations.

To numerically quantify the impact of time variable input datasets on groundwater budget, the 15-year average flux of each component has been estimated and differences between basic, transient, S1, S2, S3, and S4 simulations were represented in Figure 6. A difference of ~1.67 m^3/s was found in the mean evapotranspiration between the basic and the transient simulations. Almost the same difference (~1.70 m^3/s) was found between S2 and the transient model. This confirmed that extinction depth is the most influencing parameter, requiring a precise spatiotemporal estimation to obtain accurate predictions of the groundwater budget.

The difference in the mean inflow from the fractured aquifers component (~0.65 m^3/s) between the basic and transient models did not seem to be entirely due to the associated transient inflow parameters, but also accounted for the variable river level dataset.

Even if the difference in the averaged seawater intrusion component was relatively high (almost doubled from the basic to transient model), it should be considered negligible in absolute terms (0.02 m^3/s). The mean submarine groundwater discharge showed no appreciable changes between the scenarios, both in relative and absolute terms. Effectively, that component seems to be more affected by the non-uniform extinction depth dataset (0.16 m^3/s difference) than by the transient Tyrrhenian Sea levels (0.06 m^3/s difference), suggesting that sea level could be kept constant over the simulation time.

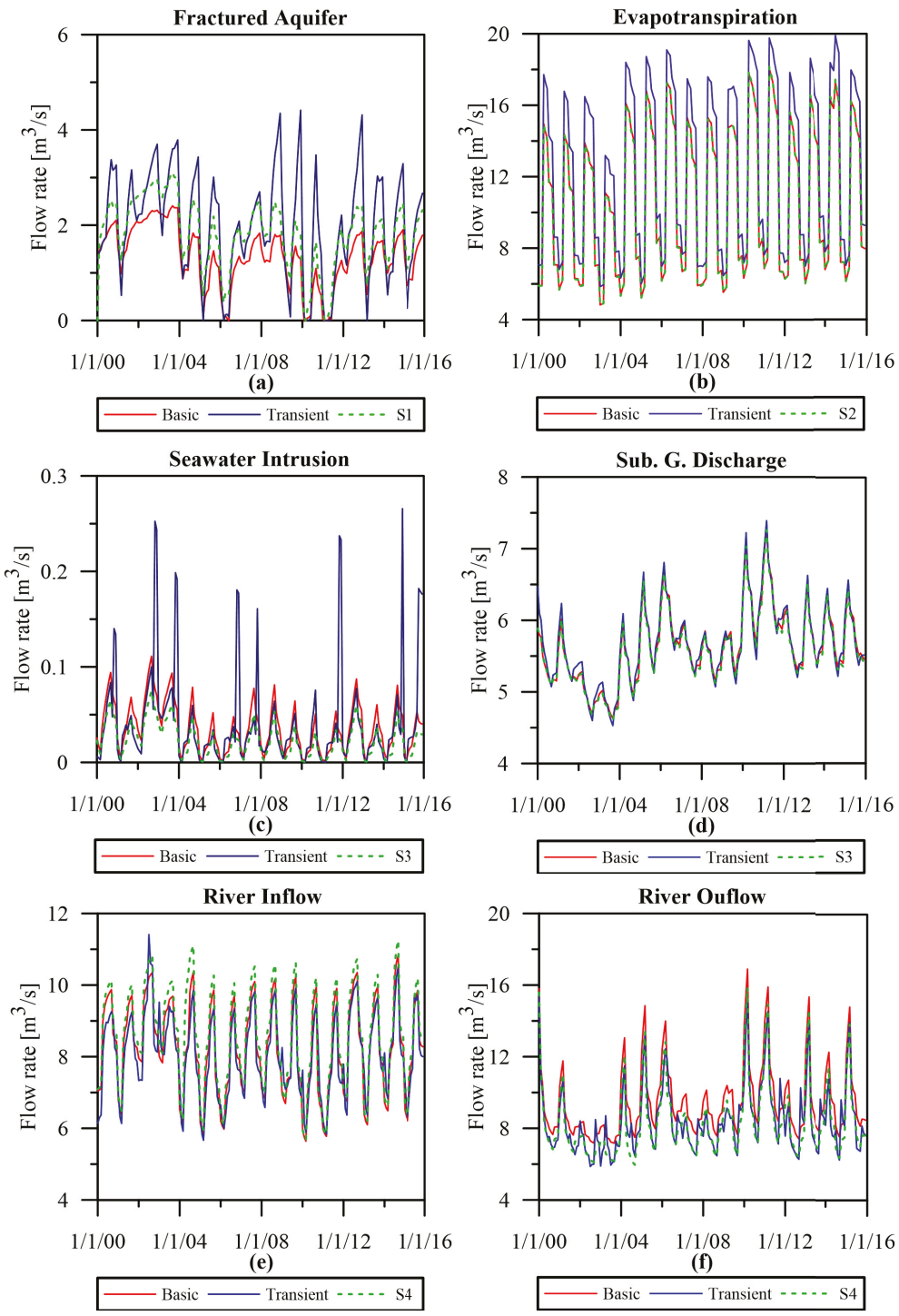

Figure 5. Comparison of the fluxes' trends over the simulation time among the basic (red line), the transient (blue line) and the S1, S2, S3, and S4 (green dashed lines) simulations: (**a**) Inflow from the fractured aquifer, (**b**) Evapotranspiration, (**c**,**d**) Seawater intrusion and Submarine groundwater discharge, (**e**,**f**) River inflow and outflow.

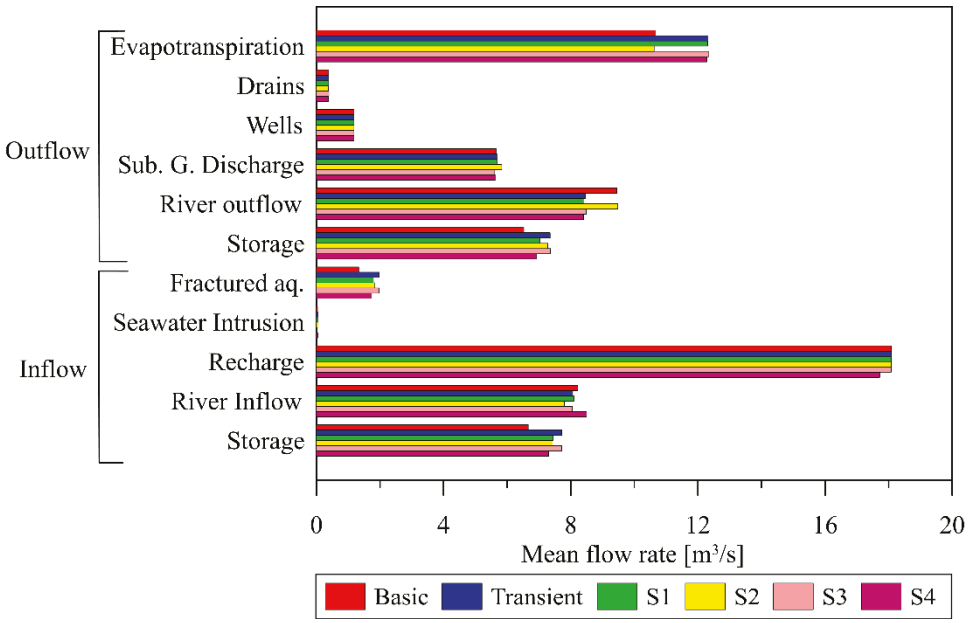

Figure 6. Comparison of the average flow rates and storage over the simulation time between: Basic, Transient, S1, S2, S3, and S4 simulations.

The same analysis can be conducted considering the mean groundwater flux towards the river (river outflow). The difference of 0.98 m^3/s between the basic and the transient simulations was mostly due to the non-uniform extinction depth rather than to the variable river level dataset: the value rose to 1.02 m^3/s between the S2 and the transient model, while it dropped to 0.05 m^3/s between the S4 and the transient model. Considering also that the mean river flux towards the unconfined aquifers (river inflow) slightly differs among the various scenarios, accounting for a variable river level dataset does not seem to be crucial.

The comparative analysis pointed out the fundamental role of the extinction depth in shifting the allocation of groundwater fluxes among different compartments, altering the contribution of each component with respect to the total budget.

Moreover, since the evaluation of each groundwater contribution underlines the pivotal role of both the recharge (with a mean flux of 18.1 m^3/s) and evapotranspiration components, the additional BIGBANG dataset has been investigated. The derived recharge and evapotranspiration trends have been calculated and compared with the transient model results (Figure 7).

The recharge flow rates strongly differ among the two models, while the evapotranspiration fluxes were more similar. The linear temporal trends show an increase in the recharge flux over time for both the PCR-GLOBWB v2.0 and the BIGBANG products, reflecting the positive trends of the hydraulic heads observed in the monitoring wells P1, P2, P3, and P4 (Figure 3). The process of groundwater recharge is driven by a decadal variability of the North Atlantic Oscillation and its robust correlation with the rainfall patterns [56]. Both the calculated evapotranspiration fluxes, controlled by interannual variability of precipitation and air temperature, showed increasing trends with a small positive shift (~0.10 m^3/s per year), highlighting that CC impact on groundwater resources is confirmed by the two independent databased here employed. Furthermore, because of the overestimation of the recharge flux due to topographic and geological heterogeneities of the Campania region, running the transient model using the BIGBANG products slightly decrease the performance parameters, with an R^2 = 0.948 and an MAE = 3.42 m, producing flooded areas during the peak recharge seasons that were not physically based.

Finally, it must be stressed that all other scenarios showed very little variation of the model performance indicators with an R^2 and an MAE that never exceeded 0.947 and 2.91 m, respectively. This is due to the low sensitivity of piezometric heads in capturing the

changes induced by evapotranspiration at the basin scale [57], while to solve this complex issue, monitoring wells with continuous heads dataloggers should be employed coupled with baseflow measurements [58].

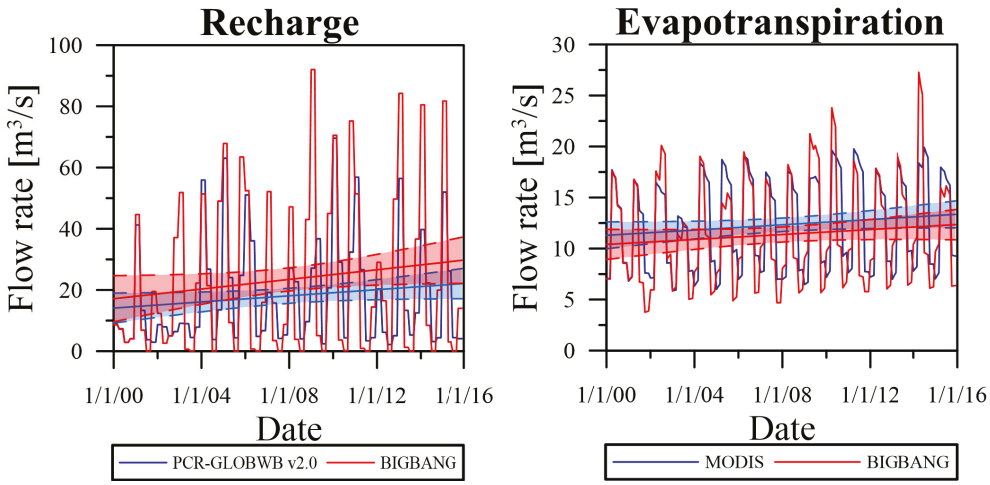

Figure 7. Left panel: comparison between the recharge rates obtained by PCR-GLOBWB v2.0 and BIGBANG, with their linear trends (solid lines); **Right panel**: comparison between the evapotranspiration rates obtain by MODIS products and BIGBANG, with their linear trends (solid lines). The coloured areas between the dashed lines represent the 95% confidence interval.

4. Conclusions

Open online datasets, along with historical observations and literature review were used to untangle the complexity of regional hydrogeological settings, supporting the implementation of a robust numerical model to describe groundwater fluxes for the unconfined aquifers of the Campania region. The quantification of the total flux of each component in the budget highlighted the pivotal role of recharge and evapotranspiration rates, with a mean flux of 18.1 and 12.3 m^3/s, respectively. Their variable patterns throughout the simulation period affected the whole hydrogeological budget, pointing out the need for their accurate estimation over time, to account for their high seasonal variability and climatic trends. Recharge can reach a value of above 60 m^3/s during wet periods, while evapotranspiration variability ranges from 5 to maximum values up to 20 m^3/s over the warm seasons. Time variable input datasets had very different effects on the components of the groundwater budget, controlling water fluxes between different compartments. Simulations pointed out that both fractured aquifers head fluctuations and non-uniform extinction depth datasets used as BCs should not be averaged. Considering transient data of extinction depth had a massive effect on the budget results, not only influencing evapotranspiration rates directly but also affecting all the other components of the groundwater budget, indirectly. Conversely, the inclusion of other datasets, namely variable river and sea levels, barely impacted the groundwater budget, not making it worth the extra effort. Therefore, the inclusion of transient BCs in a numerical model should be based on expert judgment, balancing accuracy and complexity and considering the human and computational efforts required. Finally, the results have underlined that continuous groundwater level and baseflow estimates are crucial to minimize model uncertainties and increase the reliability of groundwater budgets at the basin scale. Therefore, such measurements need to be included in an ideal groundwater monitoring network at a regional scale.

Supplementary Materials: The following supporting information can be downloaded at: https://www.mdpi.com/article/10.3390/w14162462/s1, Figure S1: The domain is limited by the Tyrrhenian Sea (light blue) and by the Apennines and the Cilento mountain range (light green). The area includes the Garigliano, Volturno, Sarno, and Sele plains (yellow), the volcanic units Vesuvio, Phlegraean Fields, and Roccamonfina (white) and the limestone units Mount Massico, Mount Maggiore, and Mounts Lattari (white). More in detail: the Garigliano plain hosts the Garigliano river, the Volturno plain hosts the Savone, Agnena, Volturno, and Regi Lagni rivers, the Sarno plain hosts the Sarno rivers, and the Sele plain hosts the Picentino, Tusciano, Sele and Calore rivers.

Author Contributions: Conceptualization, M.M. and N.C.; methodology, N.C., M.M. and M.G.; software, M.G. and N.C.; validation, M.M. and N.C.; formal analysis, M.G.; investigation, M.G.; data curation, M.G., F.R. and G.B.; writing—original draft preparation, M.G.; writing—review and editing, N.C., M.M. and F.R.; visualization, M.G. and G.B.; supervision, N.C. All authors have read and agreed to the published version of the manuscript.

Funding: This research received no external funding.

Institutional Review Board Statement: Not applicable.

Informed Consent Statement: Not applicable.

Data Availability Statement: Data will be made available by the authors upon request.

Acknowledgments: Simone Tavoni is acknowledged for helping to gather the raw data.

Conflicts of Interest: The authors declare no conflict of interest.

References

1. Blondel, J.; Aronson, J. *Biology and Wildlife of the Mediterranean Region*, 1st ed.; Oxford University Press: Oxford, UK, 1999; p. 328.
2. Lionello, P.; Scarascia, L. The relation between climate change in the Mediterranean region and global warming. *Reg. Environ. Chang.* **2018**, *18*, 1481–1493. [CrossRef]
3. Cramer, W.; Guiot, J.; Fader, M.; Garrabou, J.; Gattuso, J.P.; Iglesias, A.; Xoplaki, E. Climate change and interconnected risks to sustainable development in the Mediterranean. *Nat. Clim. Chang.* **2018**, *8*, 972–980. [CrossRef]
4. Hallegatte, S. Strategies to adapt to an uncertain climate change. *Global. Environ. Chang.* **2009**, *19*, 240–247. [CrossRef]
5. IPCC. *Climate Change 2021: The Physical Science Basis. Contribution of Working Group I to the Sixth Assessment Report of the Intergovernmental Panel on Climate Change*; Masson-Delmotte, V.P., Zhai, A., Pirani, S.L., Connors, C., Péan, S., Berger, N., Caud, Y., Chen, L., Goldfarb, M.I., Gomis, M., et al., Eds.; Cambridge University Press: Cambridge, UK; New York, NY, USA, 2021; in press. [CrossRef]
6. FitzGerald, D.M.; Fenster, M.S.; Argow, B.A.; Buynevich, I.V. Coastal impacts due to sea-level rise. *Earth Planet. Sci.* **2008**, *36*, 601–647. [CrossRef]
7. Carrasco, A.R.; Ferreira, Ó.; Roelvink, D. Coastal lagoons and rising sea level: A review. *Earth Sci.* **2016**, *154*, 356–368. [CrossRef]
8. Benjamin, J.; Rovere, A.; Fontana, A.; Furlani, S.; Vacchi, M.; Inglis, R.H.; Gehrels, R. Late Quaternary sea-level changes and early human societies in the central and eastern Mediterranean Basin: An interdisciplinary review. *Quat. Int.* **2017**, *449*, 29–57. [CrossRef]
9. Erostate, M.; Huneau, F.; Garel, E.; Ghiotti, S.; Vystavna, Y.; Garrido, M.; Pasqualini, V. Groundwater dependent ecosystems in coastal Mediterranean regions: Characterization, challenges and management for their protection. *Water Res.* **2020**, *172*, 115461. [CrossRef]
10. Famiglietti, J.S. The global groundwater crisis. *Nat. Clim. Chang.* **2014**, *4*, 945–948. [CrossRef]
11. Erturk, A.; Ekdal, A.; Gurel, M.; Karakaya, N.; Guzel, C.; Gonenc, E. Evaluating the impact of climate change on groundwater resources in a small Mediterranean watershed. *Sci. Tot. Environ.* **2014**, *499*, 437–447. [CrossRef] [PubMed]
12. Butscher, C.; Huggenberger, P. Modeling the temporal variability of karst groundwater vulnerability, with implications for climate change. *Environ. Sci. Technol.* **2009**, *43*, 1665–1669. [CrossRef]
13. Oude Essink, G.H.P.; Van Baaren, E.S.; De Louw, P.G. Effects of climate change on coastal groundwater systems: A modeling study in the Netherlands. *Water Resour. Res.* **2010**, 46. [CrossRef]
14. Mastrocicco, M.; Gervasio, M.P.; Busico, G.; Colombani, N. Natural and anthropogenic factors driving groundwater resources salinization for agricultural use in the Campania plains (Southern Italy). *Sci. Total Environ.* **2021**, *758*, 144033. [CrossRef]
15. Allen, D.M.; Mackie, D.C.; Wei, M. Groundwater and climate change: A sensitivity analysis for the Grand Forks aquifer, southern British Columbia, Canada. *Hydrogeol. J.* **2004**, *12*, 270–290. [CrossRef]
16. Zhou, Y.; Li, W. A review of regional groundwater flow modeling. *Geosci. Front.* **2011**, *2*, 205–214. [CrossRef]
17. Aghlmand, R.; Abbasi, A. Application of MODFLOW with boundary conditions analyses based on limited available observations: A case study of Birjand plain in East Iran. *Water* **2019**, *11*, 1904. [CrossRef]

18. Sun, R.J.; Johnston, R.H. *Regional Aquifer-System Analysis Program of the US Geological Survey, 1978–1992*; US Government Printing Office: Denver, CO, USA, 1994; p. 126. [CrossRef]
19. Coelho, C.D.; Faria, A.C.S.; Marques, E.A.G. Comparative analysis of different boundary conditions and their influence on numerical hydrogeological modeling of Palmital watershed, southeast Brazil. *J. Hydrol.* **2017**, *12*, 210–219. [CrossRef]
20. Bastani, M.; Harter, T. Effects of upscaling temporal resolution of groundwater flow and transport boundary conditions on the performance of nitrate-transport models at the regional management scale. *Hydrogeol. J.* **2020**, *28*, 1299–1322. [CrossRef]
21. Cushman, J.H.; Bennethum, L.S.; Hu, B.X. A primer on upscaling tools for porous media. *Adv. Water Resour.* **2002**, *25*, 1043–1067. [CrossRef]
22. Dentz, M.; Le Borgne, T.; Englert, A.; Bijeljic, B. Mixing, spreading and reaction in heterogeneous media: A brief review. *J. Contam. Hydrol.* **2011**, *120*, 1–17. [CrossRef] [PubMed]
23. Scheibe, T.D.; Murphy, E.M.; Chen, X.; Rice, A.K.; Carroll, K.C.; Palmer, B.J.; Wood, B.D. An analysis platform for multiscale hydrogeologic modeling with emphasis on hybrid multiscale methods. *Groundwater* **2015**, *53*, 38–56. [CrossRef] [PubMed]
24. Hellwig, J.; de Graaf, I.E.M.; Weiler, M.; Stahl, K. Large-scale assessment of delayed groundwater responses to drought. *Water Resour. Res.* **2020**, *56*, e2019WR025441. [CrossRef]
25. Fatichi, S.; Vivoni, E.R.; Ogden, F.L.; Ivanov, V.Y.; Mirus, B.; Gochis, D.; Downer, C.W.; Camporese, M.; Davison, J.H.; Ebel, B.A.; et al. An overview of current applications, challenges, and future trends in distributed process-based models in hydrology. *J. Hydrol.* **2016**, *537*, 45–60. [CrossRef]
26. Rau, G.C.; Cuthbert, M.O.; Post, V.E.A.; Daniel Schweizer, D.; Acworth, R.I.; Andersen, M.S.; Blum, P.; Carrara, E.; Rasmussen, T.C.; Ge, S. Future-proofing hydrogeology by revising groundwater monitoring practice. *Hydrogeol. J.* **2020**, *28*, 2963–2969. [CrossRef]
27. De Vita, P.; Fusco, F.; Tufano, R.; Cusano, D. Seasonal and event-based hydrological and slope stability modeling of pyroclastic fall deposits covering slopes in Campania (Southern Italy). *Water* **2018**, *10*, 1140. [CrossRef]
28. Corniello, A.; Ducci, D.; Ruggieri, G.; Iorio, M. Complex groundwater flow circulation in a carbonate aquifer: Mount Massico (Campania Region, Southern Italy). Synergistic hydrogeological understanding. *J. Geochem. Explor.* **2018**, *190*, 253–264. [CrossRef]
29. Mastrocicco, M.; Busico, G.; Colombani, N.; Vigliotti, M.; Ruberti, D. Modelling actual and future seawater intrusion in the Variconi coastal wetland (Italy) due to climate and landscape changes. *Water* **2019**, *11*, 1502. [CrossRef]
30. Lancia, M.; Petitta, M.; Zheng, C.; Saroli, M. Hydrogeological insights and modelling for sustainable use of a stressed carbonate aquifer in the Mediterranean area: From passive withdrawals to active management. *J. Hydrol.* **2020**, *32*, 100749. [CrossRef]
31. Brancaccio, L.; Cinque, A.; Romano, P.; Rosskopf, C.; Russo, F.; Santangelo, N.; Santo, A. Geomorphology and neotectonic evolution of a sector of the Tyrrhenian flank of the southern Apennines (Region of Naples, Italy). *Z. Geomorphol.* **1991**, *82*, 47–58.
32. Pappone, G.; Alberico, I.; Amato, V.; Aucelli, P.P.C.; Di Paola, G. Recent evolution and present-day conditions of the Campanian Coastal plains (South Italy): The case history of Sele River Coastal plain. *WIT Trans. Ecol. Envir.* **2011**, *149*, 15–27. [CrossRef]
33. Ruberti, D.; Vigliotti, M. Land use and landscape pattern changes driven by land reclamation in a coastal area: The case of Volturno delta plain, Campania region, southern Italy. *Environ. Earth Sci.* **2017**, *76*, 694. [CrossRef]
34. ISPRA. National Geological Database. 2021. Available online: http://sgi2.isprambiente.it/viewersgi2/ (accessed on 10 October 2021).
35. Corniello, A.; Ducci, D. Hydrogeochemical characterization of the main aquifer of the "Litorale Domizio-Agro Aversano NIPS" (Campania—Southern Italy). *J. Geochem. Explor.* **2014**, *137*, 1–10. [CrossRef]
36. Allocca, V.; Coda, S.; De Vita, P.; Di Rienzo, B.; Ferrara, L.; Giarra, A.; Mangoni, O.; Stellato, L.; Trifuoggi, M.; Arienzo, M. Hydrogeological and hydrogeochemical study of a volcanic-sedimentary coastal aquifer in the archaeological site of Cumae (Phlegraean Fields, southern Italy). *J. Geochem. Explor.* **2018**, *185*, 105–115. [CrossRef]
37. Stellato, L.; Coda, S.; Arienzo, M.; De Vita, P.; Di Rienzo, B.; D'Onofrio, A.; Ferrara, L.; Marzaioli, F.; Trifuoggi, M.; Allocca, V. Natural and anthropogenic groundwater contamination in a coastal volcanic-sedimentary aquifer: The case of the archaeological site of Cumae (Phlegraean Fields, Southern Italy). *Water* **2020**, *12*, 3463. [CrossRef]
38. AppEEARS Team. *Application for Extracting and Exploring Analysis Ready Samples (AppEEARS); Ver. 2.54.1. NASA EOSDIS Land Processes Distributed Active Archive Center (LP DAAC)*; USGS/Earth Resources Observation and Science (EROS) Center: Sioux Falls, SD, USA, 2020. Available online: https://lpdaacsvc.cr.usgs.gov/appeears (accessed on 10 October 2021).
39. Running, S.; Mu, Q.; Zhao, M.; Moreno, A. MOD16A2GF MODIS/Terra Net Evapotranspiration Gap-Filled 8-Day L4 Global 500m SIN Grid V006. NASA EOSDIS Land Processes DAAC. 2019. Available online: https://doi.org/10.5067/MODIS/MOD16A2GF.006 (accessed on 10 October 2021).
40. Mu, Q.; Zhao, M.; Running, S.W. Improvements to a MODIS global terrestrial evapotranspiration algorithm. *Rem. Sens Environ.* **2011**, *115*, 1781–1800. [CrossRef]
41. Shah, N.; Nachabe, M.; Ross, M. Extinction depth and evapotranspiration from ground water under selected land covers. *Groundwater* **2007**, *45*, 329–338. [CrossRef]
42. Sutanudjaja, E.H.; van Beek, R.; Wanders, N.; Wada, Y.; Bosmans, J.H.C.; Drost, N.; van der Ent, R.J.; de Graaf, I.E.M.; Hoch, J.M.; de Jong, K.; et al. PCR-GLOBWB 2: A 5 arcmin global hydrological and water resources model. *Geosci. Model Dev.* **2018**, *11*, 2429–2453. [CrossRef]
43. Harbaugh, A.W. *MODFLOW-2005, the US Geological Survey Modular Ground-Water Model: The Ground-Water Flow Process; U.S. Geological Survey Techniques and Methods 6-A16*; US Department of the Interior; US Geological Survey: Reston, VA, USA, 2005; p. 253.

44. Reimann, T.; Hill, M.E. MODFLOW-CFP: A New Conduit Flow Process for MODFLOW-2005. *Groundwater* **2009**, *47*, 321–325. [CrossRef]
45. Hill, M.C. The practical use of simplicity in developing ground water models. *Groundwater* **2006**, *44*, 775–781. [CrossRef]
46. Doherty, J. PEST-Model-Independent Parameter Estimation. Version 12. Watermark Computing. Australia. 2010. Available online: http://www.pesthomepage.org/ (accessed on 10 October 2021).
47. De Vita, P.; Allocca, V.; Celico, F.; Fabbroncino, S.; Cesaria, M.; Monacelli, G.; Musilli, I.; Piscopo, V.; Scalise, A.R.; Summa, G.; et al. Hydrogeology of continental southern Italy. *J. Maps* **2018**, *14*, 230–241. [CrossRef]
48. Russo, G.; Viggiani, C.; Viggiani, G. Geotechnical design and construction issues for Lines 1 and 6 of the Naples Underground/Geotechnische Planung und Ausführung der U-Bahnlinien 1 und 6 in Neapel. *Geomech. Tunnelbau* **2012**, *5*, 300–311. [CrossRef]
49. de Graaf, I.E.; van Beek, R.L.; Gleeson, T.; Moosdorf, N.; Schmitz, O.; Sutanudjaja, E.H.; Bierkens, M.F. A global-scale two-layer transient groundwater model: Development and application to groundwater depletion. *Adv. Water Resour.* **2017**, *102*, 53–67. [CrossRef]
50. Fan, Y.; Li, H.; Miguez-Macho, G. Global patterns of groundwater table depth. *Science* **2013**, *339*, 940–943. [CrossRef] [PubMed]
51. Braca, G.; Bussettini, M.; Ducci, D.; Lastoria, B.; Mariani, S. Evaluation of national and regional groundwater resources under climate change scenarios using a GIS-based water budget procedure. *Rend. Fis. Acc. Lincei* **2019**, *30*, 109–123. [CrossRef]
52. Brakkee, E.; Van Huijgevoort, M.H.; Bartholomeus, R.P. Improved understanding of regional groundwater drought development through time series modelling: The 2018–2019 drought in the Netherlands. *Hydrol. Earth Syst. Sci.* **2022**, *26*, 551–569. [CrossRef]
53. Ruggieri, G.; Allocca, V.; Borfecchia, F.; Cusano, D.; Marsiglia, P.; De Vita, P. Testing Evapotranspiration Estimates Based on MODIS Satellite Data in the Assessment of the Groundwater Recharge of Karst Aquifers in Southern Italy. *Water* **2021**, *13*, 118. [CrossRef]
54. Allocca, V.; Manna, F.; De Vita, P. Estimating annual groundwater recharge coefficient for karst aquifers of the southern Apennines (Italy). *Hydrol. Earth Syst. Sci.* **2014**, *18*, 803–817. [CrossRef]
55. Allocca, V.; De Vita, P.; Manna, F.; Nimmo, J.R. Groundwater recharge assessment at local and episodic scale in a soil mantled perched karst aquifer in southern Italy. *J. Hydrol.* **2015**, *529*, 843–853. [CrossRef]
56. De Vita, P.; Allocca, V.; Manna, F.; Fabbrocino, S. Coupled decadal variability of the North Atlantic Oscillation, regional rainfall and karst spring discharges in the Campania region (southern Italy). *Hydrol. Earth Syst. Sci.* **2012**, *16*, 1389–1399. [CrossRef]
57. Colombani, N.; Gaiolini, M.; Busico, G.; Postacchini, M. Quantifying the impact of evapotranspiration at the aquifer scale via groundwater modelling and MODIS data. *Water* **2021**, *13*, 950. [CrossRef]
58. Lehr, C.; Lischeid, G. Efficient screening of groundwater head monitoring data for anthropogenic effects and measurement errors. *Hydrol. Earth Syst. Sci.* **2020**, *24*, 501–513. [CrossRef]

water

MDPI

Article

Hybrid Fuzzy Multi-Criteria Analysis for Selecting Discrete Preferable Groundwater Recharge Sites

Christopher Papadopoulos [1], Mike Spiliotis [1,*], Fotios Pliakas [1], Ioannis Gkiougkis [1], Nerantzis Kazakis [2] and Basil Papadopoulos [1]

[1] Department of Civil Engineering, School of Engineering, Democritus University of Thrace, 67100 Xanthi, Greece; cpapadp@civil.duth.gr (C.P.); fpliakas@civil.duth.gr (F.P.); jgiougis@civil.duth.gr (I.G.); papadob@civil.duth.gr (B.P.)

[2] Department of Geology, School of Sciences, Aristotle University of Thessaloniki, 54124 Thessaloniki, Greece; kazakis@geo.auth.gr

* Correspondence: mspiliot@civil.duth.gr; Tel.: +30-25410-79613

Abstract: This study proposes a hybrid fuzzy multi-criteria methodology for the selection of the most preferable site for applying managed aquifer recharge (MAR) systems by utilizing floodwaters. The use of MAR can increase water resources for later water utilization in case of drought. In this multi-criteria problem, seven recharge sites are under consideration, based on nine criteria, aiming to make a final list of their relative ranking. A fuzzy analytic hierarchy process (FAHP) based on the logarithmic fuzzy preference programming (LFFP) method is used to determine the weights of criteria. LFFP is an optimization-based method that produces a priority vector from a fuzzy pairwise comparison matrix. Furthermore, fuzzy inference systems (FIS) based on the Mamdani approach are used to estimate the rating of each alternative with respect to the criterion examined, and then the final evaluation of the alternatives is obtained. A FIS is a fuzzy if–then rule-based system where the experts' qualitative knowledge is translated into numerical reasoning for each individual criterion. The proposed methodology is applied in the aquifer system of the agricultural plain located to the southeast of the city of Xanthi in the Prefecture of Xanthi, NE Greece.

Keywords: fuzzy analytic hierarchy process; fuzzy inference systems; managed aquifer recharge; Xanthi plain

1. Introduction

In recent decades, there has been growing concern about water availability, mainly due to the development of human societies and climate change [1]. Regarding the last one, trends show an increasing frequency and intensity of natural extreme events related to temperature and precipitation, such as droughts and floods [2–5].

A way of tackling low water availability challenges is the storage of water in artificial surface structures. However, this can meet only part of the increasing demand for water, mainly due to limited capacity, high evaporation losses, and competing objectives [6–9]. An alternative is groundwater recharge by utilizing excess surface water such as flood waters. Aquifers are more resistant to water supply variability related to drought than surface water supplies; however, they are under growing stress [6,10–13], especially in arid and semi-arid areas [14].

In recent years, managed aquifer recharge (MAR) systems have been increasingly used to increase groundwater availability for later use in dry seasons [15–19]. A variety of MAR techniques can be used that mainly depend on local conditions [20,21].

Scanlon et al. [12] state that two basic approaches for managing groundwater storage include: (1) conjunctive use (CU) of surface water and groundwater, and (2) managed aquifer recharge (MAR), which can be considered as an extension of CU. According to Foster and van Steenbergen [22], conjunctive groundwater use with surface water resources,

in terms of practical water management, represents one of the most important responses to improving drought water supply security and for long-term climate change adaptation. Maliva [23] mentions that MAR can be viewed as a means for optimizing the use of aquifers. Dillon et al. [24] observed that the "objectives of groundwater management relate to maximizing economic utility of aquifers while sustaining the environment and providing security for meeting human needs". Maliva [23] also states that depending upon the system, recharge is performed by either applying water onto a land surface (surface spreading), subsurface discharge into the vadose zone using wells, galleries, and trenches, or by injection using wells into either confined or unconfined aquifers. Particularly, surface spreading by using floodwater (excess winter water from a river) can be an effective MAR method [25]. A common technique for this method is the use of infiltration basins, while the suitability of an area for establishing floodwater spreading depends on various factors, such as geomorphology, hydrogeology, land use, socioeconomic issues, environmental impacts, etc., [26]. Recharge may also be induced by pumping groundwater close to connected surface water bodies (induced recharge). Modifications of the land surface and stream channels, such as by the removal (or change of) vegetation and construction of dams and levees, are also used to intentionally increase aquifer recharge.

A common issue that needs to be dealt with in applying MAR systems is the selection of suitable sites. Obviously, this is a problem of multi-criteria nature, in which an alternative or several alternative potential site/sites for applying MAR are considered based on a series of criteria, which may be divided into various categories. A variety of studies address this decision problem by the use of remote sensing and/or GIS techniques to produce a map with suitable zones for applying MAR (e.g., [27–29]). Other research provides advanced integrated methodologies by combining the GIS capabilities with multi-criteria methods (e.g., [30–35]). In such surveys, a weighted thematic layer for each criterion is produced. The criteria have been initially divided into classes (ranges) and each point of the grid obtains a score based on its classification into the classes. Then, a final map can be generated with overlay techniques using crisp operators of Boolean logic. Although these approaches are very significant and have been widely used, they are not always applicable. The main reason is the low data availability. The generation of thematic layers is based on interpolation methods, and therefore a small sample with respect to each criterion may diminish the reliability of interpolation results.

Fuzzy logic and fuzzy set theory were introduced by Zadeh [36] as a generalization of Aristotle's logic and/or classical set theory. In Aristotle's logic, a statement can be only true or false and, in classical set theory, an element x (or an individual) either belongs {1} or does not belong {0} to a given set and thus, it is described by two values [37]. In contrast to dual logic, fuzzy logic is many-valued and manipulates the concept of partial truth [38] and, in fuzzy set theory, an element x can partially participate in a (fuzzy) set, which means that it can obtain all the values in a closed unit interval [0, 1]. The principles of fuzzy logic and sets are the mathematical representation of human thinking and reasoning where truth may appear as an inference from inaccurate or partial knowledge, dealing with uncertainty due to vagueness. A variety of methodologies based on the principles of fuzzy logic and sets have been developed which incorporate the uncertainty of complex issues by the use of either autonomous fuzzy tools or hybrid analytical methods.

In particular, fuzzy logic and the theory of fuzzy sets have had an extensive use in hydrologic analysis and the analysis of hydrological multi-criteria problems since the early application of Bogardi et al. [39], in which fuzziness was used for partial satisfaction of objectives in regional water resources management, until the present [40]. The recent studies of Kazakis et al. [41], Kourgialas et al. [42], and Spiliotis et al. [43] are given as some examples of hybrid fuzzy multi-criteria methodologies. In these studies, the analysis can be carried out in order to either spatially address the examined multi-criteria problem, producing suitable fuzzy maps, or categorize points (alternatives) that can belong to several categories to some degree. This wide use of fuzzy logic and sets is due to the ability to simulate human reasoning in its use of approximate information, and to mathematize

the uncertainty and vagueness in decision-making [44,45]. Furthermore, the use of fuzzy logic and sets in multi-criteria decision-making (MCDM) can express the gray zone of the decision and manage imprecise information (e.g., the score of criteria, the available resources), etc.

Regarding the selection problem of suitable recharge sites, most research uses fuzzy operators and/or fuzzy if–then rule-based systems in a GIS environment in order to produce a map with fuzzy suitable zones (e.g., [46–52]). However, the use of such models in combination with hybrid fuzzy multi-criteria methods to address this problem is an open issue.

The main proposal of this study is the ranking of seven alternatives representing suitable sites for applying MAR systems using floodwaters via a hybrid fuzzy multi-criteria methodology, in the context of increasing the local groundwater resources for later water use in case of drought. As described in the following section, the local conditions of the case study favor the application of floodwater spreading using infiltration basins. The evaluation of the alternatives was based on nine criteria that were selected based on the local conditions and the type of MAR. The weights of criteria were obtained through a fuzzy analytic hierarchy process (FAHP)-based methodology; however, they are crisp numbers. Fuzzy inference systems (FIS) were used in the rating of each alternative with respect to each criterion. The use of FIS was preferred since the objective function regarding the criteria was unknown. The composition of criteria was achieved through a simple aggregated model where a final ranking of the alternatives was obtained. The case study refers to the aquifer system of the agricultural plain located to the southeast of the city of Xanthi in northern Greece.

2. Case Study

The study area is the aquifer system of the agricultural plain located to the southeast of the city of Xanthi in the Prefecture of Xanthi, NE Greece (Figure 1). The wider region of study area is located within the boundaries of the tertiary Vistonida basin [53], while as presented in Figure 2 (modified map based on geological map of [54]), the aquifer system is hosted in the alluvial plain consisting of loam, clays, sands, gravels, etc. Gravels and sands of Pleiocene–Pleistocene origin occur in the north of study area, while Pleiocene brackish sediments, mainly consisting of sand and clay, with no wide surface spread, occur near Vistonida Lagoon. Clastic sediments of the Eocene and Oligocene, consisting of conglomerate breccia, limestones, and mollasic formations, occur in both the south and north of study area, while the background consists of igneous rocks that underlie andesitic rocks of the same geological period.

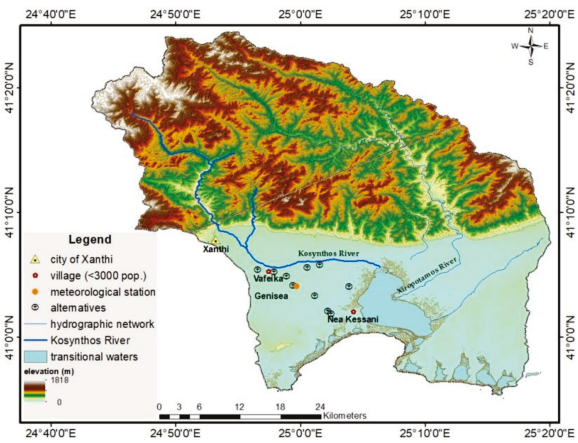

Figure 1. Geomorphology of the wider area and the alternative sites.

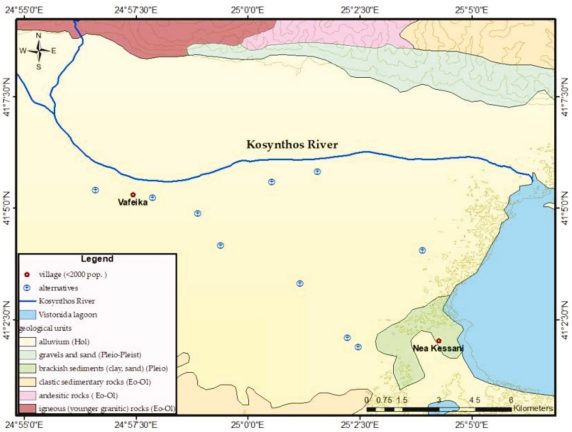

Figure 2. Geological formations of the area under consideration (modified map based on geological map of [54].

Geological formations of the alluvial plain range from fine to silty clay in the SE–E direction towards Vistonida Lagoon [53,55]. Regarding the geological structure and hydrogeological conditions, relevant assessments have shown that [56,57]:

(1) Three main geological formations are presented: (a) the upper formation (8–80 m in thickness), of low permeability, consisting of clayey sand which interchanges at certain locations with gravel sand of little thickness, (b) the intermediate aquifer formation (10–70 in thickness), consisting of permeable gravel sand, considered as a shallow confined aquifer, in some locations changing to semi-confined aquifer, and (c) the lower impermeable formation consisting of clayey silt in depth of 30–90 m;
(2) Transmissivity, T, ranges from 90 to 915 (m^2/day), while the storage coefficient, S, ranges from 2.4×10^{-4} to 8.75×10^{-2};
(3) The shallow aquifer system is naturally recharged, mainly from direct infiltration of precipitation and partially from percolation of the River Kosynthos (upstream zone of coarse-grained deposits);
(4) The groundwater flow has a SE direction, being almost identical to that of the old riverbed's direction in the area;
(5) The groundwater main recharge axes appear to be in a S–SE direction towards Vistonida Lagoon;
(6) The high quality of the water of the River Kosynthos gives rise to its use for artificial recharge purposes.

The climatic conditions of the wider area differ in the lowlands from those in the mountains [58]. Based on precipitation and temperature records from the meteorological station of Genisea (41°04′07″ N–24°59′44″ E) located in the study area, the mean annual cumulative precipitation is 605.6 mm in the period 1966–2018. The available temperature data concern the period of 1988–2018, in which the mean annual temperature was 14.4 °C, while mean temperature of the summer months was 23.9 °C. In the wider region, both wet periods (that caused flood events such as the flood of the Kosynthos River in 1996) and drought periods have occurred. In fact, a drought period might have had an effect on groundwater levels of the examined aquifer. Particularly, the groundwater level in January of the shallow aquifer is significantly related to drought in the previous hydrological year and drought in the first trimester of the current hydrological year [59].

The exploitation of the aquifer system mainly takes place in the south of the riverbed of the Kosynthos River where there is a significant number of irrigation wells. Most of these wells there are not deeper than 50 m, while there are a few shallow wells (up to 10 m) that are not in use any more [58,60]. According to Diamantis et al. [60], the annual pumping volume is estimated at 48×10^6 m^3 approximately. The spatial distribution of the irrigation wells and other detailed information regarding the study area can be found in the studies of Diamantis et al. [60] and Pisinaras [58].

3. Materials and Methods

The development of the proposed hybrid fuzzy methodology refers to the intermediate formation of the case study. It can only be applied in unconfined aquifers and where there is an underlying drainage axis. In addition, the application of the methodology requires the presence of an adjacent river whose excess water during the flood period can be utilized without burdening the ecological supply. Last, in order for each alternative to be evaluated, the lithological profile and hydraulic characteristics of both the vadose zone and saturated zone had to be available. Each alternative represents a potential site for MAR application where there is a well with available hydrogeological data. The alternatives were considered through the nine criteria described below in ascending order of importance. The selected criteria can be added or subtracted depending on the specific conditions of an area, while there is no limit in number of the examined alternatives.

3.1. Criteria Description

Ecological status (C_1): This refers to the status of the Kosynthos River. Based on River Basin Management Plans [61], the riverbed of Kosynthos is divided into sections characterized by different ecological status. Each alternative may be supplied water for applying MAR by a different section. The worst case is unknown ecological status, while the best case is high ecological status.

Slope (%) (C_2): Slope is a commonly-used criterion in identification of suitable sites for applying MAR. Obviously, the steeper the slope, the less desirableare conditions for applying MAR. The dividing of slope into classes is based on previous studies (e.g., [35,62]); however, the classes of slope were adjusted to the case study area, which is characterized by smooth slopes.

Distance from hydrographic network (m) (C_3): This refers to the distance between each alternative and a source with available water for MAR. Only the distance from the Kosynthos River was considered since the water of Vistonida Lagoon is unsuitable due to its connection with coastal water surfaces (Figure 3). In the research of Farhadian et al. [63], the distance from rivers is also used, while in other research (e.g., [35]) the distance from drainage networks is taken into account.

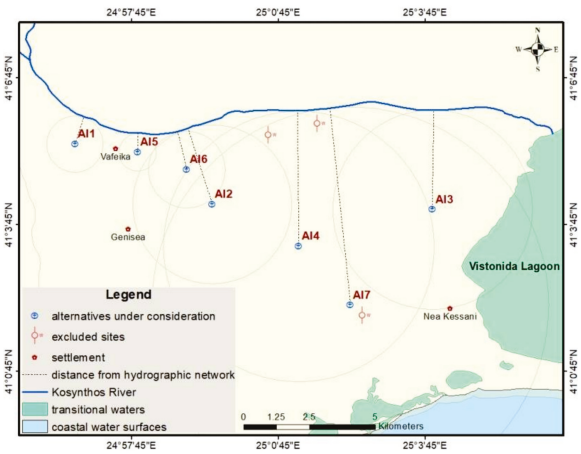

Figure 3. Distance from the hydrographic network (from the Kosynthos River) of each alternative.

Distance from road network (m) (C_4): This criterion may affect the suitability of an area for applying MAR either in a negative or a positive way. For instance, it is desirable a recharge site is a minimum distance from highways and freeways in order for potential groundwater pollution to be avoided [52]. However, this holds in the case of short distance (a few hundred meters) between the recharge site under consideration (alternative) and the potential pollution source. On the other hand, if the distance between the alternatives and road network is in the order of kilometers, where there is in fact no danger of groundwater pollution, then an easy and fast access to the recharge site is desirable [63]. In this study,

the distance of the alternatives from the highway was in the order of kilometers; therefore, the shorter distance, the higher the rating of the alternative. Figure 4 presents a map with the distances in kilometers of each alternative from the highway.

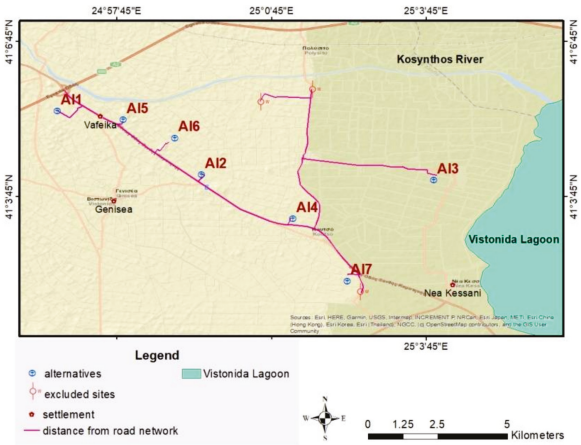

Figure 4. Distance from the road network of each alternative (based on World Street map).

Transmissivity (m^2/day) (C_5): This is a common hydrogeological parameter used in studies regarding the selection of suitable recharge sites [32,35,52,64], since it takes into account both the (horizontal) hydraulic conductivity (K) and the saturated thickness of the aquifer (b). High transmissivity values favor the recharge process since transmissivity (T) is defined as T = Kb (m^2/day). According to Pisinaras [58], in the study area, T ranges between 25 and 2950 (m^2/day).

Storativity (C_6): Another hydrogeological criterion used in site selection for applying MAR is storativity (S) [65]. The storativity of each alternative in the study area was obtained based on previous research [56–58], where storage coefficient values varied from 10^{-2} to 10^{-4}. The lower the S-values, the more unfavorable conditions are for applying MAR.

Hydraulic resistance (C_7): This is a critical hydrological criterion because in its calculation, $c = \sum_{i=1}^{n} d_i/K_i$, the (vertical) hydraulic conductivity (K) (m/days) of each sedimentary layer and its thickness (d) (m) are introduced. Kazakis [35] suggests the use of (log values) hydraulic resistance to take into account the permeability of the entire thickness of the vadose zone. High c-values indicate unsuitable recharge sites. It is noted that in the case of confined aquifers, this criterion cannot be used. The estimation of c-values of the alternatives was based on the research of Pisinaras [58], in which stratigraphic columns regarding the examined alternatives are available.

Type of aquifer (C_8): As aforementioned, the hydraulic resistance does not refer to confined aquifers. Thus, the classes of this criterion are considered to be crisp. That is, an alternative has the highest rating (10) when its aquifer is unconfined (or/and leakage aquifer), otherwise it is zero. Based on the available stratigraphic columns [58], there were confined underlying aquifers in the cases of three alternatives and, thus, these alternatives were excluded from the analysis. The aquifers of the other seven alternatives were unconfined or/and leakage (semi-confined) aquifers.

Piezometry (C_9): Piezometry and the type of aquifer are essential (hydrogeological) criteria for applying MAR systems. When a recharge axis is underlying an alternative, then this recharge site is unsuitable and vice versa. The identification of the study area regarding the recharge axes and the drainage axes was based on previous research [56–58].

On that point, it should be noted that the proposed methodology has been developed in order to analyze both large and small datasets with various hydrogeological parameters. Hence, some parameters such as aquifer type (e.g., confined) have been included in order to help to this analysis. Initially, all available information (lithological profiles, hydraulic parameters, etc.) was selected, and after the first screening, the alternatives with no

available profiles were eliminated and thus, ten alternatives remained. Based on the lithological profiles, three of ten alternatives overlie confined aquifers, and hence, these alternatives were excluded from the analysis (Figures 3 and 4). On balance, the following preparatory steps were carried out (Figure 5):

(1) Literature review and building of a detailed database including hydrogeological, morphological, etc., data;
(2) The points with lithological profiles and hydraulic data of the aquifer and vadose zone were chosen for the application and development of the methodology. The other sites were eliminated;
(3) Tensites were then chosen, of which 3 referred to confined aquifers, and for this reason they were excluded from the analysis;
(4) The method was applied to the final chosen sites (7 in total) and the most suitable for MAR application was determined.

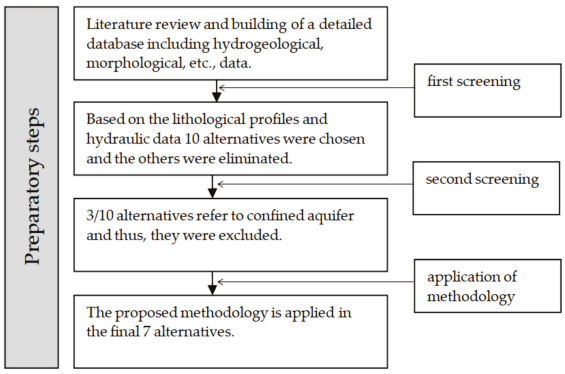

Figure 5. Preparatory steps for screening of the final alternatives.

3.2. Fuzzy Analytic Hierarchy Process—FAHP

As aforementioned, fuzzy logic has a wide use in multi-criteria analysis and has been applied to several hydrological issues. The basic concepts of fuzzy logic and sets, such as the membership function, α-cuts, fuzzy number [66], extension principle [67,68] and max–min composition of fuzzy relations [69], are presented in Appendix A. The fuzzy methods used in this study are based on these concepts.

One of the most used methods for quantification of the significance of criteria is the analytic hierarchy process (AHP) suggested by Saaty [70]. As is known, the AHP is based on pairwise comparisons between criteria (or/and alternatives), where a positive reciprocal pairwise comparison matrix $\boldsymbol{A_{nxn}}$ is constructed. A fundamental scale is used [70] in order to numerically express the initial experts' judgments regarding the relative criteria importance (ratios of weights (w_i/w_j)); however, it is not the only one [71]. Based on the eigenvalue theory from linear algebra, Saaty [70] developed the eigenvector method (EVM) in order to obtain a unique solution to derive the weights of criteria (or alternatives) from a $\boldsymbol{A_{nxn}}$. This is the principal eigenvector $\boldsymbol{w}$ determined by solving the system of equations:

$$(\boldsymbol{A_{nxn}} - \lambda_{\max}\boldsymbol{I})\boldsymbol{w} = 0 \Leftrightarrow \boldsymbol{A_{nxn}}\boldsymbol{w} = \lambda_{\max}\boldsymbol{w} \quad (1)$$

where $\boldsymbol{I}$ is the unit matrix and $\lambda_{\max}$ is the principle eigenvalue of $\boldsymbol{A_{nxn}}$.

Given that the initial judgments cannot be identical to the ratios of weights, the $\boldsymbol{A_{nxn}}$ is not fully consistent. Therefore, the validation of AHP is based on the measure of the consistency of the $\boldsymbol{A_{nxn}}$. For this reason, the consistency index CI = $(\lambda_{\max} - n)/(n-1)$ is estimated. Then, the CI-index is divided with a predefined index (RI), the value of which depends on the number of criteria n.

Fuzzy set theory is the most widely used approach integrated with the AHP [72]. The use of fuzziness can incorporate the inherent uncertainty in the assessments of pairwise comparison between criteria, derived by the subjectivity in the quantification of the ra-

tios expressing the relative importance of the decision elements (weights of criteria and ratings/scores of alternatives).

To cope with the uncertainty of imprecise judgments, Chang [73] used a fuzzy pairwise comparison matrix and then he used extent analysis to extract a crisp priority vector. An advantage of the Chang method is its computational simplicity.

However, even if extent analysis has been widely used (e.g., [74–77]), it has a major drawback. This is the fact that a weight of a criterion may obtain zero value, and hence it makes no sense for such a criterion to be under consideration [78]. In addition, extent analysis produces a priority vector, which may be quite different from the true one, and thus the weights obtained are not representative regarding the relative importance of decision criteria.

Mikhailov [79], extending his previous research [80], suggests a method for derivation of crisp weights from a matrix with fuzzy judgments, by applying a fuzzy preference programming (FPP)-based nonlinear method (optimization approach). In fact, the method of Mikhailov [79] is based on (fuzzy) flexible programming; that is, the uncertainty appears in the constant term of the fuzzy constraints [68].

Let us consider the following reciprocal matrix $\widetilde{\boldsymbol{A}}_{\boldsymbol{nxn}}$ with fuzzy pairwise comparisons between n criteria:

$$\widetilde{A} = \left(\widetilde{a}_{ij}\right)_{nxn} \begin{array}{c} \begin{array}{ccccc} C_1 & C_2 & C_3 & \dots & C_n \end{array} \\ \begin{bmatrix} 1 & (l_{12}, m_{12}, u_{12}) & (l_{13}, m_{13}, u_{13}) & \dots & (l_{1n}, m_{1n}, u_{1n}) \\ (l_{21}, m_{21}, u_{21}) & 1 & (l_{23}, m_{23}, u_{23}) & \dots & (l_{2n}, m_{2n}, u_{2n}) \\ (l_{31}, m_{31}, u_{21}) & (l_{32}, m_{32}, u_{22}) & 1 & \dots & (l_{3n}, m_{3n}, u_{3n}) \\ \dots & \dots & \dots & \dots & \dots \\ (l_{n1}, m_{n1}, u_{n1}) & (l_{n2}, m_{n2}, u_{n2}) & (l_{n2}, m_{n2}, u_{n2}) & \dots & 1 \end{bmatrix} \end{array} \begin{array}{c} C_1 \\ C_2 \\ C_3 \\ \vdots \\ C_n \end{array} \tag{2}$$

where C_i (for i = 1, ... , n) are the criteria, $\widetilde{a}_{ij} = 1/\widetilde{a}_{ji} = w_i/w_j$, that is $l_{ij} = 1/u_{ji}$, $m_{ij} = 1/m_{ji}$ and $u_{ij} = 1/l_{ji}$ for $l_{ij} \le m_{ij} \le u_{ji}$ and for all $i, j = 1, 2, \dots, n,\ j \ne i$.

In order to obtain crisp weights whose ratios are approximately included in the initial fuzzy judgments ($l_{ij} \widetilde{\le} w_i/w_j \widetilde{\le} u_{ij}$), the following membership function is introduced by Mikhailov [79]:

$$\mu_{ij}(w_i/w_j) = \begin{cases} \frac{(w_i/w_j) - l_{ij}}{m_{ij} - l_{ij}}, & l_{ij} < (w_i/w_j) \le m_{ij} \\ \frac{u_{ij} - (w_i/w_j)}{u_{ij} - m_{ij}}, & u_{ij} > (w_i/w_j) \ge m_{ij} \end{cases} \tag{3}$$

where $\mu_{ij}(w_i/w_j)$ denotes the degree of satisfaction (membership) to which the ratio (w_i/w_j) belongs to fuzzy judgment $\widetilde{a}_{ij}$.

In order to determine a global evaluation from individual membership functions [81], a proper fuzzy operator, that is the min intersection, is used with respect to the above fuzzy inequalities. The min intersection is preferred because it secures a common satisfaction of all the selected membership functions [82,83]. Furthermore, in this study, the use of min intersection can linearize the decision problem

$$\lambda = \min\left\{\mu_{ij}(w_i/w_j) | i = 1, \dots, n-1, j = i+1, \dots, n\right\} \tag{4}$$

where λ is the degree of the common satisfaction to which the crisp priority vector satisfies simultaneously each fuzzy pairwise comparison.

Assuming that the decision-maker looks forward to the highest membership degree of the ratio of weights in the fuzzy judgments $\widetilde{a}_{ij}$, Mikhailov [79] and Mikhailov and Tsvetinov [84] maximize λ under the constraint that the total sum of weights must be equal to the unit (normalization constraint) and the positivity constraint in their values:

$$\begin{aligned}
&\max \lambda \\
&s.t. \\
&\begin{cases} \min\limits_{ij}\left[\mu_{ij}\left(w_i/w_j\right)\right] \geq \lambda, \;\; i=1,\ldots,n-1, \;\; j=i+1,\ldots,n \\ \sum\limits_{i=1}^{n} w_i = 1 \\ w_i \geq 0, \;\; i=1,\ldots,n \end{cases}
\end{aligned} \tag{5}$$

In the case of a positive λ-value, all solution ratios completely satisfy the fuzzy judgments, while a negative λ-value indicates strongly inconsistent initial judgments [79].

This paper applies the logarithmic fuzzy preference programming (LFPP)-based methodology for fuzzy AHP priority derivation proposed by Wang and Chin [85].The LFPP-based nonlinear method is preferred over the FFP-based nonlinear method because (a) it can ensure nonnegative values of membership function and hence, it produces a unique optimal solution and, (b) the same priority vectors are derived; either the upper triangular elements of a fuzzy pairwise comparison matrix are used or the lower ones.

Wang and Chin [85] addressed the drawbacks of Mikhailov's method [79]. Initially, they used logarithmed values in fuzzy judgments, which can be justified based on the extension principle, and the strict monotony of the (increasing) function $\ln \widetilde{a}_{ij}$ [86]:

$$\ln \widetilde{a}_{ij} \approx \left(\ln l_{ij},\ \ln m_{ij},\ \ln u_{ij}\right) \tag{6}$$

Equation (6) is an approximation of the fuzzy judgments $\ln \widetilde{a}_{ij}$ considered as fuzzy triangular numbers, since due to the logarithmic transformation the linearity does not hold. The membership function $\mu_{ij}(\ln \widetilde{a}_{ij})$ of the triangular fuzzy number can be expressed by the following Equation (7) [85].

$$\mu_{ij}\left(\ln\left(w_i/w_j\right)\right) = \begin{cases} \frac{\ln\left(w_i/w_j\right)-\ln l_{ij}}{\ln m_{ij}-\ln l_{ij}}, \;\; \ln\left(w_i/w_j\right) \leq \ln m_{ij} \\ \frac{\ln u_{ij}-\ln\left(w_i/w_j\right)}{\ln u_{ij}-\ln m_{ij}}, \;\; \ln\left(w_i/w_j\right) \geq \ln m_{ij} \end{cases} \tag{7}$$

Following Mikhailov's approach [79], it would be desirable to construct an optimization problem (Equation (8)) in which the parameter $\lambda = min\left\{\mu_{ij}\left(\ln\left(w_i/w_j\right)\right)\right.$ for $i = 1, \ldots, n-1$ and $j = i+1, \ldots, n$ to be maximized.

$$\begin{cases} \max\lambda \\ s.t.\ \mu_{ij}\left(\ln\left(w_i/w_j\right)\right) \geq \lambda \\ \quad w_i \geq 0,\ i=1,\ldots,n \end{cases} \Leftrightarrow \begin{cases} \max 1-\lambda \\ s.t.\ \ln w_i - \ln w_j - \lambda\left(\ln\left(m_{ij}/l_{ij}\right)\right) \geq \ln l_{ij} \\ \quad \ln w_j - \ln w_i - \lambda\left(\ln\left(u_{ij}/m_{ij}\right)\right) \geq -\ln u_{ij} \\ \quad w_i \geq 0,\ i=1,\ldots,n \end{cases} \tag{8}$$

For simplicity reasons, in the above optimization problem, the normalization constraint might be carried out after the solution. Nevertheless, a negative λ-value can still occur, which means that the inequalities of Equation (8) do not simultaneously hold. In other words, there is no an optimal solution (priority vector) to satisfy all the fuzzy judgments at the same time. Thus, according to Wang and Chin [85], two nonnegative deviation variables, δ_{ij} and η_{ij}, are introduced whose values must obviously be minimum. Therefore, the optimization problem applied in this research takes the following form:

$$\begin{aligned}
&\text{Minimize } (1-\lambda)^2 + M\textstyle\sum_{i=1}^{n-1}\sum_{j=i+1}^{n}\left(\delta_{ij}^2+n_{ij}^2\right) \\
&s.t. \\
&\begin{cases} x_i - x_j - \lambda\left(\ln\left(\frac{m_{ij}}{l_{ij}}\right)\right) + \delta_{ij} \geq lnl_{ij}, \quad i=1,\ldots,n-1,\ j=i+1,\ldots,n \\ x_j - x_i - \lambda\left(\ln\left(\frac{u_{ij}}{m_{ij}}\right)\right) + n_{ij} \geq -lnu_{ij}, \quad i=1,\ldots,n-1,\ j=i+1,\ldots,n \\ \lambda, x_i \geq 0, \quad i=1,\ldots,n-1,\ j=i+1,\ldots,n \end{cases}
\end{aligned} \tag{9}$$

where M is a specific constant term aiming for nonnegativity of λ, and to hold the values of deviation variables low, $x_i = lnw_i, lnw_j = x_j$.

The nonlinear objective function of Equation (9) focuses on minimizing the deviation variables, and after the priorities' derivation, the normalization of weights takes place (Equation (10)) in order to produce optimal normalized weight values.

$$w_i = \frac{\exp\left(x_i^*\right)}{\sum_{j=1}^{n} \exp\left(x_j^*\right)}, \; i = 1, \ldots, n \tag{10}$$

where $x_i^* (i = 1, \ldots, n)$ is the optimal solution of Equation (9).

The uniqueness of the obtained optimal priority vector holds due to the convexity of the λ and the linearity of constraints. The other advantage of the LFFP based-nonlinear method (Equations (6)–(10)), which is the alignment of priorities regardless of the triangular part of the comparison matrix used, can be easily proved [85] after some simple algebraic transformation.

3.3. Fuzzy Inference Systems for the Evaluation of the Alternatives' Rating

This research uses the fuzzy inference system (FIS) based on Mamdani's approach [87] for the evaluation of the alternatives. In this study, the use of such a system was preferred because the function for the criteria synthesis was unknown. With the use of FIS, the ranges of criteria can be fuzzified as well. The input variable of the FIS was the examined criterion and the output variable was the rating of each alternative with respect to the examined criterion. Both the input and the output variables of the FIS were divided into classes (ranges), which were considered fuzzy sets (fuzzy trapezoidal numbers) and described by linguistic variables. Briefly, the linguistic variables (Figure 6) quantify the natural language characterizing the words by fuzzy sets defined in the universe of discourse in which the variable is defined [69]. Thus, each alternative, based on its numeric value regarding the examined criterion, takes a membership degree of belonging to each fuzzy class (range) of the criterion. The rating (R) of an alternative, concerning the examined criterion, depended on the activation degree of the fuzzy if–then rules designed by the experts. It is pointed out that a FIS was designed for each criterion that was examined.

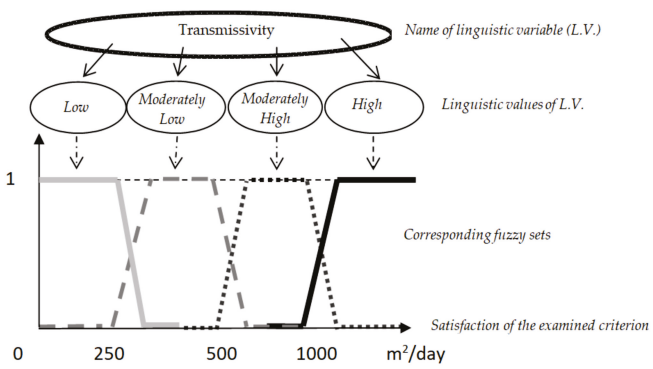

Figure 6. Transmissivity divided into four fuzzy classes described by linguistic variables.

The general structure of a FIS consists of the following components [88,89]:

(1) A fuzzifier. The degree to which the input data (the numeric value of the alternative with respect the examined criterion) satisfy the fuzzy rule is calculated. In this step, the classes of the input variables (criteria) are fuzzified.
(2) An inference engine module. A series of fuzzy if–then rules is modulated. Based on the satisfaction degree described in the previous step and the selected fuzzy implication, the fuzzy rules fire strength to infer knowledge. Thus, a fuzzy conclusion is calculated for each rule.

(3) Aggregation. All fuzzy conclusions inferred by all fuzzy rules are combined into a final fuzzy conclusion.
(4) A defuzzifier. The fuzzy output (inferred knowledge) is translated to crisp output (rating of each alternative with respect to the examined criterion).

From a mathematical point of view, a FIS, based on the Mamdani model, is composed of the premise (antecedent if–part) and conclusion (consequent then–part). It can be formulated as follows [82]:

$$Ru(k): If\ x_1\ is\ A_1^k\ and\ x_2\ is\ A_2^k \ldots and\ x_z\ is\ A_z^k\ then\ y\ is\ B^k \tag{11}$$

where A_z^k is a fuzzy set in Universe $U \subset \mathbb{R}$ (input variables of the model), B^k is a fuzzy set in Universe $Z \subset \mathbb{R}$ (output variables of the model), $(x_1, x_2, \ldots, x_z)^T \in U$, $y \in Z$ and k is the fuzzy rule kth. The above linguistic rule describes a mapping from $U_1 \times U_2 \times \ldots \times U_z$ to Z [88].

In this research, the antecedent of the fuzzy if–then rule includes only one input variable:

$$Ru(k): \ If\ x\ is\ A^k\ then\ y\ is\ B^k \tag{12}$$

The contribution of the rule kth, $Ru(k)$, to the output (inferred conclusion) of the model is also a fuzzy set which may be represented by a fuzzy implication. Here, the common engineering fuzzy implications of the algebraic product (Equation (13)) and the min implication (Equation (14)) are used, which are suited to inference on the basis of phenomenological information [90,91]. The min fuzzy implication is recommended in the case that there is no distinction between cause and effect [90].

$$\mu_{Ru^k}(x, y) = \mu_{A^k}(x) \cdot \mu_{B^k}(y) \tag{13}$$

$$\mu_{Ru^k}(x, y) = \min\{\mu_{A^k}(x),\ \mu_{B^k}(y)\} \tag{14}$$

Let a fuzzy rule consists of two fuzzy propositions as follows:

$$\left.\begin{array}{l} Fuzzy\ proposition\ 1:\ x\ is\ A'^k \\ Fuzzy\ proposition\ 2:\ Ru- > If\ x\ is\ A^k\ then\ y\ is\ B^k \end{array}\right\} Conclusion:\ y\ is\ B'^k \tag{15}$$

Then, according to the generalized modus ponens (GMP) concept [66], a new fuzzy proposition should be inferred such that the closer A'^k to A^k, the closer B'^k to B^k. Therefore, based on the concept of GMP, a fuzzy conclusion can be defined for each fuzzy rule with respect to the given input:

$$\mu_{B'^k}(y) = \sup_{x \in X} t\ [\mu_{A'^k}(x),\ \mu_{Ru^k}(x, y)] \tag{16}$$

Other t-norms, instead of the algebraic product, could be used (Equation (17)). The following Equation (17) is in fact a max–min composition in case the input is a vector. Practically, it holds:

$$\mu_{B'^k}(y) = \max_{x \in X} [\mu_{A'^k}(x) \wedge \mu_{Ru^k}(x, y)] = \mu_{A'^k \circ Ru^k}(y) \tag{17}$$

In the case that the input data of the model are crisp numbers (fuzzy singleton), it holds:

$$\mu_{A'^k}(x) = \begin{cases} 1\ if\ x = x* \\ 0\ \ otherwise \end{cases} \tag{18}$$

where x^* is a point in its universe.

Consequently, based on the fuzzy implication process, a fuzzy conclusion corresponds to each fuzzy rule. In order to obtain a final fuzzy conclusion regarding the examined criterion, all the fuzzy conclusions must be combined. This procedure is called the aggregation process and is carried out by using an operator which, in this research, is the max union.

In conclusion, in a fuzzy inference system based on the Mamdani model, the fuzzy implication of algebraic product, the algebraic product for all t-norms, and the fuzzy max union are selected. In the case of crisp input data, the Mamdani's product inference engine is described in Equation (19) [69]. In the case that the min fuzzy implication, min for all t-norm operators and the max union are selected, then the fuzzy output of the system is expressed by Equation (20).

$$\mu_{B'}(y) = \max_{k=1}^{L}[\mu_{A^k}(x_i*) \cdot \mu_{B^k}(y)] \tag{19}$$

$$\mu_{B'}(y) = \max_{k=1}^{L}\left[\min\left\{\mu_{A_i^k}(x_i*), \mu_{B^k}(y)\right\}\right] \tag{20}$$

As mentioned above, the output of the described fuzzy inference system is a fuzzy set B'^k. The last process leading to the decision (which, in this research, is the rating of an alternative with respect to the examined criterion) is the defuzzification of the fuzzy output. Here, the defuzzification method of centroid calculation is selected, which counts the gravity center (centroid) y^* as the output of the fuzzy rule-based system.

$$y* = \frac{\sum_{i=1}^{n} y_i \mu(y_i)}{\sum_{i=1}^{n} \mu(y_i)} \tag{21}$$

4. Implementation and Results

A hybrid fuzzy multi-criteria methodology was implemented in this research to solve the problem of selection of the more suitable site for applying MAR, choosing between seven (7) alternatives (Al) under the consideration of nine (9) criteria (C). Thus, the research's final goal was a relative rank order list of the suitability of the examined alternatives. The methodology included the following steps:

(1) Based on the experts' knowledge, a fuzzy reciprocal pairwise comparison matrix $\widetilde{\boldsymbol{A}}_{9x9}$ (Equation (2)) was generated regarding the examined (nine) criteria. Table 1 presents the elements of Saaty's scale [70] as triangular fuzzy numbers (TFN) (Equation (6)), while the fuzzy judgments of the matrix $\widetilde{\boldsymbol{A}}_{9x9}$ are presented in Equation (24).

(2) The optimization problem described in Equation (9) was built and solved by the use of the optimization software LINGO and the weights of criteria (priority vector) were estimated as crisp numbers. Then, the priority vector was normalized based on Equation (10). For space saving reasons, only an example of a pair of inequalities is given regarding the criteria of transmissivity (C_5) and piezometry (C_9). Based on Equation (24) presented below, transmissivity was considered moderate less important in comparison to piezometry; that is $\ln(w_5/w_9) \approx \left(\frac{1}{4}, \frac{1}{3}, \frac{1}{2}\right)$. Therefore, it holds:

$$\begin{aligned} &\ln w_5 - \ln w_9 - \lambda(\ln((1/3)/(1/4))) + \delta_{59} \geq \ln(1/4) \\ &\ln w_9 - \ln w_5 - \lambda(\ln((1/2)/(1/3)) + n_{59} \geq -\ln(1/2) \end{aligned}$$

As aforementioned, the parameter M aims to achieve a nonnegative value λ and a small deviation from the fuzzy inequalities constraints which define the fuzzy spread (support set) of each fuzzy judgment. The M-value should ensure a balance between the λ-value and the values of deviation variables [86]. The ideal solution is λ = 1 and $\sum_{i=1}^{9-1}\sum_{j=i+1}^{9}\left(\delta_{ij}^2 + n_{ij}^2\right)$ = 0; however, in the real world this is a rare condition [86]. The optimization problem was solved for several M-values. For M = 0.2 it holds: λ = 0.6069 and $\sum_{i=1}^{9-1}\sum_{j=i+1}^{9}\left(\delta_{ij}^2 + n_{ij}^2\right)$ = 2.763, for M = 0.5 and hence: λ = 0.317 and $\sum_{i=1}^{9-1}\sum_{j=i+1}^{9}\left(\delta_{ij}^2 + n_{ij}^2\right)$ = 1.807.

For or $M = 1$ it holds: $\lambda = 0.0407$ and $\sum_{i=1}^{9-1} \sum_{j=i+1}^{9} \left(\delta_{ij}^2 + n_{ij}^2\right) = 1.172$, while for $M > 2$ the solutions of deviations converged on $\sum_{i=1}^{9-1} \sum_{j=i+1}^{9} \left(\delta_{ij}^2 + n_{ij}^2\right) = 1.096$ and, the parameter $\lambda = 0$.

Therefore, the M-value selected in this study was $M = 0.5$ since it led to a balanced solution. The solution of the priority vector for $M = 0.5$ before the normalization was $\boldsymbol{W}_{\widetilde{A}}^{*}$ = (21.7949, 21.1237, 15.3198, 15.3198, 10.8694, 4.0643, 3.9769, 3.8704, 1.6641), while the normalized weights are presented in Table 2.

Let us verify the above fuzzy constraints regarding the criteria C_5 and C_9. According to the results (for $M = 0.5$), the deviation variables δ_{59} and n_{59} are zero, therefore:

$$\ln(10.8694) - \ln(21.7949) - 0.3174(\ln((1/3)/(1/4))) + 0.0 \geq \ln(1/4) \;\Leftrightarrow\; -0.78703 \geq -1.38629$$
$$\ln(21.7949) - \ln(10.8694) - 0.3174(\ln((1/2)/(1/3))) + 0.0 \geq -\ln(1/2) \;\Leftrightarrow\; 1.35574 \geq 0.69315$$

which holds.

(3) A Mamdani fuzzy inference system, included in the Fuzzy Logic Toolbox of MATLAB, was designed for each criterion. Initially, based on the experts' judgments, the classes of the examined criteria were fuzzified. The number of classes was determined by using the empirical rule of Sturges [92], which is a common technique in hydrology (Equation (22)):

$$q = 1.33 \log N \tag{22}$$

where q is the number of classes and N is the number of data (the numeric value of each alternative regarding the examined criterion, i.e., $N = 7$).

Then, a system of fuzzy if–then rules (with one input variable, e.g., if slope is low then rating is high) was built (Equation (12)). Both the algebraic product and the min implication were selected to be used in the fuzzy inference process (Equations (19) and (20)). All fuzzy output variables of all rules were combined into a fuzzy conclusion with the max union. Finally, the aggregated fuzzy output was defuzzified based on Equation (21), which is the rating of the each alternative, with respect to each criterion. For the calculation of the rating (R) based on the designed FIS, a simple code was written in MATLAB, which fed the FIS with crisp input data.

(4) The rating (R) of each alternative was multiplied with the weight of the examined criterion. The final evaluation (final score) of each alternative with respect of all criteria was achieved based on an aggregative model described as follows:

$$Al_{u.c.} = \sum_{i=1}^{n} w_i \times R_i \tag{23}$$

where $Al_{u.c.}$ is the alternative under consideration, w_i is the weight of the criterion i (for $n = 9$) and R_i is the estimated (by the corresponding FIS) rating of $Al_{u.c.}$ regarding the criterion i.

(5) Based on Equation (23), a rank list of the alternatives (from the most suitable site to the least suitable site for applying MAR) was obtained by using both the algebraic product (Equation (19)) and min implication (Equation (20)) (Table 3). It is noted that although the M-value adopted in this study is equal to 0.5, the results based on $M = 1$ are also presented in Table 3.

As shown in the above Table 1, the fuzzy spread increased as the domination between two criteria became stronger. Particularly, a lower fuzzy spread (0.5) corresponds to a judgment of equal importance, "about 1", while a higher fuzzy spread (2.0) corresponds to a judgment of extreme importance, "about 9". The authors used this increasing fuzziness on judgments because a wide fuzzy spread in an area of weak domination (i.e., from equal up to moderate importance) may lead to a large overlapping and therefore, two criteria may be considered of "about equal" importance even though they have a weak domination each other (e.g., w_i/w_j = "about 2" or "about 3"). Furthermore, it seems more convenient

to accurately *adjudicate* if two conditions are equal or about equal than to determine the degree of how important a condition is against the other in the case that the importance of the two conditions significantly differs. For instance, a decision maker (DM) might decide more comfortably that $\widetilde{a}_{1,2}$ = "about 2", which means that w_1/w_2 might be equal to 3 or equal to 1. On the other hand, in the case that a criterion is much more important than another, making such a judgment that $\widetilde{a}_{1,7}$ = "about 7", the real ratio of weights may be equal to 5 or 9, which also denotes significant importance.

Table 1. Triangular fuzzy numbers (TFN) for the pairwise comparison of the criteria regarding their relative importance.

Relative Importance of Two Criteria	TFN
Equal	(0.5, 1, 1.5)
Moderate	(2, 3, 4)
Strong	(3.75, 5, 6.25)
Very strong	(5.5, 7, 8.5)
Extreme	(7, 9, 9)
Intermediate values	(1.25, 2, 2.75), (3, 4, 5), (4.75, 6, 7.25), (6.5, 8, 9)

It is worth mentioning that several fuzzy spreads were tested. Particularly, constant spreads for the whole scale of Table 1 were used when either the fuzziness was equal to one (e.g., 2, 3, 4) or equal to two (e.g., (1, 3, 5). The tests showed that the weights of the less important criteria increased as the fuzziness increased.

$$\widetilde{A} = \begin{array}{c} \begin{array}{ccccccccc} C1 & C2 & C3 & C4 & C5 & C6 & C7 & C8 & C9 \end{array} \\ \left[\begin{array}{ccccccccc}
1 & \left(\frac{1}{4},\frac{1}{3},\frac{1}{2}\right) & \left(\frac{1}{5},\frac{1}{4},\frac{1}{3}\right) & \left(\frac{1}{6.25},\frac{1}{5},\frac{1}{3.75}\right) & \left(\frac{1}{8.5},\frac{1}{7},\frac{1}{5.5}\right) & \left(\frac{1}{9},\frac{1}{8},\frac{1}{6.5}\right) & \left(\frac{1}{9},\frac{1}{8},\frac{1}{6.5}\right) & \left(\frac{1}{9},\frac{1}{9},\frac{1}{7}\right) & \left(\frac{1}{9},\frac{1}{9},\frac{1}{7}\right) \\
(2,3,4) & 1 & \left(\frac{1}{2.75},\frac{1}{2},\frac{1}{1.25}\right) & (2,3,4) & \left(\frac{1}{5},\frac{1}{4},\frac{1}{3}\right) & \left(\frac{1}{6.25},\frac{1}{5},\frac{1}{3.75}\right) & \left(\frac{1}{6.25},\frac{1}{5},\frac{1}{3.75}\right) & \left(\frac{1}{8.5},\frac{1}{7},\frac{1}{5.5}\right) & \left(\frac{1}{9},\frac{1}{8},\frac{1}{6.5}\right) \\
(3,4,5) & (1.25,2,2.75) & 1 & \left(\frac{1}{2.75},\frac{1}{2},\frac{1}{1.25}\right) & \left(\frac{1}{5},\frac{1}{4},\frac{1}{3}\right) & \left(\frac{1}{6.25},\frac{1}{5},\frac{1}{3.75}\right) & \left(\frac{1}{6.25},\frac{1}{5},\frac{1}{3.75}\right) & \left(\frac{1}{7.25},\frac{1}{6},\frac{1}{4.75}\right) & \left(\frac{1}{7.25},\frac{1}{6},\frac{1}{4.75}\right) \\
(3.75,5,6.25) & \left(\frac{1}{4},\frac{1}{3},\frac{1}{2}\right) & (1.25,2,2.75) & 1 & \left(\frac{1}{4},\frac{1}{3},\frac{1}{2}\right) & \left(\frac{1}{5},\frac{1}{4},\frac{1}{3}\right) & \left(\frac{1}{5},\frac{1}{4},\frac{1}{3}\right) & \left(\frac{1}{6.25},\frac{1}{5},\frac{1}{3.75}\right) & \left(\frac{1}{6.25},\frac{1}{5},\frac{1}{3.75}\right) \\
(5.5,7,8.5) & (3,4,5) & (3,4,5) & (2,3,4) & 1 & \left(\frac{1}{2.75},\frac{1}{2},\frac{1}{1.25}\right) & \left(\frac{1}{2.75},\frac{1}{2},\frac{1}{1.25}\right) & \left(\frac{1}{4},\frac{1}{3},\frac{1}{2}\right) & \left(\frac{1}{4},\frac{1}{3},\frac{1}{2}\right) \\
(6.5,8,9) & (3.75,5,6.25) & (3.75,5,6.25) & (3,4,5) & (1.25,2,2.75) & 1 & \left(\frac{1}{1.5},1,\frac{1}{0.5}\right) & \left(\frac{1}{2.75},\frac{1}{2},\frac{1}{1.25}\right) & \left(\frac{1}{2.75},\frac{1}{2},\frac{1}{1.25}\right) \\
(6.5,8,9) & (3.75,5,6.25) & (3.75,5,6.25) & (3,4,5) & (1.25,2,2.75) & (0.5,1,1.5) & 1 & \left(\frac{1}{2.75},\frac{1}{2},\frac{1}{1.25}\right) & \left(\frac{1}{2.75},\frac{1}{2},\frac{1}{1.25}\right) \\
(7,9,9) & (5.5,7,8.5) & (4.75,6,7.25) & (3.75,5,6.25) & (2,3,4) & (1.25,2,2.75) & (1.25,2,2.75) & 1 & \left(\frac{1}{1.5},1,\frac{1}{0.5}\right) \\
(7,9,9) & (6.5,8,9) & (4.75,6,7.25) & (3.75,5,6.25) & (2,3,4) & (1.25,2,2.75) & (1.25,2,2.75) & (0.5,1,1.5) & 1
\end{array}\right] \end{array} \tag{24}$$

The following Figure 7 illustrates the scale of the fuzzy judgments of Table 1. For instance, based on Equation (24), the fuzzy pairwise comparison $\widetilde{a}_{5,9} = \widetilde{\frac{1}{3}} \Leftrightarrow w_5/w_9 = \widetilde{\frac{1}{3}} \Leftrightarrow \widetilde{a}_{9,5} = \widetilde{3} \Leftrightarrow w_9/w_5 = \widetilde{3}$ between the criteria C_5 (transmissivity) and C_9 (piezometry) means that piezometry was "about 3" times more significant than transmissivity.

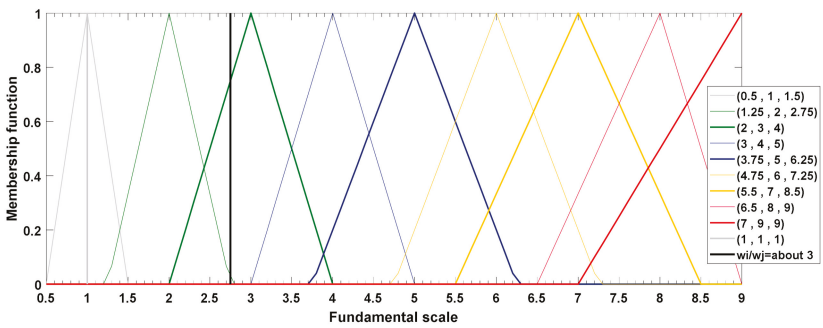

Figure 7. Graphical representation of the intensities of the relative importance of two criteria as triangular fuzzy numbers (TFN).

However, an ideal weight ratio (w_5/w_9) between these two criteria exists, which is a crisp number. As aforementioned, the ideal weight ratio of two criteria must be included in the corresponding fuzzy judgment (i.e., the support set of the TFN), or the deviations from the fuzzy thresholds should be small. In the investigation at hand, the black line in Figure 7 is assumed to be this ideal crisp weight ratio w_1/w_5.

The rating of alternatives, the weights before and after normalization, as well as the initial ranges (classes) with their corresponding linguistic variables of the criteria, are presented in Table 2 below. As aforementioned, in the FAHP of Wang and Chin [85], the final weights of criteria are crisp numbers. Based on the experts' knowledge, the criteria were divided into four crisp classes based on Equation (22). Then, the classes of each criterion were fuzzified and described by linguistic variables (low, moderately low, moderately high, high). These fuzzy classes are illustrated in Figures 8–10.

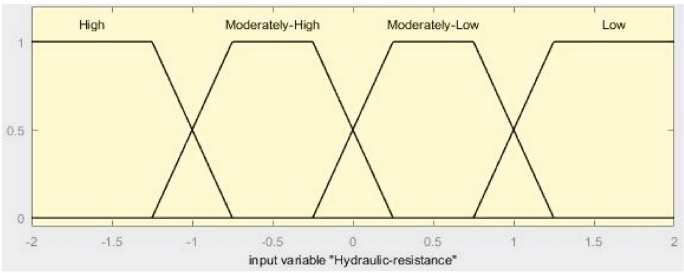

(**a**)

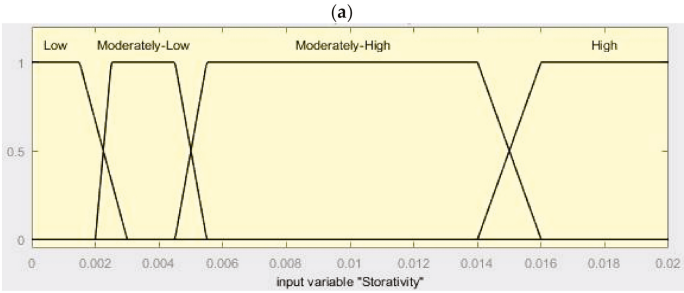

(**b**)

Figure 8. Fuzzy classes described by linguistic variables regarding the criteria (**a**) hydraulic resistance (C_7) and (**b**) storativity (C_6).

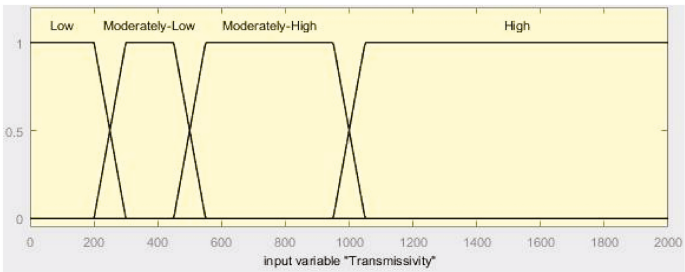

(**a**)

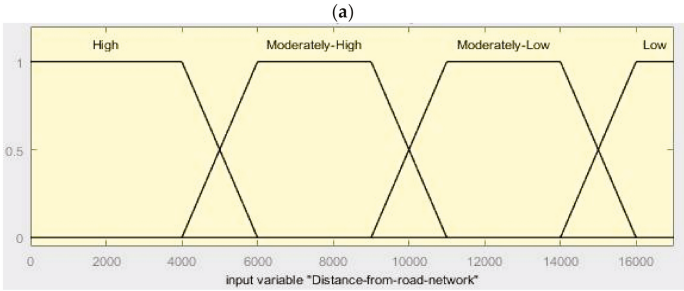

(**b**)

Figure 9. Fuzzy classes described by linguistic variables regarding the criteria (**a**) transmissivity (C_5) and (**b**) distance from road network (C_4).

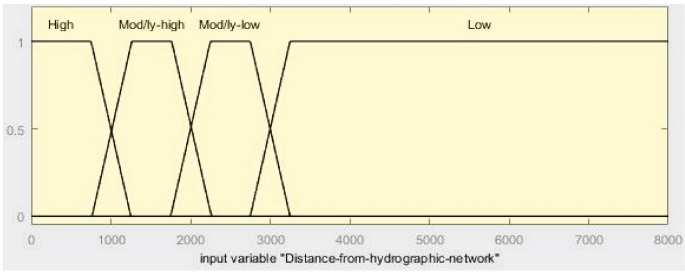

(**a**)

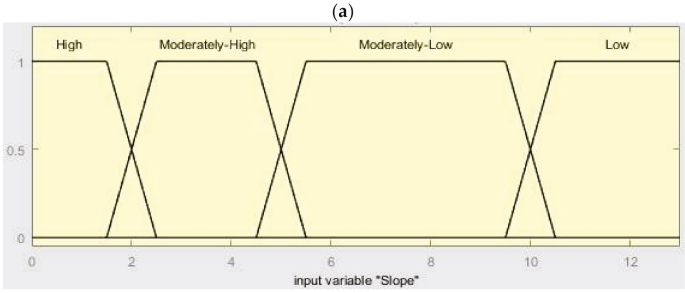

(**b**)

Figure 10. Fuzzy classes described by linguistic variables regarding the criteria (**a**) distance from hydrographic network (C_3) and (**b**) slope (C_2).

Table 2. Crisp weights of criteria and the rating of alternatives with respect to the classes of criteria. The crisp classes have been fuzzified in FIS.

Criteria	Classes	Linguistic Variable	Rating	Weight	Normalized Weight
C_1		High Good Moderate Deficient Worse Unknown	10 8 6 4 2 0	1.6641	0.0169
C_2	0–2 2–5 5–10 >10	High Moderately high Moderately low Low	10 7.5 5 2.5	3.8704	0.0394
C_3	<1000 1000–2000 2000–3000 >3000	High Moderately high Moderately low Low	10 7.5 5 2.5	3.9769	0.0405
C_4	0–5000 5000–10,000 10,000–15,000 >15,000	High Moderately high Moderately low Low	10 7.5 5 2.5	4.0643	0.0414
C_5	>1000 500–1000 250–500 0–250	High Moderately high Moderately low Low	10 7.5 5 2.5	10.8694	0.1109
C_6	>0.015 0.005–0.015 0.0025–0.005 0–0.0025	High Moderately high Moderately low Low	10 7.5 5 2.5	15.3198	0.1563
C_7	<−1 −1–0 0–1 >1	High Moderately high Moderately low Low	10 7.5 5 2.5	15.3198	0.1563

Table 2. *Cont.*

Criteria	Classes	Linguistic Variable	Rating	Weight	Normalized Weight
C_8	1 0	High Low	10 0	21.1237	0.2155
C_9	1 0	High Low	10 0	21.7949	0.2223

As noted, the classes of piezometry, type of aquifer, and ecological status are crisp. Regarding the criteria of piezometry and type of aquifer, two classes were considered and are presented in Appendix B (Figure A2). Therefore, the rating of these alternatives can be either 10 or 0. The criterion of ecological status was divided into six classes based on the relevant national River Basin Management Plans [60]. Since these three criteria divided into crisp classes, the ratings of the alternatives were calculated without the use of FIS.

Table 3 and Figure 11 present the final rating of the alternatives resulting from using either the min implication or the fuzzy implication of the algebraic product, for $M = 1$ and $M = 2$. As shown in Table 3, the ranking order of the alternatives ($Al_5 > Al_2 > Al_1 > Al_4 > Al_7 > Al_6 > Al_3$) was identical in almost all cases. A slight variation between the latter options took place when the min implication was used, and the M-value was equal to $M = 1$ ($Al_5 > Al_2 > Al_1 > Al_4 > Al_7 > Al_3 > Al_6$).

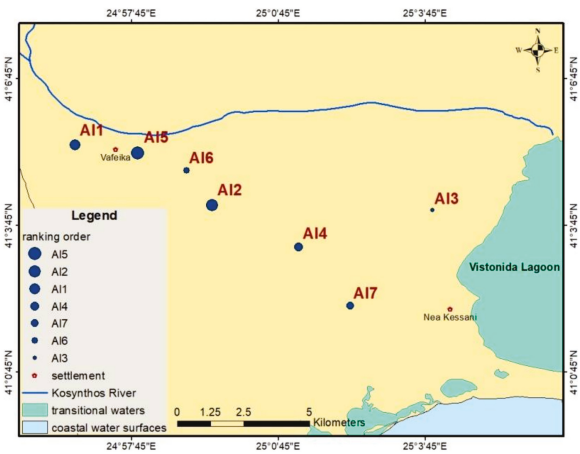

Figure 11. Final evaluation of alternatives.

Table 3. Final evaluation of the alternatives based on Mamdani product and min implication.

Ranking Order/ Implication	Alg. Prod. (M = 0.5)	Min (M = 0.5)	Alg. Prod. (M = 1)	Min (M = 1)
Al_5	8.0317	8.0320	7.9846	7.9792
Al_2	7.9859	7.9932	7.9355	7.9370
Al_1	7.7936	7.7877	7.7329	7.7191
Al_4	7.3382	7.3611	7.2765	7.2939
Al_7	6.5145	6.5179	6.4232	6.4228
Al_6	4.6199	4.6045	4.5888	4.5712
Al_3	4.5822	4.5829	4.5508	4.7090

5. Discussion

According to the results (Table 3 and Figure 11), the more favorable sites ($Al_5 > Al_2 > Al_1$) for applying floodwater spreading were located, in general, in the northwest

of the study area. Particularly, Al_5 was the most preferable alternative in all cases. In contrast, the final ratings of the alternatives located in the southeast part of the area under investigation were low (less favorable alternatives). This may be partly explained by the composition of geological formations which range from fine to silty clay in the SE–E direction towards Vistonida Lagoon [53,55]. However, this is not an absolute condition due to the significant variability of alluvial composition in the study area [58] on the one hand, and the contribution of the other criteria in the analysis on the other. For instance, the alternatives A_1 and Al_6 were less preferable than Al_2. Certainly, in the case of evaluating just a few alternatives, the best alternative might be identified on the basis of traditional hydrogeological analysis even though the criteria weights would not be taken into account. However, the more alternatives and criteria, the more complexity for the selection of the most preferable recharge site by an expert. Moreover, it is desirable that the MAR application is as effective as possible given its not negligible cost [93], and thus the solution of the selection problem should really be the best. As pointed out, the proposed methodology can be applied on both a large and small number of alternatives/criteria and this is a merit of the proposed methodology.

The local conditions of the case study (e.g., sparsely populated flat area) favor the application of flood spreading methods through infiltration basins, inasmuch as the excess winter water of the Kosynthos River might be used. Thus, the criteria were selected according to this type of MAR focusing on the hydrogeological local characteristics. Other criteria, such as socioeconomic and technical criteria, were not taken into account, as they are more in line with the design and implementation of MAR. It is worth mentioning that all alternatives were located south of the Kosynthos River. This is due to the fact that the Kosynthos River is the north hydraulic boundary of the aquifer system in the Xanthi plain [56–58].

The criteria weights were obtained through the FAHP–LFFP-based nonlinear method. Thus, in contrast to the conventional AHP, fuzziness was used to incorporate the uncertainty from the subjectivity of the initial experts' judgments. Using the FAHP–LFFP-based nonlinear method, a potential zero weight value was avoided and the non negativity of the λ-value was ensured, generating a unique optimal crisp priority vector. Besides, by using the FAHP–LFFP-based nonlinear method, the analysis could be performed either on the upper triangular elements of the fuzzy pairwise comparison matrix or on the lower ones. However, fuzzy weights can be obtained with the use of other methods (e.g., [94]).

An interesting point for discussion is the fuzziness of the initial judgments. In this study, an increasing fuzzy spread (width) was adopted regarding the scale of relative importance between two criteria. A reason for this was to avoid a large overlapping in the weak domination area that could lead to assigning almost equal importance to criteria even though there was a weak or moderately weak domination between the two criteria. Moreover, it seems more comfortable for a DM to assess that two conditions are equal or about equal than to assign the degree of their relative importance when their importance significantly differs. It is worth mentioning that after several tests on fuzzy spreads, which for space saving reasons are not presented, it was found that by increasing the fuzziness, the weights of the less important criteria increased (i.e., distance from road network, distance from hydrographic network, slope, and ecological status).

Regarding the parameter M used in the FAHP–LFFP method, it aims to ensure the non-negativity of parameter λ and to allow little deviation from fuzzy inequalities constraints, and hence an optimal solution that simultaneously satisfies all the fuzzy judgments can be achieved. An interesting point is that for $M > 2$, the solutions of deviations converged on a unit which had the lowest value in comparison with the solutions of deviation for $M < 2$. However, the λ-value was zero, which means that the inequalities of Equation (8) did not simultaneously hold, and thus these values were not used. The M-value selected was $M = 0.5$ because it produced a more balanced solution between the λ-value and the total deviations than those that were produced when $M = 1$ and $M = 0.2$ were used. In the calculation of the λ-value, the fuzzy min intersection was used because using the other

widely used t-norm (algebraic product) resulted in a lower satisfaction degree of the fuzzy pairwise comparisons.

The ratings of the alternatives with respect to each criterion were based on using fuzzy inferences systems based on the Mamdani approach. The use of such systems was preferred in this study in order for the ranges (classes) of criteria to be fuzzified. The ranges of criteria were modulated on the basis of the available information (e.g., min–max values of each criterion regarding the case study) and of the experts' knowledge. Therefore, it seemed more reasonable to use fuzzy thresholds of the ranges than crisp ones for taking into account the uncertainty derived from the lack of information and imprecise knowledge.

Another reason for using FIS is that, there are not precise and well-known objective functions for each criterion, as in the usual multi-objective problems.

On the other hand, the selection problem examined in this study could be solved based on the exclusive use of FIS; however, this choice was not preferred because it would lead to a complex system of fuzzy if-then rules.

In this study, each FIS is based on a simple system of fuzzy if-then rules, where only an input variable, has been used (Equation (12)). Therefore, neither t-conorms nor t-norms were used in the antecedent if-part. As the fuzzy implication is concerned, both the two widely used fuzzy implications were used. That is, the Mamdani implication, in which the t-norm of algebraic product is used, and the min implication, in which the t-norm of min intersection is used. In general, in case of no distinction between cause and effect, the min fuzzy implication is recommended. However, several other fuzzy implications can be used [95], the appropriate selection of which is an open issue [90]. For the composition of the fuzzy rules, the widely used t-conorm of max union was preferred. However, other t-conorms can also be tested. The fuzzy output of each FIS method is defuzzified by selecting the centroid method, which is considered a balanced solution given that it counts the gravity center.

The synthesis of criteria with respect of each alternative was achieved based on a simple additive model, in which the rating (the defuzzified output of the FIS) of each alternative is multiplied with the normalized weight with respect of each criterion. The total sum is the final evaluation (final score) of each alternative. The alternative with the highest score is the solution to the decision-making problem. Other (fuzzy) multi attributes decision-making (MADM) methods might be used for the synthesis of criteria and the final ranking of alternatives using the weights derived by the FAHP–LFFP-based nonlinear method (e.g., fuzzy TOPSIS, fuzzy ELECTRE, fuzzy pattern recognition). However, the use of such methods would have increased the complexity of the solution process on one hand and more information would have been required on the other.

The FAHP–LFFP method and the FIS were applied to the examined problem for the first time. According to Table 3, the solution (ranking order of the alternatives) did not changed regardless of which *M*-value or fuzzy inference engine was used, except in the case of min implication, in which the less preferable alternatives exchanged order. Thus, based on the knowledge of previous studies [53,55–58,60] regarding the hydrogeological conditions of the case study, and by taking into account the stability of the solution, the results of the proposed methodology are considered reliable. It would be of great interest if these results were compared with those of other (hybrid) multi-criteria methods that could be applied in the composition of criteria (e.g., fuzzy ELECTRE, fuzzy pattern recognition).

6. Conclusions

This research applied a hybrid fuzzy multi-criteria methodology to select preferable site for applying MAR systems in the context of increasing the local groundwater availability for later water use in case of drought occurrence. Fuzzy set theory and fuzzy logic were used both in the determination of criteria weights and in the evaluation of alternatives, thus incorporating the uncertainties derived from the subjectivity and the lack of information.

The proposed methodology was applied in a flat agricultural area in the southeast of Xanthi city, northern Greece, where a significant number of irrigation wells draw from the

shallow aquifer system. The local conditions favor the implementation of flood spreading through infiltration basins utilizing excess winter water of the Kosynthos River.

The results show that:

(1) The more preferable sites are located in the northwestern part of the study area near the Kosynthos River, while the most preferable is the Al_5 alternative. This mainly holds due to the hydrological conditions of the northwestern part, which are more favorable than the southeastern ones for groundwater recharge. However, this is not an absolute condition due to the intense diversity of geological formations. In addition, the contribution of the analysis of the other criteria also affected the final rank list.

(2) The proposed methodology can be used for distinguishing discrete preferable points (alternatives) for MAR application without limitation in number of the examined alternatives. In addition, the selected criteria can be added or subtracted depending on specific local conditions. In case of application of another type of MAR the selected criteria should be adjusted as well. Certainly, in the case of a small number (<10) of alternatives to study, a classical hydrogeological analysis may lead to the selection of the most preferable alternative. However, in that case, the criteria weights would not be taken into account and thus, there would be the possibility of not obtaining an efficient and comprehensive solution. On the other hand, in the case of a large number of examined alternatives and criteria, where the complexity increased, the proposed methodology might be also a useful tool for ranking discrete alternatives. Other than that, it could be used as an alternative way to identify suitable recharge sites in case of low data availability.

(3) The applicability of the methodology requires lithological profile and hydraulic characteristics of both vadose and saturated zones, while it can be applied only in unconfined aquifers and where there is an underlying drainage axis. Furthermore, the application of this type of MAR requires the presence of a river whose excess waters can be utilized. Thus, after a preparatory screening, seven alternatives satisfied all the assumptions and criteria were finally evaluated.

(4) In general, the use of fuzzy logic in AHP can incorporate the uncertainty from the subjectivity of the initial experts' judgments, while the fuzzy version of AHP implemented in this paper (FAHP–LFFP-based nonlinear method) can ensure a unique and optimal solution.

(5) Fuzzy inference systems (FIS) based on Mamdani's approach are used in order to determine the rating of each alternative, since the objective function (or value function) regarding each examined criterion is unknown. In addition, with use of FIS, the classes of criteria are fuzzified, and this fact is more reasonable to describe the real conditions.

Author Contributions: Conceptualization, C.P., M.S., F.P., I.G., N.K. and B.P.; methodology, C.P., M.S., F.P., I.G., N.K. and B.P.; software, C.P. and M.S.; investigation, C.P., M.S., F.P., I.G., N.K. and B.P.; resources, C.P., M.S., F.P., I.G., N.K. and B.P.; writing—original draft preparation, C.P., M.S., F.P., I.G., N.K. and B.P.; writing—review and editing, C.P., M.S., F.P., I.G., N.K. and B.P. All authors have read and agreed to the published version of the manuscript.

Funding: This research was co-financed by Greece and the European Union (European Social Fund—ESF) through the Operational Programme "Human Resources Development, Education and Lifelong Learning" in the context of the project "Strengthening Human Resources Research Potential via Doctorate Research" (MIS-5000432), implemented by the State Scholarships Foundation (IKΥ).

Conflicts of Interest: The authors declare no conflict of interest.

Appendix A

Each mapping from the Universe X into the [0, 1] is a *fuzzy set*. An element x of a fuzzy set $\widetilde{A}$ is expressed either by the membership function, $\mu_{\widetilde{A}}(x)$, or by α-cuts, ${}^{\alpha}\widetilde{A}$. The α-cuts are crisp sets defined as follows:

$$ {}^{\alpha}\widetilde{A} = \left\{ x \in X : \mu_{\widetilde{A}}(x) \geq \alpha \right\} \tag{A1} $$

If $\alpha = 0$, then it holds $\mu_{\widetilde{A}}(x) > 0$ for all the elements $x \in X$.

A special kind of fuzzy sets comprises *fuzzy numbers*. A *fuzzy number* $\widetilde{Z} \subset \mathbb{R}$ satisfies the following properties [65]:

(1) $\widetilde{Z}$ is a normal set, i.e., $\exists x \in X$ such that $\mu_{\widetilde{Z}}(x) = 1$;
(2) ${}^{\alpha}Z$ must be a closed interval $\forall \alpha \in (0, 1]$;
(3) the strong zero cut, ${}^{0+}Z$, which is called the support set of $\widetilde{Z}$, must be bounded.

The second property implies that a fuzzy number $\widetilde{Z}$ is a convex set as well.

There are many types of fuzzy numbers. Trapezoidal fuzzy numbers are based on four points (elements of the set of real numbers $\mathbb{R}$), while triangular fuzzy numbers are based on three points (elements of $\mathbb{R}$). Typical shapes of these fuzzy numbers are presented in the Appendix A in Figure A1a,b, correspondingly. The membership function of a trapezoidal fuzzy number is described as follows:

$$ \mu_{\widetilde{Z}}(x) = \begin{cases} (x-l)/c_1 & if\ l \leq x < m \\ 1 & if\ m \leq x \leq n \\ (u-x)/c_2 & if\ n \leq x \leq u \\ 0 & otherwise \end{cases} \tag{A2} $$

where $(x - l)/c_1$ is a continuous from the left and increasing function from $(l, m) \to [0, 1]$ and $(u - x)/c_2$ is a continuous from the right and decreasing function from $(n, u) \to [0, 1]$. The parameters c_1 and c_2 denote the fuzzy spreads of the fuzzy numbers. In the case of trapezoidal fuzzy number (Figure A1a), it holds $c_1 = m - l$ and $c_2 = u - n$. In the case of triangular fuzzy numbers (Figure A1b), it holds $m = n$, and therefore, $c_1 = m - l$ and $c_2 = u - m$.

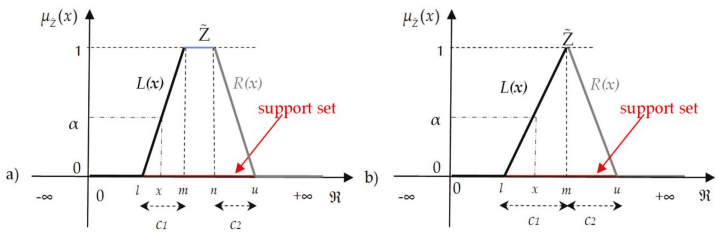

Figure A1. Typical shapes of (**a**) trapezoidal and (**b**) triangular fuzzy numbers.

In fuzzy set theory, the principle that extends all crisp mathematical concepts to fuzzy sets is named *extension principle*. With the use of the extension principle, all operations of the crisp functions between fuzzy sets (fuzzy numbers) are allowed [66].

Let X be a Cartesian product of universes $X = X_1 \times \ldots \times X_n$ and $\widetilde{A}_1, \ldots, \widetilde{A}_n$ be fuzzy sets in $X_1 \times X_2 \times \ldots \times X_n$, correspondingly. If $f : X_1 \times \ldots \times X_n \to Y$, $y = f(x_1, \ldots, x_n)$, then a fuzzy set $\widetilde{B}$ in Y can be defined as follows [67]:

$$ \widetilde{B} = \{(y, \mu_{\mathrm{B}}(y)) | y = f(x_1, \ldots x_n), (x_1, \ldots x_n) \in X\} \tag{A3} $$

where

$$\mu_{\widetilde{B}}(y) = \begin{cases} \sup\limits_{(x_1,\ldots,x_n)\in f^{-1}(y)} & \min\left\{\mu_{\widetilde{A}_1}(x_1),\ldots,\mu_{\widetilde{A}_n}(x_n)\ for\ f^{-1}(y) \neq \varnothing \right. \\ 0 & otherwise \end{cases} \tag{A4}$$

where f^{-1} is the inverse of f.

In the case of n = 1, then $f : X \to Y$, therefore it holds:

$$\widetilde{B} = f(\widetilde{A}) = \{(y, \mu_{\mathrm{B}}(y)) | y = f(x) \in X\} \tag{A5}$$

where

$$\mu_{\widetilde{B}}(y) = \begin{cases} \sup\limits_{x\in f^{-1}(y)} \mu_{\widetilde{A}_1}(x), & for f^{-1}(y) \neq \varnothing \\ 0 & otherwise \end{cases} \tag{A6}$$

The extension principle allows all algebraic operations between fuzzy sets to be performed. The relation between fuzzy sets is described by a crisp function.

In the general case, a fuzzy function is performed and a fuzzy relation (Equation (A7)), which is a fuzzy set, is produced even though the input is crisp number.

$$\widetilde{R} = \left\{\left((x,y), \mu_{\widetilde{R}}(x,y)\right) | (x,y) = f(x) \in XxY\right\} \tag{A7}$$

The generalization of the extension principle, i.e., a fuzzy mapping from X to universe Y, $\widetilde{f} : X \to Y$, is achieved with the use of *composition* of $R_1(X, Y)$ and $R_2(Y, Z)$:

$$\mu_{\widetilde{R}_1 \circ \widetilde{R}_2}(z) = \bigcup_{y\in Y}\left[\min\left\{\mu_{\widetilde{R}_1}(x,y), \mu_{\widetilde{R}_2}(y,z)\right\}\right] x \in X, y \in Y, z \in Z \tag{A8}$$

where $\widetilde{R}_1(x,y)$, $(x,y) \in XxY$ and $\widetilde{R}_2(y,z)$, $(y,z) \in YxZ$ are two fuzzy relations [68]. By using the minimum intersection, the widely used *max–min composition* is produced. The use of algebraic product as fuzzy intersection in the composition is common too. The membership function $\mu_{\widetilde{R}_1 \circ \widetilde{R}_2}(z)$ denotes the membership grades of the elements of the related fuzzy sets.

Appendix B

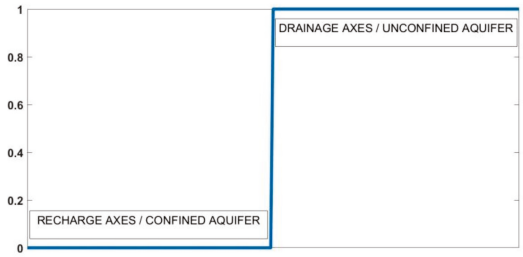

Figure A2. Typical shape of the crisp ranges regarding the criteria of piezometry (C_9) and type of aquifer (C_8).

References

1. Vörösmarty, C.J.; Green, P.; Salisbury, J.; Lammers, R.B. Global Water Resources: Vulnerability from Climate Change and Population Growth. *Science* **2000**, *289*, 284–288. [CrossRef]
2. Tebaldi, C.; Hayhoe, K.; Arblaster, J.M.; Meehl, G.A. Going to the extremes. *Clim. Chang.* **2006**, *79*, 185–211. [CrossRef]
3. Taylor, R.G.; Scanlon, B.; Döll, P.; Rodell, M.; Van Beek, R.; Wada, Y.; Longuevergne, L.; Leblanc, M.; Famiglietti, J.S.; Edmunds, M.; et al. Ground water and climate change. *Nat. Clim. Chang.* **2013**, *3*, 322–329. [CrossRef]
4. Zwiers, F.W.; Alexander, L.V.; Hegerl, G.C.; Knutson, T.R.; Kossin, J.P.; Naveau, P.; Nicholls, N.; Schär, C.; Seneviratne, S.I.; Zhang, X. Climate extremes: Challenges in estimating and understanding recent changes in the frequency and intensity of

extreme climate and weather events. In *Climate Science for Serving Society*; Asrar, G.R., Hurrell, J.W., Eds.; Springer: Dordrecht, The Netherlands, 2013; pp. 339–389, ISBN 978-94-007-6691-4.
5. Wuebbles, D.; Meehl, G.; Hayhoe, K.; Karl, T.R.; Kunkel, K.; Santer, B.; Wehner, M.; Colle, B.; Fischer, E.M.; Fu, R.; et al. CMIP5Climate Model Analyses: Climate Extremes in the United States. *Bull. Am. Meteor. Soc.* **2013**, *95*, 571–583. [CrossRef]
6. Bouwer, H. Artificial recharge of groundwater:hydrogeology and engineering. *Hydrogeol. J.* **2000**, *10*, 121–142.
7. Maliva, R.G.; Guo, W.; Missimer, T.M. Aquifer storage and recovery: Recent hydrogeological advances and system performance. *Water Environ. Res.* **2006**, *78*, 2428–2435. [CrossRef]
8. Jager, H.I.; Smith, B.T. Sustainable Reservoir Operation: Can We Generate Hydropower and Preserve Ecosystem Values? *River Res. Appl.* **2008**, *24*, 340–352. [CrossRef]
9. Minsley, B.J.; Ajo-Franklin, J.; Mukhopadhyay, A.; Morgan, F.D. Hydrogeophysical Methods for Analyzing Aquifer Storage and Recovery Systems. *Groundwater* **2011**, *49*, 250–269. [CrossRef]
10. Giordano, M. Global Groundwater? Issues and Solutions. *Annu. Rev. Environ. Resour.* **2009**, *34*, 153–178. [CrossRef]
11. Kundzewicz, Z.W.; Doll, P. Will groundwater ease freshwater stress under climate change? *Hydrol. Sci. J.* **2009**, *54*, 665–675. [CrossRef]
12. Scanlon, B.R.; Reedy, R.C.; Faunt, C.C.; Pool, D.; Uhlman, K. Enhancing drought resilience with conjunctive use and managed aquifer recharge in California and Arizona. *Environ. Res. Lett.* **2016**, *11*, 035013.
13. de Graaf, I.E.M.; Gleeson, T.; Rens van Beek, L.P.H.; Sutanudjaja, E.H.; Bierkens, M.F.P. Environmental Flow Limits to Global Groundwater Pumping. *Nature* **2019**, *574*, 90–94. [CrossRef]
14. Dillon, P. Future management of aquifer recharge. *Hydrogeol. J.* **2005**, *13*, 313–316. [CrossRef]
15. Niswonger, R.G.; Morway, E.D.; Triana, E.; Huntington, J.L. Managed aquifer recharge through off-season irrigation in agricultural regions. *Water Resour. Res.* **2017**, *53*, 6970–6992. [CrossRef]
16. California Department of Water Resources. Using Flood Water for Managed Aquifer Recharge to Support Sustainable Water Resources. White Paper. 26 June 2018, p. 54. Available online: https://ui.adsabs.harvard.edu/abs/2018AGUFM.H51X1679M/abstract (accessed on 30 December 2021).
17. Dillon, P.; Stuyfzand, P.; Grischek, T.; Lluria, M.; Pyne, R.D.G.; Jain, R.C.; Bear, J.; Schwarz, J.; Wang, W.; Fernandez, E.; et al. Sixty years of global progress in managed aquifer recharge. *Hydrogeol. J.* **2019**, *27*, 1–30. [CrossRef]
18. Wendt, D.E.; Van Loon, A.F.; Scanlon, B.R.; Hannah, D.M. Managed Aquifer Recharge as a Drought Mitigation Strategy in Heavily-Stressed Aquifers. *Environ. Res. Lett.* **2021**, *16*, 014046. [CrossRef]
19. Zhao, M.; Boll, J.; Adam, J.C.; King, A.B. Can Managed Aquifer Recharge Overcome Multiple Droughts? *Water* **2021**, *13*, 2278. [CrossRef]
20. Gale, I.N.; Dillon, P. *Strategies for Managed Aquifer Recharge (MAR) in Semi-Arid Areas*; United Nations Educational, Scientific and Cultural Organisation (UNESCO): Paris, France, 2005; p. 30.
21. Ringleb, J.; Sallwey, J.; Stefan, C. Assessment of Managed Aquifer Recharge through Modeling—A Review. *Water* **2016**, *8*, 579. [CrossRef]
22. Foster, S.; van Steenbergen, F. Conjunctive groundwater use: A 'lost opportunity' for water management in the developingworld? *Hydrogeol. J.* **2011**, *19*, 959–962. [CrossRef]
23. Maliva, R.G. *Antropogenic Aquifer Recharge*; WSP Methods in Water Resources Evaluation Series No. 5; Springer: Cham, Switzerland, 2020; p. 861. [CrossRef]
24. Dillon, P.; Escalante, E.F.; Tuinhof, A. *Management of Aquifer Recharge and Discharge Processes and Aquifer Storage Equilibrium*; Groundwater Governance Thematic Paper 4; GEF-FAO: Rome, Italy, 2012.
25. Pakparvar, M.; Walraevens, K.; Cheraghi, S.A.M.; Cornelis, W.; Gabriels, D.; Kowsar, S.A. Assessment of groundwater recharge influenced by floodwater spreading: An intergrated approach with limited accessible data. *Hydrol. Sci. J.* **2017**, *62*, 147–164. [CrossRef]
26. Hashemi, H.; Berndtsson, R.; Persson, M. Artificial recharge by floodwater spreading estimated by water balancesand groundwater modeling in arid Iran. *Hydrol. Sci. J.* **2015**, *60*, 336–350. [CrossRef]
27. Saraf, A.K.; Choudhury, P.R. Integrated remote sensing and GIS for ground waterexploration and identification of artificial recharge sites. *Int. J. Remote Sens.* **1998**, *19*, 1825–1841. [CrossRef]
28. Al Saud, M. Mapping potential areas for groundwater storage in Wadi Aurnah Basin, western Arabian Peninsula, using remote sensing and geographic information system techniques. *Hydrogeol. J.* **2010**, *18*, 1481–1495. [CrossRef]
29. Senanayake, I.P.; Dissanayake, D.M.D.O.K.; Mayadunna, B.B.; Weerasekera, W.L. An approach to delineate groundwater recharge potential sites in Ambalantota, Sri Lanka using GIS techniques. *Geosci. Front.* **2016**, *7*, 115–124. [CrossRef]
30. Chenini, I.; Ben Mammou, A.; El May, M. Groundwater Recharge Zone Mapping Using GIS-Based Multi-criteria Analysis: A Case Study in Central Tunisia (Maknassy Basin). *Water Resour. Manag.* **2010**, *24*, 921–939. [CrossRef]
31. Chowdhury, A.; Jha, M.K.; Chowdary, V.M. Delineation of groundwater recharge zones and identification of artificial recharge sites in West Medinipur district, West Bengal, using RS, GIS and MCDM techniques. *Environ. Earth Sci.* **2010**, *59*, 1209–1222. [CrossRef]
32. Nasiri, H.; DarvishiBoloorani, A.; FarajiSabokbar, H.A.; Jafari, H.R.; Hamzeh, M.; Rafi, Y. Determining the most suitable areas for artificial groundwater recharge via an integrated PROMETHEE II-AHP method in GIS environment (case study: Garabaygan Basin, Iran). *Environ. Monit. Assess.* **2013**, *185*, 707–718. [CrossRef]

33. Valverde, J.P.B.; Blank, C.; Roidt, M.; Schneider, L.; Stefan, C. Application of a GIS Multi-Criteria Decision Analysis for the Identification of Intrinsic Suitable Sites in Costa Rica for the Application of Managed Aquifer Recharge (MAR) through Spreading Methods. *Water* **2016**, *8*, 391. [CrossRef]
34. Selvarani, A.G.; Maheswaran, G.; Elangovan, K. Identification of artificial recharge sites for Noyyal River Basin using GIS and remote sensing. *J. Indian Soc. Remote Sens.* **2017**, *45*, 67–77. [CrossRef]
35. Kazakis, N. Delineation of Suitable Zones for the Application of Managed Aquifer Recharge (MAR) in Coastal Aquifers Using Quantitative Parameters and the Analytical Hierarchy Process. *Water* **2018**, *10*, 804. [CrossRef]
36. Zadeh, L.A. Fuzzy sets. *Inf. Control* **1965**, *8*, 338–353.
37. Zimmermann, H.-J. Advanced Review. Fuzzy set theory. *WIREs Comput. Stat.* **2010**, *2*, 317–332. [CrossRef]
38. Garg, H. A Hybrid GA-GSA Algorithm for Optimizing the Performance of an Industrial System by Utilizing Uncertain Data. In *Handbook of Research on Artificial Intelligence Techniques and Algorithms*; Pandian, V., Ed.; IGI Global: Hershey, PE, USA, 2015; pp. 620–654. [CrossRef]
39. Bogardi, I.; Duckstein, L.; Bardossy, A. Regional management of an aquifer under fuzzy environmental objectives. *Water Resour. Res.* **1983**, *19*, 1394–1402. [CrossRef]
40. Kambalimath, S.; Deka, P.C. A basic review of fuzzy logic applications in hydrology and water resources. *Appl. Water Sci.* **2020**, *10*, 191. [CrossRef]
41. Kazakis, N.; Spiliotis, M.; Voudouris, K.; Pliakas, F.K.; Papadopoulos, B. A fuzzy multicriteria categorization of the GALDIT method to assess seawater intrusion vulnerability of coastal aquifers. *Sci. Total Environ.* **2018**, *621*, 524–534. [CrossRef]
42. Kourgialas, N.N.; Anyfanti, I.; Karatzas, G.P.; Dokou, Z. An integrated method for assessing drought prone areas-Water efficiency practices for a climate resilient Mediterranean agriculture. *Sci. Total Environ.* **2018**, *625*, 1290–1300. [CrossRef]
43. Spiliotis, M.; Iglesias, A.; Garrote, L. A multicriteria fuzzy pattern recognition approach for assessing the vulnerability to drought: Mediterranean region. *Evol. Syst.* **2021**, *12*, 109–122. [CrossRef]
44. Chan, F.T.S.; Kumar, N. Global supplier development considering risk factors using fuzzy extended AHP-based approach. *Omega* **2007**, *35*, 417–431. [CrossRef]
45. Chan, F.T.S.; Kumar, N.; Tiwari, M.K.; Lau, H.C.W.; Choy, K.L. Global supplier selection: A fuzzy-AHP approach. *Int. J. Prod. Res.* **2008**, *46*, 3825–3857. [CrossRef]
46. Saravi, M.M.; Malekian, A.; Nouri, B. Identification of Suitable Sites for Groundwater Recharge. In Proceedings of the 2nd International Conference on Water Resources & Arid Environment, Riyadh, Saudi Arabia, 26–29 November 2006; pp. 1–5.
47. Ghayoumian, J.; MohseniSaravi, M.; Feiznia, S.; Nouri, B.; Malekian, A. Application of GIS techniques to determine areas most suitable for artificial groundwater recharge in a coastal aquifer in southern Iran. *J. Asian Earth Sci.* **2007**, *30*, 364–374. [CrossRef]
48. Riad, P.H.; Billib, M.H.; Hasan, A.A.; Omar, M.A. Overlay Weighted Model and Fuzzy Logic to Determine the Best Locations for Artificial Recharge of Groundwater in a Semi-Arid Area in Egypt. *Nile Basin Water Sci. Eng. J.* **2011**, *4*, 24–35.
49. Malekmohammadi, B.; Mehrian, M.R.; Jafari, H.R. Site selection for managed aquifer recharge using fuzzy rules: Integrating geographical information system (GIS) tools and multi-criteria decision making. *Hydrogeol. J.* **2012**, *20*, 1393–1405. [CrossRef]
50. Dashtpagerdi, M.M.; Vagharfard, H.; Honarbakhsh, A.; Khoorani, A. GIS Based Fuzzy Logic Approach for Identification of Groundwater Artificial Recharge Site. *Open J. Geol.* **2013**, *3*, 379–383. [CrossRef]
51. Selvarani, A.G.; Maheswaran, G.; Elangovan, K. Identification of Artificial Recharge Sites For Noyyal Watershed Using GIS And Fuzzy Logic. *Int. J. Appl. Eng. Res.* **2015**, *10*, 11189–11208.
52. Ghasemi, A.; Saghafian, B.; Golian, S. Optimal location of artificial recharge of treated wastewater using fuzzy logic approach. *J. Water Supply Res. Technol.* **2017**, *66*, 141–156. [CrossRef]
53. Pliakas, F.; Kallioras, A.; Damianidis, P.; Kostakakis, P. Evaluation of precipitation effects on groundwater levels in a Mediterranean alluvial plain based on hydrogeological conceptualization. *Environ. Earth Sci.* **2015**, *74*, 3573–3588. [CrossRef]
54. Dimadis, E.; Zachos, S. *Geological Map of Rhodope Massif*; Institute of Geology and Mineral Exploration (IGME), Regional Subdivision of Eastern Macedonia—Thrace: Xanthi, Greece, 1986.
55. Sakkas, I.; Diamantis, I.; Pliakas, F. *Groundwater Artificial Recharge Study of Xanthi-Rhodope Aquifers (in Thrace, Greece)*; Greek Ministry of Agriculture Research Project, Final Report; Sections of Geotechnical Engineering and Hydraulics of the Civil Engineering Department of Democritus University of Thrace: Xanthi, Greece, 1998. (In Greek)
56. Pliakas, F.; Diamantis, I.; Petalas, C. Results from a Groundwater Artificial Recharge Application in Polysitos Aquifer at Xanthi Plain Region (Greece) by Reactivating Old Stream Beds. In Proceedings of the 5th Greek National Hydrogeological Conference, Nicosia, Cyprus, 12−14 November 1999; pp. 97–113. (In Greek).
57. Pliakas, F.; Petalas, C.; Diamantis, I.; Kallioras, A. Modeling of groundwater artificial recharge by reactivating an on old streambed. *Water Resour. Manag.* **2005**, *19*, 279–294.
58. Pisinaras, V. Ανάπτυξη ΕνόςΠλαισίου ΟλοκληρωμένηςΔιαχείρισης Πολύπλοκων Συστημάτων ΥπόγειωνΥδατικών πόρων [Development of a Methodology Framework for Integrated Management of Complex Groundwater Systems]. Ph.D. Thesis, Democritus University of Thrace, Xanthi, Greece, June 2008. (In Greek).
59. Papadopoulos, C.; Spiliotis, M.; Gkiougkis, I.; Pliakas, F.; Papadopoulos, B. Fuzzy linear regression analysis for groundwater response to meteorological drought in the aquifer system of Xanthi plain, NE Greece. *J. Hydroinform.* **2021**, *23*, 1112–1129. [CrossRef]

60. Diamantis, I.; Pliakas, F.; Petalas, C. The contribution of artificial recharge as a remedy procedure regarding the impacts of various interventions on the natural environment of plain regions. The case study in Thrace, Greece. In Proceedings of the International Symposium on Engineering Geology and the Environment, Organized by the Greek National Group of the International Association for Engineering Geology and the Environment (IAEG), Athens, Greece, 23–27 June 1997; pp. 2663–2667.
61. Special Secretariat for Water. *River Basin Management Plans of Thrace Water District (GR12)*; Ministry of Environmental and Energy: Athens, Greece, 2017.
62. Krishnamurthy, J.; Kkumar, N.V.; Jayaraman, V.; Manivel, M. An approach to demarcate ground water potential zones through remote sensing and geographic information system. *Int. J. Remote Sens.* **1996**, *17*, 1867–1884.
63. Farhadian, M.; Bozorg-Haddad, O.; Pazoki, M.; Loaiciga, H.A. Locating and Prioritizing Suitable Places forthe Implementation of Artificial Groundwater Recharge Plans. *J. Irrig. Drain. Eng.* **2017**, *143*, 04017018.
64. Ghayoumian, J.; Ghermezcheshmeh, B.; Feiznia, S.; Noroozi, A.A. Integrating GIS and DSS for identification of suitable areas for artificial recharge, case study Meimeh Basin, Isfahan. Iran. *Environ. Geol.* **2005**, *47*, 493–500.
65. Jasrotia, A.S.; Kumar, R.; Saraf, A.K. Delineation of groundwater recharge sites using integrated remote sensing and GIS in Jammu district, India. *Int. J. Remote Sens.* **2007**, *28*, 5019–5036.
66. Klir, G.J.; Yuan, B. *Fuzzy Sets and Fuzzy Logic. Theory and Applications*; Prentice Hall: Hoboken, NJ, USA, 1995.
67. Ross, T.J. *Fuzzy Logic with Engineering Applications*, 3rd ed.; John Wiley & Sons: West Sussex, UK, 2010; p. 585.
68. Zimmerman, H.-J. *Fuzzy Set Theory and Its Applications*, 4th ed.; Springer Science & Business Media: New York, NY, USA, 2001; p. 514.
69. Wang, L.-X. *A Course in Fuzzy Systems and Control*; Prentice Hall: Hoboken, NJ, USA, 1997; p. 424.
70. Saaty, T.L. *The Analytic Hierarchy Process*; McGraw-Hill: New York, NY, USA, 1980.
71. Pöyhönen, M.A.; Hämäläinen, R.P.; Salo, A.A. An Experiment on the Numerical Modeling of Verbal Ratio Statements. *J. Multi-Criteria Decis. Anal.* **1997**, *6*, 1–10.
72. Ho, W.; Ma, X. The state-of-the-art integrations and applications of the analytic hierarchy process. *Eur. J. Oper. Res.* **2018**, *267*, 399–414. [CrossRef]
73. Chang, D.-Y. Applications of the extent analysis method on fuzzy AHP. Theory and Methodology. *Eur. J. Oper. Res.* **1996**, *95*, 649–655.
74. Kwong, C.K.; Bai, H. Determining the importance weights for the customer requirements in QFD using a fuzzy AHP with anextent analysis approach. *IIE Trans.* **2003**, *35*, 619–626.
75. Kahraman, C.; Ruan, D.; Dogan, I. Fuzzy group decision making for facility location selection. *Inf. Sci.* **2003**, *157*, 135–153.
76. Kahraman, C.; Ertay, T.; Buyukozkan, G. A fuzzy optimization model for QFD planning process using analytic network approach. *Eur. J. Oper. Res.* **2006**, *171*, 390–411.
77. Srdjevic, B.; Medeiros, Y.D.P. Fuzzy AHP Assessment of Water Management Plan. *Water Resour. Manag.* **2008**, *22*, 877–894. [CrossRef]
78. Wang, Y.-M.; Luo, Y.; Hua, Z. On the extent analysis method for fuzzy AHP and its applications. *Eur. J. Oper. Res.* **2008**, *186*, 735–747. [CrossRef]
79. Mikhailov, L. Deriving priorities from fuzzy pairwise comparison judgements. *Fuzzy Sets Syst.* **2003**, *134*, 365–385. [CrossRef]
80. Mikhailov, L. A fuzzy programming method for deriving priorities in the analytic hierarchy process. *J. Oper. Res. Soc.* **2000**, *51*, 341–349. [CrossRef]
81. Li, L.; Lai, K.K. A fuzzy approach to the multiobjective transportation problem. *Comput. Oper. Res.* **2000**, *27*, 43–57. [CrossRef]
82. Tsakiris, G.; Spiliotis, M. Multicriteria ranking of water development scenario using a fuzzy rule based system. In Proceedings of the International Symposium on Water Resources Management: Risks and Challenges for the 21st Century, Izmir, Turkey, 2–4 September 2004.
83. Gurav, J.B.; Regulwar, D.G. Multi Objective Sustainable Irrigation Planning with Decision Parameters and Decision Variables Fuzzy in Nature. *Water Resour. Manag.* **2012**, *26*, 3005–3021. [CrossRef]
84. Mikhailov, L.; Tsvetinov, P. Evaluation of services using a fuzzy analytic hierarchy process. *Appl. Soft Comput.* **2004**, *5*, 23–33. [CrossRef]
85. Wang, Y.-M.; Chin, K.-S. Fuzzy analytic hierarchy process: A logarithmic fuzzy preference programming methodology. *Int. J. Approx. Reason.* **2011**, *52*, 541–553. [CrossRef]
86. Spiliotis, M.; Skoulikaris, C. A fuzzy AHP-outranking framework for selecting measures of river basin management plans. *Desalination Water Treat.* **2019**, *167*, 398–411. [CrossRef]
87. Mamdani, E.H.; Assilian, S. An Experiment in Linguistic Synthesis with a Fuzzy Logic Controller. *Int. J. Mach. Stud.* **1975**, *7*, 1–13. [CrossRef]
88. Yen, J.; Langari, R. *Fuzzy Logic. Intelligence, Control, and Information*; Prentice Hall: New York, NJ, USA, 1999; pp. 32–43.
89. Ojha, V.; Abraham, A.; Snasel, V. Heuristic Design of Fuzzy Inference Systems: A Review of Three Decades of Research. *Eng. Appl. Artif. Intell.* **2019**, *85*, 845–864. [CrossRef]
90. Papadopoulos, B.; Trasanides, G.; Hatzimichailidis, A.G. Optimization Method for the Selection of the Appropriate Fuzzy Implication. *J. Optim. Theory Appl.* **2007**, *134*, 135–141. [CrossRef]
91. Balopoulos, V.; Hatzimichailidis, A.; Papadopoulos, B. Distance and similarity measures for fuzzy operators. *Inf. Sci.* **2007**, *177*, 2336–2348. [CrossRef]

92. Sturges, H.A. The choice of a class interval. *J. Am. Stat. Assoc.* **1926**, *21*, 65–66. [CrossRef]
93. Amineh, Z.B.A.; Hashemian, S.J.A.D.; Magholi, A. Integrating Spatial Multi Criteria Decision Making (SMCDM) with Geographic Information Systems (GIS) for delineation of the most suitable areas for aquifer storage and recovery (ASR). *J. Hydrol.* **2017**, *551*, 577–595. [CrossRef]
94. Buckley, J.J. Fuzzy hierarchical analysis. *Fuzzy Sets Syst.* **1985**, *17*, 233–247.
95. Vemuri, N.R.; Jayaram, B. Thecomposition of fuzzy implications. *Fuzzy Sets Syst.* **2015**, *275*, 58–87. [CrossRef]

water

MDPI

Reply

Reply to Louloudis et al. Comments on "Tzampoglou, P.; Loupasakis, C. Hydrogeological Hazards in Open Pit Coal Mines–Investigating Triggering Mechanisms by Validating the European Ground Motion Service Product with Ground Truth Data. *Water* 2023, *15*, 1474"

Constantinos Loupasakis [1,*] and Ploutarchos Tzampoglou [1,2]

[1] Laboratory of Engineering Geology and Hydrogeology, Department of Geological Sciences, School of Mining and Metallurgical Engineering, National Technical University of Athens, 15780 Athens, Greece; tzampoglou.ploutarchos@ucy.ac.cy
[2] Department of Civil & Environmental Engineering, University of Cyprus, Nicosia 1678, Cyprus
* Correspondence: cloupasakis@metal.ntua.gr

The comments of Louloudis, Roumpos, Mertiri, and Kostaridis [1] refer to data related to previous studies and not the one presented in the commented paper [2]. These specific studies have been published and evaluated in numerous articles and international conferences, certifying their validity. Also, a multitude of researchers and organizations align with our viewpoint that overexploitation of the aquifer leads to the activation of land subsidence phenomena [3–7]. The scope of this study is to combine the already verified and published ground truth datasets acquired for the study of mining geohazards with the European Ground Motion Service (EGMS) InSAR dataset, aiming to cross-verify them.

Before responding, we wish to point that the authors of the comments have disclosed a clear conflict of interest, as they were employed by the Public Power Corporation of Greece and were involved as hydrogeological, mining, or geological experts in the engineering study of the Amyntaion mine.

Focusing on the current study, its scope is to combine the ground truth datasets acquired for the study of mining geohazards, namely land subsidence and landslide, with the European Ground Motion Service (EGMS) InSAR dataset, aiming to cross-verify their outcomes. The main objectives of the study are to (a) estimate the spatial distribution of the vertical deformation due to land subsidence and landslide by evaluating the EGMS InSAR datasets; (b) correlate the above data with the data obtained through the geotechnical research highlighting opposite driving failures mechanisms and main causal factors and (c) estimate the interaction between these two catastrophic events.

Regarding the accuracy of the ground water level measurements, the extent of the depression cone, and the equal-drawdown contour maps, we would like to emphasize that the wider mining area has been thoroughly studied for the past 20 years by the authors, and several field work campaigns were conducted in which over 40 boreholes were measured at the wider perimeter of the mine. The equal-drawdown contour lines maps were designed by subtracting the piezometric curves before the start of the mining activities, as reported in the PhD thesis [8] of, at that time, employee of the hydrogeological department of PPC, with the piezometric surfaces that resulted from our campaigns. These maps, along with the methodology used to create them, have been presented in five peer-reviewed papers [9–13] and six international conferences [14–19].

Regarding the irrigation drills, a drills census was conducted during our field work campaigns. The census proved that almost all the drills at the perimeter of the mine, and at more than 2 km, were inactive due to the intensive ground water drawdown. Aiming to cover the irrigation water needs, the farmers at the perimeter of the mine began pumping water from the draining canal network using electricity from the old power supply network, installed initially for the operation of the deep wells' pumps. So, the electricity consumption, used by the authors of the comments [1] as proof of pumping activity, provides false information. This fact has been repeatedly reported to the PPC's scientific personnel and it was also introduced during common on-site field visits.

As far as the extent of the depression cone caused by the mining activities, besides our above reported accurately designed piezometric contour maps, it is clearly presented in maps and cross-sections included in a recent publication [20] cowritten by the, at that time, director of the hydrogeological department of PPC, claiming that it was caused by the practically inactive irrigation drills. So, we both agree that the depression cone exists, although we disagree on its cause.

Please note that it is not just the authors' opinion that the water table drawdown extends to a distance of 2 km, affecting the settlements located at the perimeter of the mine. It is commonly accepted and published in several papers and studies [3–7] that the open pit coal mine hydraulically resembles a huge well with a diameter of 3 to 4 km and appears to be the main cause of the groundwater table level drop, not only in its immediate vicinity but also in a wider area [6], triggering land subsidence phenomena.

Regarding the landslide event, in our publication [2], we identify several preparatory and triggering factors contributing to the triggering of the failure. Although each factor was individually studied, the synergistic interaction among them was not adequately assessed, ultimately leading to the failure's manifestation. As far as the geometry of the slopes, it is provided by simple calculations. Knowing, from high-resolution satellite images, the horizontal distance between the base of the slope and the crown of the benches, as well as the height of the benches and the total depth of the mine, the steepness was calculated. A clear description of the applied procedure can be found in a previous publication [13] and is not included in this manuscript as this is not in the scope of this paper.

The statement that "*the groundwater pore pressure at this depth* (at the depth of 200 m) *is not influenced by the mine's pumping activities in the upper aquifer. Consequently, the 2017 landslide is not related to the pumping operations at the perimeter of the mine.*" proves that, as abovementioned, the multiple causal and triggering factors were not properly evaluated. According to their statement, it is clear that they do not consider the interaction of the extensive faults intersecting the site, the high piezometric loads underneath the floor of the open pit, originating from a deeper karstic aquifer, or the occurrence of the pre-existing sheared zones within the Neogene formations that all together interact and co-act with the pore pressure of the shallow semi-confined aquifer. Also, if the stability of the slopes, as stated by the comments [1], "*is not related to the pumping operations at the perimeter of the mine*", they should not have applied all the draining and pumping measures from the beginning of its operation, avoiding at the same time the occurrence of the land subsidence.

Our findings—derived through a rigorous series of processes—are thoroughly corroborated by EGMS satellite data records, confirming their validity. This particular aspect, which also constitutes the central aim of the original article under discussion, was completely overlooked by the authors of the comment report.

Finaly, we underscore that the EGMS datasets constitute a significant and reliable resource for disentangling the various causal mechanisms of ground deformations that have impacted the study area. Their provision by an independent and internationally

recognized authority ensures that the conclusions drawn are scientifically robust and impartial.

Author Contributions: Both authors analyzed the comments of Louloudis, Roumpos, Mertiri, and Kostaridis and wrote the reply. All authors have read and agreed to the published version of the manuscript.

Funding: This research received no external funding.

Data Availability Statement: Data will be made available by the authors upon request.

Conflicts of Interest: The authors declare no conflicts of interest.

References

1. Louloudis, G.; Roumpos, C.; Mertiri, E.; Kostaridis, P. Comment on Tzampoglou, P.; Loupasakis, C. Hydrogeological Hazards in Open Pit Coal Mines–Investigating Triggering Mechanisms by Validating the European Ground Motion Service Product with Ground Truth Data. *Water* 2023, *15*, 1474. *Water* **2025**, *17*, 2343. [CrossRef]
2. Tzampoglou, P.; Loupasakis, C. Hydrogeological Hazards in Open Pit Coal Mines–Investigating Triggering Mechanisms by Validating the European Ground Motion Service Product with Ground Truth Data. *Water* **2023**, *15*, 1474. [CrossRef]
3. Soulios, G.; Tsapanos, T.; Voudouris, K.; Kaklis, T.; Mattas, C.; Sotiriadis, M. Ruptures on surface and buildings due to land subsidence in Anargyri village (Florina Prefecture, Macedonia). *Environ. Earth Sci.* **2011**, *5*, 505–512.
4. Tsourlos, P. *Research for the Appearance of Surface Cracks in the Valtonera Village, Amyntaio Municipality, Florina Region*; School of Geology of the Aristotle University of Thessaloniki: Thessaloniki, Greece, 2015; p. 17.
5. Gudulas, K. Investigation of the Mechanisms of Operation of Lakes Cheimaditida and Zazari, Located in the Amyntaio Basin, of Florina County, from a Hydrogeological and Environmental Point of View. Ph.D. Thesis, Aristotle University of Thessaloniki, Thessaloniki, Greece, 2012; p. 277.
6. Stamos, A.; Giannoulopoulos, P. *Hydrogeological Report, Geotechnical Work to the Anargiri Village, Aetos Municipality, Florina Prefecture, Greece*; Institution of Geology and Mineral Exploration: Athens, Greece, 2010; p. 34.
7. Tsourlos, P.; Papazaxos, C.; Bargmeziw, G.; Koutalou, B. *Investigation and Suggestions for the Problem Created at the Fault Which as Appeared in Municipalities of Fanos and Ksino Nero*; School of Geology of the Aristotelian University of Thessaloniki: Thessaloniki, Greece, 2007.
8. Dimitrakopoulos, D. Hydrogeological Conditioning at the Amyndeon Mine. Problems Occuring During the Exploitation and their Mitigation Actions. Ph.D. Thesis, National Technical University of Athens, Athens, Greece, 2001.
9. Loupasakis, C.; Angelitsa, V.; Rozos, D.; Spanou, N. Mining geohazards—Land subsidence caused by the dewatering of opencast coal mines: The case study of the Amyntaio coal mine, Florina, Greece. *Nat. Hazards* **2014**, *70*, 675–691. [CrossRef]
10. Tzampoglou, P.; Loupasakis, C. Mining geohazards susceptibility and risk mapping: The case of the Amyntaio open-pit coal mine, West Macedonia, Greece. *Environ. Earth Sci.* **2017**, *76*, 542. [CrossRef]
11. Tzampoglou, P.; Loupasakis, C. Evaluating geological and geotechnical data for the study of land subsidence phenomena at the perimeter of the Amyntaio coalmine, Greece. *Int. J. Min. Sci. Technol.* **2018**, *28*, 601–612. [CrossRef]
12. Tzampoglou, P.; Loupasakis, C. Numerical simulation of the factors causing land subsidence due to overexploitation of the aquifer in the Amyntaio open coal mine, Greece. *HydroResearch* **2019**, *1*, 8–24. [CrossRef]
13. Loupasakis, C. Contradictive mining–Induced geocatastrophic events at open pit coal mines: The case of Amintaio coal mine, West Macedonia, Greece. *Arab. J. Geosci.* **2020**, *13*, 582. [CrossRef]
14. Tzampoglou, P.; Loupasakis, C. New data regarding the ground water level changes at the Amyntaio basin-Florina Prefecture, Greece. *Bull. Geol. Soc. Greece* **2016**, *50*, 1006–1015. [CrossRef]
15. Tzampoglou, P.; Loupasakis, C. Updated ground water piezometry data of the Amyntaio sub-basin and their effect to the manifestation of the land subsidence phenomena. In Proceedings of the 11th International Hydorgeological Congress of Greece, Athens, Greece, 4–6 October 2017.
16. Tzampoglou, P.; Loupasakis, C. Land subsidence susceptibility and hazard mapping: The case of Amyntaio Basin, Greece. In Proceedings of the Fifth International Conference on Remote Sensing and Geoinformation of the Environment (RSCy2017), Paphos, Cyprus, 20–23 March 2017; p. 104441L.
17. Tzampoglou, P.; Loupasakis, C. Land subsidence due to the overexploitation of the aquifer at the Valtonera village. *Bull. Geol. Soc. Greece* **2017**, *50*, 1006. [CrossRef]
18. Tzampoglou, P.; Loupasakis, C. Investigation of land subsidence due to the overexploitation of the aquifer at the Amyntaio basin, Greece. In Proceedings of the 3rd European Regional Conference of IAEG, Euroengeo 2020, Athens, Greece, 8–12 April 2021.

19. Tzampoglou, P.; Loupasakis, C. Land subsidence due to the overexploitation of the aquifer at the Amyntaio basin. In Proceedings of the 12th International Hydrogeological Conference, Nicosia, Cyprus, 20–22 March 2022.
20. Dimitrakopoulos, D.; Koumantakis, I. Hydrodynamic regime of Amynteon basin. Influence of open lignite mines. In Proceedings of the 11th International Hydrogeological Congress of Greece, Athens, Greece, 4–6 October 2017; pp. 101–112.

Disclaimer/Publisher's Note: The statements, opinions and data contained in all publications are solely those of the individual author(s) and contributor(s) and not of MDPI and/or the editor(s). MDPI and/or the editor(s) disclaim responsibility for any injury to people or property resulting from any ideas, methods, instructions or products referred to in the content.

water

MDPI

Comment

Comment on Tzampoglou, P.; Loupasakis, C. Hydrogeological Hazards in Open Pit Coal Mines–Investigating Triggering Mechanisms by Validating the European Ground Motion Service Product with Ground Truth Data. *Water* 2023, *15*, 1474

Georgios Louloudis *, Christos Roumpos *, Eleni Mertiri and Petros Kostaridis

Department of Mining Engineering and Closure Planning, Public Power Corporation of Greece, 10432 Athen, Greece; e.mertiri@ppcgroup.com (E.M.); p.kostaridis@ppcgroup.com (P.K.)
* Correspondence: g.louloudis@ppcgroup.com (G.L.); c.roumpos@ppcgroup.com (C.R.); Tel.: +30-697-000-5090 (G.L.); +30-697-979-9291 (C.R.)

Abstract

The commented paper uses arbitrary and unsubstantiated hypotheses to attribute land subsidence phenomena in the Amyntaion basin to the operations of the Public Power Corporation (PPC) surface coal mine, disregarding, or at least grossly underestimating, the effect of about 600 pumped deep wells for irrigation purposes all over the basin. In addition to the huge difference in the pumped quantities of water from the aquifer, ground water table lowering due to the PPC mine has negligible influence at distances over 500 m from the edge of the mine, while the areas examined in the paper are at distances of several kilometers from the edge of the mine. Furthermore, the authors attribute the landslide that occurred in the mine in 2017 to the steep excavation slopes of the mine and the increased groundwater pore pressure due to reduced peripheral pumping, which is completely inaccurate. To build their case, the authors of the commented paper disregard multiple references in research publications on the above issues, as explained in the main text of this discussion.

Keywords: land subsidence; Amyntaion basin; Copernicus; irrigation wells; pit slopes

1. Introduction

The commented paper by Tzampoglou and Loupasakis purports [1] to provide "*an excellent case study to demonstrate the reliability and value of the EGMS product*", which is not the case, in our opinion. The article does not review the reliability of the Earth Observation data from the European Ground Motion Service (EGMS) of the Copernicus European Union's Earth observation program objectively, but selectively interprets the EGMS data to confirm the main argument of the paper, which is that the mining activities are responsible for the ongoing steady ground subsidence in an area extending at distances more than 2 km from the edge of the mine, and thus affecting the villages in this area. Our claim is that extensive deep pumping for irrigation purposes in the whole valley is responsible for the ground subsidence and damage in the villages.

The "*Introduction*" section of the commented paper does not adequately place the study in a broad context, and the current state of the research field is not thoroughly reviewed, with key publications not highlighted. Although the article investigates subsidence phenomena in the Amynteon basin and the hydrogeological hazards in Open-Pit Coal

Mines, reference [2] concerns environmental contamination, and reference [3] does not refer to mines or open pits but to tailings dam failures. There are also other references that do not correspond to the relevant text. For instance, it is mentioned that "*land subsidence slowly affects extensive areas around mines*" in references [4,5]. In contrast, reference [4] refers to mine collapse and affected buildings at a 200 m distance within the mining area, and reference [5] refers to a study investigating the possibility of land subsidence occurrence and mentions that, as of the publishing date, no damages had been recorded.

Also, the key publications used to investigate the failure mechanisms triggering natural hazards are those of the authors. Similarly, the authors' publications are also the key publications cited to relate the mining dewatering wells to the groundwater level drop extending up to 2 km around the mine, and their impact on the villages of Valtonera and Anargiroi.

Overall, the paper is based on unjustified statements and misconceptions, while the arguments are inconsistent throughout the text and have serious shortcomings, as clearly demonstrated in the following paragraphs.

2. The Authors' Attempt to Attribute Ongoing Steady Subsidence in an Area Extending Several Kilometers Around the Mine to the Mining Activities of PPC, Based on Insufficient Information, Leading to Arbitrary and Unsubstantiated Hypotheses

(a) The authors claim that farming activities cause minor settlements. However, the article lacks critical information [6–9] about the locations, density, and depth of the irrigation wells, and ignores the huge difference in pumped quantities for irrigation purposes compared to the pumping quantities for mining operations. According to undisputed data (electricity consumption for irrigation purposes), the approximately 600 irrigation wells, reaching depths up to 120 m all over the basin [10,11], pump about 40–45 million cubic meters of water per year over the last 25 years, while the PPC mine removed only 4–5 million cubic meters of water per year over the last 15 years (until 2020) via a small number of wells at the perimeter of the mine. In the Amynteon basin, the greatest pressure in the aquifer comes from the irrigation wells and is estimated to be in the order of 80–85% [6]. The authors fail to include and evaluate vital data, as key publications are ignored.

Note that the "control points" of vertical displacement measurements provided by Copernicus are located in areas surrounded by a large number of irrigation wells (Figure 1), presenting an average pumping rate of 25 m^3/h (open data of irrigation wells' permits), where there is an absolute absence of mines' dewatering wells. Based on the pumping rate, the rate of irrigation consumption in Valtonera is estimated to be approximately 0.40 m^3/m^2, which corresponds to an average annual value of 8 million m^3 of groundwater abstraction for irrigation use.

Additionally, in Section 2.2 of the commented paper, "Hydrogeologic Setting", the authors mention that "It is clear that during the last three decades the operation of the mine and, secondarily, the increase of the agricultural activities radically changed the groundwater dynamics of the basin"; however, in Section 3.1, "The Land Subsidence Mechanism", it is mentioned that "the general hydrogeological conditions remain practically unchanged since 1992. The open pit keeps on operating as the main draining source while no extra irrigation wells have been drilled at the wider area". This is contradictory as it is clearly stated initially in the manuscript that there has been an increase in agricultural activities in recent decades, and thus, the groundwater dynamics are influenced by this increase.

In their reply to our comments, the authors state that "Aiming to cover the irrigation water needs the farmers at the perimeter of the mine pump water from the draining canals

network using electricity from the old power supply network installed initially for the operation of the drills' pumps. So, the electricity consumption provides false information about the pumping activities from the aquifers". This is inaccurate, as documented above, and can be disputed by the open data of the irrigation wells' permits (see also Figure 1).

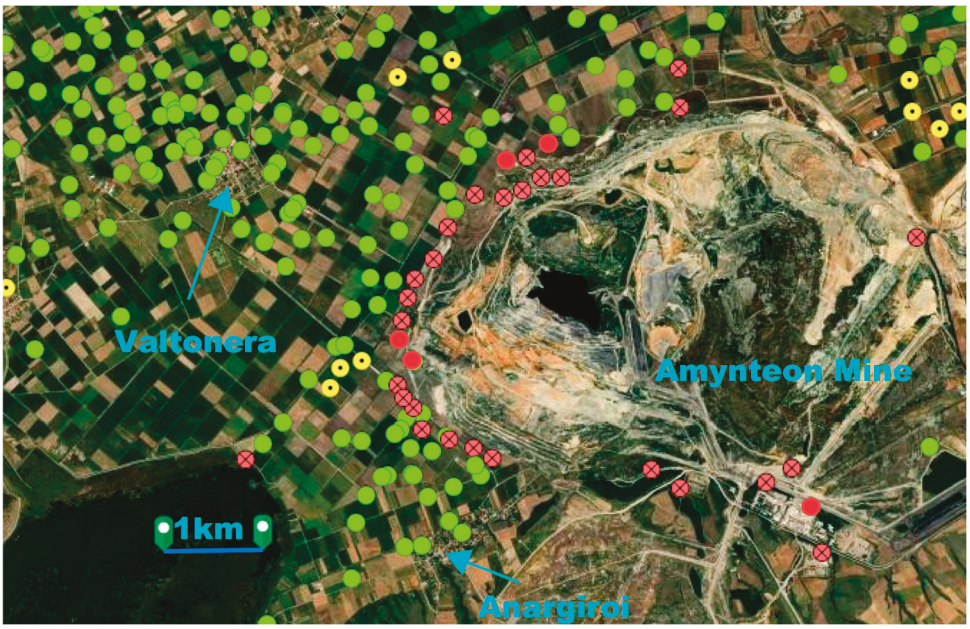

Figure 1. Irrigation pumping wells (green color) in the broader area of Amynteon (Greece) lignite mine, community pumping wells for other uses (yellow) and inactive PPC wells (have been decommissioned and sealed after the mine was decommissioned) in the perimeter (red/pink color) [7].

(b) In addition to the huge difference in the pumped quantities of water from the aquifer, ground water table lowering due to the PPC mine has negligible influence at distances over 500 m from the edge of the mine, while the areas examined in the paper are located at distances 2–8 km from the edge of the mine. The authors overlook the critical influencing factors of constant irrigation pumping over the years and the limited influence zone of the mine's dewatering measures around the mine's perimeter. Neither the mine's dewatering measures nor the mine itself can cause ground deformations at distances greater than an influence zone of a maximum of 500 m [8,12,13].

(c) Many piezometers located closer to the mine show significantly smaller groundwater table drawdown than piezometers located farther away in the valley [10]. It is thus evident that the larger values of groundwater table drawdown in the valley are caused by the operation of hundreds of irrigation wells rather than the peripheral wells of the mine [7]. This statement is also supported by the open data on groundwater table measurements in boreholes located north–northwest of the mine (Figure 2), at Valtonera village and the irrigation area between Valtonera and Pedino villages [14]. This confirms the importance of the hundreds of irrigation wells in lowering groundwater tables.

(d) The authors claim that "currently the open pit along with the surrounding draining wells operate as an oversized (4 km wide) well, continuously draining a big part of the Amyntaio basin". This is not correct as the dewatering wells were terminated in April 2020, and thus, the mine was decommissioned [8,9]. Also, according to the National Water Monitoring Network [14], it is evident that the groundwater level has been stabilized (as indicated by measurements conducted from 2018 to 2020, Figure 2).

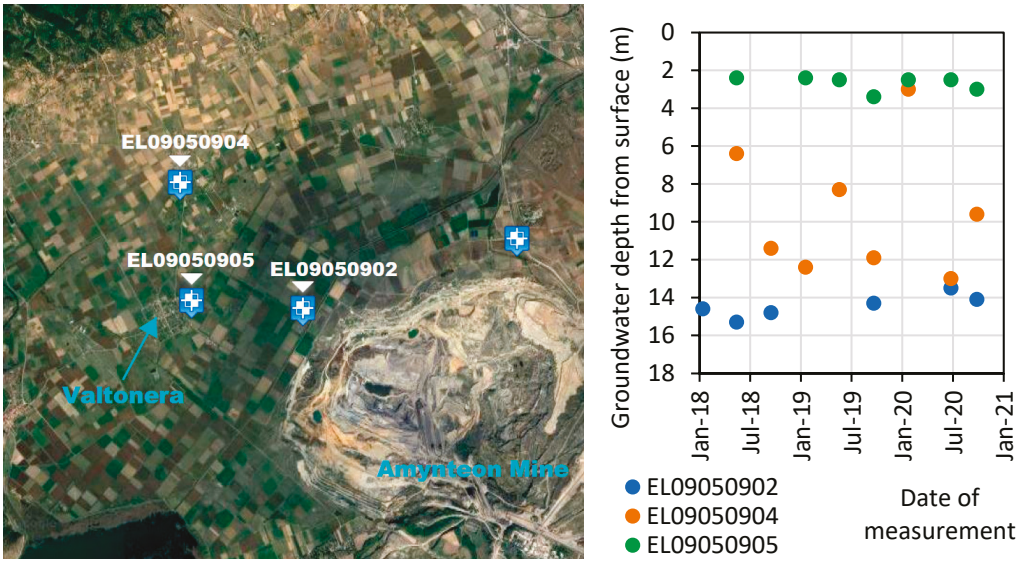

Figure 2. Monitoring of groundwater via the National Water Monitoring Network in the area near the mine. The open data concern period: 2018–2020 [14].

In their reply to our comments, the authors state that "*it is clearly presented in maps and cross sections included at a recent publication* [13] *written by the, at that time, director of the hydrogeological department of PPC, claiming that it was caused by the practically inactive irrigation drills*". This is also not correct, as in [13], it is clearly stated that the groundwater level dropdown in the valley (away from the mine's perimeter) is caused by the irrigation wells. Also, the same reference mentions that the negative water balance in the Amynteon aquifer was noticed before the beginning of the mine's pumping wells.

Also, in the authors' reply, it is stated that "It is commonly accepted that, the open pit coal mine resembles hydraulically to a huge well with a diameter of 3 to 4 km and appears to be the main cause of the groundwater table level drop not only in its immediate vicinity but also in a wider area, triggering land subsidence phenomena". This statement is supported only by a PhD thesis and a Technical Report, which, although mentioning this phenomenon, fail to justify it.

(e) Moreover, the authors mention that "*the data from May 1992 relate to the period before the operation of the open pit coal mine* [15]"; however, this is not correct as the mine was operating during that time. Based on the authors' reference [15], the groundwater drawdown during 1986 and 1992 (6-year time period) was 4–5 m and locally 6 m due to the overexploitation of the Amynteon aquifer by farmers for irrigation purposes. Note that dewatering measures were adopted to protect the surface mine during its operation after 1993. Therefore, based on the authors' reference [15], agricultural activities had a great influence on groundwater, which was evident in the area before the beginning of the mine's dewatering measures around the mine's perimeter. The authors fail to include and evaluate vital data from the publication [15] cited in their article, while other key publications, such as [6–9,14], are ignored.

(f) Figure 3 in the commented paper presents the groundwater level dropdown between certain periods, for a 23- and 24-year time period. This dropdown should be an outcome of the data processing and evaluation via piezometric maps (authors' own measurements in a three-year (3) period in 37 points). It is easy to verify that the dropdown contour lines are erroneous and do not correspond to the piezometric maps. For instance, according to the authors' piezometry, there is practically no groundwater level dropdown in the Valtonera and Anargiroi villages between the years 2014 and 2016. While comparing these measurements to those of 1992, a level dropdown of up

to 5 m can be estimated. However, the calculated dropdown level presented by the authors is 10–20 m. It is evident that the outcome of the groundwater level dropdown is not verified from the "Ground truth datasets" used in the article. The same applies to Figure 4 in the commented paper for the incorrect groundwater level dropdown maps. Additionally, the statement in Section 3.1 of the commented paper, "*. . .at Valtonera village. The observed water level drop in this area of around 10 to 20 m. . .*" is inaccurate and inconsistent with the authors' own water level measurements.

Following the argument above, it is evident that there is practically no groundwater level dropdown in the Valtonera and Anargiroi villages. Therefore, it is derived that there is no correlation between the mentioned groundwater level dropdown and the vertical deformations provided by the Copernicus Land Monitoring Service. Thus, all the related statements in the article are incorrect.

(g) The borehole network where the groundwater measurements occur is important and should be considered in the evaluation process. For the year 1992, no network is presented. According to the authors' reference [15], in 1992, the network where the measurements occurred was scarce, while there was no network in a ~3 km radius around Valtonera village, nor between Valtonera and Anargiroi villages.

(h) The authors present the groundwater table contour lines in different time periods. However, the extent of the mine presented in the satellite images does not match the real extent during the respective time period. This is crucial for conducting proper piezometric maps.

3. The Authors Attribute the Landslide Which Occurred in the Mine in 2017 to the Steep Excavation Slopes of the Mine and the Increased Groundwater Pore Pressure Due to Reduced Peripheral Pumping, Which Is Completely Inaccurate

(a) The authors relate the land subsidence phenomenon and the landslide that occurred in 2017 to the dewatering of the mine. This is inaccurate and inconsistent with the authors' own water level measurements, which clearly show that there is practically no groundwater level dropdown in the Valtonera and Anargiroi villages, as documented above. Therefore, the correlation with the vertical deformations provided by the Copernicus Land Monitoring Service does not apply, and thus, all related statements in Tzampoglou and Loupasakis (2023) are not supported by the data. Note that the locations where the vertical deformations are presented (see authors' InSAR data in relation to Figure 1 above) are contiguous with irrigation wells and at a significant distance from the mine's dewatering wells. Also note that the dewatering measures stopped in April 2020, while the irrigation wells have not yet stopped.

(b) The authors mention that "*the pumping activities directly adjacent to Anargiroi village, according to PPC* [13], *were essentially stopped in 2016, aiming to eliminate the deformation caused by overpumping at the nearby village*". However, according to the same reference, this is not accurate, as no such information is presented. Thus, the writers' outcome, where the mine's pumping activities are related to the landslide, is not supported.

(c) The authors' statement "*The drop in the groundwater level, combined with the area's general geotectonic setting, triggered extensive land subsidence in an area extending up to 2 km around the mine, causing damage to villages and infrastructure since 2002*" is not correct, because the effect of any large well is related to the magnitude of the drawdown (which in our case is 80–100 m close to the mine's perimeter) and is independent of the well diameter. Concerning the influence zone, this is also evident in hydrogeological cross sections that include water levels in boreholes [11,13]. Please note that any dropdown

in groundwater level can only enhance the stability of slopes and cannot trigger the landslide phenomenon.

(d) Based on the actual geometric data of the mining operations, all statements in the paper regarding the pit slopes and the geometry of the mine benches are inaccurate. Specifically, based on all available data and satellite images, there is no evidence to suggest that steep slopes were applied, or the excavation of the lower benches of the coal seams was prioritized, or that the excavation of the middle benches was systematically neglected. This is also verified in the Audit Findings report of the committee experts [16].

Moreover, no geometrical data are presented to support this statement. In their reply, the authors do not answer our comments and do not provide any data but only mention that they applied the Pythagorean theorem to calculate the steepness, knowing "*the horizontal distance between the base of the slope and the crown of the benches as well as the high of the benches and the total depth of the mine*". This statement is completely irrelevant to our arguments, and, of course, it is obvious that no application of the Pythagorean theorem is related to the overall slope calculation.

(e) The mine's pumping was limited at the upper aquifer (i.e., up to a depth of 100 m) that lies above the impermeable lignite strata [9], while the total depth of the mine pit exceeds 200 m, and the sliding occurred along a sub-horizontal lignite-to-clay/marl interface [17] at depth about 200 m. Thus, the groundwater pore pressure at this depth is not influenced by the mine's pumping activities in the upper aquifer. Consequently, the 2017 landslide is not related to the pumping operations at the perimeter of the mine.

In conclusion, the commented paper is based on inaccurate information and fails to present and evaluate the controversial and diverging aspects, leading to a misinterpretation of the data and, eventually, a misjudgment about the real causes of the described events. We point out that, due to the great importance and potential legal implications of these events for the operator of the mine (PPC), groundwater table levels around the mine have been monitored and studied for many years by geologists and engineers of PPC and by independent experts [10,11]; they all reach conclusions opposing the conclusions presented in the commented paper.

Author Contributions: All authors (C.R., G.L., E.M. and P.K.) analyzed the article of Tzampoglou and Loupasakis and designed and wrote the comment paper. The findings are based on the original work and analysis of all authors. All authors have read and agreed to the published version of the manuscript.

Funding: This research received no external funding.

Data Availability Statement: Data will be made available by the authors upon request.

Conflicts of Interest: All authors have been involved as hydrogeological, mining, or geological experts in the mining engineering study of the Amyntaion mine.

References

1. Tzampoglou, P.; Loupasakis, C. Hydrogeological Hazards in Open Pit Coal Mines–Investigating Triggering Mechanisms by Validating the European Ground Motion Service Product with Ground Truth Data. *Water* **2023**, *15*, 1474. [CrossRef]
2. Passariello, B.; Giuliano, V.; Quaresima, S.; Barbaro, M.; Caroli, S.; Forte, G.; Carelli, G.; Iavicoli, I. Evaluation of the environmental contamination at an abandoned mining site. *Microchem. J.* **2002**, *73*, 245–250. [CrossRef]
3. WISE_Uranium_Project. Chronology of Major Tailings Dam Failures. Available online: https://www.wise-uranium.org/mdaf.html (accessed on 8 June 2023).
4. Sun, Y.; Zhang, X.; Mao, W.; Xu, L. Mechanism and stability evaluation of goaf ground subsidence in the third mining area in Gong Changling District, China. *Arab. J. Geosci.* **2015**, *8*, 639–646. [CrossRef]

5. Wolkersdorfer, C.H.; Thiem, G. Ground water withdrawal and land subsidence in northeastern Saxony (Germany). *Mine Water Environ.* **1999**, *18*, 81–92. [CrossRef]
6. Ministry for the Environment, Energy and Climate Change. Approved River Basin Management Plan 1st Update. Available online: http://wfdver.ypeka.gr/en/management-plans-en/# (accessed on 8 June 2023).
7. Ministry for the Environment, Energy and Climate Change. Irrigation Wells. Available online: http://lmt.ypeka.gr/public_view.html (accessed on 8 June 2023).
8. Kavvadas, M.; Roumpos, C.; Servou, A.; Paraskevis, N. Geotechnical Issues in Decommissioning Surface Lignite Mines—The Case of Amyntaion Mine in Greece. *Mining* **2022**, *2*, 278–296. [CrossRef]
9. Louloudis, G.; Louloudis, E.; Roumpos, C.; Mertiri, E.; Kasfikis, G.; Chatzopoulos, K. Forecasting Development of Mine Pit Lake Water Surface Levels Based on Time Series Analysis and Neural Networks. *Mine Water Environ.* **2021**, *41*, 458–474. [CrossRef]
10. Kavvadas, M.J.; Agioutantis, Z.; Skourtsos, E.; Steiakakis, C. *Evaluation of the Causes of Surface Ruptures and Differential Settlements that Have Been Observed in the Amynteon Basin, with Emphasis on the Area Around the Mine and at Valtonera Village, Municipality of Amyntaio*; Study of the Hydrogeological Regime and the Changes in Piezometry in the Area the Amynteon Basin; Public Power Corporation: Athens, Greece, 2021; Unpublished. (In Greek)
11. Konstantopoulou, G.; Nikolaou, N.; Sabatakakis, P.; Tzima, M.; Mattheopoulos, D.; Parcharidis, I.; Karavias, A.; Gatsios, T.; Babousis, K. *Monitoring the Ground Movements in the Wider Area of the Amynteon Mine*; EAGME: Athens, Greece, 2021; Unpublished. (In Greek)
12. Stefouli, M.; Panagiotopoulou, A.; Charou, E.; Spastra, Y.; Bratsolis, E.; Madamopoulos, N.; Perantonis, S. Assessment of the Added Value of Sentinel1&2 for Mapping and Monitoring Surface Mining. In Proceedings of the 14th International Symposium of Continuous Surface Mining, Thesaloniki, Greece, 23–26 September 2018; Sideri, D., Paraskevis, N., Eds.; pp. 73–87.
13. Dimitrakopoulos, D.; Koumantakis, I. Hydrodynamic regime of Amynteon basin. Influence of the open lignite mines. In Proceedings of the 11th International Hydrogeological Congress, The Geological Society of Greece, Athens, Greece, 4–6 October 2017; pp. 101–112. (In Greek)
14. Ministry for the Environment, Energy and Climate Change. National Monitoring Water Network. Available online: http://nmwn.ypeka.gr/?q=en/content/home (accessed on 8 June 2023).
15. Dimitrakopoulos, D. Hydrogeological Conditions of Amyndeon Mine. Problems During Exploitation and Overcoming Them. Ph.D. Dissertation, National Technical University of Athens School of Mining and Metallurgical Engineering, Athens, Greece, 2001. (In Greek)
16. Papageorgiou, C.; Kavvadas, M.; Marinos, P.; Gazetas, G.; Kolovos, C.; Roumpos, C.; Machtis, K.; Chaloulos, K.; Pavlidis, S. *Experts Evaluation Report of the Committee on the Landslide of Amynteon Mine on June 10th 2017*; National Technical University of Athens (NTUA), Aristotle University of Thessaloniki (AUTH), Public Power Corporation (PPC): Athens, Greece, 2017; Unpublished. (In Greek)
17. Kavvadas, M.; Roumpos, C.; Schilizzi, P. Stability of Deep Excavation Slopes in Continuous Surface Lignite Mining Systems. *Geotech. Geol. Eng.* **2020**, *38*, 791–812. [CrossRef]

Disclaimer/Publisher's Note: The statements, opinions and data contained in all publications are solely those of the individual author(s) and contributor(s) and not of MDPI and/or the editor(s). MDPI and/or the editor(s) disclaim responsibility for any injury to people or property resulting from any ideas, methods, instructions or products referred to in the content.

MDPI AG
Grosspeteranlage 5
4052 Basel
Switzerland
Tel.: +41 61 683 77 34

Water Editorial Office
E-mail: water@mdpi.com
www.mdpi.com/journal/water

Disclaimer/Publisher's Note: The title and front matter of this reprint are at the discretion of the Guest Editors. The publisher is not responsible for their content or any associated concerns. The statements, opinions and data contained in all individual articles are solely those of the individual Editors and contributors and not of MDPI. MDPI disclaims responsibility for any injury to people or property resulting from any ideas, methods, instructions or products referred to in the content.

Academic Open
Access Publishing

mdpi.com

ISBN 978-3-7258-8376-9